



15th Physical Chemistry Conference



Effect of different acids to functionalization carbon nanotubes

A.Manafi^a.Z.Kamali^b

Department of engineering, Shahrood branch, Islamic azad university, Shahrood, Iran

^a Email: ali_manafi2005@yahoo.com

^b Email: zeynabkamaly@yahoo.com

Key words: carbon nanotubes, functionalization, functional groups

Introduction:

Chemical functionalization is a procedure used in materials science to oxidize the surface of materials. Several researchers use this technique to improve carbon nanotubes (CNTs) interaction and dispersion. The present article evaluates the effect of different functionalization methodologies on dispersion of CNTs in aqueous media. Hence, outset CNTs were immersed in two different acidic media such as H₂SO₄/HNO₃ and H₂SO₄/HNO₃/HCl. Afterwards sake survey the creation of functional groups on CNTs, used analysis of raman spectroscopy, transform fourier infrared spectroscopy. The peresence of hydroxyl and carboxylic functional groups on CNTs was proved using of this analysis. Also, it was photographed from the nanotubes by the Electron microscopy before and after the acthoi and the functionalization was identified. However, by the analysis, dispersion in aqueous media has been observed, that using from two media with 12 Molar density and heat can attraet some of the suitable functional groups on the carbon nanotubes tubes surface [1-4].

Materials and methods:

Carbon nanotubes (95%) purchased from research institute of petroleum industry, nitric acid, sulfuric acid, hydrochloric acid and ammonium hydroxide were purchased from merck germany. In the first method, the nanotubes in a mixture of sulfuric acid and nitric acid with 3 to 1 ratio for 4 hours on a magnetic agitator with a temperature of 150 ° C was placed and then rest for 20 hours on. Ammonium hydroxide is then added to the mixture using filter



paper, clear, several times washed with distilled water and the pH was brought to about 5. Flat for 4 hours in the drying oven temperature was 85 ° C . All procedures were performed with different concentrations of acids.

Apparatus:

Devices used in this project are: Scanning electron microscope (SEM), transmission electron microscopy (TEM), raman spectroscop, fourier transformed infrared spectroscopy (FT-IR).

Result and discussion:

Chemical functionalization of the surface of CNTs was investigated using different acid treatments, and its characterization was carried out using various characterization tools. The results obtained by raman spectroscopy indicated the maintenance of the structure of CNTs after oxidation. The addition of carboxyl and hydroxyl groups was confirmed by FT-IR.

Conclusion:

From the experimental results obtained for different acid treatments, it is possible to conclude that all methodologies used showed a percentage of adsorption of functional groups on the CNTs. However, by the analysis Fourier transformed infrared spectroscopy has been observed, that using from two media with 12 molar density and heat can attraet some of the suitable functional groups on the carbon nanotubes tubes surface.

Reference:

- [1]A.Osorio,I. Silveira, V.Bueno, C.Bergmann."H₂SO₄/HNO₃/HCl-Functionalization and its effect on dispersion of carbon nanotubes in aqueous media"; Applied Surface Science 255, 2008, 2485.
- [2] J.H. Lehman, M. Terrones, E. Mansfield, K.E. Hurst, V. Mcunier, "Carbon, 49".; 2011, 2581-2602.
- [3]Banerjee, MGC, Wong,"Rational chemical strategies for carbon nanotube functionalization, Chem Eur J".;9(9):1899-908, 2003.



[4]J.Bao,Q.Cheng; X.Wang, Z.Liang, B.Wang, "Zhang, Mechanical Properties of Functionalized Nanotube Buckypaper Composites", High-Performance Materials Institute, Florida State University, Tallahassee, FL 32310, USA.

15th Physical Chemistry Conference



Gold nanoparticle production optimization by a metal-tolerant bacterium as an effective clean technological approach

M. Moeinzadeh^{a*}, H. R. Karbalaeei-Heidari^a, B. Hemmateenejad^b, S. Dorostkar^b

^a Department of Biology, Faculty of Sciences, Shiraz University, Shiraz, Iran

^b Department of Chemistry, Faculty of Sciences, Shiraz University, Shiraz, Iran

Email: mitra_moeinzadeh@yahoo.com

Key word: Gold nanoparticle, Biosynthesis, Optimization.

Introduction:

The development of techniques for the synthesis of nanoparticles with well-defined size, shape and composition is a challenge and an important area of research in nanotechnology. Many microorganisms have the ability to produce inorganic nanostructures and metal nanoparticles with properties similar to chemically-synthesised materials, while exercising control over the size, shape and composition of the particles. This alternative approach to chemical synthesis procedures uses microbial systems for the production of nanosized materials. Extracellular synthesis of gold nanoparticles in the presence of bacterial cell extract has been successfully demonstrated. The possibility to manipulate the size and shape of gold nanoparticles by altering key growth parameters and incubation conditions is an interesting field and is under investigation by many researchers. The results could provide some understanding as to which parameters may have significant effect on the formation of these green and cost-effective gold nanoparticles.

Materials and methods:

The bacterial strain used in this study was isolated from Sarcheshmeh copper mine of Kerman. The bacteria was grown aerobically in nutrient broth media and incubated at 30°C and agitated at 180 rpm for 48 h. After the incubation, the supernatants were obtained by centrifugation of bacterial culture at 3000 g for 8 min and the gold ions from hydrogen tetrachloroaurate solution were added. To investigate the effect of changes in key incubation parameters to

biosynthesis of gold nanoparticles, a range of different temperatures, pH and gold ions concentration was studied, while the resulting solutions were incubated for 30 h. Control (without the gold ions only supernatant) was also run along with the experimental flask. After 30 h of incubation the cell free supernatant containing nanoparticles were obtained.

Apparatus:

It is aimed in this present work to investigate extra-cellular biosynthesis of Au NPs using bacteria, moreover, measuring the UV–visible spectra of the resulting Au NPs. Furthermore, the particles size and morphology were also monitored by the transmission electron microscopy.

Result and discussion:

Investigation of different incubation parameters revealed that optimum temperature, pH and gold ions concentration for biosynthesis of nanoparticles were 37 °C, 7.0 and 2 mM respectively. Studies of changes in incubation temperature of the solutions showed that low temperatures (4-20°C) causes no nanoparticle production and high temperatures (40-60°C) causes high reduction rate and also aggregation states. Likewise the results implied that variations in pH during exposure to Au-ions had an impact on the size of the particles. In the acidic conditions (pH 3.0-5.0), enzymes and proteins present in cell free supernatant of the bacteria are likely to be precipitate, and no gold nanoparticle production occurred. In contrast, increases in the solution pH (8.0-9.0) with the appearance of dark color showed the production of cumulative sized nanoparticles.

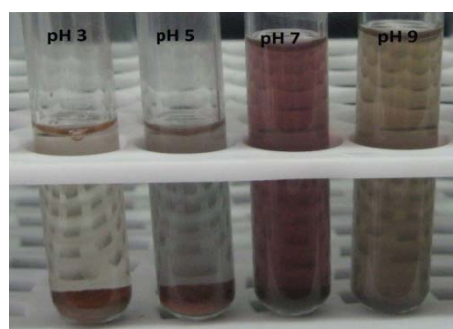


Fig. 1. Photo of Au NPs prepared by cell free supernatant with pH 3, 5, 7, 9 (from left to right), respectively:



Conclusion:

The extracellular synthesis of various sizes of gold nanoparticles in a gram positive and metal tolerant bacterium has been investigated. The rate of particle formation and therefore the size of the nanoparticles could, to an extent, be manipulated by controlling parameters such as gold ions concentration, pH of cell extract and the incubation temperature. The development of biological and chemical procedures to control the morphology of nanoparticles is an ongoing area of research. A biological process with the ability to strictly control the shape of the particles produced would therefore be an exciting prospect. However, the cellular mechanism leading to the biosynthesis of gold nanoparticles is not yet fully understood. Further research will therefore focus on the development of a fundamental understanding of the process mechanism on a cellular and molecular level, including isolation and identification of the compounds responsible for the reduction of gold ions.

Reference:

- [1] Subramanian, A. Muthukumaran, S. "Biosynthesis and characterization of gold nanoparticle using anti parkinsonian drug *Mucuna pruriens plant extract*", Int. J. Res. Pharm. Sci.; Vol-1, Issue-4, 417-420, 2010.
- [2] Prashant, M. Nisha, K. "Biosynthesis of nanoparticles: technological concepts and future applications"; J Nanopart Res 10:507–517, 2008.
- [3] Mariekie, G. "Microbial Production of Gold Nanoparticles", Gold Bulletin• 39/1, 2006.
- [4] Hussein, M.I. Aziz, M. A. E.Badr, Y.E. Mahmoud, M.A. "Biosynthesis of gold nanoparticles using *Pseudomonas aeruginosa*." Spectrochimica Acta Part A.; 67,1003–1006, 2007.



The electric field dependence of hydrogen adsorption on silicon carbide nanotube

E. Masumian, S.M. Hashemianzadeh,

Department of Chemistry, Iran University of Science and Technology, Tehran, Iran
(Email: masumiyan@gmail.com)

Keywords: Silicon Carbide Nanotube, Binding Energy, Density Functional Theory (DFT), Density of States (DOS)

Introduction:

Hydrogen is capable of carrying more energy per unit mass than fossil fuels [1], releases no pollutant material such as greenhouse gases, and also is abundant enough to be used by future generations. Nevertheless, there is an essential problem to transport this energy carrier. The researchers working on this field are looking for the materials which have high capacity to store hydrogen under ambient temperature and pressure. Recently, using Si, stable materials such as silicon carbide nanotubes (SiCNTs) have been fabricated[2]. Among their numerous capabilities, more reactivity of SiCNTs to gases particularly hydrogen due to their higher polarity than that of carbon nanotubes (CNTs) and also boron nitride nanotubes (BNTs)[3], has boosted the attention to these nanostructures to find a solution for the indispensable problem of hydrogen storage. In addition to these, applying the electric field could be a promising pathway to increase the adsorption of hydrogen on the surface of polarizable materials [1]. In this study we intend to apply a transverse electric field on SiCNT.

Methods:

We considered an armchair (5, 5) silicon nanotube. The dangling bonds were saturated by hydrogen atoms at the two ends. Our structures optimizations and the total energy calculations are based on density functional theory (DFT). To achieve more accurate data, the H₂ molecule and its nearest six silicon atoms were treated with the 6-311++G(d,p) basis set, whereas the



other atoms were treated with the 3-21G basis set. All the calculations were carried out by the MPW1PW91 exchange-correlation function, which can supply a more accurate dispersion force than B3LYP[4].

Results and Discussion:

There are four typical adsorption sites: on top of C atom, on top of Si atom, on the Si-C bond(bridge), and the middle of hexagon(hollow). All these cases have been considered for adsorption of H₂ on the SiCNT surface. Our results show that the C atom is the most favorable adsorption site. The electric field of magnitude ranges from 0 to 0.015 a.u. could enhance the binding energy from 2.17 to 4.18 Kcal/mole. Since SiCNT becomes polarized there are different electron densities on each site. We found that the higher the electron density is, the larger value of binding energy is obtained. Although some sites indicate less adsorption energy than another but their overall value implies that the adsorption is enhanced. The density of states (DOS) spectrums display that the semiconductor property of SiCNT is retained under electric field strength of 0.015 a.u.

Conclusion:

In summary we can claim that the transverse electric field increases the hydrogen adsorption on SiCNT.

References

- [1] J. Zhou, Q. Wang, Q. Sun, P. Jena, and X. S. Chen, Proc. Natl. Acad. Sci. U S A. **107**, 2801 (2010).
- [2] X. H. Sun, C.P. Li, N.B. Wong, S.T. Lee, and B.K. Teo, J. Am. Chem. Soc. **124**, 14464 (2002)
- [3] G. Mpourmpakis, G. E. Froudakis, G. P. Lithoxoos, and J. Samios, Nano Lett. **6**, 1581 (2006).
- [4] C. Lee, W. Yang, and R. G. Parr, Phys. Rev. B **37**, 785 (1988).



PANHs adsorption onto CMK-1/SDS-Fe carbon modified nanoporous sorbent by SPE-UV technique from aqueous media

M.B. Ghasemian^{a*}, M. Anbia^a, S. Shariati^b

^a Research Laboratory of Nanoporous Materials, Faculty of Chemistry, Iran University of Science and Technology, Farjam Street, Narmak, Tehran 16846, Iran

(Email: ghasemian@chem.iust.ac.ir)

^b Department of Chemistry, Science and Research Branch, Islamic Azad University, Guilan, Rasht, Iran

Keyword: PANH, 1,10-Phenanthroline, 2,2'-Bipyridine, SPE, Nanoporous sorbent, CMK-1

Introduction:

The selection of the appropriate extraction system is an important stage in the elaboration of analytical procedure. Solid-phase extraction is one of the most popular sample preparation methods. In this case, the knowledge of the interactions between isolated compounds, sorbent and elution solvents seems to be important. The selection of the appropriate sorbent is an important stage in the elaboration of the analytical method.

Methods:

In this study, a solid phase extraction (SPE) preconcentration system was developed for determination of 1,10-Phenanthroline and 2,2'-Bipyridine at ppb level. The method is based on retention of these compounds on a column of nanoporous sorbent CMK-1 modified with dodecyl sulfate sodium salt (SDS) and Fe⁺³ ions and subsequently elution with dimethyl sulfoxide (DMSO) and determination by UV-Vis at $\lambda_{\max(\text{phen})} = 264$ and $\lambda_{\max(\text{bpy})} = 280$ nm. The controllable factors such as pH, solution speed, sorbent mass, eluent volume and elution speed have been optimized applying the Taguchi method. At first, MCM-48 was synthesised as a silica nanoporous sorbent according to the synthesis procedure described by Shao et al [1]. Then CMK-1 mesoporous carbon was prepared by using MCM-48 material as template and sucrose as the carbon source. The obtained composite was then pyrolyzed in a nitrogen flow at



1173 K and kept under these conditions for 6 h to carbonize the polymer[2]. The carbon–silica composite thus obtained was washed with 1 M NaOH solution of 50% ethanol–50% H₂O twice at 363 K, in order to dissolve the silica template completely. The carbon samples obtained after the silica removal were filtered, washed with ethanol and dried at 393 K [3]. Modification with SDS aionic surfactant was carried out by treating of CMK-1 sorbent in 100mL solution of SDS surfactant at respective critical micelle concentration. The modified sample was filtered without rinsing and dried at 110 °C and then mixed with FeCl₃ in HCl 0.1 N solution under vigorous stirring for 1 h and filtered without washing and finally dried at 60 °C in order to obtain CMK-1/SDS-Fe⁺³. Next, this obtained modified nanoporous sorbent packed between two frits into a SPE glass column. Afterward, a solution included specific concentration of 1,10-Phenanthroline and 2,2'-Bipyridine passed throughout the sorbent in the SPE column [4]. The adsorption percentages of 1,10-Phenanthroline and 2,2'-Bipyridine were determined by measuring of concentration difference between primary and exited solutions[5]. Finally, certain volume of dimethyl sulfoxide (DMSO) used as eluent for recovery and desorption of 1,10-Phenanthroline and 2,2'-Bipyridine into the CMK-1/SDS-Fe sorbent and the extraction efficiencies were measured by UV-Vis[6].

Results and discussion:

These PANH compounds were selectively adsorbed in a column which was filled up with CMK-1/SDS-Fe⁺³ modified sorbent. The limits of detection for 1,10-Phenanthroline and 2,2'-Bipyridine were 8.75 and 10.1 µg/L respectively. Recovery at 25 µg/L level for 1,10-Phenanthroline and 2,2'-Bipyridine were 92.8 and 92.2% respectively. Finally, extraction and determination of 1,10-Phenanthroline and 2,2'-Bipyridine from real sample was successfully investigated.

Conclusion:

The controllable factors such as pH, solution speed, sorbent mass, eluent volume and elution speed have been optimized applying the Taguchi method. The method and CMK-1/SDS-Fe



sorbent was successfully, effectually and selectively applied to adsorption and determination of 1,10-Phenanthroline and 2,2'-Bipyridine in real water sample.

References:

- [1] Y. Shao, L. Wang, J. Zhang, M. Anpo, *Micropor. Mesopor. Mater.* 109 (2005) 20835–20841.
- [2] Mansoor Anbia, Nour Ali Mohammadi, Kaveh Mohammadi. 2010 *Journal of Hazardous Materials* 176 (1-3), pp. 965-972.
- [3] Mansoor Anbia, Maryam Lashgari. 2009 *Chemical Engineering Journal* 150 (2-3), pp. 555-560.
- [4] Mansoor Anbia, Saba Asl Hariri, *Desalination*, Volume 261, Issues 1-2, 15 October 2010, Pages 61-66.
- [5] Mansoor Anbia, Nourali Mohammadi *Desalination*, Volume 249, Issue 1, 30 November 2009, Pages 150-153.
- [6] Shabani, A.M.H., Dadfarnia, S., Dehghani, Z. - *Talanta* 2009, 79 (4), pp. 1066-1070.



A Comparative Study for Removal of Alizarin Red S from Aqueous Samples by Magnetic Nanoparticles of Fe_3O_4 , CoFe_2O_4 and Fe_3O_4 by Using Ionic Liquid as Modifier

S. Kamran* and N. Amiri Shiri

Department of Chemistry, Payame Noor University, PO Box 19395-3697 Tehran, IRAN

* E-mail: kamran_ss5@yahoo.com

Keywords: Adsorption, Alizarin Red S, Ionic liquid, Magnetic Nanoparticle

Introduction:

Dye and dye stuffs are extensively used in various areas such as textile, plastic, food, cosmetic, carpet and paper industries. Wastewaters of these industries contain dye with metals, salts, and other chemicals which may be toxic to aquatic environment. Hence, the presence of dyes in wastewaters is a major environmental problem as they are generally resistant to degradation by biological treatment methods. Many investigations have been reported using different methods for the removal of dyes from water and wastewater including biological processes, combined chemical and biochemical processes, chemical oxidation, adsorption, coagulation, and membrane treatments. Several articles have been published on the application of various nanoparticles for the treatment and remediation of pollutants in the environment [1-3].

This work focuses on comparative study for the removal of Fe_3O_4 , CoFe_2O_4 and IL- Fe_3O_4 nanoparticles as adsorbents for adsorption of alizarin red S. Adsorption isotherms, kinetic of adsorption and thermodynamic parameters were characterized.

Methods:

Aliquots of 20 mL of the dye solutions with initial concentrations of 10–100 mg L⁻¹ in the pH range of 3.0-12.0, adjusted by 0.10 mol L⁻¹ of HCl and NaOH solutions were prepared and



transferred into individual beaker. A known dosage of nanoparticles in the range of 0.01-0.03 g was added to each solution and the suspension was immediately stirred with a magnetic stirrer for a predefined period of time (1-20 minutes). After the mixing, the nanoparticles were magnetically separated and the solution was analyzed for the residual dye spectrophotometrically at 520 nm. The percent adsorption of dye, i.e. the dye-removal efficiency of IL-Fe₃O₄, was determined by using the following equation:

$$\text{Dye removal efficiency (\%)} = \frac{(C_0 - C_f)}{C_0} \times 100$$

where C_0 and C_f represent the dye concentrations (mg L⁻¹) before and after adsorption, respectively.

Results and discussion:

The mean size and the surface morphology of the nanoparticles were characterized by TEM, XRD and FTIR techniques. Adsorption studies of alizarin red S was performed under different experimental conditions in batch technique. Experimental results indicated that Fe₃O₄, CoFe₂O₄ and IL-Fe₃O₄ nanoparticles had removed more than 98% of dyes under optimum condition. The isotherm evaluations revealed that the Langmuir model attained better fits to the equilibrium data than the Freundlich model. The maximum adsorption capacities on Fe₃O₄, CoFe₂O₄ and IL-Fe₃O₄ 140.8, 192.3 and 256.4 mg g⁻¹ and Langmuir adsorption constants 0.078, 0.197, 0.28 respectively. The changes of enthalpy (ΔH) were determined to be 29.5, -65.8 and 32.2 kJ mol⁻¹ for Fe₃O₄, CoFe₂O₄ and IL-Fe₃O₄, in the same order. The applicability of two kinetic models including pseudo-first order and pseudo-second order models was estimated. Dye was desorbed from nanoparticles by alkaline solution at pH 11 for Fe₃O₄ and acidic solution at pH 3.0 for IL-Fe₃O₄ and CoFe₂O₄ nanoparticles and adsorbents were reused.

Conclusions:

Magnetic nanoadsorbents of Fe₃O₄, CoFe₂O₄ and IL-Fe₃O₄ were fabricated. The surface morphology of the nanoparticles was characterized by TEM, XRD and FTIR techniques. The



FTIR analysis demonstrated the attachment of $[C_8MIM][Br]$ on the surface of Fe_3O_4 nanoparticles was achieved via the interaction between the cationic part of $[C_8MIM][Br]$ and the surface hydroxyl groups of Fe_3O_4 . The comparative study was shown that The IL- Fe_3O_4 and $CoFe_2O_4$ nanoparticles were quite efficient as a magnetic nano-adsorbent for the fast removal of dye from aqueous solutions. Short contact time, high adsorption capacity, stability and reusability are advantages of IL- Fe_3O_4 nanoparticles and $CoFe_2O_4$ as adsorbent.

References:

- [1] G. Absalan, M. Asadi, S. Kamran, L. Sheikhan, D. M. Goltz. J. Hazard. Mater. 185, 430-441, 2011.
- [2] K. Vijayaraghavan, Y.S. Yun, Dyes Pigm. 76, 726-732, 2008.
- [3] D.K. Kim, Y. Zhang, W. Voit, K.V. Rao, M. Muhammed, J. Magn. Mater. 225, 30-36, 2001.



Study the possibility of CuO and ZnO nanoparticles for the removal of heavy metals from waste waters

Shahriar Mahdavi^{1*}, Mohsen Jalali¹, Abbas Afkhami²

1 Department of Soil Science, College of Agriculture, Bu-Ali Sina University, Hamedan, Iran

2 Department of Analytical chemistry, College of Chemistry, Bu-Ali Sina University, Hamedan, Iran

*Corresponding author: smahdaviha@yahoo.com

Abstract:

This study investigated the adsorption of Cd^{2+} , Cu^{2+} , Ni^{2+} , and Pb^{2+} from aqueous solutions with novel nanoparticle sorbents (ZnO, and CuO) using a range of experimental approaches, including, pH, competing ions, contact time, scanning electron microscopy (SEM), transmission electron microscopy (TEM). Tests were performed under batch conditions to determine the adsorption rate and uptake at equilibrium from single and multiple component solutions. The maximum uptake values (sum of four metals) in multiple component solutions were 360.6, 114.5 mg g^{-1} , for ZnO, and CuO, respectively. Sorption equilibrium isotherms could be described using the Freundlich model in some cases, whereas others isotherms did not follow this model. Furthermore, a pseudo-second order kinetic model was found to correctly describe the experimental data for all nanoparticles. Soil solution saturation indices showed that the main mechanism of sorption for Cd^{2+} and Pb^{2+} was adsorption whereas both Cu^{2+} and Ni^{2+} sorption were due adsorption and precipitation.

Key words: nanoparticles; heavy metals; removal; waste water

Introduction:

Industrial activities can lead to heavy metal contamination in surface and groundwater. Because of heavy metals toxicity to the human and persistence in environment, the need for a process to remove heavy metals has received increasing attention[1-2]. Nanoparticles have several special properties, such as high surface area and adsorption capacity, unsaturated



surfaces, simple operation, and simple production [3-4]. We selected two uncommon (CuO, ZnO) nanoparticles to evaluate the nature and properties of nanoparticles with regards to heavy metals removal. The goal of this research is therefore to investigate the kinetics and equilibrium of the uptake efficiency of Cd^{2+} , Cu^{2+} , Ni^{2+} , and Pb^{2+} from aqueous solutions using nanostructure, ZnO and CuO under batch conditions in single and multi component solutions.

Materials and methods

1. Chemicals and methods for characterization nanoparticles:

Heavy metals and particles properties analysis were carried out by using atomic absorption spectrophotometer, SEM - EDX, TEM, and BET analysis.

2. Heavy metals adsorption studies:

The Kinetic and capacity adsorption experiments were carried out in a series of 50 ml falcon tubes containing 0.05 g (2 g/L) nanostructure materials (ZnO and CuO) with 25 mL of 100 mg/L metal ions solution at their native pH.

3. Effect of contact time:

Batch experiment procedure was carried out at different shaking time of: 10, 20, 30, 40, 50, 60, 90, 120, 180 min, 24 h and other conditions was the same as adsorption studies.

4. Adsorption isotherms:

The adsorption isotherm experiments were carried out with Cd^{2+} , Cu^{2+} , Ni^{2+} , and Pb^{2+} solutions at different initial heavy metals concentrations (0, 10, 20, 30, 60, 100, 200 and 300 mg/L) at 25 °C, with 0.05 g (2 g/L) nanostructure materials and 25 mL of adsorbate at different concentration with 0.01 M NaNO_3 as background salt. The isotherms were determined on the basis of batch analysis in single and competitive modes.

5. Saturation indices and speciation of heavy metals:

The saturation indices (SI) and speciation for heavy metals in isotherm leachates (at final concentration = 300 mg/L) were calculated using the geochemical speciation model visual MINTEQ version 2.3 [5].



Results and discussions

1. Characteristics of adsorbent:

The TEM pictures showed that ZnO and CuO had a mean diameter of about 25 (rod shape) and 75 Å (spheroid), respectively. SEM was also used to examine the morphology of surfaces of adsorbents.

The results of N₂ sorption experiments showed mean surface area of particles are: 31.2, and 12.1 m²/g in ZnO and CuO, respectively.

2. Effect of contact time:

The adsorption of heavy metals on nanoadsorbents was investigated as a function of contact time (10–1440 min) at 100 mg/l initial concentrations with an initial solution pH of 5.5. It was noticed that heavy metals removal increased with time but after 120 to 180 min almost in all ions and adsorbents increasing were slow.

The pseudo-first-order did not fitted to experimental data but the pseudo –second-order kinetics plots of sorption of heavy metals were fitted best to experimental data in all two adsorbents.

3. Adsorption isotherms:

In nanoparticles and based on maximum amount of metal adsorption, the maximum metal adsorption order was found: Cu²⁺ > Cd²⁺ > Pb²⁺ > Ni²⁺ and Cd²⁺ > Cu²⁺ > Ni²⁺ > Pb²⁺ for ZnO and CuO, respectively. According to the electronegativity, the order of adsorption should have been Cu²⁺ > Ni²⁺ > Pb²⁺ > Cd²⁺ but, on the basis of electrostatics, the strongest bound should be performed by the metals with the greatest charge-to-radius ratio. This would produce a different order of performance for the same metals: Ni²⁺ > Cu²⁺ > Cd²⁺ > Pb²⁺ [6]. The above series according to the electronegativity is different from the experimentally obtained series. The observed differences are considered to be due to the specifics of ion exchange material and to the differences in the experimental techniques used [7]. This selectivity may vary according to the sources of adsorbents, kinds of metals, and experimental conditions. The difference in the series may be an indicator that adsorption is not necessarily the only



mechanism responsible for the removal of heavy metal ions from solution; precipitation of the metal hydroxides may have a significant influence in the treatment process by nanoparticles. In the multi component solutions, metals exhibit competitive adsorption on the nanoparticle. The cations sorbed from multi component solutions were mainly lower than those sorbed from the single solutions, and this was in agreement with the results reported by other authors [8]. The maximum adsorption of Cd^{2+} is 51.3, and 42 mg/g in ZnO, and CuO nanoparticles, respectively, about 57%, 64% less than that in single component system. In ZnO and CuO nanoparticles, adsorption of Ni^{2+} decreased (75% and 35%, respectively) while adsorption of Pb^{2+} increased (24% and 65%, respectively) compared with single component system. Copper adsorption increased (8%) in ZnO and decreased (89%) in CuO nanoparticles. This suggests that the adsorption of metals on the nanoparticles in multi component system is different from that in single component system.

ZnO have the highest metal uptake capacity of 360 mg/g (sum of the four adsorbed metals) followed by CuO (114.5 mg/g). Thus, it is evident that the adsorption capacity of the ZnO is significantly higher than CuO both in single and multi component solutions. There is not any published data on maximum adsorption of ZnO and CuO, so the results cannot be compared.

In order to investigate the sorption isotherm, two equilibrium models were analyzed: Langmuir and Freundlich isotherm models. None of the two models were fitted to the Cu^{2+} and Pb^{2+} isotherms in single and multi component solutions. Cadmium and Ni^{2+} sorption on nanoparticles followed good trend in Freundlich model with high correlation coefficient in single and multi component solutions. The higher correlation coefficient indicates that there is a strong positive relationship for the data, and that Cd^{2+} and Ni^{2+} experimental sorption data on all nanoparticles are well fitted to the Freundlich model.

4. Effect of sorbents on speciation and precipitation of heavy metals:

The speciation of the metals in solution is a result of competitions between different metal complexes, metal chelates and free metal ions. In single solution, almost the free metal ions dominated in solutions in all nanoparticles. The majority of the Cu^{2+} in solution was predicted to be present as OH^- complexes and about 23% of the Cd^{2+} in solution was predicted to be



present as CdCl^+ in ZnO nanoparticles. The percentage of free ion species was reduced in multi component solutions. In multi component solutions the majority of Ni, Pb, and Cu ions in solution was predicted to be present as free species and about 51% of the Cd in solution was predicted to be present as CdCl^+ . Pedersen (2002) reported the similar results for Cd^{2+} and Cu^{2+} [9]. They reported that the majority of the Cd in solution was predicted to be present as Cl^- complexes, about 90% of the Cu in solution was predicted to be present as positively charged species (Cu^{2+} , CuCl^+ and CuOH^+).

Furthermore, chemical modeling predicts that solutions SI values for all Visual MINTEQ 2.6 database Cd^{2+} and Pb^{2+} minerals are below zero both in single and multi component solutions. Therefore, the main mechanisms involved in removing Cd^{2+} and Pb^{2+} from solution are adsorption on the surface of nanoparticles. Geochemical modeling predicts that Cu^{2+} precipitates mainly as Atacamite both in single and multi component solutions in all nanoparticles. MINTEQ predicted that Ni precipitates as $\text{Ni}(\text{OH})_2$ in both single and multi component solutions.

Conclusion:

Nanoparticles can be used as an efficient technique for the removal of toxic heavy metals from wastewater. This study investigates the removal of Cd^{2+} , Cu^{2+} , Ni^{2+} , and Pb^{2+} by nanoparticles (ZnO and CuO) as new sorbents. The metal adsorption depends on the pH of the medium and maximum adsorption was occurred at pH 6. The second order model well described the kinetic data. Metal uptake decreased with decreasing pH, indicating competition of protons for binding to acidic sites. The Freundlich isotherm was able to fit some equilibrium data, whereas other data were not predicted. Our results showed that ZnO nanoparticles had much higher metal adsorption capacity among the tested nanoparticles.

References:

[1] Afkhami A, Moosavi R (2010) Adsorptive removal of Congo red, a carcinogenic textile dye, from aqueous solutions by maghemite nanoparticles. J Hazard Mater 174: 398–403.



- [2]Feng Y , Gong J-L , Zeng J-MNiu, Q-Y, Zhang H-Y, Niu Ch-G , Deng J-H, Yan M (2011) Adsorption of Cd (II) and Zn (II) from aqueous solutions using magnetic hydroxyapatite nanoparticles as adsorbents. Chem Eng J 162: 487-494.
- [3]Afkhami A, Saber-Tehrani M, Bagheri H (2010) Simultaneous removal of heavy-metal ions in wastewater samples using nano-alumina modified with 2,4-dinitrophenylhydrazine. J Hazard Mater 181: 836-844.
- [4]Navrotsky A, (2000) Nanomaterials in the environment, agriculture, and technology (NEAT). Journal of Nanoparticles Research 2:321-323.
- [5]Allison J, Novo-Gradac K (1991) MINTEQA2/PRODEFA2, A Geochemical assessment model for Environmental system:
version 3.11 databases and version 3.0. User Manual USEPA, Environmental Research Laboratory, Athens, GA
- [6] McBride MB (1994) Environmental chemistry of soils. Oxford University Press, New York
- [7]Ok Y S, Yang J E, Zhang Y-S, Kim S J , Chung D Y(2007) Heavy metal adsorption by a formulated zeolite-Portland cements mixture. J Hazard Mater147: 91-96.
- [8]Panayotova M, Velikov B (2002) Kinetics of heavy metal ions removal by use of natural zeolite. J Environ Sci Health Part A: Toxic/Hazar Subs Environ Eng 37: 139–147.
- [9]Pederson A J (2002) Evaluation of assisting agents for electrodialytic removal of Cd, Pb, Zn, Cu and Cr from MSWI fly ash. JHazardMaterB95 185-198.



Heavy metals removal from aqueous solutions using TiO₂, and MgO nanoparticles

Shahriar Mahdavi^{1*}, Mohsen Jalali¹, Abbas Afkhami²

¹ Department of Soil Science, Faculty of Agriculture, Bu-Ali Sina University, Hamedan, Iran

² Department of Analytical chemistry, Faculty of Chemistry, Bu-Ali Sina University, Hamedan, Iran

*Corresponding author: smahdaviha@yahoo.com

Abstract:

This study investigated the removal of Cd²⁺, Cu²⁺, Ni²⁺, and Pb²⁺ from aqueous solutions using nanoparticle sorbents (TiO₂, and MgO,) with a range of experimental approaches. These include, competing ions, contact time, SEM-EDX, TEM, and XRD. Experiments were performed in batch conditions to measure the removal rate and uptake at equilibrium with single and multiple component solutions. The maximum uptake values (sum of four metals) with multiple component solutions were 594.9, and 49.4 mg g⁻¹, for MgO, and TiO₂, respectively. The sorption equilibrium isotherms were described using the Freundlich and Langmuir models. The best interpretation for experiment data was given by Freundlich model for Cd²⁺, Cu²⁺, and Ni²⁺ in single and multiple component solutions. A first order kinetic model adequately described the experimental data using MgO, and TiO₂. SEM- EDX both before and after metal sorption, and MgO soil solution saturation indices (SI) with Visual MINTEQ Software indicated that the main sorption mechanism for heavy metals was attributable to adsorption and precipitation, whereas heavy metal sorption by TiO₂ adsorbents was due to adsorption.

Keyword: heavy metals; nanoparticles; removal; aqueous solutions

Introduction:

The introduction of heavy metals into water is a growing, serious environmental and public health concern, because of the toxicity of heavy metal and their non-biodegradable nature [1].



Many technologies have been developed for removing toxic heavy metals from wastewater among them adsorption of heavy metals with nanoparticles due to special properties, such as a high adsorption capacity, unsaturated surfaces, easy operation, and easy production have a great attention[2].

Materials and methods:

This study investigated the removal of Cd^{2+} , Cu^{2+} , Ni^{2+} , and Pb^{2+} from aqueous solutions using nanoparticle sorbents (TiO_2 , and MgO ,) with a range of experimental approaches. Experiments were performed in batch conditions to measure the removal rate and uptake at equilibrium with single and multiple component solutions.

Results and discussion:

TEM micrographs were used to evaluate the shape and particle sizes of the three adsorbents. TiO_2 , and MgO , particles had mean diameters of 12 nm (spheroid), and 24 nm (rod shape), respectively. The maximum metal adsorption capacity in isotherm with TiO_2 nanoparticles was found to be 120.1, 50.2, 39.3, and 21.7 mg g^{-1} for Cd^{2+} , Cu^{2+} , Ni^{2+} , and Pb^{2+} , respectively whereas for MgO the order was: Cu^{2+} (149.1) \sim Ni^{2+} (149.9) $>$ Pb^{2+} (148.6) $>$ Cd^{2+} (135 mg g^{-1}) in single mod.

Conclusion:

Nanoparticles provide an efficient method for the removal of toxic heavy metals from wastewater. The current study investigated the use of nanoparticles (TiO_2 , and MgO ,) as sorbents for the removal of Cd^{2+} , Cu^{2+} , Ni^{2+} , and Pb^{2+} . A first order model described the kinetic data well. The Freundlich isotherm fitted some equilibrium data, but other data were not well fitted. MgO is also nontoxic, noncorrosive, thermally stable, and environmentally friendly. Modeling studies and spectroscopic analyses showed that the main mechanism for heavy metal removal by TiO_2 is adsorption, whereas adsorption and precipitation both occurred with MgO .



References:

- [1] Pan, B., Qiu, H., Pan, B., Nie, G., Xiao, L., Lv, L., Zhang, W., Zhang, Q., Zheng, S. (2010). Highly efficient removal of heavy metals by polymer-supported nanosized hydrated Fe (III) oxides: Behavior and XPS study, *Water Res.*, 44, 815 – 824.
- [2] Afkhami, A., Moosavi, R. (2010). Adsorptive removal of Congo red, a carcinogenic textile dye, from aqueous solutions by maghemite nanoparticles, *J. Hazard. Mater.* 174, 398–403.



Comparison of removal of bromothymol blue from aqueous solution by rawMWCNT and Zn(OH)₂ nanoparticle loaded on activated carbon Zn(OH)₂-NP-AC: kinetic, isotherm and thermodynamic investigation of removal process

M. Ghaedi^{a*}, N. Taghavimoghadam^a, S. Naderi^a

^a Chemistry Department, Yasouj University, Yasouj, Iran

Email: www.narges.taghavi@yahoo.com

Keywords: Bromothymol blue; Zn(OH)₂-NP-AC; RawMWCNT; Kinetic; Isotherm; Thermodynamics.

Introduction:

Colored wastewater as a consequence of waste generated by applied in the textile and other industries arrive to various ecosystems. Various physical and chemical methods such as coagulation, reverse osmosis, photo-degradation, electrochemical oxidation, ozonation and adsorption, etc. Among all these methods adsorption is a popular alternative procedure, because of its low cost, simple design, easy operation and the possibility of adsorbent recycling. In this paper multiwalled carbon nanotube (rawMWCNT) and Zn(OH)₂ nanoparticle loaded on activated carbon (Zn(OH)₂-NP-AC) adsorbents applied for removal of bromothymolblue (BTB). This dye is the most appropriate pH indicator in physiological tissue and used in the investigation of the interaction of lipid with protein. It is widely applied in biomedical, biological, and chemical engineering applications. It is sometimes used to define cell walls or nuclei under the microscope. The adsorption rates were evaluated by fitting the experimental data to conventional kinetic models such as pseudo first-order, pseudo second-order and intraparticle diffusion model. The effects of temperature on the adsorption process were determined and the thermodynamic parameters such as changes in free energy (ΔG^0),



enthalpy (ΔH^0) and entropy (ΔS^0) belong to adsorption at various temperatures were calculated [1-2].

Materials and methods:

Bromothymol blue ($C_{27}H_{28}Br_2O_5S$) stock solution was prepared by dissolving its appropriate amount in double distilled water. The pH was adjusted by addition of dilute HCl and NaOH. To study the effect of important parameters like the pH, contact time, initial dye concentration and temperature on the adsorptive removal of BTB, batch experiments were conducted. For each experimental run, 50 mL of dye solution of known concentration at pH was mixed completely with optimum value. This mixture was agitated at room temperature controlled shaking water bath at constant speed.

Apparatus:

The concentration of the dye was determined at 432 nm using Jusco UV-Visible spectrophotometer model V-530, pH/Ion meter model-686, thermometer Metrohm, international ASTM sieves and Stirrer model UKA.

Result and discussion:

The effect of pH (in the range of 1-7) on BTB removal on both adsorbents was studied and further experiments were carried out at pH 2. Following optimization of variables, the kinetics of adsorption was examined by analyzing experimental data at different time intervals. Adsorption isotherms was studied at different concentrations of BTB in the range ($10\text{--}50\text{ mgL}^{-1}$) at optimum value of all variables. The increase in BTB removal efficiency by increasing temperature from 283.15 to 333.15 K in both experiment, indicate the endothermic nature of adsorption process.

Conclusion:

Adsorption studies of BTB under different experimental conditions in batch mode. The adsorption of BTB depend to adsorbent surface and amount BTB concentration, contact time



and pH of the solution. The percentage adsorption is maximal at pH value of around 2. Adsorption kinetic by two adsorbents follow pseudo-second-order kinetic. Adsorption capacity increases with temperature. The result shows that the experimental data are best correlated by Langmuir isotherm on $\text{Zn}(\text{OH})_2$ -NP-AC and rawMWCNT.

References:

- [1] NK. Amin. ; " Removal of reactive dye from aqueous solutions by adsorption onto activated carbons prepared from sugarcane bagasse pith " ; Desalination; 223, 152–161, 2008.
- [2] G. Annadurai and et al. ; " Adsorption of Reactive Dye on chitin " ; Environ Monit Assess 59, 111–119, 1999.



Synthesis of 2-substituted benzimidazoles and 2-aryl-1*H*-benzimidazoles using $[\text{Zn}(\text{bpdo})_2 \cdot 2\text{H}_2\text{O}]^{2+}$ /MCM-41 nanocatalyst under solvent-free conditions

R. Malakooti¹, M. Rostami-Nasab¹, H. A. Oskooie², M. M. Heravi², N. Karimi², A. Amouchi²,
G. Kohansal²

¹Nanochemistry Research Laboratory, Department of Chemistry, University of Birjand, Birjand, Iran

²Department of Chemistry, School of Sciences, Alzahra University, Vanak, Tehran, Iran

Email address: reihaneh.malakooti@gmail.com

Keywords: Zinc (II) complex, MCM-41, Benzimidazoles, *O*-phenylenediamine, Carboxylic acids, Aldehydes.

Introduction:

Structures containing benzimidazole have been well documented to exhibit a wide range of biological properties. This class of molecules has been found for application in several therapeutic areas such as antiparasitic [1], antifungal, antihypertensive, antitumor [2], antimicrobial [3], anti-inflammatory [4] and antiviral activities [5].

Accordingly in continuation of our previous works on synthesis of heterogeneous catalysts and heterocyclic compounds, here we wish to report the synthesis and characterization of $[\text{Zn}(\text{bpdo})_2 \cdot 2\text{H}_2\text{O}]^{2+}$ /MCM-41 used as catalyst for the synthesis of 2-substituted benzimidazoles and 2-aryl-1*H*-benzimidazoles derivatives via the simple and efficient condensation reactions of *o*-phenylenediamine with carboxylic acids under solvent-free condition at 80 °C.

Materials:

All materials were purchased from Merck and were used without further purification.

Immobilization of $[\text{Zn}(\text{bpdo})_2 \cdot 2\text{H}_2\text{O}]^{2+}$ complex within MCM-41:

0.398 mmol (0.0542 g) of ZnCl_2 and 0.7978 mmol (0.15 g) of bpdo were dissolved in 10 ml of deionized water. The solution was heated at 70 °C for 2 h. Then 1 g of MCM-41 which was



dried overnight under vacuum at 150 °C, was added to the solution of $[\text{Zn}(\text{bpdo})_2 \cdot 2\text{H}_2\text{O}]^{2+}$. The resultant mixture was stirred for 24 h at room temperature and then filtered. Finally the white precipitate was washed with deionized water.

Results and Discussion:

XRD pattern of MCM-41 shows three peaks corresponding to (100), (110) and (200) planes which are adopted with typical two-dimensional hexagonal symmetry. After grafting of the cationic complex, $[\text{Zn}(\text{bpdo})_2 \cdot 2\text{H}_2\text{O}]^{2+}$, on the surfaces of MCM-41, Fig. 1a, hexagonal symmetry is still remained. Also relative decreases are observed between the XRD intensities of the parent mesoporous and grafted sample which are originated from the complex immobilization.

Conclusion:

In conclusion, a new heterogeneous catalyst based on the cationic zinc (II) complex supported with MCM-41 is proposed. Also this study provides an efficient multi-component approach for the synthesis 2-substituted benzimidazoles and 2-aryl-1*H*-benzimidazoles. The reaction is versatile and also offers several advantages such as high yields, shorter reaction times, cleaner reaction profiles and simple experimental and work-up procedures.

Reference:

- [1]Valdez, J. Cedilo R, Hernandez-Campos A, Yopez L, Hernandez-Luis F, Navarrete-Vazquez G, Tapia A, Cortes R, Henandezc M, Castilloa R (2002) Bioorg Med Chem Lett 12:2221.
- [2]Donny WA, Rewcastle GW, Bayuley BC (1990) J Med Chem 33:814.
- [3]Fonseca T, Gigante B, Gilchrist TL (2001) Tetrahedron 57:1793.
- [4]Tan RH, Ding LC, Wei XJ (2001) China J Med Chem 11:259.
- [5]Kapinos LE, Sigel H (1999) Eur J Inorg Chem 1781.



Antimicrobial Finishing of Woolen Fabric by TiO₂/Ag Nanocomposite

A. Behzadnia ^{a*}, M. Montazer ^b

^a Textile Department, Tehran South Branch, Islamic Azad University, Tehran, Iran

^b Textile Department, Amirkabir University of Technology, Center of Excellence in Textile, Tehran, Iran, Hafez Avenue, Tehran, Iran

E-mail: amirbehzadnia@hotmail.com

Keywords: Nanocomposite, Silver, Nano TiO₂, Wool, Antibacterial activity

Introduction:

Population explosion and environmental pollution encourage researchers to seek hygienic and secure production methods to facilitate human living conditions [1]. In recent decades, there have been a lot of developments using nanotechnology in the textile industry. For instance, different kinds of antimicrobial treatments have been utilized to protect garments against harmful microorganisms [2, 3]. Among various nanoparticles, TiO₂ has attracted a great deal of scientists' attention because of its chemical stability, low cost, ease of availability, non-toxicity, and optical properties [4, 5].

Materials and Methods:

Materials: A 100% wool fabric with twill structure, and 159 g/m² fabric mass was used. Nano titanium dioxide powder (Degussa P-25) with average particle size of about 21 nm from Evonik (Germany) and silver nitrate with 99% purity from Merck (Germany) were employed to prepare the nanocomposite. Citric acid (CA) and sodium hypophosphite (SHP) with purity of more than 99% were purchased from Merck (Germany). The investigated microorganisms were *E.coli* (ATCC 11303) and *S.aureus* (ATCC 1112). Tryptic soy agar culture medium was bought from Merck (Germany).

Apparatus:

A UV-A bulb (400 W, HPA, 320nm < λ <400nm) from Philips (Belgium) was used as an artificial UV source. XRD patterns were obtained using Philips X' Pert MPD diffractometer



with a Cu generator bulb (40KV, 40 mA) (The Netherlands). SEM images and EDS spectra were obtained using XL30 scanning electron microscopy (Netherlands). An ultrasonic bath model DSA 100-XN1-2.5L, 100 W, 40 KHz (Taiwan) was used to mix the components of the impregnating bath. In addition, to create linkages between wool and carboxylic acid (CA) treated samples were cured in an oven.

Result and discussion:

After the specified contact time, antimicrobial activities of raw and the treated samples against both *E. coli* and *S. aureus* bacteria were calculated. The *S. aureus* bacterium is a pathogenic microorganism causing many diseases such as toxic shock, purulence, abscess, fibrin coagulation, and endocarditic. Moreover, it is resistant to common antimicrobial agents. Furthermore, *E. coli* bacterium which causes urinary tract and wound infections is a popular test organism. It was also confirmed that the presence of metal ions such as Ag on the TiO₂ led to a considerable improvement in the antimicrobial activity particularly in lower concentrations of nanoparticles. Ag ions increases the separation rate of photo-induced negative electrons and positive holes, providing a better photocatalytic property.

Conclusion:

This research was conducted to introduce an effective nanocomposite to produce an ideal antimicrobial wool fabric. The Ag/TiO₂ nanocomposite was successfully applied on wool surface and stabilized through citric acid as a cross-linking agent. Its antimicrobial property against two well-known pathogenic bacteria *S.aureus* and *E.coli* was evaluated. Through XRD patterns, SEM images, and EDS spectrum the presence of Ag/TiO₂ nanocomposite on the surface of treated wool samples was confirmed. Increasing the amount of Ag/TiO₂ nanocomposite, citric acid, and sodium hypophosphite concentrations lead to enhance the antimicrobial activities. Moreover, RSM was employed to investigate the impact of independent variables on antimicrobial activity.



Reference:

- [1] Y. Gao, R. Cranston, Recent Advances in Antimicrobial Treatments of Textiles, *Text. Res. J.* 78(1) (2008) 60-72.
- [2] A.P. Sawhney, K.V. Singh, S.S. Pang, Modern Applications of Nanotechnology in Textiles, *Text. Res. J.* 78(2008) 731-739.
- [3] H. Y. Ki, J. H. Kim, S. C. Kwon, S. H. Jeong, A study on multifunctional wool textiles treated with nano-sized silver, *J. Mater. Sci.* 42 (2007) 8020-8024.



Study on the effect of nano-copper oxide particles on mouse forelimb development under *in vivo* condition

Sefati Maryam¹, Parivar Kazem¹, Hayati Nasim¹, Badiei Alireza²

¹Department of biology, science and research branch, azad university, tehran, iran
(E.mail: Maryam.sefati@gmail.com)

²School of Chemistry, College of Science, University of Tehran, Tehran, Iran

Key words : Nano-copper oxide , Toxicity , Limb bud development , Organ culture

Introduction:

Nanoparticle research is currently an area of great scientific interest due to a wide variety of applications in medical fields (1). Biological characterization of nano-sized material will change with their scales because in nano-scale they could be transmitted over biological barrier such as skin, brain vessel barrier and placenta (2,3,4). Despite an increasing application of copper nanoparticles, there is a serious lack of information concerning their impact on human health and the environment (5). The aim of this study was to investigate the toxicity effects of nano-copper oxide particles on mouse limb buds in order to evaluate the effects of nano-sized copper oxide particles (25nm) on mouse forelimb development.

Materials and method:

For experiment, we used three test groups of embryos limb bud on day 15 of gestation included, (E) experimental which treated with different doses of nano-copper oxide (300, 400, 500, 600 mg/kg bw), (Sh) sham exposed with solvent which was double ionized water and (C) control. Due to research, all doses after measurement were mixed with 1cc deionized water. These suspensions were injected to the mouse in the 11th day of pregnancy. In the day of 15th, fetus were drag out from uterus and limb buds were separated. After that, several linear section were prepared. These sections were histological and



morphologically studied and statistically examined. All data were analyzed with SPSS software and all values were calculated from standard errors of means (means \pm SEM) The significance of differences among the six groups were compared using the one-way analysis of variance (AVONA). The study result revealed significant changes in forelimb development

Results:

In low doses, the number of measured index such as number of chondrocytes, red blood cells, osteocytes and total length of limbs showed significant increase, on the other hand, these index for high doses showed decrease. Karlsson et al. in 2009 did some research on effects of nano-copper oxide. Their study reveal that decreasing the size of nano-copper increases oxidative damage of DNA and cellular death (6). As oxidative damage can cause disorder in cell cycle, we observed decrease in the number of counted index in high doses. Another study about nano-copper oxide cytotoxicity in the form of suspension, reveal that when copper solve in water, reduces the fractions of viable cells, resulting in the overall inhibition of biomass growth(7). According to the experiments in high doses, because of cytotoxicity effects of nano-copper oxide we observed decreasing in most counted elements.

Conclusion:

These findings suggest that nano-copper oxide particles under low doses condition have progressive effects on the limb bud development and under high doses condition have deterrent effects on limb buds development.

Reference:

- [1] Sarkar A, Das J, Manna P, Sil P, Nano-Copper induces oxidative stress and apoptosis in kidney via both extrinsic and intrinsic pathway, Toxicology, 2011; 290(2-3): 209-218
- [2] Risha G, Boyer E, Evans B, Kuo K, Malek R, Characterization of nano-sized particles for propulsion application, MRS fall meeting, 2003; 800: 243-254
- [3] Brock J R; Nano structured materials; Science & Technology; 1997



- [4] Staples , Daniel K , Cima M, Langer R , Application of micro-and nano-electromechanical devices to drug delivery , *Pharmaceutical research* , 2006 ;23(5) :847-863
- [5] Lei R,Wu C, Yang B, Ma H , Shi C , Wang Q, Wang Q, Yuan Y, Liao M, Integrated metabolomic analysis of the nano-sized copper particle-induced hepatotoxicity and nephrotoxicity in rats: A rapid in vivo screening method for nanotoxicity, *Toxicology and Applied pharmacology* , 2008 ;223 :292-301
- [6] Pan Y , Loo G , Effect of copper deficiency on oxidative DNA damage in Jurkat T-lymphocytes , *Free Radical Biology & Medicine* ,2000 ; 28(5) : 824-832
- [7] Guanwant C , Teoh w , Marquis C , Amal R, Cytotoxic origin of copper(II) oxide nanoparticles :Comparative study with micron-sized particles , leachate , and metal salts , *ACS nano* , 2011 ; 5 (9) :7214-7215.



Preparation and characterization of polypyrrole/silver nanocomposites by interfacial chemical polymerization technique using silver ion oxidant

M. Naseh^{a*}, H. Behniafar^a

^aFaculty of Sciences, Islamic Azad University-Damghan Branch, Damghan, Iran

Email: maryam.naseh@yahoo.com

Key words: Nanocomposite, interfacial polymerization, Polypyrrole, Nanosilver.

Introduction:

Polypyrrole is an important conducting polymer with high electrical conductivity and appreciable environmental stability [1]. Research in the field of polypyrrole and other conducting polymers aims mainly at some suitable modifications of these polymers so that their applicability can be improved [2]. Some of these modifications involve preparing nano-hybrid materials [3]. This article describes the polymerization of pyrrole by silver ion oxidant in the boundary of two immiscible solvents, which can be applied for the synthesis of PPy/Ag nanocomposites. To our knowledge, no previous work has been reported to prepare PPy/Ag nanocomposites by interfacial technique in the presence of stabilizers.

Materials and methods:

All chemicals were purchased from Sigma-Aldrich and used as received, except for pyrrole, which was purified by vacuum distillation. Two anionic surfactants, i.e. sodium dodecylsulfate (SDS) and sodium poly(styrene sulfonate) (SPSS) dispersants were employed. In all systems, AgNO₃ dissolved in the aqueous phase was used as the reaction oxidant, and the reduction of Ag⁺ to metallic silver is accompanied by oxidative polymerization of pyrrole, leading to the formation of PPy/Ag nanocomposites.

Apparatus:

FT-IR spectra of the samples were recorded on a PERKIN ELMER RX I FT-IR spectrometer. XRD patterns were performed with film specimens on a Bruker Advance D5 X-ray

diffractometer with Ni-filtered Cu/K α radiation (30 kV, 25 mA). UV-vis spectra of the diluted solutions in DMSO were taken with a PERKIN ELMER PTP-1 Peltier System. TGA was performed on a Mettler TA 5000 system under N₂ at a heating rate of 20 °C.min⁻¹. The morphologies were determined with a S-A1600 SEM and a Philips EM 430T TEM.

Results and discussion:

The presence of SDS and SPSS stabilizers helps the metallic silvers to produce nano-sized and stay in the form of a stabilized nanofluid. Nearly no aggregation and then precipitation is observed in this condition. This allows the system to go to a well-dispersed nanocomposite. The TEM results clearly showed that the Ag nanoparticles were uniformly embedded into the polymer matrixes. Figure 1 shows the XRD diffractograms of the nanocomposites obtained (a), and TEM image of nanocomposite PPy/Ag prepared in the presence of SDS stabilizer (b).

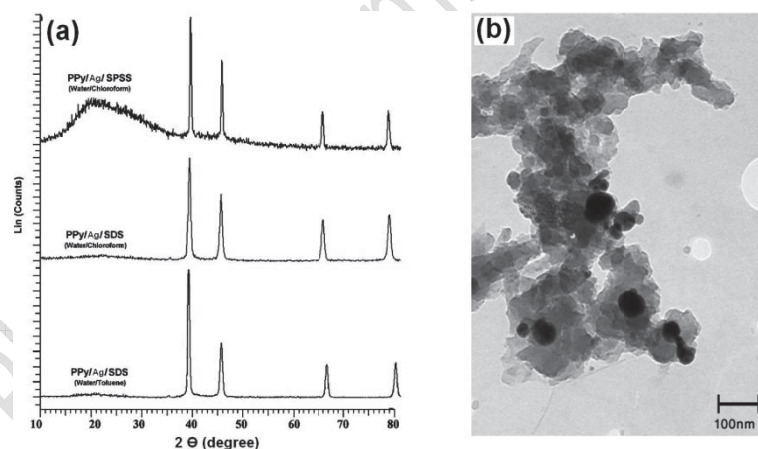


Figure 1. XRD diffractograms of the nanocomposites obtained (a), and TEM image of nanocomposite PPy/Ag prepared in the presence of SDS stabilizer (b).

Conclusion:

The oxidation of pyrrole and the formation of silver occurred simultaneously via employing AgNO₃ at the interface of water and the tested organic solvents (Toluene and chloroform) in the presence of dispersant. As a key conclusion, it should be stated that for monomer and



oxidant the further solubility coefficient difference in two solvents used, the more morphological order and the more thermostability will be.

Reference:

- [1] R.P. Mikalo, G. Appel, P. Hoffmann, D. Schmeier, " Band bending in doped conducting polypyrrole: interaction with silver", *Synth.Met.***122**, 249-261 (2001).
- [2] Aditee Joshi, S.A. Gangal, S.K. Gupta, " Ammonia sensing properties of polypyrrole thin films at room temperature", *Sens. Actuators B***156**, 938-942 (2011).
- [3] T. K.Vishnuvardhan, C.Basavaraja, S. C.Raghavendra, " Synthesis, characterization and a.c. conductivity of polypyrrole/Y2O3 composites", *Bull. Mater.Sci.***29**, 77-83 (2006).



Calculation of conductance in bilayer graphenenanoribbons under rotation

A.SalemiNajafabadi^{a*}, S.M.Fazeli^a

^aDepartment of Physics, University of Qom, Qom, Iran

Email: Hmdslm1986@yahoo.com

Key words: Graphene, nanoribbon, Conductance, Rotation.

Introduction:

Graphene is a new matter in physics and nanoscience with infinite applications. Graphene was found by Novoselov and Geim in 2004, for first time. [1] Graphene is made out of carbon atoms arranged on a honeycomb structure made out of hexagons. In graphene structure, each carbon atom has got three carbon atoms as its nearest neighbours by strongly covalent bonds. [1] It is interesting to note that graphite made out of stacks of graphene layers that are weakly coupled by van der Waals forces. The graphene structure is not a Bravais lattice but can be seen as a triangular lattice with a basis of two atoms per unit cell. [1] Recently, graphenenanoribbon is selected as an appropriate replacement of quantum nanowire due to high thermal conductivity and proper conductance; for this using, it is necessary arrange graphenenanoribbons over each other with separated conductances in experiment.

Material and methods:

Landauer-Büttiker formalism and Green function methods were used as main framework for calculation of conductance in nanoscale systems such as graphenenanoribbons in connected to leads. [2] Conductance of two graphenenanoribbons was calculated when each nanoribbon was sandwiched between two leads. This conductance was considered in different distances between graphenenanoribbons and angles of rotation, as well.

Apparatus:

Green functions were evaluated for surface and bulk samples by Sancho – Sancho approach. In their article in which this approach was introduced [3], two preferred properties for



discussing methods to evaluate kinds of Green functions, namely speed and flexibility, were discussed. Finally, computational methods were done in "FORTRAN 90".

Result and discussions:

In this research, calculation of conductance was done for bilayer graphene nanoribbons and effects of rotation & displacement of layers were also studied. It is noticeable that conductance is not linear in nanoscale systems. [2] In this work, non-linearity of conductance was observed.

Generally, couplings of graphene layers are considerable in solid state physics and nanoscience so that these layers influence of conductance of another layer in experiments and in numerical computations. [4,5] In this computation and simulation, important results are as follow:

- a) Conductance curve versus energy was depicted in different angles of rotation & displacement between twin leads and finally, coupling of two graphene layers versus angle for different displacement was studied.
- b) Maximum & minimum couplings were achieved in especial angles of rotation.
- c) Decrease of coupling between two graphene layers were observed under rotation and their displacement.

Conclusion:

As a consequence, this strength was decreased by rotating one of two graphene nanoribbons that this decrease depends on width of ribbons, but this decrease was not noticeable, such that two graphene nanoribbons over each other were not two separated nanowires.

References:

- [1] A. H. Castro Neto, F. Guinea, N. M.R. Peres, K. S. Novoselov, A. K. Geim ; RevMod Phys 81, 109 (2009)
- [2] S. Datta ; "Electronic transport in mesoscopic systems" ; Cambridge University Press (1995)
- [3] M. P. Lopez Sancho, J. M. Lopez Sancho, J. Rubio ; J. Phys. F 15, 851 (1984)



- [4] E. J. Mele ; J. Phys. D: Appl. Phys. 45, 154004 (2012)
- [5] J. Nilsson, A. H. Castro Neto, F. Guinea, N. M. R. Peres ; Phys. Rev. B 78, 045405 (2008)

15th Physical Chemistry Conference



Synthesis of magnetic nanoparticles Fe₃O₄-immobilized guanidine and its application as nanocatalyst in cyanosilylation of aldehydes

B. Atashkar, A. Rostami*, B. Tahmasbi

Department of Chemistry, Faculty of Science, University of Kurdistan, Zip Code 66177-15175, Sanandaj, Iran.

E-mail: b_atashkar@yahoo.com

Keywords: Magnetic nanocatalyst, guanidine, cyanosilylation, aldehydes,

Introduction:

Magnetic nanoparticles are efficient, readily available, high-surface-area resulting in high catalyst loading capacity and outstanding stability heterogeneous supports for catalysts^[1] More important, magnetic separation of the magnetic nanoparticles is more effective than filtration or centrifugation,^[2] simple, economical and promising for industrial applications. Among the various magnetic nanoparticles as the core magnetic support, Fe₃O₄ nanoparticles are arguably the most extensively studied because of their simple synthesis, low cost, and relatively large magnetic susceptibility. Recently preparation and application of several supported catalysts on magnetic Fe₃O₄ nanoparticles have been reported^[1]. The synthesis of novel and versatile magnetic nanocatalyst is interest in catalysis research.

Materials and methods:

Chemicals including starting materials, solvents and reagent were obtained from Merck chemical company and used without purification.

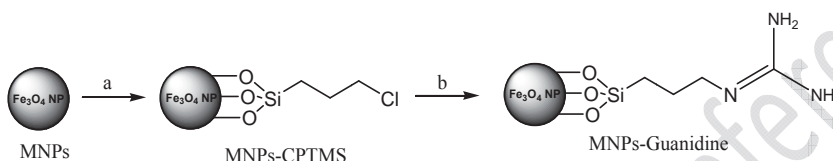
Apparatus:

Melting points were obtained in open capillary tubes and also were measured on the Electrothermal 9100 apparatus. FT-IR spectra were recorded on a Perkin Elmer RXI spectrometer. NMR spectra were recorded on a Bruker Avance DPX 250 MHz instrument.

The XRD were recorded on Philips X pert MPD Diffractometer. Images were collected using VEGA//TESCAN (SEM) and Philips microscope (EM 280, Tokyo, Japan).

Result and discussion:

The magnetic nanoparticles Fe_3O_4 -immobilized guanidine (MNPs-guanedine) was synthesized according to the procedure shown in Scheme 1.



Scheme 1. a) (3-chloropropyl)-triethoxysilane, ethanol/water, 40 °C, 8 h; b) guanidine, toluene, 28 h, reflux

The catalyst has been characterized by scanning electron microscopy (SEM), X-ray diffraction (XRD), fourier transform infrared spectroscopy (FT-IR) are shown in Figure1 and thermogravimetric analysis (TGA) and Energy dispersive X-ray spectroscopy (EDAX). A SEM image of MNPs-Guanidine is shown in Fig. 1A. It was confirmed that the catalyst was made up of nanometer-sized particles. XRD pattern of MNPs-Guanidine is shown in Fig 1B., the position and relative intensities of all peaks confirm well. The IR spectrum of MNPs-Guanidine shows peaks that are characteristic of a functionalized guanidine group, which clearly differs from that of the unfunctionalized Fe_3O_4 nanomagnets and chloropropyl-functionalized magnetic nanoparticles (Fig. 1C).

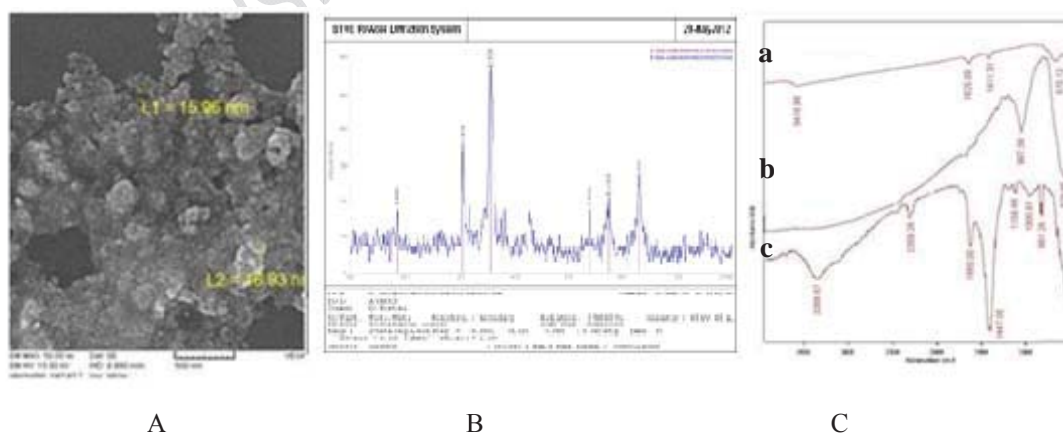


Figure 1: A) SEM image of MNP-Guanidine, B) XRD., C) FT-IR spectrum of MNP-Guanidine [insert a) Fe_3O_4 magnetic nanoparticles b) MNPs-CPTMS c) MNPs-Guanidine]



We present for the first time catalytic applications of magnetic nanoparticle-supported guanidine (MNPs-Guanedine) as a novel magnetically heterogeneous nanocatalyst for cyanosilylation^[3] of wide range of aldehydes in CH_2Cl_2 at room temperature.

Conclusion:

In conclusion, we synthesized and characterized MNPs-guanedine as robust and efficient catalyst for cyanosilylation of aldehydes with good to high yield of products under mild conditions. The catalyst can be recycled and reused for several times with little lose of activity.

Reference:

- [1] V. Polshettiwar and etal; "Magnetically recoverable nanocatalysts"; Chemical Review; 111, 3036, 2011.
- [2].C. Yavuz and etal; "Low-Field Magnetic Separation of Monodisperse Fe_3O_4 Nanocrystals"; Science; 314, 964, 2006.
- [3]R.J.H. Gregory and etal; "Cyanohydrins in Nature and the Laboratory: Biology, Preparations, and Synthetic Applications" Chemical Review; 99, 3649, 1999.



Hydrogen Storage on Boron and Nitrogen doped Silicon Carbide Nanotubes: A first principle study

Saeid Yeganegi^{a*}, Nahid Mahmoodzadeh^a, Mahnaz Nashta Hosseini^a

^aDepartment of Physical Chemistry, Faculty of Chemistry, University of Mazandaran, Babolsar, Iran

Email: sdyeaganegi@gmail.com

Key words: Adsorption, Silicon carbide nanotubes, dope, Hydrogen molecule, pristine

Introduction:

Hydrogen is being considered as an important element for future energy schemes because of its efficiency, abundance, and environmental friendliness. Silicon carbide nanotubes (SiCNTs) have been successfully first synthesized in 2001 with a Si to C ratio of 1:1 via the reaction of Si with multi-walled CNTs [1]. All SiCNTs are semiconductors and the band gap increases with increasing nanotube diameter [2,3]. In this work, we present a detailed first-principle analysis of Hydrogen molecular adsorption on a typical pristine zigzag (7, 0) SiCNT and its corresponding N_C (a N atom occupying a Carbon atom site) and B_C (a B atom occupying a Carbon atom site) doped nanotubes, by using the supercell density-functional theory (DFT).

Computational Methods:

Density functional calculations were performed using the SIESTA code [4] which solves the standard Kohn–Sham equations. The calculations were performed based on the generalized gradient approximation (GGA) with the Perdew–Burke–Ernzerhof (PBE) functional [5] and the core electrons have been treated by Troullier–Martins pseudo-potentials [6].

Results and Discussion:

At first the structures of the isolated pristine (7,0) SiCNT and Hydrogen molecule were optimized. For the subsequent calculations, the structures of the nanotube and the H₂ molecule



kept fixed while the distance between the nanotube and the center of mass of the H_2 molecule is varied (70 configurations were examined in total) to obtain the binding energy of the combined system as a function of the separation. Results show that for the parallel approach of the H_2 molecule to the center a hexagon of Si-C bonds on the nanotube is energetically more favorable than the other sites. For the perpendicular approach of the H_2 molecule, the interaction of H_2 with the C atom of Si-C bond has the lowest energy. Defected SiCNTs with a single carbon atom of the nanotube substituted by Boron or Nitrogen atoms, namely the B_C and N_C defects, were constructed and optimized. The optimized Boron-defected silicon-carbid nanotube (SiCNTB) and H_2 structures were used for the study of the adsorption of a hydrogen molecule on the B_C and N_C defected SiCNTs. The calculated binding energy and N-H equilibrium distance are -1.2 eV and 2.2 Å respectively. The calculated binding energy and B-H equilibrium distance are -0.9 eV and 2.5 Å respectively. The comparison of the results of the pristine and defected nanotube indicates that the Boron and Nitrogen substitutional defect can increase significantly the binding energy of the hydrogen to the SiCNT, -0.9 eV and -1.2 eV respectively, which is within the energy window of 0.6 to 0.2 eV desired for an ideal hydrogen storage material. Furthermore our results show that the bond lengths of H_2 exhibit only small change during its binding to the pristine and defected SiCNT.

Conclusions:

In summary, in this work studied the adsorption of the hydrogen molecule by the pristine and Boron and Nitrogen defected (7,0) SiCNTs by periodic density functional calculations (DFT). Our calculations show that the most stable adsorption site for H_2 is the perpendicular approach of a hydrogen molecule to the C atom of the nanotube and the physisorption binding energy is -0.17 eV which is not within the acceptance criteria for a suitable hydrogen storage material. The calculated binding energies for boron and nitrogen doped SiCNTs are 5 and 7 times larger than those with a pristine SiCNT which is within the energy window of an ideal hydrogen storage material. The Mulliken charge analyses reveal that the hydrogen molecule donates partially its electrons to the SiCNT.



References:

- [1] D. Lamoén and B.N.J. Persson, J. Chem. Phys. 108 (1998) 3332.
- [2] B. Xiao, J. Zhao, Y. Ding, C. Sun, Surface Science 604 (2010) 1882.
- [3] M.D. Ganji, Phys. Lett. A 372 (2008) 3277.
- [4] J. M. Soler, E. Artacho, J. D. Gale, A. García, J. Junquera, P. Ordejón, and D. Sánchez-Portal, J. Phys. Condens. Matt. 14 (2002) 2745.
- [5] J.P. Perdew, K. Burke, and M. Ernzerhof, Phys. Rev. Lett. 77 (1996) 3865.
- [6] N Troullier, J.L. Martins, Phys. Rev. B 43 (1991) 1993.



Preparation of flowerlike copper nanoparticles by chemical reduction

P. Mashayekhi^{a*}, M.Sadjadi^b

^{a,b}Department of chemistry, Science and Research branch, Islamic Azad university, Tehran, Iran.

Email: Prmashayekhi@gmail.com

Key words: Flowerlike, Copper nanoparticles, Chemical reduction, Ascorbic acid

Introduction:

The intrinsic properties of metal nanoparticles are sensitive to their composition, size, shape, crystallinity, and structure. It has been realized that many metals can now be successfully synthesized with controllable size. Recently, the intensive research motivation for the shape-controlled synthesis of metal nanoparticles are based on the fact that in many cases it allows one to fine tune the properties with a greater versatility than can be achieved otherwise. Among synthesis methods, chemical reduction is the most preferred, because this method is simple and economical, and it can realize better size and size distribution control by optimizing the experimental parameters, such as the molar ratio of the capping agent with the precursor salt and the ratio of reducing agent with the precursor salt. Here in we report a simple method for flowerlike synthesis of copper with using chemical reduction. Copper (II) sulfate was taken as the metal precursor and ascorbic acid in the presence an appropriate amount of NaOH as reducing agent and anhydride maleic as surfactant.

When (copper(II) sulfate)/(anhydride maleic) molar ratio was 100/1, flowerlike copper nanoparticles were prepared.

Materials and methods:

The three-step preparation scheme for nanoparticles starts with dissolving anhydride maleic (0.001M), in deionized water. Next copper (II) sulfate (0.1M) was dissolved in water to obtain a blue solution and added to the aqueous solution containing the surfactant (anhydride maleic) while vigorously stirring. In this step, the solution changed from blue to white. In the third

step, with constant stirring and under N₂ atmosphere mixture ascorbic acid (0.2M) and sodium hydroxide (0.2M) added to the synthesis solution. Color change occurred in the aqueous phase from white to yellow, then to olive green. When the solution color did not change, the reaction was ceased. After separation from the mixed solution, the precipitation was washed 3-4 times by de-ion water and then 2-3 times by ethanol.

Apparatus:

Morphology of copper nanoparticles were determined by scanning electron microscopy (SEM) and average size were determined by X-ray diffraction (XRD). X-ray powder diffraction (XRD) analysis was performed on a D 5000-siemens with Cu K α radiation ($\lambda=1.541\text{\AA}$) using a 30 KV operation voltage and 40 mA current. Scanning electron microscopy (SEM) images were obtained using a LEO 1430VP microscopy.

Result and discussion:

SEM and XRD pattern of copper nanoparticles characterization:

Fig.1. shows SEM images of the as-prepared Cu nanoparticles with a molar ratio 100/1 of CuSO₄/anhydride maleic.

XRD pattern of the Cu nanoparticles obtained in the typical experiment above is shown in Fig.2. Two peaks of Cu at $2\theta=43.6^\circ$, 50.8° , corresponding to the (111), (200) lattice planes are observed. All the diffraction peaks can be well indexed to face-centered cubic (fcc) Cu according to the JCPDS card No.4-836. The mean particles size is estimated by scherrer's equation to be about 21.6 – 29.12 nm.

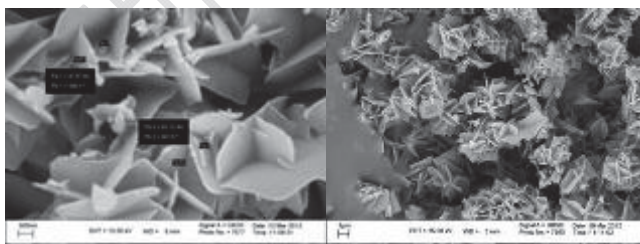


Fig.1. Typical SEM images of flowerlike copper nanoparticles

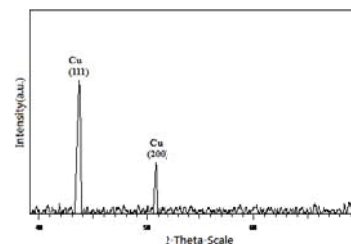


Fig.2. XRD pattern of as-prepared copper



Conclusion:

The effects of copper (II) sulfate/anhydride maleic molar ratio on morphology depositions were investigated. It is found that morphologies of copper nanoparticles can be simply controlled via change of copper (II) sulfate/anhydride maleic molar ratio.

Reference:

- [1] B. H. Han and M. Antonietti, "One-step synthesis of copper nanoparticles containing mesoporous silica by nanocasting of binuclear copper(II) complexes with cyclodextrins," *Journal of Materials Chemistry*, vol. 13, no. 7, pp. 1793–1796, 2003.
- [2] Zhang HX, Siegert U, Liu R and Cai WB 2009 *Nanoscale Res. Lett.* **4** 705
- [3] Yu W, Xie H, Chen L, Li Y and Zhang C 2009 *Nanoscale Res. Lett.* **4** 465



Study the effects of different methods for supporting Fe on Sodium Y zeolite on CNTs characteristics produced by CCVD method

A.A. Hosseini^{a*}, M. Shadfar^a, M. Pashae^a

^aState University of Mazandaran, Babolsar, P.O. Box: 47416-95447, Iran.

^{*}hos-a-pl@umz.ac.ir

Keywords: CNTs, CCVD, Zeolite, Ion-exchange, SEM.

Introduction :

Carbon nanotubes (CNTs) are allotropes of Carbon with cylindrical nanostructures which were introduced to the world by Iijima [1] in 1991. These nanomaterials have unusual properties, which are valuable for nanotechnology, electronics, optics and other fields of materials science and technology. Various techniques have been developed for synthesis of CNTs. In this work we are about to synthesize CNTs via Fe supported NaY Zeolite substrate, using CCVD (Catalytic Chemical Vapor Deposition) method [2]. Various parameters such as, catalyst nanoparticles preparation method, Fe loading and growth parameters can alter the structure and morphology of the produced CNTs [3]. In this study we investigate the effect of catalyst nanoparticles preparation process (impregnation and ion-exchange) on characteristics of CNTs.

Experimental:

The Fe-modified zeolite Y samples were prepared by ion-exchange and wet impregnation method. In wet impregnation, a solution of Iron nitrate, $\text{Fe}(\text{NO}_3)_3 \cdot 9\text{H}_2\text{O}$, in ethanol was added drop wise to a suspension of zeolite NaY and ethanol, the mixture was heated to 70°C. Three samples with different metal contents were prepared following this process. In ion-exchange method, a solution of Iron Nitrate in distilled water was prepared. In order to adjust the PH of the solution between 3-3.5 so that the Fe and Na cation exchange can take place, liquid

ammonia was added. Then, NaY zeolite was added to the solution and stirred occasionally for 24h. Samples were then filtered and dried. To synthesize CNTs, the catalyst nanoparticles were dispersed on a quartz boat placed in the middle of a horizontal furnace at a temperature of 750°C under a mixture of Argon and acetylene flowing with flow rates of 150 sccm and 15 sccm, respectively. The CNTs produced on impregnated and ion-exchanged nanoparticles were labeled I1, I2, I3 and E1, E2, E3 respectively.

Results and Discussions:

As SEM images show, Fe/Y prepared by ion-exchange was found to be of higher activity in the formation of carbon nanotubes compared with samples made by impregnation. The next noticeable characteristic of this sample is, there is much less amorphous carbon on nanotubes, compared with CNTs prepared by impregnated zeolite NaY.

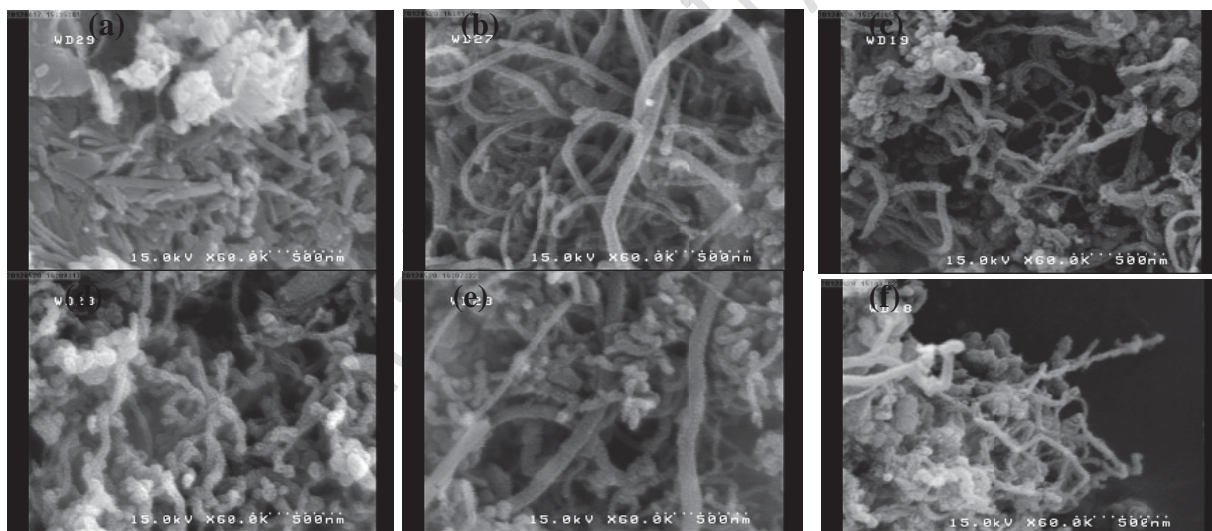


Fig.1. SEM Images of a)E1, b) E2, c)E3, d)I1, e)I2, f)I3

Conclusion:

We have shown that by using ion-exchange method for preparing catalyst nanoparticles, better results in carbon nanotubes formation can be achieved. This is as a result of good localization of metal catalyst on zeolite's body in ion-exchange method, while in impregnation the catalyst particles are located just on the pore sites of zeolite.



References:

- [1] S. Iijima, *Nature* **354**, 56 (1991)
- [2] I. Willems, Z. Konya, J.F. Colomer, G. Van Tendeloo, N. Nagaraju, K. Hernadi, J.B. Nagy, *Chem. Phys. let.* **317**, 71-76 (2000)
- [3] K.S. Triantafyllidis, S.A. Karakoulia, D. Gournis, A. Delimitis, L. Nalbandian, E. Maccallini, P. Rudolf, *Micro porous Mesoporous Mater.* **110**, 128-140 (2008)



The studies of Equilibrium Adsorption of 4-Nitroanilin from Aqueous Solution Onto Multi-Walled Carbon nanotubes

S. Khanahmadzade, F. Ghorbannejhad, M. Esmailzade

Faculty of Chemistry, Mahabad Azad University, Mahabad, Iran.

Email: F_gorbannejhad@yahoo.com

Key words: Multi Wall Carbon Nanotube, Adsorption Isotherm, pH, Dosage.

Introduction:

Carbon nanotubes (CNTs) known as a novel discovered form of carbon, and expected to be excellent adsorbents for adsorption of trace pollutants from water or air. A lot of research has been done about recovering natural habitats and reducing pollutants and because of unique physical and chemical properties of CNTs, so we intend to study the effect of pH and dosage adsorption of 4-nitroaniline and adsorption Isotherms on multi-walled carbon nanotubes (MWCNTs) in this lecture.

Materials and methods:

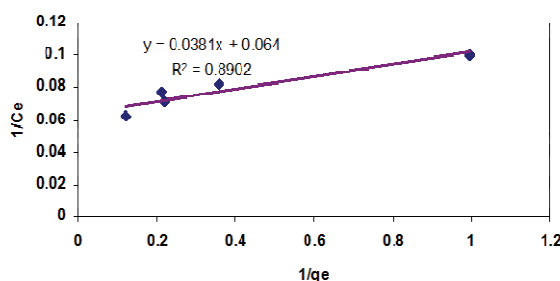
One of the most important factors in adsorption process is pH. To do so, first the zero charge point (pH_{zpc}) on MWCNTs was obtained, after preparation of 10 mg/L 4-nitroaniline and addition of 400 mg/L MWCNTs, pH of the solution was measured and its voltage was recorded. Then, the pH was adjusted with HCl and NaOH in the range of 2-10 then at each desired pH, the voltage was recorded. Then the diagram of pH versus voltage was drawn.

In order to study the effect of dosage, different amounts of MWCNTs (80, 160, 240, 320, 400 mg/L) were sampled separately and measured with a UV-Vis spectrophotometer. MWCNTs are used in adsorption isotherms and the **Langmuir**, **Freundlich** and **Temkin** isotherm models were used to express the adsorption phenomenon of 4-nitroaniline.

Result and discussion:

The zero charge point is about pH=6.9. with increase in solution pH until 6, adsorption percent of 4-nitroanilin increased and after that (PH=6) decreased, by increasing the MWCNTs from 80 to 320 mg/L, the adsorption of 4-nitroaniline increased and at 320 mg/L, its maximum value.

To investigate Langmuir, Freundlich, and Temkin isotherms Prepared concentrations of Solution, 3, 6, 9, 12 and 15 mg/L 4-mitroaniline, then 320 mg/L (MWCNTs) separately added to each solution. each 10min take the sample and centrifuge and measured with UV- Vis spectrophotometer, and isotherms for (MWCNTs) diagram drawn.



Langmuir isotherm diagram at the absorption of 4NA on MWCNTs
[MWCNTs]₀=320 mg/L ; pH=6

Conclusion:

CNTs have high adsorptive capacity for 4-nitroanilin and Ph has an important role in this process. Drawing Langmuir, Freundlich, and Temkin isotherm curves showed that the linear correlation coefficient of Langmuir isotherm is closer to one and is significantly more compatible compared to other two isotherms. According to consistency of figured obtained from Langmuir isotherm, it can be said that the resulted adsorption was monolayer.

Reference:

- [1] A.Srivastava, S.Talapatra, R.Vajtai & P.M.Ajayan, Nature Mater, 2004, 610-614
- [2] C.L.Mangun, Z.R Yue, adsorption of organic contaminants from water using tailored ACFs carbon, 2001, chem mater, 13[2356-2360]



15th Physical Chemistry Conference



Nano-bentonite as chemical flocculant in papermaking process

M. Mokhtari^a, H. Resalati^b, H. Kermanian^a, H. T. Jalali^{a*}

^aDepartment of Cellulose and Paper Technology, Shahid Beheshti University, Tehran, Iran

^bDepartment of Wood and Paper Technology, Agriculture and Natural Resources University of Gorgan

Email: H_Jalali@sbu.ac.ir

Key words: Nano Bentonite, Polyacrylamide, strength, CMP Pulp

Introduction:

Nano particle applications in papermaking have been developed and are highly focused for different advantages such as wet end chemistry and pigment coating[1]. Regardless of relatively higher cost, the Nano particle system have introduced more benefits than conventional that encourage paper industry to use it in more than 500 running paper machine in the last two decades, especially in high speed and modern ones[1]. Nano silica and Nano bentonite are attributed as the most widely used nano particle in pulp and paper industries. Both of them carry a negative charge so that they can interact with positively charged polyelectrolytes [2]. Addition of Nano particles to highly molecular weight polyelectrolyte in a complex retention system is emphasized to a great extent achieving improvement in paper ingredients formation resulted in strength enhancement. Effects of nano bentonite (Sodium montmorillonite) usage on strength properties of Chemi-Mechanical Pulp (CMP) in printing paper production were studied.

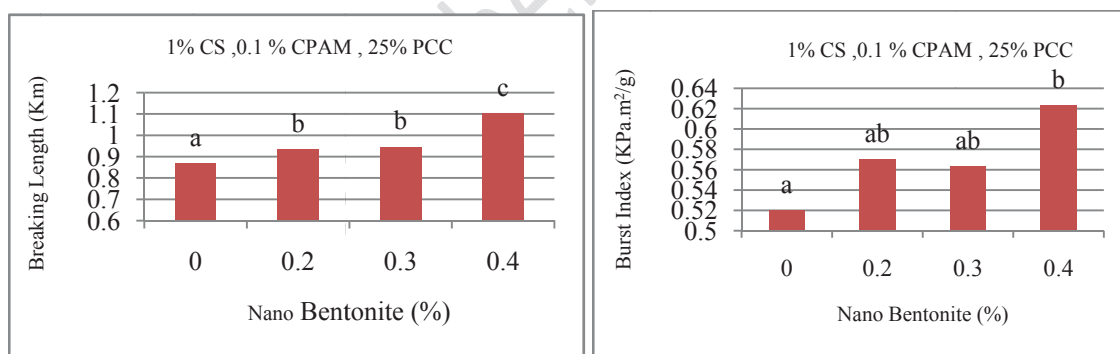
Materials and Methods:

Chemi-mechanical pulp (75% of sheet mass) was beaten to 300 ml Canadian Standard Freeness with Valley beater and precipitated calcium carbonate (~25% of sheet mass) was used as common filler. Retention of filler content in paper (~25%) was traced with trial and error. Cationic starch (CS) was gelatinized till 90 °C and used during the day. Nano bentonite slurry was allowed overnight agitation to delaminate its particle by water absorption. With

regard to importance of additives sequence combination on chemical and electrostatic interactions, cationic starch added firstly as charge neutralizer to fiber suspension followed by filler addition. Then, cationic poly acrylamide (CPAM) as filler retention aid added followed by nano bentonite particles. Hand sheet making and strength tests were done according to TAPPI test methods.

Results and Discussion:

Trend of the strength improvements with nano bentonite application could be assumed continuously which indicate effective role of the negatively charged nano particle in accumulation and distribution of CPAM-PCC agglomerates and their interaction with fiber. Anionic nano bentonite particles make more affinity for CPAM-PCC agglomerates and provide closer contact among the agglomerates. Closer and denser complexes of CPAM-PCC contribute better and uniform distribution of fiber bonding, as major factor for dry strength of paper. Statistically, the strength factors were improved significantly with nano bentonite addition compared to blank.



Effects of nano bentonite on breaking length (left) and burst index (right) of chemi-mechanical paper.

Conclusions:

Nano bentonite- CPAM complex have made improvements in breaking length and burst strength of paper composite which attribute to fine and dense flocculation of paper ingredients and finally better formation and higher bonding strength of paper compounds [3].



References:

- [1] M.A,Hubbe, Microparticle Programs for Drainage and Retention: Micro and Nanoparticles in Papermaking,Rodriguez JM(Ed), TAPPI PRESS, Georgia, Atlanta, 1-33, (2005).
- [2] I. Thorn, C. Au. Application of Wet-End Paper Chemistry, Second edition, Springer, 2009.
- [3] C, M. Gaiolas, et al., Influence of the Combined Use of Cationic Starch and Cationic polyacrylamide on the Quality of Printing Paper, TAPPI J., 5(6), 2006.



Effect of substrate temperature on Ag/C:H films prepared by PECVD devices

E..mohsensoltania* , M.Ghorannevisb , M.Shirazia

^a Faculty of physics, ISLAMIC AZAD UNIVERSITY North Tehran Branch,Iran

^b Plasma Physics Research Center, Science & Research Branch, ISLAMIC AZAD UNIVERSITY, Tehran,Iran

Email: elham_mohsensoltani@yahoo.com

Key Words: Ag , PECVD, Plasma, Sputtering, Polymerization

Introduction:

Silver is an efficacious and useful antibacterial agent. It is reported to kill over 650 bacterial strains. Silver nanoparticles could be potentially applied as bacterial resistant layers for biomedical application .This paper investigate characterization of Ag/C:H films prepared by Plasma-enhanced chemical vapor deposition (PECVD) method. Plasma polymer coatings with embedded Ag nanoparticles were deposited in low pressure DC plasma using an asymmetrical setup with an Ag electrode. The combination of plasma polymerization using Ag/CH₄ gas mixture and co-sputtering from an Ag target enables the incorporation of Ag nanoparticles in a plasma polymer matrix. The influence of the substrate temperature on properties of Ag/C:H films has been investigated. In 1988 Biederman already reviewed different plasma deposition techniques of metal/polymer composite films. Kay and Perrin et al. used a RF discharge for the deposition of gold nanoparticles of different size in a fluorocarbon matrix .Hanna Boldyryeva use DC planar magnetron deposition for the composite Ag/C:H films. [1-4]

Materials and methods:

Composite films were deposited in a vacuum chamber .The chamber contain two electrodes, anode electrode that the target of the silver (99.99% purity) is located on it with diameter of 3cm,which was connected to a DC power supply, and the cathode electrode that substrate is



located on it (silicon indimensions 1×1 cm) is connected to the ground electrode and the gap is 1Cm. More details is determined in table 1.

Sample	Pres'ower input (to (watt)	Flov (mL/min)	Flo (mL/min)	Gas Ar/CH4	Substrate mperature (0C	on Time (min)	istance of target substrate (cm)	
1	4.8×10^{-1}	12	36.20	207.30	10:1	380	120	1
2	4.8×10^{-1}	12	36.20	207.30	10:1	220	120	1

Table1: Summary of the experimental parameters used for the deposition processes

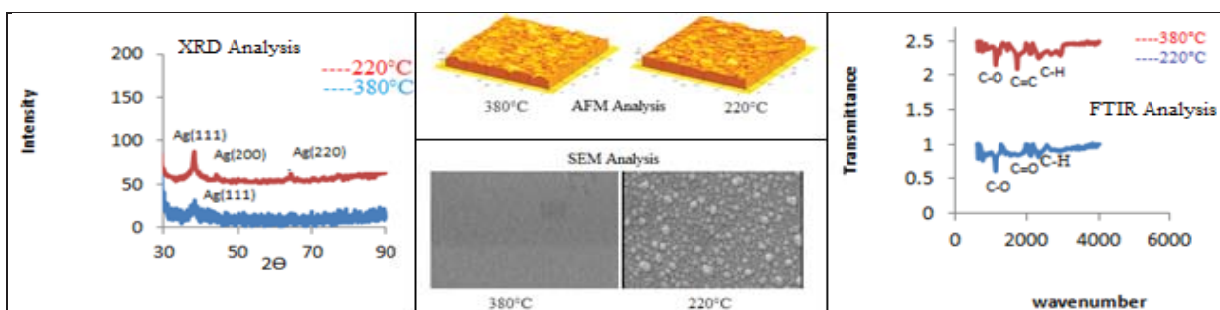
Apparatus:

The analysis techniques used to assess the material properties of the films included XRD, FTIR, SEM, AFM which one of them shows grain size, composite films and C-H link, surface roughness, surface morphology.

Result and conclusion

Since method of coating and different deposition parameters such as deposition rate, Thickness, working pressure and substrate temperature can affect the various properties of Ag/C:H thin films, in this work, The influence of the substrate temperature on properties of Ag/C:H films has been investigated and XRD, SEM, FTIR and AFM analysis were carried out. In XRD analysis for 380 oC temperature only Ag(111). peak is shown at angle of 38.354. But with decreasing of substrate temperature to 220oC , phases are composed of silver nanoparticles are formed in 38.167, 44.111 and 64.528, respectively, which form their crystal line structure are as: Ag (111), Ag (200), Ag (220). In the other hand, with decreasing substrate temperature, FWHM of XRD spectra decreases and the silver grain sizes which were calculated by Sherer formula increases, too. The increasing of substrate temperature decreases the residence time of the adsorbed specie. The deposition rate decreases upon increase of substrate temperature, so When we increase the temperature to 380 oC can be observed only one silver peak in XRD,[2]. We used FTIR analysis to identify the composition of C-H, Any absorption which is in the region of 150 ± 3000 Cm-1 is related to C-H. In FTIR analysis can be seen that in which 220°C temperature, the peaks related to the bonds CH₂, C-H, C-O, C-C are visible and in 380°C the peaks related to CH₂, C-O, C=C, C-H are observed. When we

increase the temperature will have a stronger C-H peak. Results of AFM analysis show that when the temperature increases, grain size decrease and the roughness increase. SEM analysis shows that grain size decrease with increasing of substrate temperature, too. All analysis can be seen in the figure below.



Conclusion :

In this work, we are studied the structural modifications of Ag-C:H films deposited at different substrate temperature with two precursor gas mixtures: Ar/CH₄. Our results show that with increasing of substrate temperature, the silver grain size in XRD and SEM decreases, and the surface roughness in AFM increase. And the XRD, SEM, AFM and FTIR results are in good agreements

Reference:

- [1]G.Capote; "Amorphous hydrogenated carbon films deposited by PECVD in methane atmospheres highly diluted in argon: effect of the substrate temperature" *Diamond and Related Materials* 13; 1454–1458, 2004.
- [2]E. Korner; "Formation and Distribution of Silver Nanoparticles in a Functional Plasma Polymer Matrix and Related Ag⁺ Release Properties " *Plasma Process. Polym* ;7; 619–625, 2010.



Magnetic Nanoparticle Fe₃O₄ Immobilized N-Propyl-Sulfamic Acid as Green and reusable Nanocatalyst

A. Rostami* and B. Tahmasbi

Department of Chemistry, Faculty of Science, University of Kurdistan, Zip Code 66177-15175, Sanandaj, Iran.

E-mail: Bah.tahmasbi@gmail.com and bah.tahmasbi@yahoo.com

Keywords: magnetic nanoparticles, nanocatalyst, sulfamic acid, phthalazine, solvent-free

Introduction:

Nanoparticles have recently emerged as efficient heterogeneous nanocatalysts in the organic synthesis [1]. However, particles with diameters of less than 100 nm are difficult to separate by filtration techniques. This drawback can be overcome by using magnetic nanoparticles (MNPs), which can be easily removed from the reaction mixture by magnetic separation. Magnetic nanoparticles are efficient, readily available, high-surface-area resulting in high catalyst loading capacity and outstanding stability heterogeneous supports for catalysts [2].

Materials and methods:

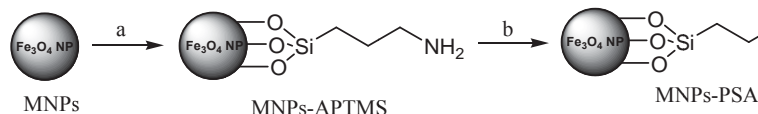
Chemicals including starting materials, solvents and reagent were obtained from Merck chemical company and used without purification.

Apparatus:

Melting points were obtained in open capillary tubes and also were measured on the Electrothermal 9100 apparatus. FT-IR spectra were recorded on a Perkin Elmer RXI spectrometer. NMR spectra were recorded on a Bruker Avance DPX 250 MHz instrument. The XRD were recorded on Philips X pert MPD Diffractometer. Images of SEM and TEM were collected using VEGA//TESCAN and Philips microscope (EM 280, Tokyo, Japan) apparatus respectively.

Result and discussion:

The MNPs-PSA was prepared according to the procedure shown in Scheme 2. Magnetite nanoparticles (Fe_3O_4) were prepared by coprecipitation of iron(II) and iron(III) ions in basic solution at 85 °C using the method described [3].



Scheme 2. Synthesis of MNPs-PSA; a) 3-aminopropyl- triethoxysilane, ethanol/water, rt, 8 h; b) chlorosulfuric acid, dichloromethane, 2 h, rt

The catalyst has been characterized by scanning electron microscopy (SEM), X-ray diffraction (XRD), fourier transform infrared spectroscopy (FT-IR) are shown in Figure1 and thermogravimetric analysis (TGA). A SEM image of MNPs-PSA is shown in Fig. 1A. It was confirmed that the catalyst was made up of nanometer-sized particles. The IR spectrum of MNPs-PSA shows peaks that are characteristic of a functionalized SA group, which clearly differs from that of the unfunctionalized Fe_3O_4 nanomagnets and aminopropyl-functionalized magnetic nanoparticles (Fig. 1D). Herein, we report catalytic applications of magnetic nanoparticle-supported sulfamic acid (MNPs-PSA) as a magnetically heterogeneous nanocatalyst for synthesis of phthalazine derivatives [4].

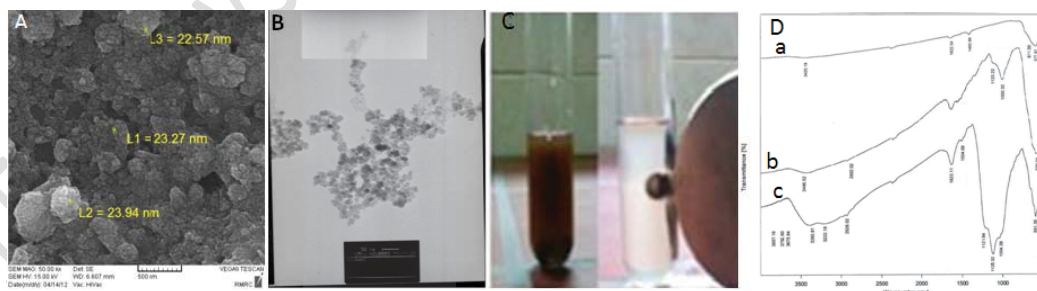


Figure 1: A) SEM image of MNPs-PSA, B) TEM image of Fe_3O_4 , C) catalyst separated by external magnetic field from the reaction mixture. D) FT-IR spectrum of MNPs-PSA [insert a) Fe_3O_4 magnetic nanoparticles b) MNPs–APTMs c) MNPs-PSA]



Conclusion:

In summary, the notable advantages of this method are easily separation of nanocatalyst by with the assistance of an external magnetic field from the reaction mixture and reused for several consecutive runs without significant loss of their catalytic efficiency (Figure 1c).

Reference:

- [1]D. Astruc and etal; "Nanoparticles as Recyclable Catalysts: The frontier between homogeneous and heterogeneous catalysis"; Angewandte Chemie International Edition; 44, 2005, 7852.
- [2]V. Polshettiwar and etal; "Magnetically recoverable nanocatalysts"; Chemical Review; 111, 3036, 2011.
- [3]X. Liu and etal; "Preparation and characterization of amino-silane modified superparamagnetic silica nanospheres". Journal of Magnetism and Magnetic Materials; 270, 2004, 1.
- [4]E. Mosaddegh and etal; "A rapid, one-pot, four-component route to 2*H*-indazolo[2,1-*b*]phthalazine-triones"; Tetrahedron Letters; 52, 2011, 488.



Synthesis and collation of NiO nanoparticles by base and acid and nonstructural investigation via XRD, FTIR and SEM techniques

F.Ashrafi¹, A. Bahari², A.Babanezhad¹, K.Taghavi^{2*} and F.Moosavi¹

¹Department of Chemistry, Payam Noor University of Sari, Mazandaran, Iran

²Department of Physics, University of Mazandaran, Babolsar, Iran

E-mail: k.taghavit@yahoo.com

Keywords: NiO, Nanoparticle, Sol- gel, FTIR, SEM.

Introduction:

Among all oxides, the nanoscale NiO has been widely used in catalysis, battery cathodes, gas sensor, and magnetic materials [1, 2]. In this work we were used of sol- gel method for prepared NiO with crystalline walls by the utilization of citric acid (CA) and NaOH base. The properties of the final products strongly depend on the metal precursors.

Materials and methods:

In the first synthesis, 3.52 g (Ni (NO₃)₂.6H₂O) and 3.16 g CA were dissolved in dilute water separately. Then the nickel solution was added to another until PH approached 1. After 120 h stirring, the obtained highly viscous residual was dried at 100°C. CA is used as a ligand. Its structure prevents the close contact of individual particles. In the second synthesis, (Ni (NO₃)₂.6H₂O) was dissolved in dilute water to form solution 0.7 M. Then solution of 2M NaOH and amount of PEG was added slowly drop wise, under stirring into the solution until PH approached 8. The obtained green precipitate was rinsed with dilute water until PH was 7 and dried at 100°C. The final product of both synthesis was annealed at 300 and 700°C.

Result and discussion:

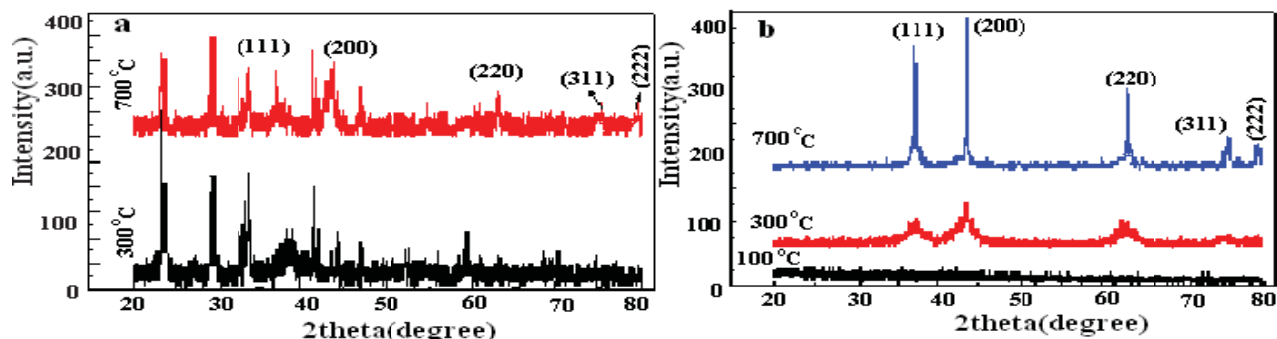


Figure 1: XRD patterns of NiO nanoparticles obtained by (a) NaOH and (b) CA.

The samples structure was quite amorphous at 100°C but it leads to crystallization structure at 300°C (Figure 1). All of the five dominated peaks at high temperatures indicate the NiO face-centered cubic phases. These peaks were grown with increase of temperature. These issues indicate the nanoparticles size increased which confirmed by calculation of Debye- Scherrer equation: $D = \frac{K\lambda}{\beta \cos \theta}$. The size avrage of synthesized nanoparticles in the presence of NaOH and CA was estimated 27 and 43nm, respectively.

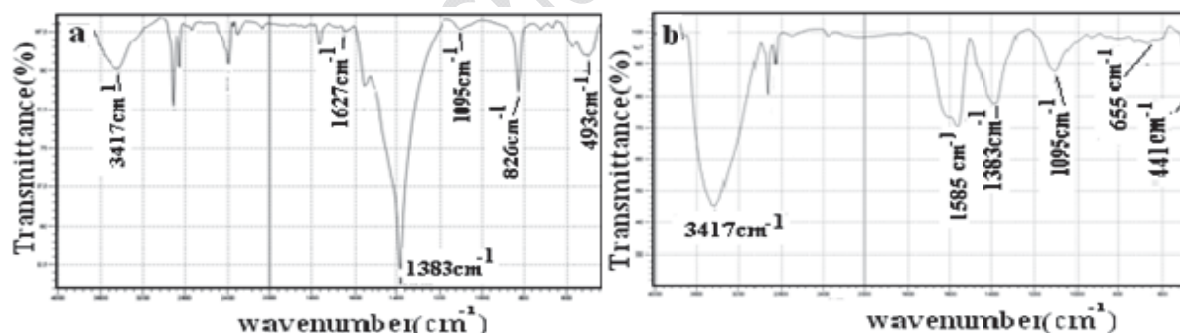


Figure 2: FTIR spectra of NiO nanoparticles at 300°C and obtained by (a) NaOH and (b) CA.

In figure 2, the broad absorption band centered at about 3417cm⁻¹ could be due to the O-H stretching vibrations which were confirmed by H-O-H bending mode at 1585 and 1627cm⁻¹. The bands at 3466 and 1383 cm⁻¹ indicate that the calcined powders tend to physically absorb water and carbonate ions, respectively. The broad absorption bands at 441cm⁻¹ and 493cm⁻¹ are assigned to Ni-O stretching vibration modes. FTIR peaks for base are sharper than acid.

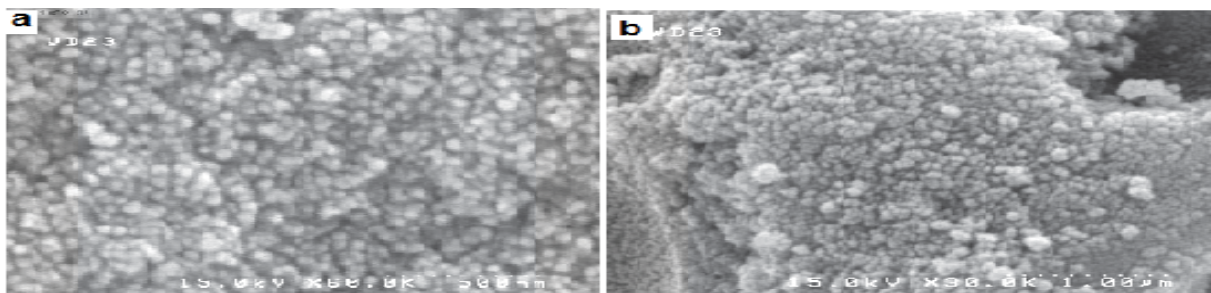


Figure 3: SEM images of calcined NiO nanoparticles synthesized by (a) CA and (b) NaOH.

As it seen in figure 3, the prepared NiO nanoparticles by CA are spherical and bigger and more uniform than NaOH.

Conclusion:

Synthesis of NiO nanoparticles in the presence of CA led to production of pure, more uniform and more spherical, which is more suitable for applications such as catalysts and gas sensors.

References:

- [1] Y. Wu, Y. He, T. Wu, T. Chen, W. Weng, H. Wan, "Materials Letters", 61. 3174–3178, 2007.
- [2] I. Hotovy, J. Huran, L. Spiess, "Materials Science", 39. 2609 – 2612, 2004.



Fabrication and Synthesizes of LSCO Nano composite via sol-gel method

NedaGhorbanzadeh^{*,1}, Ali Bahari² and Morteza Yaghoobi³

¹Department of Physics, Islamic Azad University, Fars Science and Research branch, Iran

²Department of Physics, Islamic Azad University, Mazandaran Science and Research branch, Iran

³Department of Physics, Islamic Azad University, Hamadan Science and research branch, Iran

*E-mail: Nedagh25@hotmail.com

Introduction:

Nanoparticle of $\text{La}_{0.5}\text{Sr}_{0.5}\text{CoO}_3$ (LSCO), a complex perovskite-type oxide has been synthesized by using sol-gel method. In this study, the effects of LSCO on both Nano electro mechanical and Nanostructural properties have been investigated [1]. We have performed a series of experiments to synthesis LSCO nanoparticles by using sol-gel method and study the sample structures via X-Powder and AFM techniques. These systems can show different behaviors at different temperatures and the rate of precursors [2].

Experimental Procedures and Details:

To synthesis of LSCO materials, $(\text{La}_{0.5}\text{Sr}_{0.5})\text{CoO}_3$, $(\text{La}(\text{NO}_3)_3 \cdot 6\text{H}_2\text{O})$, $(\text{Co}(\text{NO}_3)_2 \cdot 6\text{H}_2\text{O})$, $(\text{Sr}(\text{NO}_3)_2)$ have been used. These precursors were dissolved in distilled water at 90°C with the La/Sr/Co ratio of 1/1/2, followed by the addition of 0-5 wt. % polyvinyl alcohol. The resulting solution (after 48-60 h stirring) was refluxed for 24 h at $100\text{--}105^\circ\text{C}$. During reflux, the solution concentration was modified to be 0.3-0.5 M by distillation. Shortly after that, prepared colloidal solution was dried in 85°C in oven over 6 days. The procedures have been annealed at $500, 700$, and 900°C temperatures.

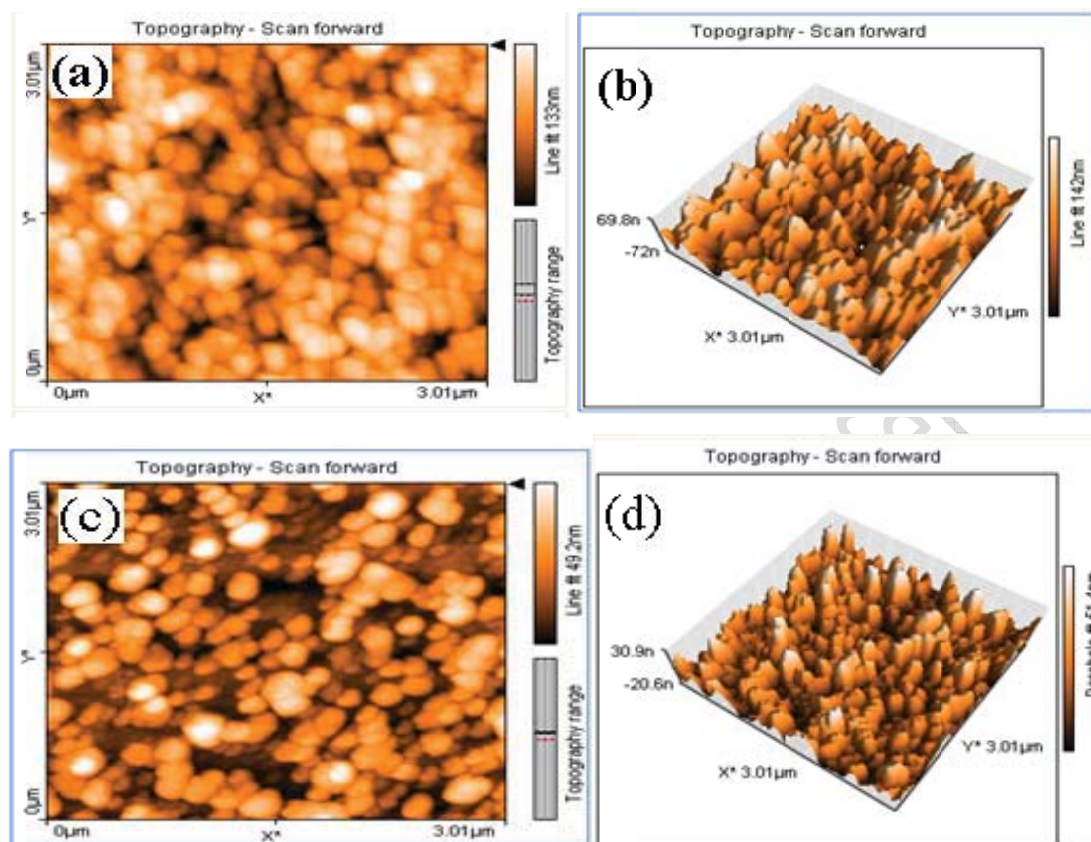


Fig.1.AFM images of LSCO annealed at (a,b) room temperature and (c,d) 900°C on two and three dimensional.

Figure 1a shows an uniform structure with fine nanoparticles at high temperatures. In contrast, as shown in figure 1c nanoparticles were clung to the other phases at high temperatures, in which the size of nanoparticles was increased. Growing of LSCO nanoparticles in cavities of silica matrix as a separate phase was displayed in figures 1b and d.

Conclusions:

The obtained results indicated that the LSCO with amorphous structure can be used as a good gate dielectric material for the future of MISFET (Metal Insulator Semiconductor Field Effect Transistor) transistor [2, 3]. Some issues are threatening the use of ultrathin silicon dioxide as a suitable gate dielectric of current and next CMOS (Complementary Metal Semiconductor) transistors due to leakage and tunneling currents and boron diffusion through the ultrathin gate dielectric [3]. The results of recent research indicate that the introduction of LSCO



nanoparticles in silicon matrix results in change of dielectric structure of a number of insulator materials. Outcomes of this study can be utilized in cases alike 3D memory devices, Nano scale fluidity control systems and Nano scale electro-producers.

References:

- [1] A. Bahari, P. Morgen and Z. Li,, Surface Science, 602,(2008),2315.
- [2] Z. Xinhua, L. Zhiguo and M. Naiben, Journal of Materials Chemistry, 20, (2010),4015.
- [3] j. S. Yu and T. He, International Journal of Hydrogen Energy, 36, (2011), 6894.



Nano structural LSCO as a good dielectric

N. Ghorbanzadeh^{*,1}, A. Bahari² and M. Yaghoobi³

¹Department of Physics, Islamic Azad University, Fars Science and Research branch, Iran

²Department of Physics, Islamic Azad University, Mazandaran Science and Research branch, Iran

³Department of Physics, Islamic Azad University, Hamadan Science and research branch, Iran

*E-mail: Nedagh25@hotmail.com

Introduction:

Nonvolatile memories based on ferroelectric capacitors show much promise because they exhibit a spontaneous polarization that can be reversed by an electric field [1]. Among ferroelectric materials, La (Sr,Co)O₃ is extensively researched. Although LSCO has many advantages such as high remanent polarization, low temperature crystallization. The most important problem of LSCO-based capacitors was the polarization fatigue. The results of recent research indicate that the introduction of LSCO nanoparticles in silicon matrix results in change of dielectric structure of a number of insulator materials [2].

Experimental Procedures and Details:

As starting precursors, reagent grade compounds were employed: (La_{0.5}Sr_{0.5}) CoO₃, (La (NO₃)₃·6H₂O), (Co (NO₃)₂·6H₂O), (Sr (NO₃)₂) as LSCO sources, absolute polyvinyl alcohol reagent (PVA) as solvent. These precursors were dissolved in distilled water at 100 °C with the La/Sr/Co ratio of 1/1/2, followed by the addition of 0-5wt% polyvinyl alcohol (PVA). The resulting solution (after 65-72 h stirring) was refluxed for 24 h at 110-120 °C. During reflux, the solution concentration was modified to be 0.5 M by distillation. Shortly after that, prepared colloidal solution was dried in 83 °C in oven over 5 days. The procedures have been repeated at 300, 500, and 900 °C annealed temperatures.

Result and discussion:

In Figure 1 the thickness of Nano crystallites (LSCO) is obtained via X-Powder method. Following Scherrer equation, the crystallite sizes have been determined for milled samples.

$$D = \frac{K\lambda}{\beta \cos \theta}$$

Debye – Scherrer equation

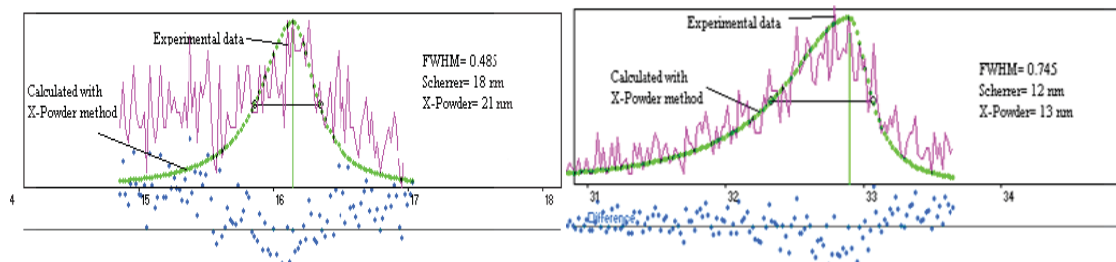


Fig.1. The size of LSCO (1:1:2) 18-12 nm determined by using X-powder method.

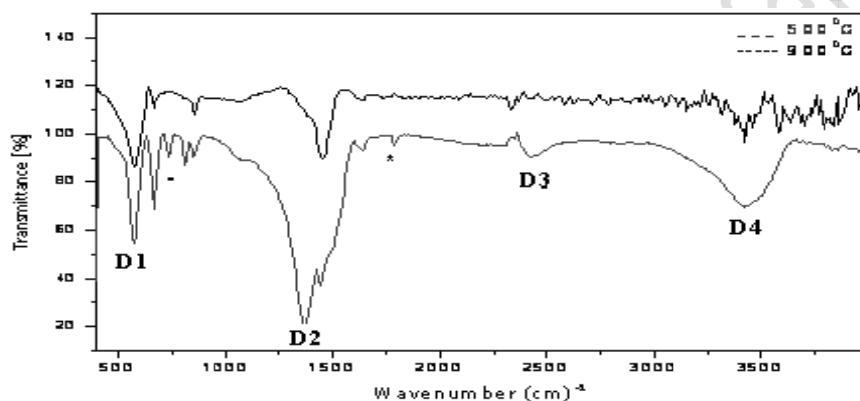


Fig.2. FTIR spectra of LSCO at 500 and 900°C. D1, D2, D3, D4 depths are explained in the text.

In Figure 2 the band at 570 cm⁻¹ related to absorbed water molecules, which can interact through hydrogen bonds with Lanthanide groups (La-OH), shows reduction of intensity at higher temperature (D₁). The band at about 1360 cm⁻¹ is due to the fact that the annealed powders tend to physically absorb water and carbonate ions (D₂). The broad absorption band centered at about 3417cm⁻¹ could be due to the O-H stretching vibrations which were confirmed by H-O-H bending mode at 2422 and 2298 cm⁻¹(D₃,D₄).

Conclusions:

The obtained results indicated that the LSCO with amorphous structure can reduced the leakage, tunneling currents and be used as a good gate dielectric material for the future of MISFET transistor(IC). Outcomes of this study can be utilized in cases alike 3D memory devices, Nano scale fluidity control systems and Nano scale electro-producers.



References:

- [1] M. A. Rodriquez, T. J. Boyle, B. A. Hernandez, C. D. Buchheit, and M. O. Eatough, *J. Mater. Res.*, vol. 11, no. 9, pp. 2282-2287, (1996).
- [2] M. G. Blanchin et al., *J. Sol-Gel Sci. Technol.* **47**, 165, (2008).

15th Physical Chemistry Conference



Magnetic Nanoparticles Catalyzed *N*-Tert-Butoxycarbonylation of Amines and Amine Derivatives

Soghra B. Sajirani^{a*}, Jafar Akbari^b, Jafar M. Nezhad^a and Akbar Heydari^c

^aChemistry Department, Shahr-e-Qods Branch, Islamic Azad University, Tehran, Iran

^bChemistry Department, Buinzahra Branch, Islamic Azad University, Buinzahra, Tehran, Iran

^cResearch center for organic chemical synthesis, No. 10. First-Kosar St. Tohid St, Tehran, Iran

Email: oaganic400@yahoo.com

Keywords: (Boc)₂O, chemoselective, magnetic nanoparticles, protection, recycling.

Introduction:

Because of increasing environmental concerns, the development of a clean synthetic procedure has become a crucial and demanding research. In this sense, heterogeneous organic reactions have many advantages, such as ease of handling, separation, recycling, and environmentally safe disposal [1]. Nanoparticles as heterogeneous catalysts have attracted a great deal of attention in recent years because of their interesting structure and high catalytic activities [2]. In this context, magnetic particles, in particular, have emerged as one of the most useful heterogeneous catalysts because of their numerous applications in nanocatalysis, biotechnology, and medicine [3]. Additionally, the magnetic properties make possible the complete recovery of the catalyst by means of an external magnetic field [4]. A large variety of protective groups have been developed. Among them, the tert-butoxycarbonyl (t-Boc) group is frequently used as a protecting group for amine in synthetic organic/peptide chemistry due to its stability towards catalytic hydrogenolysis and extreme resistance to basic and nucleophilic conditions. Various reagents and methods have been reported for the *N*-tert-butoxycarbonylation of amines.

Materials and methods:

Amine (2 mmol) was added to a magnetically stirred mixture of (Boc)₂O (2 mmol) and γ -Fe₂O₃@SiO₂ nano (5 mol%), and the mixture was stirred at room temperature. The reaction



was monitored by TLC. After the completion of reaction, the *N*-Boc product was separated from the reaction mixture by extraction with CH₂Cl₂ and vacuum dried. Then the products were identified by using NMR in CDCl₃. The γ -Fe₂O₃ nanocatalyst was separated by external magnet and reused for further reactions. Afterward, the products were identified by NMR, and physical data (mp) by comparison with those reported in the literature.

Apparatus:

The scanning electron microscope SEM 500NM Requipment company JEOL model EX90A.

Result and discussion:

Initially, Aniline reacted with (Boc)₂O instantaneously at room temperature in the presence of 5 mol% γ -Fe₂O₃@SiO₂ under solvent free condition and a white precipitate of tert-butyl-*N*-phenyl carbamate is formed. No competitive side reactions leading to the formation of isocyanate, urea, or *N,N*-di-Boc derivatives were detected. The chosen amount of catalyst (5 mol %) was found to be sufficient for an optimal result, but increasing the quantity of catalyst brought no substantial improvement. In the absence of catalyst, longer reaction time (90 min) was observed with lower isolated yield of tert-butyl-*N*-phenyl carbamate.

Conclusion:

This study was extended to a wide range of structurally diverse amines including open-chain, cyclic, aromatic and heteroaromatic, as well as β -amino alcohols and α -amino acid esters which underwent the reaction smoothly with (Boc)₂O. The method can be applied for the conversion of poorly reactive amines, such as chloroaniline and bromoaniline, as well as the sterically hindered tertbutylamine, into the corresponding *N*-Boc derivatives. The chemoselectivity of γ -Fe₂O₃ was assessed by performing *N*-Boc protection of amines in bifunctional compounds.

References:

[1] Ikegami, S.; Hamamoto, H. Novel Recycling System for Organic Synthesis *via* Designer Polymer-Gel Catalysts. *Chem. Rev.* **2009**, *109*(2), 583-593.



- [2] Scheuermann, G.M.; Rumi, L.; Steurer, P.; Bannwarth, W.; Mulhaupt, R. Palladium Nanoparticles on Graphite Oxide and Its Functionalized Graphene Derivatives as Highly Active Catalysts for the Suzuki-Miyaura Coupling Reaction. *J. Am. Chem. Soc.* **2009**, *131*(23), 8262-8270.
- [3] Shi, F.; Tse, M.K.; Zhou, S.L.; Pohl, M.M.; Radnik, J.; Hubner, S.; Jahnisch, K.; Bruckner, A.; Beller, M. Green and Efficient Synthesis of Sulfonamides Catalyzed by Nano-Ru/Fe₃O₄. *J. Am. Chem. Soc.* **2009**, *131*(5), 1775-1779.
- [4] Hu, A.G.; Yee, G.T.; Lin, W.B. Magnetically Recoverable Chiral Catalysts Immobilized on Magnetite Nanoparticles for Asymmetric Hydrogenation of Aromatic Ketones. *J. Am. Chem. Soc.* **2005**, *127*(36), 12486-12487.



Production and investigation of four phase semiconductor layer($\text{Al}/\text{AgNO}_3/\text{glass}$) by PVD method

S.Gharanizade^a, H.Kangarlou^b

a,b Faculty of sciences, Islamic Azad university, Urmia Branch, Urmia, Iran

Email:somagharani@yahoo.com

Email:hkangarloo@yahoo.com

Abstract:

According to the increasing advancement of nanotechnology and ample use of nanostructure layers in various fields like optic pieces, photic devices, solar cells, and biological drugs; manufacturing better and more commodious layers seems necessary. In this survey, aluminum has been layered and deposited on silver nitrate on glass using PVD method. Atomic force microscope (AFM), X-ray diffraction (XRD), and Scanning electron microscope (SEM) analyses, and spectrophotometry were derived from this multi-layer, and through these analyses, the structure of the surface and the morphology of these layers were studied.

Key words: Multilayer semiconductors, Nanostructures, PVD(physical vapor deposition), Crystallography.

Introduction:

Basically, semiconductors are really valuable in industry. PVD is one of the most popular procedures, which is less expensive and more available in comparison to other methods. In this paper, the four layers of $\text{Al}/\text{AgNO}_3/\text{glass}$ were built and deposited over the substrate of glass (SiO_2), (air is one of the layers). Thin layers on aluminum are widely used in electric devices, and the optical features of AgNO_3 nanoparticle on dielectrics are very amazing. And also the anti-bacteria effects of silver oxides like have been known for a long time.

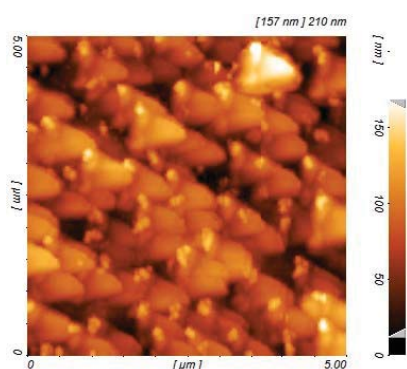
These four layers are made by ETS 160 with PVD method. Glass was chosen as the substrate and the angle of deposition was chosen vertically for these four layers. The size of the layer

was 2.54*7.62 mm, with 1 to 1.2 mm thickness. The substrate was washed and any pollution was removed from it through being washed in ultrasonic bath. The thickness of the layer was calculated by crystal quartz style. Temperature and pressure were chosen 100⁰ C, and 10⁻⁶ torr respectively. The currency needed for evaporation was 100-120A. We see the specifications of all the four layers in the following table.

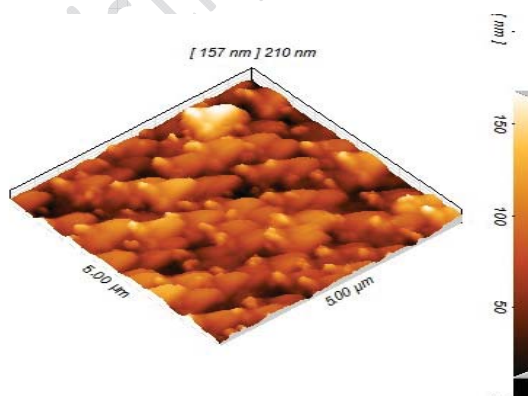
Multilayer	Thickness(nm)	Pressure
Al/AgNO ₃ /glass	~153.3	~10 ⁻⁶

Discussion:

The AFM two-dimensional image of the sample shows that clusters of AgNO₃ and the particles of Al are light and dark yellow and the voids are very obvious as black spots.



AFM 2D image

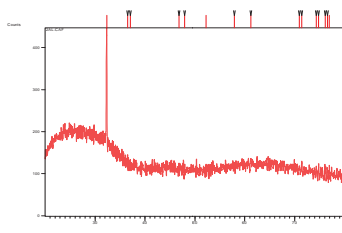


AFM 3D image

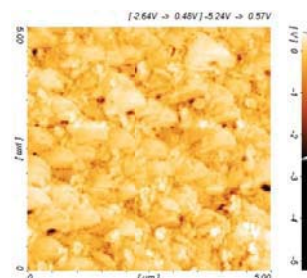
In AFM 3D image we see that the particles of Al are deposited on clusters of AgNO₃ (silver nitrate), and the empty spots of the voids are seen in black color. The thickness of the layer is 157nm on average.

In the phase image, the colors of yellow and black spots were changed which shows that there is no monotony in the so-called layer and this shows oxidation of the sample.

XRD of sample

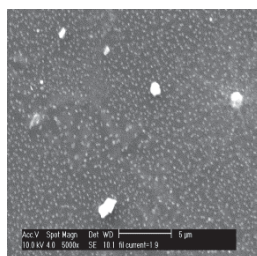


AFM phase image

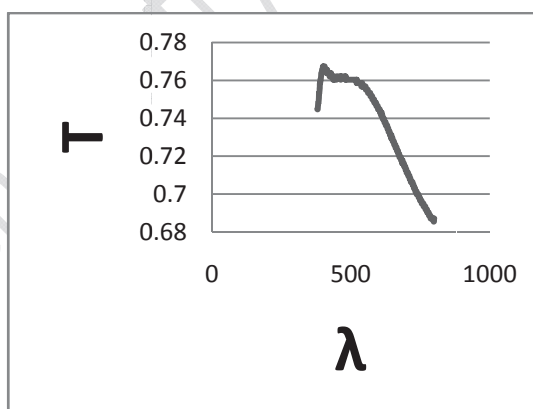


It is seen in XRD that the sample has changed from amorphous to crystallized form. The most significant peak is Al (32.32°). In addition, smaller peaks are related to AgNO_3 and Al_2O_3 . This sample is crystallized.

In SEM images we see that the surface is full of tiny grains and voids and in some spots, AgNO_3 clusters and nanoparticle are seen together and bigger which is in complete accordance with AFM images.



SEM image



Transmittance chart

It is obvious from transmittance and absorption charts that there is a peak in 400 nm wavelength with transmittance of 76%. We are encountered with high transmittance that is because of formation voids and impurities in layer.

Conclusion:

The abundance of voids is due to the thickness that was chosen for Al, and Al has a preferred peak. The direction for crystallography is highly dependent on the temperature and the



thickness of the layer. AFM and SEM images are completely in accordance with each other. XRD chart is very noisy due to the glass substrate.

References:

- [1] Weifeng wei, Xuhui Mao, Luis A. Ortiz and Donald R. Sadoway, Oriented silver oxide nanostructures synthesized through a template-free electrochemical route, *Journal of Materials Chemistry*, (2010).
- [2] Bilberg K, Malte H, Wanq T, Baatrup E, Silver nanoparticle and silver nitrate cause respiratory stress in Eurasian perch (*Perca fluviatilis*), *ELSEVIER*, (2010).
- [3] p. Quintana, A. I. Oliva, O. Ceh, Ecorona, Thickness effects on aluminum thin films, *superficies y v acio*, (1999).
- [4] Jong Hyan seo, Corrosion protection Al data line in TFT-LCD using chemical conversion coating, *solid state phenomena a vols*, 124-126 (2007).
- [5] J. P. Sullivan, J. C. Barbou, The Electrical properties of Native and deposited thin Aluminum oxide layers on Aluminum: Hydration effect, (2002).
- [6] Fran Clark, Youngx. can, Multifunctional nanostructure formation on pure Al surface during electrochemical oxidation a fluorine-based electrolyte, *American scientific publishers*, (2012).



Fabrication and Electrochemical Study of Silver and Copper Nanowires in Acidic and alkaline Environment

D. Nematollahi^a, B. khanebeygi*^b

^a Department of Chemistry, Bu-Ali Sina University, Hamedan, 651744161, Iran

^b Department of Chemistry, Islamic Azad University, Arak, 38135567, Iran

E-mail: kh.behnam@gmail.com

Keywords: Alumina template, Silver nanowire, Copper nanowire, DC deposition.

Introduction:

After Masuda and Fukuda[1] reported an ordered pore arrangement in an anodic aluminum oxide (AAO), it has been widely accepted that the AAO template is an ideal mold because it possesses many desirable characteristics, including tunable pore dimensions, good mechanical property, and good thermal stability. Moreover, especially for metal nanowires, the AAO template has been proved to be a cheap and high yield technique to produce large arrays of metals nanowires by the electrodeposition[2,3]. In this paper, anodic aluminum oxide (AAO) templates were fabricated using a two-step oxidization method and were used to grow well aligned Ag and Cu nanowires by the DC electrodeposition. The characterization of the AAO template and as-prepared nanowires were measured by scanning electron microscope (SEM) and X-ray diffraction (XRD).

Materials and methods:

High grade (99.99%) aluminum foil, and other reagents were of analytical reagent grade from Merck. The anodic alumina oxide (AAO) was fabricated by processes, one-step and two-step anodization.. Electrodeposition of nanowires was done by using the electrolytic solutions containing the following compositions: Cu (CuSO_4) and Ag (AgNO_3), with various concentrations.

Result and discussion:

Fig.1 shows SEM images of AAO anodized by one and two-step anodizing method. It can be found that AAO nanopores image of two-step anodizing show highly ordered and uniform holes (Fig.1b), but AAO nanopores image of one-step anodizing (Fig.1a) don't show appropriate properties. Fig.1c shows SEM images of silver nanowires.

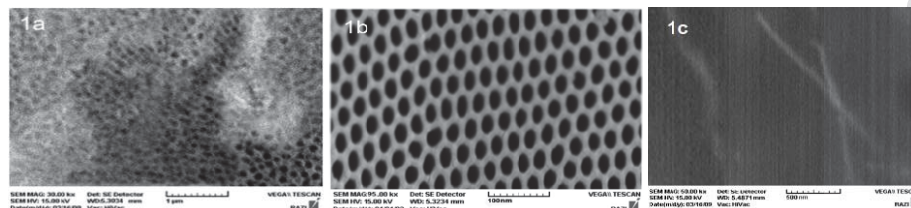


Fig. 1: SEM image of AAO, a: one-step anodizing; b: two step anodizing, c: Ag nanowires.

The XRD pattern of the nanowires product (Fig. 2) exhibited sharp peaks corresponding to the (111), (200), (220), and (311) diffraction peaks of the face centered cubic (fcc) structure of metallic Ag and Cu, respectively, indicating that the nanowires was composed of pure crystalline silver and copper.

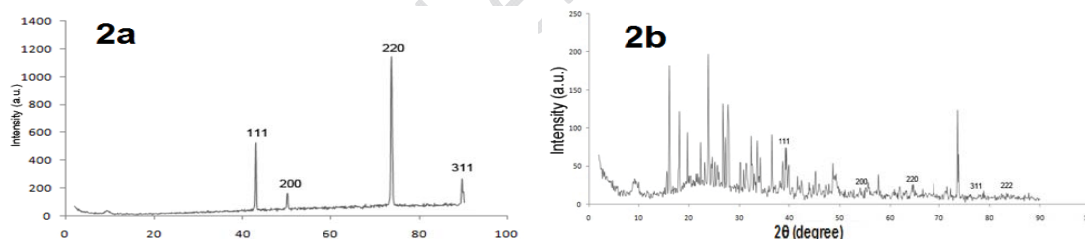


Fig. 2: The X-ray diffraction spectrum, a: Cu and b: Ag nanowire arrays embedded in the AAO template.

Typical dependencies of the amount of metal deposited into the pores of alumina are displayed in Fig. 3 and Fig. 4 for Ag and Cu nanowires, respectively. According these figures the optimize deposition condition for Ag nanowire obtained pH 8.3, time 600 s, concentration 0.2 M and current 36 mA and best optimized condition for Cu nanowire is obtained pH 1.8, time 600 s, concentration 0.2 M and current 36 mA.

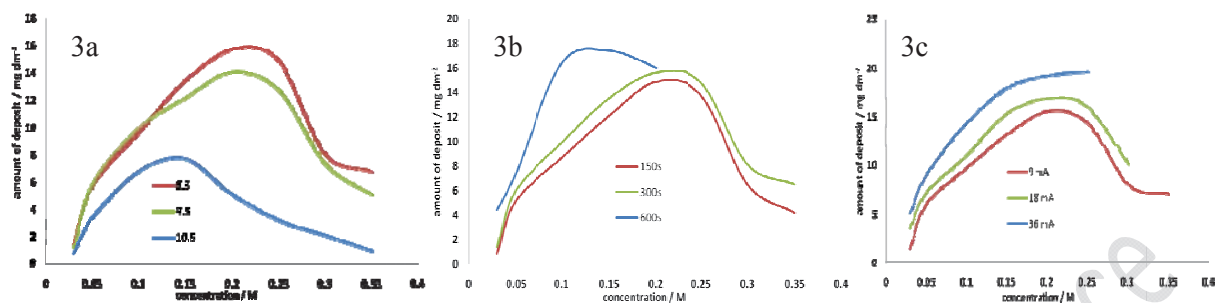


Fig. 3: Variations of the amount of silver deposited into the pores of alumina versus concentration at various a: pH, b: time and c: current.

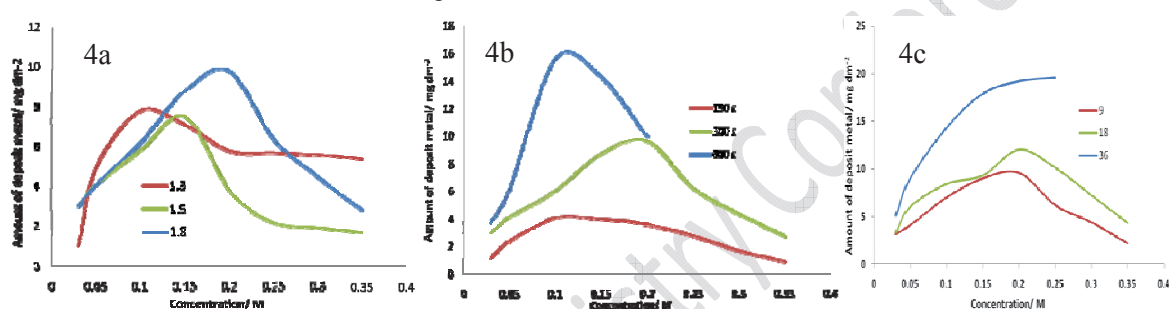


Fig. 4: Variations of the amount of copper deposited into the pores of alumina versus concentration at various a: pH, b: time and c: current.

References:

- [1] H. Masuda, M.Fukuda, Science, 268, 1466-1468, 1995.
- [2] X. SUN and et al, Mater Chem Phys, 90, 69-72, 2005.
- [3] O. Rabin and et al, Adv Funct Mater, 13, 631-638, 2003.



A new method for synthesis and characterization of Pt nanocolloid and investigation of nonlinear optical properties of this sample

E. Rusta^{a,b*}, A. Hassanzadeh^b

^a Department of Physics, Faculty of Science, Urmia University, Urmia, Iran

^b Department of Chemistry, Faculty of Science, Urmia University, Urmia, Iran

Email: Elham_rusta@yahoo.com

Key words: Nanocolloid, TEM images, UV-vis spectra, Nonlinear optics, Z-scan

Introduction:

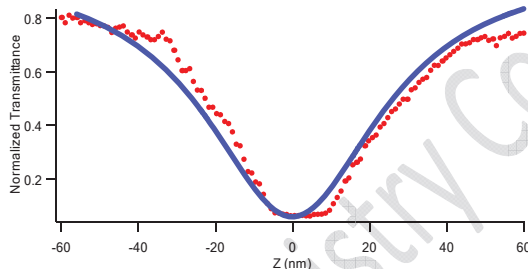
Studying of nonlinear optical properties of nanocolloids is of recent interest, due to their possible application in future high-capacity communication networks, optoelectronics and photonic devices. [1] The microscopic response of materials $\chi^{(2)}$ is related to the magnitude of the molecular nonlinearities. A fundamental requirement for second-order effects is noncentro symmetry at the molecular level. [2]

Materials and methods:

At first, we add 0.129 gr of K_2PtCl_6 in 20cc of distilled water, next put the mixture in the ultrasonic bath. Then solve 0.64 gr of $C_6H_5O_7Na_3$ in 18.5 cc of distilled water and add it over the first mixture, at first the color of mixture is yellow. Then solve 0.001 gr of $NaBH_4$ with 10 cc of distilled water and drop 3 to 4 drops of it inside of the yellow solution and put it in the ultrasonic bath for 30 minutes. Then take off the beaker of the inside of the ultrasonic bath and put it away for 2 days to form black sediment in the bottom of the beaker. After 2 days, we separate the yellow solution of black sediment then put yellow solution in the ultrasonic bath for 5 minutes next add 0.36 gr of $ZnCl_2$ and 0.36 gr of $Zn(NO_3)_2 \cdot 4H_2O$ over it and put it in the ultrasonic bath for 1 hour. After that solve 0.001gr of $NaBH_4$ in 10 cc of distilled water and drop 3 to 4 drops of it over the yellow solution and put it in the ultrasonic bath for about 2 hours and with completely solving of $NaBH_4$, the yellow color changes to dark brown and it causes the formation of Pt nanocolloid.

Results and discussion:

For proof of this sample we need to UV_vis spectra (T80 UV/Vis spectrometer) and TEM images. The UV cut-off wavelength of the sample is seen around 231.5 nm. A typical TEM image of Pt nanocolloid is done. Pt particles were all spherical and the size of these particles was within the limits of 70-80 nm. A Q-switched Nd-YAG laser was used at the fundamental wavelength of 1064 nm with the laser pulses of 8 ns. The nonlinear absorption coefficient β of Pt nanocolloid was measured by Z-scan method. Nonlinear absorption coefficient is $\beta=1.54 \times 10^{-9} \text{ mw}^{-1}$ [3].



Open aperture Z-scan curve of Pt nanocolloid

This figure shows the normalized transmission without an aperture at 532 nm. The image of this curve shows that the sample exhibits two photon absorption.

Conclusion:

From the UV-vis cut-off, it has been seen that the absence of absorption at the above region makes this sample be suitable for NLO applications and The lifetime of this sample is 1 year.

Reference:

- [1] P. Kumbhakar, M. Chattopadhyay and A. K. Mitra, Nonlinear optical properties of ZnS nanoparticles, 713209 ,2009.
- [2] Litty Irimpan,V. P. N. Nampoore, and P. Radhakrishnan, Spectral and nonlinear optical characteristics of nanocomposites of ZnO–CdS, 103, 094914 ,2008.
- [3] J. Wang, M. Sheik-Bahae, Time-resolved Z-scan measurements of optical nonlinearities, 11, 1009, 1994.



15th Physical Chemistry Conference



Synthesis and Functionalization of porous nanosilica (SBA-15) for removal of bichromate from aqueous solutions

M. ToghraeiSemiromi^{a*}, H. Faghihian^a

^aDepartment of Chemistry, Shahreza Branch, Islamic Azad University, Shahreza, Iran

*Email: Tmohadeseh1985@ymail.com

Key words: Porous Nanosilica (SBA-15), Functionalization, Adsorption, Bichromate.

Introduction:

Porous nanosilica presents high superficial areas and large uniform pores. The Stucky group synthesized the Santa Barbara Amorphous (SBA) materials in 1998 and SBA-15 has been well-known as a typical material in this family. SBA-15 mesoporous silica was prepared by pluronics P123 (PEO₂₀PPO₇₀PEO₂₀), a long chain organic structure-directing agent under highly acidic and hydrothermal conditions. It has high surface area (600–1000 m²/g), well-defined mesoporous structure and thermal stability (up to 1000K). The nanosilica wall surface of SBA-15 can be modified with organic groups to tailor their properties and achieve specific purposes. Functionalization of these materials can be carried out via grafting method in which hydroxyl groups of SBA-15 react with an organoalkoxysilane compound supporting the active functional group. Furthermore, protonated amino-functionalized mesoporous silicas are applied for the adsorptive removal of different pollutants such as chromate, arsenate and etc. Chromium compounds are extensively used in electroplating, leather industry, corrosion control, oxidation and various other industrial applications. Many approaches have been practiced in eliminating heavy metal ions, like chemical precipitation, ion exchange, adsorption, etc. Among these techniques, adsorption is a relatively easy and efficient way to remove hexavalent chromium from waste water effluents [1-3]. In this research SBA-15 was first synthesized and then functionalized. The synthesized adsorbent was used for removal of bichromate from aqueous solutions under different experimental conditions.



Materials and methods:

Tetraethylorthosilicate (TEOS, purity >98%), 3-aminopropyltriethoxysilane (APTES), N-[3-(trimethoxysilyl)-propyl] ethylene diamine (TMPED), Triblock co-polymer P123 ($\text{EO}_{20}\text{PO}_{70}\text{EO}_{20}$), H_3PO_4 (85%), toluene, HCl, NaOH, KBr, $\text{Na}_2\text{B}_4\text{O}_7 \cdot 10\text{H}_2\text{O}$ (Merk) were purchased from Merk. The stock solutions were prepared by dissolving $\text{K}_2\text{Cr}_2\text{O}_7$ and diluting to the desired concentrations using ultrapure water.

Result and discussion:

FT-IR, TGA and XRD data confirmed the efficient immobilization of amine groups on the SBA-15 surface. According to the SEM images, morphology of SBA did not change largely after functionalization with amine groups. Bichromate adsorption behavior of the resultant adsorbents was examined by a batch wise method. The effect of different parameters such as pH, contact time, anion concentration and temperature were studied and optimized. It was concluded that the adsorbent had good capacity for the studied anion. The regeneration of the adsorbent did not alter its original capacity.

Conclusion:

The characterization method showed that the new adsorbent was successfully obtained by functionalization of porous nanosilica SBA-15 through the post-grafting method. Study of its adsorption performance indicated good removal capacity for bichromate anion. The data was well fitted by the Langmuir isotherm. Maximum adsorption capacity for N-SBA-15 and NN-SBA-15 calculated from the Langmuir equations was 2.09 and 2.72 $\text{mmol} \cdot \text{g}^{-1}$ respectively. Surface organic amino groups displayed stronger affinity to bichromate at pH value of 3 compared to the other pH values, because the electrostatic interaction played a key role in the adsorption process.

Reference:

- [1] D. Zhao and et al; "Triblock Copolymer Syntheses of Mesoporous Silica with Periodic 50 to 300 Angstrom Pores"; science, 279, 548-552, 1998.



- [2] D. Zhao and etal; “Nonionic triblock and star diblock copolymer and oligomeric surfactant syntheses of highly ordered, hydrothermally stable, mesoporous silica structures”; J. Am. Chem. Soc, 120, 6024-6036, 1998.
- [3] A. Stein, and etal; “Hybrid Inorganic–Organic Mesoporous Silicates—Nanoscopic Reactors Coming of Age”; Adv. Mater, 12, 1403-1419, 2000.

15th Physical Chemistry Conference



Quantum analysis of drain source current of Gate-All-Around CdSe Nanowire Field-Effect Transistor

Seyed Ali Sedigh-Ziabari

Department of Electrical Engineering Roudbar Branch, Islamic Azad University, Roudbar, Iran

E-mail: sedigh@iauroudbar.ac.ir

Key Words: CdSe nanowire, NEGF, transmission probability.

Introduction:

The gate-all-around nanowire field-effect transistors (GAA NWFETs) are a promising option for nanometer transistors and recently they are being studied widely [1-3]. Extensive research has been carried out on the GAA NWFETs made of the semiconductors group IV such as silicon [1, 2], group III-V such as InAs and InSb [2, 3], and group II-VI such as ZnO [4]. CdSe is another option to construct GAA NWFETs [5, 6]. The electron effective mass in the CdSe is less than that in Si, and its nanowire can be covered with SiO₂ [5, 6]. In this paper, we specifically investigate the bias dependence of the drain source current in a GAA CdSe NWFET.

Device Structure :

The gate-all-around CdSe nanowire field-effect transistor oxide layer is assumed to be SiO₂ with a thickness of $d_{ox}=5$ nm. The corresponding Fermi levels would be $E_{FS}=-0.16$ eV, at thermal equilibrium. In this transistor, the channel diameter and length are taken to be $d_{ch}=5$ nm and $L_{ch}=10$ nm, respectively.

Results and discussion:

This device is simulated by the nonequilibrium Green's function (NEGF) method assuming electron's ballistic transport [7]. Figure 1(a) shows the drain-source current (I_{DS}) versus the gate-source voltage (V_{GS}) of the transistor shown of Fig. 1(a) with $L_{ch}=7$ and 10 nm, both for $V_{DS}=0.4$ V. As depicted in this figure, we may divide the I_{DS} - V_{GS} characteristic into three regions of operations in terms of V_{GS} . Region 1 includes $0 \leq V_{GS} \leq |E_{FS}|/q = 0.16$ V, region 2

covers the voltage range of $|E_{FS}/q| \leq V_{GS} \leq |(E_{FD})/q| = 0.56$ V, and region 3 includes $V_{GS} \geq |(E_{FD})/q|$. Notice $E_{FD} = E_{FS} - qV_{DS}$. To explain the device behavior in each of these three regions, we plot the channel transmission probability $T(E)$ spectra, as illustrated in Fig. 1(b). Note that the channel current is proportional to $\int dE T(E) [f_S(E - E_{FS}) - f_D(E - E_{FD})]$, wherein $f_{S,D}$ represent the source and drain occupation probabilities. Figure 1(b) shows three plots of $T(E)$ obtained for $V_{GS} = 0.1$ V (solid line) that falls in Region 1, $V_{GS} = 0.3$ V (dashes) that falls in Region 2, and $V_{GS} = 0.6$ V (dot-dash) that falls in Region 3, all three are obtained for $V_{DS} = 0.4$ V. The two blocks on the left and right represent the source with Fermi level of $E_{FS} = -0.16$ eV and the drain with Fermi level of $E_{FD} = -0.56$ eV. From the solid line in Fig. 1(b), one can realize that the contribution of $T(E)$ in the current in region 1 is limited to the electrons coming from the source with energies higher than the source Fermi level (i.e., $E \geq E_{FS}$). On the other hand, the number of electrons in this region is negligible since $f_S(E - E_{FS})|_{E > E_{FS}} \sim 0$. Hence the transistor is in the OFF state when operating in region 1. In region 2, contribution from $T(E)$ to the device current, as can be realized from the plot shown by the dashes in Fig. 1(b), mostly comes from electrons with energies $E_{FD} \leq E \leq E_{FS}$. In such condition, obviously, $f_S \sim 1$ and $f_D \sim 0$. Hence, the current for any given V_{GS} in this region, can be approximated by the area under the $T(E)$ curve for that particular V_{GS} . That is, $I_{DS}(V_{GS}) \propto \int dE T(E)|_{V_{GS}}$. In region 3, where $V_{GS} > |E_{FD}/q|$, the rate of increases in I_D decreases until $V_{GS} \rightarrow |(E_{FD} - \text{a few } kT)/q|$, after which the current saturates.

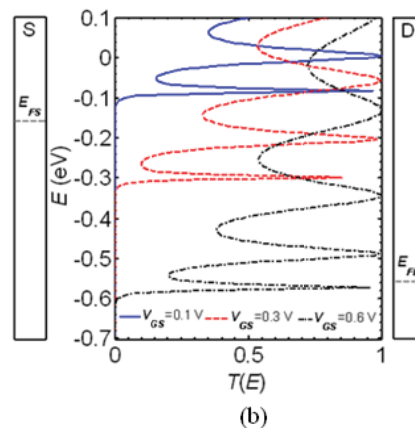
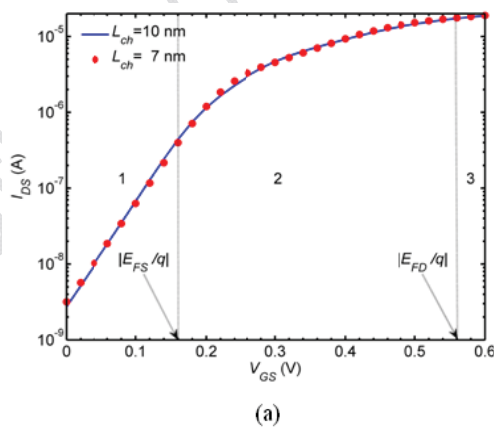




Fig. 1. (a) I_{DS} - V_{GS} characteristic for the GAA CdSe NWFET. (b) Transmission probability spectra for electrons across the channel of length L_{ch} =10 nm, for V_{GS} = 0.1 V, V_{GS} =0.3 V, and V_{GS} =0.6 V.

References:

- [1] J. Wang, A. Rahman, A. Ghosh, G. Klimeck and M. Lundstrom, "On the Validity of the Parabolic Effective-Mass Approximation for the I-V Calculation of Silicon Nanowire Transistors," *IEEE Transactions on Electron Devices*, 2005, vol. 52, 1589-1595.
- [2] M. Abul Khayer, Roger K. Lake, "Performance of *n*-Type InSb and InAs Nanowire Field-Effect Transistors," *IEEE Transactions on Electron Devices*, 2008, vol. 55, 2939-2945.
- [3] M. Abul Khayer, Roger K. Lake, "The Quantum and Classical Capacitance Limits of InSb and InAs Nanowire FETs ," *IEEE Transactions on Electron Devices*, 2009, vol. 56, 2215-2223.
- [4] Steve J. Pearton, David P. Norton, Li-Chia Tien, and Jing Guo, "Modeling and Fabrication of ZnO Nanowire Transistors," *IEEE Transactions on Electron Devices*, 2008, vol. 55, 3012-3019.
- [5] A. Khandelwal, B. Tech, CdSe NANOWIRE FIELD-EFFECT TRANSISTORS, University of Notre Dame, 2005.
- [6] A. Khandelwal, D. Jena, J. W. Grebinski, K. Leigh Hull, and M. K. Kuno, "Ultrathin CdSe Nanowire Field-Effect Transistors," *Journal of ELECTRONIC MATERIALS*, 2006, vol. 35, 170-172.
- [7] S. Datta, *Quantum Transport: Atom to Transistor*, Cambridge University Press, 2005.

A model representation for the temperature dependence of the gate-all-around Si-NW-FET threshold voltage

Seyed Ali Sedigh-Ziabari

Department of Electrical Engineering Roudbar Branch, Islamic Azad University, Roudbar, Iran

E-mail: sedigh@iauroudbar.ac.ir

Key Words: band structure, Nanowire, Threshold voltage, Temperature dependency.

Introduction:

Nanowire field effect transistors (NW-FETs), whose characteristics are dominated one-dimensional carrier transport, have attracted a great attention, in recent years [1]-[3]. Cylindrical nanowire with gate-all-around (GAA) provides full electrostatic control, and hence, leads to further device miniaturization. Many research groups have focused on the effects temperature on the NW-FETs experimentally [1]-[3]. Focus of this paper is on such a theoretical modeling for cylindrical gate-all-around Si-NW-FET threshold voltage.

The proposal model and simulation method

Figure 1 illustrates a schematic representation of gate-all-around Si-NW-FET, under study. The channel is made of a 10-nm long cylindrical Si nanowire of diameter $d_{ch}=2.75$ nm, whose crystallographic orientation is [100]. It is covered by a layer of SiO₂ of thickness $d_{ox}=1$ nm.

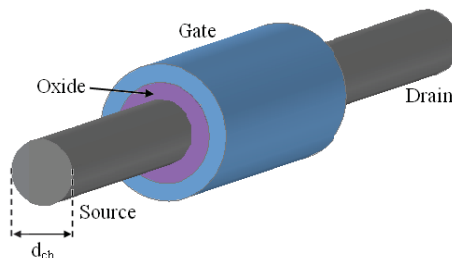


Fig. 1. Schematic representation of GAA-Si-NW-FET. The channel length and diameter are $L=10$ nm and $d_{ch}=2.75$ nm, respectively, and thickness of the gate oxide is $d_{ox}=1$ nm.

The temperature dependence of the Si lattice constant (a) can be approximated by [5]:

$$a(T) = 5.430 + 1.8138 \times 10^{-5} (T - 298.15) + 1.542 \times 10^{-9} (T - 298.15)^2 \quad (1)$$

We have taken the advantage of the similarity of (1) to the dependence of lattice constant on the compressive strain and calculated the temperature dependence of the energy band structure. In the propose model, the variation in the coupling potential is assumed to be due to the variation in temperature. As a consequence, the Hamiltonian matrix in the tight binding model is modified, accordingly. As a result of this modification the band structure and hence the resulting effective mass should be updated. Drain source current numerical simulation is based on the ballistic model by inserting the updated values of effective mass, that was first introduced by Rahman et. al. [4].

Result and discussion

The temperature dependence of the threshold voltage is shown in Fig. 2 (solid circles). This figure also illustrates that the extracted data fits excellently to the straight line (dots) represented by $V_T(T) \approx V_T(300) - KT_1(T/300 - 1)$, which in turn is similar to the one used in BSIM4.2.1 MOSFET Model [6], with $V_T(300) \approx 220$ mV and $KT_1 \approx 140$ mV/K.

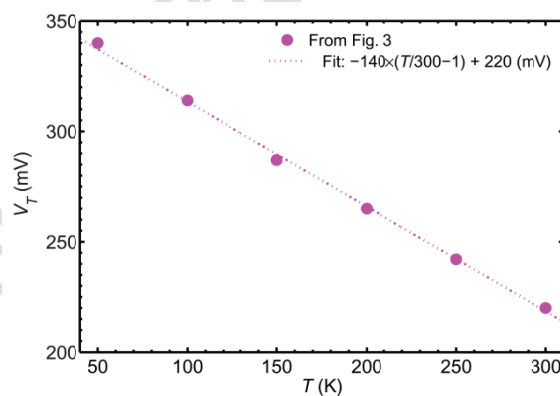


Figure 2: Temperature dependence of the threshold voltage for the Si-NW-FET of Fig. 1 under $V_{DS}=0.4$ V. Dots represent the linear fit.

References:

- [1] K. H. Cho, S. D. Suk, Y. Y. Yeoh, M. Li, K. H. Yeo, D. W. Kim, D. Park, W. S. Lee, Y. C. Jung, B. H. Hong, and S. W. Hwang, "Temperature-Dependent Characteristics of Cylindrical



Gate-All-Around Twin Silicon Nanowire MOSFETs (TSNWFETs)” *IEEE Electron Device Lett.*, vol. 28, no. 4, 2007.

[2] S. Ju, S. Kim, S. Mohammadi, and D. B. Janes, “Interface studies of ZnO nanowire transistors using low-frequency noise and temperature-dependent I - V measurements” *J. Appl. Phys. Lett.*, 2008.

[3] H. A. Nilsson, P. Caroff, C. Thelander, E. Lind, O. Karlström, and L. E. Wernersson, “Temperature dependent properties of InSb and InAs nanowire field-effect transistors ” *Appl. Phys. Lett.* **96**, 153505, 2010.

[4] Rahman A., Guo J., Datta S., and Lundstrom M., “Theory of Ballistic Nanotransistors” *IEEE Transaction on Electron Devices*, Vol. 50, No. 9, 2003.

[5] W. Martienssen and H. Warlimont, *Springer Handbook of Condensed Matter and Materials Data* (Spinger Berlin Heidelberg New York, 2004).

[6] X. Xi, K. M. Cao, H. Wan, M. Chan, C. Hu, BSIM4.2.1 MOSFET Model - user Manual, University of California, Berkeley, CA: 94720, 2001.



Electrocatalytic oxidation of formaldehyde at the surface of bimetallic Cu/Pt particles modified carbon nanotube paste electrode

J.B. Raoof*, R. Ojani, S. Aghajani, S.R. Hosseini

Department of Analytical Chemistry, Faculty of Chemistry, University of Mazandaran, 3rd Kilometer of Air Force Road, Postal Code: 47416-95447, Babolsar, Iran

Key words: Carbon nanotube, Electrocatalytic oxidation, Formaldehyde

Introduction:

The electrochemical oxidation of formaldehyde is interesting, because it is used in technologically important processes such as textile industry and electroless copper plating [1]. Platinum and its alloys are regarded as ideal catalysts for formaldehyde oxidation. However, one of the limiting factors is that Pt and its alloys have high cost. Therefore, there is a strong appetency to reduce the Pt dosage in the catalysts. Thus, in this work, we have fabricated Cu/Pt bimetallic particles onto carbon nanotube paste electrode via galvanic replacement reaction. The electrocatalytic oxidation of formaldehyde was studied at the surface of this modified electrode.

Materials and methods:

Preparation of the carbon nanotube paste electrode (CNTPE) was performed as reported previously [2]. Copper particles were electrodeposited for 15 min by using potentiostatic method in 0.1 M H₂SO₄ solution containing 0.1 M copper chloride onto CNTPE. The as-prepared substrate was used as a sacrificial matrix for deposition of Pt particles by immersing the electrode in 2.0 mM H₂PtCl₆ solution for 25 min via galvanic replacement reaction.

Results and discussion:

The morphologies of the bare CNTPE and Cu/Pt bimetallic particles modified CNTPE (Cu-Pt/MCNTPE) were characterized by SEM (Fig. 1). As can be seen in image (a), there are some holes or cavities on the electrode surface because carbon paste is porous. Image (b) shows structure of the Cu-Pt/MCNTPE, which is sufficiently decorated with Cu and Pt particles. Figure 2 (dotted line) shows a typical cyclic voltammogram of the Cu-Pt/MCNTPE during the adsorption and oxidation of bulk HCHO. Utilization of CNTs as incorporated materials into a carbon paste electrode improves the electrochemical oxidation signal of HCHO (solid line).

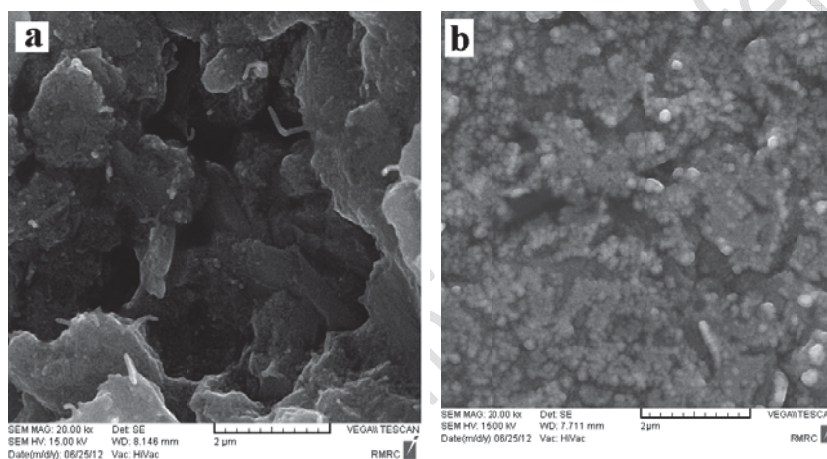


Fig. 1- SEM images of the bare CNTPE (a) and Cu-Pt/MCNTPE (b).

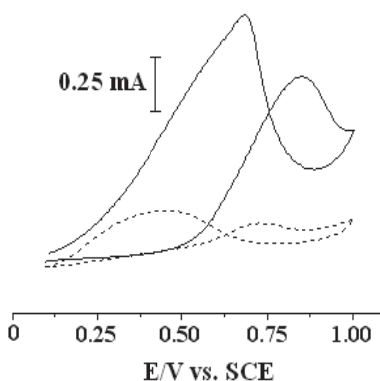


Fig 2 .Cyclic voltammograms of Cu-Pt/CPE (dotted line) and Cu-Pt/MCNTPE (solid line) in 0.5 M H₂SO₄ solution containing 0.63 M HCHO at $v=50 \text{ mVs}^{-1}$.



Conclusion:

In this work, Cu-Pt/MCNTPE was prepared by deposition of Pt particles by immersing the modified electrode in H_2PtCl_6 solution via galvanic replacement reaction. The prepared platinum particles show excellent electrocatalytic activity towards formaldehyde oxidation in acid solution.

References:

- [1] H.M. Villullas et al.; "Anodic oxidation of formaldehyde on Pt-modified SnO_2 thin film electrodes prepared by a sol-gel method"; *Electrochim Acta*; 49:3909-3916, 2004
- [2] J.B. Raoof et al.; "Highly improved electrooxidation of formaldehyde on nickel/poly (o-toluidine)/Triton X-100 film modified carbon nanotube paste electrode"; *Int. J. Hydrogen Energy*; 37, 2137-2146, 2012



Nano-Genosensor for Point Mutation Detection in Base of ELISA using nano-magnetic beads

Jahan Bakhsh Raoof^{*a}, Ezat Hamidi-Asl^a, Mohammad Saeid Hejazi^{b,c}

^aElectroanalytical Chemistry Research Laboratory, Department of Analytical Chemistry, Faculty of Chemistry, University of Mazandran, Babolsar, Iran

^bFaculty of Pharmacy, Tabriz University of Medical Sciences, Tabriz, Iran

^cDrug Applied Research Center, Tabriz University of Medical Sciences, Tabriz, Iran

* E-mail address: j.raoof@umz.ac.ir

Key words: ELISA, P53 gene, Gravi chip, Nano-magnetic beads, Genosensor

Introduction:

Genosensors have been developed recently because of their simplicity, low cost, high sensitivity, rapid analysis and compatibility with micro fabrication technology [1]. Sequence-specific detection of DNA provides the basis for detection of a wide variety of infectious and inherent disease. Electrochemical hybridization biosensors for the detection of DNA sequences reduce the assay time and simplify medical analysis [2]. The gene mutation takes place in around 60% in all humans' lifetimes [3]. Therefore, introduction of new methods for mutation detection is very important. Different methods are used to analysis the mutation status of individual tumours. The tumour suppressor p53 has been signified in a expanded number of biological processes, including cell cycle arrest, senescence, apoptosis, autophagy, metabolism, and aging. Activation of p53 in response to oncogenic stress deletes nascent tumour cells by apoptosis or senescence. Improved studying of the p53 pathway may lead to better diagnosis and treatment of cancer in the future [4].

Herein, an electrochemical DNA sensor based on a “sandwich” detection strategy is reported which involves DNA biotinylated capture probe immobilized on streptavidin coated nano-magnetic beads using screen printed electrodes (SPEs) and microfluidic based platform or gravi chip. The novelty of this work is the combination of a sensitive electrochemical platform

and a proper microfluidic with a simple and effective enzyme signal amplification technology (Enzyme-linked Immunosorbent Assays, ELISA) for detection of target DNA sequence and single nucleotide mutation in p53 tumor suppressor gene corresponding oligonucleotide.

Materials and methods:

The sequences of synthetic oligonucleotides are below: Capture probe (15mer): biotin-5'-AGT TCT GCA TCC CCA-3'; signaling probe (15mer): 5'-GGA GAG ATG CTG AGG-biotin-3'; complementary (30 mer): CCT CAG CAT CTC TCC TGG GGA TGC AGA ACT; SBM: CCT CAG CAT CTC TCC TGG GGA TGG AGA ACT; Non complementary 5'-TCC CCT ATT GAA GCA TAT CG-3'

Results and discussion:

The electrochemical measurements in SPEs were performed by the technique of differential pulse voltammetry (DPV). To investigate the analytical performances of the genosensor with synthetic oligonucleotides, a calibration experiment was designed. The DNA sensor response varied linearly between 0.01 nmol/L and 2 nmol/L. Within the linear analytical range, the sensitivity was 2.0×10^{-6} (mol/L), with an estimated detection limit of 5.90 pmol/L.

Conclusion:

In this paper a rapid and sensitive biosensor based on ELISA using a sandwich hybridization system was obtained for detection of complementary and single base mismatched oligonucleotide corresponding to a segment of p53 gene. Using of paramagnetic beads and screen printed electrodes allowed the possibility to measure pM level of DNA sequences, with high reproducibility. The specific oligonucleotide with good selectivity and more reduced analysis time can be detected by combination of this assay with microfluidic platform. The overall procedure time for gravi chip and SPE (including sample amplification, target hybridization and labeling, measurement, data presentation for 8 concentrations of target) takes approximately 2 h and 6 h, respectively.



References:

- [1] J. Wang, A. Kawde, A. Erdem, M. Salzar, *Analyst*, vol. 126, pp. 2020-2024, 2001.
- [2] J. Zhang, S. Song, L. Zhang, L. Wang, H. Wu, D. Pan, C. Fan, *J. Am. Chem. Soc.*, vol. 128, pp. 8575-8580, 2006.
- [3] T. Jiang, M. Minunni, P. Wilson, J. Zhang, A.P.F. Turner, M. Mascini, *Biosens. Bioelectron.*, vol. 20, pp. 1939–1945, 2005.
- [4] P. Nollau, C. Wagener, *Clin. Chem.*, vol. 43, pp. 1114–1128, 1997.



Morphological investigation of NBR/PVC blends reinforced with functionalized single- walled carbon nanotube

Armin Hajibaba, Ghasem Naderi*, Mirhamidreza Ghoreishy

Iran polymer and Petrochemical Institute, P.O. Box: 14965- 115, Tehran, Iran

(*) Corresponding author: g.naderi@ippi.ac.ir

Keywords: NBR/PVC, SWNT, Morphology

Introduction:

Acrylonitrile butadiene-rubber/Poly (vinyl chloride) blends are physical mixtures with wide commercial importance [1]. NBR can act as a permanent plasticizer for PVC in applications such as electrical wire, cable coating, wrapping film for the food industry, conveyor belts, domestic applications and etc. Since carbon nanotubes (CNTs) were firstly discovered by Iijima in 1991 [2], the use of CNTs as conductive fillers in polymers has attracted significantly academic and industrial interests. Up to now, CNTs have been used in diversified polymers, including thermoplastic polymers, thermosetting polymers and elastomers.

Methods:

Suspension polymerized PVC in powder form, with a K-value of 65 was provided by Bandar-e-Emam Petrochemical Company (Iran); NBR (Bound acrylonitrile content = 34%, Mooney viscosity ML (1+4) at 100°C = 41) was supplied by Kumho Petrochemical Co.Ltd (Korea); Functional SWNT powder (functionalized with carboxylic acid groups) with purity of 95% and aspect ratio of up to 1000 were obtained from research Institute of Petroleum Industry (Iran); The vulcanization curatives were of commercial grade.

The blends were characterized with the help of a scanning electron microscopy (SEM) (Leica Cambridge S 360 Model).

Dynamically vulcanized thermoplastic elastomer based on NBR/PVC with functionalized single walled carbon nanotube (SWNT) were prepared using a Brabender internal mixer at a screw speed of 50 rpm and temperature of 160°C.

Result and discussion:

Figure 1 (a-d) shows the effect of SWNTs on microstructure of NBR/PVC blends. It can be seen that with increasing the content of SWNTs diameter of droplet (NBR) get reduced and the dispersion of NBR in the PVC marching to homogenous dispersion. This reduction in droplet diameter and satisfactory dispersion of NBR in PVC in the presence of SWNTs might be relies on the viscosity ratio of phases that plays an important role in forming the structure of polymer blends that were discussed by Taylor and Wu former.

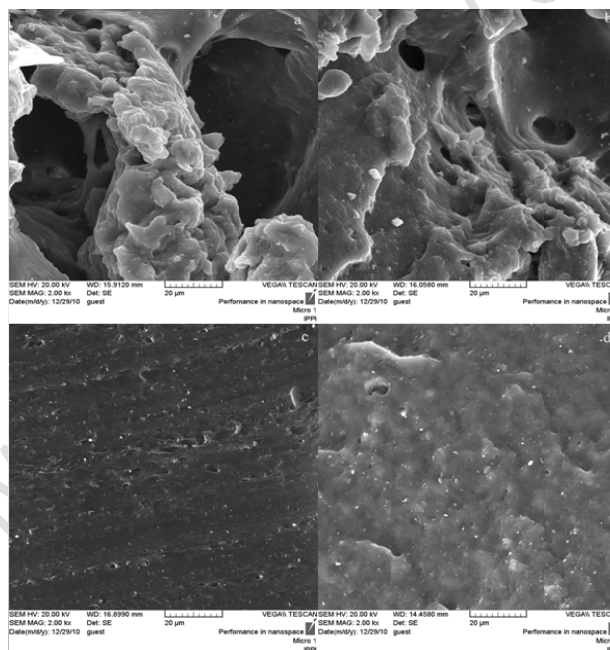


Figure 1- SEM micrographs of NBR/PVC (a), NBR/PVC/SWNT (0.5 phr) (b), NBR/PVC/SWNT (1 phr) (c) and NBR/PVC/SWNT (1.5 phr) (d)

Conclusion:

In the present article SWNTs were charged to PVC for enhancement the viscosity of PVC. Follow up this way, viscosity ratio of two phases get closer to unity. Based on Taylor and Wu



theory, when viscosity ratio of two phases in polymer blends goes to unity, the size of droplet diameter get reduced.

References:

- [1] Li H, Wang L, Song G, Gu Zh, Li P, Zhang Ch, Gao L (2010) Study of NBR/PVC/OMMT nanocomposites prepared by mechanical blending. Iran Polym J 19: 39-46
- [2] Iijima S. Nature 1991;354:56–8.



Simultaneous Determination of herbicides in Water Using Multi-Walled Carbon Nanotubes and chemometrics Methods

E.Konoz* , Z.Sedighi

Department of Chemistry, science faculty, Islamic Azad University-central Tehran Branch

Email:konozelaheh@gmail.com

Keywords: Sulfonylurea, solid-phase extraction, Multi-walled carbon nanotubes, experimental design.

Introduction:

Many research works focused on the detection of sulfonylurea herbicides at trace level, and achieved many valuable analytical techniques [1-3]. Solid phase extraction (SPE) has been the most important technique used for trace enrichment of sulfonylurea herbicides in water samples. In recent years, multi-walled carbon nanotubes (MWCNTs), was successfully observed and absorbed more attentions due to its advantage that can be used for many different goals in terms of its special chemical and physical properties. The goal of this study is to investigate the optimum trapping capability of MWCNTs for the sulfonylurea herbicides using chemometrics methods. In this work, two environmental water samples were used for evaluation including well water (east Tehran town), river water (Jajerood).

Materials and methods:

For SPE procedure 0.1 g multi-walled carbon nanotubes were packed in the 3 ml cartridge. The polypropylene upper frit and lower frit were remained at each end of the cartridge to hold the carbon nanotubes packing in place. Of the solvents, it was found that acetonitrile was the best one among methanol, acetone and dichloromethane. With the consideration of these three sulfonylurea herbicides that have poor acidity due to intrinsic characteristics, may be addition of a little acid to the elution solvent could improve the elution performance.



Result and discussion:

In this work, experimental design was used for optimization SPE procedure. It was indicated that the best pH of sample solutions was adjusted to 6.2 for well extraction. According to the results of experimental design, the best extraction performance, 13.8 mL acetonitrile containing 1% acetic acid was adopted in the followed experiments. Some important parameters of the proposed method such as linear range, correlation coefficients detection limits were also investigated under the optimal conditions for the quantitative analysis of nicosulfuron, mesosulfuron-methyl and metsulfuron-methyl. In this work, two environmental water samples were used for evaluation including well water (east Tehran town), river water (Jajerood). In a word, multi-walled carbon nanotubes has exhibited notable merits for trapping sulfonylurea herbicides, and established method would be much more competitive for the trace analysis of these herbicides in water samples.

Conclusion:

This work demonstrated the application of multiwalled carbon nanotubes used as the packing of SPE cartridge for excellent extraction of nicosulfuron, mesosulfuron-methyl and metsulfuron-methyl in water samples. Experimental design was used for optimization SPE procedure and HPLC determination. According to the found facts a sensitive, simple, and reliable method has been described for extraction and HPLC analysis which allows simultaneous determination of the these three sulfonylurea herbicides in water samples. The developed method could provide better recoveries, and lower detection limits. The facts demonstrated that it was very effective for enrichment of sulfonylurea herbicides using multi-walled carbon nanotubes.

References:

- [1] C.R. Powley, P.A. de Bernard, *J. Agric. Food Chem.* 46 (1998) 514.
- [2] J.B. Chao, J.F. Liu, M.J. Wen, J.M. Liu, Y.Q. Cai, *J. Chromatogr. A* 955 (2002) 183.
- [3] Z.L. Chen, R.S. Kookana, R. Naidu, *Chromatographia* 52 (2000) 142.



Synthesis, Modification and Application of Carbon Nanofibers for Removal of Lead from Aqueous Solution

M.Kooravand^{a*}, H.Faghihian^a

^aDepartment of Chemistry, Shahreza Branch, Islamic Azad University, Iran

Email: m.kooravand@yahoo.com

Keywords: Carbon Nanofiber, Chemical Vapor Deposition, Lead.

Introduction:

Carbon nanostructure shows exceptional adsorption capability which is significantly influenced by the pH of the solution and the nanostructure surface status. This can be controlled by the treatment processing of the nanostructure. In the present paper, a new structure of carbon nanofibers was synthesized and modified with mixture of nitric acid and sulfuric acid to enhance their cation adsorption capacity. The presence of functional groups on the carbon nanofibers was assessed. The modified carbon nanofiber was then used for adsorption of Pb^{2+} from aqueous solutions. At the optimized conditions, 211 mg.g⁻¹ of Pb^{2+} was adsorbed.

Materials and methods:

In the present paper, a new structure of carbon nanofibers was synthesized by chemical vapor deposition method on macro porous kaolin substrate surface using cyclohexanol and ferrocene as carbon source and catalyst, respectively. The process of synthesis involves the evaporation a mixture of carbon precursor and ferrocene (mass ratio 20:1), in nitrogen atmosphere [1]. Carbon nanofibers were modified with mixture of nitric acid and sulfuric acid to enhance their cation adsorption capacity. The presence of functional groups on the carbon nanofibers was assessed by FT-IR spectroscopy [2] and the surface activity of the oxidized carbon nanofiber was estimated by Boehm's titration [3]. The $pH_{(PZC)}$ of the as-synthesized and oxidized carbon nanofiber was measured [4]. The modified carbon nanofiber was then used for

adsorption of Pb^{2+} from aqueous solutions.

Apparatus:

Kaolin (Zarand mine in Semnan Region) Cyclohexanol, ferrocene, nitric acid and sulfuric acid (Merck company) FT-IR spectrophotometer (Perkin Elmer 65) Atomic adsorption spectrophotometer (PerkinElmer 300) SEM (AIS 2100, Japan)

Result and discussion:

The morphology of the product was studied by scanning electron microscopy technique. Sword like images of carbon nanofiber was observed in different parts of the SEM images (Fig.1). The synthesis of this structure has not been yet reported. The presence of functional groups on the carbon nanofibers was assessed by FT-IR spectroscopy. At the optimized conditions, 211 mg.g^{-1} of Pb^{2+} was adsorbed.

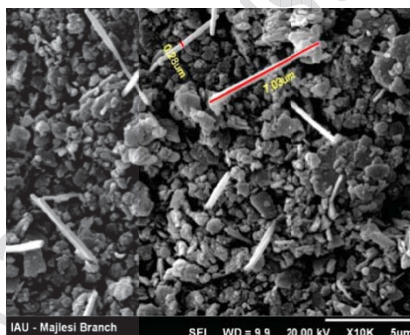


Figure 1: SEM image of carbon nano-structure.

Conclusion:

Chemical vapor deposition was used for synthesis of carbon nanofibers. The carbon nanofibers were then oxidized with nitric acid and sulfuric acid at room temperature. The results demonstrate that the adsorption capacity of the carbon nanofibers increases significantly after oxidation process. Also, increasing initial salts concentration increases the adsorption capacity of the carbon nanofibers. The structure and nature of carbon surface were changed after acidic treatment by increasing in the surface oxygen containing functional groups. The surface becomes negative and feasible for adsorption of Pb^{+2} .



Reference:

- [1] S. Musso et al. ; "Growth of vertically aligned carbon nanotubes by CVD by evaporation of carbon precursors"; *Diamond and Related Materials*;14,784-789,2005.
- [2]F.Aviles et al.;"Evaluation of mild acid oxidation treatment for MWCNT functionalization"; *Carbon*;47,2970-2975,2009.
- [3] M. Kandah et al. ; "Removal of nickel ions from water by multi-walled carbon nanotubes"; *Journal of Hazardous Materials*;146,283-288,2007.
- [4] J. Rivera-Utrilla et al. ; "Activated carbon surface modification by adsorption of bacteria and their effect on aqueous lead adsorption"; *Journal of Chemical Technology and Biotechnology*;76,1209-1215,2001.



Acetone vapor sensing characteristics of Ni-Zinc ferrite ($\text{Ni}_{0.6}\text{Zn}_{0.4}\text{Fe}_2\text{O}_4$) Nanoparticles prepared by microwave method

Y.Zohrabi, M.E.Ghazi, M. Izadifard

Department of Physics, Shahrood University of Technology, P. O. Box 3619995161, Shahrood, Iran

Email: yoneszohrabi@yahoo.com

Key words: Acetone vapor, Microwave, Gas sensing, Ni-Zinc ferrite

Introduction:

Acetone is a commonly used chemical reagent in industry. This used to dissolve plastics, purify paraffin, dehydrate tissues and for pharmaceutical applications. People may feel a headache, fatigue when the concentration of acetone in air is higher than 10,000 ppm. Additionally, the medical reports show that acetone is also harmful for diabetic patients who also have higher acetone concentrations in their blood [1]. Hence, detecting and measuring acetone concentrations in the workplace or human body are necessary for our safety and health. A large number of Nano-sized metal oxides such as SnO_2 , ZnO , WO_3 , TiO_2 , Fe_2O_3 , mixed oxides, and ferrite have shown high sensitivity to certain gases [2,3].

In recent years, the ferrites have demonstrated to be good materials for semiconductor gas sensors. Among these, nickel ferrite has shown to be a very good sensor to detect oxidizing gases like acetone [3].

Materials and methods:

In this investigation, we synthesized nanoparticles of Ni-Zinc ferrite ($\text{Ni}_{0.6}\text{Zn}_{0.4}\text{Fe}_2\text{O}_4$) by microwave method. Nickel nitrate ($(\text{Ni}(\text{NO}_3)_2 \cdot 6\text{H}_2\text{O})$), Ferric nitrate ($(\text{Fe}(\text{NO}_3)_3 \cdot 9\text{H}_2\text{O})$), Zinc nitrate ($(\text{Zn}(\text{NO}_3)_2 \cdot 6\text{H}_2\text{O})$), and urea ($(\text{CO}(\text{NH}_2)_2)$) were used as starting materials and added to the distilled water. The resultant solution was stirred magnetically at 70°C for 2h to get homogeneous mixture. Then the solution placed in a microwave oven at power 720W for 330

second. The resultant powder sintered at 700°C for 4h. The powder obtained was cold-pressed into pellet of 25 mm diameter and thickness of about 2-3 mm under the pressure of 20 ton/cm² and it was used to study the gas sensing.

Apparatus:

The electrical oven (CARBOLITE), microwave oven (LG) and Gas Sensing Rector (GSR, Nano SharghAbzarToos Company) were used to sinter, prepare and gas sensing properties of the sample respectively. XRD patterns were recorded using a B8 advance (BRUKER) x-ray diffractometer.

Results and discussion:

The x-ray diffraction pattern of the sample is presented in Fig. 1. The average crystallite size which was calculated from the pattern is about 25 nanometers. Figure 2 shows the gas sensing response of the sample at 4000 ppm acetone vapor as a function of temperature. As the figure shows, the sample has a good sensitivity to acetone vapor above 150°C.

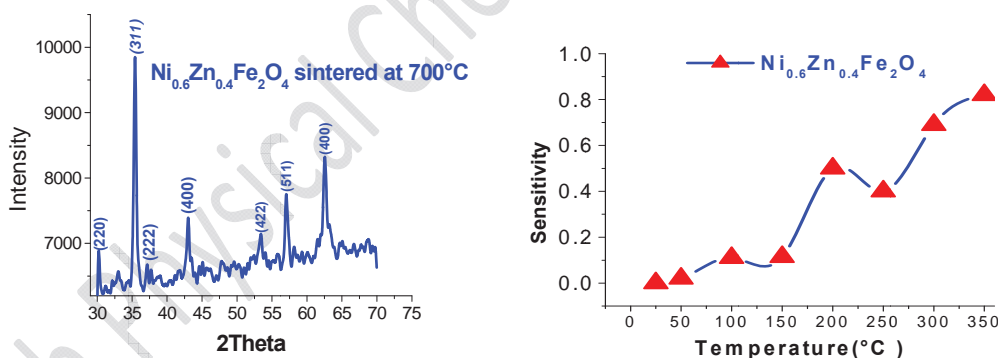


Fig. 1. X-Ray Diffraction pattern of the $\text{Ni}_{0.6}\text{Zn}_{0.4}\text{Fe}_2\text{O}_4$. **Fig. 2.** The gas sensitivity for the sample in the presence of the acetone vapor, at various temperatures.

Conclusion:



The Ni-Zn Ferrite nanoparticles can be synthesis by microwave oven method. It was shown that the nickel ferrite to be a good sensor for detection of acetone vapor especially above 150°C.

Reference:

- [1] C.C.H. Wang, Y.C.H. Weng, T.C.H. Chou ; "Acetone sensor using lead foil as working electrode"; *Sensor and Actuator B* 122(2007) 591-595.
- [2] L. Yang, Y. Xie, H. Zhao, X. Wu, Y. Wang ; "Preparation and gas sensing properties of NiFe₂O₄ semiconductor materials"; *Solid-State Electronics* 49 (2005) 1029-1033.
- [3] N. Rezlescu, N. Iftimie, E. Rezlescu, C. Doroftei, P. D. Popa ; "Semiconducting gas sensor for acetone based on the fine grained nickel ferrite"; *Sensor and actuators B* 114(2006) 427-432.
- [4] M. Sertkol, Y. Köseoglu, A. Baykal, H. Kavas, A. Bozkurt, M. S. Toprak; "Microwave synthesis and characterization of Zn-doped nickel ferrite nanoparticles"; *Journal of Alloys and Compounds* 486(2009)325-329.



Effect of nanoclay particles on the water absorption of polypropylene/Canola straw flour composites

M. Zahedi^{a*}, T. Tabarsa^a, M. Madhoushi^a, A. shakeri^b

^aDepartment of Wood and Paper Technology, Gorgan University of Agricultural Sciences & Natural Resources (GUASNR), Gorgan, Iran.

^bDepartment of Chemistry, Golestan University, Gorgan, Iran
Email: Zahedi25@yahoo.com

Key words: Nanoclay, Polypropylene, Water absorption, Canola straw.

Introduction:

Wood plastic composites (WPCs) have experienced significant market expansion in recent years as a replacement for solid wood, mainly in outdoor applications such as railings, decking, landscaping timbers, fencing, playground equipment, windows and door frames, etc. Nowadays, the consumption of plastic materials has increased enormously due to their various advantages. On one hand, the worldwide production of plastics is about 245 million tons per annum, resulting in a significant amount of municipal solid waste and most plastics take a very long time to decompose in nature the disposal of polymers after use is an important problem. On the other hand, in the wood industry, a large amount of wood waste is generated at different stages of the wood processing that this waste mainly end up in landfills (dump sites in a few areas) or burned. The volume of wood flour waste generated in the wood industry is very high, estimated at around 16% of its total production[1]. Using organo-modified montmorillonite (MMT) (commonly called “Nanoclay”) to reinforce polymer-based composites have raised great attention to academic and industrial sectors since the addition of small amount of nanoclay could substantially enhance the physical and mechanical properties of both thermoplastic and thermoset polymers. Clays are in nature organophobic, but they can be changed into organophilic by replacing the Na⁺ or Ca²⁺ cation originally present in the



galleries with one organic cation such as alkylammonium ions via an ion-exchange reaction[2].

Materials and methods:

Canola straw was obtained from canola fields in the north of Gorgan (Iran). The fibers were obtained by a local mill and screened to obtain 40–60 mesh particle sizes. Virgin polypropylene (PP) as polymer matrix was supplied by Bandar Imam Petrochemical Commercial Co., Iran, in the form of pellets with a melt flow index of 18 g/10 min and density of 0.95 g/cm³. The coupling agent, maleated polypropylene (MAPP) was obtained from Kimya Javid Sepahan Co. (Iran) in the form of pellets, which had a MFI of 64 g/ 10 min and 2% (by weight) maleic anhydride (MAH) content. Montmorillonite modified with a dimethyl, dehydrogenated tallow, quaternary ammonium (Modifier Concentration = 125 meq 100 g⁻¹ clay, d-spacing (d_{001} 31.5 Å) was obtained from Southern Clay Products Co. (USA), under trade name of Cloisite 15A. Nanoclay particles in the two level 3 and 5 percent and zero percent were used as controls.

Apparatus:

A laboratory co-rotating twin screw extruder; A hot press; A laboratory scale

Result and discussion:

One of the most important properties to be evaluated for wood-plastic composites is water absorption, since it can affect not only the mechanical properties but also biological/decay resistance and their final application. Figs. 1 shows the water absorption percentages for the composites at different periods of immersion, which vary depending upon the fiber and nano-clay loadings. The effect of clay on water absorption was investigated by using organo-clay at 0, 3 and 5 wt. %. The organo-clay, Cloisite 15A, is hydrophobic in nature and does not disperse well in water[3]. Therefore, the water absorption of wood flour/ PP composites decreased with the incorporation of organo-clay. The higher amount of clays the lower was the water uptake. Organically modified clay increases the tortuous path for water transport and as

a result water diffusivity decreases. Decreasing available space for water absorption due to occupation of void spaces in the wood flour by the polymer and nanoclay can be another mechanism for the lower water uptake of nanocomposites. The presence of organo-clay in the composite hinders the permeation of water through the composite[4]. The surface of modified clay had a tendency to immobilize some of the moisture.

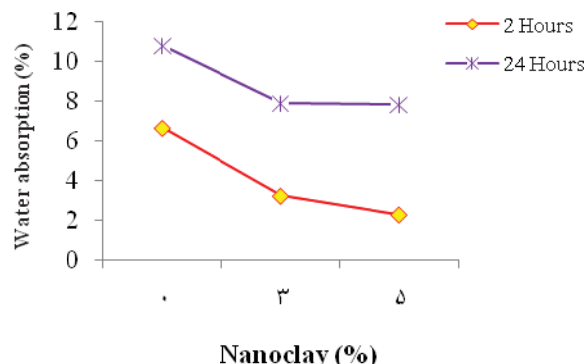


Figure 1. Water absorption (2 and 24 hours) of WPCs

Conclusion:

Base on the results of this study it can be concluded that nanoclay incorporation resulted in decreasing water absorption. The optimum ratio of nanoclay was 5%. As a consequence, it is possible to conclude that nanoclay enables to achieve better hardness strength than conventional composites.

Reference:

- [1] Arafa, I.M., Fares, M.M., Barham, A.S. 2004. Sol-gel preparation and properties of interpenetrating, encapsulating and blend silica-based urea-formaldehyde hybrid composite materials. *European polymer journal* 40; 1477-1487.
- [2] Steckel, V., Clemons, C.M., Thoemen H. 2007. Effects of Material Parameters on the Diffusion and Sorption Properties of Wood-Flour/Polypropylene Composites. *Journal of Applied Polymer Science*, 103: 752_763.
- [3] Chan, M., Lau, K., Wong, T., Ho, M., Hui, D. 2011 Mechanism of reinforcement in a nanoclay/polymer composite. *Composites: Part B* 42: 1708–1712.



- [4] Wang, L., Wang, K., Chen, L., Zhang, Y., He, C. 2006. Preparation, morphology and thermal/ mechanical properties of epoxy/clay nanoclay composite. *Composites Part A* 37: 1890–1896.

15th Physical Chemistry Conference



Effect of nanoclay particles on the hardness strength of polypropylene/Canola straw flour composites

M. Zahedi^{a*}, T. Tabarsa^a, M. Madhoushi^a, A. shakeri^b

^aDepartment of Wood and Paper Technology, Gorgan University of Agricultural Sciences & Natural Resources (GUASNR), Gorgan, Iran.

^bDepartment of Chemistry, Golestan University, Gorgan, Iran

Email: Zahedi25@yahoo.com

Key words: Nanoclay, Polypropylene, Hardness test, Extruder.

Introduction:

Environmentally friendly polymer composite materials obtained from natural bio-derived reinforcements have received considerable attention during the recent past due to cost effectiveness and increased environmental awareness and ecological concerns. One of the agricultural residues is canola straw whose cultivation had a considerable growth in Iran during the past decade. The average straw yield of canola reaches about 3 dry t/ha. It can be estimated that about 500,000 tons of canola straw is produced in Iran annually and due to the governmental policies to supply edible oil, this amount will increase in the future [1]. It is interesting to mention that canola straw has no special industrial application. Large quantities of canola straw remain in the fields every year after harvesting. Among the different nanoparticles, nanoclay is the most preferred one, owing to its high aspect ratio (1001000) and extremely high surface-to-volume ratio ($700\text{--}800\text{ m}^2\text{ g}^{-1}$), which establish significant improvements for a variety of polymers at very low filler contents (less than 5% by weight), far less than those using traditional micron-scaled fillers ($\geq 20\text{ wt\%}$)[2].

Materials and methods:

Canola straw was obtained from canola fields in the north of Iran (Gorgan, Golestan). The fibers were obtained by a local mill and screened to obtain 40–60 mesh particle sizes. Virgin polypropylene (PP) as polymer matrix was supplied by Bandar Imam Petrochemical



Commercial Co., Iran, in the form of pellets with a melt flow index of 18 g/10 min and density of 0.95 g/cm³. The coupling agent, maleated polypropylene (MAPP) was obtained from Kimya Javid Sepahan Co. (Iran) in the form of pellets, which had a MFI of 64 g/ 10 min and 2% (by weight) maleic anhydride (MAH) content. Ontmorillonite modified with a dimethyl, dehydrogenated tallow, quaternary ammonium (Modifier Concentration = 125 meq 100 g⁻¹ clay, d-spacing (d_{001} 31.5 Å) was obtained from Southern Clay Products Co. (USA), under trade name of Cloisite 15A. Nanoclay particles in the two level 3 and 5 percent and zero percent were used as controls.

Apparatus:

A laboratory co-rotating twin screw extruder; A hot press; a SCHENK–TREBEL testing machine.

Result and discussion:

Results of the hardness strengths of WPCs with varying of nanoclay showed that with incorporation of nanoclay up to 3wt% into the formulations, hardness strength significantly increased. At higher nanoclay content (5 wt. %), the values decreased (Fig. 1). The increased strength of the clay-containing samples up to 3wt% nanoclay content may be attributed to the high aspect ratio as well as surface area of stiff silicate layers in the polymer matrix that result in a higher extent of interaction with the polymer chains and good interfacial adhesion between the nanoscale clay particles and the PP matrix, so that the mobility of polymer chains is restricted under loading. The decrement of hardness strength at 5 wt. % of nanoclay could relate to the agglomeration of nanoparticles[3-4].

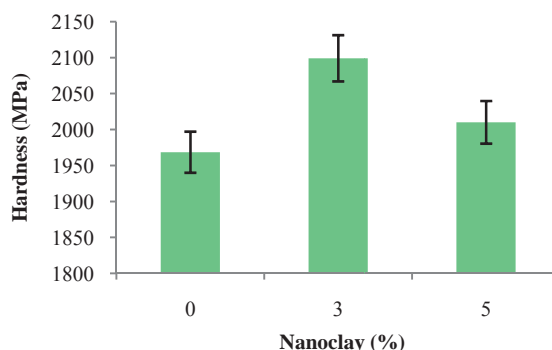


Figure 1. Hardness of various WPCs with different Nanoclay loading

Conclusion:

The results of this study indicate that hardness strength of PP/canola straw flour composites made with nanoclay increased by about 15%, with addition of 3 wt.% nanoclay, but then decreased slightly as the nanoclay content increased to 5 wt.%. The experimental results indicate that the hardness strength of WPCs could be significantly improved with an appropriate combination of polymer matrix content and nanoclay loading in the composites. As a consequence, it is possible to conclude that nanoclay enables to achieve better hardness strength than conventional composites.

Reference:

- [1] Yousefi, H., 2006. Potential of canola straw for utilizing wood and paper industries. M.S. Thesis. 2006. Department of Wood and Paper Science. Tehran University, Karaj, Iran.
- [2] Zhong, Y., Poloso, T., Hetzer, M. & De Kee, D. (2007). Enhancement of wood/polyethylene composites via compatibilization and incorporation of organoclay particles. *Journal of Polymer Engineering & Science*, 47, 797_803.
- [3] Ashori, A and Nourbakhsh, A. Performance properties of microcrystalline cellulose as a reinforcing agent in wood plastic composites. *Compos Part B* 2010; 41: 578-581.
- [4] Maji PK, Guchhait PK and Bhowmick AK. Effect of nanoclays on physico-mechanical properties and adhesion of polyester-based polyurethane nanocomposites: structure- property correlations. *J Mater Sci* 2009; 44: 5861-5871.



Synthesis and Optimization Performance of Modified Glucose Biosensor with Colloidal Gold Nanoparticles

N. Hosseinfakhrabadi^{a*}, A. A. Rohani^a, A. Farahbakhsh^b, S. Sohrabi^b, N. Ziaie^c

^a Department of Chemical Engineering, Shahrood Branch, Islamic Azad University, Shahrood, Iran.

^b Department of Chemical Engineering, Quchan Branch, Islamic Azad University, Quchan, Iran.

^c Department of Chemistry, Payam Noor University, Isfahan, Iran

E-mail: nahid.hosseinfakhrabadi@yahoo.com

Keywords: colloidal gold nanoparticles, glucose oxidase enzyme, glucose.

Introduction:

Biosensors show bio-molecular interactions at any time. In biosensors a composition is usually fixed on the biosensor chipset and the other one performs the act of identification [1]. Besides medical fields, the applications of biosensors are in other fields including bio-technology, physics, chemistry, foods safety and bio-environment control [2].

In this paper a biosensor was made based on Au_{nano}/CPE electrode (colloidal gold nanoparticles/carbon past electrode) that it was made with composition of 100mg carbon graphite powder, 300μl colloidal gold nanoparticles and 36μl paraffin oil. The biosensor was prepared by putting Au_{nano}/CPE electrode in a semi-permeable membrane containing 10mg glucose oxidase enzyme and 1ml phosphate buffer. The biosensor amperometric was done by applying 0.7V constant potential and putting it on glucose solution in (0.05-1)mM range concentration. Experiment design was performed by using Taguchi method based on both factors of glucose concentration and phosphate buffer pH and optimum values were obtained as 1mM and 6, respectively.

Materials and methods:

Glucose oxidase enzyme (35.5 Ku/mg) and colloidal gold nanoparticles (Au>48% and 24nm) was purchased from Sigma, glucose (purity:98%, molecular weight: 198.17 g/mole), paraffin



oil, carbon graphite powder (mesh<325) were obtained from Aldrich. For preparing the Au_{nano}/CPE electrode, the carbon graphite powder was heated in the furnace in 700°C for 30s. This powder is the initial material for making the electrode. The Au_{nano}/CPE electrode was prepared by adding 300μl colloidal gold nanoparticles to 100mg carbon graphite powder. After the evaporation of its water in the desiccators for 3h, 36ml paraffin oil was added to it. The Au_{nano}/CPE electrode was prepared by entering a part of this mixture into a glass tube with 4mm internal diameter. The electrical connection to the amperometric was made with a copper wire inside the electrode. This complex is put in 4°C when not in use.

Results and discussion:

Based on the comparison of the curves it may be observed that for all glucose concentration values, the maximum current occurs in pH=6. In addition, after the maximum values of the current produced, enzymatic activity in higher glucose concentrations decreased with increasing pH that is due to the formation of an improper ionic state for the substrate or the enzymatic inactivation. Experiment design with Taguchi method was done using Qualitek-4 software. The designed experiments were repeated twice in the same conditions and then were subjected to ANOVA analysis. Based on ANOVA analysis results, the most optimum values for both pH and glucose concentration factors were determined in biosensor amperometric experiments. Biosensor amperometric was done in the introduced optimum conditions and the amount of the current produced was 1.51 μA that has a negligible difference with the expected value, i.e. 1.47 μA.

Conclusions:

Using gold colloidal nanoparticles in the structure of Au_{nano}/CPE electrode not only improves conduction and electron movement, but also increases a satisfactory electrical connection between the FAD enzyme's active site and the electrode's surface increasing electron transfer.

It is found by investigating the biosensor's performance results that at very low concentrations, the enzymatic activity is lower and then it increases with gradual increasing



the glucose concentration until at a definite concentration, all enzyme's active site are filled with enzyme and the enzymatic activity reaches its maximum value.

References:

- [1]N. Ganesan, A. Gadar, M. Paranjape, J. Currie, Gold layer-based dual crosslinking procedure of glucose oxidase with ferrocene monocarboxylic acid provides a stable biosensor, *Analytical Biochemistry*, 343 (2005), 188-191.
- [2]A. Pereira, F. Fertoni, G. Neto, L. Kubota, H. Yamanaka, Reagentless biosensor for isocitrate using one step modified Pt-Ir microelectrode, *Talanta*, 53 (2001) 801–806.



Preparation and properties of biodegradable starch – ZnO nanocomposites

G.R. Kazemi Eslamian¹, B.Ganbarzadeh^{1,*}, M. Khatamian², B. Divband²

¹Food Science and Technology Department, International Aras Campus, University of Tabriz, Iran

²Inorganic Chemistry Department, Faculty of Chemistry, Tabriz University, Tabriz, Iran.

babakg1359@yahoo.com, eslamiangh@yahoo.com

Keywords: Nano biocomposite, Starch, Nano ZnO, Biodegradable

Introduction:

Increased use of synthetic packaging films has led to serious ecological problems due to their total non-biodegradability. In recent years there has been a growing interest in the use of biodegradable polymers for packaging materials in order to reduce the environmental pollution caused by plastic wastes [1, 2]. In this study, we prepared well-dispersed starch–ZnO nanocomposite. The structure and morphology of the nanocomposite was characterized by X-ray diffraction (XRD), and film properties such as water absorption, mechanical and thermal properties were also measured.

Experimental:

To completely gelatinize starch granules, 4 g of starches were suspended in distilled water (100 mL) and heated at 80 °C for 30 min. Proper amount of ZnO was slowly added to the starch solution. The mixture was stirred at 80 °C for 1 h. The solution was dried at 50 °C and the films were obtained.

Results and discussion :

The X-ray diffraction patterns of ZnO/Starch nanobiocomposites are shown in Fig. 1.

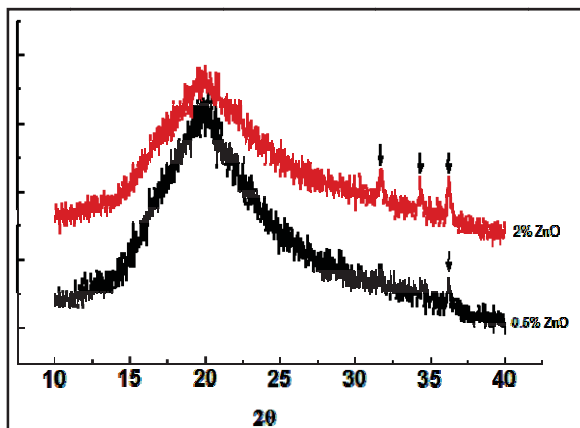


Fig. 1 The XRD pattern of nano ZnO/Starch with different ZnO containing

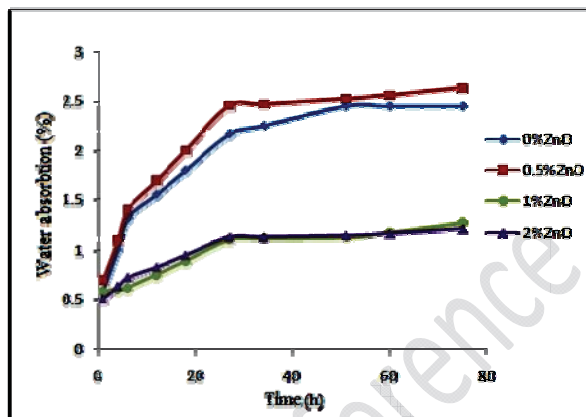


Fig. 2 the water absorption of ZnO/Starch nanocomposite films based on different amount of ZnO .

Figure 2 shows the water absorption of ZnO/Starch nanocomposite films based on different amount of ZnO. GPS/nano-ZnO bionanocomposites were prepared by incorporating nano-ZnO particles into plasticized-starch. Soluble starch played a very important role not only in the stabilization of nano-ZnO but also in the fabrication of GPS/nano-ZnO composites. The strong interaction between nano-ZnO filler and the GPS matrix contributed to the improvement of bionanocomposite properties.

Conclusion:

At a filler loading level (1 wt %), nano-ZnO enhanced glass transition temperature and mechanical properties and decrease the water absorption of GPS/nano- ZnO nanocomposites in comparison to pure GPS. These bionanocomposites have potential applications in medical, agricultural, drug release, packaging, and UV-shielding materials.

References:

- [1]X. Tang and et al; "Effects of plasticizers on the structure and properties of starch–clay nanocomposite films"; Carbohydrate Polymers; 74, 552–558, 2008.
- [2]Y.Chung and et al;"Preparation and properties of biodegradable starch-clay nanocomposites"; Carbohydrate Polymers; 79, 391–396, 2010.



15th Physical Chemistry Conference



Preparation and Properties of Starch Based-Natrolite Nanobiocomposites

G.R. Kazemi Eslamian¹, B.Ganbarzadeh^{1,*}, M. Khatamian², B. Divband²

¹Food Science and Technology Department, International Aras Campus, University of Tabriz, Iran

²Inorganic Chemistry Department, Faculty of Chemistry, Tabriz University, Tabriz, Iran.

babakg1359@yahoo.com, eslamiangh@yahoo.com

Keywords: Nano biocomposite, Starch, Zeolite, Biodegradable Polymers

Introduction:

For a long time polymers have supplied most of common packaging materials because they present several desired features like softness, lightness and transparency. However, increased use of synthetic packaging films has led to serious ecological problems due to their total non-biodegradability. In recent years there has been a growing interest in the use of biodegradable polymers for packaging materials in order to reduce the environmental pollution caused by plastic wastes [1-2]. In this study, we prepared well-dispersed starch–natrolite (GPS/Nat) nanobiocomposite. The structure and morphology of the nanocomposite was characterized by X-ray diffraction (XRD), SEM and film properties such as water absorption, mechanical and thermal properties were also measured.

Experimental:

GPS/Nat bionanocomposites were prepared by incorporating zeolite into plasticized-starch. To completely gelatinize starch granules, 4 g of starches were suspended in distilled water (100 mL) and heated at 80 °C for 30 min. Proper amount of zeolite was slowly added to the starch solution. The mixture was stirred at 90 °C for 1 h. The solution was dried at 50°C and the films were obtained.

Results and discussion:

The result of mechanical strength (Fig. 1) shows that the mechanical performances of nanobiocomposites increase by adding zeolite, the optimum loading level is 1 wt%.

The strong interaction between zeolite filler and the GPS matrix contributed to the improvement of bionanocomposite properties. At a filler loading level (1 wt%), zeolite enhanced glass transition temperature and decrease the water absorption of GPS/nano- ZnO nanocomposites in comparison to pure GPS. These bionanocomposites have potential applications in medical, agricultural, drug release, packaging, and UV-shielding materials.

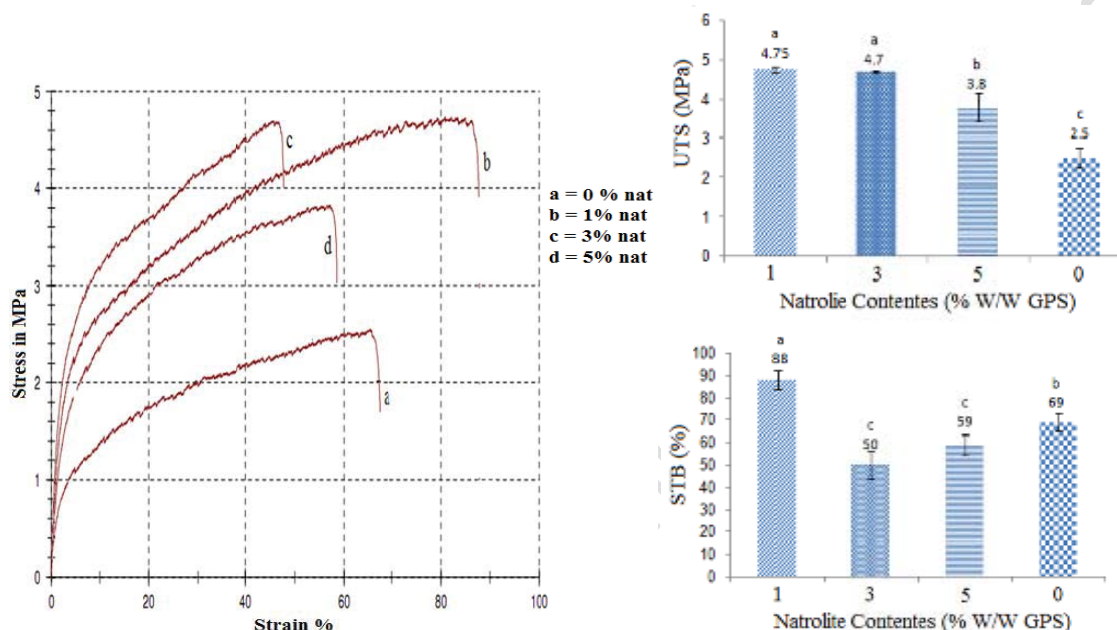


Figure 1: mechanical properties of GPS/Nat

Conclusion:

We can conclude that it is possible to use the zeolite in the polymer matrix even in reasonable quantities without loss of mechanical properties, an important fact is that we can incorporate molecules in zeolites, due to its ion exchange capacity and controlled release to prevent contamination of products which use packaging made of GPS.

References

- [1] L. Fama, et al., "Starch-vegetable fibre composites to protect food products", Carbohydrate Polymers, 75- 230- 2009.
- [2] X. Tang, et al., "Effects of plasticizers on the structure and properties of starch-clay nanocomposite films", Carbohydrate Polymers, 74, 552, 2008.



15th Physical Chemistry Conference



Effect of Kaolinite's clays on mechanical properties and dielectric constant of medium voltage insulating nanocomposites based on polyvinyl chloride (PVC)

^{*a}M. Gholipour, ^{b,c}A. Hassanzadeh

^{a,b} Department of chemistry, Faculty of science, Urmia University, Urmia, Iran

^cNanotechnology Research center of Urmia University, Urmia, Iran

Email: L.gholipour@yahoo.com

Key words: nanocomposites, nanoclays, medium voltage insulating, kaolinite

Introduction:

The field of nanotechnology is one of the most popular areas for current research and development in basically all technical disciplines. This would include microelectronics (which could now be referred to as nanoelectronics) as the critical dimension scale for modern devices is now below 100 nm. Nanocomposites are as multiphase materials, where one of the phases has nanoscale additives [1]. Although the potential use of polymer nanocomposites in electrical insulating industry has only recently begun to be searched, a great number of researches have been conducted with regards to high voltage electrical insulation performance [2]. The effects of fillers on the composite properties depend on their concentration the particle size and shape of the fillers, and their intercalation with the matrix [4]. The Kaolinite's Clay has 1:1 dioctahedral structure. In these polymer-clay nano composites can be achieved by the high surface content area of the reinforcing filler, which cause high strength, modulus, and improved thermal and barrier properties at a low clay loading level [3]. In this study, we synthesized insulator jackets nanocomposites with various relative compositions based on PVC and both natural and modified kaolinites (ZK₁ and DV) by solution intercalation method.

Materials and methods:

PVC powder, carbon black, Di-n-Octyl phthalate(Dnop plasticizer) and titanium dioxide are



industrial. Tetrahydrofuran Solvent, Stearic acid, Calcium Stearic, Zink stearat, Stearic acid and Sodium hydroxide (for syntetith of TiO_2), were supplied from Merck Chemical Co. Cetyltrimethylammonium bromide (CTAB) was obtained from Aldrich. Unlike DV nanoclay which has much more pollution, ZK_1 nanoclay is clean Kaolinite and almost pure. Nano clays are used as the supporting phase in this research and are modified by CTAB. At first, certain ratios of PVC powder and Dnop plasticizer were put in THF and mixed by magnetic mixer. Then, nanoparticles of TiO_2 was added to the given jelly solution and placed under the simple method of Ultrasonic radiation. After that, nanoclays which was put in oven in 80°C for 24 h were pour in container with some THF solution and put under ultrasonic in order to spread well its particles or atoms. Then, the above mentioned solution was added to the jelly solution and placed under ultrasonic. After 2 h mixture by magnetic mixer (for fully dispose of nanoclay atoms), it was pour in to mould and dried in room temperature. The gained product is called nano Composite Clay-Polymer. TiO_2 nanoparticles are provided according to the noted method in these references [3,2].

Result and discussion:

At 5 wt% content of nanofiller, the organic modifier increases the interaction between the nano patticles and PVC matrix which improves interfacial adhesion between particle and matrix. The decrease of the Elastic modulus may be caused by the poor interfacial adhesion between the PVC and filler phases as a result of the formation of some nanoparticle agglomerates at a higher degree of loading, leading to the retardation of crosslinks across the interfaces. The dielectric constant rises gradually with increasing the nanoclay loading in the composite. The dielectric constant of the composites with 4% nanoclay loaing reaches 4/5 at a frequency of 281.18 HZ, which is much larger than that of the pure PVC matrix [4,5].

Conclusion:

In this article, By means of intercalation of nanoclay with CTAB, the basal spacing of a natural nanoclays is expanded. because of the nanoscale silicate layers dispersed in the PVC and the stronger interactions between silicate layers and PVC, the Elastic Modulus of the



nanocomposites are greatly improved. The results reveal that the dielectric constants of the nano composites are slightly dependent on the frequency but increase rapidly with increasing nanoclay (kaolinite) loading in the composite.

Reference:

- [1] R.K. Gupta, S.N. Bhattacharya, Polymer-clay Nanocomposites: Current Status and Challenges, 50 (3) (2008) 242-267.
- [2] M. Pan, X. Shi, X. Li, H. Hu, L. Zhang, Applied Polymer Science 94, (2004) 277–286
- [3] D. Ray, S. Sengupta, S.P. Sengupta, A. K. Mohanty, M. Misra, Macromol. Mater. Eng. 291, (2006), 1513-1520
- [4] F. Pervin, Y. Zhou, M. A. Biswas, V. K. Rangari, S. Jeelani, Tuskegee, AL 36088, USA
- [5] Y. Yang, M. C, Gupta, K. L. Dudley, R. W. Lawrence, The fabrication and electrical properties of carbon nanofibre-polystyrene composites, Nanotechnology 15 (2004) 1545-1548



Decay resistance of Nano Zinc Oxide treated Cottonwood

A.Rezazadeh^{*a}, M.R.Mastri Farahani^a, A.Omidvar^a, A.A.Dejno Khalaji^b

^a Faculty of Forestry and Wood Technology, University of Agricultural Sciences and Natural Resources, Gorgan

^b Faculty of chemistry, Golestan university, Gorgan

Email: Amene_Rezazadeh@yahoo.com

Key words: White rot fungus, Brown rot fungus, Surfactant, Nano zinc oxide

Introduction:

Preparation of nanometer-size metal particles essentially increases the effective surface area of the metal in an evenly dispersed layer. If the particle size is smaller than the diameter of the wood window pit or the opening of the bordered pit, complete penetration and uniform distribution would be expected [1]. Secondly, nanometal preparations have a low viscosity. The addition of a surfactant can further increase dispersion stability by enabling liquid dispersion of higher concentrations of nanometals. Combined these properties present the potential for greater penetration and protection from more uniform particulate distribution over a wood surface [2]. In this research was used of nano zinc oxide suspension with along to polymeric surfactant of polyethylene glycol 400 and acrylic surfactant and Decay resistance of treated wood specimens with this material was investigated.

Methods:

The experimental samples were prepared from the sapwood of *Populus deltoides* with the dimension of 2×2×2 cm. To prepare suspension, nano zinc oxide powder 20 nanometer in three concentrations (0.5, 1, 1.5%) were added to beaker containing distilled water and PEG 400 (20%), Then with the speed of 40 rpm for 30 minutes were mixed by magnetic stirrer and after that, to break up agglomeration and better dispersion of nanoparticles, The suspensions were ultrasonicated for an hour. Mentioned stages for preparing suspensions with using of acrylic resin surfactant (8.4 % resin based on dry mass) were performed similarly. Then, wood

specimens impregnated with nano zinc oxide and decay resistance of all the samples were evaluated according to modified ASTM 1413 against white rot fungi of *Trametes versicolor* and brown rot fungi *Coniophora puteana* and calculated weight losses of samples.

Results and discussion:

According to results in table 1, the difference between weight loss due to decay of samples treated with nano zinc oxide with studied retention (2.61- 8.65 Kg/m³) and control was significant but no significant difference was observed between the weight losses of treated samples with increasing retention of nano zinc oxide in the presence of both surfactant. With increasing nano zinc oxide concentration, increased amount of retention.

Table 1: Average weight losses due to decay with tukey test at the confidence level of 95%

Grouping	Average weight loss	N	Retention (Kg/m ³)	Concentration (%)	Surfactant	Fungus
A	37.1	6	—	0	—	<i>T.versicolor</i>
B	25.2	6	—	0	—	<i>C.puteana</i>
C	8.8	6	2.85	0.5	Acrylic resin	<i>T.versicolor</i>
C	8.2	6	2.59	0.5	PEG 400	<i>T.versicolor</i>
C	6.2	6	2.93	0.5	Acrylic resin	<i>C.puteana</i>
C	6.1	6	2.63	0.5	PEG 400	<i>C.puteana</i>
C	4.4	6	5.49	1	PEG 400	<i>T.versicolor</i>
C	4.2	6	5.03	1	Acrylic resin	<i>T.versicolor</i>
C	3.8	6	5.40	1	PEG 400	<i>C.puteana</i>
C	3.6	6	5.25	1	Acrylic resin	<i>C.puteana</i>
C	3	6	8.52	1.5	PEG 400	<i>T.versicolor</i>
C	2.7	6	8.14	1.5	PEG 400	<i>C.puteana</i>
C	2.4	6	8.78	1.5	Acrylic resin	<i>T.versicolor</i>
C	1.9	6	8.02	1.5	Acrylic resin	<i>C.puteana</i>

Conclusion:

Treatment of wood specimens with nano zinc oxide was caused to improve decay resistance against studied white and brown rot fungi and low weight losses of all treated samples



compared with considerable weight losses of control samples indicated this subject although with increasing the percent of nano, decay resistance did not improve significantly. The use of two different types of surfactant had no significant effect on the weight loss of samples.

Reference:

- [1] M.H.Freeman and C.R.McIntyre; "Comprehensive review of copper-based wood preservatives"; Forest Product Journal; 58,11,6-27,2008.
- [2] S.N.kartal and etal; "Do the unique properties of nano metals affect leachability or efficacy against fungi&termites?"; International Biodeterioration&Biodegradation; 1-6,2009.



The Effect of Some Parameters on Photocatalytic Activity of TiO₂/M Nano Composite

Hossein Ghasemi Mobtaker^{a,b*}, Shahram Moradi Dehaghi^a, Seyed Javad Ahmadi^b

^aFaculty of Chemistry, Tehran North Branch, Islamic Azad University, Tehran-Iran

^bNSTRI, Jaber Ibn Hayan Research Laboratory, Tehran, Iran

E-mail: hosein_g@yahoo.com

Key words: TiO₂, Metal Ion Doped, Sol-Gel, Photocatalyst

Introduction:

Increasing the organic pollutants release to environment and presence of the synthetic and non-biodegradable compounds such as triazine-containing azo dyes in textile effluents are of environmental concern. Photocatalysis, because of its destructivity, low cost, milder condition, easy controllability, no-twin pollution and chemical stability appears as an efficient pollution control technology [1].

TiO₂/UV system has been considered extensively in photocatalytic processes. However, the poor quantum yield results from rapid electrons/holes recombination is a problem which restrict its widespread practical use [2]. To increase the photocatalytic efficiency of the catalyst, its surface can be modified with noble metals, such as Au, Pd, Ag, and Pt [3]. In this work, we investigated the doping effect of some transition metals and a lanthanide on photocatalytic activity of TiO₂. Acidity of the solution has also significant effect on degradation rate of organic compound and it is studied here.

Method and Material:

Metal ion doped TiO₂ was synthesized by sol-gel method and its photocatalytic activity was tested for degradation of methylorange under UV light irradiation. Ions used as dopant were Ag⁺, Cu²⁺, Ni²⁺, and Nd³⁺. The synthesized catalysts were characterized using XRD, TEM, XRF and BET. Crystal sizes for TiO₂ and Nd-doped TiO₂ were calculated about 45 and 35 nm

respectively, using Sherrer equation. Degradation process lead to final decomposition of methylorange was confirmed by UV-Visible spectrometry and LC-MS.

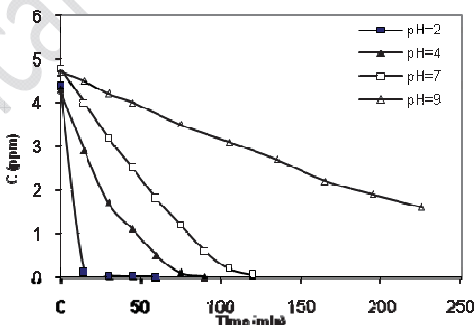
Result and discussion:

The XRD patterns show that the major part of the catalysts are anatase phase, and it contains minor phases rutile. By increasing the calcination temperature, the crystallinity of the sample decreased and some amorphous phase emerged in the matrix which caused to lower activity of the catalyst. TEM image of the Nd doped catalyst showed that the particle size distribution is in wide range, but all particles are smaller than about 50 nm. Surface area for catalysts were in 150 m²/g range. Doping with metal ions increases the activity significantly. Investigating the photocatalytic activity of doped catalysts in the same condition of concentration and pH, resulted as below



LC MS analysis showed that before degradation only the methylorange is present in the solution. After about 100 minutes the methylorange and some intermediate products are present.

Decreasing the solution pH led to increas in catalyst activity (as below)



Conclusion:

Increasing the calcinations temperature led to decrease in crystallinty of the catalyst and so decreasing the activity. Nd doped TiO₂ showed the best results so it was chosen to compare photocatalytic activity with undoped TiO₂. Decreasing the pH of the media leads to decreasing the degradation time considerably, but in alkaline media the activity was decreased.



LC-MS analysis of the solution showed fragmented species before complete degradation and confirmed complete decomposition of methyloange at the end of the process. First-order reaction kinetic was tested for degradation process and the result showed approximate accordance.

References:

- [1] Rui, X., Jia, L, Jun W., Xiaofang W., BinLiu B. W., Xiaoyu L., Xiangdong Z., Sol. Energ. Mat. Sol. C., Vol 94, pp1157–1165, 2010.
- [2] Ioannis K. K., Triantafyllos A. A., , App. Catal. B: Environ., Vol. 49, pp1–14, 2004.
- [3] Xie B., Xiong Y. R., Chen J., Chen P. C., , Catal. Commun., Vol.6, pp 699–704, 2005



[Cu(bpdo)₂.2H₂O]²⁺-supported SBA-15 nanocatalyst catalyzed synthesis of benzoxanthenone and 2-amino-chromene derivatives efficiently

R. Malakooti^a, Z. Parsaei^a, H. A. Oskooie^b, M.M.Heravi^b, M. Saeedi^b, M. Amrollah^b, A. Fallah^b

¹Nanochemistry Research Laboratory, Department of Chemistry, University of Birjand, Birjand, Iran

²Department of Chemistry, School of Sciences, Alzahra University, Vanak, Tehran, Iran

Email address: reihaneh.malakooti@gmail.com

Keywords: [Cu(bpdo)₂.2H₂O]²⁺/SBA-15, Benzoxanthenones, 2-Amino-chromenes, Solvent-free conditions, Nanocatalyst

Introduction:

Xanthenone derivatives have attracted considerable interest because they possess various pharmaceutical activities such as anti-bacterial [1], anti-inflammatory [2] and anti-viral [3]. Also 2-amino-4H-chromene derivatives are important classes of oxygenated heterocycles [4], which have attracted much interest because of the biological activities such as anticoagulant, spasmolytic, diuretic, anti-anaphylactin, anticancer, and antidiabetic activities [5].

Accordingly in continuation of our previous works on synthesis of heterogeneous catalysts and benzoxanthenone and benzopyran compounds, here we want to report the synthesis and characterization of [Cu(bpdo)₂.2H₂O]²⁺ / SBA-15 used as catalyst for the synthesis of benzoxanthenone and 2-amino-chromene derivatives by reaction of aromatic aldehydes, α/β -naphthol, dimedone or malononitrile respectively under solvent-free conditions with high yield of products moreover a simple experimental and work-up procedure without using any hazardous solvents.

Materials:

All materials were purchased from Merck and were used without further purification.



Immobilization of $[\text{Cu}(\text{bpdo})_2 \cdot 2\text{H}_2\text{O}]^{2+}$ complex within SBA-15:

0.068 gr (0.3988 mmol) of $\text{CuCl}_2 \cdot 2\text{H}_2\text{O}$ and 0.15 gr (0.7978 mmol) bpdo were solved in 10 ml of deionized water. The solution was heated at 70 °C for 2 h. Then 1 g of SBA-15 which was dried overnight under vacuum at 150 °C, was added to the solution of $[\text{Cu}(\text{bpdo})_2 \cdot 2\text{H}_2\text{O}]^{2+}$. The resultant mixture was stirred for 24 h at room temperature and then filtered. Finally the light green precipitate was washed with deionized water and dried at room temperature.

Results and Discussion:

XRD patterns of SBA-15 (Fig. 1a) shows three peaks corresponding to (100), (110) and (200) planes which are adopted with typical two-dimensional hexagonal symmetry. After grafting of the cationic complex, $[\text{Cu}(\text{bpdo})_2 \cdot 2\text{H}_2\text{O}]^{2+}$, on the surfaces of SBA-15, Figs. (1b), hexagonal symmetry are still remained. Also relative decreases are observed between the XRD intensities of the parent mesoporous and grafted samples which are originated from the complex immobilization.

Conclusion:

In conclusion, a new heterogeneous catalyst based on the cationic copper (II) complex supported with SBA-15 is proposed and its efficiency was investigated in synthesis of benzoxanthenone and 2-amino-chromene derivatives. This procedure offers several advantages such as cleaner reaction, high yields. Moreover, any hazardous solvents have not been used for these reactions.

Reference:

- [1] T. Hideu, Jpn. Tokkyo Koho JP 56005480 (1981).
- [2] H.N. Hafez, M.I. Hegab, I.S. Ahmed-Farag, A.B.A. El-Gazzar, Bioorg. Med. Chem. Lett. 18 (2008) 4538-4543
- [3] J.P. Poupelin, G. Saint-Ruf, O. Foussard, G. Narcisse, G. Uchida-Ernouf, R. Lacroix, Eur. J. Med. Chem. 13 (1978) 67-71.
- [4] Hepworth, J. D.; Gabbutt, C. D. B. M., Pergamon Press, Oxford, **1995**, 5, 301–468.
- [5] Koga, H.; Sato, H.; Ishizawa, T.; Nabata, H., US Patent 5614633, **1997**.



Preparation of polystyrene-ZnO nanocomposite via solution mixing and investigation its antibacterial property

n. dabagh^a ; B. jaleh^a ; s. azizian^b

^a Department of Physics, Faculty of sciences, Bu-Ali Sina University, Hamedan, Iran

^b Department of chemistry, Faculty of sciences, Bu-Ali Sina University, Hamedan, Iran

Email: n.dabagh@ymail.com

Key words: Zinc Oxide, Polystyrene, Nanocomposite, Antibacterial.

Introduction:

In the last few decades, much attention has been paid to preparation of organic/nanometer-sized inorganic particles nanocomposites due to their attractive mechanical, thermal, optical, electrical, magnetic properties, and potential application in the areas of plastics and rubber reinforcement, coatings, electronics, catalysis, and diagnostics. Nano-ZnO, as one of the multifunctional inorganic nanoparticles, is not only an important semiconductor material but also serves widely as catalyst for chemical reactions, photocatalysts, photoelectric conversion, antibacterial and bactericide, UV-shielding material, and photoluminescent materials. Metal oxides such as MgO, CaO, and ZnO possess antibacterial activity against some bacteria strains such as *S. aureus* and *E. coli*. ZnO nanoparticle exhibited significant antifungal properties against *Staphylococcus aureus* and *Pseudomonas aeruginosa*. The use of inorganic antibacterial agents in nonfood applications has attracted interest for the control of microbes. This study investigate the antimicrobial activity of different amounts of zinc oxides against *Aspergillus* sp. [1-5].

Materials and methods:

Polystyrene (PS, Pars Petrochemical Company, Iran) granules were first dissolved in toluene to obtain the PS solution. The Zinc oxide (ZnO, mean diameter 30nm) nanoparticles were dispersed into ethanol in an ultrasonic stirrer and then directly added into the PS solution. The



mixture was subsequently stirred. The solution mixtures were then cast into glass Petri dishes and the solvents were evaporated at room temperature. The PS-ZnO nanocomposite films were obtained with weight ratios PS:ZnO of 3:1, 4:1 and 5:1.

Apparatus:

To study the structural changes including the alteration in position and intensity of the characteristic bands Fourier transform infrared (Shimadzu FTIR spectrophotometer 8300) over the range 400- 4000 cm^{-1} was used.

Result and discussion:

To evaluate the interface affinity between PS and ZnO FTIR measurements were carried out. There is no interaction between PS and ZnO nanoparticles in the resulting composites. The antibacterial test of the prepared nanocomposite films and PS film was performed and *Aspergillus* sp. was employed in this section. The antibacterial rate of nanocomposite coatings increased with the increasing amount of ZnO nanoparticles. The generation of hydrogen peroxide by this substance after activation might be a main factor for the antimicrobial activity. While the binding of the particles on the bacteria surface due to the electrostatic forces could be one of the mechanisms of action. This study suggested that the application of PS-ZnO nanocomposite in food systems may be effective at inhibiting certain pathogens.

Conclusion:

In this work we have presented a facile method for the fabrication of PS-ZnO nanocomposite film. The ZnO amount affected the antibacterial activity of nanocomposites, whereas increasing the ZnO concentration into the nanocomposites resulted in more bacterial inhibition. This is a preliminary study that provides a starting point to determine whether the use of PS-ZnO nanocomposite has a potential in food safety.

References



- [1]E .Tang;"Preparation of styrene polymer/ZnO nanocomposite latex via miniemulsion polymerization and its antibacterial property";Colloid PolymSci; 287:1025-1032, 2009.
- [2]T.Phaechamud;"Antimicrobial activity of ZnO-doxycycline hydrogel"; ScienceAsia; 38, 64-74, 2012.
- [3]H.Kaczmarek; "Studies of photochemical transformations in polystyrene and styrene-maleic anhydride copolymer" ;Polymer Degradation and Stability; 93, 1259-1266, 2008.



Lanthanum oxide as a dielectric for the future of CMIS devices

V. Hayati, A. Bahari, A. Ramzannezhad

Department of physics, University of Mazandaran, Babolsar, Iran

E-mail: v.hayati@stu.umz.ac.ir, a.bahari@umz.ac.ir

Keywords: Nanostructures, La_2O_3 , AFM, SEM.

Introduction:

Various conditions for synthesis of pure nanoparticles have been studied, at relatively low temperatures in air atmospheres. In this way some unwanted – bonds have been created on the crystallite surface which can affect on nanostructural properties. Therefore, it is imperative production of nanotransistor devices without tunneling and leakage currents for growing of so clean and pure ultra thin films. The band gap and dielectric constant of La_2O_3 is 5.5 eV and 30 respectively [1]. La_2O_3 does not cause the degradation of dielectric constant due to its higher dielectric constant SiO_2 or Al_2O_3 . In this work we were synthesized La_2O_3 via sol-gel method.

Materials and method:

The synthesis of La_2O_3 is carried out as follows: 0.273 g of hexadecyltrimethyl ammonium bromide (CTAB) was dissolved in 30mL distilled water under stirring at room temperature. Then 0.586 g ($\text{LaCl}_3 \cdot 6\text{H}_2\text{O}$) was added. Also 0.1-0.6mL of 25% ammonia was added drop-wise to the above solution to adjust the pH value from 6-10. Along with the addition of ammonia, the solution was turned translucent colloidal right now. After 2h stirring, the system is transferred into a Teflon lined stainless steel autoclave, sealed and maintained at 80°C for 24h. The resultant white solid product was centrifuged, washed with distilled water and ethanol to remove the probable remaining ions in the final product and finally dried at 60°C .

Result and discussion:

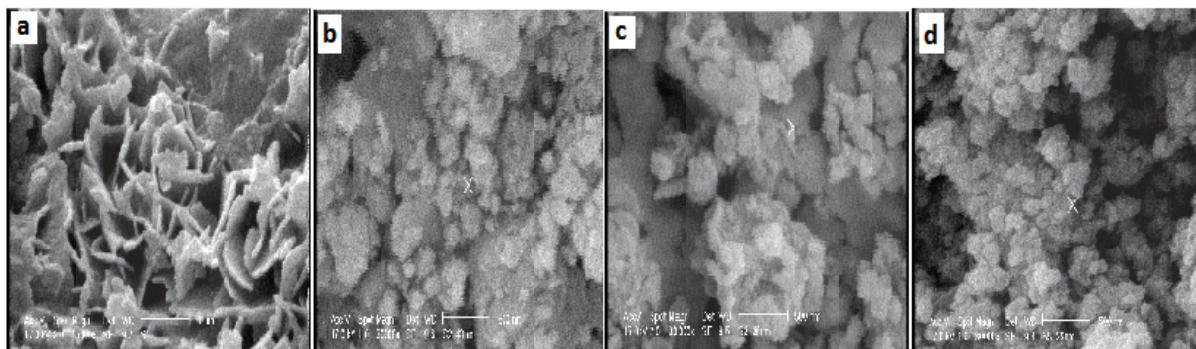


Figure 1: SEM images of the La_2O_3 films at (a) room temperature, (b) 300, (c) 600 and (d) 800°C.

The SEM images of the films show that some particles are agglomerated into clusters (Figure 1). These images reveal an amorphous or quasi amorphous structure [2] at low temperatures but it leads to crystallization structure at 300°C. The primary particles are 50-100nm in size.

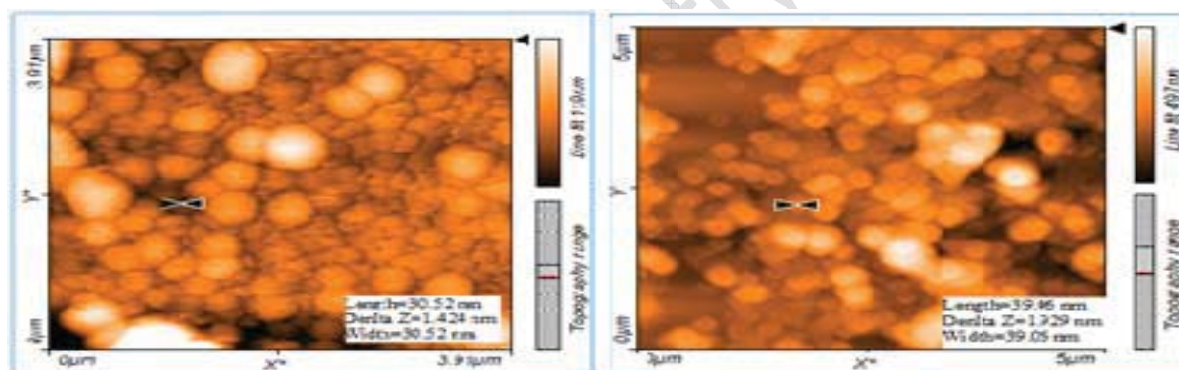


Figure 2: AFM topography images (2-D) of La_2O_3 films with different magnifications.

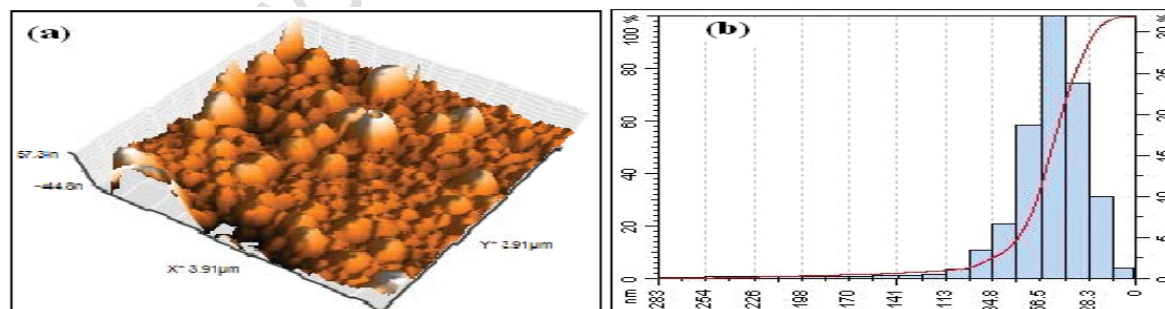


Figure 3: (a) AFM image (3-D) of the film and (b) diagram of height distribution of nanoparticles

The surface morphology of the La_2O_3 films (Figure 2) shows that uniform structure was formed at 700°C but crystalline structure was obtained at 600-800°C. The films have a dense



and fine amorphous structure at 300⁰C which makes a suitable candidate for the next CMIS (Complementary Metal-Insulator-Semiconductor) devices. These images show that films present a nano-porous morphology. The root mean square roughness of the films increased (see Figures 2 and 3). The rough surface which is usually seen at >700⁰C indicate the crystallization of induced large grain size can affect on evolution of the samples morphology. The pores distribution is also uniform and the size of the pores in the range of 20-40 nm.

Conclusion:

The obtained results exhibit a significant increase of the amorphous structures and indicate nano La₂O₃ can be used as a good insulator material to reduce leakage and tunneling currents.

References:

- [1] A Q. C. Zhang, N. Wu, C. X. Zhu, "Jpn. J. Appl. Phys.", 43 ,L1208, 2004.
- [2] A. Bahari, Z.S.Li and P. Morgen, "Surf. Sci", 600, 2966, 2006.



Sol-Gel Synthesis and Investigation of (La, Sr) CoO₃ (LSCO) Thin Films

V. Hayati¹, A. Bahari¹, A. Ramzannezhad¹, M. Ghanbari², K. Taghavi¹

¹Department of Physics, University of Mazandaran, Babolsar, Iran

²Department of Physics, Islamic Azad University, Central Tehran Branch, Iran

E-mail: v.hayati@stu.umz.ac.ir, a.bahari@umz.ac.ir

Keywords: Nano transistor, Sol-gel method, LSCO, XRD, FTIR

Introduction:

It is reported that SiO₂ thinner than 1 nm may not have the insulating properties required of a gate dielectric. It is mostly interface, with little if any bulk character [1, 2]. A shrinking of this thickness down to less than 1 nm for the next generation will lead to a couple of orders of magnitude increase in tunnelling as well as leakage currents. A very obvious alternative material is La₂O₃, due to its high dielectric constant, wide band gap and good thermal stability on silicon substrate. We have thus synthesized LSCO and studied its nanostructural properties by using XRD and FTIR techniques.

Materials and methods:

In this work we used sol-gel method for LSCO synthesis: Cobalt acetate was dissolved in acetic acid at 80°C for 20 min. As solution was stirred, strontium acetate was added. On the other container, lanthanum isopropoxide was dissolved in 2-methoxyethanol and stirred at 80°C for 20 min. The molar ratios of La: Sr: Co were 1:1:2, 2:1:1 and 1:2:1 in three different process. The latter solution was mixed with first and was stirred at 50°C for another 30 min. The silicon wafers were rinsed with ethanol to remove the SiO₂ surface layer. Then, the films were deposited by dip-coating using a withdrawal rate of 5 cm.min⁻¹. Afterward were dried at room temperature overnight, densified for 10 min at 100°C followed by a further densification at low temperature (300°C) or at higher temperature (500°C and up) for 30 min.

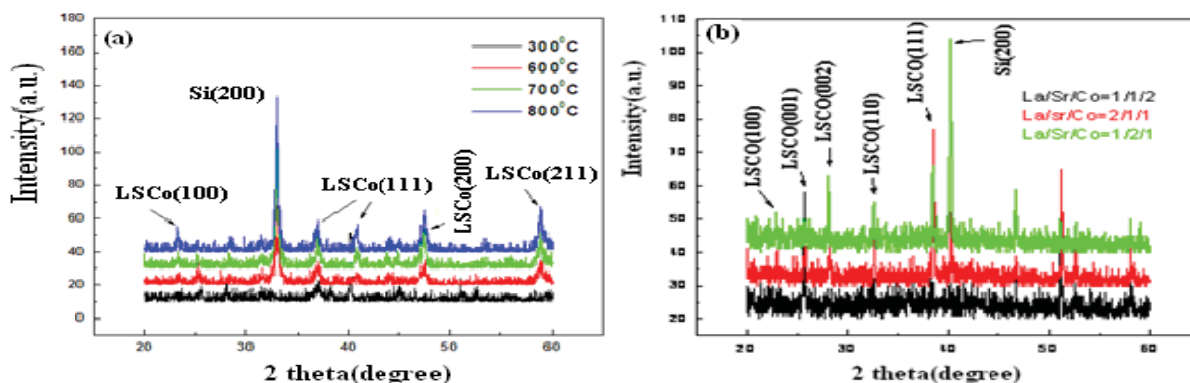


Figure 1: XRD patterns of LSCO (a): at different temperatures (La: Sr: Co = 2:1:1) and (b): at the same temperatures and different contents.

Result and discussion:

The samples structure is quite amorphous at room temperature whilst it led to crystallization structure at 300°C (Figure 1a). XRD patterns relevant to samples annealed at 300-800°C show relative growing of the peaks. These issues indicate the nanoparticles size increased. Figure 1b shows that relatively small variation of La:Sr:Co molar ratio can change structure of films.

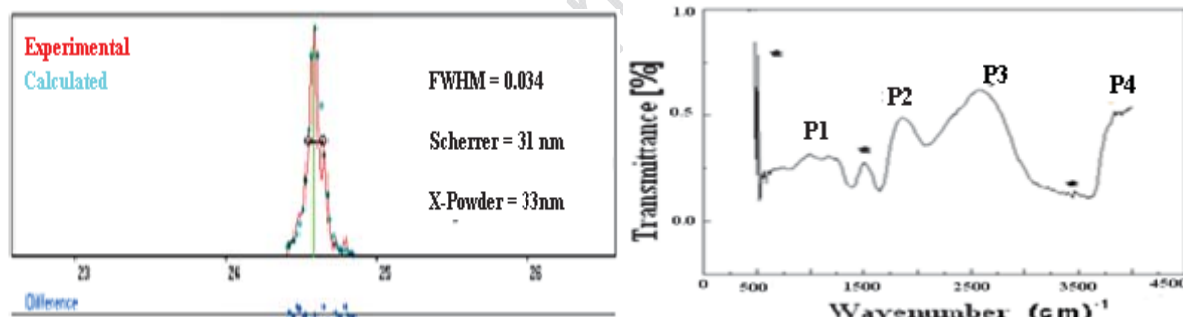


Figure 2: (Left): the size of 33 nm determined with X-powder method and (Right): FTIR spectrum of LSCO at room temperature.

In figure 2 (Left), the size of LSCO nanoparticles is estimated by using X-powder method (based on Debye-Scherrer equation: $\Gamma = \frac{K \lambda}{\beta \cos \theta}$). In figure 2(Right), the band at 3200 cm⁻¹ are assigned to hydroxyl groups (La-OH) and to O-H from water and ethanol. The O-H bending band of water in the gel is observed at 1650 cm⁻¹ and the low energy interval the La-O bond bands are found at 1061 and below 1000 cm⁻¹. This spectrum shows peaks characteristic of O-



H at the surface (3225 cm^{-1}), molecular water (1621 cm^{-1}) and La-O ($653\text{--}550\text{ cm}^{-1}$). The absorption peak at 1090 and 1010 cm^{-1} indicate the La-O-Co-Sr linkage in the powder form.

Conclusion:

In dye-sensitized solar cells, functionalization of LSCO thin films with siloxane adsorbates has been shown to be useful as a surface passivation technique that hinders the recombination processes and improves the overall efficiency of light to-electricity conversion. These results clearly demonstrate that LSCO has the potential to be succeeded as a good gate dielectric material for the future of nano transistors.

References:

- [1] A. Bahari, U. Robenhagen, P. Morgen, Z. Li, "Growth of ultrathin silicon nitride on Si (111) at low temperature", Phys. Rev, 72, 205323, 2005.
- [2] J. Hernandez, A. Mendoza – Galvan, "Formation of NiO – SiO₂ nano composite thin films by the sol – gel method", J. Nan crystalline solids, 351, 2029, 2005.

Nanotube as an Anti-HIV Deliverer?

N. Dalili Mansour^{1,*}, S. Ghorbaninezhad¹

¹Department of Chemistry, Islamic Azad University, Rasht Branch, Rasht, Iran

Email: dalili@iaurasht.ac.ir

Keywords: Nanotube, DFT, Drug Delivery, HIV.

Introduction:

One of the efficient inhibitors that have anti-HIV properties is Ganciclovir. Ganciclovir is a synthetic purine nucleoside analogue of guanine. It is structurally and pharmacologically similar to Acyclovir and is active against herpes virus [1]. To prevent drug's side effects in use, in this work the interactions between Nanotubes and these anti-HIV drugs are investigated to show if the Nanotubes are safe to deliver these drug.

Computational method:

All of calculations were performed by a personal computer which has Intel (R) core (TM) 2 quad CPU 8400 with 4GB RAM. Geometry optimization of Nanotube (6,6) with 84 atoms and acyclovir and Ganciclovir were performed with Gaussian 03 program package [2] at DFT level of theory, the B3LYP hybrid functional [3], using the standard 6-31G(d) basis set, separately. Then 8 Complexes were formed:

- Complex 1 & 3 (between Nanotube and acyclovir analogs by forming one C-N_{1,3} bond).
- Complex 2 & 4 (between Nanotube and acyclovir analogs by forming one C-S_{2,4} bond).
- Complex 5 & 7 (between Nanotube and Ganciclovir analogs by forming one C-N_{5,7} bond).
- Complex 6 & 8 (between Nanotube and Ganciclovir analogs by forming one C-S_{6,8} bond).

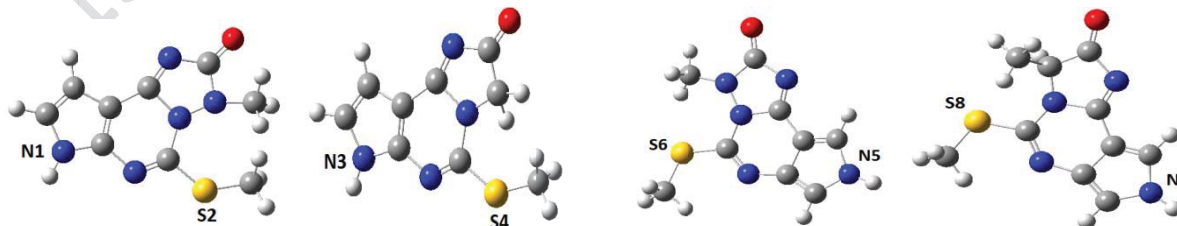


Fig. 1. Acyclovir

Fig. 2. Acyclovir analog

Fig. 3. Ganciclovir

Fig. 4. Ganciclovir analog

The formed complexes were optimized by the same method and then frequency studies and NBO analysis (Natural Bond Orbital) have been also performed [4]. For optimized complexes, bond lengths, bond angles, hybrid of atoms, occupancy and Mulliken charges were calculated.

Results and discussion:

In this work, NBO analysis was performed by B3LYP/6-31G(d) method. The results show that hyperconjugative effects can occur by donor – acceptor interactions between lone pairs of oxygen or nitrogen atom of drug as donor and σ^* or π^* orbitals of carbon of nanotube. The amount of the second-order perturbation energy for complex 7 is the highest and for complex 2 is the lowest. It becomes obvious that the complexes in which N atom formed the bond, have higher hyperconjugation energy than the complexes in which S atom form the bond. Also the results show by increasing P share in hybrid of atoms, the occupancy decreases. Note that the occupancy of LP(2) of Sulfur atom is lower than LP (1) and it shows that the p share in hybrid of LP(2) is higher. In this paper, Thermodynamic functions were calculated by frequency investigation, too. The Energy, Enthalpy, Entropy and Gibbs free energy were estimated for each complex. The results are shown in table 1. The results show that the formation reactions of complexes 4, 7 and 8 are endothermic. For the remaining complexes, the enthalpy is an assistant factor for the formation of them. In all reactions the entropy becomes less. So the entropies of all reactions are thermodynamically unfavorable factors. The obtained formation ΔG^0 of complexes 2,3,4,7 and 8 becomes positive in 298K. This indicates that these complexes could not be formed according to the second law of thermodynamics.

Agent	$\Delta G/\text{kcalmol}^{-1}$	Stability constant	Agent	$\Delta G/\text{kcalmol}^{-1}$	Stability constant
Complex1	-1.79531	1.0030	Complex5	-24656.0332	1.2082×10^{18}
Complex2	0.3985	-	Complex6	-24661.5239	1.219×10^{18}
Complex3	16.6146	-	Complex7	4934.1842	-
Complex4	9.6097	-	Complex8	24669.6533	-

Table 1. thermodynamic functions



Conclusion:

- 1- The complexes 1,5 and 6 could be formed in 298K.
- 2- There is hyperconjugative effect in all complexes between lone pairs of oxygen or nitrogen atom of drug as donor and σ^* or π^* orbitals of carbon of nanotube .
- 3- The entropies of all reactions play an unfavorable role according to the second law of thermodynamics.
- 4- The formation reactions of complexes 4,7 and 8 are endothermic.

References:

- [1] Deng H, Liu R, Ellmeier W, Choe S, Unutmaz D, Burkhart M, et al. *Nature*. 1996;381(6584):661-6.
- [2] M.J.Frigh,et al.,Gaussian 03, Revision C, 02, Gaussian Inc., Wallingford ,CT,2004.
- [3] A.D.Becke.J .chem .phy. 98 (1993)1372- 1377.
- [4] K.Kim and K.D.Jordan. J. Phy. Chem. 98(40) (1994) 10089-10094.



Investigation of Interaction between Nanotubes and Anti-Cancer Drugs

N. Dalili Mansour^{1,*}, H. Kefayati¹, F. Mahboubi¹

¹Department of Chemistry, Islamic Azad University, Rasht Branch, Rasht, Iran

* dalili@iaurasht.ac.ir

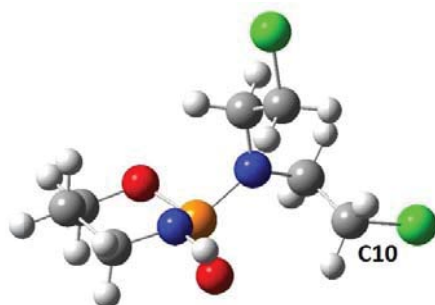
Keywords: Nanotube, Cyclozan, Ifosfamide, DFT, NBO.

Introduction:

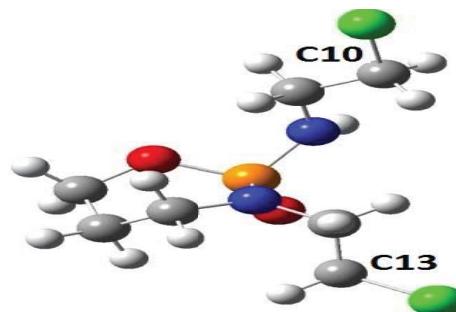
Cyclozan is used to treat various types of cancer and some autoimmune disorders. It is a "prodrug"; it is converted in the liver to active forms that have chemotherapeutic activity. The main use of Cyclozan is together with other chemotherapy agents in the treatment of lymphomas, some forms of brain cancer, leukemia and some solid tumors. It is a chemotherapy drug that works by slowing or stopping cell growth. Ifosfamide, like Cyclozan, is an oxazophosphorine alkylating agent. Following activation in the liver, ifosfamide interferes with DNA through formation of phosphotriesters and DNA-DNA crosslinks, thereby inhibiting protein synthesis and DNA synthesis. In this work the interaction between Nanotubes and these anti-CANCER drug is investigated to show if the Nanotubes are safe to deliver this drug.

Computational method:

All of calculations were performed with a personal computer which has Intel (R) core (TM) 2 quad CPU 8400 with 4GB RAM. A Nanotube (6,6) with 84 atoms are selected which react with these two drugs that including Cyclozan and Ifosfamide. Nanotube is formed by Nanotube Modeler package. The DFT Calculations have been performed using the Gaussview and Gaussian 03 by B3LYP method and 6-31G(d) standard basis set. Then complexes between Nanotube and drugs are formed and optimized by B3LYP/6-31G(d) method. The natural bond orbital (NBO) analysis and frequency calculations have been also performed for all structures using B3LYP method and the standard 6-31G(d) basis set.



Cycloxan



Ifosfamide

Results and discussion:

The obtained results show that hyperconjugative effects can occur by donor – acceptor interactions between lone pairs of oxygen or nitrogen atom in the drug as donor and σ^* or π^* orbitals of carbon in nanotube. These second – order perturbation energy can be shown by E^2 Term. In this paper, Thermodynamic functions were calculated by frequency investigation. The Energy, Enthalpy, Entropy and Gibbs free energy were estimated for each complex. These results show that all of these reactions are endothermic and in all of them, the entropy decreases. So the enthalpies and the entropies of reactions are thermodynamically unfavorable factors in the review. The obtained formation ΔG^0 of All complexes becomes positive in 298K. This indicates that these complexes could not be formed according to the second law of thermodynamics.

Conclusion:

1. In the formation reactions of all Complexes, entropies and enthalpies are thermodynamically unfavorable factors in the review.
2. ΔG^0 of formation of All complexes are positive. So in the follow of second law of Thermodynamics, these three reactions could not occur.
3. All of the reactions are endothermic reactions.
4. NBO analysis shows high hyperconjugations in all compounds.
5. By increasing p share in hybrid, the occupancy decreases.



References:

- [1] Rappeneau S, Baeza-Squiban A, Jeulin C, Marano F (March 2000).
- [2] Takimoto CH, Calvo E. "Principles of Oncologic Pharmacotherapy" in Pazdur R, Wagman LD, Camphausen KA, Hoskins WJ (Eds) Cancer Management: A Multidisciplinary Approach. 11 ed. 2008.
- [3] Shanafelt TD, Lin T, Geyer SM, et al. (June 2007). "Pentostatin, Cyclophosphamide, and rituximab regimen in older patients with chronic lymphocytic leukemia". Cancer 109 (11).



A study on synthesis of magnetic iron oxide core / ZnS shell nanoparticles

M. Keshavarz, V. Vosoughi*, Z. Ghasemi

Department of chemistry, Islamic Azad University Shahreza Branch, P.O. Box311-86145

Email: vida.vosoughi@gmail.com

Key words: nanoparticles, Fe₂O₃, ZnS, core/ shell

Introduction:

In the past decade or so, core/shell structured nanoparticles have been receiving growing research attention, due to their enhanced or combined optical, electronic, and magnetic properties compared to the single-component nanomaterials. Interests in nanocomposites of this kind originate not only from the curiosities of scientists who are exploring the mesoscopic world, but also from the ever increasing demands placed on materials synthesis performance by nanotechnology. Although much progress has been made in syntheses of core/shell nanoparticles[1,2]. In a recent report, we described the synthesis of magnetic nanoparticles iron oxide/ZnS core-shell nanoparticles. Scan electron microscopy (SEM) and Transmission electron microscopy (TEM) shows whether particles of ZnS character contains a magnetic core or not.

Materials and methods:

The reagents used for chemical synthesis γ - Fe₂O₃ nanoparticles and ZnS nanoparticles FeCl₃.6H₂O, FeSO₄.7H₂O, urea, NaOH, ZnCl₂, Na₂S are prepared by using double distilled water. The wet chemical synthesis of γ - Fe₂O₃ nanoparticles was based on hydrolysis of Fe³⁺ and Fe²⁺ salt in the presence of urea and NaOH with the following ultrasonic treatment of FeO(OH)/ Fe(OH)₂ in the sealed flask at 30°C_35°C for 10 min_30 min in order to enhance interaction between the hydrolysis products. After aging for 5h the obtained black powder was washed and dried. The calcination of the prepared Fe₃O₄ powder in air temperature 180°C_210°C led to formation of γ - Fe₂O₃ nanoparticles. The surface modification of magnetic nanoparticles (MNPs) was carried out by the reaction of NPs with sodium citrate. The mixture

was kept under ultrasonic, then stirred for 12h at temperature of 60°C under Ar protection. The precipitate washed with acetone for several time. For synthesis of ZnS nanoparticles Mercaptoethanol is used as the capping agent. A three neck reaction flask is used as reaction chamber and reaction take placed under N₂ inert gas to prevent any oxidation effect while reaction is going on. For synthesis of Fe₂O₃/ZnS core/shell MNPs, the sodium citrate modified Fe₂O₃ MNPs were re-dispersed in 100 ml deionized water and was kept under ultrasonic for 30 min, then some of former solution was added into a three-neck flask and the coating experiment was conducted according to the process product of ZnS nanoparticles.

Results and discussion

The SEM photographs of sodium citrate modified Fe₂O₃ nanoparticles coated by ZnS nanoparticles are shown in Fig.1. The SEM and TEM photographs are illustrated that the Fe₂O₃/ZnS core/shell MNPs was <100 nm. This can be explained by the fact sodium citrate modified Fe₂O₃ MNPs have smaller particle size and better dispersibility, which provided the Fe₂O₃ MNPs with larger specific surface area and surface energy.

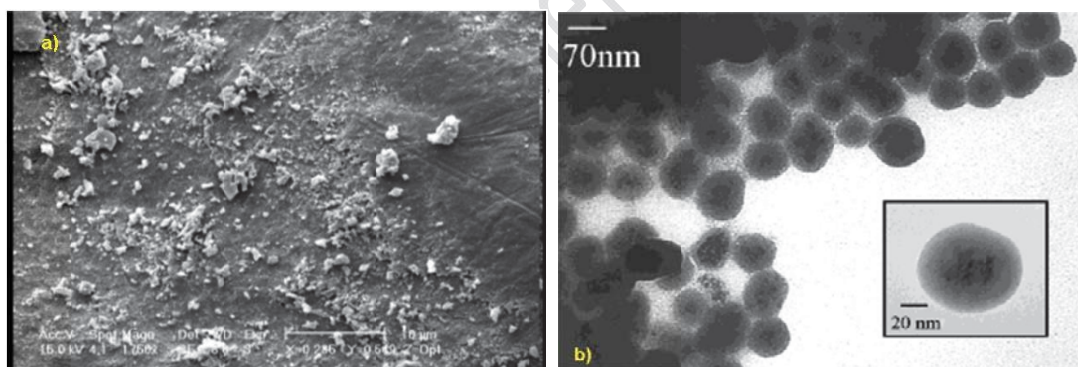


Fig.1: a) SEM image of sodium citrate modified Fe₂O₃ nanoparticles coated by ZnS nanoparticles and b) TEM image of Fe₂O₃/ZnS core/shell.

Reference:

- [1] N. Sounderya et al; “use of core/shell structured nanoparticles for biomedical applications”; Recent Patents on Biomedical Engineering; 1, 34- 42, 2008.
- [2] B. Bhattacharjee et al; “Colloidall CdSe-ZnS core-shell nanoparticles: Dependence of physical properties on initial Cd to Se concentration”; Physica E 33, 388-393, 2006.



15th Physical Chemistry Conference



Investigation Thermodynamic Function of Complexes between Nanotubes and Anti- HIV Drugs: A Theoretical Approach

S. ghorbaninezhad*^a, N. Dalili Mansour^b

^{a, b}Department of Chemistry, Islamic Azad University, Rasht Branch, Rasht, Iran

E-mail: saiedeh_ghorbany@yahoo.com

Keywords: Nanotube, Thermodynamic Functions, DFT, HIV.

Introduction:

Acquired immunodeficiency syndrome (AIDS) is the most challenging pandemic of the 21st century [1]. One of the efficient inhibitors that has anti-HIV properties, is ganciclovir. Ganciclovir is a synthetic purine nucleoside analogue of guanine. It is structurally and pharmacologically similar to acyclovir and is active against herpes virus [2]. To prevent of drug's side effects in use, in this work the interaction between Nanotubes and this anti-HIV drug is investigated to show if the Nanotubes are safe to deliver this drug.

Materials and methods:

All of the calculation were performed with a personal computer which has Intel (R) core (TM) 2 quad CPU 8400 with 4GB RAM. Geometry optimization of Nanotube (6,6) with 84 atoms and acyclovir and Ganciclovir were performed with Gaussian 03 program package [3] at DFT level of theory, the B3LYP hybrid functional [4-6], using the standard 6-31G(d) basis set. Then 8 Complexes were formed, Complex 1, 3, 5, 7 (between Nanotube and drugs by forming one C-N bond) and Complex 2, 4, 6, 8 (between Nanotube and drugs by forming one C-S bond).

Result and discussion:

NBO analysis was performed by B3LYP/6-31G (d) method. In this work, These second – order perturbation energy can be shown by ΣE^2 Term in table 1, 2. The amount of these



energies causes the stability of these complexes. In this work, The Energy, Enthalpy, Entropy and Gibbs free energy were estimated for each complex. The results are shown in table 1, 2. These results show that all of these reactions are not exothermic but in all of them, the entropy decreases. The obtained formation ΔG^0 of complex 2, 3,4,6,7, and 8 becomes positive in 298K. This indicates that these complexes could not be formed according to thermodynamic laws.

Table1: Obtained parameters from frequency study for complexes Acyclovir and energy E^2

Agent	$\Delta S/\text{kcalmol}^{-1}$	$\Delta H/\text{kcalmol}^{-1}$	$\Delta E/\text{kcalmol}^{-1}$	$\Delta G/\text{kcalmol}$	Stability constant	$\Sigma E2$
		1		-1		
Complex1	-9.3495×10^{-3}	-4.5978	-4.5971	-1.8083	1.0030	15.74
Complex2	-6.0603×10^{-3}	-1.4075	-1.4069	0.3985	-	10.77
Complex3	-0.011007	2.7553	2.7560	6.04166	-	14.75
Complex4	-5.94660	-1.22113	-1.2213	0.55095	-	11.13
Complex5	-7.48168×10^{-3}	-4.49548	-4.49548	-2.26594	1.00383	13.1
Complex6	-5.59705	-1.389307	-1.41691	-0.27861	-	10.95

Table2: Obtained parameters from frequency study Ganciclovir and energy E^2

Agent	$\Delta S/\text{kcalmol}^{-1}$	$\Delta H/\text{kcalmol}^{-1}$	$\Delta E/\text{kcalmol}^{-1}$	$\Delta G/\text{kcalmol}$	Stability constant	$\Sigma E2$
		1		-1		
Complex7	-0.01008	-0.62813	-0.62751	2.37575	-	15.97
Complex8	-8.30714	5.09282	5.09287	7.56839	-	14.97

Conclusion:

In reactions formation of all Complexes, entropies play unsuitable role to ΔG^0 become negative. ΔG^0 of formation of complexes 1 and 5 is negative. So in the follow of second law of Thermodynamic roles these two reactions can occur, in this temperature. All of the reactions aren't exothermic reactions. NBO analysis shows high hyperconjugations in all compounds.

References:

[1] G. Moyle, J. Gatell, CF. Perno et al.;" Potential for new antiretrovirals to address unmet



- needs in the management of HIV-1 infection”; AIDS Patient Care STDs; 22,459–471,2008.
- [2] 30. USP; 145, DI – 2004.
- [3] M.J. Frisch et al.;” Gaussian 03”, Revision C, 02, Gaussian Inc., Wallingford ,CT,2004.
- [4] A.D. Becke "A new mixing of Hartree- Fock and local density – functional theories" J.chem .phy. 98, 1372- 1377, 1993.
- [5] K.Kim and K.D.Jordan. "Comparson of Density Functional and MP2 Calculations on the Water Monomer and Dimer” J. Phy. Chem ; 98, 10089-10094, 1994.
- [6] A.D.Backe,"Density- functional thermo chemistry III. The role of exact exchange” J. Chem. Phys; 98, 5648- 5652, 1993.

CuO nanostructure-catalyzed oxidation of alcohol to ketone

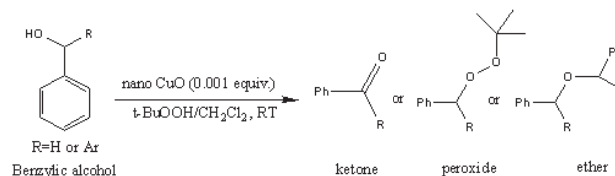
A. Tarlani*, M. Fallah

Inorganic Nanostructures and Catalysts Research Lab Chemistry & Chemical Engineering Research Center of
Iran, Tehran 14968-13151, Iran
E-mail: mahtabfallah@ccerci.ac.ir

Key words: Nanostructures, Nanocatalyst, Oxidation reaction, CuO

Introduction:

A catalyst plays a significant role in the production of chemicals today and nanomaterials have the potential for improving efficiency, selectivity and yield of catalytic process. The higher surface to volume ratio means that much more catalyst is actively participating in the reaction. Transition metal oxides are used in various applications because of their specific optical, electrical and magnetic properties. These materials represent a large class of heterogeneous catalysts widely used in many chemical reactions. Among them, copper oxide (CuO) nanostructure is a P-type semiconductor with narrow band gap of 1.2 e.V, which has a potential application in dye sensitive solar cells, gas and bio sensors, heterogeneous catalyst in many important chemical reaction such as coupling reaction and oxidation reactions. Benzylic alcohols are often used in organic synthesis either as starting materials or as protecting groups. Various systems have been used to catalyzed the oxidation such as metal-catalyzed and heteropolyacide. Oxidation of them lead to ketone, ether and peroxide compounds. In this work, firstly we have synthesized CuO nanostructures and then used as nanocatalyst for oxidation of various benzylic alcohols, are here disclosed(scheme1.)[1-3].



scheme (1)

Materials and methods:

Copper oxide nanoparticles was synthesized through solvothermal method using copper acetate as starting material and characterized by XRD, FT-IR, SEM. Oxidation reaction carried out in the presence of t-BOOH and CH₂Cl₂ as the solvent in a liquid phase condition by molar ratio of CuO nano particle (0.004 g, 0.001mmol), benzylic alcohols(1mmol) and TBHP (1.5 mmol).

The mixture was stirred at room temperature under nitrogen atmosphere for the time indicated in Table 1. Then it filtered through the short pad of alumina. Chromatography on silica eluted with petroleum ether/ethyl acetate (90/10) led to the product which was identified by HNMR .

Apparatus:

FT-IR(BRUKER), HNMR(BRUKER -AC80), SEM, XRD(BRUKER-D8ADVANC)

Result and discussion:

SEM image of the sample exhibited in fig. 1. The result of benzylic alcohol oxidation (Run 1-4) is shown in Table 1. High conversion and selectivity toward ketone were obtained at room temperature.

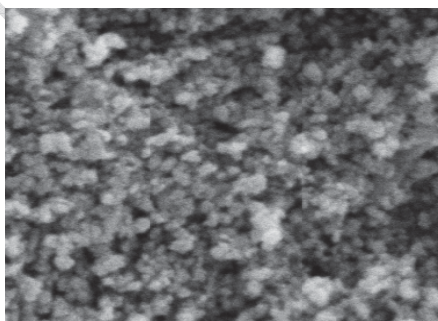


fig. 1. SEM image of CuO nanoparticles



Table. 1.

Run	alcohol	Conversion [%]	selectivity (ketone) [%]
1	benzhydrol	100	100
2	1-phenylethanol	100	100
3	Indanol	68	92
4	2,4-dichloro benzyl alcohol	100	100

Conditions: benzylic alcohol (1 mmol), catalyst (0.004 g, 0.001 mmol), RT

Conclusion:

We have shown CuO nanostructures is an efficient nanocatalyst for the production of ketones and can be obtained in high conversion and selectivity from oxidation reaction.

Reference:

- [1] M. L. Kantam and etal; "Synthesis of 1,4-dihydropyridine derivatives using nanocrystalline copper(II) oxide catalyst"; Catalysis Communications; 10, 370–372, 2009.
- [2] M. L. Kantam and etal; "Nanocrystalline copper(II) oxide catalyzed aza-Michael reaction and insertion of α -diazo compounds into N–H bonds of amines"; Tetrahedron Letters; 50, 4467–4469, 2009.
- [3] A. Tarlani and etal; "Catalytic condensation process for the preparation of organic peroxides from tert-butyl hydroperoxide and benzylic alcohols"; Applied Catalysis A: General; 315, 150-152, 2006.



Encapsulation Process in Synthesizing PolyureaMicro/nanocapsules Containing Linseed Oil and its Application in Self-Healing Coatings

M. Kouhi^{a*}, A. Mohebbi^a

^a Department of Chemical Engineering, Faculty of Engineering, ShahidBahonar University, Kerman, Iran

Email: masoume.kouhi@gmail.com

Keywords: micro/nanocapsule, self-healing, in situ polymerization, linseed oil, epoxy

Introduction:

Traditional methods for healing or repairing advanced composites needed recognition and manual intervention and were not suitable for healing invisible microcracks within the structure during its service life [1]. These cracks expose substrate to corrosive agents that result in accelerated disbonding of the polymer and flake formation from the metal coating interface [2]. In the 1980s, inspired by living systems, self-healing polymers were designed to autonomically repair invisible microcracks. The catalyst presence in the most self-healing systems to accelerate the polymerization process, as a second separated phase can lead to a major discontinuity in coating matrix. In this study, the encapsulation process of linseed oil, as an oxidative healing agent, in poly-urea formaldehyde was presented. Such coatings typically incorporate micro/nanocapsules that contain film-formers; which polymerize in the presence of air and heal the crack. Efficacy of these micro/nanocapsules in healing of cracks in an epoxy coating [3], corrosion protection and mechanical properties has been demonstrated.

Materials and methods:

130 mL of deionized water at room temperature was placed in a 400 mL beaker, along with 5 mL of 5.0% (wt/vol) poly vinyl alcohol. Under agitation, 2.50 g urea, 0.25 g ammonium chloride, and 0.25 g resorcinol were added to the aqueous solution. The pH of solution was adjusted to 3.5 by addition of 1wt% HCl solution. 30 ml of linseed oil was added slowly to



form an emulsion and allowed equilibrate under stirring conditions for 10 min before sonication. The tapered 18 mm tip sonication horn of a 1000 W ultrasonic homogenizer (Hielscher-UIP 1000) was placed in the solution, for 3 min at 30% intensity (~3.0 kJ of input energy). 6.335 g of 37 wt% formalin was added. The emulsion was slowly heated under stirring at three different rates (i.e. 500, 600, 700 rpm) and held constant for 4 h of reaction.

Apparatus:

For investigation of capsules characteristics such as Shell wall integrity, aggregation phenomena and microcapsule size, the Scanning Electron Microscopy (SEM) was used. Also the self-healing ability and corrosion performance of the scratched epoxy coating, containing linseed oil capsules, were approved by EIS and Tafel tests and the results were compared with scratch and unscratched neat one. Pull-off and Cupping tests were used for testing adhesion and flexibility respectively.

Results and discussions:

SEM images showed that the capsules were spherical in shape, and had a rough, non-porous exterior shell wall. All of synthesized capsules were in the range of 450 nm–6 μ m diameter. Scratching of neat epoxy led to severe decline in corrosion resistance of the coatings. But the capsule incorporated coating was stronger in preservation of its primary corrosion resistance, although there was a little depreciation in its corrosion behavior, along test period. In fact, this film was found to provide a very high level of protection to the underlying metal in the case of scratched neat coat. The results of polarization test were in good agreement with the results from EIS tests. A slight decrease in the adhesion strength and flexibility of cured coatings at ambient was measured for composites with included capsules. With increasing in agitation rate (i.e. using finer capsules) all capsules characteristics improved.

Conclusion:

Synthesized micro/nanocapsules in paint films released healing material, which during cracking healed cracks efficiently with satisfactory anticorrosive properties. Incorporated linseed oil



capsules through epoxy structure provided self-healing ability for coating without any catalyst requirement. With using capsules, the adhesion and flexibility decreased but the capsule incorporated coating was stronger in preservation of its primary mechanical properties. With using finer capsules, physical and chemical properties of the coatings improved.

References:

- [1] C.Challener;"The intelligence behind smart coatings"; JCT, pp. 50–55, 2005.
- [2] A.Yousefpouretal.;"Fusion bonding/welding of thermoplastic composites";J Thermoplast Compos Mater;17,303–41,2004.
- [3] M. Sternetal.;"Electrochemical Polarization: I. ATheoreticalAnalysis of the Shape of Polarization Curves";J. Electrochem. Soc.; 104,56,1957.



Surface Area Enhancement of MgO/Mg(OH)₂ by Hydrothermal process in the presence of Chiral Ionic Liquid

B. Bazri^{a*}, E. Kowsari^a

^a Department of Chemistry, Amirkabir University of Technology, Tehran, Iran

Email: bbazri@aut.ac.ir

Keywords: Magnesium oxide; Ionic liquid; Surface area; Morphology

Introduction:

The architectures and morphologies of nanostructured materials are crucial features for their physical and chemical properties [1, 2]. The ability to tune the shape of inorganic crystals is of extraordinary importance because their electronic structure, bonding, surface energy, and chemical reactivity are directly related to their surface morphology. Great interest in nanostructural materials has been focused on controlling the morphologies of materials and finding novel properties.

The synthesis of inorganic materials in Room temperature ionic liquids (RTILs) is a rather new development and has attracted increasing interest in recent years. Nevertheless, the potential of RTILs in the controlled synthesis of inorganic nanostructures with a complex form or hierarchical architectures remains to be fully explored. In this work, we present the control synthesis of MgO/Mg(OH)₂ architectures by a chiral ionic liquid-assisted hydrothermal method and enhancement in specific surface area.

Materials and Methods:

About 0.60 g of Mg(NO₃)₂·6H₂O was dissolved in 40 mL of double distilled water under vigorous stirring. Then, appropriate NaOH aqueous solution (0.2M) was added drop wise into the above solution with vigorous stirring, which would continue for 15 minutes. Then, a solution of 0.1 g of IL in 10 mL of double distilled water was added to the first solution and



stirred for about 10 minutes. Finally, the solution was transferred to a Teflon-lined autoclave. The autoclave was sealed and maintained at 130 °C and 140°C for 24 h for each sample separately, and then cooled down to room temperature. The white precipitate was separated by decantation, washed with double distilled water and dried at 60 °C.

Apparatus:

The structure and morphologies of the as-prepared product was characterized using XRD (Holland Philips Xpert X-ray diffractometer with Cu-Ka radiation), SEM (Holland Philips XL30 microscope with an accelerating voltage of 25 kV), and BET surface area (AUTOSORB-1, QUANTA CHROME).

Results and Discussion:

The XRD patterns of products manifest the high crystallinity of the samples (JCPDS Card No. 87-0653, 78-0316 for MgO and Mg(OH)₂ respectively). The SEM images of MgO/Mg(OH)₂ show novel structures of products, flake-like and porous morphologies.

BET is used to evaluate the specific surface area by fitting the absorption data to the BET model and the equation [3]. It shows significant enhancement in surface area through morphology modification of MgO/Mg(OH)₂ from 9.01 to 110.56 and 71.94(m²/g) for porous and flake-like products, respectively.

Conclusions:

In summary, new MgO/Mg(OH)₂ morphologies, have been successfully synthesized via a facile hydrothermal route assisted by a task specific basic IL, which plays an important role in fabrication of MgO/Mg(OH)₂ structures and enhancement of specific surface area. The method presented in this work is expected to help prepare other metal oxide nanomaterials. Micro/nanomaterials would be expected to have some potential applications in photocatalytic and optical electronic devices.

Reference:



- [1]Zhang, G.; Lu, X.; Wang, W.; Li, X. Chem. Mater., 2007, 19, 5207.
- [2]Ding, Y. S.; Shen, X. F.; Gomez, S.; Luo, H.; Aindow, M.; Suib, S. L. AdV. Funct. Mater., 2006, 16, 549.
- [3]G. Kickelbick.; U. Schubert, Eur. J. Inorg., Chem. (1998) 159.

15th Physical Chemistry Conference

Atomistic Simulation of Methane adsorption and diffusion in a model nanoporous carbon

Saeed Yeganegi and Fatemeh Gholampour*

Department of Physical Chemistry, Faculty of Chemistry, University of Mazandaran, Babolsar, Iran

E-mail: f_gholampour@stu.umz.ac.ir

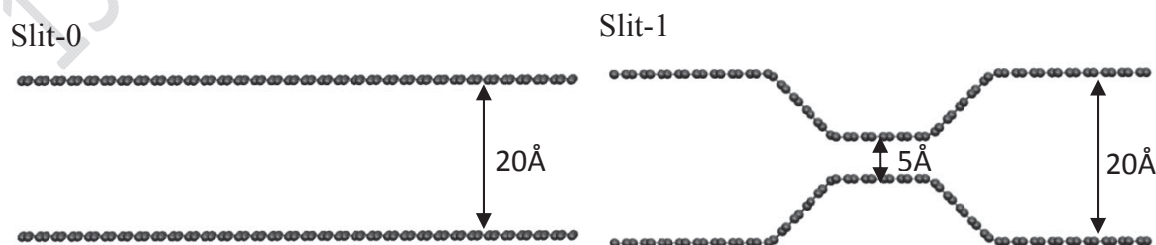
Keywords: Molecular simulation, Constricted slit, Adsorption, Diffusion

Introduction:

Nanoporous carbons (NPCs) are one of the most widely used adsorbents because of their large micropore and mesopore volumes and the high surface area. Because of the nanoscopic nature of adsorption and diffusion mechanisms in the NPCs, atomistic simulations are needed for studying these phenomena. The main problem in simulating the NPCs is modeling their amorphous structure [1]. An idealized slit-like structure has been used as a model system to study the characteristics of equilibrium adsorption as well as diffusion in porous carbon [2]. In this study we approximated the NPCs by the so-called ‘constricted slit’ pore model. We proposed this model to introduce the effect of the pore width variation in NPCs on the gas adsorption and diffusion.

Simulation details:

Three constricted slit models with constriction heights of 5, 7 and 9 Å were named with 1, 2 and 3 numbers respectively.



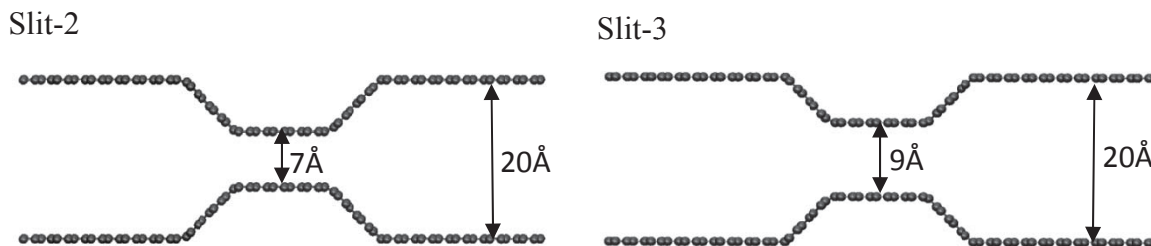


Figure 1. The studied slit models

In addition, the simple flat slit named Slit-0 was added for comparison. Figure 1 represents the studied slit models. Grand Canonical Monte Carlo (GCMC) simulations are performed for studying adsorption of methane. The all atom Lennard-Jones model were used for both carbon atoms of slits and atoms of CH₄ [3]. The simulations carried out at the temperature of 298.15 K and 12 pressures from 1 to 1000kPa. The Molecular dynamics (MD) simulations were used for examining the dynamic behavior of adsorbed methane within the constricted slits. A time step of 1fs was used for integrating the equations of motion. The MD simulations are carried out in NVT ensemble with Nose-Hoover thermostat.

Results and discussion:

The adsorption isotherms were plotted using the results of GCMC simulations. The results showed that the loading in slit-2 is the largest for all studied pressures. In slit-1, due to the small size of the pore width in the constriction region, none of CH₄ molecules can be entered in this region. One can say that introducing a constriction larger than the size of a methane molecule in the slit model of nanoporous carbon generally increases the adsorption of methane.

From MD simulations the self diffusion coefficients were calculated for adsorbed methane molecules. The diffusion coefficients for slits 2 and 3 are smaller than that of the slit-0. So, we can say that the constriction acts as a barrier of diffusion.

Conclusion:

We used GCMC and MD simulations for studying the effect of pore width variation on the adsorptive and dynamic behavior of methane within the constricted slit models of NPC. The



results were shown that introducing the constriction in which at least one CH₄ molecule can enter it, increases the adsorption and decreases the diffusion.

References:

- [1] J.C. Palmer, J.D. Moore, J.K. Brennan, K.E. Gubbins, *Adsorption* 17 (2011) 189–199.
- [2] J.C. Palmer, K.E. Gubbins, *Micropor. Mesopor. Mater.* 154 (2012) 24-37.
- [3] [23] C. J. Anderson, W. Tao, J. Jiang, S.I. Sandler, G.W. Stevens, S.E. Kentish, *Carbon* 49 (2011) 117–125.



Effect of Al-substituted on particle size and magnetic properties of $\text{Ni}_{0.6}\text{Co}_{0.4}\text{Fe}_{2-x}\text{Al}_x\text{O}_4$ ($0 \leq x \leq 0.3$) ferrite nanoparticles

A. Amirabadizadeh, T. Amirabadi

Department of Physics, University of Birjand, Birjand, Iran.

Email: amirabadi00@gmail.com

Keywords: Ferrite Nanoparticles, XRD, Magnetization.

Introduction:

Synthesis of mixed spinel ferrite nanoparticles to be one of the interesting fields of material science in material processing and technological applications, as the small size particles have some of the interesting properties as compared to bulk particles [1]. In the spinel structure, the magnetic ions are distributed among two different lattice sites, tetrahedral (A) and octahedral (B) sites. The magnetic properties of spinel ferrites, such as transition temperature and saturation magnetic moment are strongly dependent on the distribution of cations and type of doping atom. Therefore, the magnetic properties of these materials can be tailored by using the doping of the different transition metal cations. In the present work, we have study the effect of Al doping on structural and magnetical properties of $\text{Ni}_{0.6}\text{Co}_{0.4}\text{Fe}_{2-x}\text{Al}_x\text{O}_4$ ($0 \leq x \leq 0.3$) ferrite nanoparticles. Structural and magnetic properties of $\text{Ni}_{0.6}\text{Co}_{0.4}\text{Fe}_{2-x}\text{Al}_x\text{O}_4$ ferrites nanoparticles have been studied by x-Ray diffraction (XRD) and vibrating sample magnetometer (VSM). Nanoparticles of $\text{Ni}_{0.6}\text{Co}_{0.4}\text{Fe}_{2-x}\text{Al}_x\text{O}_4$ ferrite were synthesized using sol-gel method.

Experimental:

Sol-gel technique has been used to fabricate the nanoparticles of $\text{Ni}_{0.6}\text{Co}_{0.4}\text{Fe}_{2-x}\text{Al}_x\text{O}_4$ ($0 \leq x \leq 0.3$) [2]. The prepared nanoparticles were characterized using XRD and magnetization measurements were performed using VSM.

Result and Discussions:

Fig. 1 represents the XRD patterns of the $\text{Ni}_{0.6}\text{Co}_{0.4}\text{Fe}_{2-x}\text{Al}_x\text{O}_4$ ($0 \leq x \leq 0.3$). The reflection peaks observed from the samples can be well indexed with the standard pattern of the cubic spinel ferrites. The particle size of $\text{Ni}_{0.6}\text{Co}_{0.4}\text{Fe}_{2-x}\text{Al}_x\text{O}_4$ ($0 \leq x \leq 0.3$) nanoparticle was calculated from the most intense peak of XRD data using Debye Scherrer formula [1] and estimated about 26.8 , 26.4 , 26 nm, for $x=0, 0.1$ and 0.3 .

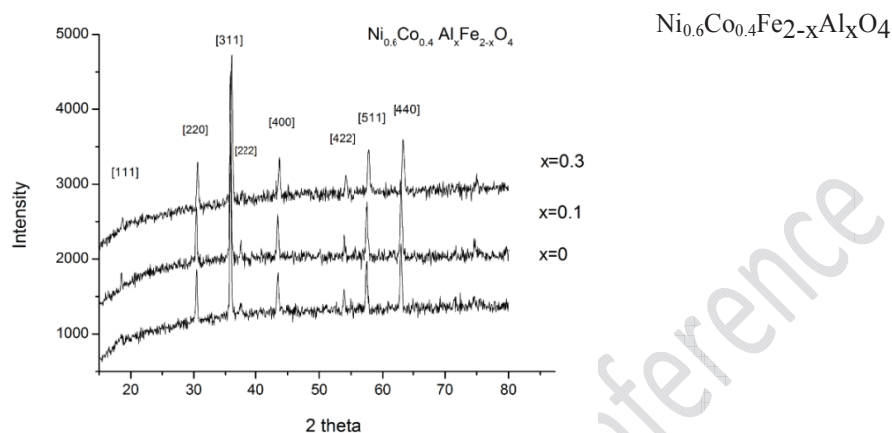
One may notice that, the particle size is slightly decreased with increasing x . It is due to the fact that the radius of the Al^{3+} ion (0.51 Å) is smaller than that of Fe^{3+} ion (0.67 Å).

The dependence of magnetization on the Al concentration (x) is measured by VSM and magnetic properties such as saturation magnetization (M_s) and H_c values for samples are given in table 1. One may notice that the M_s and H_c decrease with increasing Al concentration. It can interpret as fellows: In the spinel structure, the magnetic ions are distributed among two different lattice sites, tetrahedral (A) and octahedral (B) sites. The magnetization of these ferrites depends on the relative distribution of cations at the different sites [3]. The magnetization of either site can be reduced or increase relative to the other one by substitution of non magnetic ions in the corresponding site, in case of Al^{3+} substituted ferrites, Mazafari et al [4] studied the system of $\text{NiAl}_x\text{Fe}_{2-x}\text{O}_4$ and Kumar et al [5] studied the system of $\text{CoAl}_x\text{Fe}_{2-x}\text{O}_4$ and found that the magnetic properties decreased with increasing Al concentration. They are shown that Al ions prefer to occupy the B-sites.

Table1: Magnetic properties of $\text{Ni}_{0.6}\text{Co}_{0.4}\text{Fe}_{2-x}\text{Al}_x\text{O}_4$

Samples	M_s (emu/g)	H_c (Oe)
$\text{Ni}_{0.6}\text{Co}_{0.4}\text{Fe}_2\text{O}_4$	61	417
$\text{Ni}_{0.6}\text{Co}_{0.4}\text{Fe}_{1.9}\text{Al}_{0.1}\text{O}_4$	57	392
$\text{Ni}_{0.6}\text{Co}_{0.4}\text{Fe}_{1.7}\text{Al}_{0.3}\text{O}_4$	42	343

Fig.1: XRD pattern Of



Conclusion:

- 1- The particle size is decreased with increasing the gallium concentration in the system $\text{Ni}_{0.6}\text{Co}_{0.4}\text{Fe}_{2-x}\text{Al}_x\text{O}_4$.
- 2- Most of the Al^{3+} ions occupy the B sites in the spinel mixed ferrite.
- 3- The assumed cation distribution seems to be close to the inverse one as it possible to interpret the magnetic properties of the investigated samples according to this distribution.

References:

- [1] A. Amirabadizadeh, H. Farsi, M. Dehghani, H. Arabi, J Supecondr Nov Magn, article in press, DOI: 10.1007/s 109-011-2159-5 , 2012.
- [2] Khalid Mijasam Batoo, Shalendra Kumar, Chan Gyu Lee, Alimuddin, Current Appl. Phys. 9, 826 , 2009.
- [3] J. Smit and H.P.J. Wijn, "Ferrites", Wiley London p.140 (1959).[4] L.R. Maxwell and S.J. Pickart, *Phys. Rev.* **92** (5), 1120 ,1953.
- [4] M. Mozaffari, Z. Aboalizadeh, J. Amighian, J. of MMM, 233. 2997 (2011).
- [5] L.Kumer, M. Kar, J. of MMM 233, 2042 ,2011.



Application of Modified Sulfur Nanoparticles as a New Sorbent for Solid Phase Extraction and Determination of Linuron

F. Salehi, B. Aibaghi Esfahani*

School of Chemistry, Damghan University, Damghan, Iran

E-mail: Aibaghi@du.ac.ir

Key words: Linuron, Sulfur nanoparticles, Solid phase extraction, Preconcentration.

Introduction:

Solidphase extraction (SPE) is a routine extraction method for the pretreatment of samples with complex matrices such as seawater, because it offers the advantages of enrichment, high recovery, simplicity and high speed [1]. Recently, the use of nanoparticles (NPs) for sample extraction in SPE has garnered research interest. Compared with the micrometer-sized particles used for SPE, NPs offer a significantly higher surface area-to-volume ratio and a short diffusion route, resulting in high extraction capacity, rapid extraction dynamics, and high extraction efficiencies [2]. Nanosized sulfur particles are one class of NPs that have been widely applied in pharmaceuticals, synthesis of nanocomposites for lithium batteries, synthesis of sulfur nano wires with carbon to form hybrid materials with useful properties for gas sensor. In agricultural field, sulfur is used as a fungicide against the apple scab disease under colder conditions, in conventional culture of grapes, and several other crops [3].

Materials and methods:

In this work sulfur nanoparticles were prepared in liquid phase at normal pressure and room temperature. Sulfur powder was applied as original material, formic acid as precipitating agent, and polyethylene glycol-400 (PEG-400) as dispersing agent. The average sulfur nanoparticles size is 50~100 nm (Fig.1). This method is used to prepare sulfur nanoparticles which can be used as a sorbent for solid phase extraction.

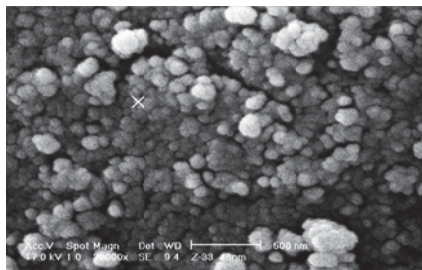


Fig. 1: SEM image of sulfur nanoparticle

SPE method is used for preconcentration and determination of Linuron in aqueous samples. For the SPE, an aqueous solution containing the analyte was adsorbed quantitatively during passage of column through modified sulfur nanoparticles sorbent. After the preconcentration and separation stage, the analyte was eluted with acetonitril and determined by (HPLC-UV).

Apparatus:

A KNAUER liquid chromatograph equipped with a UV-Vis detector was used. Separations were carried out at room temperature on a 25 cm C18 RP column preceded by a guard column. A pH meter, Metrohm 780 was employed for measuring pH values. The preconcentration system consisted of glass column (70mm height _5mm internal diameter) that connected to vacuum pumpRocker 400 was used. A Philips XL30 Scanning Electron Microscope at an accelerating voltage of 15 kV was used to obtain of SEM image of adsorbent.

Result and discussion:

In this study, a novel method, SPE-HPLC-UV, was developed for the determination of Linuron in water samples. The results showed that optimum extraction performance was achieved Acetonitril as the extraction eluent and different factors such as pH, kind and volume of buffer, sample volume, concentration of modifier, amount of sorbent, flow rate of eluent and sample solution optimazied. The linear dynamic range for determination of Linuron was $8.0 \times 10^{-10} - 8.0 \times 10^{-6} \text{ M}$ ($0.2\text{-}2000 \text{ ng.mL}^{-1}$) and the limit of detection based on three times the standard deviation of the blank was 0.086 ng.mL^{-1} .



Conclusion:

Matrix effects do not interfere with the quantification process. Compared with other extraction methods such as LLE and DLLME, combined with GC-MS, LC-MS, LC-fluorescence, and LC-UV for analysis of phenylureas in water samples, the proposed method shows low detection limits, relatively good precision, and low consumption of sample and organic solvent.

Reference:

- [1] S.Z. Mohammadi et al . ; "Flame atomic absorption spectrometric determination of trace amounts of lead, cadmium and nickel in different matrixes after solid phase extraction on modified multiwalled carbon nanotubes" ; Central European Journal of Chemistry; 8, 662-668,2010.
- [2]K. Ghanemi et al . ; "Sulfur-nanoparticle-based method for separation and preconcentration of some heavy metals in marine samples prior to flame atomic absorption spectrometry determination" ; Talanta; 85,763-769,2011.
- [3] M. Faraji et al . ; "A nanoparticle-based solid-phase extraction procedure followed by flow injection inductively coupled plasma-optical emission spectrometry to determine some heavy metal ions in water samples";Analytica Chimica Acta; 659,172-177,2010.



Functionalized nano silica as an efficient catalyst for Synthesis of chromene derivatives by multi-component reactions

Mahmood Tajbakhsh*, Heshmatollah Alinezhad, rahman hosseinzade, mohaddese kariminasab, Parizad Rezaee

Department of Inorganic Chemistry, Faculty of Chemistry, University of Mazandaran, Babolsar, Iran

E-mail: tajbakhsh@umz.ac.ir

Key words: Homogeneous base catalyst, Nano silica, Aminoethyl piperazine, Multi-component condensation

Introduction:

Base-catalyzed condensation and addition reactions are industrially important in the production of drugs, fragrances and chemical intermediates [1]. In such systems, several difficult issues arise, of which we may address to the isolation of the products, the corrosive nature of the reaction mixture and formation of large amounts of waste materials. Therefore, improved synthesis routes in terms of product purity, yield, and minimal waste formation are highly desirable. Solid acid catalysts have been extensively studied and applied in numerous reactions so far [2]; however, solid base catalysts have not been extensively studied [3]. These heterogeneous catalysts are known to suppress side reactions which include self-condensation and oligomerization, resulting in better selectivity and product yield. This means cost and energy savings for the downstream separation and purification of the product. It also avoids the complex neutralization and separation steps needed to recover the homogeneous base catalysts from the reaction mixture. The recovered solid catalysts can be readily regenerated for further use.

Materials and methods:

Nano silica was first immersed in hydrochloric acid for 24 h, and washed with deionized water, and dried under vacuum. The activated nano silica was suspended in dry toluene, and



then an excess amount of 3-chloropropyltrimethoxysilane. The suspension was mechanically stirred and refluxed, afterward, the reaction mixture was cooled to room temperature, transferred to a vacuum glass filter, and washed with ethanol and diethyl ether. The resulting solid was dried under vacuum to give nano silica bonded *n*-propyl chloride. 3-Chloropropyl nano silica and aminoethyl piperazine were added in a 50 mL round-bottomed flask contained dry toluene connected to a reflux. Afterward, the reaction mixture was cooled to room temperature, transferred to a vacuum glass filter, and washed with toluene and ethanol in turn. The resulting solid was dried under vacuum to give nano silica functionalized as a white powder.

Result and discussion:

Synthesis of 3-amino-2-cyano-1-(R)-1H-benzochromenes by reacting aromatic aldehyde derivatives, 1 or 2-naphthol and malononitrile under solvent free conditions an efficient multi-component condensation reaction utilizing base functionalized nano silica.

Conclusion:

We report here the preparation of nano silica bonded aminoethyl piperzine, as a novel heterogeneous and recyclable catalyst, from the reaction of 3-chloropropyl nano silica with aminoethyl piperazine and it's successful application in the synthesis of one-pot three-component condensation.

Reference:

- [1] G.J. Kelly, F. King, M. Kett, Green Chem. 4 (2002) 392-399.
- [2] (a) D. Choudhary, S. Paul, R. Gupta, J.H. Clark, Green Chem. 8 (2006) 479-482. (b) K. Niknam, M.A. Zolfigol, D. Saberi, H. Molaei J. Chin. Chem. Soc. 56 (2009) 1257- 1264.
- (c) F. Shirini, M.A. Zolfigol, M. Abedini Monatsh. Chem. 140 (2009) 1495-1498.
- [3] K. Tanabe, W.F. Holderich, Appl. Catal. A 181 (1999) 399-434.



Functionalized Nanoporous Silica Gel as a New Sensor for Determination of Metal Ions

Mahmood Tajbakhsh,* Rahman Hosseinzadeh, Heshmatollah Alinezhad and Parizad Rezaee

Department of Organic Chemistry, Faculty of Chemistry, University of Mazandaran, Babolsar, Iran.

E-mail: Tajbakhsh@umz.ac.ir

Key words: Functionalized nanoporous silica gel, metal ions, sensor

Introduction:

Silica-based organic – inorganic hybrids are attractive composite materials since they combine in a single solid both the properties of a rigid three-dimensional silica network with the particular chemical reactivity of the organic component(s). In particular, the design of nanoporous silica-based adsorbents for the determination of toxic heavy-metal ions in aqueous solutions is a subject that has been intensively investigated [1]. For this purpose, a variety of organic functional groups can be grafted or incorporated onto the surface of nano structured channels using ligand-functionalized organosilanes [2].

This paper describes the construction of a selective sensor, a carbon paste electrode modified with silica-based organic-inorganic hybrid materials containing thiol groups covalently attached to the solid framework *via* a alkyl chain, its properties and its application to the determination of metal ions in waste water samples.

Materials and methods:

For preparation of surface bond thiol nano silica gel ligand, a nanoporous silica gel was activated by refluxing in hydrochloric acid then washed with distilled water and dried completely. Activated silica gel with of 3-chloropropyltrimethoxysilane was refluxed in dry toluene for 24 h. The attained solid, chloropropyl silica gel, was filtered and washed with hot toluene in soxhlet and then dried in oven at 110° C. Then product was allowed to react with



piperazine and 2-mercaptopropanoic acid in refluxing toluene. The solid was filtered and washed with warm ethanol and dried at 60° C in vacuum line. Therefore, polymer-supported catalyst was synthesis and were characterized by TGA, FT-IR spectroscopy and CHN analysis.

Result and discussion:

Nanoporous silica for use in the determination of heavy metals has been the subject of extensive research recently. This work, to the best of our knowledge, is the attempt to apply modified silica gel to the selective determination of Palladium ions in the presence of other metal ions. Thus it can be concluded that the changes in the membrane potential are induced by host guest complexation, which implies molecular recognition effects at the interface of the modified electrode and the aqueous solution [3].

Conclusion:

The results of this study show that the potentiometric method provides an attractive alternative for the determination of Palladium ion. The electrode is easy to prepare, selective to Palladium over several heavy metals.

Reference:

- [1] S. Sayen, C. Gerardin, L. Rodehuser, A. Walcarius, *Electroanalysis* **2003**, 15, 422.
- [2] P. C. Pandey, S. Upadhyay, H. C. Pathak, C. Pandey, *Electroanalysis* **1999**, 11, 950.
- [3] W. Junjun, F. A. Gross, H. S. Tolbert, *J. Phys. Chem. B* **1999**, 103, 2374.



Preparation and characterization of IR spectrum LiNbO_3 nanopowders

R. Ghasemi^{*a}, A. Arab^a, M. H. Yousefi^a

^aDepartment of Physics, Malek Ashtar University of Technology, Shahin shahr, Iran

Email:ghasemich@yahoo.com

Key words: Lithium niobate, Milling, Calcination, XRD, IR

Introduction:

Lithium niobate (LiNbO_3) is an important material with applications in radar, acoustic, optic and frequency conversion. Various properties of nanoparticles have enjoyed a special status due to their different behavior in comparison with their own bulk samples [1, 2]. In order to improve properties of LiNbO_3 , its nanopowder has been prepared and its IR spectrum has been studied.

Materials and Methods:

The starting materials were Nb_2O_5 (Merck, 99 %) and Li_2CO_3 (Merck, 99%). The material was ground on ball mill via Fastmill for 4, 8 and 16 hours of milling. The four -hour- milled sample was calcined at the temperatures of 800, 900, and 1000 °C .

Apparatus:

The materials were mixed by ball mill with steel balls made in Germany and calcined at an H-T 40/14 furnace made by Naberthem in Germany. The XRD patterns were performed by X-ray diffractometer (D8ADANCE, Bruker, Germany). Further, the infrared spectrum was measured from 400 to 4000 cm^{-1} with a Nicolet 5ZPX IR spectrometer.

Results and Discussion:

Fig. 1. presents the XRD patterns of $\text{Nb}_2\text{O}_5+\text{Li}_2\text{CO}_3$ powder at different milling time. As it can be

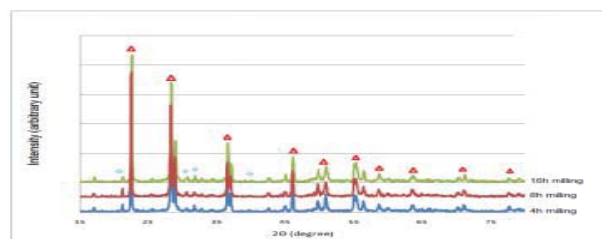


Fig.1. XRD spectra of Nb_2O_5 ▲ + Li_2CO_3 ◆ at different milling time

observed, no peak signal of LiNbO_3 (LN) implies that no reaction between Nb_2O_5 and Li_2CO_3 takes place at these milling times.

The X-ray diffraction patterns of the four-hour-milled sample that calcinated at different temperatures are shown in Fig.2.

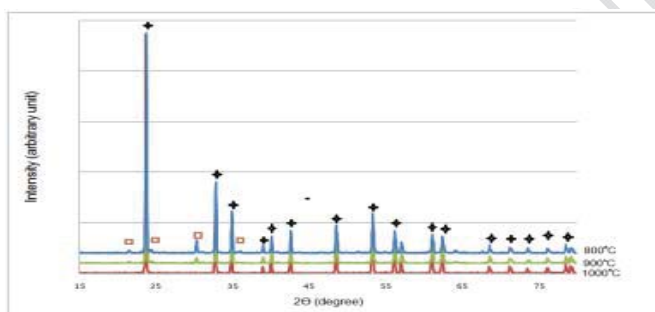


Fig.2. XRD spectra of LiNbO_3 ★ and LiNb_3O_8 □ at different temperatures

As it can be observed, at 800 and 900 °C the diffraction peaks of LiNbO_3 and the undesirable phase of LiNb_3O_8 begin to emerge. Therefore, it was necessary to increase the synthesized temperature. It is interesting to note that the sample heated at 1000 °C did reveal no impurity peaks. The formation of single phase LiNbO_3 is in agreement with its IR spectra (Fig. 3). The comparison of the IR results of this sample with similar samples shows narrow transmission peak at 1415 cm^{-1} and transmission band around 950 to 1400 cm^{-1} , which is characteristic of the LiNbO_3 crystal.

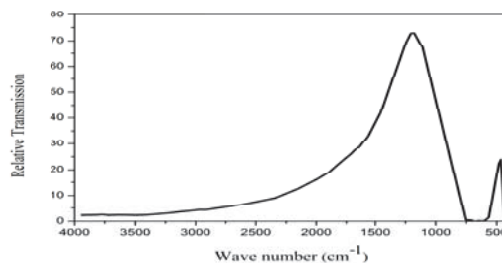


Fig.3. IR spectrum of LiNbO_3 at 1000 °C



Conclusion:

The single phase trigonal structure of LiNbO_3 nanopowder formed at 4 h milling and 1000 °C calcination temperature. The formation of single phase lithium niobate is in agreement with its IR spectra.

References:

- [1] R. S. DE Figueiredo and et al. ; “Piezoelectric lithium niobate obtained by mechanical alloying”; Journal of materials science; 17, 449 – 451, (1998).
- [2] Meinan Liu and et al. ; “An efficient approach for the direct synthesis of lithium niobate powders”; solid state Ionics; 177, 275 – 280, (2006).



Fabrication and characterization of a Nano-structured organic light emitting diode using synthesis dye

M. Ghoshni^a, A. behjat^a, B.B.F. Mirjalili^b, L. Zmani^b, F. Jafarinodushan^a

^a Department of Physics, Faculty of science, Yazd university, Yazd, Iran

^b Department of Chemistry, Faculty of science, Yazd university, Yazd, Iran

Email: maralghoshani@yahoo.com

Key words: OLED, Synthesis dye

Introduction:

In recent years, research on organic light emitting diode has been significantly increased. This is because of their possible application in large scale lighting, flexible panel and multicolor displays with low power consumption and low cost [1]. One way to obtain devices with high performance is doping polymer with dyes. The dye that doped in polymer often changes the color of radiation and increases the efficiency of device luminescence [2]. In this paper we synthesis a new dye to use in a single layer diode, with mixture of PVK, PBD and dye as an emitting layer. Then the electrical characteristics of the fabricated device are investigated.

Materials and methods:

General procedure for the synthesis of 4-(1-Naphthyl)azonaphthalin-1-amin: To 2 mmol of α -naphthylamine (0.286 mg) is added 1 mmol of sodium nitrite (0.068 mg), then 1 ml of sulfuric acid is added drop wise with stirring at room temperature until reaction is completed.

Afterward ethanol is added to mixture and the precipitate is recrystallized.

For fabricating OLED at first a 5mm wide ITO anode strip line was made by selective etching; using of hydrochloric acid (HCL) for 10-20 min. Then, the patterned anode glass was cleaned sequentially by ultra-sonication in propanol, acetone, deionized water for 10 min, respectively. Then, PEDOT:PSS as a hole injection layer was spin-coated onto the anodes and dried in the oven at 110°C for 1h. PVK, PBD, and dye dissolved in chloroform solution with (100:40:0.6) weight ratios. Then blend was spin-coated onto the prepared substrate. Finally Al was deposited by thermal evaporation as a cathode.

Apparatus:

A Keithley 2400 sourcemeter and a HR4000 spectrometer (Ocean optic) were used to record current-voltage and intensity-wavelength characteristics of the devices, simultaneously.

Result and discussion:

The current-voltage characteristics of the device is shown in Fig (1-a). This displays diode behavior for sample with synthesis dye, a nearly ohmic behavior at lower voltage and the current dramatically increases for higher voltage. It is seen that turn on voltage for sample with PEDOT:PSS decreases and current increases, because it improves the hole injection. I-V characteristic of the sample is comparable with Rubrene as a good emitting layer when we have the same OLED structure.

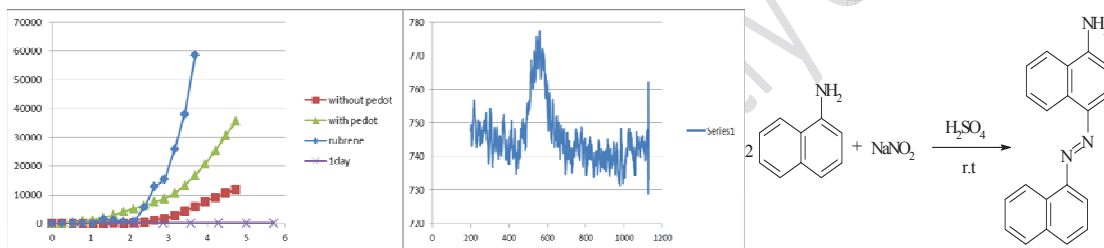


Figure 8: a) I-V characteristics b) EL spectra c) 4-(1-Naphthyl)azonaphthalin-1-amin

This sample at 10V starts to emit a yellow radiation Fig (1-b). Also the aging of the sample was studied. Fig (1-a) displays the current density decreases dramatically after one day.

Conclusion:

A new synthesis dye was used as an emitting layer in single layer OLED and as Fig 1 displays it shows diode behavior and emit yellow radiation. The life time of the device is relative short, less than one day. More work is going to be carried out on aging of the device.

Reference:

[1] P. Kopola, M. Tuomikoski, R. Suhonen, A. Maaninen, "Gravure printed organic light emitting diodes for lighting applications" ; Thin Solid Films 517, (2009) ,5757-5762.



- [2] T. Mori, H. G. Kim, T. Misutani , D. C. Lee ; "Effects of PEDOT-PSS layer on the characteristics of organic light-emitting diodes with Nile Red" ; Appl. Phys, 40, 5346(2001).

15th Physical Chemistry Conference



Application of ruthenium nanoparticle loaded on activated carbon for removal of methyl orange from aqueous solution: kinetics and isotherm study

Z. Shokoohmandi^{a*}, M. Ghaedi^b

^a Department of chemistry, Azad university ghachsaran, Ghachsaran , Iran

^b Department of chemistry, Yasouj university, Yasouj, Iran

Email: : z.sh15@yahoo.com

Key words: Ruthenium, Methyl orange, Nanoparticles, Removal.

Introduction:

The nanoparticles have very interesting physicochemical properties, such as ordered structure with high aspect ratio, ultra-light weight, high mechanical strength, etc. In recent years, there is a growing interest in the usage of nanoparticles as sorbents for organic or inorganic pollutants removal because they have significant advantages such as (i) the synthesis of them is very easy and low cost, (ii) only a little amount of nanoparticles is required for removing of the pollutants from aqueous solutions (iii) the adsorption capacity of them is relatively high. In this research ruthenium nanoparticle loaded on activated carbon has been used as adsorbent for the removal and recovery of methyl orange (MO) from wastewater. The batch studies have been carried by observing the effects of pH, concentration of the dye, amount of adsorbents, contact time and etc. The graphical correlation of various adsorption isotherm models like Langmuir, Freundlich, Tempkin have been carried out for this adsorbent. The kinetic studies suggest the process following pseudo second order kinetics and involvement of particle diffusion mechanism [1-5].

Materials and methods:



All chemicals including NaOH, HCl, KCl, Methyl Orange (MO) and activated carbon (AC) with the highest purity available are purchased from Merck, Darmstadt, Germany. An accurately weighted amount of MO was dissolved in deionized water to prepare 100 mg/L as stock solution, while the working solution was prepared by diluting this solution. Samples were collected from the adsorption bath at different time interval. its adsorbed amount (q_e (mg.g^{-1})) was calculated by the following mass balance relationship: $q_e = (C_0 - C_e)V/W$ where C_0 and C_e are the initial and equilibrium dye concentrations in solution, respectively (mg.L^{-1}), V is the volume of the solution (L) and W is the mass adsorbent (g). The obtained experimental data at various times and concentrations were fitted to different models to calculate and the kinetics and isotherm parameters of adsorption process at optimum values of all variables were investigated.

Apparatus:

During this study following pH optimization in all experiments, The pH of sample solution was adjusted by addition of HCl or NaOH using a pH/Ion meter model-686 (Metrohm) and absorption studies were carried out using Jasco UV-Visible spectrophotometer model 25-shimadzo.

Result and discussion:

the influence of variable including pH, concentration of the dye, and amount of adsorbent, contact time required for efficient removal of Methyl Orange has been investigated. in this paper, dye elimination on series of similar solution whit 50 ml volume in concentration of 12 mg.L^{-1} in the various pH from 1 to 9 was investigated and showed that in pH=3, there is maximum percent of dye elimination. synthetic studies to determinate dye absorption efficiency in optimum values namely solution with concentration of 12 mg.L^{-1} in pH=3 in the 15 time with 0.01 gr adsorbent with elovich synthetic models and intre particle diffusion was investigated and observed that dye absorption follows two-order synthetic. investigation of adsorption isotherms carried out in afew different concentration in 15 min with optimal condition of another parameters, and showed that dye absorption follow by langmuir isotherm.



Conclusion:

The ruthenium nanoparticle loaded on active carbon is identified to be an effective adsorbent for the removal of Methyl Orange from aqueous solution. It was observed that batch sorption using ruthenium nanoparticle loaded on active carbon was dependent on parameters such as initial concentration of dye, time, pH, amount of adsorbent and type of dye.

Reference:

- [1] Y. Ma, Y. Zheng, J.P. Chen, A zirconium based nanoparticle for significantly enhanced adsorption of arsenate: synthesis, characterization and performance, *J. Colloid Interface Sci.* 354 (2011) 785–792.
- [2] Y.H. Chen, Synthesis, characterization and dye adsorption of ilmenite nanoparticles, *J. Non-Cryst. Solids* 357 (2011) 136–139.
- [3] A. Ozcan, A.S. Ozcan, *J. Hazard. Mater.* 2005, 125, 252.



Introduction of new nano composite in base of nano gold particles and poly L-methionine for simultaneous determination of uric acid and xanthine

R. Ojani*, A. Alinezhad, Z. Abedi

Electroanalytical Chemistry Research Laboratory, Department of Analytical Chemistry, Faculty of Chemistry,
University of Mazandaran, Babolsar, Iran

Email: Fer-o@umz.ac.ir

Key words: Poly L-methionine (PLMT), Gold nanoparticle (AuNPs)

Introduction:

Uric acid (UA), xanthine (XA) are degradation products of purine metabolism in human and animals. Purine metabolites pathway involves transformation of $HX \rightarrow XA$, $XA \rightarrow UA$ by xanthine oxidase, so XA is intermediate and UA is the terminal product of purine degradation metabolism [1]. The concentration levels of the two products in body fluids such as human serum and urine are markers of many clinical conditions, including hyperuricemia, gout, leukemia, xanthinuria and pneumonia [2]. Gold nanoparticles are the most stable metal nanoparticles, which presented fascinating features such as the assembly of multiple types involving materials science, the behavior of individual particle, size-related electronic and optical properties (quantum size effect) and their applications to catalysis and biology [3]. With the help of a long chain molecule having suitable functional groups at both ends, the gold nanoparticles can be immobilized as an organized mono- or multiparticle layer on a solid support [4,5]. In this paper, electrochemical responses of UA and XA at the poly L-methionine(PLMT)/gold nanoparticle(AuNPs) were compared with the electrochemical responses of UA and XA at the PLMT modified electrode and GCE. Finally, modified electrode was successfully employed to detect UA and XA in the serum samples with good selectivity and high sensitivity.

Materials and methods:

UA, XA and L- methionine were purchased from Fluka. $HAuCl_4$ was obtained from merck. Cyclic voltammetric and differential pulse voltammetric measurements were accomplished



with three electrodes in (0.1mol L⁻¹) phosphate buffer solution (PBS). All experiments were accomplished at room temperature.

Apparatus:

Electrochemical experiments were accomplished using a potentiostat/galvanostat (Bhp2061-C Electrochemical Analysis System, Behpajoo, Iran). A platinum wire was used as the counter electrode. A glassy carbon as working electrode and a SCE as reference electrode were used.

Result and discussion:

In this study, GCE/PLMT/AuNPs as a new sensor was applied for simultaneous determination of UA and XA. The electrochemical behaviors of UA and XA at the modified electrode were studied by cyclic voltammetry and differential pulse voltammetry (DPV), and showed that the modified electrode exhibited excellent electrocatalytic activity toward the oxidation of these two compounds. SEM shows that when AuNPs immobilized on the electrode surface, the surface of electrode has increased compared with GCE/PLMT modified electrode. Electrochemical impedance spectroscopy (EIS) was also employed to study the surface of electrode. When nanoparticle immobilized at the GCE/PLMT modified electrode, conductivity of electrode increased. The detection limits for UA and XA were about centesimal μM . Finally, this modified electrode has been applied to simultaneous determination of UA and XA in human serum with good selectivity and high sensitivity.

Conclusion:

The experimental results reported here clearly demonstrated that the oxidation of UA and XA was facilitated by the immobilized AuNPs on PLMT modified GCE (GCE/PLMT/AuNPs) electrode compared with bulk GCE and PLMT modified electrode. Attachment of AuNPs on PLMT was characterized by SEM studies. The GCE/PLMT/AuNPs modified electrode possesses good stability, excellent sensitivity and high selectivity for simultaneous detection of UA and XA. In addition, the modified electrode also has good reproducibility and can be



applied to determination of purine derivatives in human urine samples with satisfactory results.

Reference:

- [1] T. Yamamoto, Y. Moriwaki, S. Takahashi, Clin. Chim. Acta. 356 (2005) 35.
- [2] M. Heinig, R.J. Johnson, Cleve. Clin. J. Med. 73 (2006) 1059.
- [3] M.C. Daniel, D. Astruc, Chem. Rev. 104 (2004) 293.
- [4] C.R. Raj, T. Okajima, T. Ohsaka, J. Electroanal. Chem. 543 (2003) 127.
- [5] T. Sagara, N. Kato, N. Nakashima, J. Phys. Chem. B 106 (2002) 1205.



Aniline to Polyaniline/silver nanocomposites via emulsion polymerization in the presence of *p*-phenylenediamine

Hossein Behniafar, Marziyeh Barzegar*, Roghayeh Samiaa
Department of Chemistry, Damghan University, 36715-364, Damghan, Iran
Email: barzegar.marziyeh@gmail.com

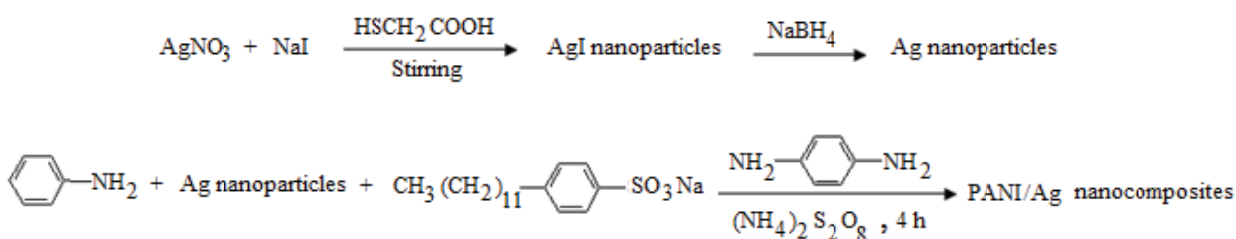
Key words: Polyaniline/silver, Nanoparticles, Nanocomposites, *p*-phenylenediamine.

Introduction:

Deposition of metal or metal oxide nanoparticles into a conducting polymer matrix is an attractive area of science [1]. The Polyaniline/silver (PANI/Ag) nanocomposites have been accelerated in the presence of a few amount of *p*-phenylenediamine (PDA) in acidic media [2,3]. This study deals with the novel synthesis of PANI/Ag nanohybrids via emulsion polymerization using PDA.

Materials and methods:

Ag nanoparticles were prepared as follows: 7.5 mL of AgNO₃ solution (0.01 M) was added to 225 mL deionized water with stirring. After 10 min of mixing, 15 mL of 2-mercaptocarboxylic acid solution (0.01 M) was added to the mixed solution and 7.5 mL of 0.01 M NaI solution was dripped into the mixed solution under vigorous stirring immediately. After 20 min of further reaction, a light yellow solution of AgI nanoparticles was obtained. Then, (0.06 g, 1.06 mmol) NaBH₄ as reducing reagent was added to AgI colloid and the mixture was kept stirred for another 30 min until AgI was thoroughly reduced and a light red colloid of Ag nanoparticles can be obtained and then acidified with HCl to 0.1 N. Aniline (0.582 g, 6 mmol), sodium dodecylbenzene sulfonate (21.78 g, 60 mmol), PDA (0.006 g, 0.06 mmol) and ammonium peroxydisulfate (1.854 g, 8 mmol) were added to the above colloid. PANI/Ag hybrid was prepared after 4 h stirring at room temperature. Acetonitrile was then added to destroy micelles and precipitate the product.



Result and discussion:

A nanocomposite of PANI/Ag was successfully synthesized by a novel strategy starting from aniline via emulsion polymerization in the presence of *p*-phenylenediamine. The hybrid prepared was fully characterized using IR, UV-vis, SEM, TEM, XRD, and TGA analyses. A uniform core-shell surface could be detected by SEM. Nanoparticles of Ag (~ 2% w/w) with size of about 20 nm were dispersed into the polymer matrix. In addition, thermo-stability of the product was not affected by this dispersion. Conductivity measurements were also done and compared with that of pure PANI.

References:

- [1] S. Bouazza, V. Alonzo, D. Hauchard. ; "Synthesis and characterization of Ag nanoparticles– polyaniline composite powder material" ; Synth. Met; 159, 1612-1619, 2009.
- [2] P. Bober, J. Stejskal, M. Trchova, J. Prokes, and I. Sapurina. ; "Oxidation of Aniline with Silver Nitrate Accelerated by *p*-Phenylenediamine: A New Route to Conducting Composites" ; Macromolecules; 43, 10406–10413, 2010.
- [3] H. D. Tran, I. Norris, H. Tsang, Y. Wang, B. Mattes, R. B. Kaner. ; "Substituted Polyaniline Nanofibers Produced via Rapid Initiated Polymerization" ; Macromolecules; 41, 7405, 2008.



Pyrrole to polypyrrole/Ag nanocomposites via emulsion polymerization

Hossein Behniafar, Marziyeh Barzegar*, Roghayeh Samiaa

Department of Chemistry, Damghan University, 36715-364, Damghan, Iran

Email: barzegar.marziyeh@gmail.com

Key words: Polypyrrole, Silver, Nanoparticles, Nanocomposites.

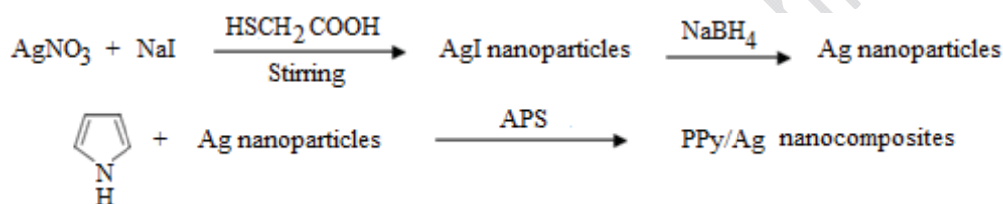
Introduction:

In recent years, the interest in the development of inorganic/organic composite has grown rapidly due to a wide range of potential use of these materials [1]. Among these materials, one important class is that in which the organic part is conducting polymers, such as polyaniline or polypyrrole [2]. Polypyrrole as one of the most promising conducting polymers has received comprehensive interests due to its excellent characteristics including easy preparation, environmental stability, high conductivity and so on. The mentioned merits lead polypyrrole to have wide potential applications in various fields, such as sensors, actuators and electric devices. On the other hand, the metal nanoparticles, such as silver, have attracted much attention in recent years due to their interesting properties and potential applications in technological fields. Silver particles have applications in catalysis, conductive inks, thick film pastes and adhesives for various electronic components, in photonics and in photography [3]. So far, various methods for Polypyrrole/silver (PPy/Ag) nanocomposites preparation have been reported. However, the preparation of them by emulsion method starting from pyrrole and silver has not been reported yet. Our target of this study is to introduce a new method for the preparation of this class of electro-active materials.

Materials and methods:

Ag nanoparticles were prepared as follows: 7.5 mL of AgNO₃ solution (0.01 M) was added to 225 mL deionized water with stirring. After 10 min of mixing, 15 mL of mercaptocarboxylic acid solution (0.01 M) was added to the mixed solution and 7.5 mL of 0.01 M NaI solution

was dripped into the mixed solution under vigorous stirring immediately. After 20 min of further reaction, a light yellow solution of AgI nanoparticles was obtained. Then, (0.06 g, 1.06 mmol) NaBH₄ as reducing reagent was added to AgI colloid and the mixture was kept stirred for another 30 min until AgI was thoroughly reduced and a light red colloid of Ag nanoparticles can be obtained and then acidified with HCl to 0.1 N. Pyrrole (0.419 g, 6 mmol), sodium dodecylbenzene sulfonate (21.78 g, 60 mmol) and ammonium peroxydisulfate (1.854 g, 8 mmol) were added to the above colloid. PPy/Ag hybrid was prepared after 4 h stirring at room temperature. Acetonitrile was then added to destroy micelles and precipitate the product.



Result and discussion:

A nanocomposite of PPy/Ag was successfully synthesized by a novel strategy starting from Pyrrole via emulsion polymerization. The hybrid prepared was fully characterized using IR, UV-vis, SEM, TEM, XRD, and TGA analyses. A uniform core-shell surface could be detected by SEM. Nanoparticles of Ag (~ 2% w/w) with size of about 20 nm were dispersed into the polymer matrix. In addition, thermo-stability of the product was not affected by this dispersion.

References:

- [1] T.K. Sarma, A. Chattopadhyay. ; "Reversible Encapsulation of Nanometer-Size Polyaniline and Polyaniline-Au-Nanoparticle Composite in Starch"; *Langmuir*; 20, 4733-4737, 2004.
- [2] S. Palaninappan, A. John. ; "Polyaniline materials by emulsion polymerization pathway"; *Prog. Polym. Sci*, 33, 732-758, 2008.



- [3] S. Jing, S. Xing, L. Yu, Y. Wu, C. Zhao. ; "Synthesis and characterization of Ag/polyaniline core-shell nanocomposites based on silver nanoparticles colloid"; Materials Letters; 61, 2794–2797, 2007.

15th Physical Chemistry Conference



Molecular Dynamics, Monte Carlo and DFT Studies of Boron-Nitride nanocones: properties investigating of $B_{10}N_{11}H_7(Thr)_2$ in Different Temperatures and Solvents

N. Hooshmand^{*a}, M. Monajjemi^a

^a Science and Research Branch, Islamic Azad University, Tehran, Iran

nhooshmand@hotmail.com

Keywords: Molecular Dynamics, Solvent Effect, DFT, $B_{10}N_{11}H_7(Thr)_2$, Nanocone, Monte Carlo

Introduction:

The fascinating novel structures of boron nitride (BN) have been intensively studied, since they have unique and interesting properties such as electronic [1] and mechanical [2] properties. Boron Nitride Nanocones (BNNCs) represent an important class of nanocnes; consist of B and N atoms. The number of electrons in combination of B and N atoms is the same as two carbon atoms, therefore they have similar properties and also in some cases, they are better candidates to predict properties compare to other composite materials. BNNCs have been investigated and synthesized [3] and shown they have very interesting properties in comparison with similar carbon nanostructure. We have proposed a $B_{10}N_{13}$ nanocone as a particular case to attach to Threonin, trough B terminated atoms to investigate thermodynamic properties.

The purpose of this work is to understand stability, atomic structure and thermochemistry properties of one of the particular Boron Nitride nanocones as $B_{10}N_{11}H_7(Thr)_2$.

Computational details

In present work, all calculations were performed using the Gaussian98 program in the electronic ground state. We used this package to study many specific properties of



$B_{10}N_{11}H_7(Thr)_2$ such as molecular energies and structures, thermodynamic properties, Multipole moment and NMR shielding in both gas phase and different solvents.

Density functional theory (DFT) is a general computational method that frequently used in computing properties of macromolecules as we applied this method to study $B_{10}N_{11}H_7(Thr)_2$. Molecular dynamics (MD) and Monte Carlo simulations are two methods for determining physical properties of macroscopic, was used in the present work. The temperature T is sequentially increased RT to 310K. Solvent effect on $B_{10}N_{11}H_7(Thr)_2$ was calculated in different solvents and five different temperatures by using the same method and basis sets.

Results and Discussion:

$B_{10}N_{13}$ nanocone as a particular case was considered to attach to Threonin (Thr), trough B terminated atoms .The resulting BN nanocones were simulated by (BN) Thr containing 10 B atoms plus 13 N atoms, to investigate stability as well as thermodynamic properties. Except for some test cases we have used DFT B3LYP level of theory for geometry optimization of $B_{10}N_{11}H_7(Thr)_2$.We have prepared our system for MD and QMC simulations for four different temperatures. In each case we followed MD and QMC simulations and performed a series of the calculations under a constant temperature and environmental setup for QMC and MD respectively. Using DFT method, the computed energetic data as well as dipole moment for various solvent. The calculated Mulliken charge and the NMR parameters were computed with concentration on active sites.

Conclusion:

In summary, an analysis of the Molecular Dynamics , Quantum Monte Carlo and DFT B3LYP calculations on $B_{10}N_{11}H_7(Thr)_2$ nanocone have been performed. This is important to fully understand the geometrical specialty of $B_{10}N_{11}H_5(Thr)_2$ nanocone and the few other recently reported faceted nanocones, more favorable energetically and stability. With regard to biochemical phenomena, the results, illustrate a new picture of the BNNCs as a favorable candidate in biological system and drug delivery instead of the other nanocompounds.



References

- [1] B. I. Yakobson and R. E. Smalley, "Fullerene Nanotubes: C_{1,000,000} and Beyond." Am. Sci. 85, 324 (1997).
- [2] J. Depres, E. Daguerre, and K. Lafdi, "Flexibility of graphene layers in carbon nanotubes" "Carbon 33, 87 (1995).
- [3] Terauchi M, Tanaka M, Suzuki K, Ogino A, Kimura K "Production of zigzag-type BN nanotubes and BN cones by thermal annealing" (2000) Chem Phys Lett 324:359.



Effect of electrodeposition frequency on magnetic properties of $\text{Co}_{0.93}\text{Sn}_{0.07}$ nanowire arrays

M. Khorshidi^a, M. Najafi^b, A.A. Rafati^{a*}

^a Department of Physical Chemistry, Faculty of Chemistry, Bu-Ali Sina University, Hamedan, Iran

^b Department of Materials Engineering, Hamedan University of Technology, Hamedan, Iran.

Email: khorshidi.mona@gmail.com

Key words: Nanowire, Coercivity, Frequency, AAO template

Introduction:

Ordered nanowires have attracted increasing attention in recent years due to their utilization as high-density magnetic recording media. AAO template had been produced by electrochemical oxidation of alumina in the presence of an acidic medium and contains a hexagonally packed two-dimensional (2D) array of cylindrical pores with a uniform size using for preparing alloy nanowires [1]. Many attempts have been focused on the fabrication of alloy nanowires in order to improve the magnetic performances of the nanowires for practical application of these materials. In this work $\text{Co}_{0.93}\text{Sn}_{0.07}$ nanowires fabricating in different frequency were investigated and effect of variation frequency on magnetic properties and structure of nanowires was shown [2].

Materials and methods:

Ordered AAO template used in this research was prepared via a conventional two-step anodization process in sulfuric acid solution. The co-electrodeposition of 0.99 M Co^{2+} and 0.01 M Sn^{2+} ions in the AAO was performed by using standard double electrode bath and ac sine wave (30 V_{P-P}) at room temperature. The $\text{Co}_{0.93}\text{Sn}_{0.07}$ nanowires array was fabricated in different electrodeposition frequency including 50, 100, 200, 300, 400, 500 and 700 Hz. The magnetic properties of nanowires were measured by the alternating gradient force magnetometer (AGFM).

Result and discussion:

The effect of the electrodeposition frequency on magnetic properties of nanowires was investigated. Fig. 1 shows the H_c value for fabricated samples in varied electrodeposition frequency with sinuous form in pH=4 before and after annealing up to 575°C. Fig.2 illustrates the electrodeposition current density regarding the time for $\text{Co}_{0.93}\text{Sn}_{0.07}$ alloy nanowires fabricated in 200 and 700 (Hz). This curve demonstrated that due to increasing frequency, the amount of electrodeposited metals decreased, causing the Co^{2+} and Sn^{2+} to reduce with less stress in nanowire structures. Fig. 3 shows the hysteresis loops for $\text{Co}_{0.93}\text{Sn}_{0.07}$ nanowires with electrodeposition frequency about 200Hz and 700 Hz, respectively. The sample fabricated in 700 Hz of electrodeposition frequency has smaller hysteresis loop and bigger coercivity because the amount of electrodeposition metal decreased. The electrodeposition frequency which was higher than 700 Hz causes the amount of electrodeposition metals to reduce, and it did not have considerable magnetic properties.

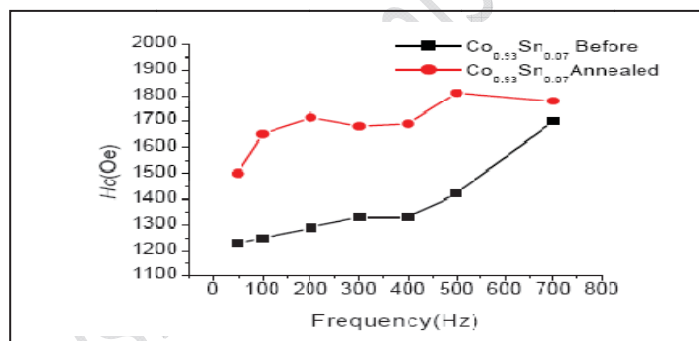


Fig. 1. The H_c value for alloy nanowire fabricating in different electrodeposition frequency before and after annealing up to 575 °C.

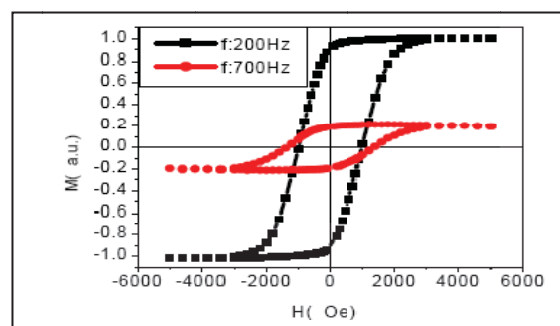
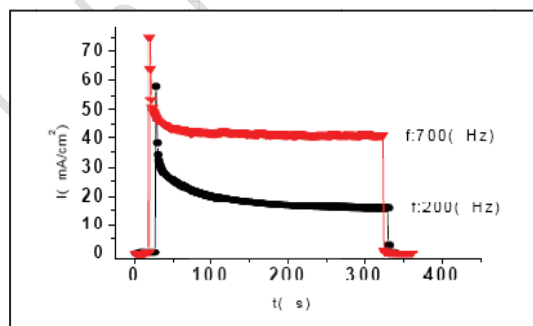


Fig. 2. The electrodeposition current density for alloy nanowires. **Fig. 3.** The normalized hysteresis loop for fabricating nanowires.



References:

- [1] W. Li and etal; Journal of Applied Physics, 97, 104306, 2005.
- [2] M. Koohbor and etal; Material Chemistry and. Physcs, 131, 728-734, 2012.

15th Physical Chemistry Conference



Optical and structural studying of Molybdenum-doped Vanadium oxide by sol-gel method

Amiri Asiabar, Maryam; Esmaili Ghodsi, Farhad

Department of physics, Faculty of sciences, Guilan University, Rasht, Iran

Email: feghods@guilan.ac.ir

Key words: Thin films, Sol-gel, Vanadium dioxide, Optical properties

Introduction:

Transition-metal oxides attract a large amount of attention because of their large variety of physical and chemical properties. Vanadium oxide thin films were identified as useful cathode materials for lithium-ion batteries due to its high capacity, high voltage and low cost. Sol-gel nano film may be appropriate because of its advantages such as high purity, simplicity of equipment and scalability. We report a facile synthesis of nano structured Vanadium oxide films by using Vanadium pentoxide and Ammonium heptamolybdate tetrahydrate powders. The aim of this work is to present a structural and optical study on Molybdenum doped Vanadium oxide thin films prepared by sol-gel dip coating rout. Structural, optical properties and molecular vibration modes were characterized by X-ray diffraction (XRD), UV-Visible, and Fourier transform infrared (FTIR) spectroscopy.

Materials and methods:

In this experiment 0.545 gr Vanadium pentoxide powder was dissolved in H₂O₂ (15%) under vigorous stir for 15 min. Then, the solution was heated in water bath. Ammonium heptamolybdate tetrahydrate powder was dissolved in a few drops of distilled water and added to the sol at 62 ° C in quantities calculated to achieve doping levels (assuming 100% substitution) 1 and 5 at.% of vanadium. A red brownish solution was formed after heat treatment in a water-bath at 70° c for 25 min. Molybdenum doped Vanadium oxide thin films deposited on the glass substrate by dip-coating technique and dried by IR dryer, then annealed at 400° C in air for 1h.

Apparatus:

Optical transmittance measurements were carried out at room temperature by using a Varian model Cary100 Scan UV–visible Spectrophotometer. The structure of the samples was determined by X-Ray diffraction (XRD) using a PW 1800 Philips diffractometer and Cu K α radiation. Fourier transform infrared spectrometer (FTIR, Bruker vector 33) operated in the range of 2.5–25 μm .

Result and discussion:

The XRD pattern of undoped and Mo-doped Vanadium oxide films is shown in Figure1. Figure 2 shows FT-IR spectroscopy. The bands at 815 cm^{-1} and 472 cm^{-1} describe the stretching of Mo-O-Mo and Mo-O respectively. The ranges of 1025 to 900 cm^{-1} are attributable to the stretching vibration of V-O bonds. A typical measured transmission spectrum of the 400° C treated films is shown in Figure 3. The thicknesses were 240, 245 and 130 nm for undoped, 1% and 5% Mo doped Vanadium oxide thin films, respectively.

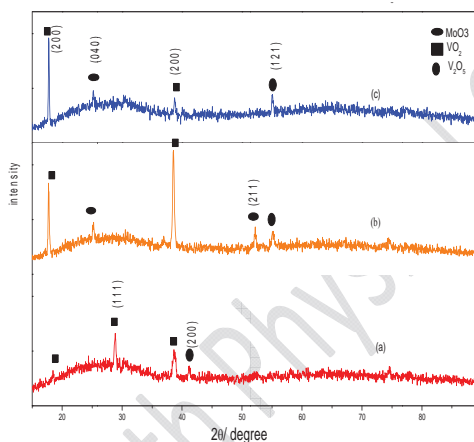


Figure1. typical XRD spectra of VO₂ films un doped (a) 1% (b) 5% (c)

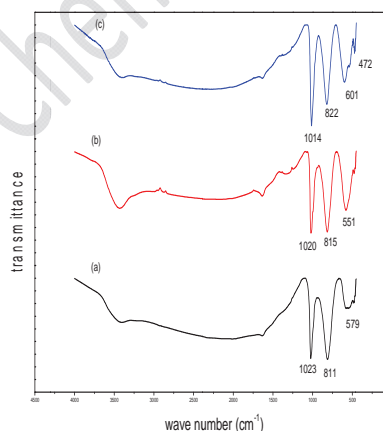


Figure2. FTIR spectra of (a) undoped (b) 1% (c) 5%

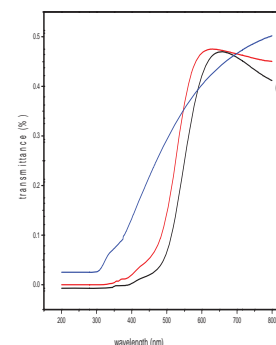


Figure3. Transmission spectrum of VO₂ thin films with un doped (a) 1% (b) and 5% (c)

Concusion:

A water-soluble molybdenum mixture added to the sol (derived from Vanadium pentoxide powder) to produce doped Vanadium oxide thin films on glass substrate. The transmittance was increased by adding dopant quantities in UV-visible spectra. A peak was appear at 472



cm⁻¹ in FT-IR spectra by adding 5% dopant. Relative peak intensity of the diffraction plane (200) at doped films are much higher when compared with the undoped Vanadium oxide film, showing fine oriented growth of Mo-doped Vanadium oxide film.

Reference:

- [1] T.J.Hanlon,J.A Coath,M.A.Richardson thin solid films 436(2003)269-272
- [2]M.Benmoussa,A.Outzourhit,R.Jourdani,A.Bennouna and E.L.Ameziane(2002)
- [3]L.Q.Mai, T.Hu, W.Chen and E.D.Gu 2006, *110*, 19083-19086



Adsorption of Crystal Violet Dye onto Carrageenan-Based Nanocomposites Adsorbent

K. Jalili¹, G.R. Mahdavinia²

¹ Department of Chemistry, Faculty of Science, Payam Noor University, Tehran, Iran

² Department of Chemistry, Faculty of Science, University of Maragheh, Maragheh, Iran

E-mail: jalili_463@yahoo.com

Keywords: Carrageenan, Nanocomposite, Crystal Violet, Adsorbent

Introduction:

Because of eco-friendly property of carrageenan with $-\text{SO}_3^-$ groups, we attempted to synthesize nanocomposite superabsorbents by introducing of this biopolymer. The current work describes the synthesis of crosslinked poly (sodium acrylate-co-acrylamide) in the presence of carrageenan biopolymer and sodium montmorillonite nanoclay. Adsorption process, an inexpensive and simple design, can be used to remove of dye contaminations from aquatic environments. In this work, we attempt to use carrageenan-based nanocomposite to remove cationic crystal violet.

Materials and Methods:

Na-MMt was dispersed into 30 mL of water and carrageenan was dissolved in clay solution under heating at 60 °C. Afterward, Neutralized acrylic acid an acrylamide monomers as well as MBA crosslinker was poured into solution and potassium persulfate initiator was added. After superabsorbent formation, it was dried. The dried samples were immersed into dye solution to adsorption kinetic.

Results and Discussion:

At first, we attempt to investigate the XRD patterns of nanocomposites by varying the clay content and the results are illustrated in Figure 1. By altering the clay content up to 10wt%

(Figure 1b and c), no distinct diffraction peak was appeared in the XRD patterns and it can be concluded that the clay layers are completely exfoliated. But, when the clay content was 14 wt% (Figure 1d), a diffractive peak was observed at $2\theta = 4.3$ and revealed that the nanoclay dispersion is in intercalated form.

According to Figure 2, the clarity of solution after adsorption confirms the adsorption of dye by carrageenan nanocomposites. The influences of the clay content on dye adsorption speed of nanocomposites are shown in Figure 3. As it is clear from figure, the clay content can affect the rate of the dye adsorption onto nanocomposites. In fact, inclusion of Na-MMt nanoclay into carrageenan-based hydrogel caused an enhancement in dye adsorption speed.

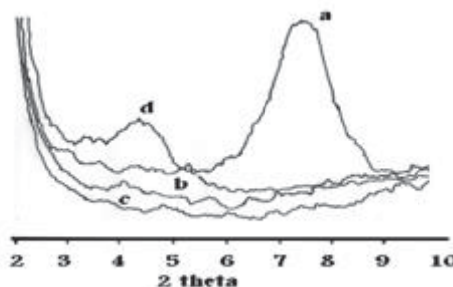


Figure 1: XRD profiles of (a) pristine clay and nanocomposites containing (b) 5, (c) 10, (d) 14 wt% of Na-MMt.



Figure 2: The Crystal violet solution before (left) and after adsorption (right).

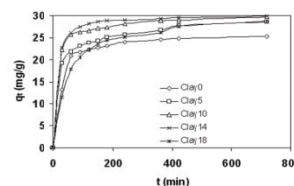


Figure 3: Dye adsorption speed of nanocomposites as a function of clay content

Conclusions:

-The XRD patterns showed that the clay dispersion type is depended on clay content. While at low content of clay, the exfoliation takes place, at high content of clay, the dispersion type is intercalation.



-The effect of Na-MMt nanoclay on dye adsorption indicated that by increasing the clay content, the dye adsorption rate and content is increased.

References:

- [1] K. Haraguchi, *Nanocomposite hydrogels*, Curr. Opin. Solid St. M., **11** (2007) 47.
- [2] E. Karadag, D. Saraydin, O. Guven, Removal of some cationic dyes from aquatic solutions by acrylamide/itaconic acid hydrogels, Water, Air, and Soil Poll., **106** (1998) 369.
- [3] P. Liu, L. Zhang, Adsorption of dyes from aqueous solutions or suspensions with clay nano-adsorbents, Sep. Purif. Technol., **58** (2007) 32.



Synthesis and Study of Nanostructural Properties of $\text{ZrO}_2\text{-CrO}_2$ Composite

M.Ghanbari^{a*}, N.Aghaeenejad^b

^aDepartment of Physics, Islamic Azad University, Shirgah Branch, Shirgah, Iran.

^bDepartment of Physics, Science and Research Branch, Islamic Azad University, Mazandaran, Iran.

E-mail: M.Ghanbaritilemi@yahoo.com

Keywords: Nanocrystalline, Ceramic composite, gate dielectric, Sol-gel method.

Introduction:

Some issues such as tunneling, leakage current and light atom penetration through the film are threatening the ultra thin SiO_2 be as a good dielectric for future industrial and electronic devices. The gate SiO_2 dielectric thickness in current complementary metal oxide semiconductor (CMOS) transistors is less than 1 nm. Such a thin gate dielectric can not prevent leakage, tunneling currents and borondiffusion. We have thus needed electrical permittivity insulators as the alternative gate dielectrics for future of CMOS devices. The $\text{ZrO}_2\text{-CrO}_2$ gate stacks with high electrical permittivity show an amorphous structure of low temperature which can fill this gap. Zirconium oxide is a very interesting material because of its thermal stability, its mechanical properties and its basic, acidic, reducing, and oxidizing surface properties. Pure zirconia has three allotropic forms monoclinic, tetragonal and cubic. Eventhough the phase boundaries are not exactly known yet as a function of temperature, many people have reported the temperature range of these phase boundaries. In this work, we have synthesized $\text{ZrO}_2\text{-CrO}_2$ which is suitable for CMOS. Its crystalline phase can be used for the potential applications of the ceramic – mesoporous structures as well[1].

Experimental procedure and details:

The $\text{ZrO}_2\text{-CrO}_2$ was prepared by adding 1M aqueous ammonia (Merk,25%) slowly into a mixed 0.1M aqueous solution of Chromium chloride (Merk \geq 99) and 0.1M Zirconium oxy-

chloride ($\text{Merk} \geq 99$) at room temperature with stirring until the PH reached 8. after 72h gelation was formed. The gel thus obtained was washed thoroughly with distilled water until chloride ion was not detected, and then was dried at 80°C for 10 h in oven and calcined at $5^\circ\text{C}/\text{min}$ to four different temperature (300 and 500°C) for 2h.

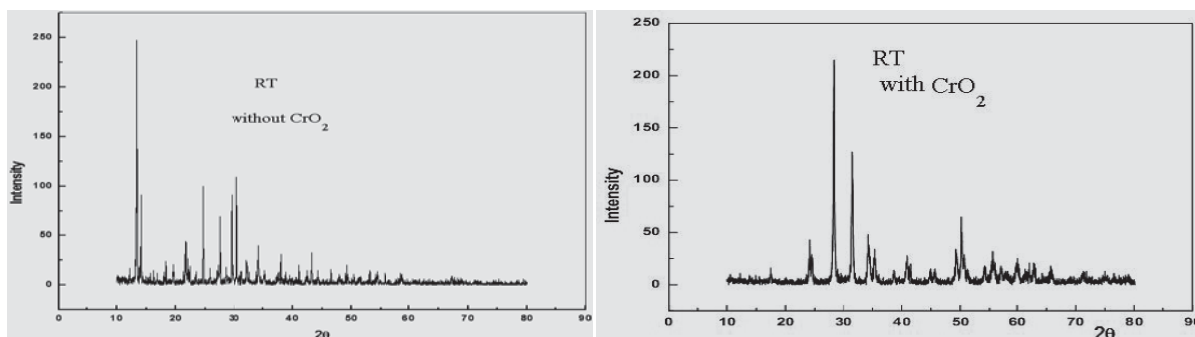


Figure 1: The XRD pattern of nanoparticles at RT without CrO_2 (Left) and with CrO_2 (Right)

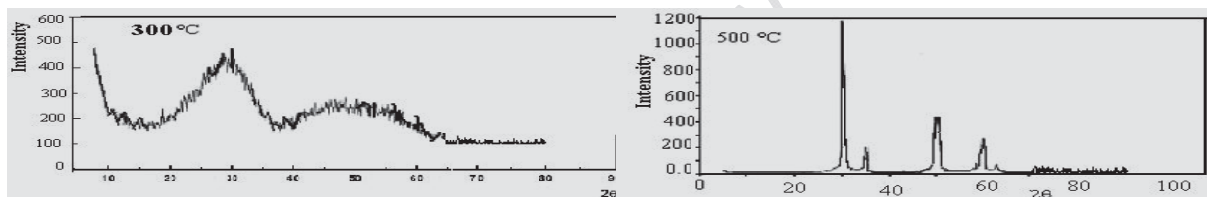


Figure 2: The XRD pattern of composite at 300°C and 500°C (50% wt ZrO_2 and 50% wt CrO_2)

Result and Discussion:

Figure 1(Left) show XRD patterns of ZrO_2 without CrO_2 . As one can see peaks at 13° , 24° , 29° , 31° and 44° attributed to the (111), (200), (220) and (311) diffraction planes of the tetragonal zirconia, and some monoclinic zirconia peak at $50^\circ - 80^\circ$. Figure 1(Right) displays the XRD pattern ZrO_2 with CrO_2 (The presence of CrO_2 (50wt%) in ZrO_2). The new peaks in comparison to figure 1(Left), attributed to CrO_2 phases. Phase beside of monoclinic, tetragonal of ZrO_2 and cubic forms of CrO_2 phase are stabilized. The size of nanoparticles is 42 nm as found with using X- Powder method. The amorphous structure is obtained at 300°C which can be used for gate dielectric of nano electronic devices. This amorphous structure has become to nano crystalline structure with heating the sample (As an example see figure 2, $T = 500^\circ\text{C}$). also, morphology of amorphous and crystalline structures is obtained by atomic force

microscopy and shown in figure 3 (a and b). There is a tendency to crystallization with increasing temperature in the figure 3(b).

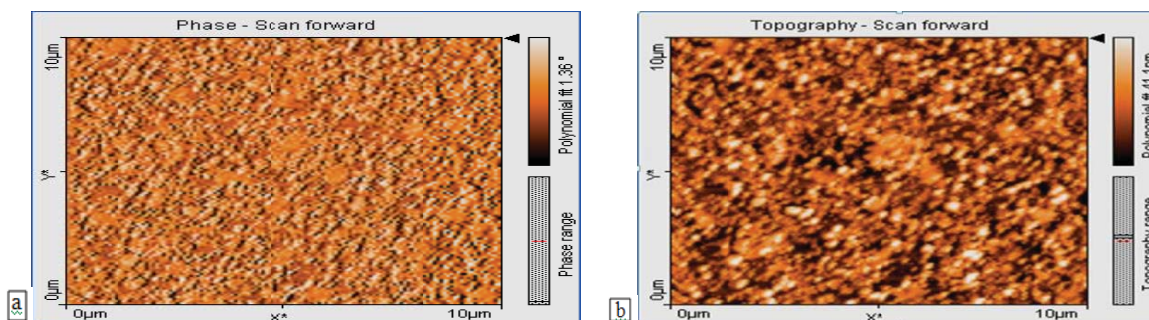


Figure 3: AFM topography images (2D) of the $\text{ZrO}_2\text{-CrO}_2$ in different magnifications. a: (300°C), b: (500°C).

Conclusion:

The amorphous structure is obtained at 300°C which can be used for gate dielectric of nano electronic devices. This amorphous structure has become to nano crystalline structure at higher temperature $T \geq 500^\circ\text{C}$ (As an example see figure 2, $T = 500^\circ\text{C}$). Moreover uniform structure is formed at 300°C in that films become dense and have a fine amorphous structure.

This point makes this compound to be a suitable candidate for the next CMOS devices. Figure 3 displays the surface morphologies of the $\text{ZrO}_2\text{-CrO}_2$, resulting from AFM characterization. In addition, XRD patterns show a broadening peak at 500°C (respect to room temperature) indicated the bigger size of the crystallites in the growth direction.

References:

- [1] A. Bahari, P. Morgen, K. Pederson, Z. Li, "Growth of a stacked silicon nitride / silicon oxide dielectric on Si (100)", J. Vac. Sci. and Technol B, 24(2006)2119.



Sorption processes of heavy metals by natural and modified bentonite using nano particles

H. Merrikhpour^{a*}, M. Jalali^a

^a Department of Soil Science, College of Agriculture, Bu-Ali Sina University, Hamadan, Iran.

E-mail: h.merrikhpour@basu.ac.ir

Key words: Adsorption; Bentonite; Modify; Nano particle.

Introduction:

Recently, the usage of natural mineral adsorbents for wastewater treatment is increasing due to their abundance and low price. One type of clay minerals is bentonite, the main component of which is montmorillonite. Its high specific surface area and cation exchange capacity makes bentonite a useful clay mineral for the decontamination of heavy metal ions [1]. Special treatment-modification cause bentonite is rendered a better adsorbent material [2]. Treatment by inorganic acids and saturation of montmorillonite by cations is the method most widely used to modify the sorptive properties of bentonite clays [3]. Simple ion-exchange reactions can significantly modify the surface properties of natural bentonite. Then the saturated bentonite with special cation (Na^+) can be replaced by nano particles.

This study aimed to investigate and comparative the sorption properties of natural Iranian bentonite, and modified bentonite with nano particles (TiO_2 , Al_2O_3), including, their removal efficiency, the sorption isotherms and the effect of the initial solution pH with Cd^{2+} , Cu^{2+} and Ni^{2+} on adsorption.

Materials and Methods:

The natural bentonite (Bent) was converted to sodium bentonite (Na-Bent). Then the modified bentonite with nano particles (Bent- TiO_2 and Bent- Al_2O_3) was synthesized by mixing the appropriate amount of nano TiO_2 and Al_2O_3 with the powder form of Na-Bent at room



temperature. The mixtures were dried at 323 K. This was followed by heating the solid material at 403K for 12 h. Finally the solid was calcined at 673K for 3 h [4]. The crystallinity and phase identification of the adsorbent were determined using X-ray diffractometry (XRD). Batch adsorption experiments were conducted with 25 mL solutions containing heavy metal ions at the desired concentrations (50 mg l^{-1}) with 0.05 g of Bent, Bent-TiO₂ and Bent-Al₂O₃, while the pH ranged from 2 to 7. In adsorption isotherms Bent, Bent-TiO₂ and Bent-Al₂O₃ were allowed to equilibrate with solutions of Cd²⁺, Cu²⁺ and Ni²⁺ of known initial concentrations ($25\text{--}600 \text{ mg L}^{-1}$). The metal concentrations in the supernatant were measured using a Varian model 220 atomic absorption spectrometer.

Results and discussion:

Because of the importance of pH on ion adsorption the dependence of Cd²⁺, Cu²⁺ and Ni²⁺ uptake on aqueous pH was studied. In all samples the uptake efficiency increased abruptly as the pH increased from 2 to 3, before increasing gradually as the pH reached 5, while the adsorption performance was almost unchanged above pH 5 where it reached a plateau.

The sorption capacity is a measure of the maximum sorption capacity that corresponds to laboratory measurements. Bentonite had a mass sorption capacity for Cd²⁺ (22.5 mg g^{-1}), Ni²⁺ (19.2 mg g^{-1}), and Cu²⁺ (17.1 mg g^{-1}). The sorption capacity for two kind of modified bentonit was greater than Ben. Ben-TiO₂ has more efficiency in all Cd²⁺ (73 mg g^{-1}), Cu²⁺ (49.4 mg g^{-1}), and Ni²⁺ (27 mg g^{-1}) adsorption capacity.

Conclusion:

In the present study, the heavy metal exchange on natural Iranian and modified bentonite was evaluated using batch systems. The modified bentonite with nano particles was highly efficient in heavy metal removal. Equilibrium studies showed that the sorption capacity for Ben-TiO₂ > Ben-Al₂O₃ > Ben for Cd²⁺, Cu²⁺ and Ni²⁺.

References:



- [1] O. Abollino et al.; “Adsorption of heavy metals on Na-montmorillonite: effect of pH and organic substances”; *Water Research*; 37,1619–1627,2003.
- [2] L. Calarge et al.; “The smectitic minerals in a bentonite deposit from Melo”; *Clay Mineral*; 38,2003.
- [3] F.R. Valenzuela et al.; “Studies on the acid activation of Brazilian smectitic clays”; *Quimica Nova*; 24,345–353,2001.
- [4] E. Amereh et al.; “Photodegradation of acetophenone and toluene in water by nano-TiO₂ powder supported on NaX zeolite”; *Materials Chemistry and Physics*; 120,356–360,2010.



On the thermal conductivity in methane-propane binary mixture in nanochannels: A non-equilibrium molecular dynamics approach

M. PourAli* and A. Maghari

Department of Physical Chemistry, University of Tehran, Tehran, Iran

Email: mpourali@khayam.ut.ac.ir

Keywords: Alkane mixture, Nanochannel, Non-Equilibrium MD, Thermal conductivity;

Introduction:

When a fluid mixture is placed in a thermal gradient, one observes a separation of the components in the mixture. This separation leads to a mole fraction gradient parallel to the thermal gradient. The phenomenological description of this situation can be made by irreversible thermodynamics [1]

$$J_q = -L_{qq} \frac{\nabla T}{T^2} - L_{q1} \frac{\nabla(\mu_1 - \mu_2)}{T}, \quad J_1 = -L_{1q} \frac{\nabla T}{T^2} - L_{11} \frac{\nabla(\mu_1 - \mu_2)}{T}$$

Where J_q and J_1 are the heat flux and diffusive molar flux of component 1, respectively, T is the temperature, μ the chemical potential and $L_{\alpha\beta}$ are the phenomenological coefficients. Throughout recent two decades, several authors have attempted to compute transport coefficients using molecular dynamics methods in multi-component systems (for review see [1]), whereas few works on thermal transport phenomena in confined media, the highly inhomogeneity of these system make such studies more difficult. In this work we have studied thermal conductivity in methane-propane binary mixtures in $8\sigma_{CH_4}$ channel by NEMD simulation.

Nemd approach:

Temperature gradient is imposed by two stochastic walls in different temperature in z direction. The thermal conductivity is the ratio of the rate of heat (kinetic energy) transfer across the system to the temperature gradient [1, 2],

$$\lambda = \frac{\Delta E_K^{in} + \Delta E_K^{out}}{2t_m A \Delta T / L_z}$$

3214

where t_m is the measurement interval, $A = L_x L_y$ is cross section. Channel is two atomic walls in x direction. Intermolecular interaction is given by the truncated Lennard–Jones potential. Bond lengths are constraint to their mean value using the SHAKE algorithm. The equations of motion are solved using the *leapfrog* algorithm with a time step of 0.002 ps. cut-off radius, r_c , is $2.5\sigma_{CH_4}$. T is 250K, $\Delta T = 150K$ and density $0.3kgm^{-3}$.

Results and Discussion:

Fig.1 show temperature and density profiles for each component in z direction in $x_{CH_4} = 0.7$. Thermal conductivities of each component and thermal conductivity of mixture in both nanochannel and bulk region at different x_{CH_4} are represented in Fig2

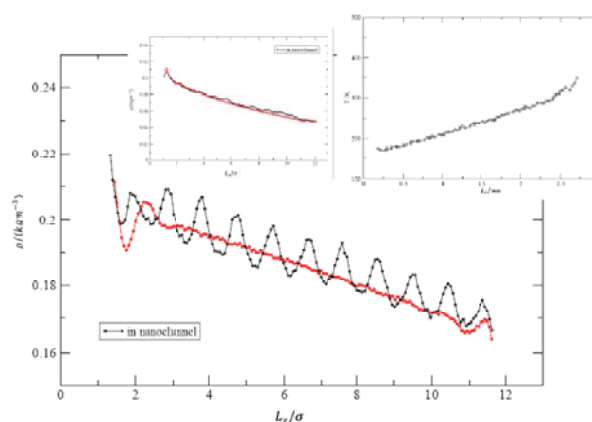


Fig.1 ρ_{CH_4} profile(main). above left is $\rho_{propane}$ profile and above right is T profile in z direction and $x_{CH_4} = 0.7$

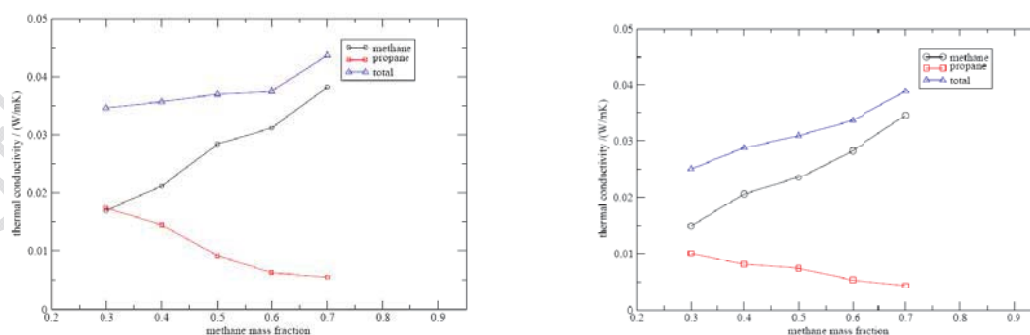


Fig2. Thermal conductivity of mixture at different x_{CH_4} for each component and thermal conductivity of mixture in nanochannel and bulk region. Left is mixture in nanochannel and right in bulk.



Conclusion:

Simulation results show that thermal conductivity in methane-propane mixture in nanochannel is higher than the same bulk mixtures. It seems walls induce inhomogeneity or layering in mixtures, especially, in lighter component and this layering causes an increase in thermal conductivity.

References:

- [1] *Thermal Nonequilibrium Phenomena in Fluid Mixtures*, Lecture Notes in Physics Vol. 584, edited by W. Köhler and S. Wiegand (Springer, Verlag, 2002)
- [2] Rappaport, D. C., 2004, *The Art of Molecular Dynamics Simulation*, 2nd ed. (Cambridge University Press).



Studying the dispersion stability of surface treated nano silica particles in a UV-curable matrix

Y.Zamani Ketek Lahijani^a, M.Mohseni ^{a*}, S.Bastani^b

^a Amirkabir University of Technology, Department of Polymer Engineering and Color Technology, Tehran, Iran

^b Department of Surface Coatings and Corrosion. Institute for Colorants, Paint and Coatings (ICPC), Tehran, Iran

Email: mmohseni@aut.ac.ir

Key words: Nano silica, Surface modification, Methacrylic Silane, Surface chemistry

Introduction:

Organic-inorganic nanocomposite coatings can be synthesized by mixing nanoparticles and organic compounds. Inorganic nano particles such as SiO₂, TiO₂, ZnO and CaCO₃ are the most commonly used nanoparticles which can improve the polymer performance. Nano silica has high hardness and can be used for the enhancement of the scratch and abrasion resistance of the coatings [1]. On the other hand, because of its low refractive index, the transparency would not be affected. Silica has polar characteristic and its surface has been covered by silanol groups. These hydrophilic groups tend to adhere to each other by hydrogen bonding and form agglomerations through the whole of polymer matrix [2,3]. In order to change nanosilica surface from hydrophilic to hydrophobic, and to have a better dispersion of nanosilica in a non polar media, surface modification using methacrylic silane coupling agent has been studied. There are many factors affecting the surface treatment reaction, including hydrolysis ratio, bath treating pH, silane to silica concentration, pre-treatment method, treatment time and temperature [4]. According to the other researches, the three first affecting factors have been investigated in this work.

Materials and methods:

A Taguchi design of experiment was utilized to statistically analyze the data and optimize the treatment processing (three affecting factors with three levels). Hence, the numbers of the experiments were decreased using Tagouchi DOE from 27 to 9. To further study, a UV-curable urethane acrylate resin was chosen to formulate a nanocomposite filled with UnT and treated particles, to evaluate the compatibility and dispersion behavior of treated particles in the resin matrix. A mixture of de-ionized (DI) water and absolute ethanol was used as the medium for silica powder treatment, and the



hydrochloric acid/acetic acid/caustic soda were used to adjust the pH. Methacryloxypropyltrimethoxy silane was poured drop-wise at the rate of 0.5 g/min. A mechanical homogenizer (IKA) was used for all samples at 19000 rpm. Finally, the coating formulation was prepared by combining organic phase (UV curable Tri functional urethane acrylate) with various amount of UnT or MPTMS treated nano silica particles.

Apparatus:

pH of each powder in the mixture of ethanol and water was determined according to ISO-787-9 standard. Apparent densities of the synthesized particles were measured using a helium pycnometer. Elemental analysis for carbon, hydrogen and nitrogen content on the modified and unmodified silica samples was employed according to ASTM-D5291. Turbidity of dispersed silica powders in the ethanol solvent was determined using a HACH 2100 AN Turbidimeter. Moreover, the absorbance spectra of the prepared coatings at 5 nm scan intervals was measured in the range of 250-800 nm by the aid of a UV-vis spectrophotometer. TEM measurement was performed to obtain information about the morphology of the hybrid material.

Result and discussion:

The results indicated that the silane/silica concentration and alkaline pH had a strong effect on the grafting of silane on the silica surface. From the measurements of pH, it was revealed that, the pH of particles changed from 3.8 for pristine silica to 4.9 and 6.9 for the lowest and the highest grafted particles respectively. Based on the elemental analysis, the carbon content of treated silica in different condition of experiments varied between 1.2 and 7.8. Nephelometric turbidity unit measurements of the suspensions conducted in a polar solvent showed that, after treatment reaction the dispersion stability of particles was varied. Also, it is concluded that the coatings including hydrophilic nano silica particles demonstrated better improvements in the UV-absorbent properties. The high transmission behavior indicated the presence of a nanoscale hybrid composite as is confirmed by TEM measurements.

Conclusion:

The purpose of this work was to study the surface chemistry of the modified silica using methacryloxypropyltrimethoxysilane. The results indicated that silane concentration had a strong



effect on the grafting of silane on the nano silica surface. The coatings containing hydrophobic nano-silica showed better improvements in the physical and morphological properties.

Reference:

- [1] S. Sepur et al; "UV curable hard coatings on plastics"; Thin Solid Films; 351, 216-219, 1999
- [2] M. Q. Zhang et al; "Effect of particle surface treatment on the tribological performance of epoxy based nanocomposites"; Wear; 253,1086-1093,2002.
- [3] T. Jesinowski et al; "Preparation of the hydrophilic/hydrophobic silica particles"; Colloids and Colloids and Surfaces A: Physicochemical and Engineering Aspects; 207, 58-49,2002.
- [4] M. Rostami et al; "Investigating the effect of pH on the surface chemistry of an amino silane treated nano silica"; Pigment & Resin Technology; 40, 363-373,2010.



Comparison of efficient removal of methyl orange and sunset yellow with Gold nanoparticle loaded on Activated Carbon: Kinetic and Isotherm study of removal process

F. Mohammadi^{a*}, M. Ghaedi^b

^a Department of chemistry, Azad university ghachsaran, Ghachsaran , Iran

^b Department of chemistry, Yasouj university, Yasouj, Iran

Email: fati.m6132@yahoo.com

Key words: Sunset yellow, Methyl orange, Gold, Kinetic.

Introduction:

Dyes are extensively used in textiles, paper, rubber, plastics, leather, cosmetics, pharmaceuticals and food industries, resulting in a steadily growing demand and production. With the increasing use of dyes, pollution from dye wastewater is becoming a serious environmental problem. A number of promising techniques have been established for elimination of heavy metals and dyes from contaminated waters. Adsorption appears to offer the best advantages, although the chemical degradation and the biodegradation approaches also find applications. The nanoparticles have very interesting physicochemical properties, such as ordered structure with high aspect ratio, ultra-light weight, high mechanical strength, electrical and thermal conductivity, and high specific surface area. They have unsaturated atoms on their surfaces, hence, they can bind readily most of the other atoms. The objective of this study was to compare the efficiency of gold nanoparticle loaded on activated carbon (Au-NP-AC) for the removal of methyl orange (MO) molecules and sunset yellow (SY) from aqueous solutions. For obtaining maximum dye removal the effect of significant parameters such as pH, concentration of MO and SY, amount of AU-AC, contact time and on removal percentage of these dyes in batch method by one at a time optimization method has been investigated [1-3].



Materials and methods:

Stock MO and SY solutions were prepared by dissolving their accurately weighted amount in double distilled water and the test solutions were prepared by diluting stock solution. All chemicals including NaOH, HCl, MO, SY and activated carbon (AC) with the highest purity available are purchased from Merck, Darmstadt, Germany. The effect of variables such as pH, amount of adsorbent, contact time, initial dye concentration and temperature on the adsorptive removal of MO and SY was investigated. The removal percentage was calculated using the following relationship: $\% \text{ removal} = ((C_0 - C_t)/C_0) \times 100$

Where C_0 (mg.L^{-1}) and C_t (mg.L^{-1}) is the dye concentration at initial and after time respectively.

Apparatus:

During this study following pH optimization in all experiments, the MO concentration was determined at 507 nm and the SY concentration was determined at 412.5 nm against a reagent blank. The pH measurements were done using pH/Ion meter model-686 (Metrohm) and absorption studies were carried out using Jasco UV-Visible spectrophotometer model 160-shimadzu.

Result and discussion:

In this work dye elimination on series of similar solution with 50 ml volume in concentration of 15 mg.L^{-1} MO and 20 mg.L^{-1} SY in the various pH from 1 to 8 was investigated and showed that in pH=2, there is maximum percent of dyes elimination. Synthetic studies to determine dye absorption efficiency in optimum values namely solution with concentration of 15 mg.L^{-1} MO in pH=2 in the 10 min with 0.005 g adsorbent and 20 mg.L^{-1} SY in pH=2 in the 10 min with 0.01 g adsorbent with Elovich synthetic models and intra particle diffusion was investigated and observed that dyes absorption follows two-order synthetic. Investigation of adsorption isotherms carried out in a few different concentration in 30 min with optimal



condition of another parameters, and showed that dyes absorption follow by langmuir isotherm.

Conclusion:

The Gold nanoparticles loaded on active carbon have been synthesized and characterized with SEM, Then these new adsorbent has been applied for removal of MO and SY. It was observed that batch sorption using Au-NP-AC was dependent on parameters such as initial concentration of dye, time, pH, dose of adsorbent and type of dye. Analysis of experimental data for the Langmuir, Freundlich and Tempkin isotherms were determined and the Langmuir model best described the equilibrium data. The kinetics process is can be successfully fitted to second-order. Therefore Gold nanoparticle loaded on activated carbon is the better adsorbent for MO than SY.

Reference:

- [1] Z. Aksu, E. Kabasakal, Sep. Purif. Technol. 57 (2003) 1.
- [2] D. Kavitha, C. Namasivayam, Chem. Eng. J. 139 (2008) 453.
- [3] M.G. Neelavannan, C. Ahmed Basha, Toxicol. Environ. Chem. 92 (2010) 1423.



Removal of sunset yellow from aqueous solution on activated carbon prepared from wood of tamarik tree: kinetics and isotherm study

F. Mohammadi^{a*}, M. Ghaedi^b

^a Department of Chemistry, Azad University Ghachsaran, Ghachsaran, Iran

^b Department of Chemistry, Yasouj university, yasouj, iran

Email: fati.m6132@yahoo.com

Key words: Tamarik tree, Sunset yellow, Kinetic, Isotherm

Introduction:

Most of the dyes are resistant to be decolorized by chemicals, heat, and light due to their complex chemical structures. Therefore, the biodegradation of dyes is a typically slow and undesired process. There are several methods available for color removal from waters and wastewaters such as membrane separation, aerobic and anaerobic degradation using various microorganisms, chemical oxidation, coagulation and flocculation, and reverse osmosis. This study investigates the potential use of activated carbon prepared from the tamarik tree for the removal of sunset yellow dye from simulated wastewater. The effects of different system variables, adsorbent dosage, initial dye concentration, pH, sieve size of adsorbent and contact time were investigated and optimal experimental conditions were ascertained. Sunset yellow contents and its removal percentage were determined using a UV-Vis spectrophotometer before and after adsorption. The results showed that as the amount of the adsorbent increased, the percentage of dye removal increased accordingly. The kinetic studies suggest the process following pseudo second order kinetics and involvement of particle diffusion mechanism. The adsorption data at equilibrium was evaluated and fitted by different isotherm models like Langmuir, Freundlich and Tempkin to evaluate the ongoing adsorption process [1-3].

Materials and methods:

All chemicals including NaOH, HCl, KCl, Sunset yellow and AC with the highest purity available are purchased from Merck. Stock Sunset yellow solution was prepared by dissolving



its accurately weighted amount in double distilled water and the test solutions were prepared by diluting stock solution. The removal percentage of Sunset yellow was calculated using the following relationship:

$$\% \text{ removal} = ((C_0 - C_t)/C_0) \times 100$$

Where C_0 (mg.L^{-1}) and C_t (mg.L^{-1}) is the dye concentration at initial and after time t respectively.

Apparatus:

During this study following pH optimization in all experiments, the Sunset yellow concentration was determined at 412.5 nm against a reagent blank. The pH measurements were done using pH/Ion meter model-686 (Metrohm) and absorption studies were carried out using Jusco UV-Visible spectrophotometer model 160-shimadzo.

Result and discussion:

in this work dye elimination on series of similar solution with 50 ml volume in concentration of 10 mg.L^{-1} in the various pH from 1 to 8 was investigated and showed that in $\text{pH}=1$, there is maximum percent of dye elimination. synthetic studies to determinate dye absorption efficiency in optimum values namely solution with concentration of 10 mg.L^{-1} in $\text{pH}=1$ in the 10 time with 0.75 gr adsorbent with elovich synthetic models and inter particle diffusion was investigated and observed that dye absorption follows two-order synthetic. investigation of adsorption isotherms carried out in a few different concentration in 60 min with optimal condition of another parameters, and showed that dye absorption follow by langmuir isotherm.

Conclusion:

active carbon prepared from the wood of tamarik tree is identified to be an effective adsorbent for the removal of Sunset yellow from aqueous solution. it was observed that bath sorption using active carbon prepared from the wood of tamarik tree was dependent on parameters such as initial concentration of dye, time, pH, amount of adsorbent and type of dye. Analysis of experimental data for the Langmuir, Freundlich and Temkin isotherms were determined and



the equilibrium data were best described by the Langmuir model. The kinetics process is can be successfully fitted to pseudo-second-order kinetic model respectively.

Reference:

- [1] Y. Zheng, S. Gao, J.Y. Ying, Adv. Mater. 19 (2007) 376.
- [2] E. Demirbas, M. Koby, M.T. Sulak, Bioresour. Technol. 99 (2008) 5368.
- [3] D. Kavitha, C. Namasivayam, Chem. Eng. J. 139 (2008) 453.

15th Physical Chemistry Conference



Zinc hydroxide nanoparticles loaded on activated carbon as adsorbent for removal of sunset yellow: kinetics and isotherm study

E. Negintaji^{a*}, M. Ghaedi^b

^a Department of chemistry, Azad university ghachsaran, Ghachsaran, Iran

^b Department of chemistry, Yasouj university, Yasouj, Iran

Email: esmat_negin@yahoo.com

Key words: Sunset yellow, Zinc hydroxide, Isotherm, Kinetic.

Introduction:

Various process industries such as textile, pulp and paper producing factories, dyeing plants, paint and ink producers use huge quantities of dyes. Decolorization of dye-containing waste waters is difficult since dyes are stable and resistant to light. For these reasons, it is necessary to find simple and inexpensive procedures for dye removal from industrial colored waste waters. Moreover, the presence of dyes in water poses aesthetic problems and may cause serious ecological problems including loss of photosynthetic activity of aquatic plants by reduced light penetration. Adsorption is one of the common and efficient waste water treatment techniques, which is based on transfer of solute molecules onto an active adsorbent surface. The adsorption is superior to other dye removal techniques in terms of initial cost, simplicity of design, and easiness of operation. Nanomaterials are becoming important owing to their special physical and chemical properties. The size, surface structure and interparticle interaction of nanomaterials concur on their unique properties and make their potential application in many areas. In order to increase the surface area of adsorbent, nanoparticles based adsorbent was selected for the dye adsorption [1-3].

Materials and methods:

The influence of variables including pH, adsorbent dosage and etc on the adsorptive removal of Sunset yellow was investigated by batch experiments. All chemicals including NaOH, HCl,



KCL, SY and activated carbon (AC) with the highest purity available are purchased from Merck, Darmstadt, Germany. Stock SY solution was prepared by dissolving its accurately weighted amount in double distilled water and the test solutions were prepared by diluting stock solution. The removal percentage of SY was calculated using the following relationship:
$$\% \text{ SY removal} = ((1 - A)/A_0) \times 100$$

Where A_0 and A is the dye Adsorption at initial and after time respectively.

Apparatus:

During this study following pH optimization in all experiments, the SY concentration was determined at 412 nm against a reagent blank. The pH measurements were done using pH/Ion meter model-686 (Metrohm) and absorption studies were carried out using Jusco UV-Visible spectrophotometer model 160-shimadzu.

Result and discussion:

in this study, dye elimination on series of similar solution with 50 ml volume in concentration of 20 mg.l^{-1} in the various pH from 1 to 9 was investigated and showed that in pH=2, there is maximum percent of dye elimination. synthetic studies to determinate dye absorption efficiency in optimum values namely solution with concentration of 20 mg.l^{-1} in pH=2 in the 10 min with 0.01 gr adsorbent with elovich synthetic models and inter particle diffusion was investigated and observed that dye absorption follows two-order synthetic. investigation of adsorption isotherms carried out in a few different concentration in 30 min with optimal condition of another parameters, and showed that dye absorption follow by langmuir isotherm.

Conclusion:

The copper sulfide nanoparticles loaded on active carbon have been synthesized and characterized with SEM, and then these new adsorbents have been applied for removal of SY. It was observed that batch sorption using $\text{ZN(OH)}_2\text{-NP-AC}$ were dependent on parameters such as initial concentration of dye, time, pH, dose of adsorbent. Analysis of experimental data



for the Langmuir, Freundlich and Temkin isotherms were determined and the equilibrium data were best described by the Langmuir model.

Reference:

- [1] Y. Zheng, S. Gao, J.Y. Ying, *Adv. Mater.* 19 (2007) 376.
- [2] E. Demirbas, M. Kobya, M.T. Sulak, *Bioresour. Technol.* 99 (2008) 5368.
- [3] D. Kavitha, C. Namasivayam, *Chem. Eng. J.* 139 (2008) 453



Characterization of Zinc oxide nanoparticle loaded on activated carbon and their efficient application for removal of murexide from aqueous solution

Z. Babaei^{a*}, M. Ghaedi^b

^a Department of chemistry, Azad university ghachsaran, Ghachsaran, Iran

^b Department of chemistry, Yasouj university, Yasouj, Iran

Email: babaei.zohre@gmail.com

Key words: Murexide, Zinc oxide, Nanoparticles, Removal.

Introduction:

Use of dyes by many industries, such as textile, paper and plastics to color their products is a common activity. Since these industries also use substantial amount of water in their processes, this results in highly colored effluent of these industries which is generally colored due to the presence of these organic chemicals. Since synthetic dyes have good solubility in water, they may frequently be found in trace quantities in industrial wastewater. Most commercial dyes are chemically stable and are difficult to be removed from wastewater. nanoparticles have very interesting physicochemical properties, such as ordered structure with high aspect ratio, ultra-light weight, high mechanical strength, high electrical conductivity, high thermal conductivity, metallic or semi-metallic behavior and high surface area. The objective of the present work is synthesis, characterization of Zinc oxide nano particle loaded on activated carbon (ZnONP-AC) as new adsorbents and its efficient applications for removal of Murexide following the optimization of variables the kinetic, thermodynamic and isotherm studied of adsorption process has been investigated, and respective values were calculated [1-3].

Materials and methods:

All chemicals including NaOH, HCl, Murexide and activated carbon (AC) with the highest purity available are purchased from Merck, Darmstadt, Germany. Stock Murexide solution



was prepared by dissolving its accurately weighted amount in double distilled water and the test solutions were prepared by diluting stock solution. The effect of variables such as pH, amount of adsorbent, contact time, initial dye concentration and temperature on the adsorptive removal of Muroxide was investigated. The obtained experimental data at various times and concentrations were fitted to different models to calculate and the kinetics and isotherm parameters of adsorption process at optimum values of all variables were investigated.

Apparatus:

During this study following pH optimization in all experiments, The pH of sample solution was adjusted by addition of HCl or NaOH using a pH/Ion meter model-686 (Metrohm) and absorption studies were carried out using Jusco UV-Visible spectrophotometer model 25-shimadzo.

Result and discussion:

in this work dye elimination on series of similar solution whit 50 ml volume in concentration of 30 mg.L⁻¹ in the various pH from 1 to 9 was investigated and showed that in pH=2, there is maximum percent of dye elimination. synthetic studies to determinate dye absorption efficiency in optimum values namely solution with concentration of 20 mg.l⁻¹ in pH=2 in the 10 time with 0.025 gr absorbent with elovich synthetic models and intre particle diffusion was investigated and observed that dye absorption follows two-order synthetic. investigation of adsorption isotherms carried out in afew different concentration in 24 min with optimal condition of another parameters, and showed that dye absorption follow by langmuir isotherm.

Conclusion:

The major interest of this study was to investigate sorption of Mugreen, from aqueous solution using muroxide nanoparticle size and temperature. The surface area and the nature of the porosity can be controlled by means of the experimental parameters. The resultant nanoparticle loaded on activated carbons has high adsorptive performance not only for small molecules, but also for large molecules. Because it is facile and effective, the novel activation



process is an advisable method for producing high quality and high performance activated carbons.

Reference:

- [1] Moreira R. F. P. M., Peruch M. G., Kuhn N. C. Adsorption of textile dyes on alumina Equilibrium studies and contact time, *Braz. J. Chem. Eng.* 15 (1), 1998.
- [2] Sarı A., Tuzen M., Biosorption of cadmium (II) from aqueous solution by red algae (*Ceramium virgatum*): Equilibrium, kinetic and thermodynamic studies, *J. Hazard. Mater.* 157, 448-454, 2008.
- [3] Anayurt R. A., Sari A., Tuzen M. Equilibrium, thermodynamic and kinetic studies on biosorption of Pb(II) and Cd(II) from aqueous solution by macrofungus (*Lactarius scrobiculatus*) biomass, *Chem. Eng. J.* 151, 255-261, 2009.



In situ synthesis of Cu₂O on cotton fabric

A. Sedighi ^{a*}, M. Montazer ^a, N. Hemmati nejad ^a

^a Textile Department, Amirkabir University of Technology, Centre of Excellence in Textile, Hafez Avenue,
Tehran, Iran

Email: ali.sedighi@aut.ac.ir

Key words: Cuprous oxide, antibacterial behavior, gas sensor, nano composite.

Introduction:

Copper (I) oxide (Cu₂O) is a metal-Oxide p-type semiconductor with a narrow indirect band gap of 2.2 eV that has potential applications in solar energy conversion, catalysis, sensors and energy storage [2]. Also antibacterial behavior of Cu₂O is interesting [1]. Here, a method for in-situ chemical synthesis of cuprous oxide nano particles on cotton fabric has been investigated through simple and cost-effective process with good washing fastness. Also the photocatalytic and antibacterial effects with physical properties of the treated fabric have been investigated.

Also gas sensors based on metal oxides are widely used for detection of gases and organic vapors [3]. Cotton fabric containing nano particles can detect ammonia gas and H₂O₂, therefore it can be considered as a sensor with small response time.

Materials and methods:

Chemical substances without further purification were used. Copper sulphate (Cu₂SO₄), ammonia (25%) and sodium hydroxide (NaOH) were purchased from Merck.

A 100% bleached cotton fabric with a weight of 118 g/m² and warp and weft yarn density of 26 and 35 yarns/cm respectively, was obtained from a local market in Tehran.

Copper sulphate dissolved in aqueous solution and then fabric entered into solution and temperature reached to 80°C within 1 h. Next, NaOH solution added in 5 steps slowly in 100°C and after 1 h in boiling temperature, solution cooled to the room temperature. Finally,



ammonia solution added and the solution color turned into dark blue. By the way cuprous nano particles were generated under continuous stirring.

Apparatus:

Synthesis, crystallography and size of copper nano particles were determined by XRD model EQuniox3000, INEL, FRANCE using Cu K α radiation ($\lambda=1.540560\text{\AA}$). The shape, size and quantity of nano metal oxide was observed on a FESEM (Hitachi S4160). FT-IR spectra of the composite were recorded by nicolet spectrometer in the range from 400 to 4000 cm^{-1} . The fabric physical properties were tested by instron instrument.

Result and discussion:

In-situ synthesis of Cu_2O on cotton fabric was obtained by chemical reduction through exhaustion method. The cellulosic chains of cotton fabric with NaOH were used as reducing agent to reduce two valences copper (Cu^{2+}) into copper (I) (Cu^+) using ammonia, as organic ligand to link metal oxide to cotton fibre.

The presence of cuprous oxide nano particles on fabric surface was approved through SEM pictures and XRD patterns. This nano Cu_2O -cotton composite is also a gas sensing polymer which can easily sense the ammonia and H_2O_2 .

Antibacterial test has been carried out according to AATCC100 against *E. coli* and *S. aureus* bacteria were obtained. The fabric tensile strain was improved because of filling behavior of metal oxide nano particles.

Conclusion:

Cotton fabric containing cuprous oxide nano particles was synthesized and characterized. Nano cuprous oxide donated some interesting and fare properties such as antibacterial and sensing behavior. Some physical properties of cotton fabric improved and higher dye adsorption was obtained.



Reference:

- [1] O. Alekseeva et al. *composites based on cellulose derivatives*”, Chemistry & chemical technology, Vol. 5, No. 4, 2011.
- [2] K.J. Lo et al, “Polyol synthesis of polycrystalline cuprous oxide nanoribbons and their growth chemistry”, J Nanopart Res (2011) 13:669–682.
- [3] P.A. Praveen Janantha et al, “Use of Cu₂O microcrystalline thin film semiconductors for gas sensing”, Proceedings of the Technical Sessions, 25 (2009) 70-76.



Theoretical Study Rate Constants and Photonic Radiation Wavelength of Electron Transfer Endohedral Metallofullerenes C₈₀ – C₈₈

Mina Dastafcan^{*1}, Avat(Arman)Taherpour²

^{1,2} Chemistry Department, Faculty of Science, Islamic Azad University, Arak Branch,
P.O. Box 38135-567, Arak, Iran
(dastafcanm@gmail.com)

Key words: Organo-metallofullerene, Free energies, ET equation, Electron Transfer

Introduction:

Fullerenes as a class of spherical carbon allotrope group have unique properties. Organometal derivatization of fullerene species is essential to construct novel organo-metallofullerene materials for a variety of applications. [1] Three new families of trimetallic nitride template endohedral metallofullerenes (TNT EMFs), based on Cerium, Praseodymium and Neodymium clusters, were synthesized by vaporizing packed graphite rods in a conventional Krätschmer – Huffman arc reactor. Each of these families of metallofullerenes was identified and characterized by mass spectroscopy, HPLC, UV/ Vis-NIR spectroscopy and cyclic voltammetry between molecules surrounding the fullerene cage. [2] Topological indices have been successfully used to relate between Electron transfer physicochemical properties of C_n derivatives such as nitride metal cluster Pr₃N@C_n (80 ≤ n ≤ 88) and some thioethers.

Mathematical Methods

Total mathematical and graphing computations were performed using Microsoft Office Excel and Matlab programs. We used Chen window for design structure this nano complexes.

Results and Discussion:

Using the number of carbon atoms within the C_n fullerenes, several valuable properties of the fullerenes can be calculated. The values were used to calculate the free energies of electron



transfer (k_{et}) and Photonic Radiation Wavelength (λ), according to the ET equation for [X-UT-Y]@[M₃N@C_{2n}]. According to the Marcus electron transfer theory, slight electronic coupling comparatively happened between the initial state (LE) and final state (CT). Hence, this is considered which the transition state is near to the passing point from LE and CT states.

Calculation:

The complexes which made from organometal derivatives and species of fullerenes can be essential to construct novel special structures for a variety of electronic applications. Using the number of carbon atoms contained within the C_n fullerenes as a topological index, some valuable characteristics of these nano structures can be calculated. C_n fullerenes were used to calculate the Rate Constants (k_{et}) and Photonic Radiation Wavelength of electron transfer (λ_{et}), according to the ET equation for [X-UT-Y]@[M₃N@C_n]. Overall, the data of the Rate Constants of electron transfer (k_{et}) as a considerable parameters, and the Photonic Radiation Wavelength of electron transfer (λ_{et}), for the new nano structures of [X-UT-Y] @ [Pr₃N@C₈₀], were determined. By increasing the number of the units which make the structure of thiocrown ether, the values of free energies decrease. To indicate to this point is important, that applying Praseodymium as one of the Lanthanids family, probably, can be introduced in electronic nano technolog. These nano complexes have not been previously reported. The results of this study could be used in designing of molecular batteries and nano electronic sensors.

References

- [1] W. Kraetschmer, L. D. Lamb, K. Fostiropoulos, and D. R. Huffman, Nature, London, 347 (1990) 354.
- [2] Manuel N. Chaur , Frederic Melin, Bevan Elliott, Amar Kumbhar , Andreas J. Athans , and Luis Echegoyen Chem. Eur. J. (2008), **14**, 4594 – 4599
- [3] A.A. Taherpour & F. Biuki , J. Inf. Displ./2011/vol.12(3) , 145-152.
- [4] A. A. Taherpour, Fullerenes, Nanotubes and Carbon Nanostructures 17(2009)26.



Molecular dynamics simulations of adsorption and separation of Methane and Carbon dioxide gases on single walled Carbon and Silicon Carbide nanotubes

M. A. Ahesteh^{a*}

^aDepartment of Chemistry, Science and Research Branch, Islamic Azad University, Khuzestan, Iran

Email: Aminahesteh@yahoo.com

Keywords: Molecular dynamics simulations, Carbon nanotube, Silicon Carbide nanotube, Adsorption isotherms.

Introduction:

Discovery of CNTs has opened a new field of research in diverse fields of science, especially Nano science and nanotechnology. Gas adsorption on single walled nanotubes has been the subject of intense attention from researchers in recent years. Several experimental and theoretical studies have been performed with the aim of understanding how adsorbed gases behave on these novel materials. Although many detailed studies related to the adsorption of small and spherical molecules on nanotubes have been performed. Interest in these systems also stems from their widespread use in the petrochemical industry. Recently, a few simulations have been carried out examining effect of the external surface of nanotube bundle on hydrogen adsorption at supercritical temperatures, and adsorption of krypton, xenon, helium and methane at subcritical temperatures. In these studies, we employed quantum mechanics in the calculations to investigate gases adsorption onto nanotubes. Adsorption and separation of methane and carbon dioxide gases onto (10, 0) carbon nanotube (CNT) and silicon carbide (SiCNT) nanotube were investigated using molecular dynamics simulations. Pure and gases fluids were studied at different temperatures (288, 293, 298, 303 and 308 K) and in the pressure ranges from 1 to 10 atm. All the adsorption isotherms obtained have a Langmuir shape (type I).

Materials and methods:

We employed Classical molecular dynamics simulations were performed using the DL_POLY 2.20 package [1]; in a canonical ensemble (NVT) and using dreiding force field [2] to describe molecular interactions, This force field used of the harmonic potential for C-O bonds in the CO₂, and C-H bonds in the CH₄. For described non-binding interactions between different atoms we employed well known Lenard-Jones potential.

$$\varphi_{LJ}(r) = 4\epsilon_{ff} \left[\left(\frac{\sigma_{ff}}{r} \right)^{12} + \left(\frac{\sigma_{ff}}{r} \right)^6 \right] \quad (1)$$

The total potential for interactions between gas molecules and SWCNTs and SWSiCNTs was calculated using the site-site interaction method.

$$\varphi_{fw} = 4\epsilon_{fw} \sum_{i=1}^{N_f} \sum_{j=1}^{N_{carbon \& SiC}} \left[\left(\frac{\varphi_w}{r_{ij}} \right)^{12} - \left(\frac{\varphi_w}{r_{ij}} \right)^6 \right] \quad (2)$$

The Verlet algorithm was used to integrate the equations of motion, and the Nose-Hoover thermostat was used to control the temperature [3]. Nanotubes were placed in the center of the simulation box, the gas molecules distributed randomly around the nanotube, with the using of the Packmol package. Furthermore, to obtain the adsorption isotherms, the gravimetric storage capacity (the absolute value of adsorption per mass of adsorbent), ρ_w , was calculated as follows:

$$\rho_w = \frac{N_{gas} \cdot m_{gas}}{N_{gas} \cdot m_{gas} + N_C \cdot m_C} \quad (3)$$

Apparatus:

In this study we used a computer to have the following characteristics. CPU i7 960QM, 4GiG Ram. GTS 250 VGA.

Results and discussion:

In the case of pure gases, results indicate that the adsorption capability of CNT is more than that of SiCNT for the adsorption of CO₂. For the mixture fluids, obtained data is interesting. In the low pressure region (less than 4 atm), CH₄ were preferentially adsorbed onto the CNT and



the opposite behavior was observed at higher pressure. In the higher region pressure, CO₂ was adsorbed more than that of CH₄.

Conclusion:

The capabilities adsorption carbon nanotubes are more from silicon carbide nanotubes and the absorption rate decreases with increasing pressure and the RDF plot also shown the absorption rate decreases with increasing pressure, and the capabilities adsorption of CH₄ at low pressures is more than that of CO₂ (less than 4 atm) and at higher pressures, (higher than 4 atm) the capabilities adsorption of CO₂ is more than that of CH₄. As results, carbon nanotubes can be separated CO₂ from CH₄ gases at higher pressures (higher than 4 atm).

References:

- [1] W.Smith, T.Forester, j.Molec.Graphics, 14, 136
- [2] SL. Mayo, BD. Olafson, WA. Goddard, j. phys. chem, 94 (1990) 8897-8909
- [3] S. Nose, J. Chem. Phys. 81(1984) 511–519



Preparation and characteristics of poly imide/titania nanocomposite

Zahra Rafiee*¹ and Sedigheh Khalili¹

¹Department of Chemistry, Yasouj University, Yasouj 75914-353, I. R. Iran

E-mail: z.rafiee@mail.yu.ac.

Key words: Poly imid, Nanoparticles, Titania, Nanocomposite

Introduction:

Nowadays, polymer-inorganic hybrid materials have become a popular topic in material science because of their unique properties [1-3]. This is related to their diphasic structure, leading to multifunctional materials. . However, increasing interest in nano-size systems (ie systems of size range 0.5-100 nm) in recent years seems to be determined both by some distinctive properties of nanoparticles themselves and by anomalous cooperative properties of systems consisting of these moieties [4]. Polyimides (PI)s, which can be prepared from a variety of starting materials by a variety of synthesis routes and posses high thermal stability, high chemical resistance and excellent mechanical properties are a promising candidate type for the matrix of these hybrids [5,6]. The high glass-transition temperature of PIs would be expected to further stabilize the nanoparticles by decreasing their mobility, thereby preventing their agglomeration into large particles.

Materials and methods:

The same molar ratios of diamine and 3,3',4,4'-tetracarboxylic benzophenone dianhydride (BTDA) were dissolved in dry NMP under nitrogen atmosphere. Adding of BTDA was in five portions and the fresh part of BTDA Then the desired amount of $\text{Ti}(\text{OEt})_4/\text{acac}$ (with molar ratios of 1:4) was added and the mixture was further stirred for 15 h. The concentration of TiO_2 were 5, 10, 15 and 20 wt.% supposing complete conversion of the $\text{Ti}(\text{OEt})_4$ to TiO_2 particles. The uniform films of pure PAA and mixed PAA with different percentage of titania



precursor were fabricated by casting onto the dust-free glass plates. After the film production, they were annealed under a dynamic air atmosphere oven at 70, each and 300°C for 12 h.

Result and discussion:

In this study, the titanium alkoxide is incorporated into PI matrix through a simpler process and good quality and well-dispersed PI/titania hybrid films with relatively high titania content are prepared. Moreover, the characteristics of morphology, optical, mechanical, and thermal properties for the hybrid films are also investigated.

Conclusion:

polyimide/titania (PI/TiO₂) nanocomposite films are synthesized by sol-gel technology. PI/TiO₂ nanocomposite films with higher titania content exhibits higher glass transition temperature and storage modulus than pure PI. Although the thermal stability of the nanocomposite films are decreased by introducing TiO₂, but the nanocomposite films still reveal pretty good thermal resista.

Reference:

- [1] J. Chen, Y. Zhou, Q. Nan, Y. Sun, X. Ye, Z. Wang, Appl. Surf. Sci. 253 (2007) 9154.
- [2] J. G. Liu, Y. Nakamura, T. Ogura, Y. Shibasaki, S. Ando, M. Ueda, Chem. Mater. 20 (2008) 273.
- [3] W. C. Liaw, K. P. Chen, Eur. Polym. J. 43 (2007) 2265.
- [4] D. Y. Godovski, Adv. Polym. Sci. 119 (1995) 79.
- [5] D. Wilson, H. D. Stengenberger, P. M. Hergenrother, Polyimides, Chapman and Hall, New York (1990).
- [6] M. X. Ding, T. B. He, New materials of polyimide, Chinese Science Press, Beijing (1998).



The first chemical synthesis Polythiophene/Ag Nanocomposite by AgNO₃

H. Behniafar, R. Samiaa*, M. Barzegar

Department of chemistry, Damghan university, 36715-364, Damghan, Iran.

Email: azamsamia@yahoo.com

Key Words: Conducting polymer, Polythiophene, Nanocomposites, chemical synthesis.

Introduction:

The interest in the development of inorganic/organic composite has grown rapidly due to the wide range of high potential application of these materials. Among the organic part is conducting polymers, such as polyaniline(PANi), polypyrrole(PPy) or polythiophene(PTh)[1]. Among electrically conducting polymers, PTh is the most important material because of their distinctive electrochemical, magnetic, and optical properties as well as their wide range of applications. Current important application areas include solar cells, supercapacitors, support materials, sensors, field effect transistors and other electronics devices[2]. Conducting polymers have redox properties and have been shown to be excellent hosts for trapping noble metal such as silver and gold. Among noble metals, silver nanoparticles have gained much interest due to its applications in catalysis, in conducting ink, as a substrate in surface enhanced Raman spectroscopy, in anticancer activity[3], optical sensor and as a potential antibacterial agent[4]. In this novel approach, no additional reducing/oxidizing agent, or surfactant was employed.

Method:

AgNO₃ was completely dissolved in H₂SO₄ (as a dopant), then thiophene was dropwise added under vigorous stirring. The molar ratio AgNO₃/thiophene was taken 1:2. Thiophene, AgNO₃ and H₂SO₄ were mixed and this reaction was carried out under N₂ atmosphere for 3h.

Results:

Ag/PTh nanocomposites have been prepared by reducing AgNO₃. The resulting products were characterized by analysis FT-IR, UV-vis, XRD, SEM, TEM.



Conclusion:

we observed a strong interaction between the Ag^+ ion and sulfur atom of thiophene ring. Therefore Ag^+ ion was reduced to Ag nanoparticles and thiophene was oxidized to polythiophen. This work provides a simple route for the synthesis of Ag/PTh nanocomposites.

References:

- [1] Ayad, M. M.; Zaki, E. Appl. Sur. Sci. 2009, 256, 787.
- [2] Sang, S. J.; Soo, J. Y.; Kee-Jung. L.; Seung, S. I. Polymer 2010, 51, 4069.
- [3] Wu, Q.; Cao, H.; Luan, Q.; Zhang, J.; Wang, Z.; Warner, J. H.; Watt, A. A. R. Inorg. Chem. 2008, 47, 5882.
- [4] Sharma, V. K.; Yngard, R. A.; Lin, Y. Adv. Colloid interface Sci. 2009, 145, 83.



Synthesis Polythiophene/Ag Nanocomposites by use of Ag presynthesized

H. Behniafar, R. Samiaa*, M. Barzegar

Department of chemistry, Damghan university, 36715-364, Damghan, Iran.

Email: azamsamia@yahoo.com

Key Words: Nanocomposite, Conjugated polymer, Polythiophene, Nanoparticle.

Introduction:

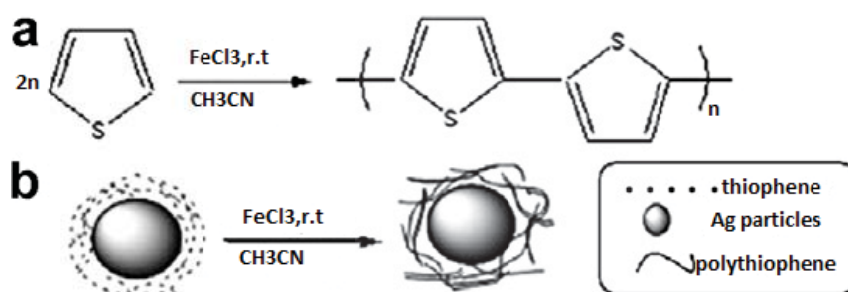
The inorganic-organic hybrids are a promising class of new materials, owing to the advantageous properties of the polymer matrix and the embedded inorganic particles. The combinations often lead to synergistic effects, resulting enhanced properties, making these materials applicable in various fields. conjugated polymers such as polypyrrole(PPy), polyaniline(PANi), have been successfully combined with different inorganic materials including metal nano particles (Ag, Au, Cu, and pd), leading to nanocomposites with high conductivity, catalytic activity, thermoelectric properties[1], etc. Polythiophene(PTh) as conducting polymer has attracted considerable attention over the past years due to numerous solid states potential applications in many fields, such as microelectronic devices, catalysts, organic field effect transistors and chemical sensors and biosensors[2]. Among nanoparticles, silver nanoparticles have gained much interest due to its applications in catalysis, in conducting ink, as a substrate in surface enhance Raman spectroscopy, in anticancer activity, optical sensor and as a potential antibacterial agent[3]. In present work, Ag nanoparticle were synthesized by reaction of silver nitrate(AgNO_3) with sodium borohydride(NaBH_4).

Method:

A Known mass of Ag prepared was finely dispersed in a conical flask containing acetonitrile(CH_3CN), after which a known quantity of thiophene was injected. A particular amount of solution FeCl_3 in CH_3CN was then added to the solution in one go. The reaction mixture was magnetically stirred at room temperature(r.t).

Results:

PThs are often considered to be useful matrices for the immobilization of the dispersed noble metal nanoparticles. The porous structure of conducting polymer allows dispersing the metal particles into the polymer matrix and generates additional electrocatalytic sites. more over, incorporation of metal nanoparticles into conducting polymers provides enhanced performance for both the "host" and "guest". The resulting Pth/Ag composites characterized by FT-IR, UV-vis; SEM, TEM and XRD.



Scheme 1. Schematic representation of the process for a) polymerization of thiophene and b) formation of PTh/Ag composites.

References:

- [1] Janaky, C.; Endrodi, B.; Kovacs, K.; Timko, M.; Sapi, A.; Visy, C. *Synth. Met.* 2010, 160, 65.
- [2] Palacios, J. C.; Cruz, G. J.; Olayo, M. G.; Chavez-Carvayar, J. A. *Surface & Coating Technology* 2009, 203, 3032.
- [3] Paulraj, P.; Janaki, K.; Sandhya, S.; Pandian, K. *Colloids and Surfaces A: Physicochem. Eng. Aspects* 2010.



Investigation of optical properties dependence to deposition angle

M. Nojavan^a , H. Kangarloo^b

^{a,b} Faculty of science , URMia Branch , Islamic Azaduniversity , URMia , IRAN.

Keywords: Magnesium fluoride; Kramers-Kronig; deposition angle; optical properties.

Introduction:

Magnesium fluoride (MgF_2) is known as a significant alkaline-earth fluoride which has been attention to, because of its ample applications as an optical material for anti-reflective (AR) coatings and polarizing light [1]. MgF_2 can be applied as anti-reflection coating material in the energy about to 3 eV, i.e, in the mid visible region and it is a good reflector material for the vacuum ultraviolet radiation [2]. MgF_2 has a good potential transmit into the VUV region (121 nm) and beyond. So it is used for UV optics and is mostly applied for Excimer laser applications [3-4]. MgF_2 has low refractive index (1.38). Magnesium Fluoride polishes well and is a hard material. So, it can be applied to be standards [5].

Experimental:

Details Magnesium fluoride thin films were deposited on glass substrates ($18 \times 18 \times 1$ mm cut from microscope slide) by resistive evaporation from Molybdenum boats at room temperature, with two different angles. The purity of Magnesium fluoride powder was 96%. An ETS 160 (Vacuum Evaporation System) coating plant with a base pressure of 3×10^{-5} mbar was used. Prior to deposition, all glass substrates were ultrasonically cleaned in heated acetone first and then in ethanol. Thickness of layers were determined by quartz crystal microbalance technique ($d = 93$ nm). The layers with deposition angle 25 and 45 degree were produced on 300 K (room temperature). Transmittance of the films was measured using VIS spectrophotometer (Hitachi U-3310) instrument. The spectrum of layers were in the range of 300–1100 nm wave length (VIS), and for using Kramers-Kronig relations [6], we extrapolated of reflectivity curves with Palik [7] data, they just reported reflectance of MgF_2 layers in long



wave length range. The optical properties such as n , k , ε_1 , ε_2 , α and Band-gap energy were obtained.

Results and discussion:

By increasing deposition angle in visible light range (300 – 1100 nm) more transmittance and less Reflectance are achieved. This is because of void formation on the layers. By increasing deposition angle more voids are formed on layer, so obtained results have more transmittance and less Reflectance. By using K-K method on Reflectivity curve and extrapolate them with Palik [7], other optical parameters were calculated. In the real part of refractive index (n) curve, there is a bump at 3.3eV for both layers. By increasing deposition angle, n decreases. All Refractive indices (k), (Imaginary part of refractive), there is a minimum at about 1.6eV for 25 degree and 45 degree. Both layers reach to a maximum at about 4eV. On the other hand higher deposition angle tends to more voids formation. Therefore tends to extinction coefficient. Both ε_1 and ε_2 are angle dependence. By increasing deposition angle dielectric property increases. By increasing deposition angle and formation of more voids on layer, absorption coefficient decreases. In order to understand how the band gap is affected by changing film deposition angle the band-gap of the films were calculated by using absorption coefficient [8]. For the layers produced in this work band energy for both layer are the same and about 3.9eV.

Conclusion:

MgF₂ nanolayers of 93 nm thickness were deposited on glass substrates conditions with two different deposition angle of 25 and 45 degrees. Optical properties and optical constants were calculated by k-k method. By increasing deposition angle because of formation more voids on layers transmittance increases and reflectance decreases. Real and imaginary part of refractive indices decreases. By increasing deposition angle dielectric property increases, therefore ε_1 and ε_2 increases. Absorption coefficient decreases by increasing deposition angle and that is



because of formation more voids on layers. Band-gap energy calculated at about 3.9 eV for both layers.

References:

- [1] O. Duyar, H.Z. Durusoy, Turk. J. Phys. 28 (2004) 139–144.
- [2] K. Ramesh Babu, Ch. Bheema Lingam (2011) Structural, thermodynamic and optical properties of MgF_2 studied from first- principles, theory, Journal of solid state chemistry 184,343-350.
- [3] Duncanson et.al. Proc.Phys.Soc. V72, p1001, 1958.
- [4] Kandil et.al. J.App.Phys. V52, p749, 1981.



Investigation of optical properties dependence to deposition angle

M. Nojavan^a , H. Kangarloo^b

^{a,b} Faculty of science , URMia Branch , Islamic Azaduniversity , URMia , IRAN.

Email:Nojavan_maryam@yahoo.com

Keywords: Magnesium fluoride; Kramers-Kronig; deposition angle; optical properties.

Introduction:

Magnesium fluoride (MgF_2) is known as a significant alkaline-earth fluoride which has been attention to, because of its ample applications as an optical material for anti-reflective (AR) coatings and polarizing light [1]. MgF_2 can be applied as anti-reflection coating material in the energy about to 3 eV, i.e. in the mid visible region and it is a good reflector material for the vacuum ultraviolet radiation [2]. MgF_2 has a good potential transmit into the VUV region (121 nm) and beyond. So it is used for UV optics and is mostly applied for Excimer laser applications [3-4]. MgF_2 has low refractive index (1.38). Magnesium Fluoride polishes well and is a hard material. So, it can be applied to be standards [5].

Experimental:

Details Magnesium fluoride thin films were deposited on glass substrates ($18 \times 18 \times 1$ mm cut from microscope slide) by resistive evaporation from Molybdenum boats at room temperature, with two different angles. The purity of Magnesium fluoride powder was 96%. An ETS 160 (Vacuum Evaporation System) coating plant with a base pressure of 3×10^{-5} mbar was used. Prior to deposition, all glass substrates were ultrasonically cleaned in heated acetone first and then in ethanol. Thickness of layers were determined by quartz crystal microbalance technique ($d = 93$ nm). The layers with deposition angle 25 and 45 degree were produced on 300 K (room temperature). Transmittance of the films was measured using VIS spectrophotometer (Hitachi U-3310) instrument. The spectrum of layers were in the range of 300–1100 nm wave length (VIS), and for using Kramers-Kronig relations [6], we extrapolated

of reflectivity curves with Palik [7] data, they just reported reflectance of MgF_2 layers in long wave length range. The optical properties such as n , k , ϵ_1 , ϵ_2 , α and Band-gap energy were obtained. Table 1 show details of layers produced in this work.

Table1: Details of MgF_2 /glass thin layers produced in this work.

sample	Deposition angle (degree)	Vacuum pressure (torr)	thickness(nm)	Deposition ($\text{\AA}^0/\text{s}$)
$\text{MgF}_2/\text{glass}$	25	3×10^{-5}	93.7	0.7
$\text{MgF}_2/\text{glass}$	45	3×10^{-5}	92.7	0.7

Results and discussion:

By increasing deposition angle in visible light range (300 – 1100 nm) more transmittance and less Reflectance are achieved. This is because of void formation on the layers.

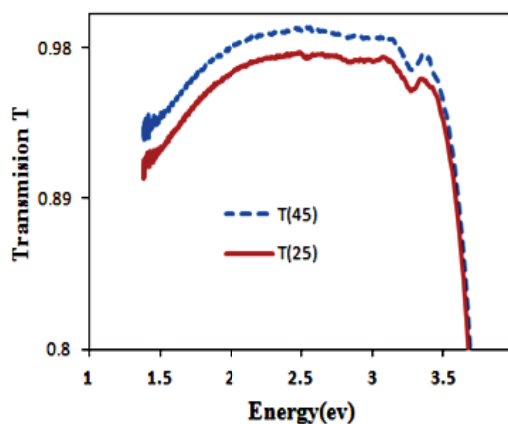
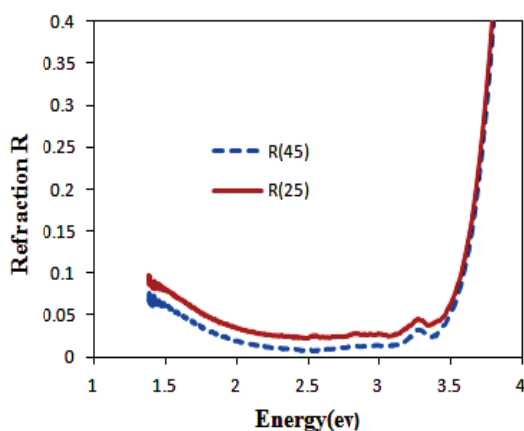


Fig1 (a). Reflectance of MgF_2 in the angle 25 and 45 **Fig1 (b).** Transmittance of MgF_2 in the angle 25 and 45

By increasing deposition angle more voids are formed on layer, so obtained results have more transmittance and less Reflectance Fig(1a,b). By using K-K method on Reflectivity curve and extrapolate them with Palik [7], other optical parameters were calculated. In the real part of refractive index (n) curve, there is a bump at 3.3eV for both layers. By increasing deposition angle, n decreases. All Refractive indices (k), (Imaginary part of refractive), there is a minimum at about 1.6eV for 25 degree and 45 degree. Both layers reach to a maximum at



about 4eV. On the other hand higher deposition angle tends to more voids formation. Therefore tends to extinction coefficient. Both ε_1 and ε_2 are angle dependence. By increasing deposition angle dielectric property increases. By increasing deposition angle and formation of more voids on layer, absorption coefficient decreases. In order to understand how the band gap is affected by changing film deposition angle the band-gap of the films were calculated by using absorption coefficient [8]. For the layers produced in this work band energy for both layer are the same and about 3.9eV.

Conclusion:

MgF₂ nanolayers of 93 nm thickness were deposited on glass substrates conditions with two different deposition angle of 25 and 45 degrees. Optical properties and optical constants were calculated by k-k method. By increasing deposition angle because of formation more voids on layers transmittance increases and reflectance decreases. Real and imaginary part of refractive indices decreases. By increasing deposition angle dielectric property increases, therefore ε_1 and ε_2 increases. Absorption coefficient decreases by increasing deposition angle and that is because of formation more voids on layers. Band-gap energy calculated at about 3.9 eV for both layers.

References:

- [1] O. Duyar, H.Z. Durusoy, Turk. J. Phys. 28 (2004) 139–144.
- [2] K. Ramesh Babu, Ch. Bheema Lingam (2011) Structural, thermodynamic and optical properties of MgF₂ studied from first- principles, theory, Journal of solid state chemistry 184,343-350.
- [3] Duncanson et.al. Proc.Phys.Soc. V72, p1001, 1958.
- [4] Kandil et.al. J.App.Phys. V52, p749, 1981.
- [5] Kashnow & McCarthy, J. .Phys.Chem. V30, P813, 1969.
- [6].H.Savaloni,H. kangarloo, j. phys. D: Appl. Phys. 40 (2007) 203.



- [7]. E. D. Plik handbook of optical constants of solids courtesy academic press inc, 1985.[8]
J. Tauc, amorphous and liquid semiconductors, plenum london, 1974.
- [8] J. Tauc, amorphous and liquid semiconductors, plenum london, 1974.
- [9] H.M. Hsiung, Texture effect of hot-pressed magnesium fluoride on optical transmittance, Materials Chemistry and Physics 81 (1) (2003) 27–32.
- [10] M. Nofar, H.R. Madaah Hosseini, H.A. Shivaee, The dependency of properties on density for hot pressed MgF_2 , Infrared physics & Technology 51 (2008) 546-549.
- [11]. H. Savaloni, H. kangarloo, j. phys. D: Appl. Phys. 40 (2007) 203.
- [12] K. Ramesh Babu, Ch. Bheema Lingam (2011) Structural, thermodynamic and optical properties of MgF_2 studied from first- principles, theory, Journal of solid state chemistry 184, 343-350.



Synthesizing and Characterizing of Silver/Copper (II) oxide Nano composite on Nylon fabric

Z. Komeili Nia¹, M. Montazer¹, M. Latifi¹

¹Textile Department, Amirkabir University of Technology, Centre of Excellence in Textile, Hafez Avenue, Tehran, Iran

Key words: In situ synthesis, Silver, Copper, Nano particles, Nylon

Introduction:

Noble metal nano particles (NPs) such as copper and silver NPs have been used in textile to improve some properties of fabric such as: mechanical, antifungal, anti microbial, flame retardant, and water repellence properties. Copper NPs were often contaminated with copper oxide due to high air sensitivity of copper NPs, unless other reagents with functional groups that form complexes with copper ions or soluble surfactants as capping agents were used. However, the effectiveness of these materials in preventing surface oxidation is poorer in case of copper than silver. Divalent copper nature against mono-valent nature of silver is one reason for such differences. Usual materials which employ to stabilize silver NPs often leave higher scope for oxygen to penetrate the surface of copper NPs.

Here we have synthesised composite of copper (II) oxide and silver NPs on nylon fabric through a simple chemical reduction method to obtain both advantages of two noble metal NPs. Also we applied copper (II) oxide NPs on nylon fabric which no report found on utilizing copper (II) oxide NPs on nylon fabric [1-3].

Materials and methods

Laboratory grade of chemical substances with purity was used without any further purification. Silver nitrate (AgNO_3), Copper sulphate (CuSO_4), ammonia, sodium hydroxide (NaOH) was purchased from Merck and nylon fabric with a weight of 90 g/m^2 , was obtained from a local market in Yazd.

1g nylon fabric were dipped in 100 mL distilled water containing different weight ratios of AgNO_3 and CuSO_4 at 90°C along with 20 mL NaOH solution (0.01 M) resulting in Ag_2O powder precipitation and after about 2 min 30 mL 2%(W) ammonia were added which leading to the preparation of copper-amine and silver-amine ($[\text{Ag}(\text{NH}_3)_2]^+$, $[\text{Cu}(\text{NH}_3)_4]^{2+}$) complex ions and exhausting was continued for 1.5 h.

Result and discussion:

Copper (II) oxide and silver NPs have colorant effects on nylon fabric and it was found that the color alter with variation in the ratio of silver to copper (II) oxide NPs which were investigated by Reflectance spectrophotometer. The treated nylon fabrics were characterized by scanning electron microscopy (SEM), X-ray Diffraction (XRD) (Fig1) and Energy Dispersive X-ray spectroscopy (EDAX) (Fig2). The treated fabrics with copper (II) oxide and silver NPs showed an antibacterial activity against *S. aureus* (Fig3) and improvement in the fabric strength.

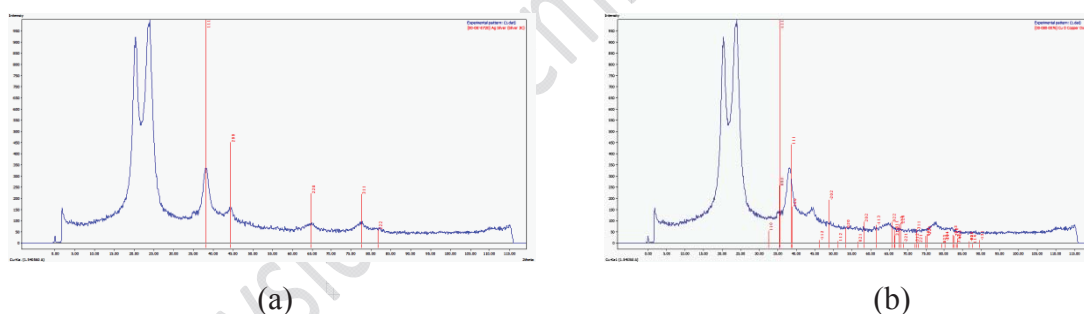


Fig1: XRD pattern of treated fabric, denoted peaks confirm the presence of a) Ag NPs and b) CuO NPs on nylon fabric

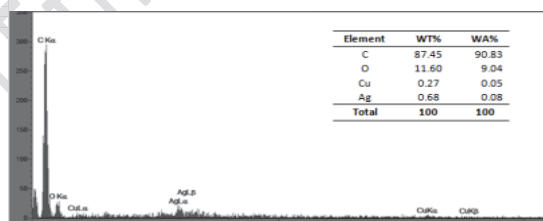


Fig2:EDAX analyzes

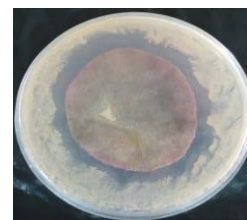


Fig 3: Antibacterial activity of treated nylon fabric against *S. aureus* bacteria



Conclusion:

Nylon/silver/copper (II) oxide nano composite was prepared by an in situ synthesis method. Silver and copper (II) oxide NPs have been synthesized on nylon fabric through using ($[\text{Ag}(\text{NH}_3)_2]^+$, $[\text{Cu}(\text{NH}_3)_4]^{2+}$) complexes reducing silver nitrate and bounding to negative groups of polyamide chains. NPs on the fabric introduce an antibacterial effect with enhanced fabric strength due to their cross linking action between the polymer chains.

Reference:

- [1] P. K. Khanna et al.; " Synthesis of hydrophilic copper nanoparticles:effect of reaction temperature"; J. Nanopart Res ; 11, 793–799, 2009.
- [2] M. Montazer et al.;" In situ synthesis of nano silver on cotton using Tollens' reagent"; J.Carbohydrate Polymers; 87,1706-1712 ,2012.
- [3] M. Grouchko.; "Synthesis of copper nanoparticles catalyzed by pre-formed silver nanoparticles"; J Nanopart Res;11,713–716. 2009.



Colored and Functional Nylon/Silver Nano composite: Synthesis and Characterization

Z. Komeili Nia¹, M. Montazer¹, M. Latifi¹

¹Textile Department, Amirkabir University of Technology, Centre of Excellence in Textile, Hafez Avenue, Tehran, Iran

Key words: Synthesis, Silver, Nano Particles, Nylon, Surface Plasmon Resonance

Introduction:

Silver nano particles (NPs) can be synthesised in different sizes and shapes including: disks, rods, prisms, wires, hexagons, cubes, bi-pyramids, tetrahedrons, hollow structures and branched particles. Various methods were employed to synthesis the NPs such as: polyol process, surfactant-assisted reduction, solvothermal synthesis, thermolysis of precursors, micelles controlling growth and photo reduction. The mentioned methods were classified in two main strategies which called Thermal and photochemical methods. Thus, the photochemical routes provide more mono-disperse samples with greater control over structural parameters. This paper describes a photochemical synthesis of silver NPs. The synthesized colloidal solutions exhibited different colors due to the localized surface plasmon resonance (LSPR) properties of metal NPs. By harnessing LSPR effect through controlling over morphology and size of metal NPs, the color of NPs colloidal solutions can alter [1-3].

Materials and methods:

Laboratory grade of chemical substances with purity was used without any further purification. Silver nitrate (AgNO₃), sodium borohydride (NaBH₄), Trisodium citrate (TSC) was purchased from Merck and nylon fabric with a weight of 90 g/m², was obtained from a local market in Yazd.

A typical experiment was carried out by the photochemical method. First, silver seeds were prepared by dropwise addition of NaBH_4 solution (0.01mM, 5 mL) to an aqueous solution of AgNO_3 (0.25mM, 100 mL) in the presence of trisodium citrate (0.25mM) under vigorous stirring. Next, the yellow silver seeds were exposed under three Philips Cleo UV Lamp HPA 400S located 1m above the silver seed solutions. The color of silver colloids changed from yellow, to dark yellow, orange and green during the irradiation process. In the next step colored fabric were prepared by exhausting method at pH=4, which 1g nylon fabric were immersed in 100 mL of each prepared colloidal solutions under vigorous stirring at 80°C for 1.5 h.

Result and discussion:

As exhibited in figure1, colloidal silver NPs solutions were prepared in different colors and then applied on nylon fabrics. The UV-visible spectrum of the solutions was studied and modified nylon fabrics were characterized by scanning electron microscopy (SEM) (Fig 2), X-ray diffraction (XRD) and Energy Dispersive X-ray spectroscopy (EDAX) analyzes. The results indicated that silver NPs were assembled on the surface of nylon fibers. It was found that silver NPs have bound to the polyamide chain of nylon fibers by the electrostatic interaction between nylon fibers and metal NPs. Also antibacterial test against *S. aureus* bacteria have been investigated.

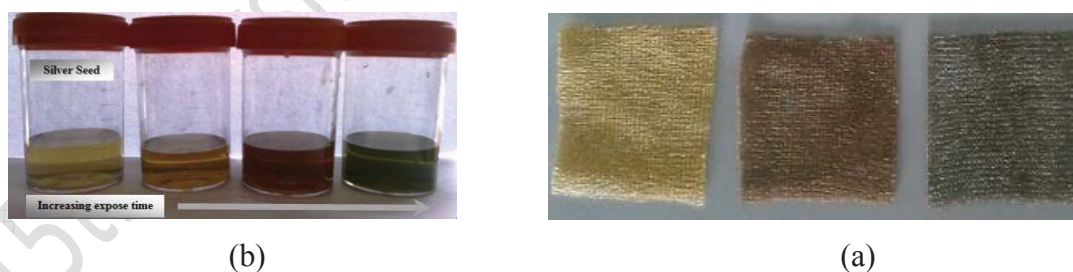
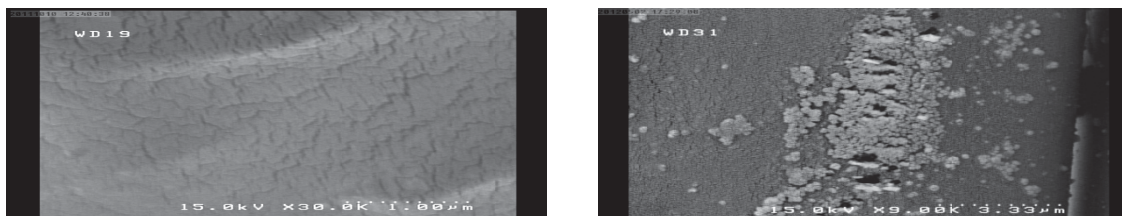


Fig 1: Digital photograph of (a) colloidal silver NPs solutions and (b) treated fabric



(b) (a)
Fig 2: SEM images of (a)raw nylon fabric (b) treated nylon fabric

Conclusion:

Silver NPs have been successfully synthesized by a photochemical method and chemically bound to polyamide chain of nylon fibers to provide different color through surface plasmon resonance effects. The treated fabric also exhibited anantibacterial activity against *S. aureus* bactria.

References:

- [1]B.Tang etal.; "Photoinduced Shape Conversion and Reconstruction of Silver Nanoprisms"; J. Phys. Chem. C; 113, 7025–7030,2009.
- [2]G.S.Metraux etal;"Rapid thermal synthesise of silver nanoparticles with chemically tailorable thickness"J.Adv.Master;17,412-415,2005.
- [3] B.Tang etal ;"Application ofanisotropic silver nanoparticles: Multifunctionalization of wool fabric"; J.Colloid and Interface Sci; 356 , 513–518.2011.



Effect of some operational parameters on discoloration of Acid Blue 113 via nano TiO₂ stabilized on concrete bed in photocatalytic process

Roya Nayebi Gavgani, Bita Ayati, Hossein Ganjidoust

Civil & Environmental Engineering Faculty, Tarbiat Modares University, Tehran, Iran

* Email: roya.nayebi@modares.ac.ir

Keywords: Titanium dioxide nanoparticle, COD, DO, ORP, AB113.

Introduction:

Textile dyes are one of the main sources of environmental pollution. More than 40 percents of consumed dyes, in different dyeing processes are released to wastewater. Dyes change the color of water and prevent light diffusion, disturbing photosynthetic and leads to destruction of aquatic ecosystem [1-2]. Modern commercial dyes are very stable and they contain high composition ratio of aromatic rings. Azo dyes represent the largest class of dyes. The release of these compounds into the environment is undesirable, not only because of their color, but also because many azo dyes and their breakdown products are toxic and/or mutagenic to life. Thus, wastewater containing synthetic azo dyes is considered serious warning for environment and removal of these pollutants has been attended in several researches [3]. Since conventional treatment methods including physical, chemical and biological, such as filtration, adsorption, coagulation and chemical oxidation are unable to degradation of these pollutants as much as environmental standards [4]. Recently, the application of advanced oxidation methods[5], such as photocatalytic reactions have been expanded for removing of toxic and non-biodegradable pollutions. Semiconductor nanostructures play an important role in developing smart materials that can simultaneously sense and destroy harmful chemical contaminants such as dyes. Some reasons for these particular properties are break down of whole pollutions, removing of various types of pollutions in short time, excreting of residuals easily and ability to carry out in room temperature and pressure [6-7].



Material and Methods:

AB113 (commercial dye) was purchased from Alvan Sabet (Iran, Hamedan) company and used without purification. TiO_2 (P25: 80% anatase, 20% rutile; 50 $\text{m}^2 \text{g}^{-1}$) was kindly supplied by Degussa Company. Also K_2CrO_7 , AgSO_4 , HgSO_4 , NaOH are Merck products, that used for the COD measurement. A laboratory-scale reactor is included plastic containers (Length=23cm, Width=16cm, Height=5cm), that concrete bed with 8 mm thickness is located inside. In this research, we used an immobilized system by concrete glue.

Apparatus:

The spectrometer had been used for spectroscopic application (Carry50, Varian Co.). The COD reactor has been applied for determining the amount of organic pollution (DRB200, Hach Co.). OPR and DO, HQC model made by Hach Co. is used.

Result and discussion:

The effects of some operational parameters such as COD, DO, ORP and dye removal were investigated under optimum conditions ($\text{TiO}_2=40\text{gr/m}^2$, $\text{pH}_{\text{in}}=9$, $C_{\text{AB113}}=75 \text{ ppm}$, $P_{\text{UV-C}}=90\text{W}$, coating method: SSP). According to the results, 92 percent of AB113 was removed in less than 5 hours. The degradation of benzylic, naphthalene and phenolic cycle are 17, 6.7 and 9.3 percents, respectively. Also changes of ORP were in accord with the DO consumption.

Conclusion:

AB113 could be successfully decolorized using immobilized TiO_2 nanoparticles photocatalysis. Benzylic, naphthalene and phenolic cycle intermediates generated during the degradation process were analyzed by spectroscopy in special wavelength and they are removed by time. Also the ORP is quickly reduced at the first 60 min and then the changes slow down. After that, it increased again. The reason is the transfer of electrons and the generation of active species.



Reference:

- [1] Rai, H.S., and etal, (2005), "Removal of dyes from the effluent of Textile and dyestuff manufacturing industry: A review of emerging techniques with dereference to biological treatment", *Critical Reviews in Environ Science and Technology*, 35:219-238.
- [2] Garcia-Montano, J., and etal, (2008), "The testing of several biological and chemical coupled treatments for cibacron red FN-R azo dye removal", *J. of Hazardous Materials*, 154:484-490.
- [3] Santos, A.B., (2005), "Reductive decolourisation of dyes by thermophilic anaerobic granular sludge", Department of Environmental Technology, Wageningen, PhD Thesis.
- [4] Kobya, M., and etal, (2003), "Treatment of textile wastewaters by electro coagulation using iron and aluminum electrodes", *J. of Hazardous Materials*, 100:163-178.
- [5] Klavarioti. M., and etal, (2009), "Removal of residual pharmaceuticals from aqueous systems by advanced oxidation processes", *Environ. Int.*, 35: 402–417.
- [6] Timothy, T., (2003), "Photocatalytic reduction of selenate and selenite: Water/wastewater treatment and the formation of nano-selenium compounds", Australia, PhD Thesis.
- [7] Konstantinou, I.K., and etal, (2004), "TiO₂-assisted photocatalytic degradation of azo dyes in aqueous solution: Kinetic and mechanistic investigations", *Apply. Catalyst B: Environmental*. 49 (1):1–14.



Synthesis of Nanostructure MCM-41 Using Stems of Phragmites Australiy Ash as Silica Sources

S.N. Azizi*, O. Rangrizrostami

Analytical Division, Faculty of Chemistry, University of Mazandaran, Babolsar, Iran

Email: oliarangrizrostami@yahoo.com

Keywords: MCM-41, Mesoporous silica, Sodium silicate, CTAB

Introduction:

Since mobile corporation have discovered nanostructured mesoporous materials known as M41S in the late 1980s [1], MCM-41, one of the M41S family, has become the best known and most interesting material. Due to its excellent properties such as high surface area, well defined regular pore shape, narrow pore size distribution, large pore volume, tunable pore size and thermal stability, MCM-41 has been utilized for chemical and environmental applications such as an adsorbent, catalyst support, ion-exchanged material and nanofilter [2]. In the present work silica was extracted from stems of Phragmites australiy ash (SPAA) using the methods of Kalapathy et al. [3] and it use for synthesis of nanostructure MCM-41.

Materials and methods:

The nanostructure MCM-41 was synthesized using stems of Phragmites australiy ash-derived sodium silicate as a silica source, cetyltrimethyl ammonium bromide (CTAB) as the pore structure-directing agents. The surfactant solution was added to the silicate solution. The pH of the mixture was adjusted to a definite value through the dropwise addition of solution of H₂SO₄. The reaction vessel was heated. Then, the solid products were recovered by filtration, washed with distilled H₂O, air-dried, and calcined.

Apparatus:

The physical properties of synthesized MCM were characterized by XRD, SEM and FT-IR.

Result and discussion:

The Stems of Phragmites australis was collected from north of Iran after preparing the ash, it analyzed with x-ray fluorescence (XRF) spectrometry to determine elemental composition. The XRF of Stems of Phragmites australis ash (SPAA) shows more than 84.02% of hydrated silica (SiO_2). This low-cost source of silica used for synthesis of nanostructure MCM-41.

The synthesized nanomaterial was characterized by the XRD, SEM, FT-IR. The X-ray diffraction patterns of extracted silica and synthesized MCM-41 are recorded which allowed us to corroborate, that the obtained mesoporous sample has a highly ordered pore system with a high porosity (Figure 1.a-b). The average particle size was calculated to be 37 nm according to Scherer equation. To support the XRD analysis, the infrared (IR) spectroscopy was used and the size and morphology of the samples were determined by SEM which indicated good morphology of the crystals (not shown).

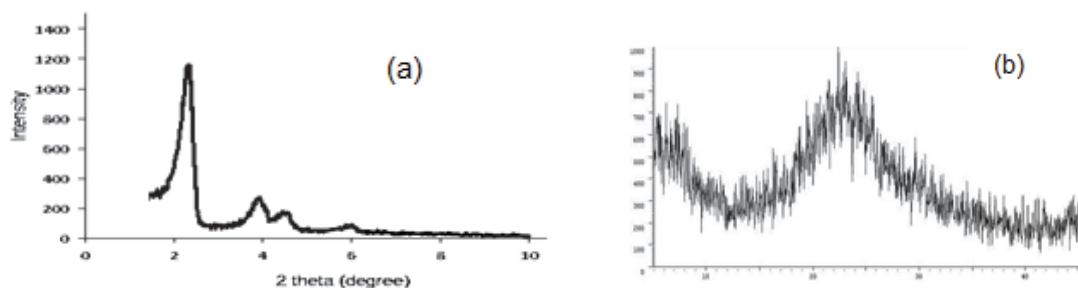


Fig. 1. (a) The XRD pattern of SPAA-MCM-41 and (b) the XRD pattern of silica extracted from Stems of Phragmites australis.

Conclusion:

In conclusion, MCM-41 was successfully synthesized from SPAA. MCM-41 contains a regular arrangement of uniform channels with nanodiameters, high specific surface area and high specific pore volume.

Reference:



- [1] Beck J. S., Vartuli C., Roth W. J. and Kresge C. T. ; "Family of mesoporous molecular sieves prepared with liquid crystal templates" ; Journal of the American Chemical Society; 114,10834-10843,1992.
- [2] Zhao S. X., Lu Q. G. and Millar J. G.; "Advances in Mesoporous Molecular Sieve MCM-41";Industrial&Engineering ChemistryResearch.; 35,2075-2090, 1996.
- [3] U. Kalapathy, A. Proctor, D. Schultz;"A Simple Methode for production of Pure Silica from Rice Hull Ash";Journal. Bioresource Technology ; 73,252-257,2000.

15th Physical Chemistry Conference



Effect of treatment process parameters on the surface characteristic of a hydrophilic nano-silica

M.kalantari^a, M.Mohseni^{a*}

^a Department of Polymer Eng. and Color Tech, Amirkabir university of technology,
Tehran, Iran

Email: mmohseni@aut.ac.ir

Key words: Nano-Silica, Treatment, Vinyl Silane, Sol-Gel, Surface Physical Chemistry

Introduction:

Nano particles and their applications is one of the most parts in science and industry nowadays. In this way polymer science has a special situation. The use of inorganic nanoparticles in polymers and coatings has attracted lots of attention from long ago due to their desired properties (especially mechanical properties) with low amounts. Silica is one of the best inorganic nano-particles for coating because of good mechanical properties & no undesirable effect on appearance and optic. But use of these nanoparticles has their own problems. High polarity and hydrophilic surface of inorganic materials leads to a high surface energy which results in incompatibility with polymeric matrix. So their expected properties may not show. Lots of efforts have been done in order to dissolve these problems. [1, 2]

Silica particles have a lot of OH groups on their surface which results a very strong hydrophilicity so it can be used as a water scavenger. To increase the hydrophobicity of surface and have more compatibility with polymers, using silane coupling agents is one the best ways. Silane molecule reacts with Silanol group via a Sol-Gel process and remains hydrophobic organic group with lower surface energy on silica. The treatment has some parameters such as temperature, time, hydrolysis ratio, silane to silica ratio & etc, so that the amount and kind of silane grafting on surface are different. 3 of these parameters were investigated. [1-4]



Materials and methods:

For this purpose nanosilica OX50 (Degussa Co.) with particle size 40nm was used. Vinyltrimethoxy silane (VTMS) which has a vinyl organic group opposite side of methoxy inorganic group was used from Dynalosilane Company. The treatment was performed on the high shear with homogenizer and the reflux conditions during 3 hours. Silane was added continuously during 15 minutes after pH justifying.

Apparatus:

Density and surface pH of treated particles was determined by helium picnometer and digital pH meter. For discussion about amount of grafted silane, elemental analysis (CHN) was used for some samples. To determine the changes of surface hydrophilicity and its characteristics, behavior of treated particles in solvents was investigated using UV-Vis spectrophotometer and Turbidimeter. At last for discussion about particle size on nano silica after treatment in polymers TEM microscopy was performed.

Result and discussion:

Samples Conditions	nT									
pH of treatment	---	- 3	- 6	- 9	- 6	- 9	- 3	- 9	- 3	- 6
Hydrolysis Ratio	---	/3 : 1	/3 : 1	/3 : 1	: 1	: 1	: 1	: 1	: 1	: 1
Silane/silica ratio	---	/10 : 1	: 1	0 : 1	/10 : 1	: 1	0 : 1	/10 : 1	: 1	0 : 1
Particle surface pH	.10	.96	.29	.19	.80	.54	.82	.13	.33	.58
Particle density (gr/cm ³)	.26	.86	.89	.43	.85	.74	.66	.88	.76	.88
Carbon analysis	---	.01	---	.13	---	.02	---	---	---	---



First investigations confirmed the existence of silane on the treated silica. Results of treated particles pH were more alkali surface via decreasing in OH groups. Densitometries showed increasing of particle density via addition of organic chains on inorganic silica and reduce the mass in the terms of increasing volume. CHN analysis determined quantitative amount of silane on some samples of treated silica and better conditions were performed. Turbidity values and spectrophotometer spectra showed increasing in compatibility with solvents, better wet ability, better and more durable dispersions. TEM microscopy determined the particle size of treated silica on average of 60-80 nm.

Conclusion:

Treatment of nano silica is very effective on its surface characteristics. Best treatment conditions are pH less than 4 or more than 6, more silane/silica ratio and 1:1 hydrolysis ratio. Silane/silica ratio has most and hydrolysis ratio has less effect on amount of grafted silane. Types of grafting of silane are different in various conditions. All the samples after treatment have better compatibility with solvents and so polymers. The treatment process leads to have fine nano particles with much better properties and fewer problems in applications.

Reference:

- [1] M.kalantari; "Effect of nano-silica treatment with vinyl-silane coupling agents on the interfacial properties and scratch resistance of UV-curable polyurethane acrylate resins," Amirkabir university of technology, 2012.
- [2] Teofil Jesionowski; "Preparation of the hydrophilic/hydrophobic silica particles," Colloid and surface: 207, 49-58, 2002.
- [3] Chang Hun Lee; "Preparation and characterization of surface modified silica nanoparticles with organo-silane compounds"; Colloids and Surfaces; 384,318-322, 2011.
- [4] Rostami, Z. Ranjbar, M. Mohseni; "Investigating the interfacial interaction of different aminosilane treated nano silicas with a polyurethane coating"; Applied Surface Science; 257,899-904,2010.



Simulation insights into the thermal conductivity of carbon nanotubes bundles and carbon nanocomposites: A reverse non-equilibrium molecular dynamics study

M. R. Gharib-Zahedi^a, M. Alaghemandi^b, M. Tafazzoli^{a,*}

^a Department of Chemistry, Sharif University of Technology, 11365-9516 Tehran, Iran

^b Lehrstuhl für Theoretische Chemie, Fakultät für Chemie, Universität Duisburg-Essen, D-45117 Essen, Germany

Email: tafazzoli@sharif.edu

Abstract:

Understanding and modeling thermal transport properties in nanostructured materials is an important concern for the design of high-performance nanoscale devices for specific applications. Individual carbon nanotubes (CNTs) typically self-assemble into bundles containing tens to hundreds of hexagonally close-packed nanotubes [1]. The thermal conductivity of the bundles in the direction perpendicular to the tube axis is considerable less than the parallel value. This reduction is due to those phonons, as predominant energy carriers in carbon nanostructures, which scattered at the interfaces. Here, in this study, we have chosen a (10, 10) nanotubes bundle. Using reverse non-equilibrium molecular dynamics simulations (RNEMD) [2], the thermal conductivity of the CNT bundle is investigated. The measured thermal conductivities showed a value of about $0.5 \text{ W m}^{-1} \text{ K}^{-1}$ in the direction perpendicular to the tube axis at 300 K, while the parallel values are about two to three orders of magnitude larger [3]. Thus, although individual CNTs possess high axial conductivity as a best conductor, the bundles of CNTs act as an insulator in the perpendicular direction of tube axis i.e., anisotropy in the thermal conductivity. In addition to the neat CNTs bundles, we have also studied the CNT-polymer and graphene-polymer nanocomposites to understand the origin of the relatively low thermal conductivity in the nanocomposites. The main reason is the high interfacial thermal resistance between the nanotubes and the polymer which hinders heat to be transferred from the slow-conducting polymer into the fast-conducting nanotubes and back into the polymer.



Key words: Carbon Nanotubes, Molecular Dynamics, Nanostructures, Polymer Nanocomposite, Thermal Conductivity

References:

- [1] A. Thess, R. Lee, P. Nikolaev, H. Dai, P. Petit, J. Robert, C. Xu, Y. H. Lee, S. G. Kim, A. G. Rinzler, D. T. Colbert, G. E. Scuseria, D. Tomanek, J. E. Fischer, R. E. Smalley, *Science* 273 (1996) 483
- [2] F. Müller-Plathe, *J. Chem. Phys.* 106 (1997) 6082
- [3] M. Alaghemandi, E. Algaer, M.C. Bohm, F. Müller -Plathe, *Nanotechnology* 20 (2009) 115704

Acidic Nanomagnet as a Green Catalyst for the Synthesis 1,2,4,5-Tetrasubstituted Imidazole

N. Azizi*, M. Maryami, A. Rahimzadeh Oskooee

Chemistry and Chemical Engineering Research Center of Iran, P.O. Box 14335-186, Tehran, Iran

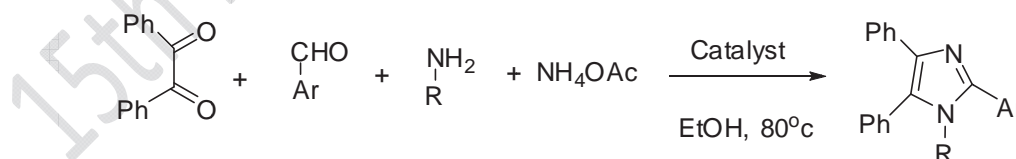
E-mail: azizi@ccerci.ac.ir

Keywords: Green Catalyst, Easy work-up, Nanomagnet, Imidazole

Introduction:

Imidazoles are the core structures of many biological systems such as histidine, histamine and biotin, an active component in drug chemistry, pesticides [1]. In recent years, there are growing interests on the catalytic properties of transition metal nanoparticles because of their large surface area and a great ratio of atoms remaining at the surface [2]. Although many researchers have been done, there is still the paramount challenge for the wide application of transition metal nanoparticle as catalysts in the industry, i.e. how to separate and recycle them completely from the products.

Through out of our investigation, on one-pot multicomponent reaction, herein we report a simple highly versatile and efficient synthesis of 1,2,4,5-tetrasubstituted imidazoles by four component cyclocondensation of 1,2-dicarbonyl compounds with aldehyde, primary amine, and ammonium acetate, as ammonia source using functional nano $\text{Fe}_3\text{O}_4(\text{Fe}_3\text{O}_4\text{-pr-SO}_3\text{H})$ as catalyst in ethanol at moderate temperature.



Scheme 1. Synthesis of 1,2,4,5-substituted imidazoles

Materials and methods:

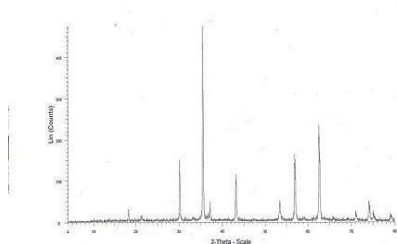
All reagents and solvents were used without further purification. The iron (II) chloride tetrahydrate ($\text{FeCl}_2 \cdot 4\text{H}_2\text{O}$, 99.7%), iron (III) chloride hexahydrate ($\text{FeCl}_3 \cdot 6\text{H}_2\text{O}$, 99.0%), ammonia ($\text{NH}_3 \cdot \text{H}_2\text{O}$, 25 wt.% - 28 wt.%), and ethanol ($\text{C}_2\text{H}_5\text{OH}$, 99.7%) are all commercially available. Distilled water is also used for preparation of the solutions.

Apparatus:

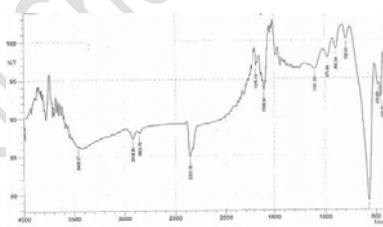
The determination of the size and shape distribution of nanometer size particles can be addressed with several techniques such as scanning electronic microscopy (SEM), Powder X-ray diffraction (XRD) and Fourier transform infrared (FT-IR).

Result and discussion:

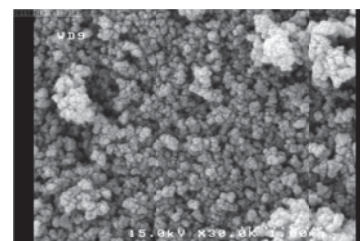
Magnetic nanoparticles of 30–40 nm in size were prepared by a coprecipitation method [2]. The-SH functionalization has been made post-synthetically using 3-mercaptopropyltrimethoxysilane as sulfur precursor and its oxidation to $-\text{SO}_3\text{H}$ has been done according to the literature report [3].



طیف Fe_3O_4 - XRD



طیف Fe_3O_4 - IR



طیف Fe_3O_4 - SEM

Conclusion:

In conclusion, a one-pot, multicomponent methodology has been developed for the synthesis of 1,2,4,5-tetrasubstituted imidazoles catalyzed by nano(Fe_3O_4 -pr- SO_3H) as catalyst in good yields. The mild reaction conditions, easy work-up, clean reaction profiles and cost efficiency render this approach as an interesting alternative to the existing methods.

References:



- [1] Z. Wang, P. Xiao, B. Shen, N. He, *Synthesis of Palladium-Coated Magnetic Nanoparticle and Its Application in Heck Reaction*, Colloids and Surfaces A: Physicochem. Eng. Aspects, **276** (2006) 116–121.
- [2] I. Martinez---Mera, M.E. Espinosa, R. Perez---Hernandez, J. Arenas---Alatorre, *Mater. Lett.*, **61**, (2007), 4447.
- [3] I. Diaz, C. Marquez-Alvarez, F. Mohino, J. Perez-Pariente, E. Sastre, *J. Catal.* **193** (2000) 283.



Synthesis and application of mesoporous poly (*N*-vinyl-2- pyrrolidone) containing palladium nanoparticles.

R.JavadKalbasi, H.Johari

Department of Chemistry, Islamic Azad University, Shahreza Branch, 311-86145 Shahreza, Isfahan, Iran

E-mail: rkalbasi@iaush.ac.ir

Key words: Pd nanoparticles, Poly(*N*-vinyl-2-pyrrolidone), KIT-5, mesoporous silica.

Introduction:

Palladium nanoparticles have become of increasing scientific interest as catalysts for carbon–carbon bond-forming reactions methodologies in advanced organic synthesis. In catalytic applications, a uniform dispersion of nanoparticles and an effective control of particle size are usually expected. They must be embedded in a matrix such as polymer or macromolecular organic ligand. In addition, to avoid the problems associated with metal nanoparticles such as homogeneity, recyclability, and the separation of the catalyst from reaction system, some other works have focused on immobilizing metal nanoparticles on suitable support materials such as immobilization in pores of heterogeneous supports like ordered mesoporous silica [1].

Ordered mesoporous silica materials have received considerable attention because of their unique structures with organized porosity, high specific surface area, and specific pore volume, which make them available to a wide range of applications in the areas of adsorption, separation, sensing, and catalysis. Among the mesoporous materials, materials that consist of interconnected large-pore cage-type mesoporous systems with three-dimensional (3D) porous networks are highly interesting and promise supports for heterogeneous catalysis. Among them, KIT-5, is highly well-ordered cage type mesoporous with cubic Fm3m close packed symmetry, high surface area, large pores, and a high specific pore volume [2].

Materials and methods:

1-Preparation of poly(*N*-vinyl-2-pyrrolidone)/KIT-5 (PVP/KIT-5): *N*-Vinyl-2-pyrrolidone (NVP) (0.5 mL, 4.6 mmol) and KIT-5 (0.5 g) in 7 mL tetrahydrofuran (THF) were placed



dinaround bottom flask. Benzoylperoxide(3mol%,0.034g)was added and the mixture was heated to 65–70 1C for 5h while being stirred under N₂ gas. There sulting white fine powder composite (PVP/KIT-5) was collectedby filtration, was hed several times with THF and finally dried at 601 Cunder reduced pressure 2-Preparation of mesoporous poly (N-vinyl-2-pyrrolidone):In order to obtain purely organic mesoporous polymer, the PVP/KIT-5 composite was stirrer in HF for 6 h and the salid was filtered and wahed with HF (10%).

Apparatus:

The X-ray diffraction pattern of samples were determined using a Brukerdiffractometer (D8 Advance) with Ni-filtered copper radiation ($K_{\alpha}=1.5406 \text{ \AA}$) and 2θ range of 5-80°. FT-IR spectra of the samples, on KBr pellets were recorded with a Nicolet single beam FT-IR (Impact 400D) spectrometer in the range of 400-4000 cm^{-1} at room temperature.

Result and discussion:

The FT-IR spectrum of mesoporousPVP, showed the characteristic peaks for the PVP and showed that the silica groups were successfully removed from the PVP. The XRDpattern of a peak at around $2\theta = 2^{\circ}$ is corresponded to cage-shaped structure and regular pores of PVP which prove the successful formation of mesoporous PVP.

Conclusion:

In this work, we have investigated the critical parameters thatinfluence the synthesis of ordered mesoporous polymeric materialsusing porous silica templates. It was found that the mostimportant factors are the hydrophobic coating of the silica porewalls, crosslinking of the monomers.The formation of highly crosslinked polymersinside the mesoporous silica template faithfully replicatedthe 3D pore system in the resulting rigid polymeric framework. The polymeric framework retained an ordered mesoporouspolymeric structure after release from the template by HF.



References

- [1] R.J. Kalbasi, N. Mosadegh, Synthesis and characterization of Pd-poly(N-vinyl-2-pyrrolidone)/ KIT-5 nanocomposite as a polymer-inorganic hybrid catalyst for the Suzuki-Miyaura cross-coupling reaction, *J. Solid State Chem.* 184, 2011, 3095-3094.
- [2] D. Heung Choi, R. Ryoo, Template synthesis of ordered mesoporous organic polymeric materials using hydrophobic silylated KIT-6 mesoporous silica, *J. Mater. Chem.* 20, 2010, 5544-5550.



Removal of Cu(II) from aqueous solution by adsorption onto Polyacrylamide/KIT-6 NanoComposite

R. JavadKalbasi^{*}, Z. Jahanpour

Department of Chemistry, Shahreza Branch, Islamic Azad University, 311-86145 Shahreza, Isfahan, Iran

E-mail: rkalbasi@iaush.ac.ir

Key words: Polyacrylamide, Nanocomposite, Adsorbent, Cu(II), Water

Introduction:

Ordered mesoporous silica materials have received considerable attention because of their unique structures with organized porosity, high specific surface area, and specific pore volume, which make them available to a wide range of applications in the areas of adsorption, separation, sensing, and catalysis [1]. Among them, KIT-6, is highly well-ordered three-dimensional (3D) type mesoporous with cubic Ia3d close packed symmetry, high surface area, large pores, and a high specific pore volume[2].

Polymer/mesoporous nanocomposite materials have long been extensively studied for their combined advantages of mesoporous inorganic materials (e.g. thermal stability) and organic polymers (e.g. pH stability and chemical functionality) [3]. Moreover, surface functionalization of mesoporous silica with polymer groups is important for practical applications in adsorption of pollutant owing to the inert nature of the amorphous silica surface.

Materials and methods:

Preparation of KIT-6: in a typical synthesis, P123 and n-butanoland 37 wt% HCl the weight ratio of 1:1:2 were dissolved in 270 g (15 mol) of distilled water. To this mixture, 0.061 mol of TEOS was added. The mixture was stirred at 45⁰C for 24 h. Subsequently, the reaction mixture was heated for 24 h at 95⁰C under static conditions for hydrothermal treatment. The



solid product was then filtered, washed with deionized water and dried at 100 °C. Finally, the samples were calcined to remove the template.

Preparation of polyacryl amide/KIT-6 in a typical synthesis, 0.5 g KIT-6 and 0.25 g acryl amide in 7 mL THF were placed in a round bottom flask. 0.025 g Benzoyl peroxide was added and the mixture was heated to 70–75 °C for 5 h while stirring.

Apparatus:

The X-ray diffraction pattern of samples were determined using a Bruker diffractometer (D8 Advance) with Ni-filtered copper radiation ($K_{\alpha}=1.5406 \text{ \AA}$) and 2θ range of 5–80°. FT-IR spectra of the samples, on KBr pellets were recorded with a Nicolet single beam FT-IR (Impact 400D) spectrometer in the range of 400–4000 cm^{-1} at room temperature.

Result and discussion:

The FT-IR spectra of mesoporous PVP, showed the characteristic peaks for the PVP and showed that the silica groups were successfully removed from the PVP. The presence XRD pattern of a peak at around $2\theta = 2$ is corresponded to cage-shaped structure and regular pores of PVP which prove the successful formation of mesoporous PVP.

Conclusion:

This investigation has focused on the application of the Polymer/KIT-6 as adsorbent for the separation and removal of pollutant metal ions. Therefore, polyacrylamide/KIT-6 as a novel heterogeneous nanocomposite was successfully used as an adsorbent for removal of Cu(II) from aqueous solution.

References

- [1] R. J. Kalbasi, N. Mosaddegh, "Synthesis and characterization of palladium poly (N-vinyl-2-pyrrolidone)/KIT-5 nanocomposite for Heck reaction", J. Mater. Res. Bull. 47, 2012, 160.



- [2] R. J. Kalbasi, N. Mosaddegh, "Palladium Nanoparticles Supported on Poly(2-hydroxy ethyl methacrylate)/KIT-6 Composite as an Efficient and Reusable Catalyst for Suzuki–Miyaura Reaction in Water", *J. Inorg. Organomet. Polym.* 22, 2012, 404.
- [3] R. J. Kalbasi, M. Kolehdozan, M. Rezaei, "Synthesis and characterization of PVAm/SBA-15 as a novel organic–inorganic hybrid basic catalyst", *J. Mater. Chem. Physics.* 125, 2011, 784



Production and investigation about nanostructures of PbS thin films

F.Akbarbeiglou*^a, H.Kangarlou^a

^aFaculty of Science, Urmia Branch, Islamic Azad University, Urmia, Iran

(Email: F_akbarbeygloo@yahoo.com)

Keywords: Thin films, Lead sulfide, Deposition time, Deposition temperature.

Introduction:

PbS is a IV-VI semiconductor and has a narrow band gap. Due to the narrow gap, Lead sulfide absorbs infrared radiation therefore it can be used in infrared detector. This material is not only used in various fields such as photography and optical absorption sensors but also is used as light resistance, Temperature and moisture sensors, Solar control and decorative coatings. For these properties and applications of PbS, many Researchers have turned to more study and understand the properties of these materials through various processes such as physical vapor deposition, Sputtering, Chemical vapor deposition and chemical bath deposition. CBD method is more commonly used by researchers because of its low cost and easy to handle. CBD method does not require sophisticated tools and capable of yielding a thin film with good quality on large surfaces.

Characteristics of thin films obtained, are strongly associated with the properties of materials used for to prepare of thin film, Techniques were used for deposition, growth Conditions and kind of the substrates used [1-7].

Optical properties of narrow gap semiconductors are considered, hence in this study, we reviewed and studied the effect of deposition time and deposition temperature on the optical properties, crystal structure and morphology of chemically deposited PbS layers.

Experimental:

For deposition of PbS thin films, lead acetate was used as Pb^{2+} and thiourea as S^{2-} source in an alkaline medium. For this, 50 ml solutions of 0.1 M lead acetate, and 0.1 M thiourea were mixed together. The pH of the bath was adjusted to 10 by drop-wise addition of ammonia. The



distilled water was added to the solution to achieve a total volume of 100 ml. The ultrasonically cleaned glass substrates were dipped in the bath. To obtain the films, one substrate vertically immersed into the solution, supported on the wall of the beaker at 28°C (room temperature), and one other substrate vertically immersed into the solution, supported on the wall of the beaker at 55°C. Time of deposition was 20 min for layers. After deposition, the substrates were taken out and rinsed with distilled water, dried and placed into a desicator. Surface morphology, nanostructures and optical properties of thin layers was studied by using AFM, XRD and Spectrophotometer analysis respectively.

Results and discussion:

1. Surface morphology:

As it can be seen from 2D AFM figures, by increasing deposition temperature, PbS grain will migrate on surface and coalescence happens that tends to growth of bigger clusters of surface. It observed from 3D AFM images of layers, by increasing deposition temperature for same deposition time, morphology of layers changes completely from needle like grains to canonical grains and roughness in creases.

2. Structural analysis:

We understood from XRD figures, both of layers are amorphous and there are no clear crystallographic peaks on patterns. XRD patterns are very noisy, and there is a wide peak at 25 degree, that depends to amorphous glass substrate.

3. Optical properties:

It can be seen from transmittance and reflectance of layers, by increasing deposition temperature grains have surface diffusion and coalescences happens that tends to formation of bigger grains and more voids between them, so transmittance increases and reflectance decreases.

Conclusions :

PbS thin layer were deposited on glass substrate at 20 min deposition time and two different temperature of 28°C temperature and 55°C deposition temperature and same other deposition



conditions, by CBD method. By increasing deposition temperature morphology of PbS/glass thin layers changes from needle like grains to canonical grains and more voids between them. Roughness increases by increasing deposition temperature. Layers are amorphous and by increasing deposition temperature from room to 55°C, transmittance of layers increases and reflectance decreases.

References:

- [1] M.M.Abbas, A.Ab-M.Shehab. Effect of deposition time on the optical characteristics of chemically deposited nanostructure PbS thin films, *Energy procedia* 6 (2011) 241-250.
- [2] N.S.Belova, A.A.Rempel. PbS Nanoparticles: Synthesis and size determination by X-ray diffraction, *inorganic materials* 40 (2004) 3-10.
- [3] M.A.Barote, A.A.Yadav. Characterization and photoelectrochemical properties of chemical bath deposited n-PbS thin films, *Digest journal of nanomaterials and biostructures*, 2011, p. 979-990.
- [4] S.Mahmoud, O.Hamid. Growth and characterization of lead-sulfide films deposited on glass substrates, *FIZIKA A (Zagreb)*, 10 (2001) 1, 21-30.
- [5] A.U.Ubale, A.R.Junghare. Thickness dependent structural, electrical and optical properties of chemically deposited nanoparticle PbS thin films, *Turk J Phys*, 31 (2007), 279-286.
- [6] S.Seghaier, N.Kamoun. Structural and optical properties of PbS thin films deposited by chemical bath deposition, *Materials chemistry and Physics*, 97 (2006) 71-80.
- [7] J.J.Valenzuela-Jauregui, R.Ramirez-Bon. Optical properties of PbS thin films chemically deposited at different temperatures, *Thin Solid Films*, 441 (2003) 104-110.



Magnetic properties of zigzag and ladder Ti nanochains under pressure: An ab-initio study

H. Galavani, M. Jafari

K.N.Toosi University of Technology , Tehran, Iran

Email: galavani_3333@yahoo.com

Key words: Nanochain, Magnetic moment, Zigzag, Ladder

Introduction:

Ti nanowires were manufactured experimentally by different methods [1]. In nanotechnology, ultrathin nanowires or nanochains have fundamental and practical rules. In this work the effect of pressure on the magnetic moment and the bulk modulus of the zigzag and ladder Ti nanochains was investigated. The effect of pressure on the physical properties of materials is largely been studied theoretically [2] and experimentally [3].

Materials and methods:

All the calculations were performed within the framework of density functional theory using the full-potential linearized augmented plane wave plus local orbital (FLAPW+lo) in the Wine2k package [4]. Exchange and correlation effects were treated using the generalized gradient approximation (GGA). We have used supercell approach for simulation of zigzag and ladder titanium nanochains, and the distance between the atomic wires is taken to be about 10Å, which is sufficient to eliminate the inter wire interactions. We employed amount of RMT=2.22, k-point=500, $R_{mt}K_{max}=8$ and RMT=1.92, k-point=2000, $R_{mt}K_{max}=8$ for zigzag and ladder titanium nanochains simulation respectively in magnetic stat (FM) and P=0GPa. The bulk modulus is one of the most important parameters that characterize the bulk property of a material system [5]. Using 3 dimensional Birch-Murnaghan state equations and data produced by our calculations for different volumes, the volume modules (B_o) for zigzag and

ladder structures are respectively 147 and 127 GPa, and its derivative (B'_0) are 6.05 and 6.5 GPa. When we talk about the pressure in solids, in fact, it is a macroscopic quantity that can change the volume. The volume variation can be negative (Contraction) or positive (expansion) regarding the equilibrium volume.

Result and discussion:

From the Figure1, it can be seen zigzag and ladder titanium nanochains in equilibrium distance $h=2.64\text{\AA}$ and $h=2.73\text{\AA}$ by amount of $\mu=0.15\mu_B$ and $\mu=0.9\mu_B$ for magnetic moments are stable respectively. Then by applying pressure this distance increases or decreases, so the magnetic moment of the system varies too. In diagram (a) with increasing pressure the magnetic moment changes about $0.02\mu_B$ but for expansion state this change is about $0.2\mu_B$. For ladder structure the magnetic moment is almost constant in expansion state, but in contraction states it is increased considerably as in $p=12\text{GPa}$ the $\mu=0.98\mu_B$.

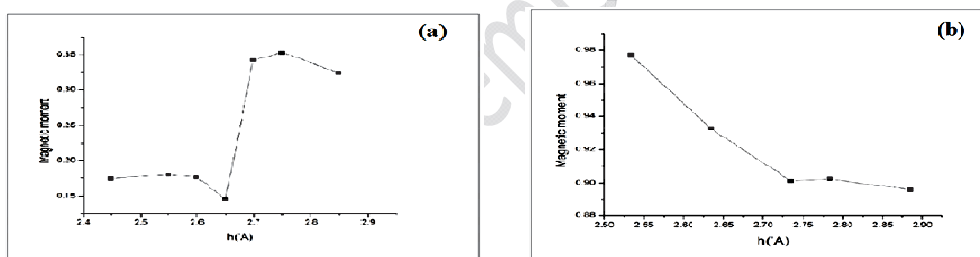


Figure1: Variation of magnetic moment in terms of varies interatomic distance $h(\text{\AA})$: a)zigzag b)ladder

Conclusion:

We investigated magnetic moment of zigzag and ladder titanium nanochains under pressure. The results showed that in the case of ladder structure, the diagram of magnetic moment versus interatomic distance descended before stable point ($h=2.73\text{\AA}$) and gets saturated after that; while in the case of zigzag structure, the diagram is saturated before stable point ($h=2.64\text{\AA}$) which is the minimum of the diagram and after that increases very sharply and then gets almost saturated. Saturated magnetic moment around the equilibrium point for nanochains (as ladder structure) is a determining factor for the application of these structures in the stable systems.



Reference:

- [1] B.J. Inkson, G. Dehm and T. Wagner *Journal of Microscopy* 214, 252 (2004).
- [2]. Kalarasse, B. Bennecer, F. Kalarasse, S. Djeroud, *J. Phys. Chem. Solids* 71 (2010) 1732.
- [3]. Ohara, G. F. Chen, I. Sakamoto, *J. Alloys. Comp* 632 (2001) 323.
- [4] P. Blaha, K. Schwarz, G. K. H. Madsen, D. Kvasnicka and J. Luitz, Vienna, Austria (2001).
- [5] Kittel C 1983 *Introduction to Solid State Physics* (New York: Wiley)



Effect of Polyaniline Nanoparticles on Thermal Behavior of Epoxy Based Thermosets

A.Omrani*, M. Yaghoubi, A. A. Rostami

Faculty of Chemistry, University of Mazandaran, P.O.Bax 453, Babolsar, Iran.

Email: Omrani@umz.ac.ir

Key words: Polyaniline Nanoparticles, Filler, Micellar Polymerization, Epoxy Resin.

Introduction:

Conductive polymers having conjugated structure have applications in various emergence areas. One of these polymers is polyaniline which its electrical properties can be controlled by doping process [1]. The conductive forms of PANI have themselves not so good mechanical properties, and for this reason they are mostly used in blends with common insulating polymers [2,3]. PANI can be used as filler to prepare micro structured electrically conducting composites materials.

In this study, polyaniline nanoparticles are prepared through micellar polymerization and its effect as nanofiller on thermal properties of epoxy resin is investigated.

Materials and methods:

In a synthetic typical route, 0.5 gr aniline (purified) was added to the solution of water-ethanol (50% w/w) with slow stirring. 4- dodecylbenzenesulfonic acid (DBSA) used as dopant and surfactant that was dissolved by stirring for 1 h. Ammonium peroxydisulfate ((NH₄)₂S₂O₈) was used as oxidante (initiator). It was separately dissolved in 10 ml solution water- ethanol (50% w/w). The polymerization was performed by the addition of the initiator solution to the micellar solution. The colour of polymerization solution changed with the process of polymerization reaction. After 24 h, methanol was added to the mixture to stop the polymerization. The precipitated nanoparticles were collected after filtering and washed by ethanol prior to be finally dried at 60°C in vacuum. The thermosetting matrix consisted of a

bisphenol A epoxy resin (Aldrich) cured with 4,4'-oxydianiline curing agent. In the present study, blends containing 1, 3, 5 wt.% PANI-DBSA were prepared and the thermal properties of the samples were studied by DSC and TGA.

Result and discussion:

In Fig.1, DSC thermograms of the uncured EP/PANI-DBSA blends are presented. A single exothermic peak was observed for the different concentrations of the conductive salt in the EP matrix. It can be observed that with an increasing amount of PANI-DBSA in the blends the maximum peak is shifted to higher temperatures, and also the curing time is increased. Our observation showed that the glass transition temperature of the epoxy matrix can be enhanced by the nanoparticles addition. Results from TGA measurements revealed that the thermal stability of the thermosets improved by the addition of polyaniline nanoparticles.

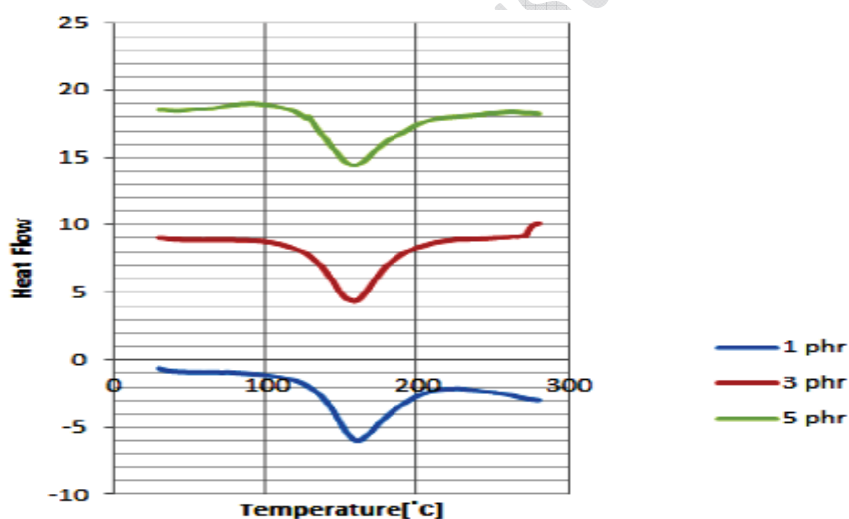


Fig.1. DSC thermogram of uncured EP/PANI-DBSA blends. Heating rate: 10°C/min.

Conclusion:

Conductive EP/PANI-DBSA blends are prepared. The thermal properties of the cured EP/PANI-DBSA blends were characterized by DSC and TGA. The results showed that the composition



having 5 wt.% of polyaniline nanoparticles present better thermal stability and the highest value of T_g .

Reference:

- [1] J. Stejskal, P. Kratochvil, A.D. Jenkins, The Formation of Polyaniline and the Nature of its Structures , Polymer, 37, (1996), 367- 369.
- [2] Y. Cao, S. Paul, A.J. Heeger, Synth. Met. 13, (1992), 91.
- [3] A.J. Heeger, Trends Polym. Sci. TRIP 3, (1995), 18.



Synthesis of well defined polymer nanocomposite by polymerically modified silica

Mojtaba Abbasian *¹, Mitra amirmanesh¹

¹Department of Science, Payame Noor University, Tehran- Iran

E-mail: amirmaneshmitra@yahoo.com

Abstract:

New organically-modified clay that contains an oligomeric styrene has been prepared and used to produce nanocomposites of poly Styrene. Intercalated nanocomposites and, in some cases, exfoliated or mixed intercalated/exfoliated nanocomposites of all of these polymers have been produced by solution method. The use of the styrene-containing clay permits the direct blending of the clay with polystyrene, without the usual need for maleation, to produce the nanocomposites. The systems have all been characterized by X-ray diffraction, transmission electron microscopy, thermogravimetric analysis. These novel new clays open new opportunities for solution blending of polymers with clays to obtain nanocomposites with important properties.

Keywords: Nanocomposite , Polystyrene, Silicate, polymerically modifier, Living radical polymerization

Introduction:

In order to produce a nanocomposite the clay must be well-dispersed throughout the polymer matrix. The clay usually has sodium cations to balance the negative charge that resides on the clay layers and this makes it difficult to incorporate an organic polymer between the clay layers. The usual treatment is to ion-exchange the sodium for an organophilic cation, such as an ammonium ion which contains at least one long alkyl chain. This treatment is usually sufficient to permit the polymer to insert between the clay layers. Clay minerals are hydrous aluminum silicates and are generally classified as phyllosilicates or layered silicates [1].The



Na-MMT clay is hydrophilic and expands the interlayer spaces readily when immersed in water. The clay surface can be converted from hydrophilic to organophilic via cation exchange of Na^+ with alkylammonium ions including primary, secondary, tertiary and quaternary alkylammonium cations under proper conditions [2-3].

Methods:

Synthesis of poly (chloromethyl styrene-co- styrene) via NMRP:

A 100 mL three-necked flask containing 10 mL styrene and p-chloromethyl styrene (50/50 v/v) and 0.15 g (0.7 mmol) benzyl peroxide and 0.13 g (90 mmol.Lit-1) TEMPO stirred at 95 °C for 4 h under argon atmosphere. Then temperature increased to 130 °C and mixture stirred for another 12 h. The mixture cooled at room temperature and the polymer recovered by filtration in ice methanol. This product was dried overnight in vacuum at room temperature.

Surface modification of montmorillonite:

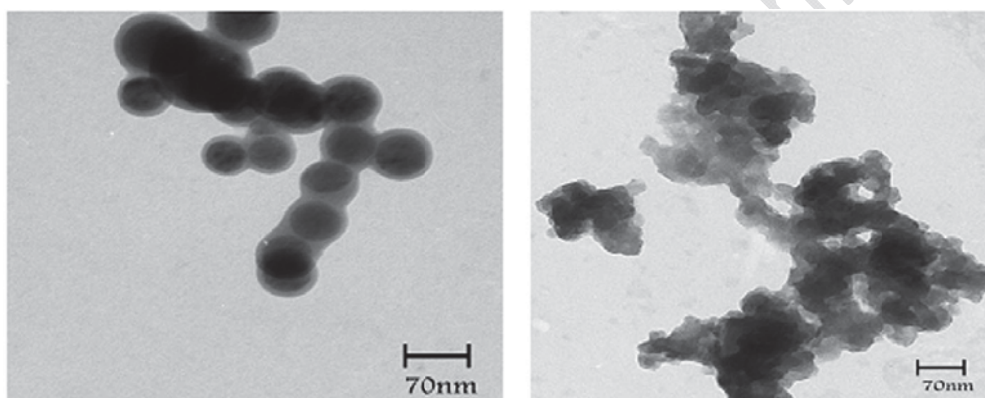
Organophilic montmorillonite (O-MMT) was obtained after treated with poly (chloromethyl styrene-co- styrene) salt ion-exchange process. Montmorillonite was first dispersed in deionized water under ultrasound for 1 h (UNICOM INSTRUMENTS, USA). The modifier was prepared in deionized water separately, and was added to the clay dispersion at an amount a little higher than the CEC of montmorillonite. The resulted suspension was intensively stirred for 10 h, and was then filtered and washed with deionized water three times. The final product was dried in vacuum oven at room temperature for 48 h and grounded into powder.

Preparation of polymer/organoclay nanocomposite:

Certain amount of organophilic montmorillonite (3 Wt %) was first dispersed in 30 mL carbon tetrachloride under ultrasound for 30 min. Then certain amount (1 g) of polystyrene that was synthesized by NMRP method dissolved in 50 mL carbon tetrachloride. The clay suspension was then slowly added to the polymeric solution under vigorously stirring. The resulted suspension was intensively stirred for 6 h at 60 °C. Then the mixture was poured into methanol for rapid precipitation. The precipitate was filtered and dried at 50 °C under vacuum for 2 days.

Result and Discussion:

This polymeric clays offer an advantage in thermal stability when compared to conventional ammonium salts. The degradation begins at higher temperatures for these systems and this may enable solution processing of polymers which require higher temperature, especially the styrene copolymer. It is clear from the TEM results that the styrene copolymer gives nanocomposites in which one can see individual clay layers. The peak heat release rate reduction shows the presence of nanodispersed clay in the polymer matrix and further indicates that the state of this nanodispersion, intercalated or exfoliated or even if the clay is largely present as clay tactoids, is not important as long as there is good nanodispersion.



TEM of polymer-clay nanocomposites were synthesized with nitroxide mediate

References:

- [1]. C.Saujanya, S.Radhakrishnan, Polymer, 2001, 42,6723.
- [2].G.Qiu,Q.Wang,C.Wang,W.Lau,Y.Guo,Sie Di,2007,14,55.
- [3].K.Wormuth,J.Colloid.Interf.Sci.,2001,241,366.



Decolonization of indigo carmine using synthesized nanocomposites zero valent iron

Z.Nooraei¹, Z.Seidabadi¹, Z.Sedighi^{1*}, F.Sakhaei^{1*}, M.E.Olya²

¹Research Institute of Ebnesina, Tehran, Iran

²Institute for color science and technology

Email: zinat_sedighi@yahoo.com and f.sakhaiii@gmail.com

Keywords: Nanozerovalent iron, Multi-wall carbon nanotubes, Nanocomposites, Decolonization

Introduction:

Nanotechnology is currently applied in a wide variety of fields, including environmental and wastewater treatment. There are very few comparative studies, in the literature among various sorbents. In this work, we report a comparison between, Ac with MWCNTs and C₁₈-Silica as sorbents for removal organic pollutant from environmental waters. Nanozerovalent iron (NZVI) technology represent of the first generations of nanoscale environmental clean up technology. Because of its tiny size, its large specific surface and its high surface reactivity. NZVI can enhance the kinetic rate of destruction of many pollutants. Most research on the degradation of dyes by NZVI has been conducted in bach experiments. We quantified the colorization effectiveness of indigo Carmine and dye wastewater by NZVI. We also determined the effect of the sorbents such as Ac and C₁₈ –Silica and MWCNTs on the destruction of dyes by NZVI particle were mixed with adsorbent as a reactive dye was investigated [1-6] .

Material and methods:

Analytical grade FeCl₃.6H₂O and NaBH₄, purchased from Merk Germany, and other agents were all purchased from Sinofharm Group Chemical Reagent, China. MWCNTs diameter of 5 – 15 nm, length of 10-20μm, purity >95% , C₁₈-Silica (pore size of 128Å°) and Carbon active (diameter of 0/15-0/85 mm). This mixture was kept at 25°C under N₂ gas for 1h reaction.



Apparatus:

The freeze-dryer system has been applied for increased efficiency zerovalent and Multi-wall carbon nanotubes are dried in oven for 2h under 120°C temperature. Surface morphology of NZVI-MWCNTs-, NZVI-C₁₈-Silica and NZVI-AC was examined by SEM (Leo1455VP). The XRD analysis were performed with a Cu K α radiation at scanning rate of 8° min⁻¹ in the 2 θ range from 4° to 84° to determine the composition of these particles.

Results and discussion:

Iron nanocomposites synthesized with the borohydride method, have been characterized with technique of SEM and XRD. According to the XRD patterns, the strong peaks 2 θ =44.90 correspond to the iron nanoparticles. The lower intensity of the samples may be due to the small particles. The average particle size of iron in MWCNTs, C₁₈-Silica CA using Debye-Scherrer formula were around 3.157, 2.788, 4.740 respectively. Therefore using MWCNTs, C₁₈-Silica, CA, as a support were effective for increasing the dispersion of the nanoparticles and avoiding the agglomeration of the metallic nanoparticles. The SEM image the most of the NZVI particles were less than 25 nm in diameter. The results shown that reductive degradation of dye in aqueous solution can be achieved in less than 25s by adding using MWCNTs, C₁₈-Silica, CA, as supported nano zero valent iron, namely nanocomposites, under ambient conditions without pH control.

Conclusion:

Our results indicate that NZVI nanocomposites can be successfully used to decolorize indigo carmine from textile dyeing manufacturing wastewater. In this study X-ray diffractometer indicate phase of Iron nanoparticles. The SEM images the most of the NZVI particles were less than 25 nm in diameter. This work proved that NZVI nanoparticles could be supported by MWCNTs, C₁₈-Silica, CA, which exerted excellent acceleration effect on indigo carmine degradation and removal. The UV spectra showed the completed degradation of dye by nanocomposites occurred within 270s under ambient condition without pH control.



References:

- [1] L.N.Shi and etal;" Removal of chromium(VI) from wastewater using bentonite-supported nanoscale zero-valent iron". *Water Res*;45, 886–892, 2011.
- [2] D.W. Elliott and etal; "Degradation of lindane by zero-valentiron nanoparticles". *Journal of Environmental Engineering*; 135, 317-324, 2009.
- [3] T.H.Zheng, and etal;" Reactivity characteristics of nanoscale zerovalent iron-silica composites for trichloroethylene remediation". *Environmental Science & Technology*; 42,4494-4499, 2008.



Evaluation of Rheological Properties of Organoclay as Water-base Drilling Fluid in Iran

M. Mohammadi^{a*}, A. Sarafi, M. Schaffie

^a Department of Chemical Engineering, faculty of Engineering, Shahid Bahonar University, Kerman, Iran

Email: mostafamohammadi6581@yahoo.com

Keywords: Nano Organoclay, Rheological, Cation Exchange Capacity (CEC), Drilling Fluid

Introduction:

Bentonite is a clay mineral produced in many places around the world. It has a significant number of applications such as preparation of green sand moulds for metal casting as a binder, as a thixotropic fluid in wall and road construction and as an additive in drilling fluids for oil-well, geothermal and water-well drilling to control viscosity and filtration properties [1]. Water bentonite suspensions have strong colloidal properties and increase liquid viscosity, behave as non-Newtonian fluids when sheared while under certain circumstances have the unique ability to gel when not sheared. The concentration of bentonite in water suspensions varies depending on the application, for example, may range between 3 and 7% in drilling fluids [2, 3] to control rheological and filtration properties. In the past years there has been significant research to study the rheological behavior of bentonite suspensions [4-6] currently there is a good understanding, however, full understanding of the mechanism of viscosity and gel generation when bentonite is added in water is still under question. After the necessary period of hydration of bentonite particles, rheology of bentonite suspensions depends among other things on bentonite concentration, the presence of ions, particularly electrolytes, temperature and pH of the suspension [1].

Rheological tests were carried out on bentonitic samples obtained from Kheirabadmine in Kerman, Iran. This is to evaluate the performance of the local clays for drilling operations in Iran. The swell index, Cation Exchange Capacity (CEC) and rheological properties of

Kheirabad mud improved by purification and organification. The study shows that beneficiated Kheirabad clay gives a good promise for drilling purposes at optimum clay concentrations. Moreover, Nano Organoclay was a proper additive with adequate rheological properties, as Oil-base Drilling fluid.

Materials and methods:

Four bentonitic samples obtained from Kheirabadmine, and swelling index of them was investigated. Then CEC of Na-bentonite sample, determined by adsorption method of ethylene di amino copper ($[\text{Cu}(\text{EDA})_2]^{+2}$). 20 gr of bentonite that commonly is used in drilling fluid, and 20 gr of nanoclay were mixed separately in 600 cc fresh water; Their viscosity measured by DV-III ULTRA viscometer in 50 rpm and 30 °C. Finally, results were compared.

Result and discussion:

Swelling index of four samples A, B, C and D from Kheirabadmine, was determined to be 10, 20, 12 and 26, respectively; also, it was 19 for common bentonite (E) that is used in drilling fluid. Therefore, sample D was selected to be compared by Sample E. CEC from these samples was obtained to be 78 and 61 for D and E, respectively. Moreover, for produced nanoclay, swelling index and CEC was 37 and 103, respectively. Fig. 1 shows the viscosity measurement in 50 rpm and 30°C, for D (nanoclay) and E samples.

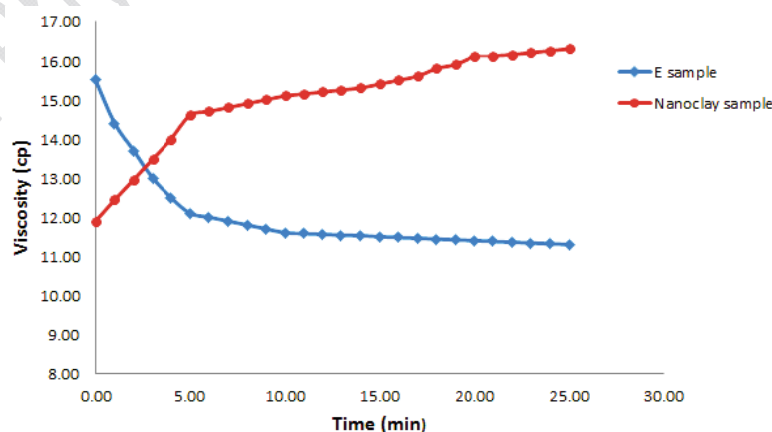




Fig. 1. Viscosity of nanoclay and E samples

Viscosity from D sample, increasing by time and it decreases for E sample, because the alteration structure in nanoclay (e.g. high swelling index and CEC than D sample) is the best reason for this treatment. On the other hand, nanoclay is to some extent rheopectic and E sample have more thixotropic property in 25 min.

Conclusion:

Since the sample which has high swelling index has more Na-bentonite, it is best for production of nanoclay; the produced nanoclay has higher swelling index and CEC than common bentonite (E). Also, nanoclay has more rheopectic property than Na-bentonite. This characteristic causes that during drilling operation stop, viscosity increases, and by keeping cutting in suspension prevent drill stem from sticking.

Reference:

- [1] V.C. Kelessidis, R. Maglione.; Modeling rheological behavior of bentonite suspensions as Casson and Robertson–Stiff fluids using Newtonian and true shear rates in Couette viscometry; Powder Technology 168, 134–147, 2006.
- [2] A.T. Bourgoyne, M.E. Chenevert, K.K. Millheim, F.S. Young Jr.; Applied Drilling Engineering; SPE Textbook Series, vol. 2, Richardson, 1991.
- [3] E.C. Bingham, Fluidity and Plasticity.; McGraw-Hill, New York, 1922.
- [4] R. Maglione, G. Robotti, R. Romagnoli.; In-situ rheological characterization of drilling mud, SPE J. 5 (2000) 377–386.
- [5] T.S. Mihalakis, P.G. Makri, V.C. Kelessidis, G.E. Christidis, A.E. Foscolos, C.E. Papanikolaou.; Improving rheological and filtration properties of drilling muds with addition of greek lignite; Paper presented at the 7th National Congress on Mechanics; June 24–26, Chania, Greece, 2004.
- [6] V.C. Kelessidis, T.S. Mihalakis, C. Tsamantaki; Rheology and rheological parameter determination of bentonite–water and bentonite–lignite–water mixtures at low and high temperatures; Paper presented at the 7th World Congress in Chem. Engineering, Glasgow,



July 10–14, 2005.

Ab - initio investigation of Tramadol adsorption on the single - walled carbon nanotube

A . Rakeb^{a*} , Z . Nikfarjam ^a

^a Department of chemistry , Veterinary directorate general , Bushehr , Iran

Email: a.rakeb@gmail.com

Key words: DFT, carbon nanotube, Tramadol, adsorption.

Introduction:

Structure tramadol closely resembles a stripped down version of codeine. Both codeine and tramadol share the 3-methyl ether group, and both compounds are metabolized along the same hepatic pathway and mechanism to the stronger opioid, phenol agonist analogs. Tramadol hydrochloride is a centrally-acting synthetic analgesic used to treat moderate to moderately-severe pain. The drug has a wide range of applications, including treatment of rheumatoid arthritis, restless legs syndrome and fibromyalgia .

Computational chemistry methods can be used as the analysis of nano materials [1]. Developments in electronic structure methods, in particular in density functional theory (DFT), with the continuous increase of available computing capacities to deliver unprecedented power to computational experiments on atomistic level. Robustness of DFT makes this technique the method of choice in assisting the design and development of the next generation of devices for nano scale applications. The underlying principle of DFT is that the total energy of the system is a unique functional of the electron density, hence it is natural that there exist a large number of computer programs that are designed for calculations of the total energy [2].

Computational Method:

For computing Ab-initio is used because this method is the best mathematical approximation for real system. In this method the real Hamilton is used and the experiential parameter is not used. Density Functional Theory (DFT) is the exactitude method of Ab-initio. Energy of n electrons system is the basis of density possibility. In fact energy is $E(\rho)$ and density is $\rho(r)$. Density Functional is polar matrix. This method is named Density Functional Method (DFT). Electron energy of a system in DFT method according to the kohn-sham equation is $E = e_t + e_v + e_j + e_{xc}$. e_t is kinetically energy, e_v is potential energy of nucleon – electron and nucleon – nucleon, e_j is expulsion of electron – electron and e_{xc} is correlation and interchange of electron. All calculated in gas phase with Gaussian 09 package of program by B3LYP method at 6-311++G** standard basis set.

Results and Discussion

Given the change of gap energy to the up side in chart 2 we can conclude that adsorption beginning from 1 Å and reaches to its peak in 5 Å. for closer examination of this issue we have plotted the gap energy and the system overall energy and both energy showed excellent adjustment.

Figure 1. structure of CNT and Tramadol (absorption site)

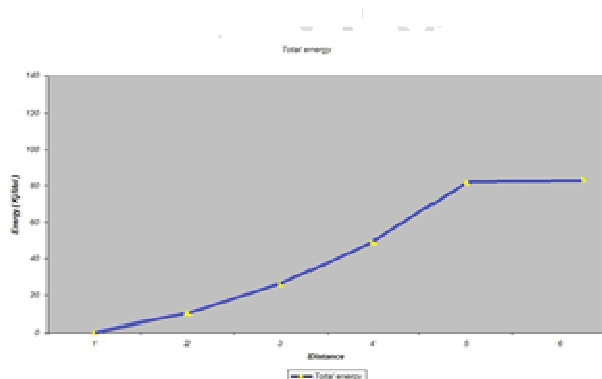


Chart 1. Total energy of CNT and tramadol system (KJ/Mol)

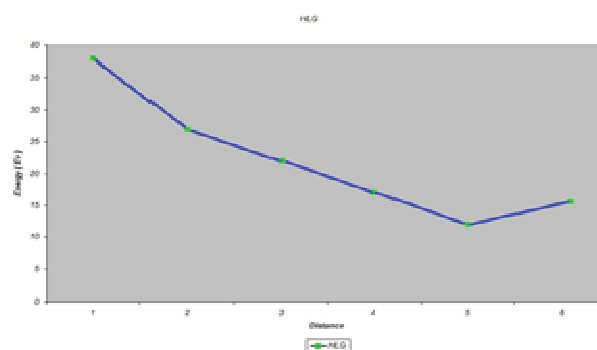


Chart 2. HOMO – LUMO - GAP energy (KJ/Mol)

Conclusions:



In this paper, it has been investigated the most stable structure of tramadol with CNT in different places of the molecule. To gain this purpose, the total energy of system has been calculated in different places from 5 Å of molecule to carbon termination and then in different points to 5 Å from carbon termination of CNT. Based on theoretical observation and reviewing the HLG energy, we found the stable place in termination of CNT. Diagrams of energy is plotted in Chart 1 and 2. HLG parameter has been calculated. The results show that the most stable structure has the greatest value of Homo-Lumo energy.

References :

- [1] B. Sitharaman, R.D. Bolskar, I. Rusakova, L.J. Wilson, Nano Lett. 4 (2004) 2373.
- [2] G.R. Mettam, L.B. Adams, A.D. Becke, Phys. Rev. A 38 (1998) 3098.



Study of morphology and optical properties of PVDF films after addition of Au nanoparticles

B. Jaleh^a, F. Bazak^a, A. A. Yousefi^b, M. J. Torkamany^c

^a Department of Physics, Bu Ali Sina University, Hamedan, Iran

^b Iran Polymer and Petrochemical Institute, Tehran, Iran

^c Iranian National Center For Laser Science and Technology (INLC), Tehran, Iran

bkjaleh@yahoo.com

Key words: polyvinylidene fluoride, Au Nanoparticle, β -Phase.

Introduction:

Within the last two decades poly (vinylidene fluoride) has been extensively studied. This is because of the extraordinary pyroelectric and piezoelectric properties. Polyvinylidene fluoride (PVDF) is a semicrystalline polymer with five different crystalline structures having high permittivity, excellent thermal stability. Consequently, PVDF finds widespread applications in transducers, sensors, actuators and MEMS [1-3]. NPs of noble metals like Au recognized to exhibit optical properties. Metal-Polymer nanocomposites have recently received great interest because of their potential applications in nanoelectronic devices, sensors and optical devices.

Materials and methods:

PVDF (MW=534000), in powder form was purchased from Sigma Aldrich. Dimethylformamide (DMF) (Merck) of purity 99.5% was used as solvent. N-Methyl-2-pyrrolidone (NMP) was used as second solvent too. In this work, Au-NPs have been produced by laser ablation of a gold metal plate (99.999%) [4]. Nanocomposites of PVDF/Au were prepared by a solution mixing technique for different Au-NPs concentrations. The prepared films were studied by UV-Vis and SEM analysis.

Apparatus:



The UV-visible measurements were performed at room temperature by a Perkin Elmer 550ES from 300 to 800 nm with a resolution of 1 nm. Morphology and particle dispersion was investigated by scanning electron microscopy (SEM) (Cam scan MV2300).

Result and discussion:

The images of the surface of pure PVDF and PVDF nanocomposites shows spherulitic crystal structure of PVDF; The size of these spherulites decreased with the further increase of Au-NPs content. The UV-Vis spectra shows a surface plasmon resonance (SPR) band centered around 537 nm, the absorption spectra are essentially in agreement with that of chemically prepared gold nanoparticles. optical band gap for pure PVDF and its nanocomposite films has been determined. The value of E_g decreases from 4.62 eV for pure PVDF to 2 eV for PVDF/0.5% Au nanocomposite. Such a decrease in the value of E_g can be attributed to the formation of trap levels between the HOMO (Highest Occupied Molecular Orbital) and LUMO (Unoccupied Molecular Orbital) energy states. The presence of the nanoparticles introduce many states into the polymer's HOMO-LUMO gap, making the lower energy transitions possible and results in the reduction of optical band gap.

Conclusion:

The PVDF/Au nanocomposites were prepared by mixing of Au-NPs in NMP and PVDF solution. The nanocomposite films were studied by various methods. Scanning electron microscope (SEM) micrographs showed spherulitic crystal structure of PVDF [3]. The spherulitic morphology of the pure PVDF is maintained for PVDF nanocomposites; the size of spherulites decreases by increase in weight fraction of Au nanoparticles. The optical band gap values (E_g) deduced from UV-Visible absorption spectra were found to reduce from 4.62 eV in pure PVDF to 2 eV after embedding 0.5 wt% of Au nanoparticles.

Reference:

- [1] Salimi, A.; Yousefi, A. A. Polym Test 2003, 22, 696.
- [2] Novinger, A. J. Macromolecules 1982, 15, 40.



[3] Bendetti, E.; Catanorchi, S.; Dalessio, A.; Moggi, G.; Vergamini, P.; Parcalla, M.; Ciardelli, G. *Polym Int* 1996, 41, 35.

[4] Alvarez M M *et al* 1997 *J. Phys. Chem. B* 101 3706.

15th Physical Chemistry Conference



Applying Homogeneous Precipitation for Synthesis and Physicochemical Characterization of CuO/CeO₂/Al₂O₃ and CuO/ZrO₂/Al₂O₃ Nanopowders

M. Abdollahifar^{a,b}, M. Haghighi^{a,b*}, H. Ajamein^{a,b}

^a Chemical Engineering Faculty, Sahand University of Technology, Tabriz, Iran

^b Reactor and Catalysis Research Center (RCRC), Sahand University of Technology, Tabriz, Iran

*Email: haghighi@sut.ac.ir

Keywords: Homogeneous Precipitation, CuO/CeO₂/Al₂O₃, CuO/ZrO₂/Al₂O₃, Nanopowder.

Introduction:

Alumina supported copper oxide composites are widely applied in variety of organic and inorganic catalytic reactions such as CO, hydrocarbon and alcohol oxidation as well as NO_x and SO₂ reduction reactions [1,2]. In this research, effect ZrO₂ and CeO₂ on the physicochemical properties of two ternary CuO/ZrO₂/Al₂O₃ and CuO/CeO₂/Al₂O₃ composites were studied.

Materials and methods:

CuO/ZrO₂/Al₂O₃ and CuO/CeO₂/Al₂O₃ composites were prepared by homogenous precipitation method from nitrate form of consumed metals. Different analysis such as XRD, FESEM, FT-IR and BET were carried out to describe their various characteristics.

Result and discussion:

X-ray diffraction patterns were shown in Figure 1 for both CuO/ZrO₂/Al₂O₃ and CuO/CeO₂/Al₂O₃ composites. Strong peaks of CuO were observed in $2\theta=35.5$ and 38.8 . For CeO₂, only the weak diffraction peak could be observed at 28.7 . It is true in case of ZrO₂ which its weak peak was depicted at 30.3 . No peaks were monitored for Al₂O₃ because of its little amount. FESEM images were illustrated in Figure 2. They described the nanometer particles morphology of both CuO/CeO₂/Al₂O₃ and CuO/ZrO₂/Al₂O₃ composites. Figure 3

shows the comparison of the specific surface area of nanopowders. The specific surface area of $\text{CuO/ZrO}_2/\text{Al}_2\text{O}_3$ is about 16% higher than $\text{CuO/CeO}_2/\text{Al}_2\text{O}_3$. The FT-IR analysis results were depicted in Figure 4. Bands at 520 cm^{-1} shows metal oxides while bands in range of 1400-2200 can be assigned to alumina which was not detected in XRD analysis.

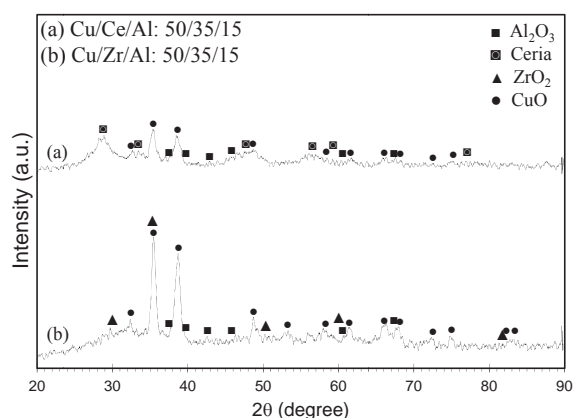


Figure 9: XRD patterns of nanopowders.

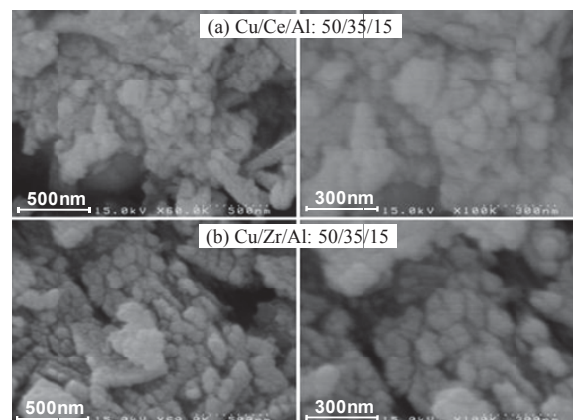


Figure 10: FESEM images of nanopowders.

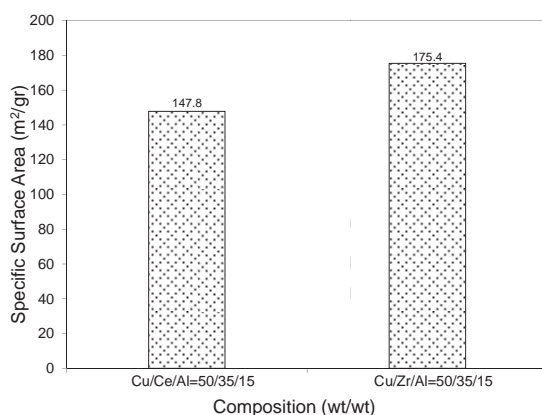


Figure 11: BET surface area of nanopowders.

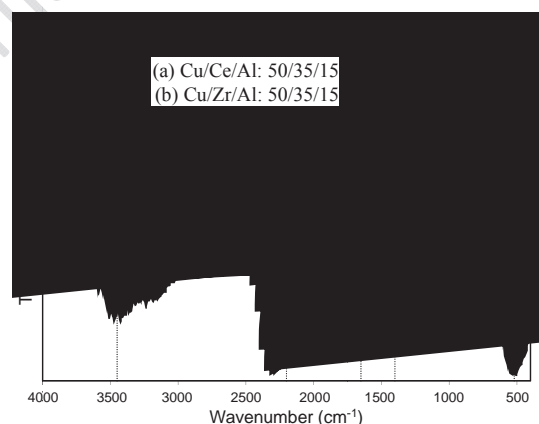


Figure 12: FTIR spectra of nanopowders.

Conclusion:

Two ternary $\text{CuO/ZrO}_2/\text{Al}_2\text{O}_3$ and $\text{CuO/CeO}_2/\text{Al}_2\text{O}_3$ nanomaterials were prepared by conventional homogeneous precipitation method. The physicochemical characteristics analyses determine the existence of components, their crystallinity, and morphological



properties. It can be concluded that homogeneous precipitation could be an efficient method for alumina supported copper oxide composites.

References:

- [1] M. He, M. Luo and P. Fang, "Characterization of CuO Species and Thermal Solid-Solid Interaction in CuO/CeO₂-Al₂O₃ Catalyst by In-Situ XRD, Raman Spectroscopy and TPR", *Journal of Rare Earths*, 24, (2), 188-192, 2006.
- [2] H. Zou, S. Chen and W. Lin, "Effect of pretreatment methods on the performance of Cu-Zr-Ce-O catalyst for CO selective oxidation", *Journal of Natural Gas Chemistry*, 17, (2), 208-211, 2008.



Ultrasound Assisted Urea-Nitrates Combustion Synthesis and Physicochemical Characterization of CuO/ZnO/Al₂O₃ Nanopowder

H. Ajamein^{a,b}, M. Haghighi^{a,b*}, M. Abdollahifar^{a,b}

^a Chemical Engineering Faculty, Sahand University of Technology, Tabriz, Iran

^b Reactor and Catalysis Research Center (RCRC), Sahand University of Technology, Tabriz, Iran

*Email: haghighi@sut.ac.ir

Keywords: Ultrasound, Urea-Nitrates Combustion, CuO/ZnO/Al₂O₃, Nanopowder.

Introduction:

Combustion synthesis is one of the recent novel methods to produce nanomaterials. It is very advantageous because of applying inexpensive raw materials, fast and simple methodology and achieving fine porous powders with high homogeneity [1]. Its efficiency will be increased when assisted by ultrasonic method [2]. In this research, ternary CuO/ZnO/Al₂O₃ nanopowder was prepared by ultrasonic assisted combustion and its physicochemical characteristics were investigated by various analyses.

Materials and methods:

Ternary CuO/ZnO/Al₂O₃ nanocomposites with composition of 30/50/20 were prepared by urea-nitrite combustion and ultrasonic assisted urea-nitrite combustion. Various kinds of analyses such as XRD, FESEM, FT-IR and BET, were applied to characterize their physicochemical properties like crystallinity, surface area, material detection and surface morphology.

Result and discussion:

Figure 1 illustrates the X-ray diffraction patterns for CuO/ZnO/Al₂O₃ nanomaterial. Identified peaks observed at $2\theta=38.5$, 38.8 and $2\theta=31.7$, 36.2 demonstrated the existence of CuO and ZnO, respectively. No identified peaks were observed for Al₂O₃. In Figure 2 the FESEM

images were depicted for synthesized nanomaterials. It proves that the particles in both methods were in nanometre ranges. The surface area for these nanocomposites was calculated by BET analysis and shown in Figure 3. As expected, the surface area for composite made by ultrasound- combustion method was more than one made by combustion method. The FT-IR test results were shown in Figure 4. Bands at 430-675 cm^{-1} and 1400-1650 cm^{-1} could be assigned to metal oxides and alumina which was not detected in XRD patterns.

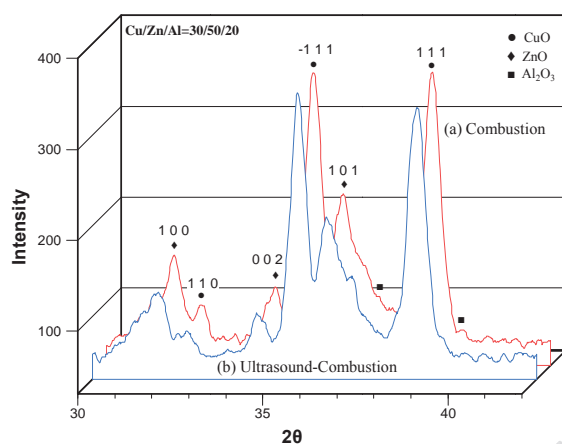


Figure 13: XRD patterns of CuO/ZnO/Al₂O₃ nanopowders.

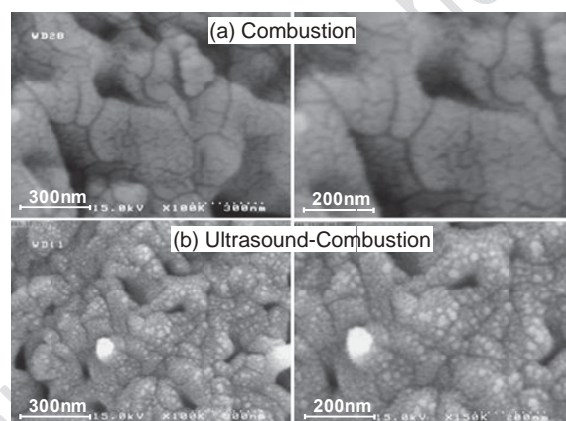


Figure 14: FESEM images of CuO/ZnO/Al₂O₃ nanopowders.

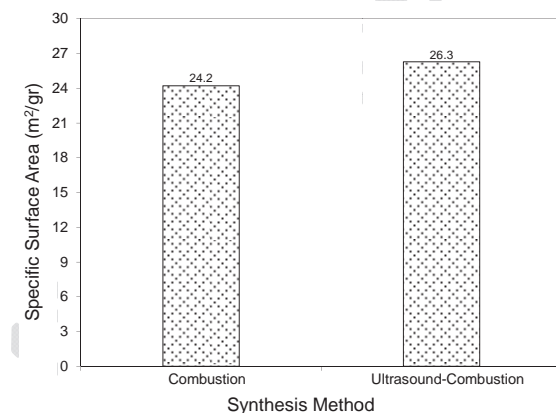


Figure 15: BET surface area of CuO/ZnO/Al₂O₃ nanopowders.

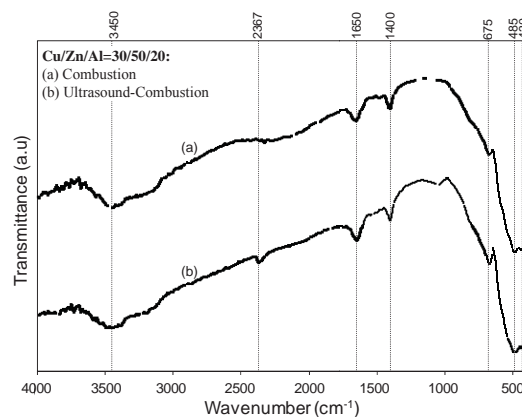


Figure 16: FTIR spectra of CuO/ZnO/Al₂O₃ nanopowders.



Conclusion:

A ternary CuO/ZnO/Al₂O₃ nanomaterial was prepared by two novel synthesis methods: urea-nitrate combustion and ultrasonic assisted combustion. Their physicochemical characterisations were investigated by various analyses such as XRD, FT-IR, BET and FESEM. It was found out using ultrasonic post treatment for material synthesized by combustion method increase the surface area and crystallinity of particles.

References:

- [1] T. Hu et al., "Preparation of a Cu–Ce–O Catalyst by Urea Combustion for Removing CO from Hydrogen", Chinese Journal of Catalysis, 28, (10), 844-846, 2007.
- [2] S. Bennici, A. Gervasini and V. Ragaini, "Preparation of highly dispersed CuO catalysts on oxide supports for de-NO_x reactions", Ultrasonics Sonochemistry, 10, (2), 61-64, 2003.



Experimental investigation on electrical conductivity of Fe₃O₄ nanofluids

H. Khandan Fadafan ^a, M. Adli ^{b,*}, M. Benam ^b

^a Department of Physics, University of Golestan, Gorgan, Iran.

^b Department of Physics, Payame Noor University, 19395-3697 Tehran, I. R. of Iran

Email: maryamadli914@yahoo.com

Key words: Magnetic liquid, Magnetite nanofluid, Fe₃O₄ nanofluid, Electrical conductivity.

Introduction:

Ferromagnetic liquids, ferrofluids, are stable colloidal suspensions of single domain particles of ferromagnetic materials. These relatively new materials have a wide range of applications in modern technology and behave as smart fluids due to their unique features [1-3]. Although ferrofluids have been the subject of numerous investigations during past two decades, their electrical properties have not received enough attention. The present work is an attempt to fill the gap of knowledge on the electrical conductivity (EC) of nanofluids constituted of Fe₃O₄ (magnetite) nanoparticles. For this purpose, the EC of magnetite ferrofluid was measured at different volume fractions and selected temperatures.

Experimental and method:

The magnetite nanofluid was synthesized by chemical co-precipitation technique using Tetramethyl ammonium hydroxide as surfactant [2]. To obtain the best conditions for the formation of Fe₃O₄ nanoparticles, different conditions were performed (table 1). The products were characterized by X-ray diffraction (Mo-K_α radiation, $\lambda=0.7092$ Å), Fourier transform infrared spectroscopy, and transmission electronic microscopy. The electrical conductivity of the nanofluids was measured using Wagtech Ec-meter model Con 11.

Table1. Different conditions in the synthesis of magnetite nanoparticles.

Sample	pH (initial)	pH (final)	Synthesis temperature (°C)
I	6	4	30
II	6	10	30
III	1	10	30
IV	1	10	70

Results and discussion:

Fig. 1.a shows the XRD patterns of all samples prepared under different conditions. This figure confirms the lack of any impurity compound and shows that the best condition for synthesis is belong to sample IV. The TEM image of Fe₃O₄ nanoparticles (Fig. 1.b) shows that the size of nanocrystals is about 15 to 20 nm and the FTIR analysis (Fig. 1.c) reveals that the Fe₃O₄ nanoparticles are free of organic contaminants. Fig. 2 shows the effective EC of Fe₃O₄ nanofluid as a function of temperature (Fig. 2.a) and volume fraction (Fig. 2.b). It can be seen that the EC linearly increases with increasing temperature especially at higher volume fractions and increases linearly with increasing volume fraction at all temperatures. These results are attributed to aggregation of nanoparticles in electric field and their Brownian motion at various temperatures [3].

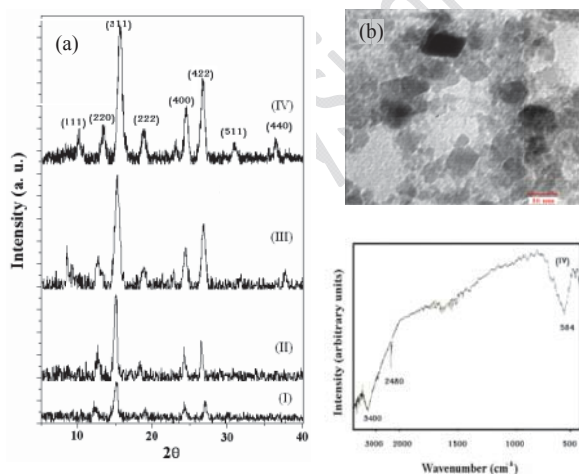


Figure 1. (a) XRD, (b) TEM, and (c) FTIR results of magnetite nanoparticles at room temperature.

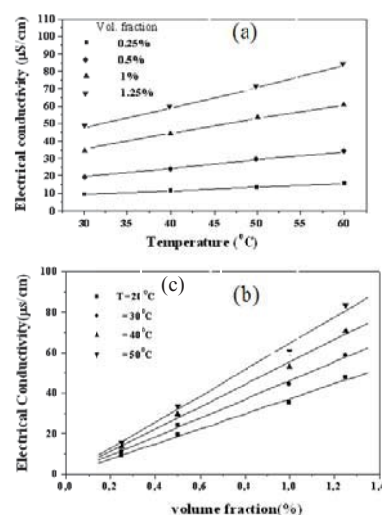


Figure 2. EC of magnetite nanofluid as a function of (a) temperature and (b) volume fraction.



Conclusion

Magnetite nanoparticles were successfully synthesized by chemical co-precipitation method in different conditions. XRD pattern confirms the purity of magnetite phase and TEM images show that the size of nanoparticles is about 15 to 20 nm. The EC measurements of nanofluid show the increase of EC with increase in volume fraction at all temperatures. Moreover, with increasing temperature, the EC linearly increases especially at higher volume fractions. The observed behavior can be explained due to aggregation of nanoparticles in electric field and their Brownian motion at various temperatures.

References:

- [1] Q. Li et al; Exp. Therm. Fluid Sci. 33, 591-596, 2009.
- [2] M. Abareshi et al; J. Magn. Magn. Mater.; 322, 3895-3901, 2010.
- [3] S. Ganguly et al; Powder Technol.; 196, 326-330, 2009.



CaF₂ Nanoparticles: Synthesis and Characterization

M. Esmailipour^{*a}, K. Tahvildari^a, H. Nabipour^b

^aDepartment of Chemistry, Islamic Azad University, North Tehran Branch, Tehran, Iran

^bDepartment of Chemistry, Islamic Azad University, Takestan Branch, Takestan, Iran

(Email: m.esmailipour@yahoo.com)

Key words: Synthesis, Characterization, Nanoparticles, Calcium fluoride.

Introduction:

It has been well-established that alkali earth metal (AEM) fluorides MF₂, where M = Ca, Sr or Ba, should be very attractive host crystals for some applications. These applications may be as Ln and transition metal laser activators since they possess a broad optical transparency region, moderate Raman gain coefficients, relatively small linear and non-linear refractive indices, and rather flat curvature of the refractive index dispersion over a wide wavelength range in the near IR [1]. The aim of the present study was to prepare nano-sized calcium fluoride (CaF₂). Nanoparticles were synthesized by co-precipitation method. The synthesized nanocrystals were characterized by X-ray diffraction (XRD), Fourier transform infrared spectroscopy (FTIR), scanning electron microscopy (SEM).

Materials and methods:

Calcium chloride hexahydrate, ammonium fluoride were prepared in ethanol. CaCl₂ (0.01 mol) was dissolved in 50 ml ethanol taken in 250 ml conical flask. NH₄F (0.02 mol) was added into the flask under vigorous stirring on a magnetic stirrer. The mixed solution was stirred for 3 h to gradually transform the transparent reaction mixture into opaque white suspension gradually. Then, the mixture was centrifuged for 15 min at 4000 rpm and washed three times with water via centrifugation to eliminate the residual chloride and the ammonium ions. Finally the solid product was extracted and then kept in a desiccator over P₂O₅.

Result and discussion:

Powder X-ray diffraction (XRD):

The XRD patterns of CaF_2 nanoparticles and SEM are shown in Fig. 1,2 The nanoparticles size obtained in the range 20–30 nm.

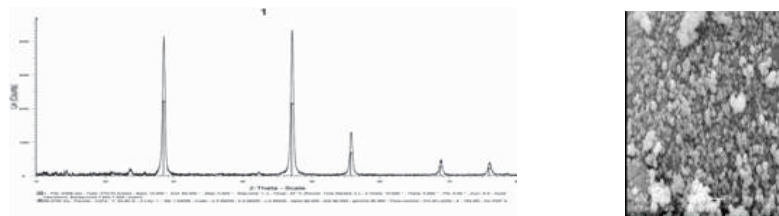


Fig 2. SEM images and XRD of CaF_2 nanoparticles synthesized by co-precipitation method

Fourier transform infrared spectrum (FTIR):

Although the synthesized CaF_2 was a white powder, its purity was further examined by means of FT-IR spectrometry. The peak at 443 cm^{-1} in the FT-IR spectrum in Fig. 3 was assigned to the Ca–F stretching vibration of CaF_2 . The spectrum shows strong IR absorption bands at $\sim 3423\text{ cm}^{-1}$ which is characteristic of H–O–H bending of the H_2O molecules revealing the presence hydroxyl groups in the as prepared sample.

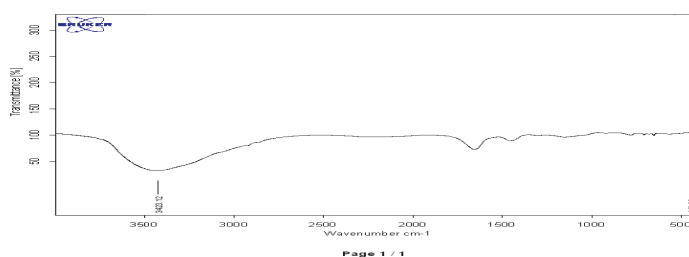


Fig 3. FT-IR spectrum of CaF_2 nanoparticles

Conclusions:

In conclusion, the current report describes the synthesis of pure phase CaF_2 nanoparticles in uniform diameter of $\sim 20\text{ nm}$ by co- precipitation method. It is noteworthy that the co-precipitation method is effective for obtained pure phase nanomaterials with controllable size, uniform morphology and shape. Resulting nanocrystals have been characterized using spectroscopy data.



Reference:

- [1] Kaminskii, A.A., (1981 and 1990), *Laser Crystals, Their Physics and Properties.*, Springer, Berlin, 139-155.

15th Physical Chemistry Conference



Technical and Economical Evaluation Use of Nano Oil in Agricultural Tractor Engines Compared with Conventional Oil

Gh. Nasiri-Khuzani*^a, M. A. Asoodar ^a, M. Rahnema ^a, H. Sharifnasab ^b

^a Department of Agricultural Engineering, University of Agriculture and Natural Resources Ramin, Khouzestan
Iran

^b Scientific Board of Agricultural Engineering Research Institute, Karaj, Alborz Iran

E-mail: Ghasemnassiri63@gmail.com

Key Words: Engine Parts, Wear, Nano-Diamond, Fuel Consumption

Introduction:

Machinery management tries to control maintenance and operation costs by reducing agricultural machinery damages. Higher costs of repair and engine maintenance push engineers to employ technology. Today Nanotechnology has important role to reduce engine wear costs by using nano particles in engine oils. Nano-lubrication therefore can be defined as the art and science necessary to control adhesion, friction, and wear of surfaces coming into contacts at the micro/nano-scale [3]. Nano diamond is one of these additives which could practice less engine wear, special at high dust and haze conditions in agricultural demand with high loads.

Materials and methods:

To study the effect of nano oil on agricultural engines, performance eight Massey Ferguson 399 model tractors manufactured in Iran were used in 2011. These tractors were similar in operating conditions, moreover each block of experiment was based on hours and years of operation and maintenance conditions. Nano oil was used in four tractor engines and Behran turbo .diesel oil with similar nano oil characteristics was utilized for other tractor engines Sampling was taken at 65, 90, 115, 150 interval hours of operation. Subsequently, each sample



was analyzed by atomic absorption spectrometry, particle quantifier (PQ), total base number (TBN), viscosity, fuel and water pollution tests were also applied.

Result and discussion:

Results showed that using of nano diamond in agricultural tractor engines as an oil additive reduced wear in cylinders, gaskets, drive shafts, gears, camshaft and valve mechanisms by 68 percent gaskets and exhaust ,bearing ,Also this additive reduced the wear in piston ring .valve by 64 percent. Lee et al. (2009) found that the friction coefficient of the nano-oil was less than that pure oil over the entire orbiting speed ranges between 300 and 3000 rpm [2]. Hsiao et al (2009) previously reported a large reduction in the friction appeared after adding 2% or/and 3% of the nano-diamond lubricant additive to a base oil [1]. Durability of the nano-oil utilized in agricultural tractor engines was 22 percent more than conventional oil. Fuel consumption reduced 21 percent and viscosity loss was 24 percent lower compared to conventional oil. It can be concluded that the use of nano-diamond additive reduces the total costs of fuel and oil by 24 percent.

Conclusion:

In summary, nano-diamond particle resulted in an improvement of anti-scuffing performance in the engine oil. As a result of various tests, the nano-particles in lubrication oil improved the lubricating performance on the friction surfaces by reducing wear on metal surface.

References:

- [1] Y.Hsiao and et al; "The anti-scuffing performance of diamond nano-particles as an oil additive"; Wear; Kun Shan University; China; 956-967; 2009.
- [2] J.Lee and et al; "Application of fullerene-added nano-oil for lubrication enhancement in friction surfaces"; Elsevier; Tribology International 21; Figure 5; 2009.
- [3] MH.Stephen; "Nano-lubrication: concept and design"; Elsevier; Tribology International; 1-9, 2004.



Sono-synthesis of Nanocomposite (TiO₂-Cu₂O) and Their Application in Degradation of Surfactants from Aqueous Solution by Sunlight

A. Talebian, N. Ghows, M.H. Entezari*

Department of Chemistry, Ferdowsi University of Mashhad, 91775, Mashhad, Iran

*Email: moh_entezari@yahoo.com

Keywords: TiO₂-Cu₂O nanocomposite, Ultrasound, Visible light, Detergent, degradation

Introduction:

Water pollution caused by synthetic surfactants has been increasing during the past few years due to their extensive use in household, industry, and etc. [1]. Releasing detergents into environmental lead to significant effects due to their toxicity and hinder from the dissolution of atmospheric oxygen into natural waters and the sedimentation of floating particles [1]. Hence, great attention has been paid on their efficient degradation. Different methods such as biodegradation, ozonation, and ultrasound have been reported to their decomposition [2]. But, they have some disadvantages such as enhancing foam formation, resisting to degradation, using of expensive energy sources, and forming by-products with higher toxicity [1, 2]. For this reason, photoassisted destruction would be desirable to completely eliminate surfactants from the effluents and the opportunity for solar light utilization.

Cu₂O is a fascinating material with ideal band gap energy (2.0 eV) [3] in the solar cells, photocatalysis and etc. However, its photocatalytic activity is limited because of recombination of the hole and electron. In order to improve the photo-efficiency and enhance its catalytic properties, it has been combined with other materials such as TiO₂ [3].

In this study, a method has developed to produce TiO₂-Cu₂O nano-composite under ultrasound in order to exploit the maximum optical absorption in the visible range and increase the highest photocatalytic efficiency for the degradation and mineralization of the selected



detergent. In addition, easier workup, better control in preparation of nano-composite can be considered as advantageous of this study.

Materials and methods:

The nanocomposite of $\text{TiO}_2\text{-Cu}_2\text{O}$ was prepared by the hydrolysis of titanium butoxide and reduction of copper acetate under different conditions of ultrasound. The precipitate was separated, washed, and dried. Then, the photocatalytic degradation of dodecylbenzenesulfonate (DBS) and sodium dodecyl sulfate (SDS) under sunlight was performed under different conditions

Apparatus:

The nanocomposite was synthesized under ultrasonic irradiation. It was characterized by XRD, TEM, FT-IR spectroscopy, EDAX. The concentration of detergents was monitored with UV-Vis spectrophotometer at $\lambda_{\text{max}} = 224\text{nm}$ (DBS) and at 652 nm for SDS (the colour agent was methylene blue for SDS). COD analyses were carried out according to the dichromate method.

Result and discussion:

The results of EDAX, FT-IR, TEM and XRD measurements confirm the crystallinity and purity of nanocomposit. The XRD patterns indicated that size nanoparticles to be about 8.4 nm. In this study, the preparation method has an important role on the structure and properties of the composites. It is confirmed that sonication would favor the formation of nanocomposite with highest photocatalytic activity and mineralization of DBS and SDS on the surface of catalyst under the solar light. The extent of degradation depends on the operating conditions employed such as the type and concentration of catalyst, and etc. In addition, the $\text{TiO}_2\text{-Cu}_2\text{O}$ exhibited better photocatalytic activity than Cu_2O or TiO_2 alone with decreasing COD and increasing their mineralization. The lowering of COD could be effectively improved by increasing the treatment time. Also, the data obtained from the degradation experiments were fitted to the first-order kinetics and their adsorption obeyed the the Langmuir equation.



Conclusion:

A method has developed to produce $\text{TiO}_2\text{-Cu}_2\text{O}$ nano-composite under ultrasound for obtaining the maximum optical absorption in the visible range and the highest photocatalytic efficiency for mineralization of DBS and SDS. The extent of degradation depends on the operating conditions employed such as the type, concentration of catalyst, and etc. Their degradation in the presence of $\text{TiO}_2\text{-Cu}_2\text{O}$ was better than TiO_2 and Cu_2O alone with lowering of COD.

References:

- [1] A. Amat; etal; "Photo-Fenton reaction for the abatement of commercial surfactants in a solar pilot plant"; *Solar Energy*; 77, 559–566, 2004.
- [2] L. Yang; etal; " Degradation of alkylbenzene sulfonate surfactants by pulsed ultrasound"; *J. Phys. Chem. B*; 109, 16203-16209, 2005.
- [3] F. Niu; etal; "In Situ Loading of Cu_2O Nanoparticles on a Hydroxyl Group Rich TiO_2 Precursor as an Excellent Catalyst for the Ullmann Reaction" ; *Nano Res*; 3(11), 757–763, 2010.



Synthesis and Characterization of Tungsten Oxide Intercalation Nanohybrids

M. Afsharpour*

*Chemistry & Chemical Engineering Research Center of Iran, Tehran, Iran

afsharpour@ccerci.ac.ir

Keywords: Tungsten oxide, nanohybrid, catalyst

Introduction:

Inorganic-organic hybrid materials, especially metal oxides are the main concern of many current research projects, owing to their potential applications in catalysis, sorption, photochemistry and electronics [1]. The synthesis of inorganic-organic hybrids by intercalation of organic ligands into layered tungsten oxide has been extensively explored [2-4]. Organic components act as a ligand incorporated into the metal oxide backbone. Furthermore, such organic-inorganic hybrid materials have a new properties arising from the interplay of two components. In this work we describe our attempts to synthesize new tungsten oxide nanohybrids by intercalation of organic ligands, 4-aminobenzoic acid (PABA), 1,4-diaminobenzene (DAB), 1,4-benzodicarboxylic acid (BDC), between oxide layers.

Synthesis:

A mixture of 1mmol of yellow tungstic acid and 1mmol of each ligands in a solution containing ethanol and water was stirred for approximately 24h, until solid powder was obtained. The product was collected by filtration and dried at room temperature.

Result and discussion:

On the basis of X-ray diffraction, scanning electron microscopy, thermogravimetry and infrared results, a possible arrangement of organic ligands in the interlayer space of tungsten

oxide has been proposed. By replacing the interlayer water molecules under mild condition with organic ligands a control over the morphology can be gained.

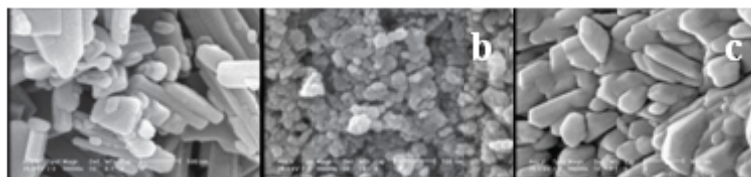


Fig. 1 SEM images of synthesized nanohybrids. (a) $\text{WO}_3\cdot\text{BDC}$, (b) $\text{WO}_3\cdot\text{PABA}$ (c) $\text{WO}_3\cdot\text{DAB}$.

Results shows that our nanocatalysts could successfully catalyzed the epoxidation of the selected olefins with high reactivity (78-96%) and selectivity (97-98%). It indicated that the additional electron density donation from the ligand to the Mo center significantly weakens the Mo-O bonds. On the basis of these observations, it seems that the differences in the electron-donor capability of the ligands play a role with a slight implication in the rate and activity of the catalysts. The weaker Mo-O bond shows higher conversion based on the electron-donor capability of ligands.

Conclusion:

These nanohybrids are prepared by replacing the interlayer water molecules under mild condition with organic ligands. They are new forms of tungsten oxide hybrid which can be recommended as a suitable catalyst for epoxidation of olefins.

References:

- [1] A. P. Wight et al; Design and Preparation of Organic-Inorganic Hybrid Catalysts; *Chem. Rev.*; 102, 3589-3614, 2002.
- [2] B. Ingham et al; Layered Tungsten Oxide-Based Organic-Inorganic Hybrid Materials; *J. Phys. Chem. B*; 109, 4936-4940, 2005.
- [3] S. V. Chong et al; Novel materials based on organic-tungsten oxide hybrid systems; *Current Applied Physics*; 4, 197-201, 2004.



Selective Oxidation Catalysts Based on Carbon Nanotubes with Covalently Attached to Molybdenum Oxides

M. Afsharpour*

*Chemistry & Chemical Engineering Research Center of Iran, Tehran, Iran

afsharpour@ccerci.ac.ir

Keywords: Carbon nanotube, molybdenum oxide, catalyst

Introduction:

Selective oxidation of organic compounds is an extremely important and useful reaction in the chemical industry. Following discovery of carbon nanotubes, they have been studied extensively in versatile fields because of their novel structural characteristics. Carbon nanotubes based on transition metal derivatives are being also widely studied, among them molybdenum oxide MoO_3 is an oxide which have been used for the development of materials potentially useful for catalysis, electrodes and sensors.

Here we describe the rapid and facile chemically controlled deposition of MoO_3 in the cavity of CNTs.

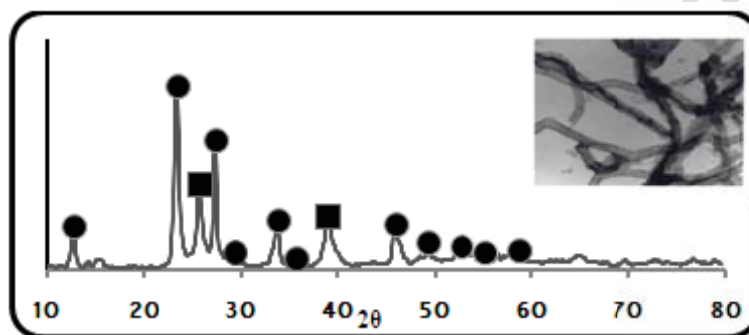
Synthesis:

Here, we use the simplest opening method for nanotubes by catalytic oxidation in the presence of peroxomolybdenum precursor. This experiment is easily perform in one-step method by refluxing MWNTs with MoO_5 complex at 60°C .

Result and discussion:

It is suggested that three distinct stages maybe exist during the filling of MoO_3 into MWNTs based on our observation. In the first stage of immersion, MoO_5 solution was functionalized and opened the end of the MWNTs. In the second stage of the treatment, the MoO_5 solution was

soaked into the empty cavity of MWNTs. The inner cavity acted as a reactor with sucked MoO_5 solution and the MoO_5 solution was then functionalized the inner surface of MWNTs and nucleated to be MoO_5 nanocrystals. In the third stage of the calcinations at 300°C in air, the MoO_3 nanocrystals in the inner cavity further grew up and yield a filling formed by a series of spherical nanoparticles. According to the conservation of mass, the amount of MoO_3 nanoparticles filled in the cavity is consistent with the concentration of MoO_5 solution. So, the amount of MoO_3 nanoparticles filled in the MWNTs can be controlled by changing the concentration of MoO_5 solution.



Conclusion:

In this paper, MoO_3/CNTs hybrids were prepared due to the strong chemical bonding of molybdenum oxide on carbon materials. In one step, the CNTs applied to functionalize and then the functionalized nanotubes were decorated with MoO_3 nanoparticles. MoO_3 were found to show a strong interaction with CNTs and resulting MoO_3/CNTs hybrids were proven to be a good catalyst for alcohol oxidation. The selectivity of the hybrid was found to increase dramatically when MoO_3 react with functional group of CNTs.

References:

- [1] J. M. Planeix et al; Application of Carbon Nanotubes as Supports in Heterogeneous Catalysis; J. Am. Chem. Soc; 116,7935-7,1994.
- [2] F K. Jurkschat et al; Multiwalled Carbon Nanotubes with Molybdenum Dioxide Nanoplugs; Small; 2,95-98,2006.



The effect of multi wall carbon nano tubes on NMRI mouse anterior limb bud development in in vivo systems

Kazem Parivar PhD¹, Nasim Hayati Roodbari PhD², Alireza Badieli PhD³,
Shiva Afshani MSc⁴

¹Professor, Department of Biology, Science and Research branch, Islamic Azad university, Tehran, Iran

²Assistant professor, Department of Biology, Science and Research branch, Islamic Azad university, Tehran, Iran

³Associate professor, School of Chemistry, College of Science, University of Tehran, Tehran, Iran

⁴MSc, Department of Biology, Science and Research branch, Islamic Azad university, Tehran, Iran

Abstract:

Aim: Carbon nano tubes are used in biosensor technology, tissue scaffold, drug delivery and tissue engineering in biological sciences. Scope of this research was investigation on the effects of multi wall carbon nano tubes in NMRI mouse anterior limb bud development in vivo.

Key words: multi wall carbon nano tubes, anterior limb bud, chondrogenesis.

Material and Methods:

In this technique we used 20 pregnant NMRI mice groups: control, sham and experimental. In vivo technique in pregnant mice was used in the animals received different doses of carbon nano tubes (0.5,1 mg/mouse) on day 11 of gestation intraperitoneally. Then the limb buds were amputated from mouse embryos on day 15 of gestation for morphological and histological studies.

Results:

Our research demonstrated that number of hypertrophied chondrocytes and chondrocytes increased ($P < 0.001$) in stylopod, zeugopod and autopod areas also cell division increased



($P < 0.001$) in stylopod, zeugopod areas. Muscle cells decreased ($P < 0.001$) in tree zones of limb bud when compared with control and sham groups.

Conclusion:

Our results indicate that injection of multi wall carbon nano tubes in these doses accelerate chondrogenesis in mouse anterior limb bud, and decrease differentiation of muscle cells.

Effect of Catalyst on Grows of Diomond-like Carbon by HFCVD

Z.Purrajabi^{*a}, M.Ghoranneviss^b, M.Aghaie^c

^a Department of Chemistry, Science and Research Branch, Islamic Azad University, Tehran, Iran

^b Plasma Physics Research Center, Science and Research Branch, Islamic Azad University, Tehran, Iran

^c Faculty of Chemistry, North Tehran Branch, Islamic Azad University, Tehran, Iran

(H.purrajabi@gmail.com)

Diomond-like carbon (DLC) is a metastable form of amorphous carbon containing a significant fraction of sp^3 bonds. It can have a high mechanical hardness, chemical inertness, optical transparency, and it is a wide band gap semiconductor [1].

In this work DLCs were grown on silicon substrate that coated with Ni and Au nanocatalyst by hot filament chemical vapor deposition (HFCVD) technique. A combination of CH_4/H_2 renders the growth of carbon nanostructures. Catalytic layers and DLCs were characterized by SEM and Raman spectroscopy.

Raman spectroscopy is an effective technique for the characterization of DLC structure [2], all carbon materials such as DLC coatings indicate features in Raman spectra, named as D and G peaks. In amorphous carbons, the intensity ratio I_D/I_G is related to the size of the sp^2 phase organized in rings [3].

In this study, the above ratio for the two samples with various catalysts were compared.

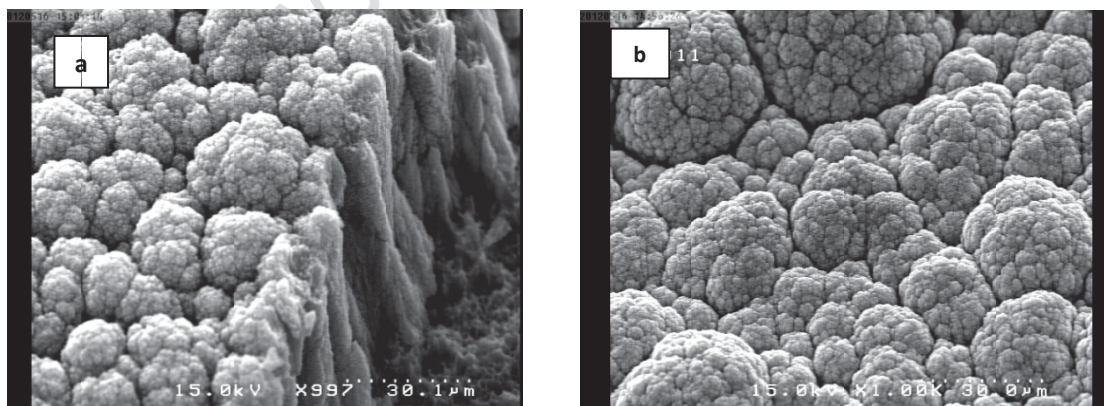


Figure 1- SEM images of the DLC deposited on (a) Au ,(b) Ni nanoparticles

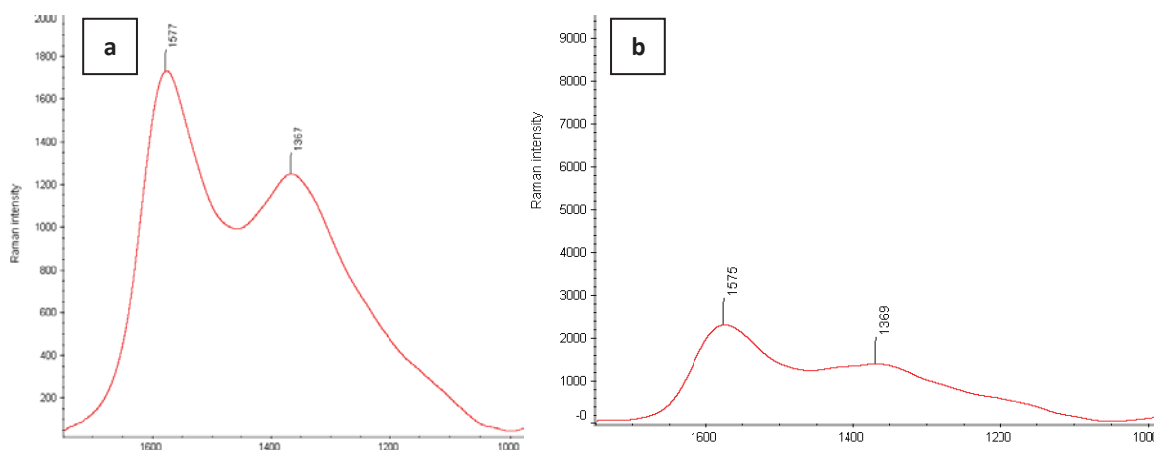


Figure 2- Raman spectra for DLC coating on: (a) Au , (b) Ni nanoparticles

Keywords: Diamond like carbon, DLC, HFCVD, Raman sepectroscopy

References:

- [1] J. Rabertson, Mater.Sci.Eng. R37 (2002) 129-281
- [2] W. G. Cui, Q. B. Lai, L. Zhang, F. M. Wang, Surf. Coat. Tech. 2010, 205, 1995–1999.
- [3] F. Tuinstra, J. L. Koenig, J. Chem. Phys. 1970, 53, 1126.
- [4] J. Q. Chen, J. A. Freitas Jr., D. L. Meeker, *Diamond Relat Mater.* 2000, 9, 48–55.
- [5] M. Kahn, M. ^ekada, Th. Schoberl, R. Berghauser, Ch. Mitterer, Ch. Bauer, W. Waldhauser, E. Brandstatter, Thin Solid Films, 2009, 517, 6502–6507.



Calculation of optical properties of multi layers semiconductors by Kramers-Kronig method

S. Ghahramani^{a*}, H. Kangarloo^a

^aFaculty of science, Urmia branch, Islamic Azad University, Urmia, Iran

E-Mail: SoghraGhahramani@gmail.com

Key words: Multilayer semiconductors, Magnesium fluoride, Titanium dioxide, Kramers-Kronig.

Introduction:

Thin films producing technologies are developing rapidly and nowadays nano techniques are using in producing them. Thin films mechanical properties are much dependent on microstructure and chemical composition, so it depends on deposition technology. Conditions of thin films before deposition, deposition conditions and coatings are important [1, 2].

The use of magnesium fluoride as a support for different catalytic materials, transition metal oxides and binary systems, more over for metallic catalysts [3-9] is appealing. MgF_2 is a nonconductor with a wide band gap and has good thermal stability and considerable hardness also it is an optical material which stands transparent in a broad band of photon energies [10].

TiO_2 films under ultraviolet light act as antibacterial, deodorizing and self-cleaning (Matsubara et al 1995; Negishi et al 1995; Kikushi et al 1997). Conversely, the band-gap energy of TiO_2 is $\sim 3.2\text{eV}$, so, UV illumination is essential to photo activate this semiconductor which is a weakness of it. A number of techniques used to prepare films based on TiO_2 . TiO_2 has widely been studied as a good form material for solar cell, water splitting, and Photo catalysts [11-15]. In this paper we calculate optical properties of multi layers semiconductors such as $MgF_2/MgF_2/\text{glass}$ and $MgF_2/TiO_2/\text{glass}$ by Kramers-Kronig method.

Experimental Details:



Magnesium fluoride and Titanium dioxide thin films were deposited on glass substrates by resistive evaporation from Molybdenum and Tungsten boats for MgF_2 and TiO_2 respectively at room temperature and high vacuum conditions. An ETS 160 (Vacuum Evaporation System) coating plant with a base pressure of $\sim 10^{-6}$ mbar was used. Thickness of layers was determined by quartz crystal microbalance technique. In second step for sample one, we used rotating $\text{MgF}_2/\text{glass}$ as substrate and we coat MgF_2 on substrate that tends to heterogeneous $\text{MgF}_2/\text{MgF}_2/\text{glass}$ layer. For sample two, MgF_2 powder with normal deposition angle coated on $\text{TiO}_2/\text{glass}$ substrate and tends to four phase $\text{MgF}_2/\text{TiO}_2/\text{glass}$ thin layer. Transmittance of the films was measured by using VIS spectrophotometer (Hitachi U – 3310) instrument. The spect of layers were in the range of 300–1100 nm wave length (VIS), and for using Kramers-Kronig relations [16], we extrapolated of reflectivity curves with bulk standard samples [17]. The optical properties such as n , k , ϵ_1 , ϵ_2 , α (absorption coefficient) and Band-gap energy were obtained. There was a good agreement between them.

Results and discussion:

Transmittance and reflectance curves of layers in visible light range are different for layers. By changing material of last layer real part of reflective index n , completely changes. Imaginary parts of refractive indices k , have same trend for both samples. Real and imaginary parts of dielectric constants respectively ϵ_1 and ϵ_2 for samples are completely different. In general second sample shows higher dielectric property. According to absorption coefficient, Sample two in general shows higher absorption coefficient. That is because of formation more void on sample one by rotating substrate and of course TiO_2 had an ideal deposition angle that tends to less voids on layer. The value of band gap is 3.8eV for sample one and 3.9eV for sample two, that is in agreement with dielectric constants and other optical properties.

Conclusion:

$\text{MgF}_2/\text{MgF}_2/\text{glass}$ and $\text{MgF}_2/\text{TiO}_2/\text{glass}$ multi layers were produced in this work at room temperature and HV conditions. Reflectivity and transmittance of layers are completely different. By using Kramers-Kronig relations on reflectivity curves optical parameters



calculated $\text{MgF}_2/\text{TiO}_2/\text{glass}$ layer in general showed higher dielectric property. That is because of gettering property of Ti atoms. Band gap is about 3.9 eV for this layer. For $\text{MgF}_2/\text{MgF}_2$ glass band gap is about 3.8 eV that is much more less than a bulk MgF_2 (10.8 eV) almost insulator, so by nanometric deposition we can produce semiconductors of MgF_2 .

References:

- [1] G. Ottermann, J. Otto, U. Jeschkowski, O. Anderson, M. Heming, K. Bange, Mater. Res. Soc. Symp. Proc. 308 (1993) 69.
- [2] J.K. Fu, G. Atanassov, Y.S. Dai, F.H. Tan, Z.X. Mo, J. Non-cryst. Solids 218 (1997) 403.
- [3] J. Haber and M. Wojciechowska, J. Catal. 110 (1988) 23.
- [4] J. Haber and M. Wojciechowska, Catal. Lett. 10 (1991) 271.
- [5] M. Wojciechowska, W. Gut and V. Szymenderska, Catal. Lett. 7 (1990) 431.
- [6] M. Wojciechowska, S. Łomnicki, J. Bartoszewicz and J. Goslar, J. Chem. Soc. Faraday Trans. 91 (1997) 2207.
- [7] M. Wojciechowska, J. Haber and S. Łomnicki, J. Mol. Catal. 141 (1999) 155.
- [8] M. Wojciechowska, M. Pietrowski, S. Łomnicki and B. Czajka, Catal. Lett. 46 (1997) 63.
- [9] M. Wojciechowska, M. Pietrowski and S. Łomnicki, J. Chem. Soc. Chem. Commun. (1999) 463.
- [10] M. Scrocco, Phys. Rev. B 33, 7228 (1986)
- [11] Kudo A, Miseki Y (2009) Chem Soc Rev 38:253
- [12] Fujishima A, Zhang X, Tryk DA (2008) Surf Sci Rep 63:515
- [13] Macwan DP, Dave PN, Chaturvedi S (2011) J Mater Sci 46:3669. doi:10.1007/s10853-011-5378-y
- [14] Ni M, Leung MKH, Leung DY, Sumathy K (2007) Renew Sust Energy Rev 11:40
- [15] Zou J, Zhang Q, Huang K, Marzari N (2010) J Phys Chem C 114:10725
- [16] H. Savaloni, H. Kangarloo, J. Phys. D: Appl. Phys. 40 (2007) 203
- [17] E.D. Palik handbook of optical constant of solids, courtesy academic press inc, 1985



15th Physical Chemistry Conference



Synthesis of Magnetite Anion-exchange Nanoparticles and Their Application for Separation and Preconcentration of Methyl Phosphonic Acid

B. Maddah, M. Cheraghvasi

Department of Chemistry, Imam Hossein University, Tehran, Iran.

Tel +98 2177104952, Fax +98 2177104930

bozorgmaddah@yahoo.com

Introduction:

The Chemical Weapons Convention (CWC), which came into force in April 1997, forbids the development, production, stockpiling, or use of chemical weapons (CW) [1]. Among Chemical Warfare Agents (CWA), nerve agents are known to be highly toxic and powerful inhibitors of acetylcholinesterase. The nonvolatile and highly polar Methylphosphonic acid is a poor UV absorber. Moreover, since it is readily soluble in water, its presence can be expected in soil and water of contaminated regions with nerve agents. In order to measure the ultratrace level of MPA in water, an analytical method with low limit of detection (LOD) level is required. Solid-phase extraction (SPE) has been widely used for its high selectivity and good reproducibility [2, 3]. Detection of Ultra traces of alkylphosphonic acids are unique challenges for the analytical chemists. In this paper, we explored a new method to direct extraction of MPA from water by magnetite amine-nanoparticles as a sorbent in solid phase extraction.

Experimental:

Chemicals

MPA was purchased from the Aldrich Chemical Co. The derivatization reagent bis(trimethyl silyl) trifluoroacetamide (BSFTA) was obtained from ACROS. sodium nitrate, potassium chloride, silver nitrate, ammonia, acetic acid, nitric acid, hydrochloric acid, Ferric chloride

hexahydrate ($\text{FeCl}_3 \cdot 6\text{H}_2\text{O}$), ferrous chloride tetrahydrate ($\text{FeCl}_2 \cdot 4\text{H}_2\text{O}$), Tetraethyl orthosilicate (TEOS) and 3-Aminopropyl triethoxysilane (APTES), toluene, methanol and ethanol.

Apparatus:

A Varian Model 3400 capillary GC system, vibrating sample magnetometry (VSM) system (LDJ9600, Troy, USA), X-ray diffractometer (XRD, Bruker D8 Discover, Germany), Fourier Transform-Infrared Spectrometer (FT-IR, Perkin Elmer, spectrum 100).

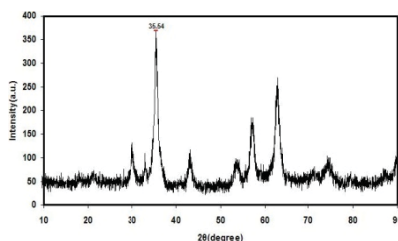
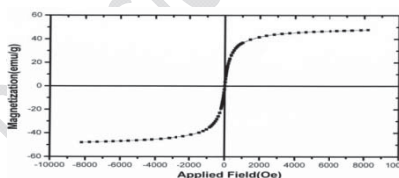
Synthesis of magnetite nanoparticles with functional amine group:

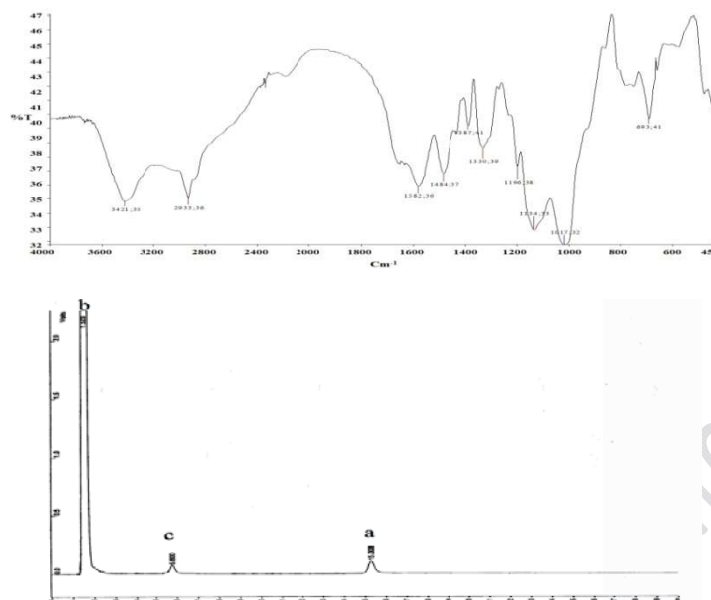
First, the Fe_3O_4 magnetite nanoparticles (MNPs) were synthesized using a co-precipitation method. Then, the MNPs were coated with silica (SMNP), followed by an amine coating [4].

Procedure of extraction, elution and determination of MPA:

AMNPs (0.10 g) were dispersed in 20 mL standard solutions in a beaker to form a suspension with the aid of ultrasonication. AMNPs (0.10 g) were dispersed in 20 mL standard solutions in a beaker to form a suspension with the aid of ultrasonication. The extracted ions were stripped from the using 1 mL solution of Methanol:Ammonia (80:20 v/v). BSFTA derivative of MPA obtained was analyzed by GC.

Results and discussion:





Conclusion:

NH₂-(CH₂)₃-SiO₂-Fe₃O₄ NPs as sorbent can be easily synthesized. Due to very high surface areas, short diffusion route and magnetically-assisted separability of these NPs high adsorption capacities can obtain in a very short time. Results presented in this work demonstrate the possibilities offered by the anion-exchange NPs as a sample preparation method for trace analysis amounts of MPA in water samples. The optimized methods are fast, sensitive, accurate and simple.

References:

- [1] Convention on the prohibition of the development, production, Stockpiling, use of Chemical Weapons and their Destruction, (1997) Technical Secretariat of the Organization of prohibition of chemical Weapons
- [2] McDowall, R.D., (1989), Sample preparation for biomedical analysis. *J. Chromatogr. B*, 492: 3.
- [3] Bielicka-Daszkiwicz, K., Voelkel, A., Szejner, M., Osypiuk, J., (2006), Extraction properties of new polymeric sorbents in SPE/GC analysis of phenol and hydroquinone from water samples. *Chemosphere.*, 62:890.



- [4]Jang, J.H., Lim, H.B., (2010), Characterization and analytical application of surface modified magnetic nanoparticles, *Microchemical J.*, 94: 148

15th Physical Chemistry Conference



Structural Evolution of Nanocrystalline Ti-Ni-Cu Shape Memory Alloys Synthesized by Mechanical Alloying

Fatemeh Alijani, Rasool Amini, Morteza Alizadeh

¹Department of Materials Science and Engineering, Shiraz University of Technology, 3619995161, Shiraz, Iran

E-mail: f.alijani@gmail.com

Keywords: TiNiCu shape memory alloys; mechanical alloying; amorphous phase

Introduction:

Equiatomic NiTi compounds are widely used in medical and engineering applications, due to their shape memory effect (SME), superelasticity (SE) and biocompatibility. However, by partial replacement of Ni with Cu, not only the composition sensitivity of the alloy reduces [1], but also the corrosion resistance of the alloy can be improved and the transformation behavior and shape memory characteristics can be affected. Since there exist limited reports on the TiNiCu formation by mechanical alloying (MA) [2, 3], more attention is needed on the production, characterization, and properties investigation of these smart materials. In the present work, the structural evolution and morphological changes during the milling cycle of the mechanically alloyed Ti-41Ni-9Cu compound were investigated.

Experimental Procedure:

High purity elemental titanium, nickel and copper powders were mixed with the atomic ratio of 50:41:9 and then mechanically alloyed in a planetary ball mill with tempered steel vials and balls under argon atmosphere. The milling was performed at room temperature with the speed of 450 rpm and the ball-to-powder mass ratio of 20:1. The phase constituent and structural properties of the powders were studied by using powder X-ray diffraction (XRD, Pananalytical, X'pert Pro MPD) with the CuK α (λ = 0.154 nm) radiations. The Rietveld refinement was performed using the MAUD software package version 2.26. Finally, the

evolution of particles morphology and size was studied by scanning electron microscopy (SEM, FEI, Nova Nanosem 430).

Results and Discussion:

Fig. 1a shows the XRD pattern of the as-milled powders at various milling time. As it can be seen from the figure, by starting the milling process, the peaks sharpness and broadening of the starting materials are reduced and increased, respectively. By progression of milling, the alloying process is done and the peaks of the initial materials are completely eliminated after 24 hours of milling. Based on the XRD peaks broadening of the as-milled powders, particularly 48 h, the development of nano-size structures (Fig. 1b), introduction of high amount of lattice strain (Fig. 1c), and also the existence of high quantity of amorphous phase are evident.

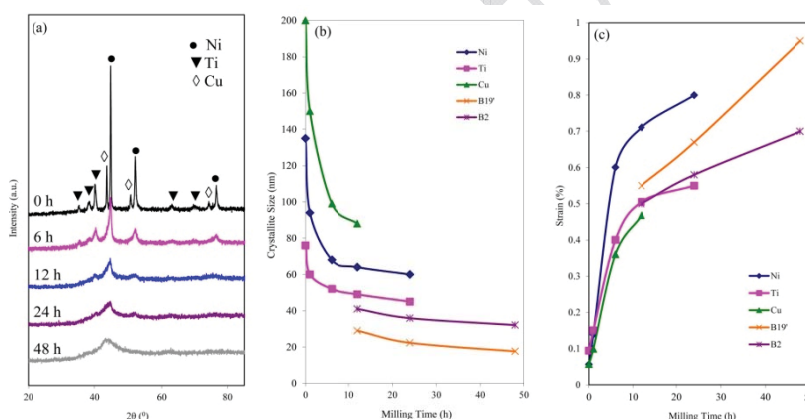


Fig. 1 (a) XRD pattern of the as-milled powders; (b) The variation of Crystallite size and (c) lattice strain of the present crystalline phase as a function of milling time.

The SEM images of the as-milled powders (Fig. 2) show clearly the mechanism of MA (e.g. cold welding and fracturing).

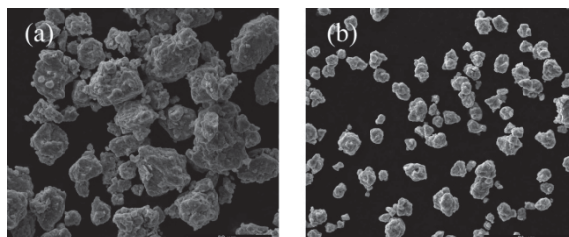




Fig. 2 SEM images of the powders milled for a) 6h and b) 24h.

Conclusions :

In the present work, the structural properties of the amorphous/nanocrystalline Ti-41Ni-9Cu alloys were evaluated. According to the results, nanocrystallization rapidly occurred and the high amount of micro-strains and lattice defects were created during the milling cycle. Moreover, the amount of the amorphous phase was increased considerably. By milling evolution, the powders morphology was changed and the average particles size was initially increased, then reduced.

References:

- [1] D. C. Lagoudas, Shape memory alloys modeling and engineering applications, Springer, Texas, 2008.
- [2] M. Valeanu, M. Lucaci, A.D. Crisan, M. Sofronie, L. Leonat, V. Kuncser, J. Alloys Compd. 509 (2011) 4495-4498.
- [3] R. Amini, F. Alijani, M. Ghaffari, M. Alizadeh, A.K. Okay, J. Alloys Compd., 538 (2012) 253–257.



Evolution of Phase Transformation in Nanocrystalline/Amorphous Ti-41Ni-9Cu Shape Memory Alloys Synthesized by Ball Milling

Fatemeh Alijani, Rasool Amini, Morteza Alizadeh

Department of Materials Science and Engineering, Shiraz University of Technology, 3619995161, Shiraz, Iran

E-mail: f.alijani@gmail.com

Keywords: TiNiCu shape memory alloys; mechanical alloying; phase transformation

Introduction:

In comparison to binary NiTi shape memory alloys (SMAs), TiNiCu alloys exhibit more favorable properties such as small transformation hysteresis and higher corrosion resistance. Accordingly, these smart materials are widely used in different fields like electronics and medical applications [1]. In the present work, phase transformation of the alloying system during the milling process was investigated.

Experimental Procedure:

High purity elemental titanium, nickel and copper powders were mixed with the atomic ratio of 50:41:9 and then mechanically alloyed in a planetary ball mill under argon atmosphere. The milling was performed at room temperature with the speed of 450 rpm and the ball-to-powder mass ratio of 20:1. The phase constituent and structural properties of the powders were studied by powder X-ray diffraction (XRD, Pananalytical, X'pert Pro MPD) with the CuK α ($\lambda = 0.154$ nm) radiations. The quantitative analyses were done according to previous work [2]. Then, to investigate the microstructural features of the as-milled powders, selected powder particles were characterized by a high-resolution transmission electron microscope (HRTEM, FEI, Tecnai G2 F30).

Results and Discussion:

Fig. 1a shows the XRD spectra of the as-milled powders at selected milling time. As it can be seen, by milling initiation, due to the development of nano-size structure and introduction of

high quantity levels of micro-strain, the peaks sharpness reduces and their broadening increases considerably. More focus on the XRD profiles indicates that, by increasing the milling time, because of the dissolution of Cu and especially Ti into the Ni lattice and consequently solid solution formation, the diffraction lines of Ni shift toward lower angles. The variation of phase content by milling time is depicted in Fig. 1b. Although the stress-induced martensite (B19') is formed due to severe plastic deformation, the high temperature B2 phase is also created due to temperature rising during milling process. By comparing the XRD patterns of 48 h and 96 h powders at Fig. 1a, it can be seen that the mechano-crystallization of the amorphous phase to the more stable crystalline B2 and B19' phases occurs during this milling interval.

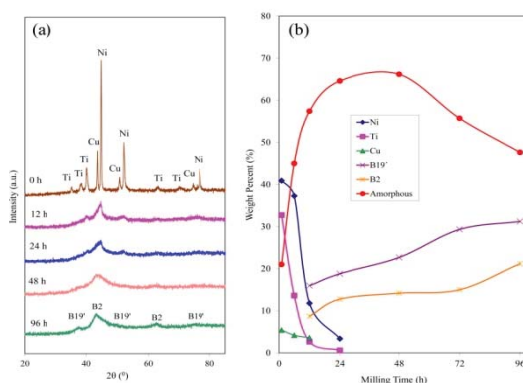


Fig. 1 (a) XRD pattern of the as-milled powders; (b) The quantity of the crystalline and amorphous phases as a function of milling time.

The HRTEM image of the powders milled for 96 h indicates a combination of crystalline and amorphous phases in the powder structure which is confirmed by the continuous polycrystalline rings and amorphous halo pattern of the SAD pattern.

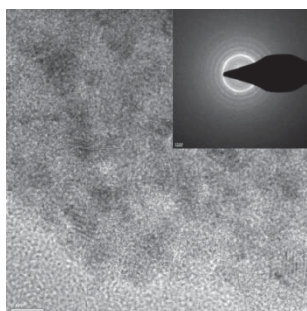


Fig. 2 TEM image and corresponding SAD pattern of the 96h-milled powders.



Conclusions:

In the present work, the phase transformation of the amorphous/nanocrystalline Ti-41Ni-9Cu alloys was studied. According to the results, the Ni solid solution, amorphous and nanocrystalline B2 and B19' phases were formed during the milling. By milling continuation, mechano-crystallization of the amorphous phase to B2 and B19' occurred.

References:

- [1] K. Otsuka, C. M. Wayman, Shape Memory Materials, Cambridge University press, Cambridge, 1998.
- [2] R. Amini, F. Alijani, M. Ghaffari, M. Alizadeh, A.K. Okyay, J. Alloys Compd., 538 (2012) 253–257.



15th Physical Chemistry Conference



Investigation of optical and structural properties of Mn doped ZnO nanoparticles, synthesized at 0°C

R. Lotfi Orimi, K. Khosravi

Dep.of Physics, University of Golestan, Gorgan, Iran

Abstract:

Un-doped and Mn doped ZnO nanoparticles were synthesized by simple chemical precipitation method at 0°C. The Mn doped ZnO nanoparticles were prepared with various Zn concentration (1%, 3%, 5%, and 7%) and were characterized by X-ray diffraction (XRD), UV-Vis spectra and photoluminescence (PL). By comparing the XRD spectra it was found that XRD patterns of un doped ZnO nanocrystals were similar to those of Mn doped ZnO nanocrystals, improving that the nanocrystal Mn ions were substituted for Zn atoms. It was found also that the size of the Mn doped ZnO nanocrystals increased from 5 to 12 nm when the concentration of Mn was increased. The UV-Vis spectra peaks were shown a small red shift when the concentration of Mn was increased.

Keywords: optical properties, Mn doped, ZnO nanoparticles, band gap

Introduction:

ZnO is a wide band gap (3.37 eV) compound material with large exciton binding energy (60 meV) [1]. This metallic oxide material with dual properties, semiconducting and piezoelectric properties [2,3], is a unique material that exhibits novel application in optoelectronics, sensors and medical sciences [4]. However, it was found that the presence of impurity can dramatically affect the electrical and optical properties of the nanostructures. In addition detailed reports for ZnO nanoparticles, doped with transition metals, Mn [5], Cu [6], Ti [7] demonstrate that the doping effect increases strongly the optical and electrical properties of ZnO nanoparticles. In this paper we report the synthesis and characterization of pure and Mn doped ZnO nanoparticles.

Experimental:

The synthesis of ZnO and ZnO:Mn nanoparticles was performed by three following steps: First, 1.76 g of $\text{Zn}(\text{Ac})_2 \cdot 2\text{H}_2\text{O}$ and 1 mmol $\text{Mn}(\text{Ac})_2$ was added into a breaker with 160ml ethanol under magnetic stirring at 70 °C. Then a solution of 0.8 g NaOH in 160 ml ethanol was added dropwise into the above solution at 0 °C under rigorous magnetic stirring for 1 h. In the third step, 0.5 oleic acid was added into the solution as capping material to avoid agglomeration of the nanoparticles. The precipitate was collected by centrifugation of the solution and finally, precipitate was washed by acetone and deionized water sequentially. Then, wet precipitate was dried in vacuum at room temperature to obtain the white (undoped case) and brown –black (Mn doped case) powder.

Results and discussion:

The XRD patterns of un doped and Mn doped ZnO with various Mn concentration are shown in Fig.1. All the XRD peaks are indexed to hexagonal wurtzite phase of ZnO. The peaks broadening in the XRD pattern clearly indicate that nanoparticles are present in the sample. By comparing these patterns, it is found that there are the peaks correspond to tetragonal crystal structure in samples with 1% and 3% belong to secondary phase ZnMn_2O_4 . In the higher doping percentage (5% and 7%) the other secondary phase, Mn_3O_4 with tetragonal structure, are formed. According to Deby-Scherrer formula[8] the highest peak in XRD patterns of different Mn concentration(0% -7%) at 36.3° gives the ZnO nanoparticle diameter of 5-12 nm. Fig.2 displays the UV-Vis absorbance

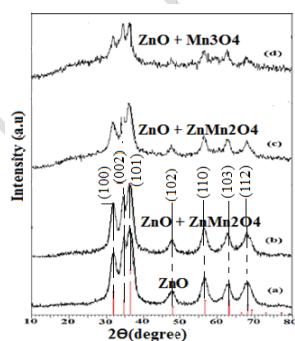


Fig.1 XRD patterns of ZnO:Mn under different

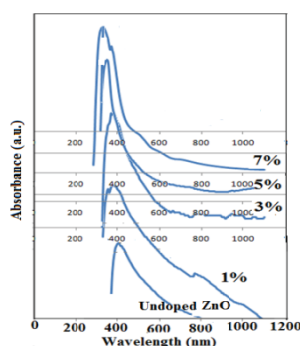


Fig.2 UV-Vis spectra of Mn doped ZnO

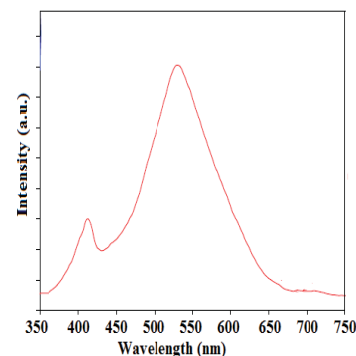


Fig.3 PL spectra of Mn doped ZnO



Mn concentration :a) 0%, b)1%, c) 3%, d) 5%.

nanoparticles by different Mn concentration

nanoparticles

spectra of un doped and Mn doped ZnO nanoparticles by different concentration of Mn. It is clear that with increase of 0, 1, 3, 5, 7 at % Mn concentration, the optical energy band gap of sample increase, a blue shift in energy band gap, which may be explained by Burstein-Moss shift[9].

Fig.3 shows PL emission spectra of undoped ZnO nanoparticles with a strong green emission attributed to oxygen vacancies which is due to synthesis conditions[10] .

Conclusion:

In this study the Mn doped ZnO nanoparticles synthesized at 0° C and were characterized by XRD and UV-Vis absorbance spectra. it is found that there are the peaks correspond to tetragonal crystal structure in samples with 1% and 3% belong to secondary phase ZnMn₂O₄ and in the higher doping percentage (5% and 7%) the other secondary phase, Mn₃O₄ with tetragonal structure, are formed. UV-Vis absorbance spectra is shown that with increase of 0-7 at % Mn concentration, the optical energy band gap of sample increase, a blue shift in energy band gap. the PL emission spectra of undoped ZnO nanoparticles shows a strong green emission peak, attributed to oxygen vacancies, which is due to synthesis conditions

References:

- [1] O. Madelung, Data in Science and technology: Semiconductors(springer, Berlin, 1992).
- [2] E. Fortunato, P. Barquinha, A. Pimental, A. Marques, L. Pereira, R. Martins, Thin Solid Films 487 (2005) 205-211.
- [3] H. Gong, J. Wang, C.H. Ong, F.R. Zhu, Sens. Actuators B115(2006)247-251.
- [4] R. F. Service, Science (1997) 276.
- [5] Yao-Ming Hao, Shi-Yun Lou, Shao-Min Zhou, Rui-Jian Yuan, Gong-Yu Zhu, Ning Lig, Nano Science Research Letters (2012) 7,100.
- [6] T.S. Hemg, S.P. Lau.S.F. Yu, S.H. Tsang, K.S. Teng, J.S. Chen, Journal of Applied Physics,(2008) 104,103104
- [7] N. Samaele, P. Amompitoksuk, S.Suwanboon, Material Letters, 64(4), (2010), 500-2.



- [8] H.P. Klug, L.E. Alexander, X-ray Diffraction procedure..., Wiley, New York, 1974, P. 662.
- [9] E. Burstein, Phys. Rev. 93 (1954) 632.
- [10] D.C. Reynolds, D. C. Look, B. Jogai and H. Morkoç, Solid State Commun.101, 1997, pp.643

15th Physical Chemistry Conference



Morphology Prediction of Ternary Blends and Their Nanocomposites via Thermodynamic Approach

A. Rostami^{*a}, H. Nazockdast^b, M. Karimi^c

^{*a} Polymer Engineering Department, Amirkabir University of Technology, mahshahr campus, mahshahr, Iran

^b Polymer Engineering Department, Amirkabir University of Technology, Tehran, Iran

^c Textile Engineering Department, Amirkabir University of Technology, Tehran, Iran

arostami@aut.ac.ir

Keywords: Ternary blends, Nanocomposites, Morphology, Thermodynamic Approach

Introduction:

The properties of ternary blends are controlled by their morphology, so it is necessary to predict it. Hobbs et al. [1] used Harkin's spreading coefficient concept to predict the phase morphology of different ternary blends. For a ternary system with A as the continues phase and B and C as the dispersed phases, the spreading coefficients λ_{BC} and λ_{CB} are defined as:

$$\lambda_{BC} = \gamma_{AC} - \gamma_{AB} - \gamma_{BC} \quad (1)$$

$$\lambda_{CB} = \gamma_{AB} - \gamma_{AC} - \gamma_{BC} \quad (2)$$

where γ_{ij} is the interfacial tension between i and j phases. A positive value of λ_{BC} and negative value of λ_{CB} will lead to encapsulation of C phase by the B phase. If λ_{BC} and λ_{CB} are both negative, two minor components form separate dispersed phases. In the case, both λ_{CB} and λ_{BC} are negative and λ_{AC} is positive one phase will partially encapsulate the other phase.

Materials:

Poly(methyl metacrylate) (PMMA) from LG chemical Co., polystyrene (PS) from DongbuHannong Chemical Co., and Commercial polypropylene (PP) from Marun Petrochemical Co. were used in this work. The CNTs used in this study were commercially available as multiwall carbon nanotubes (MWNTs), NC-7000, from Nanocyl Inc., Belgium.

Result and discussion:

Morphology Prediction by Thermodynamic Approach:

The morphology of the blends was predicted by using the spreading coefficient concept. First, interfacial tensions (γ_{ij}) data were calculated for the three polymer–polymer interfaces present in the blends, i.e. PMMA-PS, PS-PP, and PMMA-PP and their nanocomposites using the harmonic mean equation.

$$\gamma_{ij} = \gamma_i + \gamma_j - \frac{4\gamma_i^p \gamma_j^p}{\gamma_i^p + \gamma_j^p} - \frac{4\gamma_i^d \gamma_j^d}{\gamma_i^d + \gamma_j^d} \quad (3)$$

where γ_{ij} is the interfacial tension between components i and j, γ_{ij} is the surface tension of component i, γ_i^d and γ_i^p are dispersive fraction and polar fraction of surface tension of the component i, respectively. The data used in these calculations are shown in Table 1 and 2.

Table 1: Data for the surface tension, dispersive fraction and polar fraction of samples components

Polymer	γ (mN/m)	γ^d	γ^p	$d\gamma/dT$
PMMA	31.6	20.8	10.8	-0.071
PS	27.7	15.6	12.1	-0.072
PP	24.7	9	15.7	-0.056
PMMA/CNTs	50.7	45.7	5	-0.071
PS/CNTs	32.3	18.9	13.4	-0.072
PP/CNTs	24.4	3.8	20.6	-0.056

Table 2: Data for the Interfacial tension value

Polymer pair	Interfacial tension value
PMMA-PS	1.400
PMMA-PP	9.030
PS-PP	3.833
PMMA/CNTs-PS/CNTs	30.389
PMMA/CNTs-PP/CNTs	66.401
PS/CNTs-PP/CNTs	21.504

The calculated values of interfacial tensions were used to obtain the spreading coefficient (λ) and relative interfacial energy (RIE) values to predict the morphology of the PMMA/PS/PP

ternary polymer blend in the presence and absence of CNTs. The obtained data are shown in Table 5 and 6.

Table 3: Data for the Harkins spreading coefficient

Polymer pair	Harkins spreading coefficient (λ)
PMMA/PS	-6.596
PS/PP	3.796
PP/PS	-11.464
PMMA-CNTs/PS-CNTs	-75.286
PS-CNTs/PP-CNTs	14.508
PP-CNTs/PS-CNTs	-57.517

According to Table 3, spreading coefficient (λ) and relative interfacial energy (RIE) for the neat samples in 220°C are in the order of:

$$\lambda_{PS/PP} > \lambda_{PP/PS}$$

The results suggested a core-shell type morphology, in which PS shell encapsulated the PP phase. By addition of CNTs, $\lambda_{PS/CNTs-PP/CNTs}$ is still greater than $\lambda_{PP/CNTs-PS/CNTs}$, suggesting that the morphology of this sample is not changed in presence of CNTs.

Sem Results:

Figure 1 shows SEM micrographs of PMMA/PS/PP (80/05/15) in which the PS phase was etched by cyclohexane. As it can be seen, the ternary blend shows a core-shell morphology. The PS was found to encapsulate the PP.

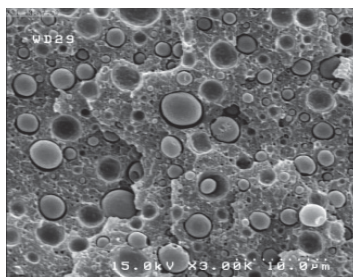


Figure 1: SEM micrograph of 80/05/15 ternary blend of PMMA/PS/PP



Conclusions:

SEM micrographs of PMMA/PS/PP ternary blend showed a core-shell type morphology. Thermodynamic method is used to determine the morphology in ternary blends and their Nanocomposites.

Reference:

- [1] Hobbs, S. Y.; Dekkers, M. E. J.; Watkins, V. H. Polymer 1988, 29, 1598.

15th Physical Chemistry Conference



Development of a New Chitosan Nanofiber Mats Containing Silver Sulfadiazine for Burn Dressing

N. S. Tehrani^{a*}, R. Faridi-Majidi^b, H. Attar^{a,c}, M. Rezayat^{b,c}

^a Department of Chemical Engineering-Biotechnology, Science and Research Branch, Islamic Azad University, Tehran, Iran

^b Department of Medical Nanotechnology, School of Advanced Medical Technologies, Tehran University of Medical Sciences, Tehran, Iran

^c Department of Biotechnology, Pharmaceutical Science branch, Islamic Azad University, Tehran, Iran

Email: * Neda.sTehrani@gmail.com

Keywords: Burn-dressing, Chitosan, Nanofibers, Electrospinning

Introduction:

Wound healing is a complex process that often requires treatment with antibiotics. Protection from environmental factors can be accomplished by covering the wound with wound dressings. Silver sulfadiazine (AgSD) is an effective and widely used antibiotic for burn injuries in human. Chitosan (CS) is a biopolymer that has been well known as being able to accelerate the healing of wound in human [1, 2].

In the present study we successfully prepared and analyzed chitosan/poly ethylene oxide (PEO) nanofiber containing silver sulfadiazine (AgSD) via electrospinning.

Materials and methods:

CS/PEO solutions were prepared by dissolving CS and PEO in 70% acetic acid at ratios of CS to PEO of 90/10, 80/20 and 70/30. AgSD powder was also dissolved in 70% acetic acid. Then the solution was mixed with the CS/PEO solutions at ratio of 1:2.

The electrospinning processes were carried out using Electroris (FNM Ltd., Iran, www.fnm.ir) as an electrospinner. Then, the obtained mats were analyzed by SEM and UV-vis spectrophotometer to study the nanofibers sizes and amount of AgSD.

Result and discussion:

Chitosan-based nanofibers containing different ratios of chitosan/polyethylene oxide (PEO) and AgSD as an antibacterial agent were successfully electrospun from 70% aqueous acetic acid solutions to overcome current limitations in silver sulfadiazine (AgSD) cream for treating acute burn wounds. Figure 1 presents the SEM image of nanofibers obtained from electrospinning of CS/PEO solutions in 70 % acetic acid at ratio of 90/10 containing AgSD.

The UV-vis spectroscopy of the AgSD showed absorption band at 266 nm demonstrating the presence of AgSD. The results show that when the concentration of chitosan was increased we had a better absorbance of AgSD. The absorbance of CS/PEO nanofiber solution at the ratio of 90/10 was 0.629. With a CS/PEO ratio of 70/30 and decreasing the amount of chitosan, we achieved a 0.536. The most likely reason for this difference is that with the increasing amount of chitosan, the solubility of the drug is enhanced.

The results also show that nanofibers have more absorbance compared to polymer solutions that is very likely due to error in weighing nanofibers.

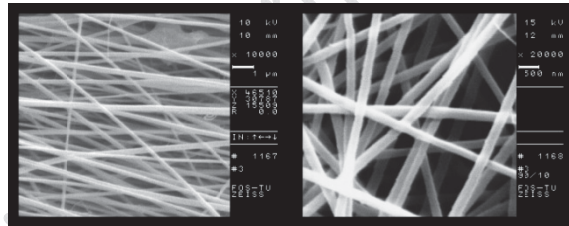


Figure 1. SEM micrographs of nanofibers obtained from electrospinning of CS/PEO solution in 70 % acetic acid at ratio of 90/10 containing AgSD from experiment No. 2

Conclusion:

Chitosan-based nanofibers can be fabricated by electrospinning of a 70% aqueous acetic acid solution with different ratios of CS/PEO containing AgSD. Due to biodegradability, biocompatibility, antibacterial and excellent biological properties of chitosan, the obtained nanofibers containing AgSD may be a good potential candidate for burn dressing with antibacterial capability to prevent an injured skin from infections.



Reference:

- [1] E .R. Kenaway, J .M. Layman, J.R. Watkins, G.L. Bowlin, J.A. Matthews, D.G. Simpson, G.E. Wnek, *Biomaterials* 24 (2003) 907.
- [2] G. Verreck, I. Chun, J. Rosenblatt, J. Petters, A. Van Dijck, J. Mensch, *J. Control. Rel.* 92(2003) 349.

15th Physical Chemistry Conference



Preparation of Chitosan Based Nanofibers as a Potential Burn Dressing by Electrospinning

N. S. Tehrani^a, R. Faridi-Majidi^{b*}, H. Attar^{a,c}, M. Rezayat^{b,c}

^a Department of Chemical Engineering-Biotechnology, Science and Research Branch, Islamic Azad University, Tehran, Iran

^b Department of Medical Nanotechnology, School of Advanced Medical Technologies, Tehran University of Medical Sciences, Tehran, Iran

^cDepartment of Biotechnology, Pharmaceutical Science branch, Islamic Azad University, Tehran, Iran

Email: * refaridi@tums.ac.ir

Keywords: Burn-dressing, Chitosan, Nanofibers, Electrospinning

Introduction:

To accelerate the healing process of wounds, the wounded area needs to be protected from environmental factors. The goal of wound dressing is to produce an ideal structure with high porosity but at the same time be a good barrier. Chitosan is a biopolymer that has been well known as being able to accelerate the healing of wound in human [1, 2].

In the present study we successfully prepared and analyzed chitosan/poly ethylene oxide (PEO) nanofiber containing silver sulfadiazine (AgSD) via electrospinning.

Materials and methods:

CS/PEO solutions were prepared by dissolving CS and PEO in 70% acetic acid at ratios of CS to PEO of 90/10, 80/20 and 70/30. AgSD powder was also dissolved in 70% acetic acid. Then the solution was mixed with the CS/PEO solutions at ratio of 1:2.

The electrospinning processes were carried out using Electroris (FNM Ltd., Iran, www.fnm.ir) as an electrospinner. Then, the obtained mats were analyzed by SEM and TEM to study the nanofibers sizes and morphologies.

Result and discussion:

Chitosan-based nanofibers containing different ratio of CS/PEO and AgSD as an antibacterial agent were successfully electrospun from 70% aqueous acetic acid solutions. CS concentration had a significant effect on the average fiber diameter as shown in figure1. The average fiber diameter decreased from 327nm to 184 nm in the presence of AgSD and from 233 nm to 130nm in the absence of AgSD when the CS concentration was increased.

Figure 2 presents the TEM images of nanofibers obtained from electrospinning of CS/PEO solution in 70 % acetic acid containing AgSD.

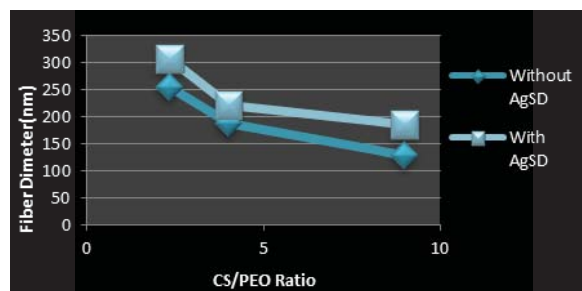


Figure1:effect of CS/PEO ratio on average nanofiber diameter in the presence and absence of AgSD



Fig 2: TEM micrographs of nanofibers obtained from electrospinning of CS/PEO solution in 70 % acetic acid at ratio of 70/30 and the presence of nanoparticles.

Conclusion:

Chitosan-based nanofibers can be fabricated by electrospinning of a 70% aqueous acetic acid solution with different ratios of CS/PEO containing AgSD. Due to biodegradability, biocompatibility, antibacterial and excellent biological properties of chitosan, the obtained nanofibers containing AgSD may be a good potential candidate for burn dressing with antibacterial capability to prevent an injured skin from infections.



Reference:

- [1] E .R. Kenaway, J .M. Layman, J.R. Watkins, G.L. Bowlin, J.A. Matthews, D.G. Simpson, G.E. Wnek, *Biomaterials* 24 (2003) 907.
- [2] G. Verreck, I. Chun, J. Rosenblatt, J. Petters, A. Van Dijck, J. Mensch, *J. Control. Rel.* 92(2003) 349.

15th Physical Chemistry Conference



Synthesis, characterization and photocatalytic activity of Mg/ZnO-SnO₂ nanoparticles

M.A. Behnajady, Y. Tohidi^{*}, N. Modirshahla

Department of Chemistry, Faculty of Science, Tabriz Branch, Islamic Azad University, Tabriz, Iran

Email: yasamin_tohidi@yahoo.com

Keywords: Advanced oxidation, Nanoparticles, Photocatalysis, ZnO-SnO₂.

Introduction:

Dyes found in wastewater are well known for their toxicity and pose a threat to human health through contamination of water supplies, thus they should be removed [1]. Among different water purification processes photocatalytic degradation of dyes by using nanostructured photocatalysts (TiO₂, ZnO,...) and UV irradiation has attracted extensive attention. However, the high degree of recombination of photogenerated electron-hole pairs restricts their application. Therefore lowering the recombination of electron-hole pairs is of a great interest. Coupling two semiconductor particles with different band gap widths and/or loading metals on the surface of semiconductors have been reported to be a beneficial way to achieve this goal [2,3]. Thus, the objective of this study is to prepare Mg/ZnO-SnO₂ nanoparticles and to characterize this new composite material and evaluate its photocatalytic activity in contrast to ZnO-SnO₂ coupled oxide for degradation of Methyl Orange (MO) as a model pollutant. Also the effect of different operational parameters on the photocatalytic activity has been studied.

Materials and methods:

Co-precipitation method has been employed to synthesize ZnO-SnO₂ coupled nanoparticles using ZnSO₄.7H₂O and SnCl₄.5H₂O as precursors. Then, Mg has been loaded on the coupled nanoparticles by impregnation method. For the photodegradation of MO a solution containing a known concentration of MO and photocatalyst (ZnO-SnO₂ or Mg/ZnO-SnO₂) was irradiated



under the UV light (15W, UV-C, $\lambda_{\max}=254\text{nm}$, manufactured by Philips), then MO concentration was analyzed by UV-Vis spectrophotometer (Pharmacia Biotech, Ultraspec 2000).

Results and discussion:

The synthesized nanoparticles were characterized by XRD, FESEM, TEM and DRS methods. The phases and mean grain sizes of nanosized photocatalysts were determined according to the XRD results by using the Shcerrer formula. TEM and FESEM images demonstrated that the synthesized samples were nanosized and spherical in shape. The DRS spectra exhibited a blue shift for Mg loaded ZnO-SnO₂ in contrast to ZnO-SnO₂ sample and thus greater redox capacity of the catalyst. The photocatalytic activity measurements indicated that Mg loaded ZnO-SnO₂ with 0.8% mol Mg and calcined at 350°C exhibited superior photocatalytic activity to ZnO-SnO₂. The study of the effect of operational parameters (catalyst dosage, MO concentration, pH and light intensity) on photocatalytic activity of Mg/ZnO-SnO₂ nanoparticles indicated that the highest removal percentage of MO was achieved with 800 mg L⁻¹ of photocatalyst, 10 mg L⁻¹ of MO at pH = 4.5 and light intensity of 62.2 W m⁻².

Conclusion:

Our results showed that Mg/ZnO-SnO₂ is a nanosized material and have a better photocatalytic activity than ZnO-SnO₂ i.e. metal loading would be an effective way to improve the photocatalytic activity of photocatalysts. Also it was found that after setting the operational parameters at their desired values its photocatalytic activity will further improve.

Reference:

- [1] S. Ahmed et al.; "Advances in heterogeneous photocatalytic degradation of phenols and dyes in wastewater: A review"; Water, Air, and Soil Pollution; 215, 3-29, 2011.
- [2] L. Zheng et al.; "Network structured SnO₂/ZnO heterojunction nanocatalyst with high photocatalytic activity"; Inorganic Chemistry; 48, 1819-1825, 2009.



[3] H. Wang et al.; "High photocatalytic activity of silver-loaded ZnO-SnO₂ coupled catalysts"; Chemical Engineering Journal; 146, 355-361, 2009.

Finite temperature Casimir interaction between a perfectly conducting surface and a permeable surface

Badrosadat Ojaghi Dogahe^a

^aDepartment of Physics, Science faculty, University of Isfahan, Esfahan, Iran

Email: ojaghi.8489@gmail.com

Keywords: Casimir interaction, Finite temperature, Path integral approach, mixed boundary condition (mixed B.C.)

Introduction:

Casimir interaction is an important phenomenon which should be considered in constructing Nano-devices, MEMS and NEMS. The attraction force between two perfectly conducting flat plates at zero temperature for the first time was defined by Casimir: $F(T = 0, H) = -\frac{\pi\hbar c A}{480H^4}$

Where A is the area and H is the separation of the plates.

We study the finite temperature Casimir force between two *flat* surfaces of mean separation H , in which the Dirichlet (D) boundary condition is imposed on one surface and the Neumann (N) boundary condition on the other one (i.e. mixed B.C.). this force is repulsive as Boyer has shown [1].

Methods:

We suppose two flat plates. To study the system at a finite temperature T , we use the Matsubara formalism [2]. By means of Path integral approach the logarithm of partition function will be

$$\ln Z_{ND} = -A \sum_{n=-\infty}^{\infty} \int \frac{d^2 p}{(2\pi)^2} \ln [1 + e^{-2H\sqrt{p^2 + \omega_n^2}}]$$

The normal Casimir force per unit area reads

$$\frac{F(T, H)}{A} = \frac{1}{\beta A} \frac{\partial \ln Z}{\partial H}$$

$$= -\frac{1}{\beta} \sum_{n=-\infty}^{\infty} \int \frac{d^2 p}{(2\pi)^2} \frac{-\sqrt{p^2 + \omega_n^2}}{1 + e^{-2H\sqrt{p^2 + \omega_n^2}}}$$

Results:

We have plotted normal repulsive force F as a function of H for various T (Figure 1). For very low temperatures, the normal Casimir force still scales as H^{-4} . At intermediate temperatures, e.g. $T = 50$ K, two regimes $F \propto H^{-4}$ and $F \propto H^{-3}$ are distinguishable. Increasing the temperature, one can observe the $F \propto H^{-3}$ regime for smaller values of H .

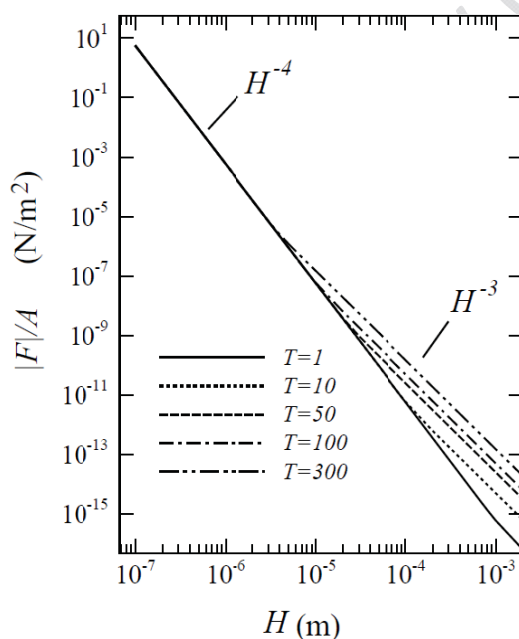


Figure (1)

Conclusion:

By considering finite temperature, T , we study the casimir force per unit area for mixed boundary condition. Then we plot the force as a function of separation, H , for various values of temperature, T . One can see from this figure that at small distances, which are less than a



micron, the main contribution to the interaction comes from quantum fluctuations of the scalar field, while at large distances thermal fluctuations have the most contribution.

References:

- [1] Boyer, T.H., Van der Waals forces and zero-point energy for dielectric and permeable materials. *Physical Review A*, 1974. **9**(5): p. 2078.
- [2] J. I. Kapusta, *Finite-Temperature Field Theory* (Cambridge University Press, Cambridge, 1989).

15th Physical Chemistry Conference



Nanosilica Containing Polypropylene/Liquid Crystalline Polymer Blend

Reza Foudazi, Hossein Nazockdast

Polymer Engineering Department, Amirkabir University of Technology, Tehran, Iran

Email: r.foudazi@gmail.com

Introduction:

Polymer blends comprising of a flexible matrix and small amount of liquid crystalline polymers (LCP) are of industrial and academic interests because the dispersed LCP phase can lead to easier processing and enhanced mechanical properties (e.g. [1]). It has been found that inorganic solid particles can be used for compatibilizing polymer blends [2]. It has been shown [3] that the hydrophobic nanosilica enhances the fibrillation process of LCP in PP/LCP blends. The thickening effect of nanosilica in polypropylene matrix was suggested to be the reason of this observation. Zhang et al. [4] also studied the effect of hydrophobic and hydrophilic nanosilica on PP/LCP blends and reported that only hydrophobic type silica enhances the fibrillation of LCP phase. In the present work, the effects of fumed silica concentration on the rheology and morphology of both PP matrix and PP/LCP blend are studied in order to provide a deeper insight into compatibilization and/or thickening effect of nano-silica on P/LCP blend.

Materials and Methods:

An isotactic polypropylene, Moplen HP500H obtained from Arak petrochemicals, with melt flow rate (MFR) of 1.8, was used as matrix. The dispersed phase was a thermotropic liquid crystalline polymer, Vectra A950 (from Hoechst-Celanese) with a nominal melting point of 280°C. Fumed nanosilica, Aerosil 200 (Hydrophilic, BET of $200 \pm 25 \text{ m}^2/\text{g}$, particle size of 12nm) and Aerosil R816 (Hydrophobic, BET of $190 \pm 20 \text{ m}^2/\text{g}$, particle size of 12nm) were kindly supplied by Degussa GmbH.

Two different series of samples were prepared by melt blending in a Brabender internal mixer: (1) PP/silica nanocomposites, and (2) PP/LCP/silica hybrid blends. The PP/LCP blend with 85/15 weight fraction was selected to study the effect of different nanosilica concentrations (1,

2 and 3wt.%) on its rheology and morphology. The transmission electron microscopy (TEM), Philips EM 208 operating at 100kV was used to study the aggregate size and location of nanosilica in the samples prepared by cryomicrotoming. CamScan model MV2300 scanning electron microscopy (SEM) was employed to study the morphology of cryofractured blend samples. The rheological measurements were performed at 290°C with a stress/strain controlled rheometer, Paar Physica model UDS 200, equipped with parallel plate geometry with 25mm diameter and 1mm gap under a continuous flow of nitrogen.

Results and Discussion:

The analysis of rheological results showed that hydrophobic silica has higher tendency for aggregation and forms bigger and denser aggregates. The lower percolation threshold and the higher fractal dimension ($d_f \approx 2$) for hydrophilic silica are due to its stronger particle-particle interaction rather than polymer-particle interaction compared to hydrophobic one ($d_f \approx 1.9$). While the hydrophobic silica has lower thickening capability and lower coalescence hindrance caused by aggregates, it locates at the interface of PP/LCP blend (Fig. 1) and results in smaller droplet size (Fig. 2) and higher elasticity in comparison to hydrophilic silica.

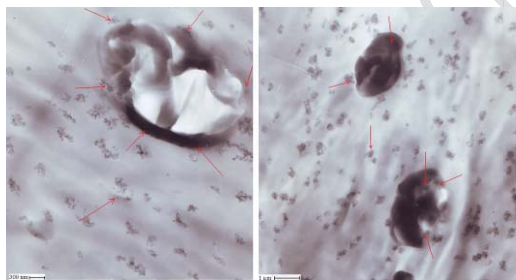


Fig. 1: TEM micrograph of (left) PP/ LCP/ hydrophobic, and (right) PP/ LCP/ hydrophilic silica

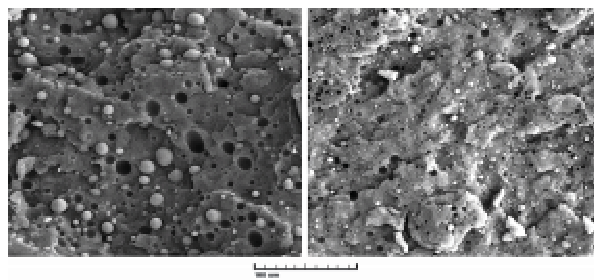


Fig. 2: SEM micrograph of 3wt.% (left) hydrophilic, and (right) hydrophobic silica containing PP/ LCP

The results suggest that the hydrophobic silica has a compatibilization capability for PP/LCP blend, while the hydrophilic silica mostly works as a thickening agent and suppresses the coalescence (Fig. 3). Fig. 4 suggests that the stress transfer due to enhanced interfacial adhesion is improved by hydrophobic silica more than hydrophilic one.

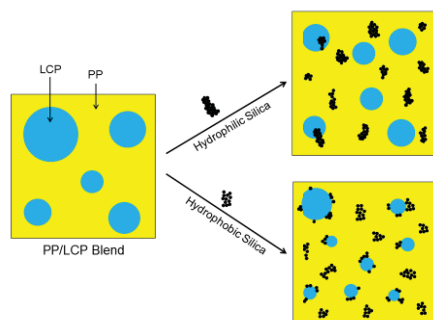


Fig. 3: Schematic of hydrophobic versus hydrophilic function in PP/LCP blend

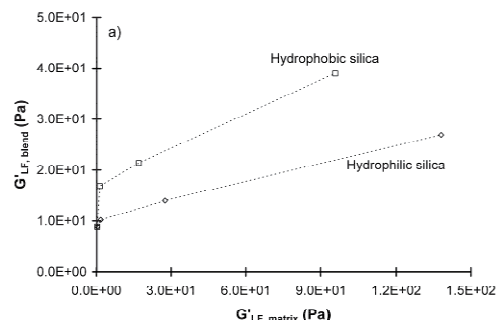


Fig. 4: Variation of G' of PP/ LCP/ silica samples versus G' of PP/ silica nanocomposites at low frequency

References

- [1] W.N. Kim, M.M. Denn, *J. Rheol.*, **36**, 1477 (1992).
- [2] S.S. Ray, S. Pouliot, M. Bousmina, L.A. Utracki, *Polymer*, **45**, 8403 (2004).
- [3] M.W. Lee, X. Hu, C.Y. Yue, L. Li, K.C. Tam, K. Nakayama, *J. Appl. Polym. Sci.*, **86**, 2070 (2002).
- [4] L. Zhang, K.C. Tam, L.H. Gan, C.Y. Yue, Y.C. Lam, X. Hu, *J. Appl. Polym. Sci.*, **87**, 1484 (2003).



Catalytic performance and characterization of Fe-V/TiO₂-SiO₂ nano catalysts promoted with Zn

Mostafa Feyzi*, Fatanh Jafari

Faculty of Chemistry, Razi University, Kermanshah, Iran.

*Corresponding Authors Emails: Dalahoo2011@yahoo.com

Key word: sol–gel, oxidation reactions, Characterization

Introduction:

The Fe-V/TiO₂-SiO₂ nano catalysts promoted with zinc were prepared by sol–gel method. The effects of different wt.% of Zn, synthesis temperature and calcination conditions on the structure and morphology of Fe-V/SiO₂-TiO₂ nano catalysts were investigated. The catalyst was employed for oxidation reactions. These catalysts with magnetite core can recovery after reactions by a magnet from the medium of reaction. Characterization of catalysts were done using XRD, FT-IR, Vibrating sample magnetometer (VSM) and and N₂ physisorption measurements such as the specific surface area, pore volume and pore diameter.

The type of support plays an important role on the catalytic properties and for a given reaction, the activity and selectivity of the catalyst can be improved by the use of an appropriate support [1]. Thus intrinsic being characteristics of both titania and silica support can be explored fully by using them in combination. Therefore the combined TiO₂–SiO₂ mixed oxide represents a novel class of materials that have attracted much attention recently as a support [2,3]. These catalysts are used in different formulations, among which vanadia supported on titania is known to be efficient catalyst in partial oxidation of hydrocarbons.

Catalyst preparation:

The catalysts used in present study were prepared by a combination of sol- gel and impregnation method. At first Fe(NO₃)₃.9 H₂O have been dissolved in ethanol, to a stirred solution tetraethyl orthosilicate (TEOS) and titanium isopropoxide (TIP), have been dissolved

in ethanol, slowly added in drops. To the obtained solution has been added oxalic acid that has been dissolved in ethanol. The obtained gels have been dried n at 90 °C, for 10 h and calcined in 450 °C for 6 h, to give the Fe/TiO₂-SiO₂ catalyst and then promoted with V and Zn.

Results:

The preparation conditions are effective on porosity and surface area of Fe-V/TiO₂-SiO₂ promoted with zinc nano catalyst. The obtained results are specific surface are=168.3m²g⁻¹, pore diameter= 0.065Å and pore volume=15.5cm³g⁻¹. The XRD pattern for nano catalyst revealed the Fe₂O₃ phase is present at rhombohedral form while the SiO₂ phase is present at tetragonal system. Scherrer equation was shown that nano catalyst has a particle size about 56 nm and the M_s factor of nano catalyst which was determined by VSM technique is equal to

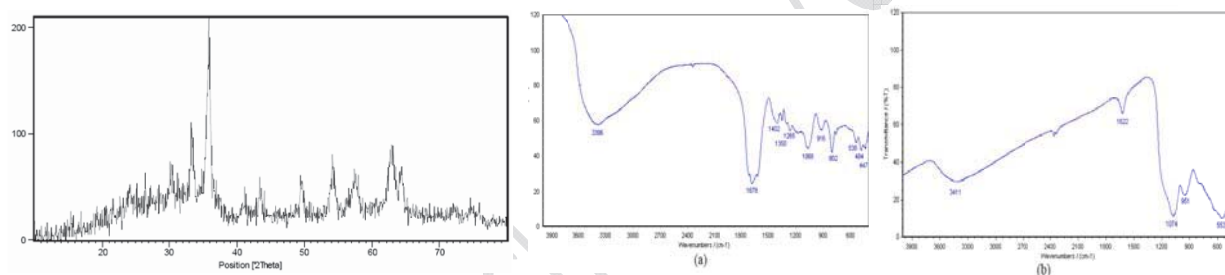


Fig.1, XRD pattern of nano catalyst , **Fig.2**, FT-IR spectra of (a) precursor, (b) after calcination

Fig.2, shows the infrared spectra of the precursor and the Fe-V/TiO₂-SiO₂ promoted with zinc. Fig. exhibits vibration bands corresponding to Ti-O-Si at 916, 951 cm⁻¹ of precursor and Fe-V/TiO₂-SiO₂ promoted with zinc nano catalyst respectively. Hysteresis curves were collected in a field range of ±10000kOe. The measured the M_s are reported 10/173emu/gr.

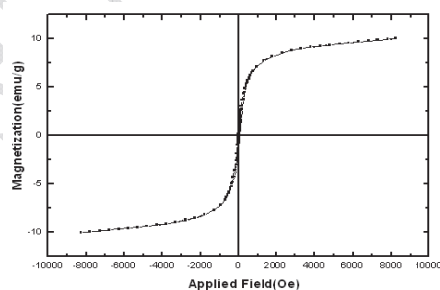
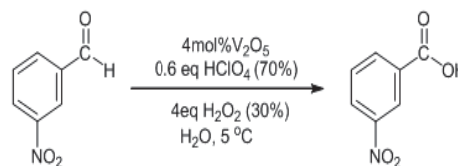


Fig.3, Magnetic hysteresis of catalyst



Oxidation reaction with Fe-V/TiO₂-SiO₂ promoted with zinc



Results are shown the used catalyst decreasing reaction time comparison with V_2O_5 from 7.5 h, resulted time with this catalyst to 3.5 h.

Reference:

- [1] H. Hu, I.E. Waches, J. Phys. Chem. 99 (1995) 10911–10922.
- [2] M.S. Rana, S.K. Maity, J. Ancheyta, G. Murli Dhar, T.S.R. Prasada Rao, Appl. Catal. A 253 (2003) 165–176.
- [3] S.K. Samantaray, K.M. Parida, Appl. Catal. A 211 (2001) 175–187.



Electrochemical Synthesis and Electrochemical Characteristic of Graphene-Supported Pt Nanoparticles for Methanol Oxidation

Karim Kakaei^{a,*}

^a Department of Chemistry, Faculty of Science, University Of Maragheh, P.O. Box. 55181-83111, Maragheh, Iran

E-mail address: k_kakaei56@yahoo.com, kakaei@maragheh.ac.ir

Key words: electrochemical exfoliation, graphene, platinum nanoparticles, methanol oxidation,

Introduction:

Direct methanol fuel cells (DMFCs) are considered one of the most promising power sources for applications in electric vehicles and electronic portable devices, due to their high power density, relatively quick startup, rapid response to varying loading, and low operating temperature.

The new form of carbon, which they call graphene, has very intriguing physical properties that suggest it could have a wide variety of applications. Graphene has received significant attention in recent years due to their unique electronic, physical, mechanical, thermal and chemical properties, such as high surface area, excellent conductivity, ease of functionalization and potentially low manufacturing cost since their discovery in 2004. So, graphene -supported Pt nanoparticles with 10 wt. % metal loading are prepared by sodium borohydride reduction method and the electrochemical characteristic of Pt /graphene is studied carefully and compared with commercial Pt/C (E-TEK) under methanol oxidation[1-4].

Material and methods:

The graphite rod was inserted as anode into the ionic liquid (IL) /water solution, placed parallel to the Pt wire as counter-electrode with a separation of 1 cm. the ionic liquid Urea choline chloride was mixed with water at 1:1 ratio. Static potentials of 5 V were applied to the two electrodes using a DC power supply. The synthesis of Pt nanoparticles dispersed onto



graphene (Pt/graphene) was carried out by chemical reduction of platinum on to graphene oxide (GO).

Result and Discussion:

We report a Pt/graphene catalyst for the methanol oxidation. Graphene is synthesized from graphite electrodes using ionic liquid-assisted electrochemical exfoliation. X-ray diffractometer and scanning electron microscopy technique are used to investigate the crystallite size and the surface morphologies respectively. The electrochemical characteristics of the Pt/graphene and commercial Pt/C catalysts are investigated by cyclic voltammetry (CV) in nitrogen saturated sulfuric acid aqueous solutions and in mixed sulfuric acid and methanol aqueous solutions. Furthermore, Pt/graphene exhibited a better sensitivity, signal-to-noise ratio

Conclusion:

We have developed a unified one-pot electrochemistry method to prepare graphene sheets from the exfoliation graphite electrode. Pt was reduced by sodium borohydride reduction method with ethylenediaminetetraacetic acid disodium salt (EDTA-2Na) on carbon graphene to use as (DMFC) catalysts. The methanol electroactivity in the Pt/graphene electrocatalyst was found to be 1.81 times higher than in the Pt/C electrode. SEM results confirmed the 'urchin' structure of graphene sheets with few layers.

References:

- [1] A.S. Arico, S. Srinivasan, V. Antonucci, Fuel Cells, 1 (2001) 133-161.
- [2] K.Y. Chan, J. Ding, J.W. Ren, S.A. Cheng, K.Y. Tsang, J. Mater. Chem., 14 (2004) 505-516.
- [3] V. Mehta, S.J. Cooper, J. Power Sources, 114 (2003) 32-53.
- [4] A. Hamnett, Catal.Today, 38 (1997) 445-457.



Ultrasonic irradiation and magnetic polymeric sorbent for complete removal of p-nitrophenol

M.H. Entezari^{a*}, T. Ebrahimi^b

a Department of Chemistry, Ferdowsi University of Mashhad, 91775, Mashhad, Iran

b Department of Chemistry, Ferdowsi University of Mashhad, 91775, Mashhad, Iran

E-mail: moh-entezari@yahoo.com

Key words: Ultrasound, P-nitrophenol, Nanomagnetic sorbent

Introduction:

P-Nitrophenol is considered priority toxic pollutants by the United States Environmental Protection Agency and the maximum allowed concentration in water is in the range of 1–20 ppb. The ever increasing discharge of these compounds into the environment has caused various problems in water and wastewater treatment systems because they can not be effectively treated by traditional technologies such as biological degradation, solvent extraction, and adsorption [1,2].

Materials and methods:

The sorbent used in this study was magnetic polymeric sorbent that used for removal of P-nitrophenol from aqueous solution. Then, the sorbent and solution were separated by centrifuge. After separation, the concentration of pollutant was determined by UV–vis spectrophotometer.

Apparatus:

The ultrasonic irradiation with equipment operating at 20 kHz (W- 450 D), X-ray diffractometer (XRD, Philips PW1800), Fourier transform infrared (FT-IR) spectrometer (Avatar 370). Transmission electron microscopy (TeM, *Leo 912 AB*), Scanning electron microscopy (SEM). UV–vis spectrophotometer (Unico 2800), centrifuge by Universal 320 (Hettich Zentrifugen Germany).



Result and discussion:

In this work, a combination of resin and magnetic nanoparticles were used as a sorbent for the removal of p-nitrophenol from aqueous solution in the presence and absence of ultrasound. The characteristics were studied by FT-IR, TEM, SEM, and XRD. The results showed that the nanoparticles with dimensions of about 10 nm were uniformly coated on the surface of resin. The presence of magnetic nanoparticles on the surface of polymeric resin gave a magnetic property to the sorbent particles with a high interaction with external magnetic field for easy separation. Various parameters such as the amount of sorbent, pH, contact time, intensity, temperature and the initial concentration were investigated in the presence and absence of ultrasound. The concentration of p-nitrophenol was measured in different samples under various conditions by UV-vis spectroscopy. The results indicated that the removal of p-nitrophenol was more effective with combined sorbents than the single components (Fe_3O_4 or resin). The experimental results were well fitted with Langmuir and Freundlich adsorption isotherm models and the removal kinetics followed the pseudo second order model.

Conclusions:

The present study clearly shows that the magnetic polymeric sorbent under this study is an effective sorbent for p-Nitrophenol removal from aqueous solution. This removal was enhanced in the presence of ultrasound. The shear forces generated during the cavitations process appear to be mostly responsible for this enhancement. Sorption capacity and sorption rate are strongly dependent on the applied conditions such as temperature, dose of sorbent, and ultrasonic intensity. The kinetics of sorption obeyed the pseudo-second-order.

Reference:

- [1] M.R Haghighi-Podeh, S.K. Bhattacharya. Water Sci.Technol. 34 (1996)345
- [2] Z.Wu, Y. Cong, M. Zhou, T. Tan. Chem.Eng.j.106(2005)83



15th Physical Chemistry Conference



Study Effective Parameters onto Swelling of Hydrogel Nanocomposite

Maryam teymori^{1*}, Mohammad Sadeghi²

^{1,2} Department of Chemistry, Science Faculty, Islamic Azad University, Arak Branch, Arak, Iran

E-mail: m_teymori90@yahoo.com

Abstract:

In continuation of our studies, graft polymerization of pectin and acrylic acid (AA) and acrylamide (AAm) in the presence of montmorillonite using methylenebisacrylamide (MBA) as a crosslinking agent and ammonium persulfate (APS) as an initiator, the influence of the all factors effecting onto reaction of the copolymerization were systematically optimized to achieve a superabsorbent hydrogel nanocomposite with maximum water absorbency (430 g/g).

Keywords: Hydrogel nanocomposite, Clay, Polymerization, Absorbency, Superabsorbent

Introduction:

Superabsorbents can absorb a large amount of water compared with general water-absorbing materials in which the absorbed water is hardly removable even under some pressure. Because of these excellent characteristics, superabsorbents are widely used in health, agriculture and horticulture and have aroused considerable interest and researches¹⁻³ since the first superabsorbent polymer was reported by the US Department of Agriculture in 1961[1]. It is significant for reducing the production cost and improving the comprehensive water-absorbent properties of the superabsorbent materials to graft-copolymerize the superabsorbent resin onto montmorillonite in order to fabricate a composite consisting of polymer and montmorillonite ultrafine particles. In a previous paper, we reported the synthesis of pectin *graft*-acrylic acid/montmorillonite and poly(acrylamide) superabsorbent composites.

Experimental:

The influence of the effective agents on the water absorbency of the Nanocomposite:

The amount and variety of the chemical agents will affect on the water absorbency of superabsorbent composites. Figure 1 to 4 depicts the effect of the amount of MBA, APS,

AA/AAm and pectin on the swelling [1]. The effect of the concentration of MMT on the water absorbency for the pectin-g-poly(AA-co-AAm)/MMT hydrogel nanocomposite is also shown in Figure 5. The effect of MMT amount and MBA concentration showed that with increase of these parameters, the water absorbency of the superabsorbent nanocomposite was decreased[2]. We attempted to optimize the reaction conditions to obtain hydrogel nanocomposite with higher swelling values. Therefore, the maximum water absorbency (430 g/g) was achieved [2-3].

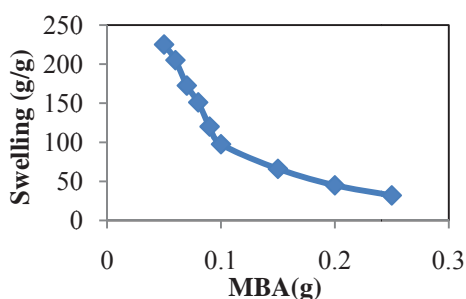


Figure 1

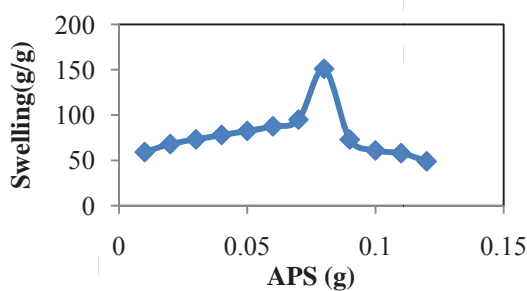


Figure 2

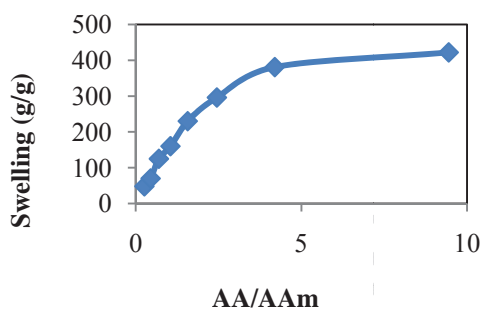


Figure 3

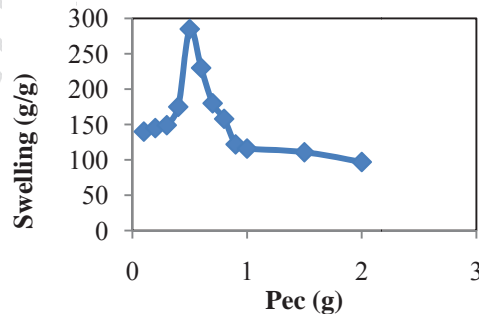


Figure 4

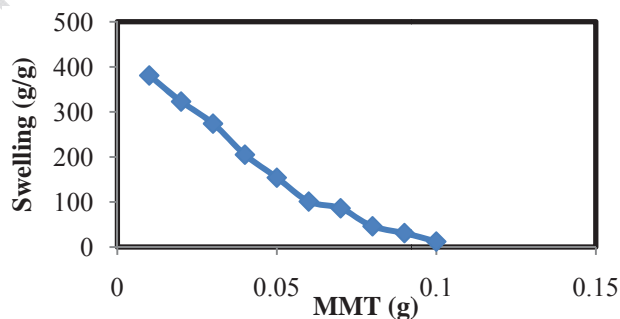


Figure 5



Conclusions:

A novel pectin-graft-poly(AA-co-AAm)MMT superabsorbent nanocomposite with water absorbency 430 times (g g^{-1} sample) was synthesized by graft copolymerization reaction among ratio AA/AAm monomer (5 g), pectin (0/5 g) and montmorillonite ultrafine powder (0/01 g) with initiator (0.07 g), crosslinker (0.05 g) at temperature 60 °C for 120 min.

References:

- [1]. Lee, W.F. and Lin, G.H. J. Appl. Polym. Sci., 79: 1665–1674,1999.
- [2]. Athawale, V.D. and Lele, V. Carbohydr. Polym., 35: 21–27,2004.
- [3]. Chen, J. and Zhao, Y., J. Appl. Polym. Sci., 75: 808–814,2008.



Study Effective Parameters on to Swelling of Hydrogel Nanocomposite And Diagrams

Maryam teymori^{1*}, Mohammad Sadeghi²

^{1,2} Department of Chemistry, Science Faculty, Islamic Azad University, Arak Branch, Arak, Iran

E-mail m_teymori90@yahoo.com

Abstract:

In this paper, A novel superabsorbent nanocomposite based on pectin has been prepared via graft copolymerization of acrylic monomers in the presence of montmorillonite clay powder. Evidence of grafting and montmorillonite interaction was obtained by comparison of FTIR, TGA and DSC spectra of the initial substrates and the superabsorbent nanocomposite.

Keywords: Hydrogel nanocomposite, Clay, Optimization

Introduction:

Superabsorbents can absorb a large amount of water compared with general water-absorbing materials in which the absorbed water is hardly removable even under some pressure. Because of these excellent characteristics, superabsorbents are widely used in health, agriculture and horticulture and have aroused considerable interest and researches¹⁻³ since the first superabsorbent polymer was reported by the US Department of Agriculture in 1961[1]

Experimental:

Preparation of Hydrogel Nanocomposite:

Pectin-g-poly(AA-coAAM)/MMT superabsorbent composite was synthesized the following steps. In a four-neck round-bottom flask equipped with a mechanical stirrer, condenser, thermometer and nitrogen line, dried pectin (0.5 g) was dispersed in distilled water (40ml). After purging with nitrogen for 20min to remove the dissolved oxygen, the pectin solution was heated to 65 °C in a water bath for 10 min under stirring to form pectin slurry. The ammonium

persulphate initiator was added (0.2 g, 5 ml) and the pectin slurry continued to react for 10min at 65 °C. When the colour of the pectin slurry changed from orange to yellow, the monomers–Crosslinker– montmorillonite mixed solution was added, and the reaction mixture was stirred for 120 min to ensure the completion of graft copolymerization.

Results and Discussion:

For identification of the product, FTIR, SEM, TG and DSC spectroscopies were used(fig 1-4). The FTIR spectra of initial substrates and composite graft copolymer are depicted in Figure 1. Fig. In the layer silicate structure, -OH groups show absorption bands at 3628-3675 cm^{-1} . The broad band at 3200-3400 cm^{-1} is due to stretching of -OH groups of the polysaccharide. In the spectrum of the nanocomposite (Fig 1b), new absorption peaks at 1653 and 1714 cm^{-1} are appeared. The characteristic band at 1653 cm^{-1} is due to C=O asymmetric stretching in carboxylate anion that is reconfirmed by another peak at 1435 cm^{-1} which is related to the symmetric stretching mode of the carboxylate groups [2-3].

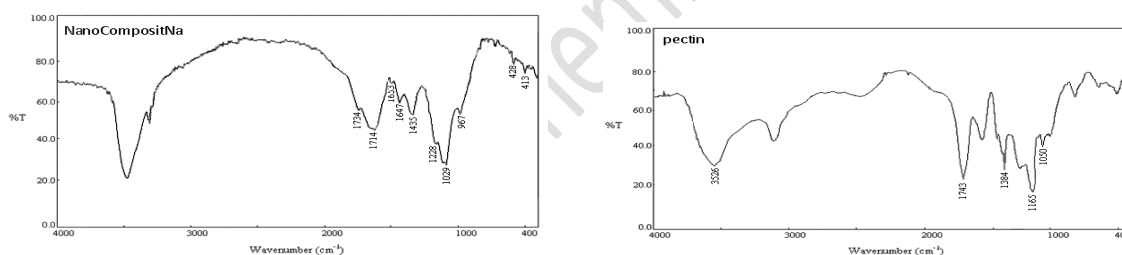


Figure 1. FTIR spectra of (a) pectin , nanocomposite(b)

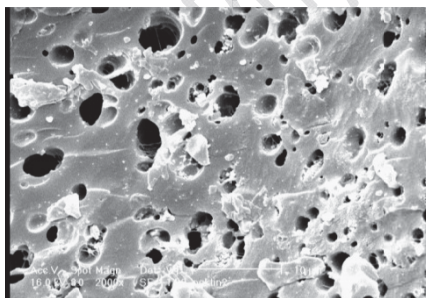


Figure 2

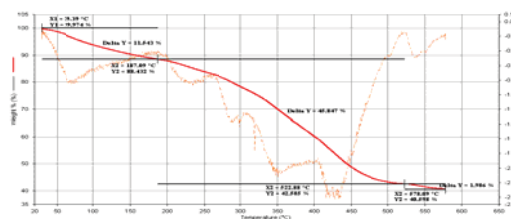


Figure 3

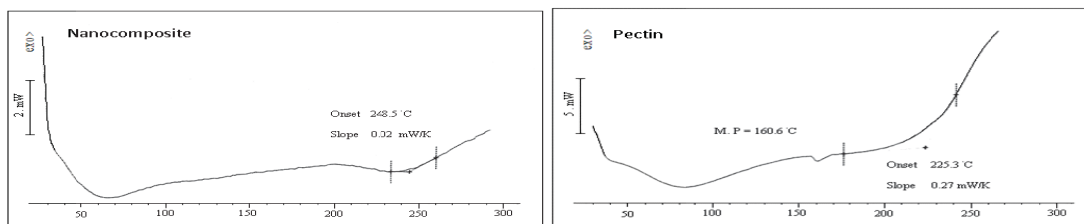


Figure 4. DSC of (a) pectin , nanocomposite(b)

Conclusion:

A novel superabsorbent nanocomposite was prepared by graft copolymerization of AA and AAm onto pectin in the presence of a crosslinking agent. Evidence of grafting and montmorillonite interaction was obtained by comparison of FTIR, TGA and DSC spectra of initial substrates and superabsorbent nanocomposite. The resultant superabsorbent nanocomposite had a large degree of water absorbency.

References:

- [1]. Lee, W.F. and Lin, G.H. J. Appl. Polym. Sci., 79: 1665–1674,1999.
- [2]. Athawale, V.D. and Lele, V. Carbohydr. Polym., 35: 21–27,2004.
- [3]. Chen, J. and Zhao, Y., J. Appl. Polym. Sci., 75: 808–814,2008.

Synthesis of nanoparticles silica sulfuric acid (NPs SiO₂-OSO₃H): a solid phase acidic catalyst for synthesis of biscoumarin derivatives

T. Ziya*, B. Sadeghi, A. Elkhani

Department of Chemistry, Islamic Azad University, Yazd Branch, Yazd, Iran

Key words: nanoparticles, Aldehydes, silica sulfuric acid, biscoumarin

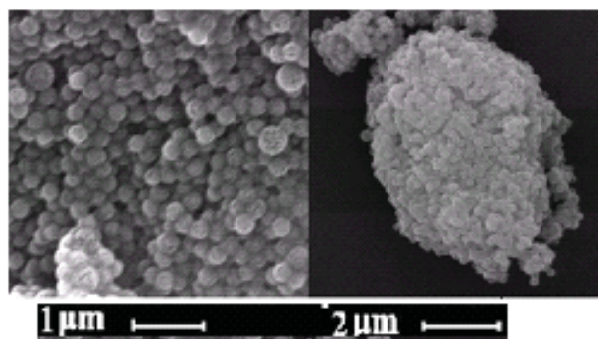
Introduction:

In the last few years, literature has highlighted the importance of nanosized materials in several scientific and technological areas, and many research councils have intensified investments in nanotechnology for the coming years [1]. Coumarins play an important role in both natural and synthetic organic chemistry because of their potential applications in fragrance, pharmaceutical and agrochemical industries [2]. We have now used nanoparticle silica sulfuric acid (NPs SiO₂-OSO₃H) as a new rapid method affording excellent yield and using solid phase acidic green catalyst for the synthesis of biscoumarin derivatives at reflux in water.

Methods:

Synthesis of SiO₂-OSO₃H nanocrystals :

Chlorosulfonic acid (23.3 g) was dropwise added over 30 min via a syringe to nanosilica gel powder (60 g) in a 100 ml flask at 0° C. The reaction mixture was then stirred for 30 min. Finally, the white powder was separated. The product was characterised by SEM (Scheme 1).



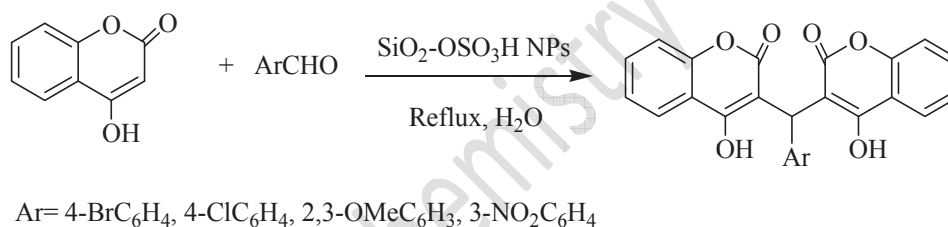
Scheme 1 The SEM images of NPs SiO₂-OSO₃H.

General procedure for synthesis of biscoumarin derivatives:

In a typical experiment, an aldehyde (1 mmol), 4-hydroxycoumarin (2 mmol) and silica sulfuric acid (0.006g) were refluxed in water with vigorous stirring. After completion of the reaction as monitored by TLC, the reaction mixture was cooled to room temperature. The crude product was recrystallized from ethanol to give the pure desired product.

Results and discussion:

In continuation of our investigations of the application of nanocatalyst in organic synthesis [3,4] we have investigated the synthesis of biscoumarin derivatives by the condensation of an aromatic aldehyde and 4-hydroxycoumarin, in the presence of 0.006 g NPs SiO₂-OSO₃H catalyst (Scheme 2).



Scheme 2 Synthesis of biscoumarin derivatives

Conclusion:

The present method offers several advantages including high yields of product, a safe environmentally benign non toxic and inexpensive heterogeneous nanocatalyst and an easy experimental workup procedure.

References:

- [1] (a) A. Yamaguchi, F. Uejo, T. Yoda, T. Uchida, Y. Tanamura, T. Yamashita, N. Teramae, Nat. Mater. 3, 337, 2004; (b) P. Claus, A. Bruckner, C. Mohr, H. Hofmeister, J. Am. Chem. Soc. 122, 11430, 2000
- [2] JW. Hinman, H. Hoeksema, EL. Caron, WG. Jackson; J. Am. Chem. Soc; 78, 1072, 1956.
- [3] B. Sadeghi, A. Hassanabadi and S, Bidaki, J. Chem. Res., 35, 666, 2011,
- [4] B. Sadeghi, A. Hassanabadi and E, Taghvatalab, J. Chem. Res., 35, 707, 2011,



15th Physical Chemistry Conference



Preparation and electrochemical capacitive behaviors of nanostructured molybdenum oxide

S. Moghiminia^{a,*}, H. Farsi^{a,b}, H. Raissi^{a,b}

^a Department of Chemistry, University of Birjand, P.O. Box: 97175-615, Birjand, Iran

^b Solar Energy Research Department, University of Birjand, Birjand, Iran

Email: shmoghminia@yahoo.com

Key words: Nanostructure, molybdenum oxide, pseudocapacitor

Introduction:

Molybdenum oxide is a wide band gap n-type semiconductor which plays an important role in technological applications because of its structural and electronic properties. Due to its crystal structure, molybdenum oxide has widely used as cathode materials for lithium ion batteries. Since of different oxidation numbers of molybdenum, this is expectable that molybdenum oxide be a good candidate for pseudocapacitor, an electronic device which has a higher power density and long cycle life compared to batteries and a higher energy density compared to conventional capacitors. Several methods have been developed for preparing nanostructured molybdenum oxide. In this study, we used potentiodynamic electrodeposition, a facile method which has several advantages like the low cost and good sticking of deposited materials to the current collector and investigated the pH and electrolyte composition effects on the pseudocapacitive behavior of nanostructured molybdenum oxide [1-3].

Materials and methods:

Na₂MoO₄, H₂SO₄ and Na₂SO₄ were Merck products and were used without further purifications and all solutions prepared using double-distilled water. The electrodeposition bath was prepared by dissolving appropriate amounts of Na₂MoO₄ and H₂SO₄ in double distilled water to have a solution of 0.04 M Na₂MoO₄ and 0.01 M H₂SO₄. The morphology of deposited materials was studied by Atomic Force Microscopy, AFM. The capacitive behaviors



of as-deposited materials were investigated in the solutions with different combinations of Na_2SO_4 and H_2SO_4 using cyclic voltammetry, galvanostatic charge/discharge curves and electrochemical impedance spectroscopy.

Apparatus:

Electrodeposition, cyclic voltammetry, and galvanostatic charge/discharge tests were performed by a Solartron Electrochemical interface SI1287. Electrochemical impedance spectroscopy studies were carried out by a Solartron Phase Gain Analyzer SI 1260. All electrochemical experiments were carried out via a standard three electrodes cell containing of an Ag/AgCl electrode, a platinum grid and a piece of stainless steel or nanostructured molybdenum oxide-coated stainless steel as reference, auxiliary and working electrodes, respectively. Surface morphological studies were carried out with scanning probe micrographs, obtained with a Dual Scope SPM (DME, Denmark).

Results and discussion:

In this study, nanostructured molybdenum oxide was potentiodynamically deposited onto a stainless steel surface from an aqueous bath by cycling the potential between 0 and -0.75 V vs. Ag/AgCl. The deposit consisted of particulates in the range of 30 to 80 nm. Electrochemical studies under galvanostatic charge/discharge and also impedance spectroscopy revealed capacitive behavior in the potential range of -0.3 to -0.55 V vs. Ag/AgCl with the value of 477 Fg^{-1} at 0.1 mA/cm^2 . An equivalent circuit comprising of three parallel branches consisting of double layer capacitance, Warburg impedance and a constant phase element signifying pseudo-capacitance each coupled with their corresponding resistances was fitted to the experimental findings and the magnitudes of the elements were derived.

Conclusion:

Our studies depicted that increasing acid concentration to 0.02 M had favorable effect on the capacity of nanostructured molybdenum oxide while beyond that the effect was detrimental. Capacitance around 600 Fg^{-1} was recorded in the potential range of 0 to -0.55 V vs. Ag/AgCl.



References:

- [1] H. Farsi, F. Gopal, H. Raissi, S. Moghiminia, *J. Solid State Electrochem.*, **14** (2010) 643.
- [2] H. Farsi, F. Gopal, H. Raissi, S. Moghiminia, *J. Solid State Electrochem.*, **14** (2010) 681.
- [3] T.M. McEvoy, K.J. Stevenson, *Analytica Chimica Acta*, **496** (2003) 39.

15th Physical Chemistry Conference



One Pot Synthesis of 2-Amino-2-Chromene Derivatives with Zinc Oxide Nanoparticles as a Reusable Catalyst

Z. Sadeghi,* B. Sadeghi

Department of Chemistry, Islamic Azad University, Yazd Branch, Yazd, Iran

Email: sadeghi.zahra28@gmail.com

Key words: ZnO nanoparticles, Aldehydes, Chromene, One- pot Synthesis

Introduction

In the last few years, literature has highlighted the importance of nanosized materials in several scientific and technological areas, and many research councils have intensified investments in nanotechnology for the coming years [1]. Surface of metal oxides exhibit both Lewis acid and Lewis base character [2]. High yield, selectivity and recyclability have been reported for a variety of nanocatalyst based organic reactions [3]. Among inorganic nanoparticles, the ZnO nanoparticle has received great attention because of its unique catalytic, electrical, electronic, and optical properties as well as its low cost and extensive applications [4]. 2-Amino-2-chromenes are an important class of compounds found as the main components of many naturally occurring products employed as cosmetics and pigments [5] and utilized as potential biodegradable agrochemicals [6].

Methods:

Aqueous solutions of zinc nitrates and urea were added into a flask under vigorous stirring (300 rpm/min). The molar ratio of Zn^{2+} to urea was about 1:4. In order to inhibit the growth of the ZnO crystallite during the course of precipitation, a certain amount of surfactant (SDS), was added into reaction system. Then the reaction system was heated to 95°C and maintained at that temperature. After stirring for 2 h, a semitransparent zinc hydroxide colloid was obtained. The precipitates were then filtered, washed with distilled water and alcohol for three

or four times, dried in air at 80°C, and finally calcined at 350°C for 2 h to achieve samples with 30–50nm particle size Fig.1.

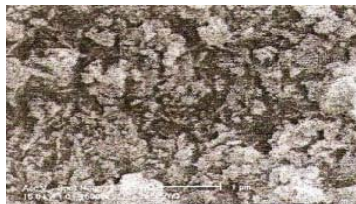
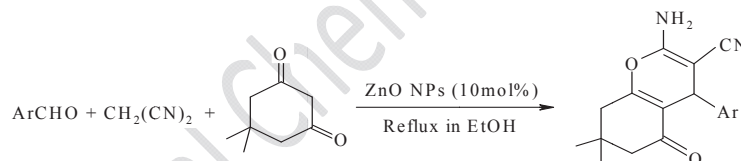


Fig 1: The SEM images of ZnO nanoparticles

Results and discussion:

In continuation of our investigation about application of solid acids [7] in organic synthesis we investigated the synthesis of chromenes in the presence of ZnO NPs as a inorganic solid acid. To optimize the reaction conditions, the reaction of benzaldehyde, dimedone and malonitrile was used as a model reaction to 2-amino-2-chromene synthesis. According to the obtained data, using the ZnO NPs (10mol%) under reflux in ethanol is the best condition. Therefore, some aldehydes, dimedone and malonitrile were subjected to chromenes (Scheme 1).



Scheme1. ZnO nanoparticles catalyzed synthesis of 2-amino-2-chromenes

Conclusion:

In conclusion, we have successfully developed an efficient Lewis acid catalyst ZnO for the synthesis of chromene derivatives. The present method offers several advantages including high yields of product, a safe environmentally benign non toxic and inexpensive heterogeneous nanocatalyst and an easy experimental workup procedure.

References:



- [1] (a) A. Yamaguchi, F. Uejo, T. Yoda, T. Uchida, Y. Tanamura, T. Yamashita, N. Teramae, *Nat. Mater.* 3 (2004) 337; (b) P. Claus, A. Bruckner, C. Mohr, H. Hofmeister, *J. Am. Chem. Soc.* 122 (2000) 11430.
- [2] K. Tanabe, *Solid Acids and Bases*, Academic Press, New York, 1970.
- [3] D. Astruc, F. Lu, J.R. Aranzaes, *Angew. Chem. Int. Ed.* 44 (2005) 7852.
- [4] E. Tang, B. Tian, E. Zheng, C. Fu, G. Cheng, *Chem. Eng. Comm.* 195 (2008) 479.
- [5] Ellis, G. P. *The Chemistry of Heterocyclic Compounds*. In *Chromenes, Chromanes and Chromones*
- [6] E. A. Hafez, M. H. Elnagdi, A. A. Elagamey, F. A. M. El-Taweel, *Heterocycles*, 26 (1987) 903.
- [7] B. Sadeghi, B. F. Mirjalili, M. M. Hashemi, *Tetrahedron Lett.* 49 (2008) 2575.



Synthesis of siliceous MCM-48 and NiO/SiO₂ mesoporous material via Ultrasound assisted sol-gel method

S.Yari^{a*}, R.Alizadeh^b, E.Fatehifar^b

a. M.sc in chemical engineering, Sahand University of Technology, Tabriz, Iran

b. Department of chemical engineering faculty, Sahand University, Tabriz, Iran

Email: Saeed.851539@gmail.com

Key words: MCM-48, NiO/SiO₂, Sol-gel, Ultrasound, Spherical particles

Introduction:

Mesoporous materials have been the focus of intense research since the discovery of the M41S class of materials in 1992 by the Mobil group [1]. Among the various classes of mesoporous materials, MCM-48 has an interpenetrating network of three-dimensional pores and hence is thought to possess favorable mass transfer kinetics compared to the unidimensional pores that occur in MCM-41 type of materials. The MCM-48 material is a favorable candidate for several catalytic reactions. The synthesis of MCM-48 is dependent on a number of factors such as temperature, stirring rate, reactant ratios, type and chain length of surfactant employed, nature of solvent and Si precursor [2]. The present work describes a synthetic approach that is based on a combination of the Modified Stöber synthesis to form non-porous silica spheres, and use the template to create a cubic structure. The catalytic properties can be adjusted by the incorporation of different metals into the MCM-48 framework. In the present study, we incorporated the Nickel-Oxide into the silica framework to determine the effect of metals on the silica structure.

Materials and methods:

First, n-Hexadecyltrimethylammonium bromide template and a certain amount of the metallic precursor (metal content 10%) was dissolved in distilled water and technical ethanol was added to the surfactant solution, a known volume of TEOS (Tetraethylorthosilicate) was added while sonication, and after 20 min, 28% ammonium hydroxide was added as a catalyst to

promote the condensation reaction. Sonication was continued for a further 45 min to get a suspension. All the above experiments were conducted at room temperature. The resulting solid was recovered by filtration and washed with distilled water and dried at 110 °C for 48h. The template was removed by calcination at 550 °C for 6 h. The synthesized Catalysts were characterized using BET, XRD, FESEM techniques.

Results and discussion:

BET analysis showed that specific surface area of silica is about 1370 m²/gr and of 10%Ni/SiO₂ is about 668 m²/gr, that shows massive surface area reduction by adding nickel special. XRD patterns were obtained between 2°-10° with a size step of 0.01 for silica and 2°-70° for 10Ni/SiO₂. The XRD patterns showed that the structure of silica tends to MCM-48, but with loading 10Ni on SiO₂, the MCM-48 structure is destroyed. Fig.1 showed that the nickel oxide is consistent with the reference code 00-022-1189. FESEM graphs represented appropriate morphology. So that SiO₂ and 10Ni/SiO₂ have spherical structures and synthetic catalysts are in the nanoscale (see Fig. 2).

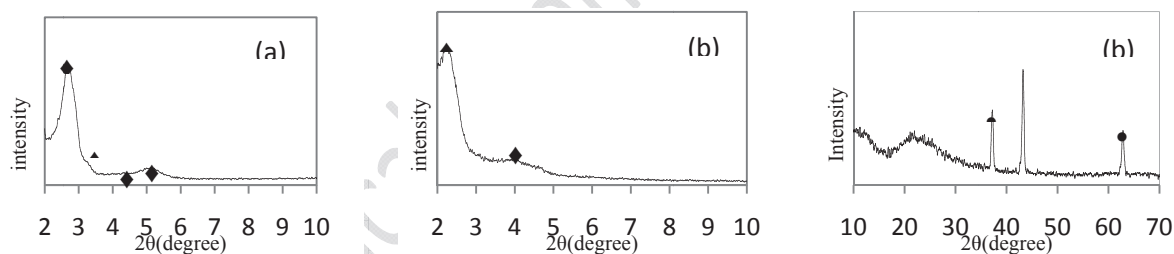


Fig. 1. XRD patterns of a) SiO₂ (MCM-48) b) 10Ni/SiO₂ (metal content 10%); (♦ SiO₂ • NiO)

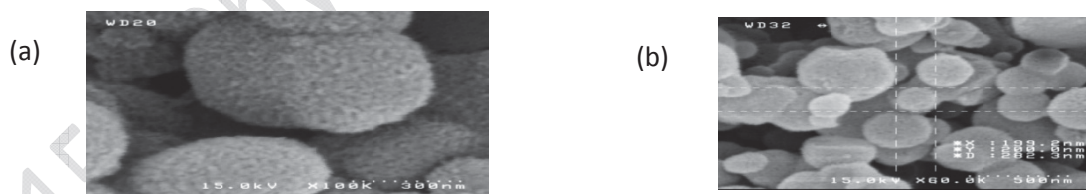


Fig. 2. FE-SEM image of a) MCM-48 b) 10Ni/SiO₂ (metal content 10%)

Conclusions:

Structure of silica which synthesized in this paper is MCM-48. However, the loading of 10% Ni can be destroyed the structure of MCM-48 that shows the structure of MCM-48 is very



sensitive to the loading of the active phase. Also with loading of nickel oxide on the silica, the particles are retained in their spherical structure. Furthermore, FESEM results represented appropriate dispersion of nickel nano-particles on silica support. The Simultaneous use of two methods sol-gel and sonication at this paper caused to have appropriate morphology and the synthesis of nanoscale particles.

Reference:

- [1] C.T.Kresge and et al; "Ordered mesoporous molecular sieves synthesized by a liquid crystal template mechanism", *Nature*, 359 (6397) (1992), pp. 710–712.



Synthesis of silica nanocomposite MSN-polyMAA for oral drug delivery

S.Amiria*, B.A.Massumib, M.Mahkamc

a Department of Chemistry, Payame Noor, Tabriz, Iran

b Department of Chemistry, Payame Noor, Tabriz, Iran

c Department of Chemistry, Azarbaijan University of Tarbiat Moallem, Tabriz, Iran

Email: s.amiri6228@gmail.com

Key words: Drug delivery, Naproxen, silica, nanocomposite.

Introduction:

The discovery of highly ordered mesoporous silica materials by scientists at the Mobil Corporation in 1992 was quickly recognized as a breakthrough that could lead to a variety of important applications. The effect of surface charge and pH on the release of The synthesis conditions for making mesoporous silica the mesoporous materials, used as a drug carrier. Naproxen, the well-known nonsteroidal anti-inflammatory drug (NSAID), was loaded into the pores of mesoporous silica modified by organic 3-(chloropropyl)-trimethoxy-silane, 4-(dimethyl amino)pyridin groups and then surface polymerization by monomer Methacrylic acid (MAA) have been successfully prepared and have been used as drug-controlled delivery system of naproxen. In addition, the naproxen release rate depended on the surface modification with the specific organic groups. materials pH-responsive drug release behavior in vitro studied in vitro release of naproxen into simulated gastric fluid (Ph=1.2) and intestinal fluid (Ph=7.4).

Materials and methods:

Silica nano particles: 60 litμ of 25% ammonia, 110 mmol was mixed in 100 mL Methanol. This mixture was allowed to reflux with stirring for 4 h. Then, it was filtered and washed. The silica was dried in furnace 150°C for 5 h.

Silica loaded with 3-chloropropyltrimethoxysilane (Si-CTS): 1 g of activated silica was mixed

with 20 mL dry toluene and 2.5 mL 3-chloropropyl trimethoxysilane. The mixture was refluxed at 70-80°C with stirring for 8 h. Then, it was filtered and washed with dry toluene, and dry acetone. The Si-CTS was dried in vacuum oven at 70°C for 3 h.

Si-CTS modified 4-(dimethyl)amino pyridin (Si-CTS-DMAP): 40 mL of dry toluene and 5 mL of 4% (v/v) 4-(dimethyl)amino pyridin solution was added into 1 g of Si-CTS. The mixture was allowed to reflux at 70-80°C under nitrogen flow condition for 8 h. Modified silica was filtered and washed with toluene. Finally, it was dried in oven vacuum at 50°C for 3 h. 0.05 g of naproxen was loading into 0.5g mesoporous silicas modified and si-nanocomposi by Freeze-Dryer device. in vitro release of proxen was into simulated gastric fluid(pH 1.2) and intestinal fluid (pH 7.4).

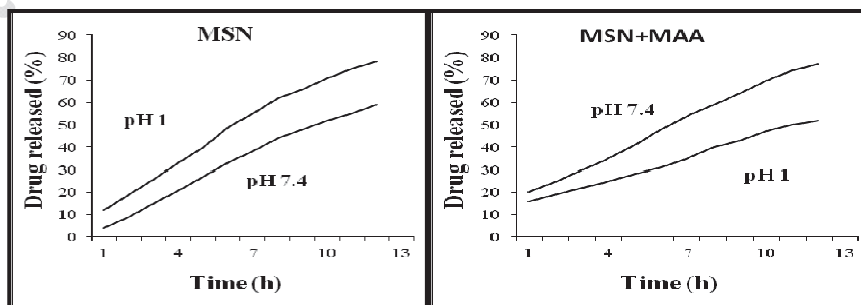
acrylamide was added into 1 g of Si-CTS-DMAP. The mixture was allowed to reflux at 50-60°C under nitrogen flow condition for 2 h.

Apparatus :

Spectrophotometer UV/Vis has been applied for determining the drug release, scanning electron microscopy (SEM) has been applied for determining scal nanopartical.

Result and discussion:

According to the results of SEM silica particals size is 54-66nm. The results of Spectrophotometer UV/Vis for rate of drug release is shown in following figure. based on the rate of drug release for nanocomposite in vitro release of naproxen into intestinal fluid (Ph=7.4) increased but mesoporous silica modified in vitro release of naproxen into simulated gastric fluid (Ph=1.2) increased.





Conclusion:

In the present work, we studied the amine-modified mesoporous silica and si-nanocomposite poly methacrylic acid loaded with anti-inflammatory drug naproxen. The obtained results show that the drug could be successfully loaded into si-nanocomposite poly methacrylic acid as well as the amine-modified silica and subsequently released from the samples si-nanocomposite poly methacrylic acid /naproxen and amine-modified silica /naproxen into the physiological solution. We observed that amount loaded into si-nanocomposite poly methacrylic acid and amine-modified silica /naproxen material was similar. Release of naproxen was faster and larger from nanocomposite sample in the Ph=7.4 than amine-modified silica /naproxen, due to larger amount of the drug trapped on the outer surface in this sample . released amount of naproxen from the amine-modified /napro sample was lower in comparison with si-nanocomposite poly methacrylic acid, as the reason of interactions of the drug with aminopropyl groups.

Reference:

- [1] A. Szegedi , M.Popova , I.Goshev , J.Miha' ly : Effect of amine functionalization of spherical MCM-41 and SBA-15 on controlled drug release , Journal of Solid State Chemistry 184 (2011) 1201–1207, Bulgaria .
- [2] i , Jeffrey I. Zink , F. Tamanoi : In vivo tumor suppression efficacy of mesoporous silicananoparticles-based drug-delivery system: enhanced efficacy by folate modification . Nanomedicine, Nanotechnology, Biology, and Medicine (2011).USA.



The effect of nanoclay particles on the mechanical properties of almond shell powder- polypropylene composite

A. Eshghi^{*a}, A. Rashno^a, M. Farsi^b, A. Lashgari^a

^aDepartment of Wood Science and Paper Technology, Karaj Branch, Islamic Azad University, Karaj, Iran

^bDepartment of Wood and Paper Science and Technology, Sari Branch, Islamic Azad University, Sari, Mazandaran, Iran

Email: Ayoub_Eshghi@yahoo.com

Keywords: Nanoclay, Almond shell flour, Composite, Mechanical properties, X-ray Diffraction

Introduction:

One of the most abundant waste materials in the west of Iran that can unlock the potentiality of these underutilized renewable materials and provide a non-food based market for the agricultural industry is almond (*Prunus dulcis amygdalus*) shells. The almond shells generated in nuts processing operation are regarded as waste material and are usually burnt, they can probably be used as fillers in FRPs. The effect of nanoclay (NC) loading (0, 2.5, and 5 phr) and almond shell flour (ASF) content (40%) on the strength properties of polypropylene composites was evaluated. The amount of maleic anhydride grafted polypropylene (PP-g-MA) was constant at 2 phr for all formulations. The Mechanical properties such as tensile, flexural were measured. Results revealed the fact that when NC and ASF were added, the flexural and tensile strengths decreased slightly. The morphology of the composites containing different levels of NC has been examined by using X-Ray Diffraction (XRD) and Scanning Electron Microscopy (SEM), respectively. XRD findings showed that with increasing NC content the peak was shifted to a lower angle, which implies formation of the intercalation morphology. The mechanical properties of the composites blends made with ASF were further supported by SEM micrographs



Materials and methods:

Polypropylene (PP) supplied by Shazand (Arak) Petrochemical Co., Iran, which has a melt flow index (MFI) of 10 g/10 min and a density of 870 kg/m³, was used as a matrix in this experiment. Maleic anhydride grafted polypropylene (PP-g-MA) as coupling agent was obtained from Solvey Co, Belgium (MFI=64 g/10 min, 0.1% maleic anhydride and density of 910 kg/m³). Almond shells (AS) were collected from a nut processing plant and the grinded using Wiley mill to produce fine powder. 60-mesh Almond shell flour (ASF) was used as filler. Montmorillonite modified with trade name Cloisite 15 A was obtained from Southern clay Products Co, USA.

Composite preparation:

The amount needed from each component were mixed, using counter-rotating twin screw extruder providing the mixing temperatures of 155-190°C in different sections of the extruder, and the rotational speed of 70 rpm. The pasty compound produced was cooled to room temperature and then grinded to produce suitable granules for further processing. Grinding was carried out in a laboratory mill. An injection molding machine set at 180°C temperature was used to prepare test samples.

Result and discussion:

The flexural strength decreases with the NC increase up to 5 phr. It is probably because of the formation of clay agglomeration and the presence of voids [1]. With incorporation of 2.5 phr NC to ASF/PP composites, the tensile strength was significantly reduced. After increasing NC up to 5 phr, the tensile strength was relatively increased. This decrease is most probably due to the low interaction between nanoparticles dispersed in the matrix [2]. With adding of NC 2.5 and 5 phr to the compound, the peak related to Cloisite 15A was weakened and shifted to lower angles which implies formation of the intercalation morphology. This means that the interlayer distance of NC increased and the interaction of the layers should be weakened. In our research, the NC could not achieve exfoliation morphology (Fig.1). Through SEM study in Fig. 2 which

is related to composite including 40% ASF and 2.5 phr NC, it has been seen that a clog of NC which is dispersed in broken matrix.

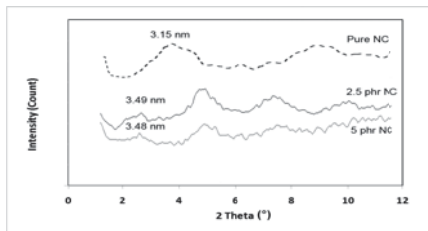


Fig. 1 XRD patterns of pure NC and composites

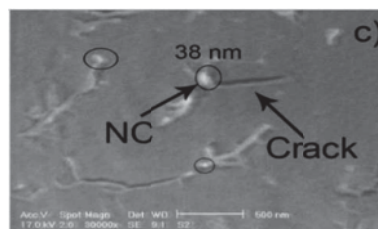


Fig. 2 SEM photomicrographs of fractured sample

Conclusion:

The influence of NC on the mechanical properties of the ASF/PP composites was investigated. The results of this study indicate that tensile and flexural strength of composites made with NC and ASF decreased by about 37.7% and 25.8%, respectively, with the addition of 2.5 phr NC, but then decreased slightly as the NC content increased to 5 phr. The SEM analysis showed heterogeneous dispersions in morphologies of ASF/PP composites containing different levels of NC. The previous findings from XRD analyses demonstrated intercalation nanocomposite structures.

Reference:

- [1]F.H. Gojny, M.H.G. Wichmann, B. Fiedler, W. Bauhofer and K. Schulte, *Compos. Part A*, 36, 1525 (2005).
- [2]F. Bensadoun, N. Kchit, C. Billotte, S. Bickerton, T. Francois, E. Ruiz, *Int. J. Polym. Sci.*, 10 (2011).



Removal amoxicillin from aqueous solutions by nanomagnetics LaSrMnO₃

M.H. Entezari*, N. Ghows, S. Ramandi, S. Taherian

Department of Chemistry, Ferdowsi University of Mashhad, 91775, Mashhad, Iran

*Email: moh_entezari@yahoo.com

Keywords: Amoxicillin, Perovskite, Ultrasound, Nanoparticles.

Introduction:

From an environmental engineering point of view, pharmaceuticals including antibiotics are a new group of manmade chemicals of concern entering the environment at concentrations such that the health effects are unknown [1]. Hence, great attention has been paid on its removal from wastewater. Available methods to deal with antibiotics compounds include activated carbon adsorption, chemical oxidation, biological digestion, photocatalytic degradation, etc [2]. However, these methods have their limitations and disadvantages. In many cases, these methods are not appropriate to use for the removal of low levels of pollutants. In addition, among different nanoparticles, there is no report on perovskite materials (ABO₃) such as Sr-doped LaMnO₃ for the removal of antibiotics pollutants. They have attracted a great interest due to its proper magnetic, catalytic properties, nontoxicity, stability at very high temperatures, high resistance and biomedical applications. In this paper, LSMO has been synthesized by ultrasound under mild conditions. Then the adsorption of amoxicillin by LSMO is investigated under different conditions due to its high efficiency and easy to use.

Materials and methods:

KMnO₄, LaCl₃. 6H₂O and Sr(NO₃)₂ were purchased from BDH Co. MnCl₂. 4H₂O, HCl, NaOH were obtained from Merck Co. KOH was obtained from Riedel Co. Antibiotic amoxicillin was purchased from Sigma. The magnetic nanoparticles were synthesized by chemical coprecipitation method in the presence of ultrasound. Then 50 mL of amoxicillin solution containing nanoparticles was stirred for removal of amoxicillin.



Apparatus:

The samples synthesized by ultrasound apparatus 20 kHz and analysed by FT-IR Spectroscopy, transmission electron microscopy (TEM), X-ray diffraction (XRD). The samples concentration determined using Spectrophotometer by method P. Nagaraja et al [3].

Result and discussion:

The XRD peaks and the FT-IR spectrum for the samples confirm a perovskite structure. The XRD patterns indicated when size nanoparticles to be about 23 nm. The TEM indicate the hexagonal structure of samples. The removal of amoxicillin over LSMO is optimized by considering the effect of important variables on the adsorption process. Based on the results, the maximum removal efficiency was attained at higher temperature and low pHs in an almost short time. The optimum time for the removal of amoxicillin was more than 90% for 50 min. In addition, the most important is the magnetic property of the nanoparticles which separated easily from aqueous solution by an external magnetic field.

Conclusion:

The removal of amoxicillin by the batch system has been investigated under different experimental conditions such as pH, amount of nanoparticles, contact time, temperature and initial concentration. Furthermore, decreasing fast concentration and efficient use of this nanoparticles under mild condition makes it an excellent candidate for industrial applications in wastewater.

References:

- [1] E. S. Elmolla, Degradation of amoxicillin, ampicillin and cloxacillin antibiotics in aqueous solution by the UV/ZnO photocatalytic process, J. of Hazardous Materials 173 (2010) 445–449
- [2] E. S. Elmolla, Photocatalytic degradation of amoxicillin, ampicillin and cloxacillin antibiotics in aqueous solution using UV/TiO₂ and UV/H₂O₂/TiO₂ photocatalysis, Desalination 252 (2010) 46–52.



- [3] P. Nagaraja, Spectrophotometric method for the determination of drugs containing phenol group by using 2,4-DNP, E-Journal of chemistry, 2010,7(2),395-402.

15th Physical Chemistry Conference



Studies on Enzymatic Biomachining of Copper by Glucose Oxidase

Mohammadreza Eskandarian^{a*}, Afzal Karimi^a, Mohammadreza Shabgard^b

^a Departments of Applied Chemistry and Chemical Engineering, University of Tabriz, Tabriz, Iran

^b Department of Mechanical Engineering, University of Tabriz, Tabriz, Iran

Email: m.r.eskandarian@gmail.com,

Key words: Biomachining, Enzyme, Glucose oxidase, Material removal, Copper.

Introduction:

Chemical machining (CM), electro-chemical machining (ECM) and electro-discharge machining (EDM) are among the conventional methods which have successful results on machining process in micro scale (micro-machining). In chemical machining, which is mostly done by strong acid and toxic substances, work risks are very high and the process often faces with many challenges [1]. In biomachining, which is one of the most recent methods of machining, bacteria such as *Acidithiobacillus ferrooxidans* are used for material removal from the piece's surface. Thus far, some studies have been carried out on this process and many advantages have been presented for it compared with other modern machining methods [2]. Despite of many advantages, biomachining has its own problems. For example, the *Acidithiobacillus ferrooxidans* bacterium used in the process can grow and act only in acidic pH (pH=1-3) and, in higher pH, its activities decrease [3]. In this work, a new method which does not have the above-mentioned problems and makes it possible to control the material removal rate and maintain surfaces integrity characteristics presented.

Materials and methods:

Glucose oxidase (GOx) type II (EC 1.1.3.4, 25 U/mg, from *Aspergillus niger*) purchased from Sigma Aldrich, Ferrous sulfate, β -D-(+)-glucose, sodium acetate, acetic acid, sulfuric acid (95-98%) purchased in analytical grad and all solutions were prepared in distilled water. In the present research, copper pieces with 99.99% purity were used. Copper pieces with the



dimensions $0.02 \times 0.02 \text{ m}^2$ were cut, abraded and washed by ethanol. Then, they were put in 250 mL erlenmeyer flasks containing 100 mL solution of $\text{Fe}_2\text{SO}_4 \cdot 7\text{H}_2\text{O}$ 0.5 g; β -D-(+)-glucose 1 g and GOx 100 U and incubated in the 130 r/min at 25°C for 10 h. Then, copper pieces were taken out of the solution and the required analyses were conducted on them.

Results and discussion:

The results of weight measurement of pieces before and after conducting the process, demonstrate that enzymatic material removal is happened and, after 10 h, 0.026 g is taken from the copper piece with 0.0004 m^2 surface. Analysis of the surface was conducted using SEM on copper pieces with similar initial surfaces and dimensions which were under machining in four different environments including acid solution of sulfuric acid, 1N, acid solution of hydrochloric acid, 1N, *Acidithiobacillus ferrooxidans* bacterial solution and enzymatic solution of this work along with the control sample. The surface morphology of the piece in enzymatic solution showed the minimum change compared with the control piece. Acidic solutions exerted the maximum change on the characteristics of copper piece surface.

Conclusion:

Experiments showed that enzymatic machining is feasible on the pure copper pieces. Enzymatic machining maintains morphological characteristics of the considered piece to a large extent. In addition to being new, noticeable advantages of the enzymatic material removal are including simplicity, controllability and low rate. Therefore, in this method, machining can be done more delicately. Also, results showed that enzymatic material removal rate is linear with time and by adjusting reaction time, the favorable material removal depth can be adjusted. In this method, the rate of material removal rate is mostly influenced by enzyme activity and depends on the production rate of hydrogen peroxide in the environment.

Reference:

- [1] Williams K, Gupta K, Wasilik M. Etch rates for micromachining processing-Part II. *Microelectromech S* 2003; 12: 761-778.



- [2] Uno Y, Kaneeda T, Yokomizo S. Fundamental study on biomachining: Machining of Metals by *Thiobacillus ferrooxidans*. JSME. Inter J Ser C 1996; 59: 837-842.
- [3] Zhang DY, Li YQ. Possibility of biological micromachining used for metal removal. Sci China Ser C 1998; 41: 151-156.

15th Physical Chemistry Conference



The effect of nanoparticles and enzyme immobilization on the performance of biosensor Sulfite, based on glassy carbon electrode

Sajjad Khakpour², Afshin Farahbakhsh^{1*}, Airin Ghoseyri²

¹Assistant Professor of Chemical Engineering, Department of Chemical Engineering, Quchan Branch, Islamic Azad University, Quchan, Iran.

²Student of MS Chemical Engineering, Department of Chemical Engineering, Quchan Branch, Islamic Azad University, Quchan, Iran.

* Email: afshin.farahbakhsh@gmail.com

Keywords: Glassy carbon electrode, detect Sulfite, nanoparticles, enzyme immobilization

Introduction:

One of the ways to detect small amounts of Sulfite is to use electrochemical sensors and using nanoparticles can also increase the efficiency and performance. When higher selectivity and accuracy is necessary we use biosensors to detect desired material. Biosensors procreate changes such as: Decreasing the time and the cost of a sample, making non-destructive tests, and decreasing the health product in chemical analysis and microbial tests. In the performance of biosensor that is based on electron transfer, the electrode uses as a Converter.[2] A biosensor contains three electrodes: Reference electrode (Ag/AgCl), Working electrode which is based on materials like glassy carbon, and Auxiliary electrode. Working electrode to make the Sulfite detectors are basically based on glassy carbon and their performance improves by gold nanoparticles, carbon nanotubes and enzyme immobilization. In this paper we investigate the effect of nanoparticles plus enzyme immobilization to improve the performance of the biosensors.

Materials and methods:

Working electrodes to make Sulfite detectors are basically based on glassy carbon and their performance improves by gold nanoparticles [3], carbon nanotubes [1] and enzyme immobilization.[4] To connect nanoparticles to the desired base, the substrate must be



polished by alumina and the electrode is made of interface materials like, dimethylformamide and ployallylaminehydrochloride film or electric deposition and with the presence of interface materials polyphenol oxidase enzyme will be immobilized on it. Mainly to make working electrode, fundamental substance is used as the electrode base which is polished before using, then the prepared nanoparticles are immobilized on the electrode base and the modified electrode will be washed with doubly distilled water, after drying the enzyme will be immobilized on it.

Result and discussion:

For a better performance of working electrodes, they must have minimum electrical resistance, maximum selectivity and highest sensitivity in low current changes. The pure glassy carbon electrode has fairly linear current peak. According to obtained curves, the performance of glassy carbon electrodes will be improved by using nanoparticles and enzyme immobilization. There is a potential peak in the curve for optimum voltage that shows maximum difference current between anode and cathode, this can be used to compare the effect of adding nanoparticles and enzyme immobilization on the performance of the system. Using gold nanoparticles and carbon nanotubes will improve the performance of the sensor, so the optimum voltage will be 2 and 3 times more than the optimum voltage of glassy carbon electrode. The enzyme selectivity and using nanoparticles in glassy carbon electrode with gold nanoparticles, carbon nanotubes, ployallylamine hydrochloride film and polyphenol oxidase enzyme, will reduce electrical resistance. The optimum amperage in this electrode is about 6 times more than optimum amperage of glassy carbon electrode, consequently the electrochemically response will be increased.

Conclusion:

Based on obtained results and curves in the glassy carbon electrode, mainly using nanoparticles leads to reduce electrical resistance and also increases the sensitivity. Using nanoparticles and immobilized enzyme will increase the electrochemically response. Comparing these modified electrodes: Glassy carbon electrode modified with gold



nanoparticles, Pure glassy carbon electrode, glassy carbon electrode modified with nanotubes and glassy carbon electrode modified with gold nanoparticles, carbon nanotubes, ployallylamine hydrochloride film and immobilized polyphenol oxidase enzyme, in the same experimental conditions, Consequently, glassy carbon electrode modified with gold nanoparticles, carbon nanotubes, ployallylamine hydrochloride film and immobilized polyphenol oxidase enzyme had the best selectivity and the most sensitivity, also it had the best performance.

Reference:

- [1] Lawrence, N.S., Deo, R.P., Wang, J., " Electrochemical determination of hydrogen sulfide at carbon nanotube modified electrodes", *Analytical Chemical Acta*, 2004, 517.
- [2] Yourong, W., Heqing, Y., Efeng, W., " The electrochemical oxidation and the quantitative determination of hydrogen sulfide on a solid polymer electrolyte-based system", *.Electoanalytical, Chem.*, 2001, 497.
- [3] Yang, B., Wang, Sh., Tian, S., Liu, L., " Determination of hydrogen sulfide in gasoline by Au nanoclusters modified glassy carbon electrode", *Electrochemistry Communications*, 2003, 11.
- [4] Sartori, E.R., Campanha, V., Filho, O.F., " Indirect determination of sulfite using a polyphenol oxidase biosensor based on a glassy carbon electrode modified with multi-walled carbon nanotubes and gold nanoparticles within a poly(allylamine hydrochloride) film", *Talanta*, 2011, 81.
- [5] Bahmani, B., Moztaarzadeh, F., Rabiee, M., Tahriri, M., " Development of an electrochemical sulfite biosensor by immobilization of sulfite oxidase on conducting polyaniline film", *Synthetic Metals*, 2010, 16



The effect of operating parameters on the photocatalytic removal of antibiotic Gentamicin at aqueous solution using UV-C irradiated TiO₂ nanoparticles

M. Shokri, M.A. Behnajady, P. Moradian*

Department of chemistry, Faculty of science, Tabriz branch, Islamic azad university, Tabriz, Iran

Email: parimoradian@yahoo.com

Key words: Gentamicin, TiO₂ Nanoparticles, Photocatalysis

Introduction:

The antibiotics group is one of the most important pharmaceuticals used worldwide for humans and veterinary purposes. The presence of broad spectrum antibiotics in aquatic environments, albeit at low concentrations, may pose serious threats to the ecosystem and human health by inducing proliferation of bacterial drug resistance [1]. Antibiotic formulation effluents are well known for the difficulty of their elimination by traditional bio-treatment methods and their important contribution to environmental pollution is due to their fluctuating and recalcitrant nature [2]. In this paper, the antibiotic gentamicin elimination using TiO₂ (Degussa P25) photocatalyst under UV-C light has been reported. The influence of operational parameters on the photocatalytic reactions, including catalytic amount of TiO₂, light intensity and pH has been studied.

Materials and methods:

The following chemicals were used: Gentamicin (a product of Alborz Darou Company). As catalysts, TiO₂ (Degussa P25, anatase:rutile 80:20, 21 nm particle size, 50 m²/g BET area), Double-distilled water (a product of Kasra Company).

For the investigation of the photocatalytic activity of UV/TiO₂ nanoparticles towards degradation of Gentamicin, a solution containing desired amounts of Gentamicin and photocatalyst were prepared and irradiated with UV-C lamp (15 W, λ_{max} =254 nm, light intensity = 17.9 W/m²).



Then the concentration of remaining Gentamicin was determined by UV-Vis spectrophotometer at $\lambda_{\text{max}} = 255 \text{ nm}$

Result and discussion:

Based on our results, the optimum TiO_2 concentration for degradation of Gentamicin antibiotic in aqueous solution is 0.12 g/L. Further increase of TiO_2 concentration above 0.12 g/L did not produce significant improvement in antibiotic degradation. This may be due to the decreasing light penetration, increasing light scattering, agglomeration, and sedimentation of TiO_2 under high catalyst concentration. The study of the effect of initial pH on degradation of Gentamicin, demonstrated that pH had a great effect on the antibiotic degradation, and the highest degradation was achieved at pH= 4. But by further increasing pH to 6 the removal percentage has dropped from about 87% to 57%. The TiO_2 surface is positively charged in acidic medium and negatively charged in alkaline medium. So, we can infer that the change in surface charge reduces the absorption of gentamicin on TiO_2 catalyst and consequently degradation of gentamicin will decrease. Also the study of the effect of light intensity showed that with increasing light intensity, concentration of pollutant will be reduced.

Conclusion:

Degradation of Gentamicin antibiotics in aqueous solution by TiO_2 photocatalysis under UV (254 nm) irradiation was studied. The amount of TiO_2 has an important influence on the reaction rate. The optimum conditions for the photocatalytic degradation of Gentamicin were found to be pH= 4, light intensity 31.6 W/m^2 and catalyst dosage of 0.12 mg/L.

Reference:

- [1] E. Hapeshi et al.; "Drugs degrading photocatalytically: Kinetics and mechanisms of ofloxacin and atenolol removal on titania suspension"; *Water Research*; 44, 1737-1746, 2010.
- [2] A. Chatzitakis et al.; "Photocatalytic degradation and drug activity reduction of Chloramphenicol"; *Water Research*; 42, 386-394, 2008.



Synthesis of NiO nanoparticles by precipitation method and their application as an effective adsorbent in the removal of Cr(VI) from aqueous solutions

M.A.Behnajady, S.Bimeghdar*, N.Modirshahla

Department of Chemistry, Faculty of Science, Tabriz Branch, Islamic Azad University, Tabriz, Iran

Email: s.bimeghdar@yahoo.com

Keywords : Adsorption, Cr(VI), NiO nanoparticles, Precipitation

Introduction:

Chromium is widely used in industrial applications such as metallurgy, battery, paper and paint manufacturing. Chromium exists in the environment both as trivalent [Cr(III)] and hexavalent [Cr(VI)] forms. However, the hexavalent form is 500 times more toxic than the trivalent form. A number of technologies have been used for removal of heavy metals from aqueous solutions, such as coagulation/flocculation, membrane filtration, oxidation, reverse osmosis, ion exchange and adsorption processes [1]. In the recent years there has been an increasing interest in the synthesis of nanosized crystalline metal oxides because of their large surface areas, unusual adsorptive properties, surface defects and fast diffusivities. NiO is one of these metal oxides and exhibits adsorption capacity for several ions. Therefore the NiO nanoparticles may be used to control the mobility of metal ions in the environment [2,3].

In this work NiO nanoparticles have been synthesized by precipitation method and characterized by XRD and TEM techniques. The efficiency of this nanoparticlese have been studied in the removal of Cr(VI) from aqueous solutions.

Materials and methods:

All the chemicals used in this study were analytical grade and used without further purification. Potassium dichromate ($K_2Cr_2O_7$), Nickel nitrate ($Ni(NO_3)_2 \cdot 6H_2O$) and NaOH



were obtained from Merck. Nickel oxide was prepared by adding a solution of nickel nitrate to a sodium hydroxide solution. The resultant gel was filtered, and then washed with deionized water several times. The gel was dried at 75°C for 15 h, then calcined at 300°C for 2 h.

Adsorption experiment of Cr(VI) on the NiO nanoparticles was carried out using 100 mL of various concentration of metal ions, at 30°C and pH= 4.7. NiO nanoparticles (0.5 g) were added to Cr(VI) solution under stirring. At the end of the adsorption period, the solution was centrifuged and analyzed by UV-vis spectroscopy in the maximum wavelength of Cr(VI).

Results and discussion:

The XRD patterns of the synthesized NiO were recorded for the identification of the samples. The crystal size of the NiO nanoparticles was estimated to be about 11 nm, which is in agreement with the TEM results. According to the results this nanoparticles are effective in removal of Cr(VI) from aqueous solutions and the capacity of this adsorbent decreases by increasing initial concentration of Cr(VI) and temperature.

Conclusion:

The results show that precipitation method is an effective way for synthesis of NiO nanoparticles. These nanoparticles by average size of 11 nm are an appropriate adsorbent for elimination of Cr(VI) from aqueous solutions. The adsorption capacity of Cr(VI) is found to decrease with increase in initial concentration of Cr(VI). This reduction is due to the saturation of the specific surface area and reduction of active sites of nano-adsorbent. Also, the results of temperature effect illustrates that the adsorption of Cr(VI) by NiO nanoparticles is an exothermic and spontaneous process.

References:

- [1] J.C Igwe et al.; "Adsorption isotherm studies of Cd(II), Pb(II) and Zn(II) ions bioremediation from aqueous solution using unmodified and EDTA-modified maize cob"; *Ecletica Quimica*; 32, 33-42, 2007.



- [2] N.M. Hosny; "Synthesis, characterization and optical band gap of NiO nanoparticles derived from anthranilic acid precursors via a thermal decomposition route"; *Polyhedron*; 30, 470-476, 2011.
- [3] T. Mahmood et al.; "Cation exchange removal of Zn from aqueous solution by NiO"; *Journal of Non-Crystalline Solids*; 357, 1016-1020, 2011.

15th Physical Chemistry Conference



Thermal Resistance Magnetic Nano Composites Based on Silicon- Resin Epoxy

S.H.Hosseini^a, M.Montazerlotf^{a*}

^aDeptment of chemistry, Faculty of Technical and Engineering, Islamic Azad university, Saveh
Branch, Felestin Square, Saveh-Iran

*Email: fg_jam@yahoo.com

Keywords: Nano composi, nano fibr carbon, nano silice, magnetic, fibrs

Introduction:

Composite is said to material that consists of two or more elements, so that they make a quality together in macroscopic scale that it doesn't occur by each of them individually, and if the dimensions of at least one of these elements is lie in nanometer scale, the nano composite terms is used for that material. The nano composites are classified based on context material to three groups as: metallic, ceramic and polymeric context. Among these the highest interest is given to nano composites with polymeric context. One of reasons to developing the nano composites with polymeric context is its unique mechanical, physical and chemical properties. Among applications of polymeric nano composites we can mention to making covers resistant to wear, covers resistant to corrosion, linings resistant to high temperatures that are used in military equipments.

Experimental:

In this research more improving thermal, mechanical and magnetic properties of nano composites was investigated. When particles are dispersed in a polymeric bed as layers, the desired properties reach to their maximum level, because these materials show unexpected increasing properties. One of these modes is using the silica particles. By adding a very low percent of these materials, a more strength composite with high thermal resistant is obtained.



When properties such as high strength and hardness with low weight and unique properties such as resistance to corrosion, mechanical resistance in high temperatures, chemical neutrality and ductility are required, it can be add carbon nano fibers.

Conclusion:

For providing absorbent materials two methods are used: 1) providing nano composites from conductive polymers that cause to increasing the dielectric coefficient; 2) using the conductive polymers with high dielectric coefficient and with conductive fillers such as graphite, black carbon and etc. those nano composites that made by this method, are used In automobile industry, aerospace, structural and home equipments and etc.

In present research, the nano particles are used as reinforcement material in optimized ratios of context matrix polymer. Also the optimized ratios of reinforcement materials were obtained based on various experiments by different ratios between constituents. The different physical conditions such as pressure, temperature, vacuum and natural conditions on aluminum plates (by dimensions 5×10) investigated for increasing the maximum contribution with surface. The investigated nano composites were include carbon nano fiber, nano silica and nano carbon tubes that were used beside metallic materials such as aluminum in a polymeric bed consist of resin, epoxy, silicon resin, phenolic resin. This improves composites properties such as lightness, viscosity, film making ability, thermal and chemical resistance, and also the new properties such as absorbing magnetic waves.

References:

- [1] Dudkin BN, Zainullin GG, Krivoschapkin PV, Krivoschapkina EF, Ryazanov MA. Glass Physics and Chemistry(2008;34:187)
- [2] Johnsen BB, Kinloch AJ, Mohammed RD, Taylor AC, Sprenger S. Polymer(2007;48:530)
- [3] Drzal LT. The interphase in epoxy composites. In: Dusek K, editor. Epoxy resinsand composites. 2nd ed. Berlin, Heidelberg: Springer;(1986.)



Removal and Separation of Calcon Dye from Wastewater by Magnetic Solid Phase Extraction with Iron Oxide Nanoparticles Modified with CTAB

R. Abbasi^a, H.Parham^b, Z.Ramazani^c

^a Department of chemistry, Islamic azad university, Omidyeh branch, Omidyeh , Iran

^b Department of chemistry, Faculty of science, Shahid chamran university, Ahvaz, Iran

^c Department of chemistry, Faculty of science, Shahid chamran university, Ahvaz, Iran

E-mail: abbasi_br@yahoo.com

Keywords: Magnetic Iron Oxide Nanoparticles, Adsorption Isotherm, Calcon, Separation, AKPC

Introduction:

Nanotechnology is beginning to allow scientists, engineers, and physicians to work at the cellular and molecular levels to produce major advances in the life sciences and healthcare. Real applications of nanostructured materials in life sciences are uncommon at the present time. However, the excellent properties of these materials when compared with their bulk counterparts provide a very promising future for their use in this field [1]. Current challenges include further research to determine methods that increase the stability of nano - particles used in remediation, and the need to develop manufacturing techniques for mass production of these materials [2]. Nanosized magnetic particles possess high performance in the separation process due to the high specific surface area and the absence of internal diffusion resistance [3].

Materials and methods:

All chemicals and reagents were of analytical grade and the solutions were prepared with bi-distilled water. Calcon, phosphoric acid (85% m/m), methanol (99.9% m/m), ammonia solution (25% m/m), Hcl (37% m/m), acetic acid (99.9% m/m), FeCl₃ (96% m/m), FeCl₂ .4H₂ O (99.9% m/m), potassium hydrogen phthalate (KHP) and cetyltrimethylammonium bromide



(CTAB) were purchased from Merck (Darmstadt, Germany). Suggested reaction for the formation of nanoparticles is as following equation(1) [16]:



Experimental conditions such as temperature, rate of ammonia addition and rate of solution stirring have critical effect on the size of nanoparticles. The particles were ageing in the solution under mechanical stirring, decanted by magnetic settling, and washed three times with distilled water. The IONPs were imaged with TEM (906E, LEO, Germany) and their sizes were in the range of 20–100 nm. Removal percent and adsorbed amount of Calcon was determined by photometric measurement of absorption of the sample solution before and after removing process at 520 nm.

Apparatus:

The spectrophotometric measurements were made with a Cary 100 spectrophotometer (Varian Manufacturer Pty Ltd, Australia). A transmission electron microscope (906E, LEO, Germany), An Accumet Model 15 pH-meter with separate glass and calomel electrodes (Fisher scientific Co.) and a super magnet (1.2 T, 10 cm × 5 cm × 2 cm) for settlement of magnetic nanoparticles were used.

Results and discussion:

The removal and preconcentration of Calcon by surfactant modified IONPs (CTAB-IONPs) showed fast separation of this dye from the bulk of the water solutions. Moreover, the removal of Calcon reached equilibrium within about 5 min. Such a fast adsorption rate could be referred to the absence of internal diffusion resistance. The adsorption process was studied by varying different regulating parameters like amount of nano adsorbent, solution pH, initial dye concentration, temperature, buffer volume, amount of CTAB, electrolyte concentration also were optimized. The effect of some other parameters such as reuseability of nano particles, tolerable volume of dye solution and interfering ions on the removal process was also investigated.



Conclusion:

In summary a fast, simple and new magnetic removal of Calcon from aqueous solution has been successfully developed with CTAB-coated IONPs as adsorbent. The adsorbent could be manipulated magnetically and exhibited high adsorption capacity and fast adsorption rates for the removal of Calcon due to the high specific surface area and the absence of internal diffusion resistance. The adsorption behavior could be described by Langmuir isotherm. The adsorbent may also be useful for the removal of other anionic dyes from aqueous solutions. The adsorbed Calcon could be desorbed using methanol solvent. The whole adsorption-desorption processes can be completed within 5 min.

References:

- [1] P. Tartaj , M.D. P. Morales, S.V. Verdaguer, T.G.L. Carreno, C. J. Serna, J. Phys. D: Appl. Phys. 36 (2003) 182.
- [2] N.Savage, M.Diallo, J.Duncan, A.Street, R.Sustich, Nanotechnolog Applications for Cean Water, William andrew inc.(2009) 347.
- [3] Y. Chang, D. Chen, Macromol. Biosci., 5(2005) 254.
- [4] M. Takafuji, S. Ide, H. Ihara, Z. Xu, Chem. Mater, 16(2004) 1977.
- [16] P. Li, D.E. Miser, S. Rabiei, R.T. Yadav, M.R. Hajaligol, Appl. Catal. B: Environ. 43(2003) 151.



Synthesis of nano-zeolite: modification of carbon paste electrode using nano-zeolite and its application for determination of dopamine

A. izadi¹, M. Abrishamkar^{2,*}

¹Department of Chemistry, Young Researchers Club, Islamic Azad University, Khouestan Science and Research Branch, Ahvaz, Iran.

² M. Abrishamkar, Department of Chemistry, Islamic Azad University, Khouestan Science and Research Branch, Ahvaz, Iran.

E-mail: M.abrishamkar@umz.ac.ir

Keywords: Nano zeolite, Determination, Modified electrode, Dopamine

Introduction:

Dopamine is one of the most significant catecholamines, plays a very important role in the functioning of the central nervous system, cardiovascular, renal and hormonal systems as well as in drug addiction and Parkinson's disease [1]. The selectivity and sensitivity seemed important in the development of any procedure for the determination of dopamine. The best way is to directly determine Dopamine without any separation steps of samples. The electrochemical methods have more advantages over the other because of the advantage of the electrode in sensing the neurotransmitters in living organisms. Electrochemical analysis on the unmodified electrodes, has limitations because of the overlapping of oxidation potentials of ascorbic acid and dopamine and hence often suffers from a pronounced fouling effect those results in rather a poor selectivity and reproducibility [2]. The use of zeolites as supported electrodes represents a good feature for preparation of modified electrode for fast, easy and cheap for electrocatalytic oxidation of dopamine. The zeolite with particle sizes of less than 100nm are referred to nano-sized zeolite. Zeolites nano particles are more efficient catalyst and adsorbent materials because of their higher surface areas comparing to the conventional micron size zeolites. By reducing of particle size, diffusion path lengths will be decreased and active site will be accessible readily [3-4]. Our research intends to introduce a novel

synthesized zeolite modified carbon paste electrode based on Ni ions for electrocatalytic oxidation and determination of dopamine using electrochemical methods.

Materials and methods:

The ZSM-5 nano-zeolite was synthesized in our laboratory. Sodium aluminate was from Fison. Graphite powder, nickel chloride, potassium chloride were from Fluka. Silicic acid, tetrapropyl ammonium hydroxide (TPAOH), dopamine, sodium nitrate, ascorbic acid and sodium hydroxide used in this work were also purchased from Merck. All reagents were of analytical grade and used as received without further purification.

Apparatus:

A potentiostat/galvanostat (sama 500-c Electrochemical Analysis system, sama, Iran). SCE electrode as reference electrode, a platinum wire as the auxiliary electrode and Ni/ZMCPE as the working electrode were used.

Result and discussion:

The detection limits and linear dynamic ranges for dopamine using differential pulse voltammetry method was 3.5×10^{-6} M (LOD), 8.0×10^{-5} - 9.0×10^{-4} (LDR) respectively Fig.1. The diffusion coefficient for dopamine using chronoamperometry method was calculated $7.745 \times 10^{-6} \text{ cm}^2 \cdot \text{s}^{-1}$ Fig.2

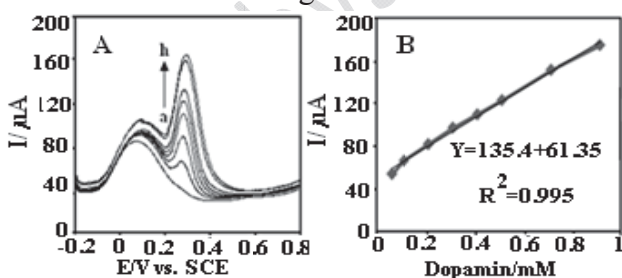


Figure 1: (A), The DPVs of dopamine in various concentrations a) 0.0, to h) 0.9 mM in the presence of 0.8 mM ascorbic acid on the surface of NiZMCPE and (B) the peak current vs. dopamine concentration from (A).

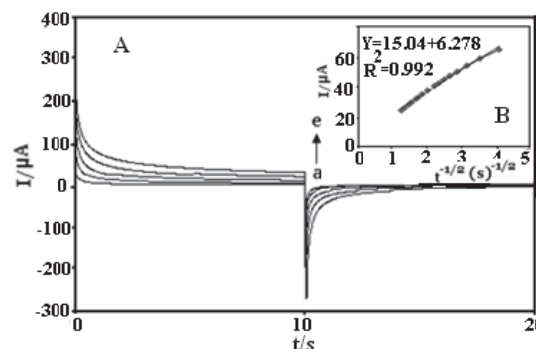


Figure 2: (A) CAs of NiZMCPE in the absent (a) and presence of dopamine, and (B) oxidation current of dopamine vs. $t^{1/2}$.



Conclusion:

In this study determination of dopamine in the presence of ascorbic acid was investigated using zeolite modified carbon paste electrode. The catalytic oxidation and determination of dopamine was studied using differential pulse voltammetric and chronoamperometry methods. Obtained results show that the oxidation peaks of ascorbic acid and dopamine were well separated at the surface of carbon paste electrode modified with Ni-zeolite.

References:

- [1] D. R. Shankaran et al; "Simultaneous determination of ascorbic acid and dopamine at a sol-gel composite electrode"; Sensors and Actuators B; 94, 73-80, 2003.
- [2] V.S. Vasantha et al, "Electrocatalysis and simultaneous detection of dopamine and ascorbic acid using poly (3, 4-ethylenedioxy) thiophene film modified electrodes"; Journal of Electroanalytical Chemistry; 592, 77-87, 2006.
- [3] S.N. Azizi et al; "Novel nano-zeolite modified carbon paste electrode for electrocatalytic oxidation of methanol"; Monatsh Chem; 10, 85-89, 2011
- [4] N. Goyal et al; "Comparison of spherical nano gold and nano gold plates for the oxidation of dopamine and ascorbic acid"; Journal of Electroanalytical Chemistry; 631, 58-92, 2009.



Recovery and Synthesis of Nano-Silver Particles from Medical Wastes

Elham Cheraghi^{a*}, Bahram Keyvani^a, Arman Sedghi^b

^a Chemistry Department, Faculty of Engineering, Islamic Azad University, Saveh Branch, P.O.Box 39187/366, Saveh, Iran.

*Email: cheraghyelham@yahoo.com

^b Material Engineering Department, Faculty of Engineering, Islamic Azad University, Saveh Branch, P.O.Box 39187/366, Saveh, Iran.

Key words: Silver nano-particles, Medical waste, Silver recovery, Zinc powder

Introduction:

The recovery of silver in the form of nano-particles from medical wastes is reported in this work. Waste solutions rich in silver from industrial or medical sources may be treated primarily with zinc powder. Silver recovery was then followed by the use of suitable mineral acid like nitric acid through vigorous leaching reaction to yield silver nitrate as precursor. Silver nano-particles were eventually synthesized by treatment of the precursor with sodium citrate solution. The FTIR (spectrum RXI Perkin Elmer) of the product as well as the results from XRD (made by Philips, modeled of pw 1800) analysis confirm successful formation of silver. The SEM (made by Japan, modeled of S-4160) images show that nano particles of silver are formed. There has been tremendous research activities reported on the recovery of precious metals like silver in the literatures. Metallic silver may be formed by treatment of X-ray photographic films with sodium cyanide in an oxidizing environment at room temperature [1]. The recovery of silver from various salts including $\text{Ce}(\text{SO}_4)_2$ and NaClO by electrolysis and electrochemical methods has been reported elsewhere [2-3]. Silver nano particles could be formed with or without the use of dispersing agents from silver nitrate solutions with ammonium hydroxide [4].



Experimental:

All chemicals used in this work including nitric acid, sodium chloride, sodium citrate and zinc are of laboratory grade. The SEM model s-4160 made by japan was used to study the morphology of the nano silver particles. The FTIR model perkin elmer made by japan was used to study the formation of silver. Waste solution rich in silver from medical sources was treated primarily with ca. 5 g zinc powder. Silver recovery was then followed by the use of suitable mineral acid like con-nitric acid through vigorous leaching reaction to yield black silver nitrate precipitate. The precipitates were filtered and rinsed with cold distilled water. This was then dissolved in distilled water as precursor. The precursor was added dropwise to a sodium citrate solution (200 mmol/lit) at room temperature through constant stirring until nano-silver particles were formed .

Conclusion:

Literatures are addressing to several research activities reported on the recovery of precious metals like silver from industrial wastes. However, conversion of recyclable silver into nano particles is unique. Medical wastes are employed to recover silver in the form of nano-particles. The sample was primarily treated with zinc powder. Silver recovery was then pursued by the use of nitric acid through leaching reaction. The freshly formed silver nitrate was considered as precursor. Silver nano-particles were eventually synthesized by treatment of the precursor with sodium citrate solution. The FTIR spectrum of the product and the results from XRD(modeled of japan ,modeled by japan) analysis confirm successful formation of silver. The SEM images show that nano particles of silver are formed

References:

- [1] Moreno, Garcia,R.,”silver recovery by $\text{NaCN}+\text{H}_2\text{O}_2$ “,*Hydrometallurgy* 1986,16(3)395-400
- [2] Treshkova S.G., Prodan E.A. , “silver recovery by $\text{Ce}(\text{so}_4)_2$ ” , *Tekh.Kino. Telev*5 1988(14-18)



- [3] Moreno, Garcia,R.,”Nisli ,G., toskali,D., Yenigul , B.,and Duran ,C., “silver recovery by Naclo “,”VIIIth National symposium on chemistry and chemical Engineering, stambul,1992(341-345)
- [4] Kuya,M.K.,Nova,Quim.,” asilver recovery by Naclo”,1993,16(5) 474-476
- Waste; United States Patent 4437889

15th Physical Chemistry Conference



Enhanced activity and selectivity of Au/ZnO catalysts containing low CuO content for preferential oxidation of CO in H₂ rich streams

Amir Alihoseinzadeh^{*a}, Abbas Ali Khodadadi^a, Yadollah Mortazavi^a

^a Oil & Gas Processing Centre of Excellence, School of Chemical Engineering, College of Engineering,
University of Tehran, P.O. Box 11365-4563, Tehran, Iran

Email: a.a.hoseinzadeh@ut.ac.ir

Keywords: PEM fuel cell, Preferential oxidation, Au, CuO, ZnO.

Introduction:

The preferential oxidation of CO in H₂-rich gas (PROX) is an effective way to purify feed for the polymer-electrolyte-membrane fuel cells (PEMFCs). It has been reported that the Au supported catalysts have proper activity and selectivity for PROX within operation range of fuel processor (80-150 °C) [1]. So far, many studies have focused on various supports for Au catalysts, in order to achieving better performance in PROX reaction conditions [2]. In this work, Au/CuO-ZnO is introduced as a novel catalyst and the effects of CuO loading on CO conversion and O₂ selectivity are investigated.

Experimental:

The CuO-ZnO support was prepared by co-precipitation method. Also for supplementary experiments ZnO support synthesized with similar method. The Au catalyst was loaded on the prepared CuO-ZnO support using a deposition-precipitation method. The aqueous solution of HAuCl₄ and 0.1 M Na₂CO₃.1H₂O was simultaneously added dropwise into the suspended powder of support at 50°C while pH was maintained at 8. The slurry was then filtered, washed and dried at 100°C, followed by crushing and sieving to a mesh size of 50-120. The final catalysts is denoted as xAu/yCuO-ZnO, where x= 2 wt%, and y= 0, 0.5, 1, 2 and 5 wt%.

The catalytic performance of the catalysts was measured in a fixed-bed quartz microreactor using 0.1 g of catalyst. A gas mixture containing 1.0% CO, 40.0% H₂ and 1.0% O₂ balanced

with Ar with a GHSV= 30000 ml/g.h was used as PROX feed in a temperature range of 30-200°C. The effluent from the reactor was analyzed by a Shimadzu GC-8A gas chromatograph with a methanizer and an FID detector. Furthermore a Vector 22 FTIR instrument equipped with a gas cell and KBr windows performed online measurements.

Results:

The effects of CuO loading on 2Au/ZnO catalysts are presented in Figures 1. As is observed in Figure 1 optimal content of CuO in 2Au/ZnO structure, significantly enhances activity and selectivity similar to the results reported by Mozer et al for Au-Cu/Al₂O₃ catalysts [3]. Comparing 2Au/1CuO-ZnO with 2Au/0.5CuO-ZnO, the former catalyst shows higher activity at higher temperature. However, with respect to the common temperature range for the PROX, i.e. 80-150°C, this catalyst has the best performance compared to the others, 100% CO conversion at 80-105°C, and 63% at 150°C.

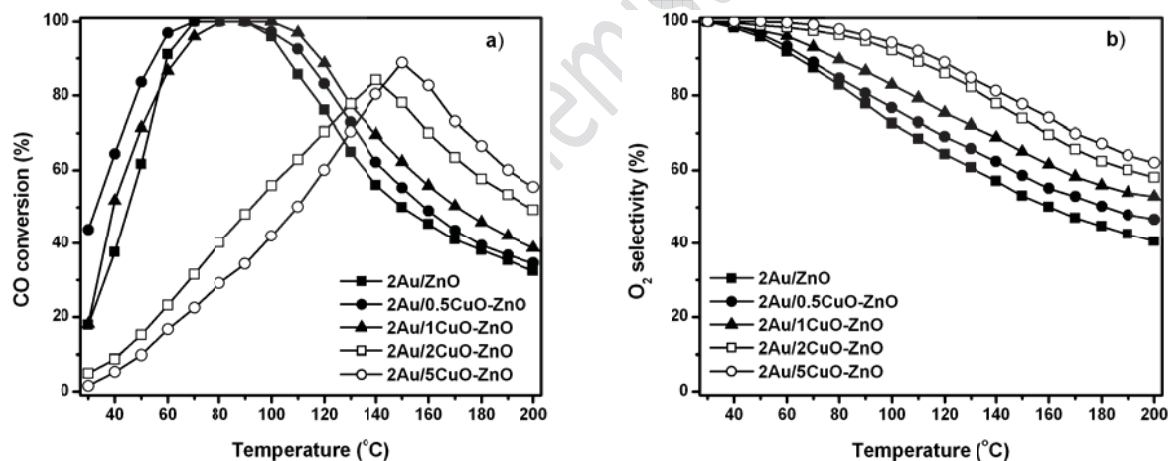


Figure 1: Effect of CuO loading on activity (a), and selectivity (b) of 2Au/ZnO catalysts.

Conclusion:

CuO-ZnO supports are prepared by co-precipitation method and Au is dispersed by deposition-precipitation on the support. A low amount of CuO in 2Au/CuO-ZnO catalysts shows enhanced CO conversion in the range of PROX reaction temperature of 80-150°C, and



causes higher selectivity. An increase in Au/CuO ratio enhances the activity of catalysts, due possibly to changes in electronic and/or geometric properties of Au nanoparticles.

References:

- [1] D. Cameron, R. Holliday, D. Thompson; "Gold's future role in fuel cell systems"; *Journal of Power Sources*; 118, 298–303, 2003.
- [2] E.D. Park, D. Lee, H.C. Lee; "Recent progress in selective CO removal in a H₂-rich stream"; *Catalysis Today*; 139, 280-290, 2009.
- [3] T.S. Mozer, D.A. Dziuba, C.T.P. Vieira, F.B. Passos; "The effect of copper on the selective carbon monoxide oxidation over alumina supported gold catalysts"; *Journal of Power Sources*; 187, 209–215, 2009.



Effect of nanofluid on natural convection fluid flow and heat transfer in an enclosure containing a heated circular cylinder

Ali Akbar Abbasian Arani^a, Mohammad Hemmat Esfe*^a

^aDepartment of mechanical engineering, University of Kashan, Kashan, Iran.

E-mail: M.hemmatesfe@gmail.com

Keywords: Nanofluid, Natural convection, circular cylinder, Heat transfer

Introduction:

Research and study about free convection is an essential issue because of its applications in industry. Some of important applications of free convection include the following: Radioactive waste materials disposal [1] and nuclear reactors cooling [2].

Application of nanofluids inside the cavities has been investigated by many researchers, due to importance of using nanofluids to enhance heat transfer and therefore effects of different nanofluids parameters such as type of nanofluid, volume fraction of nanofluid, and its temperature on heat transfer and stream characteristics has been studied. Free convection fluid flow and heat transfer of various water based nanofluids in a square cavity with an inside thin heater has been investigated numerically by Mahmoodi [8]. Due to lack of extensive research on nanofluids heat transfer inside a cavity with a hot square cylinder, and also considering application this geometry in industrial application, purpose of this study is to investigate this geometry with respect to different effective factors like strength and weakness of buoyancy force, type of suspended particles, and volume fraction of nanoparticles. Results of this study are presented in the form of temperature and stream contours and different figures.

Numerical modeling:

Schematic of the problem is shown in Figure 1. A hot cylinder with radius r and different positions at a high constant temperature (T_h) is considered to be located inside the cavity and the side lids are remained at a low constant temperature (T_c). The upper and lower lids are also insulated.

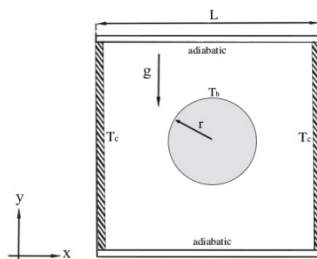


Figure 17. Schematic of the problem

Nanofluids used in this problem are considered to be incompressible and Newtonian and the stream is laminar and steady in all areas of the cavity. Except for the density which varies according to the Boussinesq approximation, other thermophysical properties of water and nanofluid are assumed to be constant.

Numerical approach:

In this study the governing equations (mass, momentum and energy) have been discretized using the finite volume method and the SIMPLE algorithm has been used to couple velocity and pressure fields.

Results and discussion:

The impact of the presence of nanoparticles, radius and position of heated block, Ra number and type of nanofluid on the flow field and heat transfer characteristics inside the enclosure were discussed. The study has been carried out for the Rayleigh number between 10^3 and 10^7 while solid volume fraction of nanoparticles changed from 0 to 0.08. It was found that, increasing solid volume fraction and Ra number caused a noticeable enhancement in the rate of heat transfer. Also the value of ψ_{\max} inside the cavity containing nanofluid significantly increase compared to the cavity filled with the base fluid. On the other hand increasing radius of the hot circular cylinder, difference in values of Nusselt number between base fluid and nanofluid significantly increases.

Conclusion:

Numerical simulation was carried out and the following results were extracted:



- 1) addition of nanoparticles to the base fluid increases the amount of heat transfer in all points of the lid and amount of this increase is more at upper areas of the lids.
- 2) increasing Ra number caused a noticeable enhancement in the rate of heat transfer.
- 3) with increasing of solid volume fraction, the effect of the type of nanoparticles is higher.

References:

- [1]E. Bilgen “Natural convection in cavities with a thin fin on the hot wall”, International Journal of Heat and Mass Transfer. Vol. 48. pp. 3493–3505, (2005).
- [2]E. Bilgen “Natural convection in enclosures with partial partitions”, Renewable Energy. Vol. 26. pp. 257 – 270, (2002).
- [3]M. Mahmoodi “Numerical simulation of free convection of nanofluid in a square cavity with an inside heater”, International Journal of Thermal Sciences. Vol. 50. pp. 2161–2175, (2011).



Poly(3-methylthiophene)/TiO₂ Nanocomposites via Inverted Emulsion

H. Behniafar*, E. Mohammadi Hacheroood,

*School of Chemistry, Damghan University, 36715-364, Damghan, Iran.

E-mail: h_behniafar@du.ac.ir

Key words: Polymer-based nanocomposites, Poly(3-methylthiophene), TiO₂, Inverted emulsion

Introduction:

Poly(3-methylthiophene) (P3MTh) as one of the most important semiconductors has some electrochromism, thermochromism and solvatochromism properties [1]. Moreover, it has been demonstrated that many characteristics of polymer semiconductors can be improved by the presence of nanosized particles. Nano-TiO₂ can be used in energy converter in solar cells, gas sensors, photochemical degradation of toxic chemicals, capacitors, and waste water purification. For TiO₂, catalytic activity is dramatically increased at particles sizes below 20 nm [2].

Materials and methods:

3-Methylthiophene was purified by distillation. Toluene or chloroform (15 mL), sodium dodecylbenzenesulfonate (0.35 g, 1 mmol) and nanosized TiO₂ (0.05 g) were added to a round-bottomed flask, respectively. FeCl₃ oxidant (14.15 g, 87.22 mmol) dissolved in deionized water (5 mL) was then poured into the flask. Next, the solution of the monomer (0.6 mL, 6.23 mmol) in toluene or chloroform (5 mL) was added dropwise to the vessel. The reaction mixture was finally poured into methanol nonsolvent to precipitate the P3MTh/TiO₂ nanocomposite.

Apparatus:

FT-IR spectra of the samples were recorded on a PERKIN ELMER RX I FT-IR spectrometer. XRD patterns were performed with film specimens on a Bruker Advance D5 X-ray diffractometer with Ni-filtered Cu/K α radiation (30 kV, 25 mA). UV-vis spectra of the diluted

solutions in DMSO were taken with a PERKIN ELMER PTP-1 Peltier System. TGA was performed on a Mettler TA 5000 system under N₂ at a heating rate of 20 °C.min⁻¹. The morphologies were determined with a S-A1600 SEM and a Philips EM 430T TEM.

Results and discussion:

To characterize the products obtained, FT-IR, UV-vis, TGA, XRD, SEM and TEM analyses were performed. A well-dispersion of the nano-TiO₂ powders could be observed into the polymer matrix. In addition, the nanohybrid samples, especially P3MTh/TiO₂ prepared in chloroform solvent, showed more thermostability than the pure sample. For example, Figure 1 shows the FT-IR spectra of the samples compared with each other (a) and TEM image of P3MTh/TiO₂nanocomposite prepared in toluene (b).

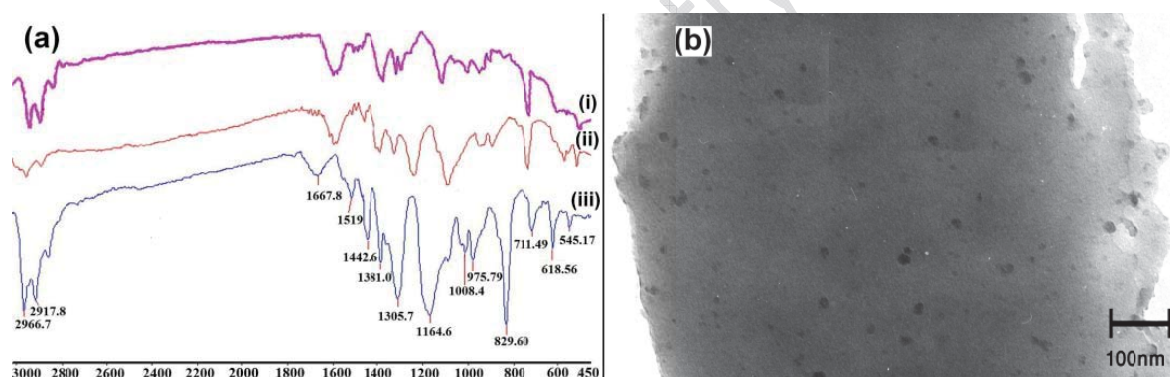


Figure 1.(a) FT-IR spectra of the samples: (i) P3MTh/TiO₂prepared in CHCl₃ (ii) P3MTh/TiO₂prepared in toluene (iii) pure P3MTh/TiO₂; (b) TEM image of P3MTh/TiO₂prepared in toluene.

Conclusion:

Preparation and characterization of P3MTh/TiO₂nanocompositeswas successfullyperformed by an inverted emulsion pathway. Herein, a solution of monomer and surfactant in an organic solvent played the role of continuous phase and an aqueous solution of oxidant played the role ofdispersed phase. In sum, this technique could be a good choice to prepare an important class of polymer-based nanomaterials.



Reference:

- [1] M. Granstron.; K. Pentrisch.; A. C. Arias.; A. Lux.; M. R. Aandersson.; R. H. Friend., "Laminated fabrication of polymeric photovoltaic diodes" *Nature*; 395, 257-260, 1998.
- [2] F. Garnier.; R. Hajlaoui.; A. Yassar.; P. Srivastava.; "All-Polymer Field-Effect Transistor Realized by Printing Techniques" *Science*; 265, 1684-1686, 1994.

15th Physical Chemistry Conference



Surface Plasmon Resonance of Silver Nanoparticles for determination of ascorbic acid in food and Pharmaceutical Samples

K. Zarei*, S. Moghaddari

School of Chemistry, Damghan University, Damghan, Iran

E-mail: zarei@du.ac.ir

Keywords: Silver nanoparticles, Ascorbic acid, Spectrophotometric determination, Plasmon resonance

Introduction:

Ascorbic acid (Vitamin C), a water-soluble vitamin, is important in forming collagen, a protein that gives structure to bones, muscles and blood vessels. Fruits and vegetables constitute the principle source of vitamin in most human [1].

Metal nanoparticles such as silver nanoparticles (AgNPs) have been found wide applications for analytical purposes due to the unique optical and electric properties. These properties contain the collective oscillation of conductive electrons under the excitation of a light beam known as localized surface plasmon resonance (LSPR). This phenomenon depends on the size, shape and dielectric environment of nanoparticles, metal nanoparticles exhibit a strong UV-Vis absorption band [2]. Therefore, the geometry of metal nanoparticles would provide important control over linear and nonlinear optical properties. The primary consequences of LSPR excitation are selective photon absorption, and local electromagnetic field enhancement.

Materials and methods:

In 10 mL volumetric flask, 1.5 mL of PVP 0.4 (g/L), 1 mL robinson buffer (PH=9.5), different concentration of the analyte and 1mL of AgNO₃ 0.01 M were added, then it was mixed and transferred into a 1 cm glass spectrophotometric cell. Then the absorbance was measured at 440 nm.

Apparatus:

The UV-Vis spectra were recorded on the Perkin Elmer (Lambda 25) spectrophotometer and 1.0 cm glass cell is used. Measurement of pH were made with a Metrohm model 827 pH meter.

Result and discussion:

The method is based on the reaction of ascorbic acid with the oxidizing agent (silver nitrate) in the presence PVP (Polyvinylpyrrolidone) and a slightly basic medium. In this condition silver nanoparticles is formed.

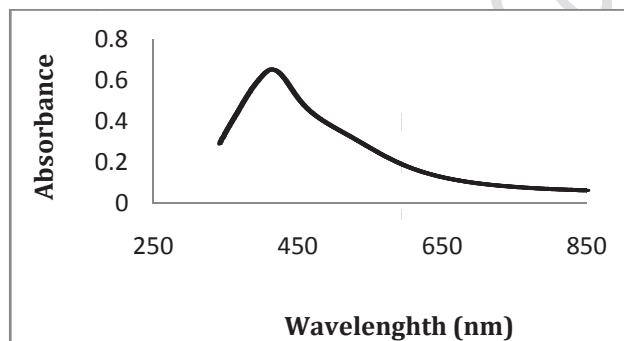


Figure 1: Absorbance spectra of AgNPs formed by reaction of ascorbic acid with AgNO_3 in the optimum conditions

The optimum reaction conditions were: robinson buffer (PH=9.5), 1.5 ml PVP 0.4 (g/L) and 10^{-3} M AgNO_3 , the linear dynamic range for ascorbic acid was obtained as 1×10^{-8} - 6×10^{-5} M. The detection limit of the method was 8×10^{-9} M. This method is more sensitive than previous reported spectrophotometric works [1]. The proposed method was successfully applied to the determination of ascorbic acid in some powdered drink mixture and vitamin C tablet.

Conclusion:

A simple and highly sensitive spectrophotometric method for AA was established. In this method the changes of SPR band at maximum wavelength of silver nanoparticles (440 nm) is



monitored. The proposed method, was applied to assay of AA in pharmaceutical samples and different vitamin C tablets.

Reference:

- [1] M. Nejati-Yazdinejad. ; "Indirect determination of ascorbic acid (vitamin C) by spectrophotometric method" ; International Journal of Food Science and Technology; 42,1402-1407,2007.
- [2] J. Tashkhourian et al . ; "Application of silver nanoparticles and principal component-artificial neural network models for simultaneous determination of levodopa and benserazide hydrochloride by a kinetic spectrophotometric method" ; Spectrochimica Acta, Part A; 82, 25-30,2011.



Preparation and Magnetic Properties of Nanostructured $\text{Mn}_{0.5}\text{Zn}_{0.5}\text{Fe}_2\text{O}_4$ in Silica Matrix

M. Abedini¹, A. Amirabadizade¹, H. Farsi^{2,3}

¹ Physics Department, University of Birjand, P.O. Box: 97175-615, Birjand, Iran

² Department of Chemistry, University of Birjand, P.O. Box: 97175-615, Birjand, Iran

³ Solar Energy Research Department, University of Birjand, Birjand, Iran

E-mail: m_abedini65@yahoo.com

Keywords: Nanostructure, Ferrite, $\text{Mn}_{0.5}\text{Zn}_{0.5}\text{Fe}_2\text{O}_4$, Silica

Introduction:

Nanomaterials represent a novel class of materials with physical and chemical properties that are different from those of the bulk material. Due to the small dimensions of nanocrystals, an important fraction of the atoms is on the surface, which induces properties that are different from polycrystalline material obtained through conventional methods. The embedding of magnetic nanocrystals in inorganic or organic matrices is of great interest in practical applications, due to the high-performance (optical, catalytic, magnetic, etc.) properties of these nanocomposites. For this reason, particular interest has been shown recently in developing synthesis methods that make it possible to obtain such nanomaterials. The sol-gel synthesis method makes it possible to obtain magnetic nanoparticles dispersed in inorganic matrices, by hindering the growth of the nanocrystallites in the pores of the matrix, as well as their aggregation. In this work, we prepared manganese-zinc ferrite in silica matrix via a modified sol-gel method which is developed in our laboratory and then the effect of annealing temperature on the magnetic properties of prepared ferrite was investigated.

Materials and Methods:

$\text{Mn}(\text{NO}_3)_2$, $\text{Zn}(\text{NO}_3)_2$, $\text{Fe}_2(\text{NO}_3)_3$, ethylene glycol and tetraethylorthosilicate were purchased from Merck company and used without any further purifications. Nanostructured

$\text{Mn}_{0.5}\text{Zn}_{0.5}\text{Fe}_2\text{O}_4$ ferrite in silica matrix was prepared by making a sol containing of appropriate amounts of $\text{Mn}(\text{NO}_3)_2$, $\text{Zn}(\text{NO}_3)_2$, $\text{Fe}_2(\text{NO}_3)_3$, ethylene glycol and tetraethylorthosilicate. To determine calcination temperature and to find what happen during calcination, dried gel was analyzed by TGA and DTA studies. The crystal structure and morphology of prepared materials were verified by XRD and TEM analysis. Vibrating sample magnetometric, VSM, is used for study of magnetic properties of prepared ferrite.

Result and Discussions:

Thermal gravimetric analysis showed all chemical reactions for ferrite formation take place up to 400 °C, Figure 1-a. XRD pattern analysis showed that an amorphous material is formed for sample annealed at 650°C whereas the clear XRD patterns are observed at 800 and 1000°C for samples as annealing temperature verifying formation of $\text{Mn}_{0.5}\text{Zn}_{0.5}\text{Fe}_2\text{O}_4$ ferrite. TEM images illustrated that ferrite nanoparticles have been made inside silica matrix. VSM analysis depicted that the prepared nanomaterials show a ferrite magnetic behavior which is depend to the annealing temperature (figure 1-b).

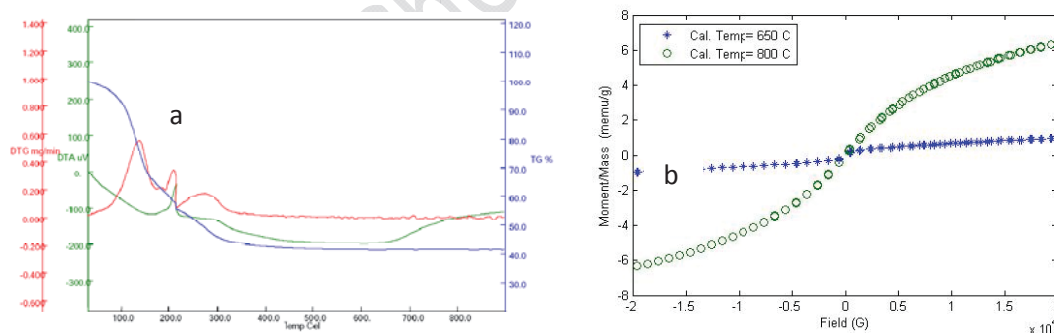


Figure 1: a) TGA and DTA of prepared gels, b) Hysteresis loops at room temperature for prepared nanostructure ferrite inside the silica matrix annealed at 650 and 800°C.

Conclusions:

Our studies illustrated that silica matrix prepares a template for forming ferrite's nanoparticles. Also, the magnetic properties of prepared ferrite inside the silica matrix is depend to the annealing temperature.



References

- [1] C. Caizer, J. Magn. Magn. Mater., **320** (2008) 1056.
- [2] K.Parekh,R.V. Upadhyay, L. Belova, K.V. Roa, Nanotechnology, **17** (2006) 5970.
- [3] C.-G. Stefanita, “*From Bulk to Nano: The Many Sides of Magnetism*”, 2008, Springer-Verlag Berlin Heidelberg.

15th Physical Chemistry Conference



Sonochemically Synthesis of NiMo/Al₂O₃-ZrO₂ Nanocatalyst with High ZrO₂-Content for Hydrodesulphurization of Thiophene

P. Jabbarnezhad^{a,b}, M. Haghighi^{a,b*}

^a Chemical Engineering Faculty, Sahand University of Technology, Tabriz, Iran

^b Reactor and Catalysis Research Center (RCRC), Sahand University of Technology, Tabriz, Iran

*Email: haghighi@sut.ac.ir

Keywords: NiMo/Al₂O₃-ZrO₂, Sonosynthesis, Nanocatalyst, Hydrodesulphurization.

Introduction:

The demand for lower sulphur content in fuels requires the synthesis of more active hydrodesulphurization (HDS) catalysts [1]. The conventionally used NiMo catalysts are supported onto γ -Al₂O₃ and they are prepared by impregnation method [2]. At this work, a series of high-performance HDS nanocatalysts were prepared by supporting NiMoS on Al₂O₃-ZrO₂ (ZrO₂: 17, 20, 30 wt %) and HDS activity of the catalysts were evaluated.

Materials and methods:

Highly dispersed NiMoS/Al₂O₃-ZrO₂ (ZrO₂: 17, 20, 30 wt %) nanocatalysts were prepared by the sonochemical decomposition of molybdenum hexacarbonyl and nickel acetate in the presence of sulphur and Al₂O₃-ZrO₂ support and characterized by XRD, FESEM, FTIR and surface area analyzer BET. The HDS activity tests were performed in a stirred reactor at 160°C and atmospheric pressure for 2 h (1 wt% thiophene in decane as a model fuel).

Result and discussion:

The XRD patterns of the samples are shown in Figure 1. The peaks related to MoS₂ (JCPDS No: 00-017-0744) and Ni₃S₂ are not appeared at catalysts. This feature could be due to high dispersion of this Species over the mixed oxides supports. In FESEM images as shown in Figure 2 nanoscale particles is visible and BET analyze (Figure 3) presented the surface area

of the samples was decreased with increasing ZrO₂ content. Thiophene HDS activities of nanocatalysts as a function of ZrO₂ contents are illustrated in Figure 4. It could be observed that the Al₂O₃-ZrO₂(ZrO₂: 17%) supported NiMo nanocatalysts exhibited higher catalytic activities than that of other catalysts and residual thiophene (44 ppm) is in agreement with environmental standards for sulphur content in fuels.

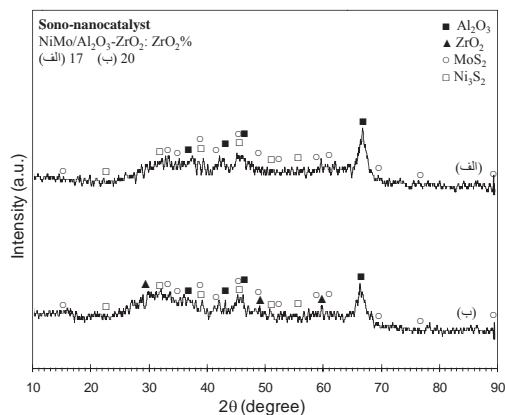


Figure 18: XRD patterns of NiMo/Al₂O₃-ZrO₂ nanocatalyst with high ZrO₂-content.

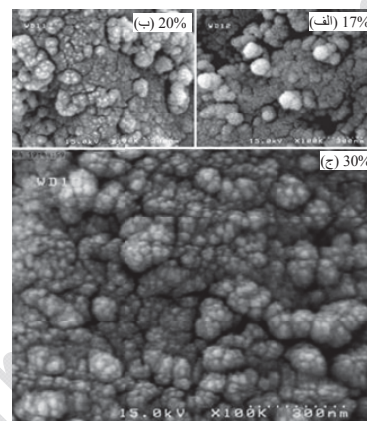


Figure 19: FESEM images of NiMo/Al₂O₃-ZrO₂ nanocatalyst with high ZrO₂-content.

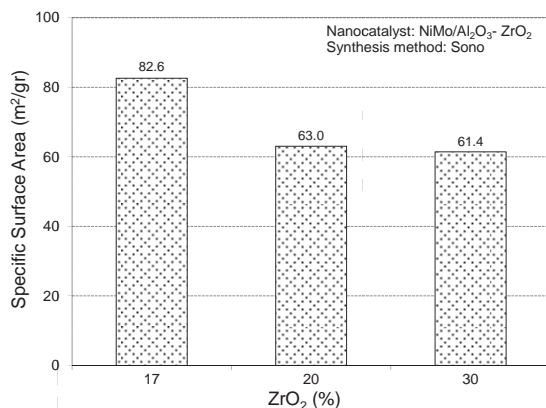


Figure 20: BET surface area of NiMo/Al₂O₃-ZrO₂ nanocatalyst with high ZrO₂-content.

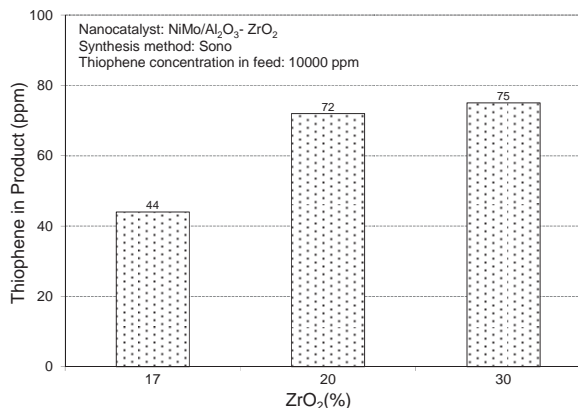


Figure 21: Hydrodesulphurization of thiophene over NiMo/Al₂O₃-ZrO₂ nanocatalyst.

Conclusion:

In this study, it has been shown that sonolysis is an effective technique to prepare NiMoS/Al₂O₃-ZrO₂ (ZrO₂: 17, 20, 30 wt %) nanocatalysts. XRD patterns of nanocatalysts



showed high dispersion of active metal on support. In FESEM images nanoscale particles was seen. The HDS activity of sonochemical catalysts exhibited high catalytic activities. When the ZrO_2 content was 17wt%, nanocatalyst presented the highest hydrodesulfurization activities.

References

- [1] T.A. Zepeda et al., " Effect of Al and Ti content in HMS material on the catalytic activity of NiMo and CoMo hydrotreating catalysts in the HDS of DBT ", Microporous and Mesoporous Materials, 111, 157-170, 2008.
- [2] D. Zhang et a., "Preparation, characterization and hydrotreating performances of ZrO_2 - Al_2O_3 supported NiMo catalysts", Catalysis Today, 149, 62–68, 2010.



Nano-Perovskites of $\text{LaFe}_{(1.0, 1.2, 1.5 \text{ or } 1.7)}\text{O}_{(3+\delta)}$ as Catalyst of CO and UHC

Z. Ramezani, A. Malekzadeh

School of Chemistry, Damghan University, Damghan, Iran

E-mail: Malekzadeh@du.ac.ir

Keywords: perovskite, Excess Iron, Exhaust Gas, XRD, Citric acid.

Introduction:

The catalytic converter is used for purification of automotive exhaust gas (unburned hydrocarbons (UHC), carbon monoxide (CO) and nitrogen oxides (NO_x)). Lanthanum-transition metal perovskites (LaBO_3) are proved to be effective catalysts for the catalytic oxidation of hydrocarbons, CO and ammonia. They are also considered to be promising materials for application as electrode materials in solid oxide fuel cells. LaFeO_3 is well-known LaBO_3 perovskite oxide which consists of FeO_6 octahedra units with La^{3+} ions inserted between these units [1-3]. Based on the target applications, different synthesis methods have been used as alternative for solid state reactions and mechanical chemical solid reaction, including coprecipitation, combustion, sol-gel, sonochemical and thermal decomposition. The samples were characterized by FT-IR, XRD and UV-Vis spectrometry. In our case crystallite size of the samples was calculated to be in range of 37-45 nm using XRD data.

Materials and methods:

In this work, we prepared $\text{LaFe}_{1+x}\text{O}_{3+\delta}$ perovskites with $x = 0.0, 0.2, 0.5, 0.7$ using citrate method and examined as catalysts for the carbon monoxide and ethane oxidation at the temperature range of 100 - 800°C. A solution containing metal nitrate precursor with appropriate concentration and citric acid equal to the total number of mole of nitrate ions in 20 mL distilled water were used for preparation of the samples [4]. Solutions were evaporated at 80°C overnight. Thus the obtained spongy and friable materials were completely powdered

and subsequently dried at 150 and then 200°C, overnight. Samples were calcined at 900°C for 5 h.

Apparatus:

The precursor and the calcined powders were characterized by XRD, in a 2θ range from 10° to 90° at room temperature using Cu-K α radiation (Advance-D8). IR spectra were obtained over the frequency range from 1850 to 450 cm⁻¹, using a model RXI Perkin-Elmer spectrophotometer.

Result and discussion:

Figure 1 shows the XRD pattern of LaFe_{1+x}O_{3+δ} samples. The pattern of LaFeO₃ is indexed as orthorhombic perovskite-type LaFeO₃ and shows a high degree of crystallinity. Pattern of the FT-IR spectrum is in consistent with the results. Increase in non-stoichiometric of iron leads to decrease in the perovskite phase formation. The UV-Vis spectroscopy verified the presence of Fe³⁺ ion which confirms the existence of Fe₂O₃ phase.

The catalytic activities are reported in Figure 2. Catalytic tests indicated that in the investigated temperature range the catalysts show reasonable activity. The catalytic properties increase from stoichiometric LaFeO₃ to LaFe_{1.7}O₃. The most activity was attained at Fe:La ratio of 1.2:1; i.e. LaFe_{1.2}O₃ sample. The LaFe_{1.5}O₃ and LaFe_{1.7}O₃ catalysts show less catalytic activity in comparison with LaFe_{1.2}O₃.

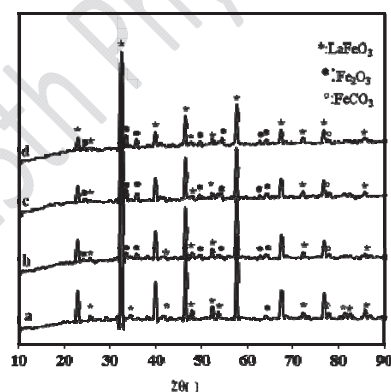


Figure 1: XRD pattern of LaFe_{1+x}O_{3+δ} (a) x= 0.0, (b) x= 0.2, (c) x= 0.5, (d) x= 0.7

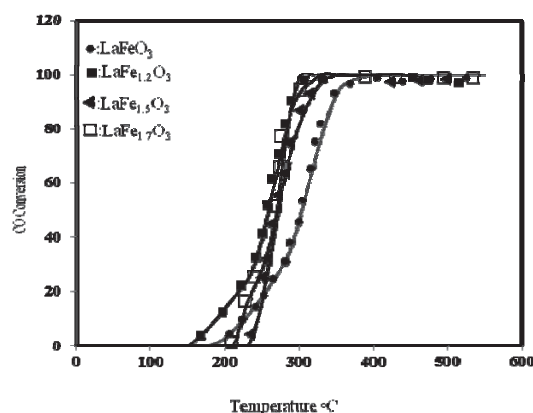


Figure 2: CO conversion to CO₂



References:

- [1] M. Sivakumar, A. Gedanken, W. Zhong, Y. H. Jiang, Y. W. Du, I. Brukental, D. Bhattacharya, Y. Yeshurun, I. Nowik, "Sonochemical synthesis of nanocrystalline LaFeO_3 ", J. Mater. chem, **14** (2004) 764-769.
- [2] M. J. Lee, J. H. Jun, J. S. Jung, Y. R. Kim, S. H. Lee, "Catalytic Activities of Perovskite-type LaBO_3 ($B = \text{Fe, Co, Ni}$) Oxides for Partial Oxidation of Methane", Bull. Korean Chem. Soc, **26** (2005) 1591-1596.
- [3] M. B. Bellakki, V. Manivannan, "Solution combustion synthesis of (La, K) FeO_3 orthoferrite ceramics: structural and magnetic property studies", Bull. Mater. Sci, **33** (2010) 611-618.
- [4] M. Khazaei, A. Malekzadeh, F. Amini, Y. Mortazavi, A. Khodadadi, "Effect of citric acid concentration as emulsifier on perovskite phase formation of nano-sized SrMnO_3 and SrCoO_3 samples", Cryst. Res. Technol, **45** (2010) 1064-1068.



Effect of TiO_2 , Fe_3O_4 and Al_2O_3 nanoparticles on phosphorus removal from aqueous solution

S. Moharami^{a*} and M. Jalai^a

^aDepartment of Soil Science, College of Agriculture, Bu-Ali Sina University, Hamedan, Iran

(Email: sm_moharami@yahoo.com)

Abstract:

Phosphorus (P) removal from aqueous solutions was investigated using TiO_2 , Fe_3O_4 and Al_2O_3 . Adsorption studied was performed to determine the optimum operation conditions such as adsorption time, pH and adsorbent dosage. The Langmuir equation was used to describe the sorption and desorption isotherms P onto adsorbents. The maximum adsorption capacity of P was 51.7, 35.2, and 25.6 mg g^{-1} for TiO_2 , Fe_3O_4 and Al_2O_3 , respectively.

Keywords: Nanoparticles, removal, sorption, desorption, phosphorus.

Introduction:

The role of phosphorus (P) in causing eutrophication in natural waters has been well recognized for decades. However, immobilization and/or control of non-point P in the surrounding soils for a water body remain a challenging environmental issue [1-3]. The use of nanoparticles (NPs) for water treatment processes is now a reality: a long list of materials based on nanostructures are today in the market or under final research steps [4], even though the worldwide tendency to decrease the permitted level of contamination in drinking water is a big challenge for the environmental researchers [5]. Some nanomaterials such as nano zero valance iron (Fe^0), F_2O_3 , Fe_3O_4 , TiO_2 , SiO_2 and Al_2O_3 are the most common of these materials extended the variety of adsorbent. In this study, removal of phosphorus by TiO_2 , Fe_3O_4 and Al_2O_3 in solution was investigated.

Materials and methods:



The adsorbents used in the present investigation were TiO_2 , Al_2O_3 and Fe_3O_4 . The uptake of P on the adsorbents was carried out using the batch method. The adsorption properties of adsorbents were evaluated by depending on different conditions such as adsorption time, pH value and adsorbents dosage. The adsorption isotherms of the P with adsorbents were determined based on batch analysis. Adsorbents were allowed to equilibrate with solutions at different initial P concentrations (0, 5, 10, 20, 40, 60, 100, 150, 200 and 250 mg L^{-1}). The pH values of the solutions were adjusted to 5.45. Desorption experiments were performed immediately following the completion of sorption experiments using 0.01 M CaCl_2 solution. The Langmuir equation was used to describe the sorption isotherms P onto adsorbents using the nonlinear procedure with Sigmaplot statistical software package version 10.0.

Results and discussions :

In the present study, results showed that the adsorption of P has gradual increase with contact time until 180min for adsorbents, and then the removal percent became constant. From the calculated removal percents, the efficiency of Al_2O_3 for P was higher than the others (40%). The removal percent of P TiO_2 and Fe_3O_4 was 38 and 38% respectively at optimum contact time. Long et al. [6] showed that adsorption time P by magnetic Fe-Zr binary was less than 2 h. The maximum removal of P, take place at pH 4 in all adsorbents. Results showed that the removal of P increased with increasing the adsorbents dose. Also, the amount of P sorbed per unit weight of adsorbents decreased with the increasing amount of sorbents dose. Phosphorus sorption increased with increasing amounts of P added. The percentage of P adsorbed decreased with the increasing levels of added P onto adsorbents (except TiO_2). Figure 1 show sorption and retention isotherms of P onto adsorbents. Phosphorus sorption capacity for TiO_2 (28.3 mg g^{-1}) that was greater than Fe_3O_4 (24.4 mg g^{-1}) and Al_2O_3 (21.5 mg g^{-1}). Vecente et al. [7] described that magnetic nano achieved an adsorption maximum of 18.83 (mg P g^{-1}). The highest percentage of desorbed P was observed from Al_2O_3 (6.5%), while the lowest percentage of desorbed P was determined in Fe_3O_4 (5.9%), and TiO_2 (2.8%). Sorption of P result onto adsorbents was well described by the Langmuir model. According to the Q (mg g^{-1})

parameter, maximum sorption capacity adsorbents are arranged in the following sequence, $\text{TiO}_2 > \text{Fe}_3\text{O}_4 > \text{Al}_2\text{O}_3$.

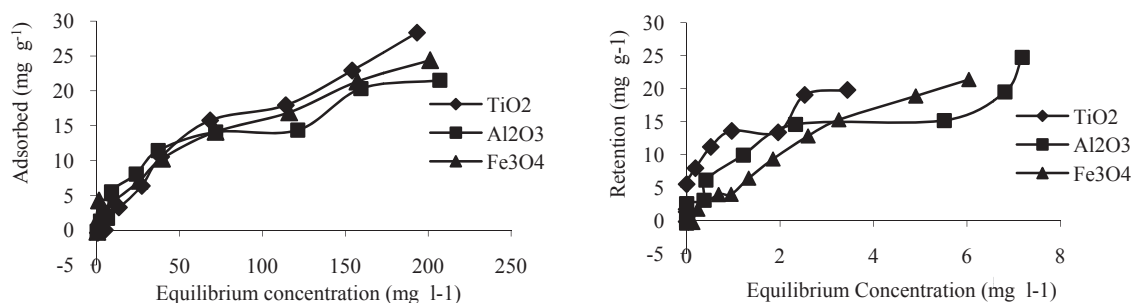


Figure 1. Sorption and retention isotherms of P onto adsorbents

References:

- [1] Daniel, T.C., Sharpley, A.N., Lemunyon, J.L. 1998. *J. Environ. Qual.* 27, 251–257.
- [2] Sharpley, A.N., Rekolainen, S. 1997. CAB International, Wallingford, pp. 1–53.
- [3] Gilliam, J.W. 1995. *Ecol. Eng.* 5, 405–414
- [4] Nowack, B., Bucheli, T.D. 2007. *Environ. Pollut.* 150, 5–22.
- [5] Jia, K., Pan, B., Lva, L., Zhang, Q., Wang, X., Pan, B., Zhang, W. 2009. *J. Colloid Interface Sci.* 331, 453–457.
- [6] Long, F., Gong, J.L., Zeng, G.M., Chen, L., Wang, X.Y., Deng, J.H., Niu, Q.Y., Zhang, H.Y., Zhang, Z.R. 2011. *Chem. Eng. J.* 171, 448–455
- [7] Vicente, I.D., Merino-Martos, A., Luis Cruz-Pizarro, L., Vicente, J.D. 2010 *J. Hazard. Mater.* 181, 375–381.



Cesium sorption studies on mesoporous MCM-41 impregnated with potassium zinc hexacyanoferrate

H. Sepehrian^{a*}, S. Vashnia^b, R. Cheraghali^b, H. Tavakoli^c

^a NFCRS, Nuclear Science and Technology Research Institute, AEOL, Tehran, Iran

^b Chemistry Department, Islamic Azad University, Saveh Branch, Saveh, Iran

^c Faculty of Science, Islamic Azad University, Nour Branch, Nour, Iran

Email: hsepehrian@aeoi.org.ir

Keywords : Mesoporous MCM-41, Zinc hexacyanoferrate, Cesium sorption

Introduction:

The management of radioactive wastes has become a major concern, particularly with regard to the release of radioactive materials in the environment. ¹³⁷Cs and ¹³⁵Cs are among the main fission products in radioactive wastes [1]. Among various inorganic ion-exchange materials exhibiting selective sorption properties for radiocesium, the hexacyanoferrates of transition elements have been studied extensively due to the stabilizing effect of the large cesium ion on the crystal structure of the sorbent. MCM-41 is one of the important inorganic adsorbents, which possess unique features such as large uniform pore sizes (1.5–10 nm), highly ordered nanochannels and large surface areas (~1500 m²/g), and large pore volume with regular hexagonal structure [2]. In this work, Mesoporous MCM-41 was chosen for supporting potassium zinc hexacyanoferrate (KZnCF) to prepare a new Cs-selective material.

Materials and Methods:

The KZnCF-loaded mesoporous MCM-41 (KZnCF-MCM-41) adsorbent was prepared by repetitious batch precipitation reaction of Zn²⁺ with [Fe(CN)]⁴⁻. Adsorption studies of the cesium ion on the KZnCF-MCM-41 adsorbent was carried out using batch method. In this procedure, 20 mg of the adsorbent material was added to a 20 mL solution of 5-250 mg.L⁻¹ cesium ions. The pH of the solution was adjusted with HCl and NaOH for pH 1-12. The



suspension was stirred for preselected period of time using a water shaker bath. Then it was filtered and the amount of cesium ion was determined by atomic absorption spectrometer.

Apparatus:

A Philips X'pert powder diffractometer system with Cu-K α ($\lambda=1.541$ Å) radiation was used for X-ray studies. Nitrogen adsorption studies were made with a Quantachrome NOVA 2200e instrument. pH measurements were made with a Schott CG841 pH-meter (Germany). Quantitative determination of the cesium ion was made using an atomic absorption spectrometer (AAS) of Varian model SpectrAA-200. A waterbath shaker model CH-4311 (Infors AG) was used in adsorption studies.

Result and discussion:

The synthesized sample has been characterized by X-ray diffraction, nitrogen adsorption/desorption measurement. The XRD pattern shown the successful loading of KZnCF onto MCM-41 pores and BET specific surface area and total pore volume of 585 m²/g and 0.43 cm³/g for KZnCF-MCM-41 was calculated by nitrogen adsorption/desorption studies, respectively.

The cesium adsorption results show that KZnCF-MCM-41 adsorbent has more sorption capacity than the amorphous KZnCF. For more investigations, the effects of the various parameters like contact time, temperature, initial pH value of the solution, nitric acid concentration and initial concentration of the cesium ion in the solution on the adsorption efficiencies of KZnCF-MCM-41 have been studied by batch experiments. Cesium adsorption depended to initial pH of solution and nitric acid concentration. The optimal Cs adsorption was found at pH 4.35 and/or 0.1 M HNO₃.

Conclusion:

KZnCF-loaded mesoporous MCM-41 with Zn/Fe mole ratio 2 has been successfully synthesized by a simple route and is a promising adsorbent for Cs removal from aqueous



solutions. The high surface area of the synthesized adsorbent endow the adsorbent with an improved adsorption ability of 139.1 mg.g^{-1} and fast kinetics of less than 30 min for Cs.

References:

- [1]S. Milonjic, et al.; "Sorption cesium on copper hexacyanoferrate/polymer/silica composites in batch and dynamic conditions"; Journal of radioanalytical and nuclear chemistry; 252, 497-501, 2002.
- [2]J.S. Beck, et al.; "A new family of mesoporous molecular sieves prepared with liquid crystal templates"; Journal of American Chemical Society; 114, 10834-10843, 1992.



Supporting of potassium lead hexacyanoferrate on mesoporous MCM-41 as strontium adsorbent: isotherm, kinetic and thermodynamic studies

H. Sepehrian^{a*}, S. Vashnia^b, R. Cheraghali^b, H. Tavakoli^c

^a NFCRS, Nuclear Science and Technology Research Institute, AEOL, Tehran, Iran

^b Chemistry Department, Islamic Azad University, Saveh Branch, Saveh, Iran

^c Faculty of Science, Islamic Azad University, Nour Branch, Nour, Iran

Email: hsepehrian@aeoi.org.ir

Keywords: Mesoporous MCM-41, Lead hexacyanoferrate, Strontium sorption studies

Introduction:

The management of radioactive wastes has become a major concern, particularly with regard to the release of radioactive materials in the environment. Liquids may be decontaminated using solid sorbents, that the radionuclides being concentrated under smaller volumes of solid residues [1]. The most frequently used agents for precipitation of Cs and Sr radionuclides are transition metal hexacyanoferrate (II, III) which exhibit high sorption selectivity toward these radionuclides and especially that from salinity solution [2].

In this work, mesoporous MCM-41 was chosen for supporting potassium lead hexacyanoferrate (KPbCF) to prepare a new Sr-selective material.

Materials and Methods:

The KPbCF-loaded mesoporous MCM-41 (KPbCF-MCM-41) adsorbent was prepared by repetitious batch precipitation reaction of Pb^{2+} with $[\text{Fe}(\text{CN})]^{4-}$. Adsorption studies of the strontium ion on the KPbCF-MCM-41 adsorbent was carried out using batch method. In this procedure, 20 mg of the adsorbent material was added to a 20 mL solution of 5-250 mg.L^{-1} strontium ions. The pH of the solution was adjusted with HCl and NaOH for pH 1-12. The suspension was stirred for preselected period of time using a water shaker bath. Then it was filtered and the amount of strontium ion was determined by atomic absorption spectrometer.



Apparatus:

A Philips X'pert powder diffractometer system with Cu-K α ($\lambda=1.541$ Å) radiation was used for X-ray studies. Nitrogen adsorption studies were made with a Quantachrome NOVA 2200e instrument. pH measurements were made with a Schott CG841 pH-meter (Germany). Quantitative determination of the strontium ion was made using an atomic absorption spectrometer (AAS) of Varian model SpectrAA-200. A waterbath shaker model CH-4311 (Infors AG) was used in adsorption studies.

Result and discussion:

The XRD pattern shown the successful loading of KPbCF onto MCM-41 pores and BET specific surface area and total pore volume of 771 m²/g and 0.46 cm³/g for mesoporous MCM-41 and 366 m²/g and 0.27 cm³/g for KPbCF-MCM-41, was calculated by nitrogen adsorption/desorption studies, respectively.

The strontium sorption results show that KPbCF-MCM-41 adsorbent has more than the amorphous KPbCF. For more investigations, the effects of the various parameters like contact time, temperature, initial pH value of the solution, nitric acid concentration, initial concentration of the strontium ion and other coexisting cations in the solution on the adsorption efficiencies of KPbCF-MCM-41 have been studied systematically by batch experiments. Strontium adsorption depended to initial pH of solution and nitric acid concentration. The optimal Sr adsorption was found at pH 8-10 and/or 0.2-1.0 M HNO₃.

Adsorption isotherm of KPbCF-MCM-41 was studied and the fitted results indicated that the Langmuir model could well represent the adsorption process.

Conclusion:

KPbCF-loaded mesoporous MCM-41 (KPbCF-MCM-41) with Pb/Fe mole ratio 2 has been successfully synthesized by a simple route and is a promising adsorbent for Sr removal from aqueous solutions. The modification of MCM-41 by potassium lead hexacyanoferrate is rapid, simple and inexpensive method compared the modification by organic modifiers. The high



surface area of the synthesized adsorbent endow the adsorbent with an improved adsorption ability of 141.2 mg.g^{-1} and fast kinetics of less than 30 min for Sr.

References:

- [1] S. Milonjic and et al.; "Sorption cesium on copper hexacyanoferrate/polymer/silica composites in batch and dynamic conditions"; Journal of radioanalytical and nuclear chemistry; 252, 497-501, 2002.
- [2] L. Vrtoch and et al.; "Sorption of cesium from water solutions on potassium nickel hexacyanoferrate-modified Agaricus bisporus mushroom biomass"; Journal of radioanalytical and nuclear chemistry; 287, 853-862, 2011.



Synthesis of zirconia nanoparticles in presence of citric acid or starch as emulsifier

H. Bojari*, A. Malekzadeh, M. Ghiasi

School of chemistry, Damghan University, Damghan, P.O. Box 36715/364, I. R. Iran

E-mail: malekzadeh@du.ac.ir

Keywords: Emulsifier, Nanoparticle, Starch, Citric Acid, Thermal decomposition.

Introduction:

The zirconium oxide nanoparticles (zirconia) are known as conductive or semi-conductive metal oxides. Zirconia exhibits several crystalline modifications: monoclinic, tetragonal, cubic and rhombic. The martensitic transformation from the tetragonal to the monoclinic structure has great importance in ceramic and catalytic applications of zirconia. Ultrafine zirconia particles have been synthesized via various methods such as sol-gel processing, chemical vapor synthesis, precipitation from inorganic salt solutions, microwave plasma synthesis and etc [1]. Zirconia's most naturally occurring form, with a monoclinic crystalline structure, is the rare mineral baddeleyite. The high temperature cubic crystalline form, also called cubic zirconia (CZ), is rarely found in nature as mineral tazheranite (Zr,Ti,Ca)O₂ and a doubtful mineral arkelite [2].

Materials and methods:

Samples were prepared by drying of a solution of ZrO(NO₃)₂·2H₂O in presence of organic emulsifier of citric acid or starch. The materials were calcined at 600°C and subsequently at 900°C for 5 h by a heating rate of 10°C/min from room temperature. The samples were characterized by FT-IR spectroscopy, XRD and TG/DTA.

Results and discussions:

Cubic Nano-nonstoichiometric ZrO_{2.12} with diameters 6-9 nm is synthesized on calcination at 600°C in presence of citric acid. A same sample with crystallite sizes of 20-24 nm, however, is

prepared in presence of starch. Results were confirmed by the FT-IR and XRD studies. The formation of the nonstoichiometric $\text{ZrO}_{2.12}$ was also confirmed by the TG/DTA studies. The crystallite size of the samples was calculated by the Scherrer and Williamson-Hall equations using XRD data [3, 4]. Increase in the calcination temperature, however, causes a tetragonal or monoclinic stoichiometric zirconia with diameters 20-25 nm to form.

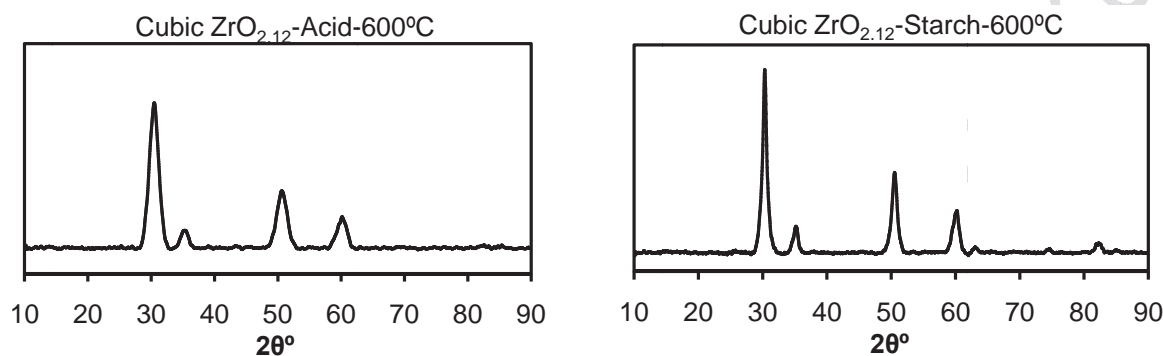


Fig. 1: XRD patterns of the samples that were calcined at 600°C for 5 h.

Conclusion:

A Cubic Nano-nonstoichiometric $\text{ZrO}_{2.12}$ with a smaller crystallite size is synthesized in presence of citric acid in compared to starch upon calcining at 600°C. A phase transition with crystallite size increasing is occurred on increase of the calcination temperature to 900°C.

References:

- [1] M. Salavati-Niasari, M.Dadkhah, F. Davar. "Synthesis and characterization of pure cubic zirconium oxide Nanocrystals by decomposition of bis-aqua, tris-acetylacetonato zirconium(IV) nitrate as new precursor complex". Inorg. Chem;362 (2009) 3969-3974.
- [2] G.Y. Guo, Y.L. Chen."A nearly pure monoclinic Nano crystalline zirconia".J. Solid State Chem; 178 (2005) 1675.
- [3] H. Wang, G. Lia, Y. Xue, L. Lia, "Hydrated surface structure and its impacts on the stabilization of t-ZrO₂". Journal of Solid State Chemistry; 180 (2007) 2790–2797.



- [4] R.Zhang, X.Zhang, Sh. Hu. "*High temperature and pressure chemical sensors based on Zr/ZrO₂ electrode prepared by nanostructured ZrO₂ film at Zr wire*". Sens. Actuators, B; 149 (2010) 143-154.

15th Physical Chemistry Conference



Synthesis of lanthanum oxide nanoparticles in presence of citric acid or starch as emulsifier

H. Bojari*, A. Malekzadeh, M. Ghiasi

School of chemistry, Damghan University, Damghan, P.O. Box 36715/364, I. R. Iran

E-mail: malekzadeh@du.ac.ir

Keywords: Lanthanum oxide, Nano-particles, Citric acid, Starch, Emulsifier.

Introduction:

Lanthanum oxide is an odorless, white solid that is insoluble in water, but soluble in dilute acid. It is hygroscopic; under atmosphere, it absorbs moisture over time and converts to lanthanum hydroxide. It has p-type semi-conducting properties because its resistivity decreases with an increase in temperature, average room temperature resistivity is 10 kΩ·cm. At low temperatures, it has an A-M₂O₃ hexagonal crystal structure and at high temperatures it converts to a C-M₂O₃ cubic crystal structure. [1].

Materials and methods:

Samples were prepared by a method similar to the so-called citrate method using lanthanum nitrate, citric acid or starch as emulsifier [2]. A dried solution of the samples was calcined at 600 and 900°C. The products were characterized by the FT-IR, XRD and TG/DTA studies. The specific surface area of samples was measured by the BET method.

Result and discussion:

In the FT-IR spectra of the samples calcined at 600°C bands are present in the ν(O–C–O) vibrations range (data not shown). Thus, the calcination did not lead to formation of oxide material. The thermal behavior of the as-prepared samples that were dried at 200°C were studied by (TG/DTA) from ambient temperature to 800°C in the air atmosphere. Three steps

weight loss was reported for the lanthanum carbonate Nano-particles, which are at ca. 125°C (weight loss ~6.9%), 480°C (weight loss ~19.0%) and 590°C (weight loss ~10.4%), respectively, with an overall weight loss of 36.3%. The weight losses was related to the evaporation of H₂O molecules in the La₂(CO₃)₃·1.7H₂O, and then evolution of CO₂ during the thermal decomposition. Thus, thermal treatment at 600°C leads to a partial transformation to oxy-carbonate (La₂O₂CO₃) and finally to La₂O₃ upon calcining at 900°C. Results were also confirmed by XRD analysis. The final step for the formation of the La₂O₃ is observed to take place at a lower temperature in presence of starch in compared to the citric acid.

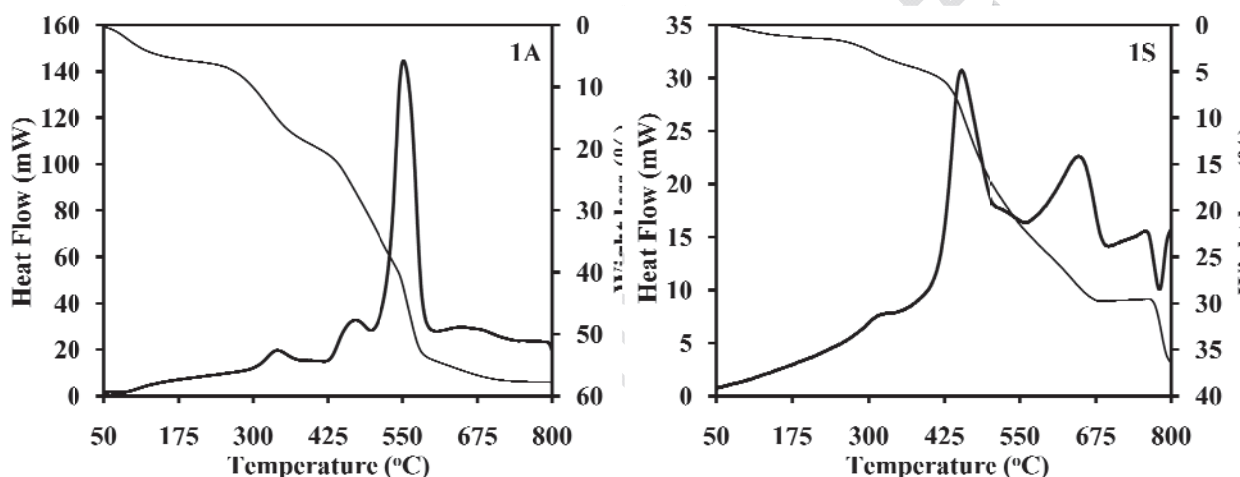


Fig. 1. Thermal gravimetric and differential thermal analyses (TG/DTA) of dried samples.

The crystallite size of the samples was calculated by the Scherrer and Williamson-Hall equation using XRD data and was found to be in range of 18-25 nm and 45-50 nm upon calcination at 600°C and 900°C, respectively.

Conclusion:

In comparison with the citric acid, a more crystalline phase with a higher specific surface area is formed using starch as emulsifier. Crystallite size was found to be independent of the emulsifier.

References:



- [1][R. Vali, S.M. Hosseini, First-principles study of structural, dynamical, and dielectric properties of A-La₂O₃, *Computational Materials Science* 31 (2004) 125–130].
- [2]M. Khazaei, A. Malekzadeh, F. Amini, Y. Mortazavi, and A. Khodadadi, *Cryst. Res. Technol.* **45**, 1064 (2010); M. Ghiasi and A. Malekzadeh, *Cryst.Res. Technol.* **47**, 471 (2012).

15th Physical Chemistry Conference



preparation and drug release kinetic studies of Fluoxetine-loaded PEG-coated Fe₃O₄ nanoparticles

R. Omid Rad^a *, F. Hosseinpour Rajabi^a , B. Vasheghani Farahani^a

^a Department of chemistry, Faculty of sciences, IKIU, Qazvin, Iran

Email: reyhan.omidirad@gmail.com

key words: Drug delivery, Magnetite nanoparticles, Polyethylene glycol, Fluoxetine

Introduction:

Recently, Fe₃O₄ magnetic nanoparticles is widely used in the field of biology and medicine due to their advantages such as chemical stability, low toxicity and ultra-fine size, etc. Bare magnetite nanoparticles tend to agglomerate due to their large surface area/volume ratio. To prevent nanoparticle agglomeration a variety of polymeric coatings have been applied to nanoparticles. Of these polymers, PEG has been identified as being effective. The surface-modified Fe₃O₄ nanoparticles were explored as drug carriers. Many drugs have problems of poor stability, water insolubility and so on. Good drug carriers play an important role in resolving these problems. In this research, we prepared one kind of novel nano-scale carrier for fluoxetine, using Fe₃O₄ nanoparticles as core and PEG as a polymeric shell and fluoxetine as drug to form drug-loaded magnetic nanoparticles. [1-3]

Materials and methods:

Materials was PEG -1000, FeCl₃.6H₂O, Na₂SO₃ and pure fluoxetine powder . Magnetite nanoparticles were prepared using reduction -precipitation method [4] and functionalized the magnetite surface with hydroxyl group, and then modified with PEG. The Fe₃O₄:PEG ratio was 1:2 (w/w). magnetite nanoparticles and drug were mixed in organic solution and stirred for 10 h. The PEG-Fe₃O₄:drug ratio was 2:1 (w/w) . The modified MNPs were deposited using an external magnetic field. The application of PEG-coated Fe₃O₄ nanoparticles as carriers of naproxen was evaluated by measuring its drug content, drug entrapment efficiency and in vitro drug release at PH 1.9 and 7.4.



Apparatus:

The morphology, structure and characteristic of the prepared nanoparticles were studied by FE-SEM (hitachi s-4160), TEM (zeiss, CEM902A), FTIR (Bruker, Tensor 27) and UV-VIS (CAMSPEC M350).

Result and discussion:

Particles with a roughly spherical shape and an average diameter of 20 nm were observed. Drug entrapment efficiency was about $(60 \pm 0.22)\%$. Accumulative release of drug in chloride buffer after 8 h was about 66% whereas the loaded naproxen was further released reaching about 100% at pH 7.4 within 2 h. It is likely due to the faster dissociation of hydrogen bonding between drug and PEG at higher pH. Hydrogen bonds between Fluoxetine and PEG are formed as a result of hydrogen bonding between the aminic protons of Fluoxetine and the ether oxygen of PEG. Drug release followed Higuchi model at two PH and drug release mechanism followed super case II transport in acidic medium whereas anomalous/non-Fickian transport was observed in alkaline medium.

Conclusion:

Spherical magnetite particles were prepared and successfully modified with PEG and confirmed by FTIR. The drug loading was confirmed by FTIR and release behavior *in vitro* was investigated. The results indicated that these PEG-Fe₃O₄ drug carriers have a high drug loading capacity and favorable release property for fluoxetine.

Reference:

- [1] L.-Y. Zhang and et al, J. Current Applied Physics. 10 (2010) 828–833
- [2] D.T.K. Dung and et al, J. Physics: Conference Series. 187 (2009) 012036
- [3] C. Sun and et al, J. Nanomedicine (Lond). 3 (2010) 495–505
- [4] Sh. Qu and et al, J. Colloid and Interface Science. 215 (1999) 190-192



On the chemical synthesis and drug delivery response of naproxen-loaded PAA/PEG interpolymer complex-coated magnetite nanoparticles

R. Omidirad^a*, F. Hosseinpour Rajabi^a, B. Vasheghani Farahani^a

^a Department of chemistry, Faculty of sciences, IKIU, Qazvin, Iran

Email: reyhan.omidirad@gmail.com

key words: Drug delivery, Magnetite nanoparticles, Interpolymer complex, Naproxen

Introduction:

Recently, Fe₃O₄ magnetic nanoparticles is widely used in the field of biology and medicine due to their advantages such as chemical stability, low toxicity and ultra-fine size, etc. Bare magnetite nanoparticles tend to agglomerate due to their large surface area/volume ratio. To prevent nanoparticle agglomeration a variety of polymeric coatings have been applied to nanoparticles. Polyacrylic acid (PAA) is well-known for its biocompatibility, and is widely used in drug delivery systems, especially as a mucoadhesive drug carrier. The high water solubility of PAA limits its use as a carrier for the sustained release of drugs. Interpolymer complexation of PAA with polyethylene glycol (PEG) reduce this solubility. Interpolymer complexes (IPCs) between PAA and PEG are formed as a result of hydrogen bonding between the acidic protons of PAA and the ether oxygen of PEG. Many drugs have problems of poor stability, water insolubility and so on. Good drug carriers play an important role in resolving these problems. In this research, we prepared one kind of novel nano-scale carrier for naproxen, using Fe₃O₄ nanoparticles as core and PAA/PEG IPC as a polymeric shell and naproxen as drug to form naproxen-loaded magnetic nanoparticles. [1-3]

Materials and methods:

Materials was PEG-4000, PAA-10000, FeCl₃·6H₂O, Na₂SO₃ and pure naproxen powder. Magnetite nanoparticles were prepared using reduction-precipitation method and



functionalized the magnetite surface with hydroxyl group. IPC of PAA/PEG was prepared in citrate buffer pH 3.5. magnetite nanoparticles and PAA/PEG IPC and naproxen were mixed in organic solution, and then adjusted to pH 10 to disruption of hydrogen bonding between the PEG and the PAA. The Fe₃O₄:PAA/PEG IPC:drug ratio was 1:2:0.5 (w/w) . The suspension was shaken vigorously for 24 h, during which evaporation of organic phase was prevented, then adjusted to pH 3.5 to reforming hydrogen bonds between the PAA and the PEG and drug in order to entrapping drug . The application of PAA/PEG IPC-coated Fe₃O₄ nanoparticles as carriers of naproxen was evaluated by measuring its drug entrapment efficiency and in vitro drug release at PH 1.9 and 7.4.

Apparatus:

The morphology, structure and characteristic of the prepared nanoparticles were studied by FE-SEM (hitachi s-4160), TEM (zeiss, CEM902A), FTIR (Bruker, Tensor 27) and UV-VIS (CAMSPEC M350).

Result and discussion:

Particles with a roughly spherical shape and an average diameter of 43 nm were observed. Drug entrapment efficiency was about (64±0.15)%. Accumulative release of drug in chloride buffer after 8 h was about 45% whereas the loaded naproxen was further released reaching about 100% at pH 7.4 within 2 h. It is likely due to the faster dissociation of hydrogen bonding between drug and PAA/PEG at higher pH. Hydrogen bonds between naproxen and PAA/PEG are formed as a result of hydrogen bonding between the acidic protons of naproxen and PAA and the ether oxygen atoms of PEG. The drug release followed Higuchi model at two PH and drug release mechanism followed fickian diffusion in acidic medium whereas anomalous/non-Fickian transport was observed in alkaline medium.

Conclusion:

Spherical magnetite particles were prepared and successfully modified with PAA/PEG IPC and confirmed by FTIR. The drug loading was confirmed by FTIR and release behavior *in*



vitro was investigated . The results indicated that these drug carriers have a high drug loading capacity and favorable release property for naproxen.

Reference:

- [1] L.-Y. Zhang and et al, J. Current Applied Physics. 10 (2010) 828–833
- [2] C. Sun and et al, J. Nanomedicine (Lond). 3 (2010) 495–505
- [3] B. Vasheghani Farahani and et al, J. Polymer International. 60 (2011) 279-283

15th Physical Chemistry Conference



Physical and mechanical properties of polyurethane/polyhedral oligomeric silsesquioxane (PU/POSS) nanocomposite

M. A. Mokhtari Farsi^{*a}, M. Mohseni^a

^a Department of polymer engineering and color technology, Amirkabir university of technology, Tehran, Iran

Email: mmohseni@aut.ac.ir

Keywords : Polyhedral Oligomeric Silsesquioxane, POSS, Polyurethane, Nano composite,

Introduction:

Polyurethane clear coats are widely used in automotive industries. Incorporation of nano particles have shown to improve the properties of these resins leading to appropriate mechanical properties and high transparency provided that the dispersion process is well accomplished. However, nano particles have usually high aggregation tendency which make them difficult to disperse. In recent years, Polyhedral Oligomeric Silsesquioxanes (POSS) have emerged as a new type of silica structure with structural size of 1-3 nm, which have functional site and are capable of being dissolved in solvent or vehicle. POSS does not possess conventional difficulty of nano particles. Moreover, these materials are able to act as fire retardant, surface energy reducer, corrosion inhibitor. The main advantage of these nanostructures is their ability to enhance the cross-linking density. In this study hybrid coatings based on polyurethane/polyhedral oligomeric silsesquioxane were synthesized. The reaction with POSS has been done by the use of DBTL as catalyst. Furthermore partial chemical reaction of POSS active sites with NCO part of polyurethane was proved. The effects induced by POSS content on chemical, physical and mechanical properties in surface and bulk of blank polyurethane coating versus polyurethane containing 1, 3, 5 percent were investigated.

Materials and methods:

AL0125 (the POSS type) (Hybrid plastic, USA) was used without any purification. 0.045, 0.13, 0.21 gr of POSS were used in order to make 1, 3 and 5 percent of hybrid coatings



respectively. Polyol and isocyanate (Bayer, Germany) were used as received. Butyl acetate and DBTL (Bayer, Germany) was used as solvent and catalyst respectively.

Apparatus:

The reaction of POSS with PU was studied by FTIR. The DMTA and Tensile experiments were conducted for evaluating mechanical properties of nano composites. The micro indentation and Nano indentation methods were used for studying the surface properties of coatings. Optical properties of coatings have been investigated by the optical microscopy and Turbidometry. Atomic force microscopy (AFM) was applied for investigation of surface topology and roughness.

Result and discussion:

According to FTIR results, the reaction between alcoholic group of POSS and isocyanate occurred. The investigation into mechanical properties of POSS/PU coating by DMTA, tensile and micro Indentation showed an upward trend in mechanical properties by increasing the POSS concentration such as modulus, Tg, cross-link density and Viker's hardness. On the other hand by increasing the POSS concentration up to 5 percent the mechanical properties depreciated which is believed to the aggregation. The nano indentation data indicated that there was a decreasing trend in mechanical properties of coating by increasing the POSS concentration. This might be related to the POSS migration into the surface due to the incompatibility with polyurethane matrix at higher loadings. This observation was further confirmed by increase in roughness as obtained by AFM.

Conclusion:

Partially reacted POSS/PU nano composite was successfully synthesized. Mechanical properties of the hybrid coating were reinforced by POSS up to 3%. On the other hands there is an opposite behaviors in higher concentration as well as surface of the coating. It seems that properties in surface are affected by migration of non reacted POSS into surface.



Reference:

- [1] Y.S. Lai and etc, Structural and electrochemical properties of polyurethanes/polyhedral oligomeric silsesquioxanes (PU/POSS) hybrid coatings on aluminum alloys, *Materials Chemistry and Physics* 117 (2009) 91–98.
- [2] Samy A and etc , Recent advances in synthesis, characterization and rheological properties of polyurethanes and POSS/polyurethane nanocomposites, *Progress in Polymer Science* 34 (2009) 1283–1332.

15th Physical Chemistry Conference



Synthesis of Nanozeolite NaA Using Barley Husk Silica: Mercury Removal from Babolrood River and Industrial Wastewater

Amir. Joorabdoozha^{a*}, Seyed. Naser. Azizi^a

^a Analytical Division, Faculty of Chemistry, University of Mazandaran, Babolsar, Iran

Email: amir.umz2011@gmail.com

Key words: Barley, Mercury, Nanozeolite, Hydride generation.

Introduction:

Barley husk silica (BHS) in amorphous phase with 85% purity was extracted from barley husk ash (BHA). The BHS was used effectively as a new source of silica for the synthesis of nanozeolite NaA. The nanozeolite in pure phase has been synthesized from a gel aluminosilicate with high alkalinity at low temperature, without adding any organic additives. In this study, the application of synthesized NaA nanozeolite from barley husk silica (BHS) for mercury removal from standard and real aqueous solutions were investigated. The crystallization of NaA nanozeolite from BHS was characterized by X-ray diffraction (XRD), scanning electron microscopy (SEM), and FTIR techniques. Moreover, concentration of Hg^{2+} ions in the aqueous solutions was analyzed by hydride generation atomic absorption spectroscopy method. Efficiency of mercury (II) adsorption from real solutions onto the nano-sized NaA zeolite was 98%. The standard and real samples experiments showed that NaA nanozeolite was capable of Hg^{2+} ions removal from the aqueous solutions.

Materials and Methods:

Barley husk was washed thoroughly with distilled water to remove the adhered soil and dust and dried at 100 °C overnight. Then, Kalapathy et al. method [1] was used for extraction of silica from BHA. BHS was used as a silica source for the synthesis of NaA nanozeolite.



The NaA nanozeolite was synthesized by hydrothermal crystallization at low temperature. A typical synthesis mixture with the initial composition $6\text{Na}_2\text{O}/1.5\text{SiO}_2/1\text{Al}_2\text{O}_3/200\text{H}_2\text{O}$ was prepared by mixing the freshly prepared homogeneous aluminate and silicate solutions [2].

The real samples were filtered through millipore ($0.2\mu\text{m}$) filter. Ion exchange process for mercury removal was carried out under optimum conditions ($\text{pH}=8$ and contact time= 60 min) and stirring at 1000 rpm , by contacting 0.01 g of NaA nanozeolite with 10 mL of real solution. Thereafter, the liquid was separated from NaA nanozeolite by centrifuging at 15000 rpm and 30 min . Mercury (II) concentrations were determined by hydride generation atomic absorption spectrophotometer (Model GBC-932, Australia made). The detection limit was 0.2 ppb .

Apparatus:

The extracted silica and the nanozeolite samples were evaluated by XRD spectrometry (GBC MMA). It was scanned for 2θ ranging from 5° to 50° with CuK α radiation and an acceleration voltage of 35.4 kV and current of 45 mA at a rate of $5^\circ/\text{min}$. Moreover, Field-emission scanning electron microscopy (FE-SEM) images were provided using a HITACHI, S-4160 field-emission electron microscope operating at 15 kV for indicating the morphology of samples.

Result & Discussion:

The wastewaters from Bandar Emam Petrochemical center and Babolrood River in Babolsar have been selected for the removal of mercury (II) ions. The initial concentration of the Hg^{2+} ions in the wastewater of Bandar Emam Petrochemical center and Babolrood River were 85.67 and 20.62 ppb , respectively. After the interaction of this mercury (II) solutions with 0.01 g NaA nanozeolite, the final concentration of Hg^{2+} ions were reduced to 1.243 and 0.274 ppb , respectively.

Conclusion:

In this research, the BHS in amorphous phase (85% purity) was prepared from barley husk and used as a new source of silica for the synthesis of NaA nanozeolite. The synthesized NaA



nanozeolite can be employed as an environmentally friendly adsorbent for the removal of mercury from standard and real aqueous solutions. The adsorption process depends on pH and contact time between adsorbate-adsorbent which found to have the optimized values 8 and 60 min, respectively. As it could be expected, it was shown that Hg uptake by NaA nanozeolite occurred faster and more effective.

References:

- [1] U. Kalapathy, A. Proctor, J. Shultz, Bioresour. Technol. 73,257-262,2000.
- [2] E.P. Parry, J. Catal. 2,371-376,1963.



Cold Wall Chemical Vapour Deposition Reactor Design for Synthesis of Carbon Nanotubes: Parametric Study

S. Aghamohammadi^{a, b}, M. Haghighi^{a, b*}

^a Chemical Engineering Faculty, Sahand University of Technology, Tabriz, Iran

^b Reactor and Catalysis Research Center (RCRC), Sahand University of Technology, Tabriz, Iran

*Email: haghighi@sut.ac.ir

Keywords: Nano Material, Chemical Vapor Deposition, Cold Wall, Carbon Nanotubes.

Introduction:

Chemical vapour deposition (CVD) is one of the most popular used techniques for the production of nanoparticles [1]. In this work, results are reported on parametric modelling approach to synthesize multi-walled carbon nanotubes (MWCNs) using a cold wall CVD reactor. Effects of substrate temperature, rotating disk velocity and inlet gas composition on average growth rate of carbon nanotubes were investigated.

Methods:

The process gases Xylene (C_8H_{10}) and Hydrogen (H_2) and the carrier gas Argon (Ar) enter the reactor at 310 K. Laminar flow and low pressure conditions are necessary to synthesize CVD products of better quality. The carbon solid deposition rate is governed by a mixture of volumetric and wall surface reactions. The mixture velocity at the inlet is 0.022 m/s. The top wall is heated to 200°C and side walls of the reactor are maintained at 70°C. This can be a representative of a cold wall reactor in which only the substrate is heated to high temperatures, while the remaining reactor walls are maintained at low temperatures. Figure1 demonstrates the schematic of the CVD reactor configuration.

Result and discussion:

Figure 2 presents the growth rate of carbon solid on side walls. It can be seen that by implementing cold wall reactor no solid carbon was deposited on side walls [2]. It was found there is not a wide change in average deposition rate by changing the rotating substrate

velocity. Table 1 shows the effect of mass fraction of Xylene in the process gas on average growth rate of carbon nanotubes. Deposition rate grows by increasing the concentration of C_8H_{10} . Table 2 depicts the influence of substrate temperature on solid carbon deposition rate. As the temperature increases, the average growth rate decreases. Thus, CVD synthesis of carbon nanotubes should be done at lower temperatures.

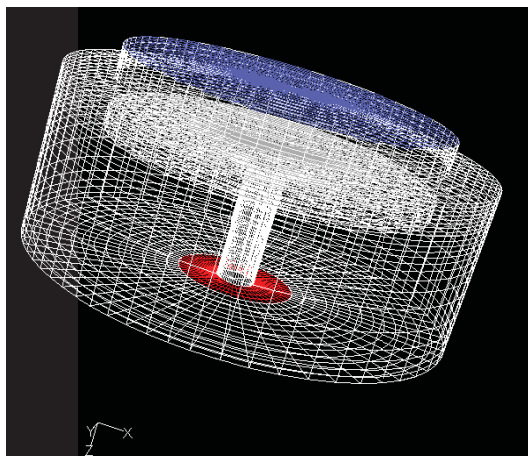


Figure 22: Schematic of the CVD reactor configuration

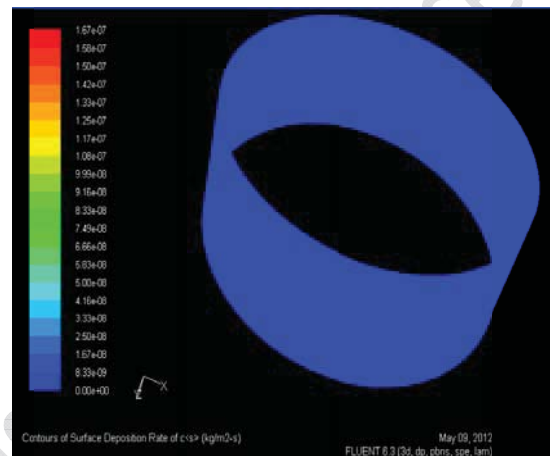


Figure 23: Growth rate of carbon solid on side walls.

Table 1: Average growth rate vs. mass fraction of C_8H_{10}

Mass Fraction of Inlet Gas (C_8H_{10} : H_2 : Ar)	Average Growth Rate on Rotating Substrate ($kg/m^2 \cdot hr$)
0.02: 0.1: 0.87	9.6457832e-08
0.03: 0.1: 0.86	1.6254147e-07
0.04: 0.1: 0.85	1.9386428e-07
0.05: 0.1: 0.84	2.4292711e-07
0.06: 0.1: 0.83	2.9223173e-07

Table 2: Average growth rate vs. Substrate Temperature

Substrate Temperature (k)	Growth Rate on Rotating Substrate ($kg/m^2 \cdot hr$)
1100	1.5132241e-07
1000	1.6623189e-07
900	1.8445184e-07
800	2.0715056e-07
700	2.3619445e-07

Conclusion:

MWCNs applications range from use in new high strength composites to use in advanced electronics applications as transistors, field emitters, and sensors. Parametric study of CVD synthesis method in a promising cold wall reactor indicated that lower temperature and higher concentration of Xylene in the reactant gas favour the growth rate on rotating substrate.



References:

- [1] P. Finnie et al., "Optimization of methane cold wall chemical vapor deposition for the production of single walled carbon nanotubes and devices", *Carbon*, 44, (15), 3199-3206, 2006.
- [2] C. Zhang et al., "The efficient synthesis of carbon nano-onions using chemical vapor deposition on an unsupported Ni-Fe alloy catalyst", *Carbon*, 49, (4), 1151-1158, 2011.



Study of Physicochemical Behavior of Annealed TiO₂ Nanotubes

S. Miraghaei^{a*}, F. Ashrafizadeh^a, M. Santamaria^b, F. Di Quarto^b

^a Department of Materials Engineering, Isfahan University of Technology, 84156 Isfahan, Iran

^b Department of Civil and Environmental Engineering, University of Palermo, 90128 Palermo, Italy

E-mail: s-miraghaei@ma.iut.ac.ir

Key words: Nanotubes, TiO₂, Anodization, Photocurrent, Capacitance, physicochemical

Introduction:

TiO₂ NanoTubes (TNTs) have been appealed a lot of attention during the last decade among researchers. Among previous studies, there have been a plenty of reports regarding TNTs mechanism of formation and their physicochemical properties before and after annealing [1]. It has been tried to explain, to some extent, the electrochemical and photo-electrochemical behavior of annealed TNTs. Regardless of some noticeable achievements, still there are several contradictions and ambiguity about the mechanism of photocurrent and capacitance formation in TNTs. Our previous reports on the physicochemical behavior of titanium oxide nanotubes [2] have explained the origin of some electrochemical and photo-electrochemical properties of TNTs before and after annealing. Also, the effect of anodically and thermally formed oxide layers below nanotubes on physicochemical response of the whole system has been evaluated [3]. In the present work, it has been tried to study, in more detail, the physicochemical behavior of annealed TiO₂ nanotubes. Finally, qualitative models were presented for better describing the mechanism of photoresponse and capacitance of annealed TNTs.

Materials and Methods:

To prepare TiO₂ nanotubes, titanium foils were anodized in an electrochemical cell using ethylene glycol electrolyte and a platinum mesh as the cathode. Cell voltage (45 V) was kept constant during anodization for different times to form nanotubes of different lengths. Field-



emission scanning electron microscope (Carl Zeiss ULTRA55) was used to examine the morphology and geometry of nanotube arrays. Photo-electrochemical characterizations were conducted using photocurrent spectroscopy technique [3]. Differential admittance measurements were conducted using a PARSTAT 2263 instrument in 0.5 M K₂SO₄ solution.

Results and Discussion:

Photocurrent spectroscopy revealed that, at constant potentials, photocurrent depends on photon wavelength and also the geometry of nanotubes. There is an optimum length for TNTs at which the maximum photocurrent generates. Photocurrent at constant wavelengths is independent of potential in the anodic potentials but is highly affected by potential in the cathodic region with respect to the flat band potential. Similarly, capacitance of TNTs shows different behaviors in the anodic and cathodic potentials. In the anodic region, capacitance is low and can be described using Mott-schottky model, but in the cathodic potentials TNTs behave as a supercapacitors showing very high values for capacitance which also depends on the nanotubes length.

Conclusion:

A model presented for describing photoresponse of titania nanotubes shows that in anodic potentials, separation and transportation of photocarriers are both independent of electrode potential due to the size and geometry of nanotubes. In this case, electrons diffuse through tube walls to reach to the substrate to generate photocurrent. In the cathodic region, direction of electrical field within TNTs reversed which results in a great cathodic current opposing anodic photocurrent. The model also shows that in anodic potentials capacitance is controlled by the behavior of barrier layer beneath nanotubes but in the cathodic region, capacitance is determined by the double layer capacitance expanded over the entire active surface of TNTs that makes the electrode a supercapacitor.

References:

- [1] P. Roy, S. Berger, P. Schmuki, *Angew. Chem. Int. Ed.*, 50, 2904 (2011).



- [2] S. Miraghaei, F. Ashrafizadeh, K. Raeissi, M. Santamaria, F. Di Quarto, *Electrochem. Solid State Lett.*, 14, K8 (2011).
- [3] S. Miraghaei, F. Ashrafizadeh, M. Santamaria, F. Di Quarto, K. Shimizu, *J. Electrochem. Soc.*, 158, K197 (2011).

15th Physical Chemistry Conference



TiO₂/Fe:Ag nano composite: Synthesis and photo catalytic activity

T. Harifi*^a, M. Montazer^a

^aTextile Department, Amirkabir University of Technology, Center of Excellence in Textile, Hafez Avenue,
Tehran, Iran

E-mail: tina_harify@yahoo.com

Keywords: Photo catalyst, TiO₂/Fe:Ag nano composite, Antibacterial property

Introduction:

The photo catalytic activity of TiO₂, as one of the most promising photo catalysts, is limited by fast photoelectron–hole pair recombination and low interfacial charge-transfer rates of photo generated carriers [1]. In order to solve these problems, some transition metals have been employed for enhancing the photo catalytic activity of the titanium dioxide [2]. Also numerous efforts have been made to improve the photo response of TiO₂ by noble metal nanoparticles loading [3]. Therefore, enlightened by the respective advantages of transition metal doping and deposition of noble metal [4], in this study the idea of combining Fe³⁺ cations doping and Ag nanoparticles deposition was considered, aiming to develop a new photo catalyst with higher performance, which have been rarely reported till now.

Materials and Methods:

Fe³⁺ doped TiO₂ deposited with Ag (TiO₂/Fe:Ag nano composite) was successfully prepared with simple wet impregnation method, using TiO₂ P25 Degussa as a precursor and Fe(NO₃)₃·9H₂O as a dopant. Photo deposition of silver on TiO₂/Fe nanoparticles was carried out by adding AgNO₃.

Apparatus:

The synthesized product was characterized by X-ray diffraction (XRD), Energy dispersive X-ray spectroscopy (EDX) and Scanning electron microscopy (SEM). To analyze the light



absorption of the prepared photo catalyst, UV-Vis reflectance spectra were obtained. The photo catalytic degradation of Methylene Blue was evaluated by spectrophotometric analysis.

Result and Discussion:

The results demonstrated that size of the as prepared anatase $\text{TiO}_2/\text{Fe}:\text{Ag}$ was in the nano regime. No significant characteristic peak of iron and Ag was observed, indicating low amount of iron presented in the lattice of TiO_2 and sparse distribution of Ag on TiO_2/Fe surface. UV-Vis diffuse reflectance spectra showed enhancement of light absorption in visible region. The Fe^{3+} and Ag have synergistically improved the photo catalytic activity of TiO_2 for photo degradation of Methylene Blue under both ultraviolet and sunlight irradiation. The co-operation of the Fe^{3+} and Ag in the narrowing of the band gap, promoting the separation of the photo generated electrons and holes and accelerating the transmission of photo current carriers is presumed to be the probable mechanism resulted in higher photo catalytic activity. Furthermore, the synthesized photo catalyst is expected to show higher antibacterial property compared with non-doped TiO_2 due to the presence of Ag nanoparticles.

Conclusion:

$\text{TiO}_2/\text{Fe}:\text{Ag}$ nano composite with high photo catalytic activity and antibacterial property was successfully prepared by facile wet impregnation method. The synthesized photo catalyst showed both high ultraviolet and visible light photo catalytic activity in degrading Methylene Blue. The benefit of doped Fe^{3+} and loaded Ag particles was due to their capability in inhibiting the recombination of photo electron-hole pair and narrowing the band gap.

Reference:

- [1] S. Bzdón et al.; "Radiation-induced synthesis of Fe-doped TiO_2 : Characterization and catalytic properties"; Radiation Physics and Chemistry; 81, 322-330, 2012.
- [2] K. Naeem et al.; "Preparation of Fe^{3+} doped TiO_2 nanoparticles and its photo catalytic activity under UV light"; Physica B; 405, 221-226, 2010.



- [3] S. Ko et al.; "Photochemical synthesis and photo catalytic activity in simulated solar light of nanosized Ag doped TiO₂ nanoparticle composite"; *Composites: Part B*; 42, 579-583, 2011.
- [4] L. Qin et al.; "Ag/Fe:TiO₂ nano-catalysts prepared by Fe ion implantation and Ag nanoparticle deposition by electron beam irradiation", *Nuclear Instruments and Methods in Physics Research B*; 267, 1077–1080, 2009.

15th Physical Chemistry Conference



Simultaneous Synthesize of Nano-Silver and Polyester Hydrolysis in Alkali Media along with Nano TiO₂ Application

V. Allahyarzadeh^{a*}, M. Montazer^a, N. Hemmatinejad^a, N. Samadi^b

^a Textile Department, Amirkabir University of Technology, Hafez Avenue, Tehran, Iran.

^b Faculty of Pharmacy, Tehran University of Medical Science, Tehran, Iran.

(E-mail: vidaallahyar@aut.ac.ir)

Key Words: Silver Nano Particles, Nano Titanium Dioxide, Polyester, Antimicrobial Activity.

Introduction:

Silver nano particles have attracted much attention because of distinctive properties with developing of numerous synthesis approaches [1]. Nano titanium dioxide (NTO) particles have been widely investigated due to their photo catalytic activity and ability to absorb ultra-violet irradiation [2]. The stability of nano particles on polyester fabrics (PET) is low due to the lack of functional groups [3]. Thus, it is necessary to create some functional groups on the polymer chains of PET. The chemical surface modification, such as alkali hydrolysis, increases PET functionality by introducing hydroxyl and carboxylic groups onto the fabric surface to impart new specifications to the fabric, such as better binding to nano-TiO₂ particles [4-5]. In the present work, to achieve multifunctional PET fabric, in situ synthesis of silver nanoparticles along with application of TiO₂ nanoparticles has been done in one step with alkaline hydrolysis of polyester fabric. In addition, the properties of the treated fabric such as antimicrobial activity, self cleaning, wettability, tensile strength and bending rigidity have been studied and reported.

Methods:

The polyester (PET) fabric was hydrolyzed in alkali media with assistant of cationic surfactant (cetyl trimethyl ammonium bromide) to increase polyester fabric surface activity producing ethylene glycol as reducing agent to synthesize nano silver and to enhance nano titanium dioxide adsorption on the PET fabric. The properties of the treated PET fabric have been



characterized by FTIR spectroscopy, X-Ray Diffraction, Field Emission Scanning Electron Microscopy (FESEM) and energy-dispersive X-ray (EDX) and water droplet adsorption, antibacterial properties, weight loss, self-cleaning, tensile strength and bending rigidity have been studied.

Result and discussion:

The weight of the treated PET samples was reduced and their wettability was improved due to introduction of hydrophilic groups on the PET surface as a result of alkaline hydrolysis. The FTIR spectroscopy showed more intense peaks related to the hydroxyl and carboxyl groups. XRD patterns confirmed the presence of silver and TiO₂ nano particles with crystal size of 10 nm on the fabric surface. Field Emission Scanning Electron Microscopy (FESEM) showed the fabric surface and distribution of the nano particles on the fibers surface with the average size of 54 nm. Additionally, the presence of nano silver and nano TiO₂ on the PET fabric surface was proved by EDX. Also, the treated fabrics indicated excellent antibacterial activity against *Staphylococcus aureus* and *Escherichia coli* proved the possible in situ synthesis of silver nano particle with alkaline hydrolysis of PET fabric. Alkaline hydrolysis of PET fabrics produced ethylene glycol led to reduction of silver ions to silver nano particles. Introducing functional groups on the PET fabrics enhanced absorption of nano-TiO₂ particles on the PET fabric and the photo catalytic activity of nano-TiO₂ particles on the PET fabric was confirmed by the degradation of Methylene Blue under daylight irradiation. Interestingly, the tensile strength of the treated fabrics was improved even with the action of alkali and surface hydrolysis.

Conclusion:

In this paper, a novel idea is introduced to achieve antibacterial PET fabric with good handle properties. The weight of the treated PET samples was reduced as the action of alkali hydrolysis that is confirmed by FTIR with improved wettability. FESEM, EDX and XRD patterns confirmed the presence of nano particle on the treated samples. The treated fabrics



showed excellent antibacterial properties against *S.aureus* and *E.coli*. Self-cleaning properties of TiO₂ treated samples was good with improved tensile strength.

Reference:

- [1] R.Dastjerdi, M.Montazer, S.Shahsavan. Colloids and Surfaces A: Physicochem. Eng. Aspects, 345, 202, 2009.
- [2] R.Dastjerdi, M.Montazer. Colloids And Surfaces B: Biointerfaces, 79, 5, 2010.
- [3] D. Mihailovic, Z. Saponjic, M. Radoicic, T. Radetic, P. Jovancic, J. Nedeljkovic, M. Radetic, Carbohydr Polym, 79, 526, 2010.
- [4] S.Hashemizad, M. Montazer, A.Rashidi. J. Appl.Poly. Sci., 2011.
- [5] M.Dhinakaran, B.S.Dasaradan, V.Subrasmnism. JTATM, 6, 1, 2010.



Thermal Stable and Self-Cleaning Hollow Fiber PET Nonwoven Using Nanoclay/Nano TiO₂/Poly Siloxane Composites

M. Asadi*^a, M. Montazer^a, N. Hemmatinejad^a

^a Textile Department, Amirkabir University of Technology, Centre of Excellence in Textile, Hafez Avenue, Tehran, Iran
E-mail: m_asadi@aut.ac.ir

Keywords: Nanoclay, Nano TiO₂, Hollow fiber PET Nonwoven, Thermal stability, Self-cleaning

Introduction:

Surface modification of nonwoven PET is very important due to its importance and application in various fields such as: hygiene, medical, filters, carpet backing, insulation and others. Polymer/layered silicate nano composites have been recognized as one of the most promising research fields in materials chemistry because of their unique properties, such as enhanced mechanical property, increased thermal stability, improved gas barrier property, and reduced flammability. In recent years nano titanium dioxide/nano clay composites has attracted much attention as photo catalysts in special applications. This paper describes a method for surface modification of hollow fiber PET nonwoven using nano clay, nano TiO₂ and poly siloxane softener through conventional exhaustion-dry-cure method. The effect of presence and absence of nano clay on the fabric surfaces modification was investigated. Thermal stability and mechanical strength of the treated fabrics were also investigated [1-4].

Materials and methods:

PET Hollow fiber nonwoven with 170g/m² Den. The organically modified montmorillonite clay (Cloisite 20A), Nano titanium dioxide with the anatase crystalline structure and average particle size of 21nm was purchased from Evonik Co. (Germany), dispersing agent (nonionic) based on poly acrylate and alkyl phosphate from Alkemi Co., Water-based polyester polyurethane resin namely Asupret E-Pol purchased from Asutex Co (Spain).

The fabric samples were first scoured with 1g/L non anionic detergent at 60 °C for 20 min, rinsed with cold water, and dried at ambient temperature. Different concentrations of nanoclay, dispersing agent, nano TiO₂, polysiloxane, polyurethane resin were dispersed in water by sonication for 10 min at 60 °C. Then all pre-washed fabric samples were immersed in the prepared bath for 20 min, then dried at 90 °C followed by curing at 150 °C for 5 min.

Results and discussion:

The nonwoven morphology and presence of nano clay and nano TiO₂ on the PET surface observed with SEM, ATR and EDS. XRD patterns of nano clay powder, treated and untreated PET nonwoven was obtained. D-spacing of nano clay sheets was increased with intercalation siloxane between layers of nano clay (Fig1-a). Thermal gravimetric analysis (TGA) and derivatives weight was employed to investigate the thermal decomposition behavior of the treated samples (Fig1-b, 1-c). Self-cleaning properties of PET nonwoven treated by TiO₂/nano clay/poly siloxane composites was followed by degradation of methylene blue under daylight irradiation at ambient temperature. The nonwoven tensile strength also measured with using a tensile tester (Instron, England).

Small dye degradation under daylight irradiation has appeared on the control samples. The samples treated with poly siloxane showed low staining. By increasing of TiO₂ up to 2 g/L the degradation of Methylene Blue was increased. However, with adding nano clay and polyurethane resin, staining increased but had no negative effect on the self-cleaning property. PET/nano clay/TiO₂/poly siloxane/resin has been showed good thermal stability than PET nonwoven.

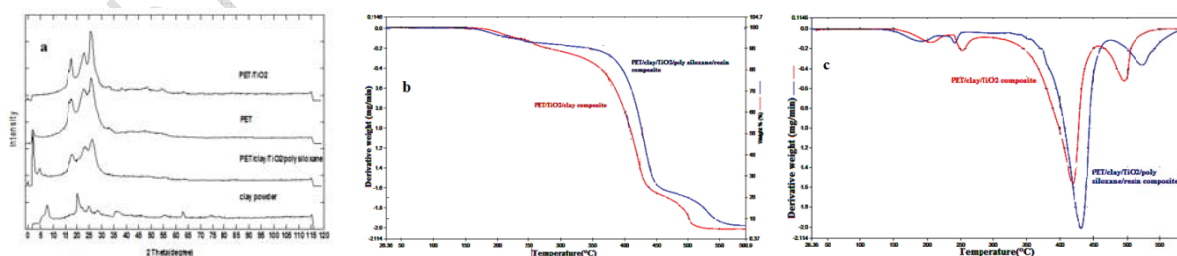


Fig1. a) XRD analysis of PET/clay/TiO₂/poly siloxane composites, b) TGA curves, c) DTG curves



Conclusion:

The obtained results showed that increasing the concentration of the polyurethane resin and nano clay content in the bath had a considerable influence on the add-on percentage. Application of clay/ TiO₂/ poly siloxane nano composites on the fabric surfaces improved self-cleaning property, thermal stability and mechanical strength as compared to the samples treated with the compounds alone.

References:

- [1] L.Yuan, D. Huang, "TiO₂/Montmorillonite Nanocomposite for Removal of Organic Pollutant", J.Appl. Clay Sci., 53, 272-278, 2011.
- [2] F. Carosio, J. Alongi, F. Frach , "Influence of Surface Activation by Plasma and Nanoparticle Adsorption on the Morphology, Thermal Stability and Combustion Behavior of PET Fabrics", J. Euro. Polym., 47, 893-902, 2011.
- [3] P. Kiliaris, C.D. Papaspyrides, "Polymer/layered Silicate (clay) Nanocomposites: An Overview of Flame Retardancy", Prog. Polym.Sci., 35, 902–958, 2010.
- [4] A. Bozzi, T. Yuranova, J.Kiwi, "Self-cleaning of Wool-Polyamide and PolyesterTextile by TiO₂-Rutile Modification Under Daylight Irradiation at Ambient Temperature", J. Photochem. A: Chem., 172, 27–43, 2005.



Applying Non-Thermal Plasma to Synthesis of Nanostructured Ni/Al₂O₃-MgO Catalyst for Syngas Production from CH₄/CO₂

N. Rahemi^{a,b}, M. Haghighi^{a,b}, A. A. Babaluo^{a,c}, M. Fallah Jafari^d, P. Estifae^{a,b}

^a Chemical Engineering Faculty, Sahand University of Technology, Tabriz, Iran

^b Reactor and Catalysis Research Center (RCRC), Sahand University of Technology, Tabriz, Iran

^c Nanostructure Material Research Center (NMRC), Sahand University of Technology, Tabriz, Iran

^d National Iranian Oil Refining & Distribution Company (NIORDC), Tehran, Iran

*Email: haghighi@sut.ac.ir

Keywords: Ni/Al₂O₃-MgO, CH₄/CO₂ Reforming, Syngas, Nanocatalyst, Plasma.

Introduction:

Non thermal plasma treatment of catalysts has a significant effect on the formation of small size and high dispersed nanocatalysts [1-3]. In this context we investigate how this method affects on the properties of Ni/Al₂O₃-MgO nanocatalyst used in syngas production from CH₄/CO₂.

Materials and methods:

Two Ni(10wt%)/Al₂O₃-MgO(10wt%) catalysts were prepared by impregnation with and without non-thermal plasma treatment. The non-thermal plasma treatment time was 15 min and the treatment was repeated for three times in order to get a uniformly treated powder. XRD, FESEM, TEM, BET and FTIR techniques have been used to investigate the effect of the non-thermal plasma on the structure of Ni/Al₂O₃-MgO nanocatalyst.

Result and discussion:

FESEM micrograph (Figure 1) of plasma treatment for Ni/Al₂O₃-MgO nanocatalyst shows smoothened nanocatalyst particles, larger contacting interface, and flat morphology that are in agreement with literature [4]. High interaction between support and Ni can be concluded from

TEM micrograph (Figure 2) of plasma catalyst. This observation is due to static electric repulsion during the plasma treatment [5].

Catalytic experiments were evaluated in the temperature range of 550–850°C in the quartz packed bed reactor. The effect of operating conditions such as temperature, CH₄/CO₂ ratio, GHSV on synthesis gas, yield, H₂/CO ratio and stability test has also been studied.

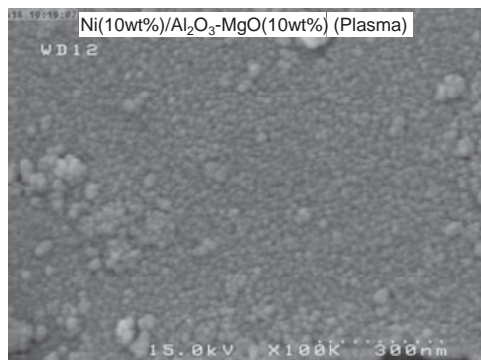


Figure 24: FESEM image of Ni/Al₂O₃-MgO.

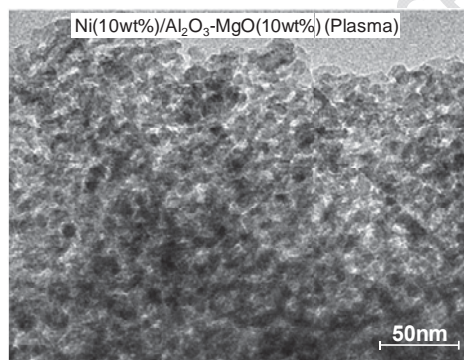


Figure 25: TEM image of Ni/Al₂O₃-MgO.

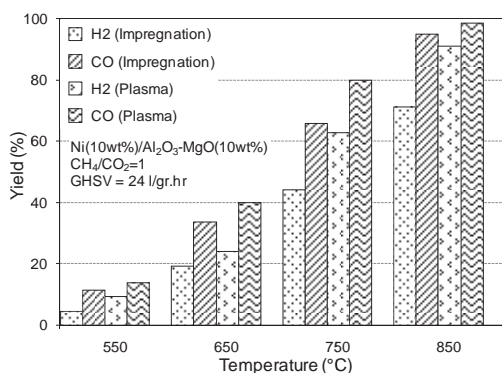


Figure 26: H₂ and CO yields over synthesized nanocatalysts at different temperatures.

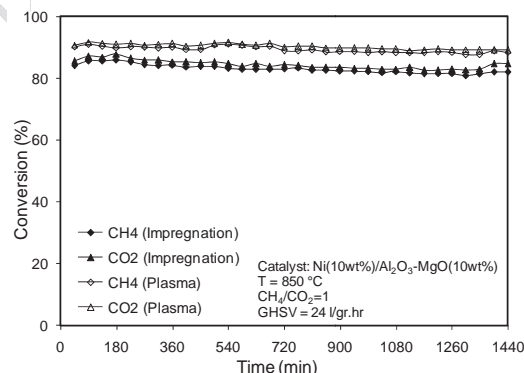


Figure 27: Time on stream performance of synthesized nanocatalysts.

As seen in Figure 3 plasma treated nanocatalyst always had higher activity than that of the conventional catalyst in term of H₂ and CO production. Yield of H₂ and CO increased with increasing temperature due to highly endothermicity of CO₂ reforming, the increasing of temperature is beneficial to conversion of CH₄ and CO₂. As seen in Figure 4 the plasma treated sample is very stable in terms of CH₄ and CO₂ conversion but impregnated



nanocatalyst show a slight deactivation during testing. This confirms effect of plasma in creation of anti-coke catalysts.

References:

- [1]Y.-P. Zhang et al., "A novel plasma-treated Pt/NaZSM-5 catalyst for NO reduction by methane", *Catalysis Communications*, 5, (1), 35-39, 2004.
- [2]C.-j. Liu et al., "Characterization of plasma treated Pd/HZSM-5 catalyst for methane combustion", *Applied Catalysis B: Environmental*, 47, (2), 95-100, 2004.
- [3]J.-g. Wang et al., "Partial oxidation of methane to syngas over glow discharge plasma treated Ni-Fe/Al₂O₃ catalyst", *Catalysis Today*, 89, (1-2), 183-191, 2004.
- [4]X. Zhu et al., "Structure and reactivity of plasma treated Ni/Al₂O₃ catalyst for CO₂ reforming of methane", *Applied Catalysis B: Environmental*, 81, (1-2), 132-140, 2008.
- [5] Z.-j. Wang et al., "CO₂ reforming of methane over argon plasma reduced Rh/Al₂O₃ catalyst: a case study of alternative catalyst reduction via non-hydrogen plasmas", *Green Chemistry*, 9, 554-559, 2007.



Ultrasound Assisted Synthesis and Characterization of Nanostructured MnNiSAPO-34 Catalyst Used in MTO Process

M. Charghand^{a,b}, M. Haghighi^{a,b}, A. Alizadeh Eslami^{a,b}

^a Chemical Engineering Faculty, Sahand University of Technology, Tabriz, Iran

^b Reactor and Catalysis Research Center (RCRC), Sahand University of Technology, Tabriz, Iran

*Email: haghighi@sut.ac.ir

Keywords: Methanol, Olefins, MTO, MnNiSAPO-34, Hydrothermal, Ultrasound.

Introduction:

The methanol to olefins process is regarded as a powerful indirect technology to convert fossil resources to value added products [1]. Among the Silica-Alumina-Phosphate molecular sieves, SAPO-34 has received much attention since it reveals higher selectivity for C₂-C₄ hydrocarbons [2]. In this research, we developed nanostructured MnNiSAPO-34 catalyst via sono-chemical method to boost the conversion and stability.

Materials and methods:

Aluminum isopropoxide was mixed with TEAOH (as structure directing agent). After stirring for 1.5 h, fumed silica, and phosphoric acid was added drop wise to the mixture. Finally the sonicated and homogeneous gel with the portion of Al₂O₃/SiO₂/P₂O₅/TEAOH/H₂O= 1/0.3/1/3/50 was heated in a hydrothermal autoclave for 48 hours. The crystallization and morphology of the prepared catalyst were characterized by XRD, and FESEM analysis, the conversion and selectivity were considered in particular.

Result and discussion:

The XRD pattern of MnNiSAPO-34 (Figure 1) matches the CHA structure type [3]. Sharp peaks confirm the narrow crystal size (~20 nm) which is calculated by Scherrer equation. FESEM micrographs (Figure 2) offer a great order of crystallinity and a good dispersion of

metal particles on the surface of SAPO-34. This can be initiated by positive effect of ultrasonic synthesis in nucleation process.

Catalyst performance test was carried out in a U-shape quartz micro reactor at atmospheric pressure. Methanol conversion (Figure 3) is almost 100% for ultrasonic assisted synthesis in reaction temperature (300-500°C). The selectivity (Figure 4), at 350°C with 100% conversion, was 83%, 60%, and 27% for olefins, ethylene, and propylene respectively.

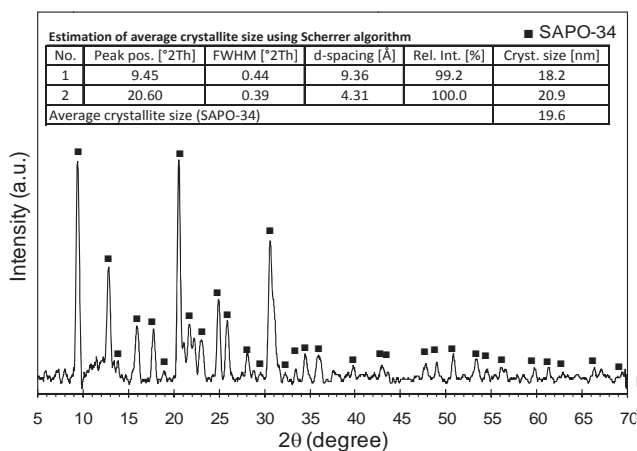


Figure 28: XRD pattern of MnNiSAPO-34.

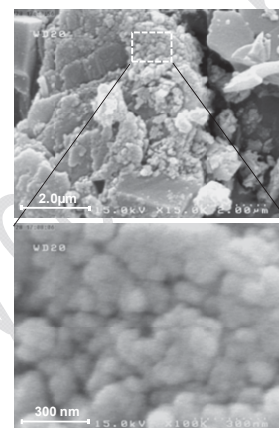


Figure 29: FESEM image of MnNiSAPO-34.

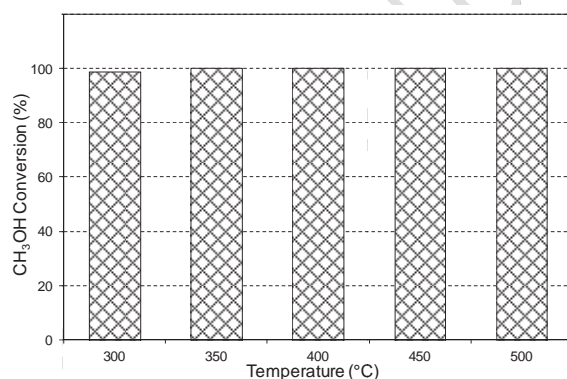


Figure 30: Methanol conversion over MnNiSAPO-34 catalyst.

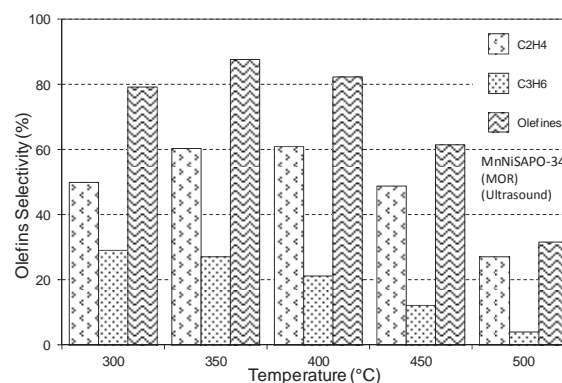


Figure 31: Olefins selectivities over MnNiSAPO-34 catalyst.



Conclusion:

For this study MnNiSAPO-34 catalyst were synthesized by sono-chemical method. Results confirmed narrow pore size which leads the catalyst cages to be shape selective for cracking of oligomers, and the reaction can progress further at lower temperatures. This also decreases the costs of energy supplying as well.

References:

- [1] Z. Liu and J. Liang, "Methanol to olefin conversion catalysts", *Current Opinion in Solid State and Materials Science*, 4, (1), 80-84, 1999.
- [2] S. Wilson and P. Barger, "The characteristics of SAPO-34 which influence the conversion of methanol to light olefins", *Microporous and Mesoporous Materials*, 29, (1-2), 117-126, 1999.
- [3] J. Tan et al., "Crystallization and Si incorporation mechanisms of SAPO-34", *Microporous and Mesoporous Materials*, 53, (1-3), 97-108, 2002.



Catalytic Performance of Ni-Co/Al₂O₃-MgO-ZrO₂ Nanocatalyst toward CO₂ Reforming of CH₄: Effect of ZrO₂ Precursor

S. M. Sajjadi^{a,b}, M. Haghighi^{a,b*}, F. Rahmani^{a,b}

^a Chemical Engineering Faculty, Sahand University of Technology, Tabriz, Iran

^b Reactor and Catalysis Research Center (RCRC), Sahand University of Technology, Tabriz, Iran

*Email: haghighi@sut.ac.ir

Keywords: Ni-Co/Al₂O₃-MgO-ZrO₂, Sol-Gel, CO₂ Reforming, Syngas, Nanocatalyst.

Introduction:

The main catalyst for CO₂ reforming of CH₄ is Ni-based catalyst. However, their major drawback, high amount of coke formation, leads to rapid deactivation [1-2]. In order to evaluate the effect of zirconia precursor in the catalytic properties and activity, Ni(10wt%)-Co(5wt%)/Al₂O₃-MgO-ZrO₂ nanocatalyst with two different zirconia precursor, zirconyl nitrate hydrate (ZNH) and zirconyl nitrate solution (ZNS) was synthesized by sol-gel method.

Materials and methods:

Al-tri-sec-butoxide, zirconyl nitrate solution and Mg(NO₃)₂.6H₂O were employed as support precursors. Ni(NO₃)₃.6H₂O and Co(NO₃)₃.6H₂O were used as active phase and promoter precursors, respectively. Isopropanol and acetyl acetone were used as solvent and gelling agent, respectively [3].

The nanocatalysts were characterized by XRD, FESEM, BET and FTIR analysis and tested in U-shaped fixed-bed quartz reactor, stoichiometric feed ratio and 550-850°C. In this paper the nanocatalyst synthesized using ZNH is called NCZNH, and the other sample which employed ZNS is called NCZNS.

Result and discussion:

XRD patterns in Figure 1a and b reveal that NCZNS has a suitable crystalline structure which improves catalytic activity. In contrast, the amorphous behaviour was intensified in the NCZNH. FESEM images in Figure 2a and b indicate that employing of ZNS leads to uniform

and homogeneous particle size. These features are attributed to peptization of zirconyl nitrate by nitric acid.

As illustrated in Figures 3 and 4, both nanocatalysts show high activity and stability. However, the NCZNS exhibited better catalytic performance. Furthermore, the mentioned nanocatalyst produces the high amount of syngas in all of the investigated temperature ranges. The excellent catalytic performance of NCZNS is related to the better characterization.

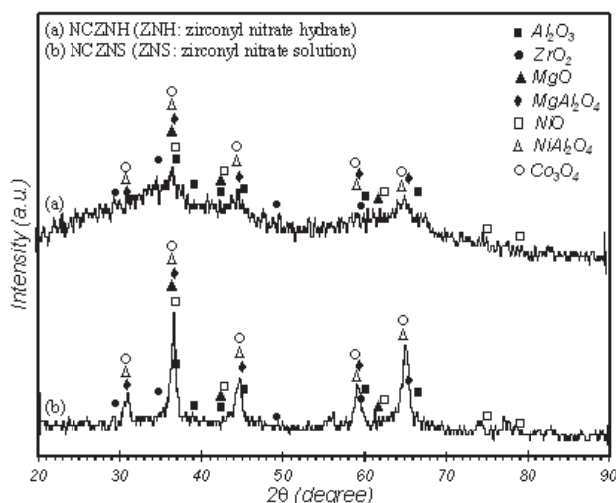


Figure 32: XRD patterns of Ni-Co/Al₂O₃-MgO-ZrO₂ nanocatalyst using different ZrO₂ precursor.

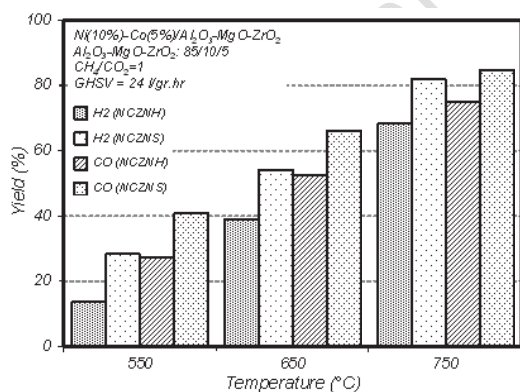


Figure 34: H₂ and CO yield over Ni-Co/Al₂O₃-MgO-ZrO₂ nanocatalyst.

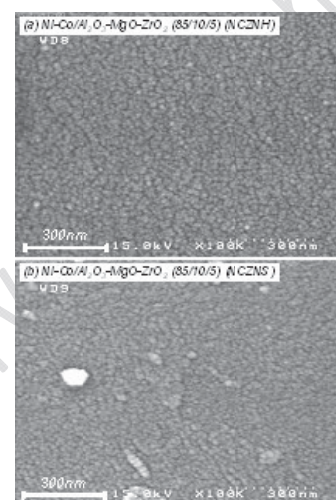


Figure 33: FESEM of Ni-Co/Al₂O₃-MgO-ZrO₂ nanocatalyst using different ZrO₂ precursor.

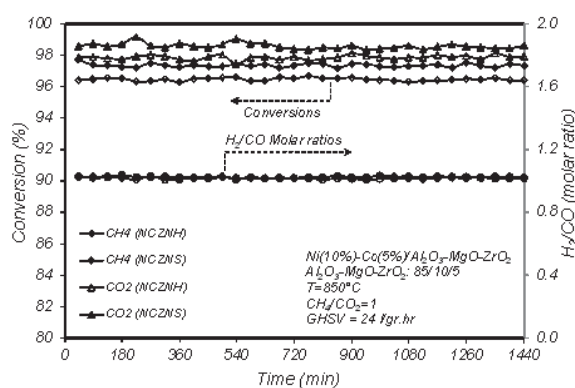


Figure 35: Time on stream performance of Ni-Co/Al₂O₃-MgO-ZrO₂ nanocatalyst.



Conclusion:

NCZNS exhibited suitable crystalline structure and uniform and homogeneous particle size. This nanocatalyst also shows high catalytic activity and stability during 1440 min. Therefore, ZNS is a suitable zirconia precursor for preparation of Ni-Co/Al₂O₃-MgO-ZrO₂ nanocatalyst.

References:

- [1] Hao, Z., et al., "Characterization of aerogel Ni/Al₂O₃ catalysts and investigation on their stability for CH₄-CO₂ reforming in a fluidized bed", Fuel Processing Technology, 90, (1), 113-121, 2009.
- [2] Alonso, D., et al., "Ni, Co and bimetallic Ni-Co catalysts for the dry reforming of methane", Applied Catalysis A: General, 371, (1-2), 54-59, 2009.
- [3] Tang, S., et al., "CO₂ Reforming of Methane to Synthesis Gas over Sol-Gel-made Ni/□-Al₂O₃ Catalysts from Organ metallic Precursors", Journal of Catalysis, 194, (2), 424-430, 2000.



Plasma Assisted Synthesis of Nanostructured Pt/Al₂O₃-CeO₂ Catalyst Used for Waste Gas Stream Treatment

F. Rahmani^{a,b}, M. Haghighi^{a,b*}, P. Estifae^{a,b}

^a Chemical Engineering Faculty, Sahand University of Technology, Tabriz, Iran

^b Reactor and Catalysis Research Center (RCRC), Sahand University of Technology, Tabriz, Iran

*Email: haghighi@sut.ac.ir

Keywords: Pt/Al₂O₃-CeO₂, VOCs, Toluene, Total oxidation, Plasma.

Introduction:

Emission control of VOCs is one of the priorities for environmental catalysis. Supported noble metals especially platinum on γ -Al₂O₃ catalysts have been conventionally synthesized for the oxidation of VOCs [1]. However, the duration of these catalysts is not enough for industrial applications [2]. In this research, to improve the catalyst properties and the catalytic performance, ceria as suitable promoter and plasma treatment with the catalyst preparation were applied.

Materials and methods:

To this aim, the Pt (1 wt%)/CeO₂ (30 wt%)-Al₂O₃ catalyst was prepared by impregnation and modified by glow discharge plasma. The prepared nanocatalyst was characterized by XRD, FESEM, BET and FTIR techniques, and its catalytic performance was evaluated by the catalytic oxidation of toluene in an atmospheric U-shape Pyrex micro reactor.

Result and discussion:

The XRD patterns confirmed the formation of cerium oxide as the crystalline phase on alumina with the average crystallite size of 8.1–8.7 nm, derived by Scherrer equation. In addition, platinum oxide was not observed which could be due to high dispersion of this metal on the support. Morphological analysis indicated that the synthesized nanocatalyst had

particles in nano-ranges with the average size of 64.8 nm. BET surface area measurements showed that the nanocatalyst had large surface area for catalytic application.

The catalytic results showed that the synthesized nanocatalyst had high activity, low light-off temperature and good stability in terms of toluene elimination as a result of plasma modification which result in improved morphology and anti coke properties. It was observed that the complete destruction (about 100%) of toluene was achieved at 210°C.

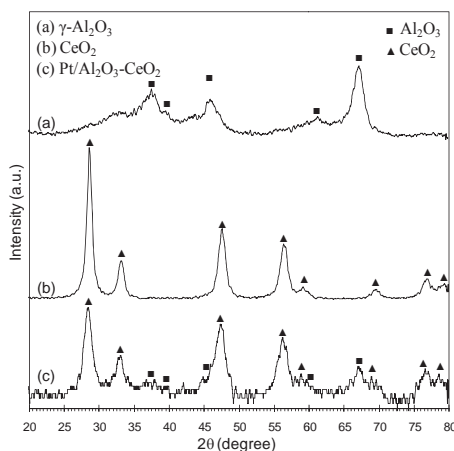


Figure 36: XRD patterns of γ - Al_2O_3 , CeO_2 and $\text{Pt}/\text{Al}_2\text{O}_3$ - CeO_2 nanocatalyst.

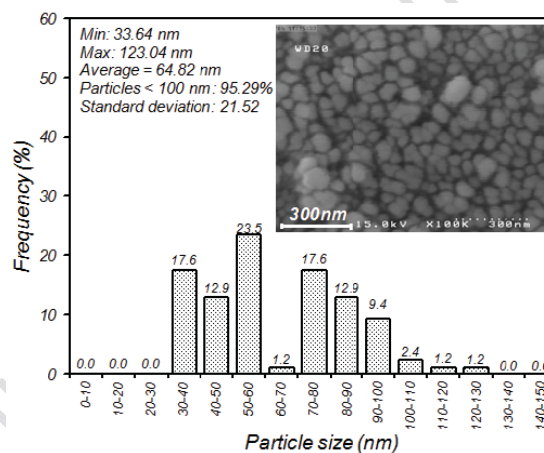


Figure 37: FESEM image and size distribution histogram of $\text{Pt}/\text{Al}_2\text{O}_3$ - CeO_2 nanocatalyst.

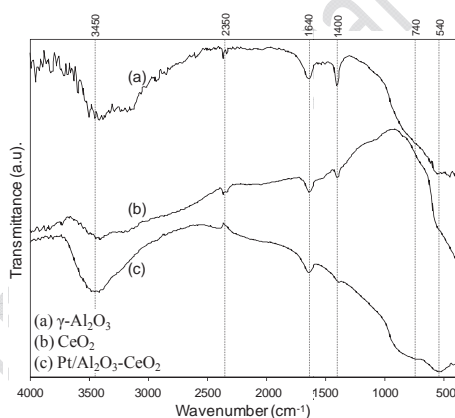


Figure 38: FTIR spectra of γ - Al_2O_3 , CeO_2 and $\text{Pt}/\text{Al}_2\text{O}_3$ - CeO_2 nanocatalyst.

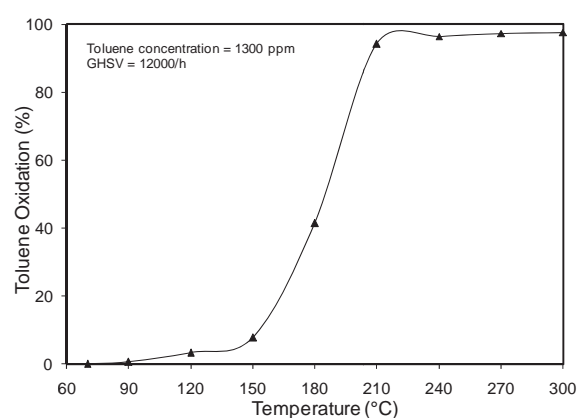


Figure 39: Oxidation performance of $\text{Pt}/\text{Al}_2\text{O}_3$ - CeO_2 nanocatalyst.



Conclusion:

Pt (1% wt)/Al₂O₃-CeO₂ (30% wt) nanocatalyst was prepared by impregnation and modified by glow discharge plasma in order to toluene oxidation. The low temperature catalytic activity and complete removal efficiency of toluene with high stability was achieved over the glow discharge plasma treated catalyst. Therefore, the plasma treated impregnation method is leading to an excellent preparation of supported catalysts, esp., those for VOCs oxidation.

References:

- [1] H. S. Kim et al., "Complete Benzene Oxidation over Pt–Pd Bimetal Catalyst Supported on γ -alumina: Influence of Pt–Pd Ratio on the Catalytic Activity", *Applied Catalysis A: General*, 280, (2), 125-131, 2005.
- [2] S. F. Tahir et al., "Catalytic Destruction of Volatile Organic Compound Emissions by Platinum Based Catalyst", *Chemosphere*, 38, (9), 2109-2116, 1999.



Ionic liquid-assisted formation of Co₃O₄ nanoparticles

S. Dabaghi^{a*}, A. Ahmadpour^a, F. F. Bamoharram^b, M. M. Heravi^c

^a Department of Chemical Engineering, Ferdowsi University of Mashhad, Mashhad, Iran

^b Department of Chemistry, Mashhad Branch-Islamic Azad University, Mashhad, Iran

^c Department of Chemistry, School of Sciences, Alzahra University, Tehran, Iran

E-mail: sh_dabaghi82@yahoo.com

Keywords : Cobalt Oxide, Nanomaterials, Ionic Liquids, X-ray diffraction

Introduction:

Nanosized transition metal oxides often exhibit enhanced physical, chemical, thermal, electrical, optical, or magnetic properties. A good example is crystalline cobalt oxide with nanometer-scale, an advanced material with wide potential applications as heterogeneous catalysis, Li-ion rechargeable batteries and so on. Traditional methods for the synthesis of Co₃O₄ need some special instruments, harsh conditions, and relatively high performance temperature. Therefore, there is a need for more effort towards the preparation of the spinel-type nano Co₃O₄ [1].

Ionic liquids seem to be well positioned to address the challenge of preparing Co₃O₄ nanoparticles, due to their negligible vapour pressure, recyclability, extended temperature range in the liquid state, low toxicity, high ionic conductivity, a wide range of viscosities and high chemical and thermal stability. In recent years, ionic liquids have been discovered to be excellent media in the formation and stabilization of metallic or metal oxide nano-sized objects [2].

Materials and methods:

Cobalt nitrate (Co(NO₃)₂·6H₂O), sodium hydroxide (NaOH) and hydrogen peroxide (H₂O₂) were purchased from Merc Company and used without further purification. Ionic liquid (1-hexyl-3-methylimidazolium hydroxide ([HMIM]OH) was synthesized according to the

literature. In a typical reaction, 0.7 g of $\text{Co}(\text{NO}_3)_2 \cdot 6\text{H}_2\text{O}$ was dissolved in the mixture of distilled water and $[\text{HMIM}]\text{OH}$. Then, 4mL of NaOH was added dropwise into the above solution with continuous stirring. After that, H_2O_2 was dropped in the mixture and mixed solution was maintained stirring at room temperature for 2h. The black–brown precipitate was separated by centrifugation and washed several times.

Result and discussion:

The XRD patterns of the product is shown in Figure 1. All diffraction peaks of the sample can be indexed to the cubic spinel Co_3O_4 . No characteristic peaks of impurity phases such as CoO and CoOOH are present, indicating high purity of the final products.

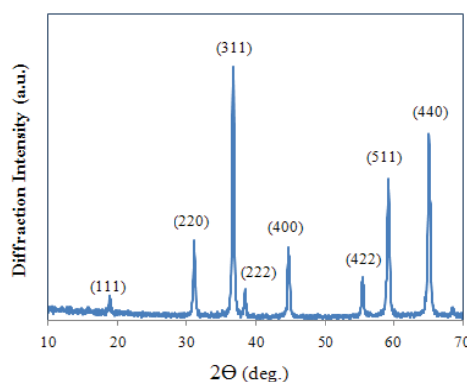


Figure 1: XRD pattern of the Co_3O_4 nanoparticles.

The FTIR spectrum of the final product also confirms the formation of Co_3O_4 nanocrystals. The cobalt oxide nanoparticles were also characterized by scanning electron microscopy (SEM). It can be seen remarkably that the sample consisted of a large quantity of dispersive nanoparticles with the size ranged from 20 to 40 nm.

Conclusion:

In this article, we describe a simple and facile method to prepare Co_3O_4 nanoparticles using $\text{Co}(\text{NO}_3)_2 \cdot 6\text{H}_2\text{O}$ and NaOH in the presence of an ionic liquid 1-hexyl-3-methylimidazolium hydroxide ($[\text{HMIM}]\text{OH}$) by a facile oxidation route. This route has promoted the reaction to



act at room temperature and simplified the reaction procedures. The ionic liquid [HMIM]OH has a significant influence on the reaction as an assisted agent.

Reference:

- [1] N. N. Binitha and etal; “Simple synthesis of Co_3O_4 nanoflakes using a low temperature sol–gel method suitable for photodegradation of dyes”; J Sol-Gel Sci Technol; 53, 466, 2010.
- [2] G. Clavel and etal; “Synthesis of Cyano-Bridged Magnetic Nanoparticles Using Room-Temperature Ionic Liquids”; Chem. Eur. J; 12, 3798, 2006.



Preparation and optical properties of Porphyrin nanoparticles

A. Eslami*, Z. Seyedi

Faculty of Chemistry, University of Mazandaran, P.O. Box 47416-95447, Babolsar, Iran

Email: Eslami@umz.ac.ir

Key word: Nanoparticle, Ion association, Porphyrin, Optical properties

Introduction:

Recent research entails investigations of non-covalent organic assemblies or aggregates on nanometer scales because their optical properties significantly differ from those of monomeric species [1]. Porphyrin nanoparticles are promising components of chemical advanced materials because of the rich photochemistry, stability and proven catalytic activity [2]. In particular, water soluble porphyrins are very interesting because their self-aggregation can be conveniently controlled by screening the charge repulsion through the ionic strength and pH [3]. In the present study, we attempt to prepare nanoparticles of a water-soluble porphyrin bearing a long alkyl chain as peripheral groups.

For this, an ion association method was employed in which formation of nano-sized particles occurs through ion pairing between moderately hydrophilic cationic porphyrin and tetraphenylborate (TPB) which acts as a hydrophobic anion.

Materials and method:

meso-Tetrakis(1-nonylpyridinium-4-yl)porphyrin chloride (TNPyP) was prepared based on a previous report. , Poly vinyl pyrrolidone (PVP; average Mw = 10,000 Aldrich) and sodium tetraphenylborate (Na TPB) were used as received.

The TNPyP nanoparticles have been synthesized by ion association method at room temperature. TNPyP solution was added to a solution of PVP and TFB under ultrasonic and sonication was continued for 15 min.



Instruments:

The size of nanoparticles was determined using a Malvern dynamic light scattering instrument. UV-Vis spectra were obtained by a Double Beam UV-Vis Spectrophotometer Braic 2100M. The fluorescence spectra were obtained by Perkin Elemer LS-5 luminescence spectrometer.

Result and discussion:

TNPyP nanoparticles were synthesized by ion association technique. In this process, PVP acts as a stabilizer and prevents particle agglomeration. These nanoparticles were stable in solution without precipitation for 30 days. The UV-Vis spectra exhibited large red shift compared to TNPyP solutions and the fluorescence spectra exhibited increase resolution compared to TNPyP solution.

Conclusion:

Ion association between TNPyP and TFB in aqueous solution produced TNPyP nanoparticles with narrow size distribution. This method prepared porphyrin under controlled aggregation. UV-Vis spectra of TNPyP nanoparticle exhibited a large red shift compared to aqueous solution of TNPyP and the fluorescence spectra exhibited high resolution compared to porphyrin solution.

References:

- [1] X. Gong , T. Milic , C.Xu , J. D. Batteas , C. M. Drain, J. Am. Chem. Soc. 124 (2002) 14290
- [2] Z. Ou, H.Yao, K.Kimura, J. Photochem. Photobio. A 189 (2007) 7
- [3] M. A. Castriano, A. Romeo , V. Villari , N. Micali , L. M. Scolaro, J. Phys. Chem. B 108 (2004) 9054



Preparation of MWCNT-Al₂O₃ hybrid for the production of nanoemulsion with the application in enhanced oil recovery

S.Khosravani^a, M.Alaei^{b*}, A.Ramazani^a, M.Ershadi^a, A.M.Rashidi^b

^a Department of Chemistry, University of Zanjan, Zanjan, P.O. Box: 45195-313, IRAN

^b Nanotechnology Research Center, Research Institute of Petroleum Industry (RIPI), P.O. Box:
14665-1998 Tehran, Tehran, I.R
Email: alaiem@ripi.com

Keywords: Nanoemulsion; Alumina; CNT-Al₂O₃ hybrid; Carbon nanotubes (CNT)

Introduction:

Nanoscience is the study of phenomena on a nanometer scale [1]. Carbon nanotubes (CNTs) have exceptional mechanical properties, particularly high tensile strength and light weight. CNT are being widely used as a support material for applications in heterogeneous catalysis [2], fuel cells [3] and sensors. Up to now, Al₂O₃ nanoparticles can be synthesized by many different methods, such as co-precipitation, sol-gel [4], thermal decomposition. But the descriptions concerning the preparation of Al₂O₃ nanoparticles by use of water-in-oil microemulsion have been limited [5]. Nanoemulsions are metastable dispersions of submicron droplets that have a significant surface tension, one of these applications is that the resulting nanoemulsions can be used in enhanced oil recovery [6].

Materials and methods:

Synthesis of CNTs-Al₂O₃ hybrid:

To prepare alumina nanoparticle, ammonia solution and sorbitol (solution A) added drop by drop to AlCl₃ and distilled water (solution B) and were mixed by magnetically stirring and adjusted the pH=10 with ammonia solution in this stage added opening cap MWCNT prepared by HNO₃ under the reflux condition for 18h, to make MWCNTs-Al₂O₃ hybrid, poured it to the hydrothermal cell to the temperature at 140°C for 24 h. The precipitates filtered and were

repeatedly washed using distilled water until neutralized. The as-prepared powder was dried in oven at 60°C overnight. Finally, the product was calcined at 800°C for 6 h under argon atmosphere Preparation of nanoemulsion:

Small amount of hybrid MWCNT-Al₂O₃ (spatula tip) is taken and triplet it weight of surfactant is taken and is added to 100 ml of distilled water and is mixed by magnetically stirring, then hybrid is added and sample dish is kept in ultrasonic bath. For preparation of nanoemulsion three types of surfactants, Triton X-100, cetyl Trimethyl Ammonium Bromide (CTAB), Sodium Dodecyl Benzene sulfonic Acid (SDBS), kerosene and n-butanol were used.

Result and discussion:

Figure 1 presents FE-SEM images of the as-prepared MWCNT-Al₂O₃ hybrid (10%) and (50%) respectively. It can be seen well-defined coating of MWCNTs with Al₂O₃ nanoparticles in the both hybrid with very good distribution.

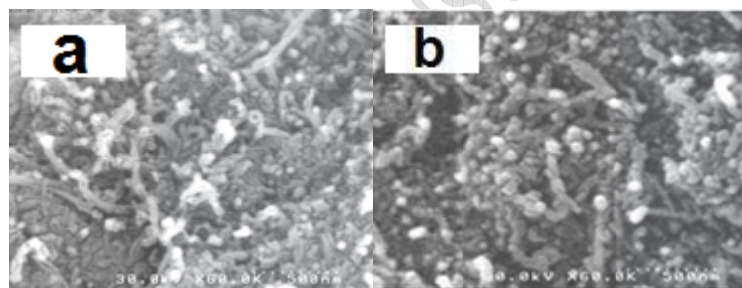


Figure 1.FE-SEM of the prepared a: MWCNT-Al₂O₃ hybrid (10%) and b: MWCNT-Al₂O₃ hybrid (50%)

Nanoemulsion that was prepared with MWCNT-Al₂O₃ hybrid (50%) has better stability in comparison to the nanoemulsion that was prepared with MWCNT-Al₂O₃ hybrid (10%).

Conclusions:

In this research, we have proposed an economical method for the preparation of MWCNT-Al₂O₃ hybrid in order to the production of nanoemulsion for enhanced oil recovery. Our results indicated that the as-prepared emulsion that was prepared with 50% hybrid is more stable than the other sample that was prepared with 10% hybrid.



References:

- [1] S. Chaturvedi, P.N. Dave, N.K. Shah. Journal of Saudi Chemical Society, 2011.
- [2] P. Serp, M. Corrias, P. Kalck, Appl. Catal. A-Gen. 253 (2003) 337.
- [3] J.S. Ye, H.F. Cui, Y. Wen, W.D. Zhang, G.Q. Xu, F.S. Sheu, Microchim. Acta 152 (2006) 267.
- [4] T. Horiuchi, T. Osaki, T. Sugiyama, K. Suzuki, T. Mori. Journal of Non-Crystalline Solids, 291 (2001) 187–198.

15th Physical Chemistry Conference

Molecular Dynamics Simulation of the Melting Process in Na₂₂ K₃₃ Nanoalloy

F. Arianfar*, M. Asgari , H. Behnejad

School of Chemistry, University College of Science, University of Tehran, Tehran, Iran

Email: Arianfar.fatemeh@gmail.com

Abstract

In this work, the melting process of (Na₂₂K₃₃) nanoalloy is studied and compared using dynamical criteria. We have used these criteria to evaluate thermal behavior of (Na₂₂K₃₃) nanoalloy and obtain an estimated value for its melting temperature through analyzing all these criteria.

Keyword: Nanoalloy, Molecular dynamics, Melting process criterion.

Computational method

In order to study melting process, several MD simulation in NVT ensemble are done starting from system's global minimum and incrementing from low temperatures to high temperature. Using Gupta potential to describe interaction between particles phase space trajectory saved as output to calculate properties of the system.

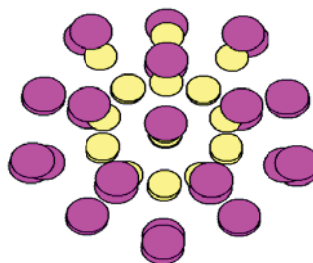


Fig.1.Optimal Structure of (Na₂₂K₃₃) Nanoalloys.

Results and discussion

Different criteria can be employed to study melting process of a system that are divided into three groups as follows: thermodynamical, geometrical and dynamical criterion.

I. Dynamics criteria:

a. velocity autocorrelation function

Velocity autocorrelation function, $c(t) = \langle v(t_0)v(t) \rangle$, demonstrates how the present velocity of a particle is related to its previous value, and how it is effective on its subsequent velocity. In this work, we calculate Velocity autocorrelation function of (Na₂₂K₃₃) nanoalloy constituent atoms of each nanoalloy individually using following relation.

Velocity autocorrelation function, $c(t) = \langle v(t_0)v(t) \rangle$, demonstrates how the present velocity of a particle is related to its previous value, and how it is effective on its subsequent velocity.

In this work, we calculate Velocity autocorrelation function of (Na₂₂K₃₃) nanoalloy constituent atoms of each nanoalloy individually using following relation^[1].

$$C^{(i)}(t) = \frac{\langle v_i(t_0)v_i(t+t_0) \rangle}{\langle v_i(t_0)v_i(t_0) \rangle} \quad (1)$$

Velocity autocorrelation function, $c(t) = \langle v(t_0)v(t) \rangle$, demonstrates how the present velocity of a particle is related to its previous value, and how it is effective on its subsequent velocity. In this work, we calculate Velocity autocorrelation function of (Na₂₂K₃₃) nanoalloy constituent atoms of each nanoalloy individually using relation (1).

b. Power spectrum

Another useful quantity which can be handled to study of dynamical behavior of nanoalloys is power spectrum, $\Omega(\omega)$, that can be calculate from velocity autocorrelation function by a Fourier transform as follows^[3].

$$\Omega^{(i)}(\omega) = 2 \int_0^\infty C^{(i)}(t) \cos(\omega t) dt \quad (2)$$

Spectroscopically, the infrared spectra of the system belong to vibrational motions of atoms, so this function can project out the underlying frequencies of the individual atoms in this region^[2].

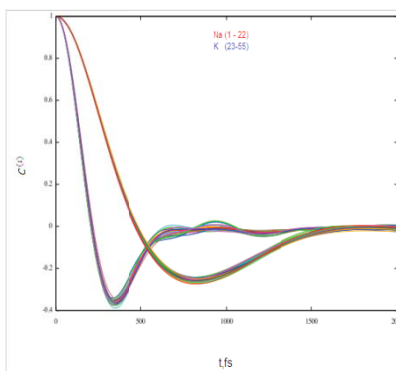


Fig.2. Velocity autocorrelation functions of all constitute atoms of (Na₂₂K₃₃) in temperature 200 °K.

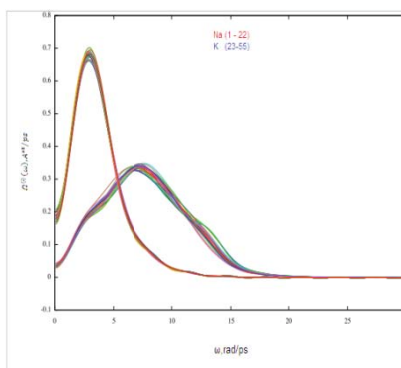


Fig.3Power spectrums of constitute atoms of (Na₂₂ K₃₃) in temperature 200 ° K.

Conclusions:

The results of our simulations show the melting temperature of (Na₂₂K₃₃) nanoalloy to be around 200°K by using of dynamical criteria .

References:

- [1] Haile, J. M. (1992) Molecular dynamics simulation: Elementary methods Wiley-Inter science.
- [2] Hsu, P.J.,J.S.Luo,etal.(2008). "Melting Scenario in metallic clusters". The Journal of Chemical Physics.**129**(19):194302-15.
- [3]Jellinek,J.,T. L. Beck, etal. (1986)."Solid-liquid phase changes in simulated iso energetic Ar[sub 13]". The Journal of Chemical Physics **84**(5):2783-2794.



Molecular Dynamics Simulation of the Melting Process in Au₁₅Ag₄₀ Nanoalloy.

F. Arianfar*, M. Asgari , H. Behnejad

School of Chemistry, University College of Science, University of Tehran, Tehran, Iran

Email: Arianfar.fatemeh@gmail.com

Keyword: Nanoalloy, Molecular dynamics, Melting process criterion

Abstract:

In this work, the melting process of (Au₁₅Ag₄₀) nanoalloy is studied and compared using different thermo dynamical and geometrical criteria. We have used these criteria to evaluate thermal behavior of (Au₁₅Ag₄₀) nanoalloy and obtain an estimated value for its melting temperature through analyzing all these criteria.

Computational method

In order to study melting process, several MD simulation^[2] in NVT ensemble are done starting from system's global minimum and incrementing from low temperatures to high temperature. Using Gupta potential to describe interaction between particles phase space trajectory saved as output to calculate properties of the system.

Results and discussion

Different criteria can be employed to study melting process of a system that are divided into three groups as follows: thermo dynamical, geometrical and dynamical criterion.

I. Thermodynamics criteria:

II. Caloric curve;

As a thermo dynamical criterion^[1], the caloric curve of nanoalloy (Au₁₅Ag₄₀) shows the variation of mean internal energy with temperature for a canonical ensemble. As shown in

Fig.1, increasing the configuration energy with temperature deviates from linear regime after $T=500^{\circ}\text{K}$. This status continues up to $T=535^{\circ}\text{K}$ in which the configuration energy increasing in linear again.

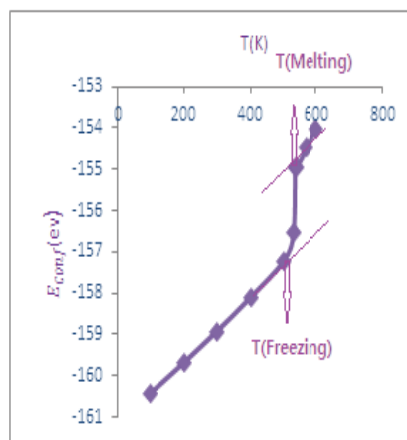


Fig.1. Caloric Curve of the $(\text{Au}_{15}\text{Ag}_{40})$ Nanoalloys

a. Heat capacity:

In canonical ensemble, this quantity is related to energy fluctuations^[2].

$$C_v(T) = \frac{\langle E_{total}^2 \rangle_t - \langle E_{total} \rangle_t^2}{k_B T^2} \quad (1)$$

As shown in the fig.2, the heat capacity increases with temperature straightly by a mild slope initially. Although, the highest pick on heat specific graph (530°K) is defined as melting temperature, but it should be considered that there is still solid phase at this and even higher than this temperature and coexistence will be extended up to 535°K .

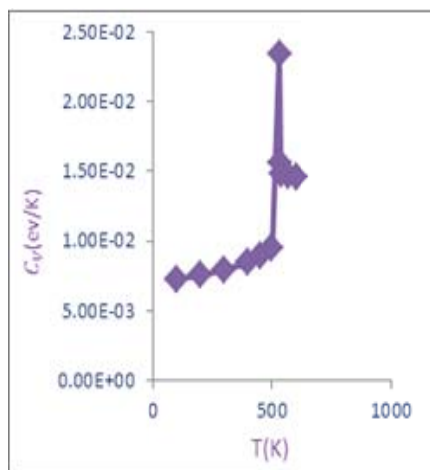


Fig.2. Heat capacity of Au₁₅Ag₄₀) versus temperature.

II. Geometrical criteria:

The distance fluctuation criteria;

Distance fluctuation may also be used as a geometrical criterion to determine of the melting point in nanoalloys. In this work, we study the root-mean-square (rms) relative bond length fluctuation, δ , which is also known as the Lindemann-Like parameter^[3].

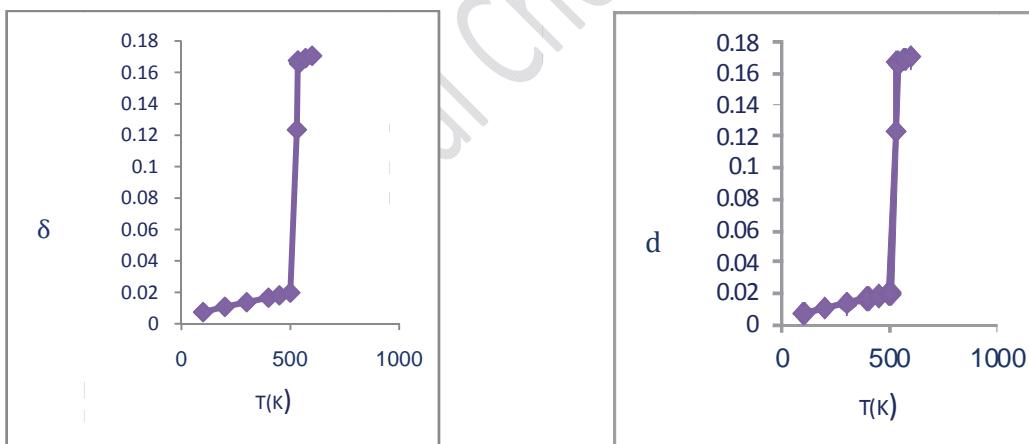


Fig. 3 . The distance fluctuations of(Au₁₅ Ag₄₀) Nanoalloys as a function of temperature.

Conclusions

The results of all our simulations show the melting temperature of (Au₁₅Ag₄₀) nanoalloy to be around 535°K by using all of thermo dynamical, geometrical and criteria.



References

- [1] Ferrando, R.J. Jellinek, et al; (2008). "Nanoalloys: From Theory to Application of Alloy Cluster and Nanoparticles. Chemical Reviews **108**(3): 845-910.
- [2] Haile, J.M. (1992) Molecular dynamics simulation: Elementary methods Wiley-Inter science.
- [3] Lindemann, F. A. (1910). Phys. Z. **11**:609.



Optimization of bovine serum albumin fibrillation: use of response surface methodology and simple Congored testing

Amir Arasteh^a, Mehran Habibi-Rezaei*^b, Azadeh Ebrahim-Habibi^c, Ali Akbar Moosavi-Movahedi^d

^aDepartment of Biology, Science and Research Branch, Islamic Azad University, Tehran, Iran

^{b*}Department of Biotechnology, Faculty of Science, University of Tehran, Tehran, 14155-6455, Iran

^cEndocrinology and Metabolism Research Center, Tehran University of Medical Sciences, Tehran, Iran

^dInstitute of Biochemistry and Biophysics, University of Tehran, Tehran, Iran

Email: mhabibi@khayam.ut.ac.ir

Key Words: Bovine Serum Albumin, Fibrillation, Optimization, Congored

Introduction:

Amyloid fibrils are considered as nanostructures that could be formed by the self-assembly of peptides and proteins [1]. In recent years, amyloid fibrils are being used as experimental nanomaterials [2]. From this point of view, increasing aggregation amount could be desirable. In this study, bovine serum albumin was used as a model protein whose aggregation process was optimized.

Materials and Methods:

Response surface methodology (RSM) was used in a design that contained a total of 30 experimental trials. The first 24 were organized in a factorial design and from 25 to 30 involve the replications of the central points. Data obtained from RSM were subjected to the analysis of variance (ANOVA) and analyzed using a second order polynomial equation. Subsequent testing of the suggested experimental parameters was done *in vitro* with Congo red spectrophotometric assay [1].

Results and discussion:



Protein concentration, pH, temperature and time of incubation were the variables used in this experiment. Responses were assessed by measuring absorbance in 540 nm (characteristic of amyloid formation), maximal wavelength and absorbance in maximal wavelength. Concomitant effects of variables were assessed in surface plots that each considered two of the variables. Interestingly, the pattern obtained by monitoring absorbance in 540 nm and absorbance in maximal wavelength were identical.

Conclusions:

Use of Congo red spectrophotometric test, as a simple and affordable assay could be suggested as a first test for assessing fibril formation of proteins. Absorbance in maximal wavelength could be used as a significant indication for fibril formation.

References:

- [1] Holm NK, Jespersen SK, Thomassen LV, Wolff TY, Sehgal P, Thomsen LA, Christiansen G, Andersen CB, Knudsen AD, Otzen DE (2007) Aggregation and fibrillation of bovine serum albumin. *Biochimica et Biophysica Acta (BBA)-Proteins & Proteomics* 1774:1128-1138
- [2] Pilkington SM, Roberts SJ, Meade SJ, Gerrard JA (2010) Amyloid fibrils as a nanoscaffold for enzyme immobilization. *Biotechnology progress* 26:93-100



Dye Adsorption isotherm modeling onto Functionalized Nanoporous Silica

Majid Hamzehloo^{*}, Bahman Hasanazade, Afsaneh Shahbazi, Alireza Badiei

School of Chemistry, College of Science, University of Tehran, P.O. Box 14155-6455, Tehran, Iran.

¹ Corresponding author

Introduction:

The preparation of nano-structured silicas since 1992 until now has opened a wide field of applications. In comparison with other nano-structured silica materials, SBA-15 exhibits thicker pore wall, higher pore volumes, and wider pores. The silica wall surface of nanoporous silica can be modified with organic groups to tailor their properties and achieve specific purposes. Among the main uses of nanoporous silicas, it is well-known the design of adsorbents for environmental cleanup and many reports can be found [3, 4, 5]. Removal of dyes from aqueous solutions is one of the major problems on wastewater treatment because they are mostly toxic. Malachite green, a triphenylmethane dye, has been widely used for the dyeing of leather, wool and silk as well as used as a fungicide and antiseptic in aquaculture industry to control fish parasites and disease [3]. But recently, MG has been found exhibiting carcinogenic, genotoxic, mutagenic and teratogenic properties. Among the techniques for removal of dyes from wastewater, adsorption has been proved to be an effective and attractive process because of its inexpensive nature and ease of operation.

Methods:

SBA-15 nanoporous silica was synthesis of SBA-15 similar to that described in the literature by using Pluronic P123 nonionic surfactant as a structure directing agent and tetraethyl orthosilicate under acidic conditions [1, 2]. In a typical surface modification process, calcined SBA-15 (5 g) was refluxed in dry toluene (200 mL). After 2 h of stirring and refluxing, APTES (5.5 mL) was slowly added to the mixture and refluxed at 100 °C for 24 h. amine-modified mesoporous (NH₂-SBA-15) were collected by filtration. Subsequently, NH₂-SBA-15 (5 g) was suspended into the flask containing carboxylic ligand under argon condition. The



pore size and wall thickness of mesoporous SBA-15 were obtained by X-ray diffraction (XRD), N₂ adsorption-desorption, and FTIR.

The adsorption capacity of the material was investigated in synthesized wastewater. The equilibrium adsorption capacity of adsorbent for dye was studied and extrapolated using linear Freundlich and Langmuir isotherms.

Results and discussion:

The results of XRD, nitrogen adsorption-desorption, and FTIR spectroscopy confirmed that the organic functional groups were successfully grafted on the SBA-15 surfaces.

The behavior of the adsorbent for the adsorption of MG dye from aqueous solutions was showed that the overall process was fast and the kinetic was well-fitted by pseudo-second-order kinetic model. The obtained experimental data were well agreed with Freundlich model. Therefore, the maximum amount of multi-layer dye adsorbed could be predicted as 120 mg/g. This study shows that the functionalized silica with carboxylic groups is promising sorbent for the removal of cationic dye from aquatic solutions.

Conclusions:

The nanoporous SBA-15 functionalized with carboxylic groups can be used in the adsorption and separation of MG and other cationic dye from aqueous solutions. This adsorbent may be promising in the field of the removal of dyes from drinking waters and industrial wastewaters.

References:

- [1] Badii, A., H. Goldooz, G. M. Ziarani and A. Abbasi (2011), J. Colloid Interface Sci., Vol. 357, No. 1.
- [2] Shahbazi, A., H. Younesi and A. Badii (2011), Chem. Eng. J., Vol. 168, No. 2.
- [3] C.-H. Huang, K.-P. Chang, H.-D. Ou, Y.-C. Chiang, C.-F. Wang, , Microporous and Mesoporous Materials 141(2011) .109-102.
- [4] P.V. Messina, P.C. Schulz, Journal of Colloid and Interface Science 299(2006) .320-305



- [5] X. Wu, K.N. Hui, K.S. Hui, S.K. Lee, W. Zhou, R. Chen, D.H. Hwang ,Y.R. Cho, Y.G. Son, *Chemical Engineering Journal* 180(2012) .98-91.

15th Physical Chemistry Conference



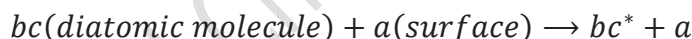
Quantum scattering theory of diatomic molecules with nanolayers

A. Maghari , N. Safaei

Department of Chemistry, University of Tehran, Tehran, Iran

(Email: Safaei@ut.ac.ir)

In this work, we have theoretically studied the adsorption and scattering of diatomic molecules on nano surfaces by solving the Lippmann-Schwinger equation, which have been previously studied by monte-carlo and molecular dynamics simulations [1,2]. Scattering of atoms and molecules from a surface when gas – phonon interactions are negligible (stationary surface) enables a comparison between very accurate experimental results and theoretical ones obtained by exact quantum mechanical scattering calculations. Such a comparison props the interaction potential of the atom or molecules with a solid surface and enlights the dynamical processes, which accrue on the solid surface. In the scattering of molecules from the stationary surfaces and nanolayers, presence of surface enables energy transfer among the degrees of freedom of the incoming molecules (excitation channel of scattering).[3,4]



In this work, we used the Lippmann-Shewinger equation for calculating the transition matrix elements in momentum space for scattering of diatomic molecule from the corrugated nano-surface. We have used here the Morse potential in normal direction (z-direction) of a corrugated surface with primitive translation vectors a_0, b_0 :

$$V(x, y, z) = V(z) \times \cos\left(\frac{2\pi x}{a_0}\right) \times \cos\left(\frac{2\pi y}{b_0}\right), \quad (1)$$

$$V(z) = De[e^{-2a\bar{z}} - 2e^{-a\bar{z}}]$$

We assume that the potential interaction between surface and diatomic molecule divides in two terms, including interaction of each atom with surface, i.e.

$$V = Vac + Vab$$

By this assumption the transition matrix element can be written as:

$$\langle p' | T | p \rangle = \langle p' | Tab | p \rangle + \langle p' | Tac | p \rangle \quad (2)$$

Using the first Born approximation, the T-matrix can be obtained as

$$\langle p' | \mathcal{T}ab | p \rangle = \langle p' | Vab | p \rangle, \quad \langle p' | \mathcal{T}ac | p \rangle = \langle p' | Vac | p \rangle \quad (3)$$

For a potential of the form $(X, Y, Z) = V(Z) \times V(X) \times V(Y)$, the T-matrix element is obtained as follows:

$$\begin{aligned} \langle p' | \mathcal{T}ac | p \rangle = & \int d\bar{k}_1' e^{-i(p\bar{z}-p\bar{z}')\bar{k}_1'} Vac(\bar{k}_1') \\ & \times \int d\bar{k}_2' e^{-i(p\bar{y}-p\bar{y}')\bar{k}_2'} Vac(\bar{k}_2') \\ & \times \int d\bar{k}_3' e^{-i(p\bar{x}-p\bar{x}')\bar{k}_3'} Vac(\bar{k}_3') \\ & \times \int dr' \Phi^*(r') \Phi(r') \int \eta(r', \theta', \varphi') Y^*(\theta', \varphi') Y(\theta', \varphi') d\varphi' d\theta' \end{aligned} \quad (4)$$

where

$$\eta(r', \theta', \varphi') = e^{-i(p\bar{z}-p\bar{z}')\alpha(\theta', \varphi')r'} e^{-i(p\bar{y}-p\bar{y}')\beta(\theta, \varphi)r'} e^{-i(p\bar{x}-p\bar{x}')\gamma(\theta', \varphi')r'} \quad (5)$$

$\Phi(r')$ and $Y(\theta', \varphi')$ are vibrational-rotational and rotational wave functions for a diatomic molecule in ground state. The star notation stands for the excited states. By substituting Eq. (1) into (4), the transition matrix elements for Morse potential of corrugated surface are calculated as:

$$\begin{aligned} \langle p' | \mathcal{T}ac | p \rangle = & De \left[\left(\frac{e^{[i(p\bar{z}'-p\bar{z})-2a]k_{1c}]-1}}{-ip\bar{z}'-ip\bar{z}-2a} \right) - 2 \left(\frac{e^{[i(p\bar{z}'-p\bar{z})-a]k_{1c}]-1}}{-ip\bar{z}'-ip\bar{z}-a} \right) \right] \\ & \times \frac{\sqrt{2\pi}}{2} \left[\delta \left(p\bar{y} - p\bar{y}' - \frac{2\pi}{b_0} \right) + \delta \left(p\bar{y} - p\bar{y}' + \frac{2\pi}{b_0} \right) \right] \\ & \times \frac{\sqrt{2\pi}}{2} \left[\delta \left(p\bar{x} - p\bar{x}' - \frac{2\pi}{a_0} \right) + \delta \left(p\bar{x} - p\bar{x}' + \frac{2\pi}{a_0} \right) \right] \end{aligned} \quad (6)$$

$\times \psi$

Where

$$\psi = \int dr' \Phi^*(r') \Phi(r') \int \eta(r', \theta', \varphi') Y^*(\theta', \varphi') Y(\theta', \varphi') d\varphi' d\theta' \quad (7)$$

The result for $\langle p' | \mathcal{T}ab | p \rangle$ is similar to $\langle p' | \mathcal{T}ac | p \rangle$.

References:

- [1] M. R. Wattenbarger, V. A. Bloomfield, D. F. Evans, *Macromolecules*, 25 (1), (1992)



- [2] Vivek P. Raut, Madhuri A. Agashe, Steven J. Stuart, and Robert A. Latour, *Langmuir*, 21, (2005)
- [3] U. Peskin and N. Moiseyev, *J. Chem. Phys.*, 96, 3 (1992)
- [4] E. Engdahl, N. Moiseyev and T. Maniv, *J. Chem. Phys.*, 94, 1636 (1991)

15th Physical Chemistry Conference



Quantum Mechanics & Spectroscopy



Three-particle quantum scattering via separable potentials: Application to statistical mechanics

V. Moheb Maleki and A. Maghari

Department of Physical Chemistry, College of Science, University of Tehran, Tehran, Iran

E-mail: vahdat_mohebmaleki@yahoo.com

Abstract:

In the present work, we have calculated three-body system transition matrices in the presence of a non-local separable potential and any other scattering properties such as poles of transition matrix, phase shift, cross sections, time delay, cross sections and collision integrals. Analytical expressions for some equilibrium thermodynamics properties, such as the Helmholtz free energy and heat capacities as well as some non-equilibrium thermophysical properties, such as collision cross sections and transport collision integrals have been studied.

Keywords: Faddeev equation, Three-body scattering, thermophysical properties

Introduction:

From the Faddeev point of view, in a three-body system there are three different two-body subsystems. The idea is to sum up the pair forces in each two-body subsystem to infinite order, and then in a second step among all three particles. The approach based on the direct use of the Lippmann-Schwinger equation is found to be inapplicable in this case. In fact, it can be shown that even for a two-particle system the Lippmann-Schwinger equation does not have unique solution, if we take in to account the motion of the center of mass of the system. A similar indeterminacy in the solution of the Lippmann-Schwinger equations is also found for systems consisting of three or more particles. In recent works, the scattering properties of a two-body system with zero and non-zero angular momentum via a separable potential of rank 2 was calculated and then applied to obtain the equilibrium statistical mechanical properties of fluids. A generalized formulation for the partial-wave scattering wavefunction and its properties, such as the phase shift and time delay, subjected to the potential scattering in a given partial-wave form factor with arbitrary angular momentum has recently been

developed. Our generalization also allows for the calculation of the non-equilibrium thermodynamic properties as well as equilibrium thermodynamic properties. In this work our previous results of three-body scattering properties have been used in the framework of quantum statistical mechanics and of the corresponding kinetic theory to calculate the equilibrium and non-equilibrium thermophysical properties.

The Faddeev Method:

The indeterminacy of the Lippmann-Schwinger equations can be removed by means of an appropriate rearrangement of the equations; the equations obtained as the result of such a rearrangement are usually called Faddeev equations. We now adopt the following notation and conventions for a system of three non-relativistic spinless particles: Let the initial state consist of particle 1 impinging on a bound state of 2 and 3. The split-up of the hamiltonian corresponding to this arrangement is

$$\begin{aligned} H &= H_1 + H'_1 \\ H_1 &= H_0 + V_{23} \quad H'_1 = V_{12} + V_{13} \end{aligned} \quad (1)$$

The Green function of the simple hamiltonian H_1 is given by

$$g_1(E) = (E - H_0 - V_{23})^{-1} \quad (2)$$

The T operator appropriate to the description of collision in which the final arrangement is again 1(2,3) is called T_{11} . The \mathbf{T} matrix is obtained from it by taking matrix elements between eigenstates of H_1 . Its equation is

$$T_{11} = H'_1 + H'_1 g_1^+ T_{11} = V_{12} + V_{13} + (V_{12} + V_{13}) g_1^+ T_{11} \quad (3)$$

T operators appropriate to rearrangements in which the final state is 2(1,3) or 3(1,2) are called T_{21} and T_{31} , respectively. They can be obtained from T_{11} by the equations

$$\begin{aligned} T_{21} &= H'_2 + H'_2 g_1^+ T_{11} = V_{23} + V_{21} + (V_{23} + V_{21}) g_1^+ T_{11} \\ T_{31} &= H'_3 + H'_3 g_1^+ T_{11} = V_{31} + V_{32} + (V_{31} + V_{32}) g_1^+ T_{11} \end{aligned} \quad (4)$$

Results and discussion:

In this work the analytical expression that we obtained for T_{11} is as follow:

$$\begin{aligned} \langle p_r, p_{23} | T_{11} | p'_r, p'_{23} \rangle \\ = \sum_{j=2}^3 \sum_{n,m,k=1}^2 \gamma_{nm}^{1j} v_k^{1j} \chi_k^{1j}(p_r, p_{23}) \chi_k^{1j}(p_r, p_{23})^* \langle \chi_n^{1j} | \chi_m^{1j} \rangle \langle \chi_k^{1j} | \Lambda^{-1} | \chi_n^{1j} \rangle \end{aligned} \quad (5)$$



where γ_{nm}^{1j} are coefficients which can be found by applying the separable potential model, v_k^{1j} is the attractive (or repulsive) coupling strength and $\chi_k^{1j}(p_r, p_{23})$ is the state of the system with angular momentum quantum number l , which is a real number in the unitary case. Analytical expression for $\chi_k^{1j}(p_r, p_{23})$, $\langle \chi_n^{1j} | \chi_m^{1j} \rangle$ and $\langle \chi_k^{1j} | \Lambda^{-1} | \chi_n^{1j} \rangle$ are as follow:

$$\chi_k^{1j}(p_r, p_{23}) = \frac{2^{2l} l! (2l+1) (a_k^{1j} a_k^{23})^{\frac{2l+1}{2}}}{\pi^{\frac{3}{2}} \Gamma(l+\frac{1}{2})} \frac{p_r^l p_{23}^l P_l(\cos\theta_{pr}) P_l(\cos\theta_{p23})}{[(a_k^{1j})^2 + p_r^2]^{l+1} [(a_k^{23})^2 + p_{23}^2]^{l+1}} \quad (6)$$

$$\langle \chi_n^{1j} | \chi_m^{1j} \rangle = \frac{1}{\pi} \left[\frac{\pi 2^{l+1} l! (2l-1)!!}{\Gamma(l+\frac{1}{2})} \right]^2 \frac{(a_n^{1j} a_m^{1j} a_n^{23} a_m^{23})^{l+\frac{1}{2}}}{(a_m^{1j} + a_n^{1j})^{2l+1} (a_m^{23} + a_n^{23})^{2l+1}} \quad (7)$$

$$\langle \chi_k^{1j} | \Lambda^{-1} | \chi_n^{1j} \rangle = \frac{4(a_m^{1j} a_n^{1j} a_m^{23} a_n^{23})^{\frac{1}{2}}}{(a_m^{23} + a_n^{23})} \frac{a_m^{1j} [(a_n^{23} + 2i\omega_n)\omega_n + a_m^{23}(\omega_n - 2ia_n^{23})]}{[(a_m^{1j})^2 - (a_n^{1j})^2] [(a_m^{23})^2 + \omega_m^2] [(a_n^{23})^2 + \omega_n^2]} \quad (8)$$

where $\Gamma(l + \frac{1}{2})$ is the gamma function and $\omega_n = \sqrt{q^2 + (a_n^{1j})^2}$ and $\omega_n = \sqrt{q^2 + (a_n^{1j})^2}$.

Moreover, the obtained expressions are applied to obtain the scattering and thermodynamics properties of three-body systems from the three-body potential model in the Faddeev approximation. The potential parameters are adjusted to fit the two-body phase shift data and then applied to calculate the third virial coefficients of some appropriate systems. By calculating these scattering properties we have extended our previous work for obtaining the analytic expressions for both equilibrium and non-equilibrium thermophysical properties of fluids at moderately densities.

References:

- [1] Maghari, A. and Dargahi, M., *J. Phys. A: Math. Theor.* **41** (2008) 275306
- [2] Maghari, A. and Tahmasbi, N., *Physica A* **382** (2007) 537
- [3] Maghari, A. and Tahmasbi, N. *J. Phys. A: Math. Gen.* **38** (2005) 4469
- [4] Newton R G., *Scattering Theory of Waves and Particles* (New York: McGraw-Hill), 1966
- [5] Phillips, A.C., *Phys. Rev.* **142** (1966) 985
- [6] Ueta, K., Miyake, H. and Bund, G.W., *Phys. Rev.* **59C** (1999) 1806.

Laser Mass Spectrometry of Alkali-Earth Halides

M. Mirian, M. Tabrizchi, F. Abyar, H. Farrokhpour

Email: mmirian66@yahoo.com

Department of Chemistry, Isfahan University of Technology, Isfahan, Iran, 84156-83111

Keywords: Time-of flight, Alkali-Earth Halides, Isotope pattern, Detection devices.

Introduction:

Time of flight (TOF) mass spectrometry is one of the most important analyzing techniques which works based on acceleration and separation of ions in vacuum. The advantage of TOF instrument is that it can readily reach mass resolving power ($m/\Delta m$) of 1000–10000 with very high efficiency compared to other detection devices including magnetic sectors, quadrupole and ion traps. In this work, mass spectra of earth alkali halides including MgCl_2 , CaCl_2 , SrCl_2 and BaCl_2 ; and their mixtures have been recorded using a laser ionization technique and a home made TOF mass spectrometer. The spectra were assigned and the effects of the laser intensity and acceleration voltages on the spectra were investigated.

Experimental:

The TOF mass spectrometer, constructed in the Isfahan University of Technology, is schematically shown in Fig.1. The solid sample coated on the repeller of the accelerator and was irradiate by laser light. The produced ions accelerated in region A and fly in a field free region. The ions are separate based on the mass to charge ratio (m/z). The chamber was under high vacuum (10^{-7} mbar).

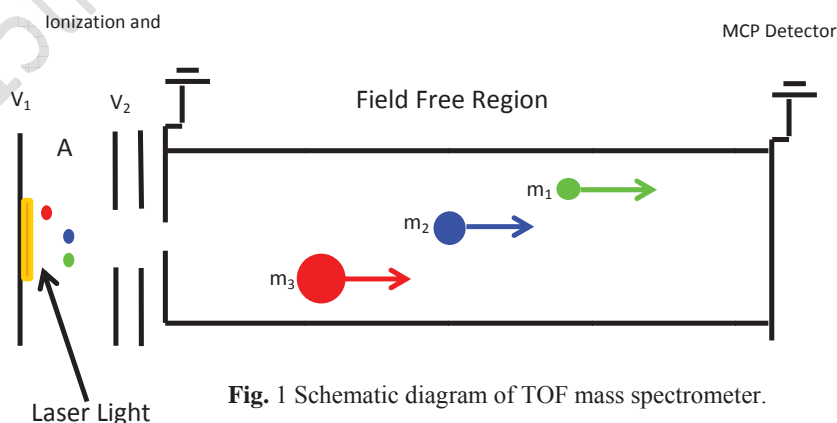


Fig. 1 Schematic diagram of TOF mass spectrometer.

Result and discussion:

Fig. 2 and 3 shows the recorded TOF spectra of SrCl_2 and BaCl_2 , respectively. Molecular ion patterns were used for assignment. Ba and Cl have five and two stable isotopes, respectively. This makes several types of BaCl^+ ion. To simulate the mass pattern of BaCl , the relative population of each isotope was calculated based on the natural abundances of each atom. The solid lines in Fig. 2 show the simulated pattern of the recorded spectrum related to Ba isotopes and the different combinations of BaCl . Fig.3 also demonstrates the TOF spectrum of SrCl . Sr^+ and SrCl^+ ions are evident in the spectrum.

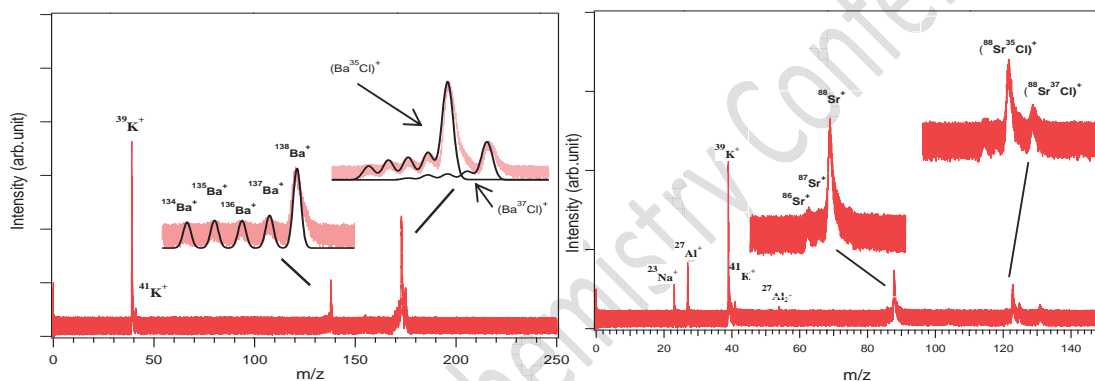


Fig.2 &3. TOF spectra of BaCl_2 and SrCl_2 .

Conclusions:

Time-of-flight mass spectra of CaCl_2 and SrCl_2 have been recorded using laser as ionization source. The spectra includes AE^+ and AEX^+ where AE and X stands for alkali earth and halide, respectively. The simulated isotope pattern confirms the mass assignment.

References:

- [1] M. Tabrizchi, Construction of a laser ionization time-of-flight mass spectrometer, Iranian Patent No. 73361, 2012.
- [2] M.Yildirima, O.Siseb, M.Doganb, H.S. Kilic, Designing multi-field linear time-of-flight mass spectrometers with higher-order space focusing, J. Mass Spectrom. 2010; 291:1–12.



Determination and comparison of formation constants of bis(4-amino-3-penten-2-onato) copper(II) and nickel(II)

M. Jamialahmadi^{*a}, S. F. Tayyari^a

^aChemistry Department, Ferdowsi University of Mashhad, Mashhad, 91775-1436, Iran

*Email: Jamialahmadimina@Yahoo.com

Keywords: bis(4-amino-3-penten-2-onato) copper(II), bis(4-amino-3-penten-2-onato) nickel(II), GAUSSIAN 03, Formation constant, B3LYP/6-311G*.

Introduction:

Information concerning the role of the metal ion in the process of chelation is of primary importance to the understanding of the nature of chemical bonding. Equilibrium constants of the various complexes, have been determined by experimental methods such as volume metric titration [1], potentiometric measurements [2,3], pH measurements with computer treatment of the data [4,5], ESR analysis [6], spectrophotometric measurements [7,8], and distribution method [9]. However, there is no experimental method for determination of β -ketoamine complexes.

The aim of this work is to calculate the formation constants of bis(4-amino-3-penten-2-onato) copper(II), (Cu(APO)₂), and bis(4-amino-3-penten-2-onato) nickel(II), Ni(APO)₂ by DFT methods. Equilibrium constant is related to the standard Gibbs free energy change for the reaction by $\Delta G^0 = -RT \ln K_f$ equation. Since, G^0 s can be obtained from Gaussian program, ΔG^0 and then K_f for each complex can be calculated.

Method of analysis:

In this study, the molecular equilibrium geometry, harmonic force field, vibrational frequencies, and thermodynamic properties of Cu(APO)₂ and Ni(APO)₂ were computed with the GAUSSIAN 03 software system [10], using 6-311G* basis sets.

Results and discussion:

The optimized geometries of trans Cu(APO)₂ and Ni(APO)₂ are shown in Fig. 1.

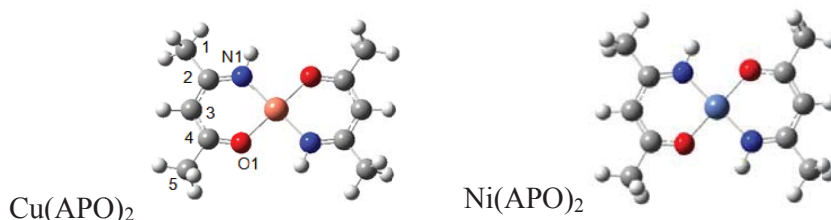
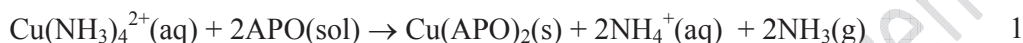


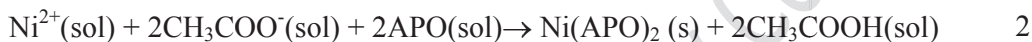
Fig. 1 The geometries of trans Cu(APO)₂ and Ni(APO)₂ optimized at B3LYP/6-311G* level.

Cu(APO)₂ is formed in ammonia media and the equation of its formation can be expressed as



The thermodynamic properties of Cu(NH₃)₄²⁺(aq), APO(sol), NH₄⁺(aq), NH₃(g), and Cu(APO)₂(g) were calculated in corresponding solvents.

Ni(APO)₂ was formed in alcoholic solutions by the equations



By using the G⁰s of all species in above equations the formation constants of Cu(APO)₂ and Ni(APO)₂ were obtained 5.57×10¹² and 9.02×10¹⁴, respectively. These results are in good agreement with the vibrational frequencies of O-M-O/N-M-N stretching bands of Cu(APO)₂ (466 cm⁻¹) [11] and Ni(APO)₂ (479 cm⁻¹) [12].

Conclusion:

The thermodynamic properties of Cu(APO)₂ and Ni(APO)₂ were computed at the B3LYP/6-311G* level and by using the G⁰s of all species involved in the preparation of Cu(APO)₂ and Ni(APO)₂, the formation constants of these complexes were calculated. According to theoretical calculations, the formation constant of Ni(APO)₂ is more than that of Cu(APO)₂. This result is in accordance with the vibrational frequencies of O-M-O/N-M-N stretching bands.

References:

- [1] L. G. Van Uitert, W. C. Fernelius, B. E. Douglas, *J. Am. Chem. Soc.* 75 (1953) 2736.
- [2] J. J. Cruywagen, A. G. Draaijer, J. B. B. Heyns, E. A. Rohwer, *Inorganica Chimica Acta* 331 (2002) 322.
- [3] M. S. Masoud, H. H. Hammud, H. Beidas, *Thermochemica Acta*, 381 (2002) 119.



- [4] J. J. Cruywagen, A.G. Draaijer, J. B. B. Heyns, E. A. Rohwer, *Inorganica Chimica Acta* 331 (2002) 322.
- [5] T. S. Planka, N. Nagy, A. Rockenbauer, L. Korecz, *Polyhedron* 19 (2000) 2049.
- [6] T. S. Planka, N. Nagy, A. Rockenbauer, L. Korecz, *Polyhedron* 20 (2001) 995.
- [7] Y. W. Lu, G. Laurent, H. Pereira, *Talanta* 62 (2004) 959.
- [8] T. Pivetta, M. D. Cannas, F. Demartin, C. Castellano, S. Vascellari, G. Verani, F. Isaia, *Inorg. Biochem.* 105 (2011) 329.
- [9] N. Kameta, H. Imura, K. Ohashi, T. Aoyama, *Polyhedron* 21 (2002) 805.
- [10] Gaussian 03, Revision B.05, M. J. Frisch, et al. Gaussian, Inc., Pittsburgh PA, 2003.
- [11] M. Jamialahmadi, S. F. Tayyari, M. H. Habibi, M. Yazdanbakhsh, S. Kadkhodaei, R. E. Sammelson, *J. Mol. Struct.* 985 (2011) 139.
- [12] M. Jamialahmadi, S. F. Tayyari, M. H. Habibi, M. Yazdanbakhsh, R. E. Sammelson, *J. Mol. Struct.* 997 (2011) 117.



Anion- π Interaction in $C_6H_3X...M^-$ ($X = H, F, CN, CH_3$, and NH_2 ; $M = Au, Ag$, and Cu) Complexes

H. Farhangian and Z. Jamshidi*

Chemistry and Chemical Engineering Research Center of Iran

P.O. Box 14335-186, Tehran, Iran

(jamshidi@ccerci.ac.ir)

Introduction:

In the last two decades the role of noncovalent interaction in nature was fully recognized. In biology, these interactions are the basis of a great deal of processes, whose efficiency is always significant. It is really important to understand and quantify these weak interactions to be able to designing new supramolecular systems. In particular, aromatic interactions play a vital role in supramolecular chemistry and biology. Aromatic rings can participate in several noncovalent interactions; C – H/ π , cation- π , anion- π , and lp/ π . The density of charge in aromatic rings can be affected by substituting hydrogen atoms by electron withdrawing groups, for instance fluorine atoms. The importance of anion- π interactions, i.e., noncovalent forces between electron deficient aromatic systems and anions, has been recognized by a great deal of theoretical and experimental investigations.

Method of Calculation:

The geometry of the complexes included in this study was fully optimized at the MP2/aug-cc-pVDZ-PPU6-311++G** level of theory. Although for comparison the ab-initio and DFT methods; DFT-D3 (B3LYP-D3, TPSS-D3, and BP86-D3) and M06-2X methods performed for $C_6H_3X...Au^-$ complexes. Relativistic effects were model using the ZORA approximation in all DFT calculations. The interaction energy is defined as the difference between the energy of a complex and sum of the energies of its components, and interaction energies were corrected for the basis set superposition error. To reveal the nature of bonds, the NBO, QTAIM, and EDA analyses were carried out on MP2 structures.

Result and Discussions:

The geometric and energetic results obtained for complexes are summarized in Table 1. In anion- π interaction two main terms contribute: electrostatic and ion-induced polarization. The

polarization term is always favorable and it does not depend on the sign of the ion. However the electrostatic term contribute as positive or negative term depends on the charge of ion and the kinds of substituting atoms in the ring. In the case of benzene, positive value of electrostatic term (due to $Q_{zz} < 0$) contributes to the total interaction energy and compensated with the ion-induced polarization term. As expected, the interaction energies of benzene with M^- atoms are small and positive, except for gold atom ($E_{C_6H_6Au^-} = -0.31$ kcal/mol). The interaction energies for trifluorobenzene and tricyanobenzene are negative. In these complexes, negative value of quadrupole changes to positive one by attaching electron-withdrawing substituents. Thus the unfavorable anion- π interaction turned into favorable. It can be investigated through energy decomposition analysis (Table 2).

Table 1. Interaction energies (in kcal/mol) and equilibrium distances (in Å) at the MP2/aug-cc-pVDZ-PPU6-311++G** level of theory

Complexes	E_{int}	R	ω	Q_{NBO}	ρ_{BCP}
$C_6H_6Cu^-$	0.63	5.111	10.62	-0.998	0.0008
$C_6H_6Ag^-$	0.38	4.826	14.58	-0.999	0.0012
$C_6H_6Au^-$	-0.31	4.076	29.19	-1.000	0.0031
$C_6H_3F_3Cu^-$	-4.77	4.000	33.75	-1.001	0.0030
$C_6H_3F_3Ag^-$	-5.40	3.976	34.05	-1.000	0.0034
$C_6H_3F_3Au^-$	-8.03	3.678	40.76	-1.000	0.0052
$C_6H_3(CN)_3Cu^-$	-16.94	3.630	63.39	-0.995	0.0048
$C_6H_3(CN)_3Ag^-$	-17.88	3.647	82.46	-0.993	0.0053
$C_6H_3(CN)_3Au^-$	-22.21	3.437	17.8	-0.989	0.0072

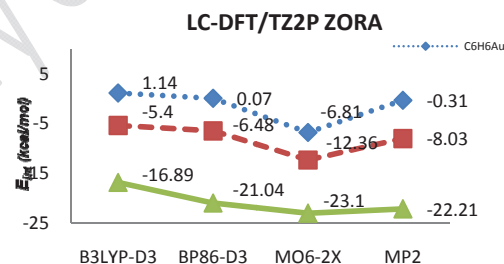


Table 2. EDA values (in kcal/mol) at the BP86-D3/TZ2P level of theory.

Complexes	E_{Pauli}	E_{elec}	E_{orb}	E_{disp}	$E_{int-BP86-D3}$	$E_{int-MP2}$
$C_6H_6Cu^-$	1.34	1.91	-1.67	-0.84	0.74	0.63
$C_6H_6Ag^-$	2.60	1.14	-1.51	-1.44	0.79	0.38
$C_6H_6Au^-$	5.77	0.28	-2.84	-3.66	-0.45	-0.31
$C_6H_3F_3Cu^-$	11.02	-9.54	-3.58	-3.44	-5.54	-4.77
$C_6H_3F_3Ag^-$	13.70	-11.77	-2.89	-4.04	-5.00	-5.40
$C_6H_3F_3Au^-$	15.31	-12.38	-4.52	-5.31	-6.90	-8.03
$C_6H_3(CN)_3Cu^-$	24.09	-29.65	-11.41	-5.66	-22.63	-16.94
$C_6H_3(CN)_3Ag^-$	27.54	-32.05	-6.15	-6.15	-21.80	-17.88
$C_6H_3(CN)_3Au^-$	29.07	-32.94	-11.22	-6.71	-21.80	-22.21

References:

- [1] Frontera, A.; Quinonero, D.; Deya, P. M. *Advanced Review*, **2011**, *1*, 440.



- [2] Lucas, X.; Frontera, A.; Quinonero, D.; Deya, P. M. *J. Phys. Chem A* **2010**, *114*, 1926.
[3] Granatier, J.; Lazar, P.; Otyepka, M.; Hobza, P. *J. Chem. Theory. Comput.* **2012**, *1*, 141.

15th Physical Chemistry Conference



Ionization of Benzene, Toluene and Xylene via Charge or Proton Transfer Reaction

Maede Darzi, Mahmoud Tabrizchi *

Department of Chemistry, Isfahan University of Technology, Isfahan, 84156-83111, Iran

Email: m-tabriz@cc.iut.ac.ir

Key words: Ion mobility spectrometry, Aromatic compounds, Charge Transfer, Proton Transfer, BTEX, NO^+ , H_3O^+ .

Introduction:

Benzene, toluene, ethylbenzene and xylene are the compounds commonly called BTEX. These volatile organic compounds (VOCs) are widely present in petroleum products, increasing the octane number [1]. BTEX are notorious due to the contamination of soil and groundwater and have harmful effects on the central nervous system. Hence, detecting and monitoring of these hazardous chemicals in ambient air has been the subject of many researches. A usual way of detecting those chemicals is ionization and identification of their ion in a mass spectrometer. In this work we compared two methods of atmospheric pressure chemical ionization, the proton transfer with H_3O^+ and the charge transfer with NO^+ for BTEX using or an ion mobility spectrometry (IMS).

Materials and methods:

The chemicals used in this study were Benzene, Toluene and Xylenes (O-xylene, P-xylene and M-xylene). Headspace vapor of liquid samples was injected into the IMS cell using a syringe pump (model 1000, New Era Pump System Inc. USA) with a speed of 0.5-3 ml/min. The IMS instrument was constructed in our laboratory at Isfahan University of Technology [2]. In IMS ions are first produced by an ionization source and then injected as an ion packet into a drift region where they are separated according to their mass, size and charge. The technique is very similar to time-of-flight mass spectrometry but it operates under atmospheric pressure. H_3O^+ is produced by corona discharge and NO^+ was generated by adding NO generated by arc to the corona discharge.

Result and discussion:

Depending on proton affinity (PA) or ionization energy (IE), the formation of MH^+ or M^+ and $M.NO^+$ are expected in atmospheric pressure chemical ionization techniques. When H_3O^+ is used, the BTEX may form MH^+ if its proton affinity is higher than that of water. However, reaction of sample with NO^+ generates M^+ , if its ionization energy is less than that of NO . Otherwise it generates $M.NO^+$ adduct. This is demonstrated in Fig. 1 where ion mobility spectra recorded with two different reactant ions were shown. Peaks 1 and 2 in benzene spectrum are the M^+ and the $M.NO^+$ adduct, respectively.

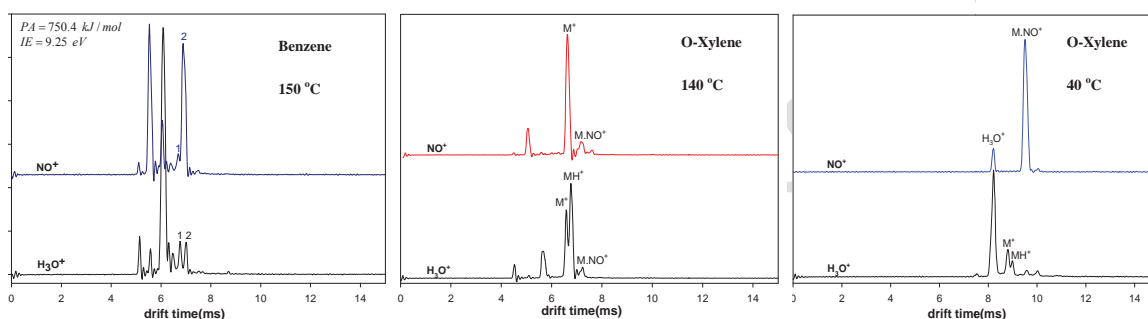


Fig.1. Ion mobility spectra of benzene and O-Xylene with H_3O^+ and NO^+ reactant ions.

For Benzene, peak 1 and 2 show MH^+ and $M.NO^+$, respectively

Benzene is weakly reacting with H_3O^+ because of low PA. It either does not produce M^+ in reaction with NO^+ due to high IE. However, it strongly forms the $M.NO^+$ adduct, hence a better sensitivity if NO^+ reactant ion is used. O-Xylene produces both MH^+ and M^+ ions due to low IE and high PA. The $M.NO^+$ adduct is small at high temperature of 140°C but it grows considerably at low temperature of 40°C.

Conclusion:

While some volatile organic compounds such as BTEX are not reacting with H_3O^+ due to low proton affinity, they react with NO^+ reactant ion to form either M^+ or $M.NO^+$ adduct. In addition, unlike H_3O^+ , the reaction of NO^+ with sample molecules is not affected strongly by humidity. Hence, the use of NO^+ as reactant ion could enhance the sensitivity and improve the selectivity of detecting BTEX.



References:

- [1] K. Badjagbo, P. Picard, S. Moore, and S. Sauve, "Direct Atmospheric Pressure Chemical Ionization-Tandem Mass Spectrometry for the Continuous Real-Time Trace Analysis of Benzene, Toluene, Ethylbenzene, and Xylenes in Ambient Air"; *Am. Soc. Mass Spectrom.*; 20,829-836, 2009.
- [2] M. Tabrizchi, *Construction of a research grade ion mobility spectrometer*, Iranian Patent No. 39074, 2007.

15th Physical Chemistry Conference



Reduced Density Gradient along Bond Paths in Different Chemical Bonds

Z. Abbasi, N. Mahmoodabadi, K. Eskandari

School of Chemistry, Damghan University, Damghan, 36716-41167, Iran

eskandari@du.ac.ir

Keywords: QTAIM, Bond Path, Reduced Density Gradient.

Introduction:

Although *chemical bond* is the cornerstone of chemistry, there is no a precise and clear-cut definition for bonds even in specialized chemistry texts. It seems the best definition has been proposed by Bader, who used electron density as an information source and introduced the concept of *bond path (BP)* [1]. According to this definition, existence of a BP in equilibrium geometry is both necessary and sufficient condition for the existence of a chemical bond. However, in contrast to Bader, several authors claimed that the presence of a BP is not necessarily indicative of attractive interactions and should be interpreted as either bonding or nonbonding, attractive or repulsive [2,3]. Another disadvantage of BP is that it cannot distinct between different type of chemical bonds. On the other hand, Johnson and co-workers developed an approach to detect noncovalent interactions based on the electron density and its derivatives [4]. In the current work, we will calculate reduced density gradient along BPs of different bonding (covalent and van der Waals) and nonbonding interactions to find a better definition for *chemical bond*.

Methods:

Molecular geometries and electronic wavefunctions were fully optimized at MP2/6-311++G(d,p) 6d level using Gaussian 03 program. The AIM2000 package was used to calculate electron density and its gradient along the BPs.

Results and Discussions:

The reduced density gradient, s , which is a fundamental quantity in DFT, defined as:

$$s = \frac{1}{(2(3\pi^2)^{\frac{1}{3}})} \frac{|\nabla\rho|}{\rho^{\frac{4}{3}}}$$

3534

This quantity has been calculated at different points at the BPs of covalent bonds (in H_2 and CO_2), van der Waals interactions (in $Ne - Ne$ and $CO_2 - CO_2$) and nonbonded $He - He$ interaction (the wavefunction of $He - He$ system has been generated from HF calculations to eliminate the dispersion contributions). As indicated in Figure 1, plotting s versus r reveals important differences between covalent, noncovalent and nonbonding interactions.

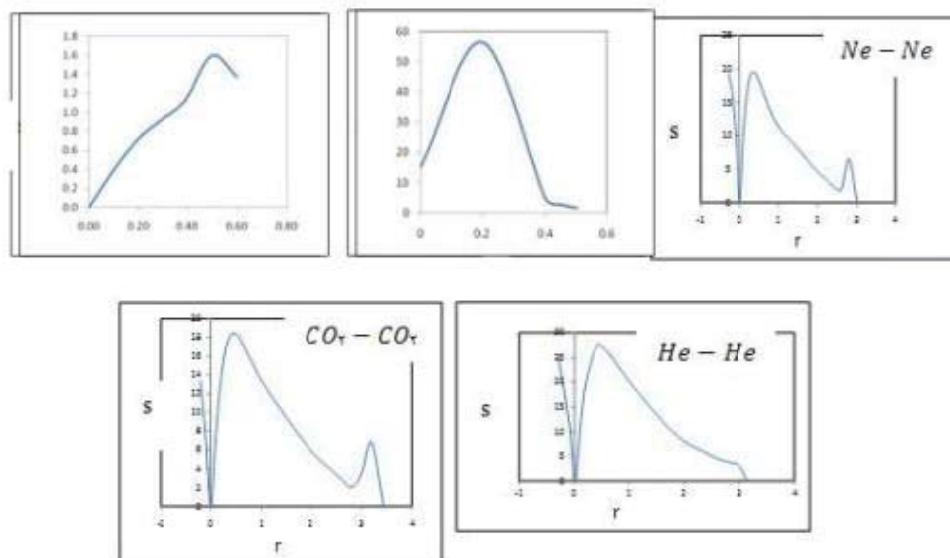


Figure 1. Reduced density gradient along BP of different bonds.

Conclusion:

Our results show that the behavior of reduced gradient is different for covalent, noncovalent and nonbonded interactions. In the covalent bonds, there is only one maximum between BCP and nucleus. But in the noncovalent bonds, there are two extrema between BCP and nucleus, one maximum and one minimum. In addition, it seems that reduced gradient is different for nonbonding interactions; as an example, the variations of reduced gradient along the BP in He_2 are completely different with attractive van der Waals interactions.

References:

- [1] R. F. W. Bader, Atoms in Molecules, A Quantum Theory, OUP, UK, 1990.
- [2] J. Cioslowski, S. T. Mixon. J. Am. Chem. Soc. 114, 4382, 1992.
- [3] J. Cioslowski, J. Am. Chem. Soc. 112, 6536, 1990.
- [4] E. R. Johnson et. al., J. Am. Chem. Soc. 132, 6498, 2010.



Electronic Structure of Protonated PAHs: Acenaphthylene and Acenaphthene

B. Saed, R. Omidyan*

Department of Chemistry, University of Isfahan, Isfahan 81746-73441, Iran

r.omidyan@sci.ui.ac.ir/b.saed@chem.ui.ac.ir

Keywords: Acenaphthene, Acenaphthylene, Protonation, RI-CC2, Charged Transfer

Introduction:

Protonated aromatic molecules, as the short lived intermediates of Electrophilic Aromatic Substitution reactions (EAS), are important in the wide range of science, environment, and ranging from stereochemistry, jet engine gas exhaust and Biomolecular building blocks such as proteins and DNA [1-4]. During the last decade, improvement of high resolution TOF-MS, advance-light sources and high-level quantum mechanic calculations such as CASPT2 and CC2, have made a convenient situation to study these important molecules. In this report, we will present the protonation effect on the electronic properties of acenaphthylene (ACYN) and also acenaphthene (ACN). Hence, the geometry and electronic excited states (S_1 , S_2) of protonation ACYN and ACN, as well as their neutral homologues, will be reasonably addressed in the present work.

Methods:

The “*ab initio*” calculations have been performed with the TURBOMOLE program package making use of the resolution-of-the-identity (RI) approximation for the evaluation of the electron-repulsion integrals. The equilibrium geometry of the protonated ACYN and ACN ground electronic states (S_0) has been determined at the MP2 level. Excitation energies and equilibrium geometry of the lowest excited singlet and triplet states (S_1 , S_2 , T_1 and T_2) have been determined at the RI-CC2 level. The calculations were performed with the cc-pVDZ and the aug-cc-pVDZ basis sets.

Results and Discussion:

The ground state geometry optimization of protonated isomers shows The C7 isomer is the most stable isomer produced from protonation of ACYN and the isomer with protonation of



C4 is the highest in energy. The proton affinity of neutral ACYN was calculated at the MP2/aug-cc-pVDZ level and the value of 8.99 eV was acquired. Among the 6 isomers of protonated ACN, the C3 isomer is the most stable of all. The isomer with the proton attached on the C4, is the highest in energy. Furthermore, the proton affinity of the ACN was also calculated to be +8.81 eV. Results of this study show that no drastic geometry deformation was found in the S_1 optimized state of neutral ACYN in respect to its ground state structure. According to RI-CC2 calculations, in both of the neutral and protonated ACYN (C7-the most stable protonated isomer), the first electronic transition (S_1-S_0) corresponds to LUMO \leftarrow HOMO and the second electronic transition (S_2-S_0) corresponds to LUMO \leftarrow HOMO-1 transition. Considering the orbitals which are participated on the S_1-S_0 transitions, the first electronic transition in neutral and some of protonated isomers of ACYN has a $\pi\pi^*$ nature. The calculated S_1-S_0 adiabatic transition energy of neutral ACYN is 2.72 eV and for protonated isomers it lies in a broad range, from the beginning of visible to the near IR. The calculated values for other protonated isomers derived from adiabatic S_2-S_0 transition energy, lie in the visible region. In relation to S_1-S_0 excitation, comparing the S_1 geometry optimized parameters of neutral ACN to the corresponding ground optimized parameters shows very small changes. Similar to neutral ACYN, the optimized geometry of neutral ACN at the ground state belongs to C_{2v} symmetry point group and its S_1 and S_2 transition energies are assigned as the $\pi\pi^*$ transition. The S_1 and S_2 transition energies of the protonated isomers of ACN lie obviously in the visible and UV region respectively. In addition, the calculations show that the S_1-S_0 ($\pi\pi^*$) transition energies in ACYN- H^+ and ACN- H^+ are effectively red-shifted compared to the neutral homologues.

Conclusion:

Protonated aromatic molecules could be divided into two classes: the first one showed short lived excited state with broad band spectra, while, the second one exhibited sharp and well structured spectra and longer lived excited state. The calculations predict that protonated ACYN and ACN are belonging to the second category with an excited state life time- long enough to observe narrow vibronic bands. The effect of spectral red- shift induced by protonation on the electronic transition energies, is due to a charge transfer character of the



excited state transition which is more pronounced in protonated ACN rather than protonated ACYN.

References:

- [1] A. Kiendler, F. Arnold, *Atmos. Environ.* 36 (2002) 2979.
- [2] A. L. Sobolewski, W. Domcke, C. Dedonder-Lardeux, C. Jouvet, *Phys. Chem. Chem. Phys.* 4 (2002) 1093.
- [3] O. V. Boyarkin, S. R. Mercier, A. Kamariotis, T. R. Rizzo, *J. Am. Chem. Soc.* 128 (2006) 2816.
- [4] S. H. Vosko, L. Wilk, M. Nusair, *Can. J. Phys.* 58 (1980) 1200.



Theoretical consider of properties of oligo (3-methyl thiophenes) terminated with formyl

H. Nikoofard^a, M. Khorrami^{a,b,*}, N. Shakour^{b,c}

^a Faculty of chemistry, Shahrood University of Technology, Shahrood, Iran

^b Department of chemistry Islamic Azad University, shahreza branch, Shahreza, Iran

^cDepartment of Chemistry, Faculty of Science, Zanjan Univrsity Zanjan, Iran

Email: monire.khorami@yahoo.com

Keywords: DFT, Conducting Polymers, Alkylthiophene, End capped, HLG

Introduction:

A variety of oligothiophenes derivatives have been synthesized and their molecular and crystal structures, self-ordering, electrochemical, photophysical, optical, and electrical properties have all been studied. In addition, their potential application to field-effect transistors, photovoltaic devices, and organic electroluminescent devices has been investigated [1]. We have already studied some properties of oligo(3-alkyl thiophenes). The researches have shown that characteristics of conjugated polymers improved clearly when they terminated with some molecular specifies. In this work, we have added formyl in both sides of chains of oligo (3-methyl thiophenes) and have considered structural and electronic properties again. We have compared these results with pervious results. Some oligoformyl-thiophenes derivatives synthesized [2].

Methods:

All calculations were done with Gaussian 03 program. We calculated full optimization on, B3LYP level of theory with the 6-31G** basis set.

Results and discussion:

The conjugated length is almost unit for all different types of substituent (1.4Å). We had found it about 3-alkyl thiophenes previously. In 3-alkylthiophenes the first bond and the last bond of the conjugated length are shorter. In other hand, it seems these two bonds haven't

intered in the conjugated length completely yet. When we insert formyl at both end of the polymer chain, these two bond lengths increase distinctly. In other way, the length of two end bond are been 1.4Å. Fig1. compare the conjugated length for hexa(3-methylthiophene) and hexa(3-methylthiophene) that terminated with formyl.

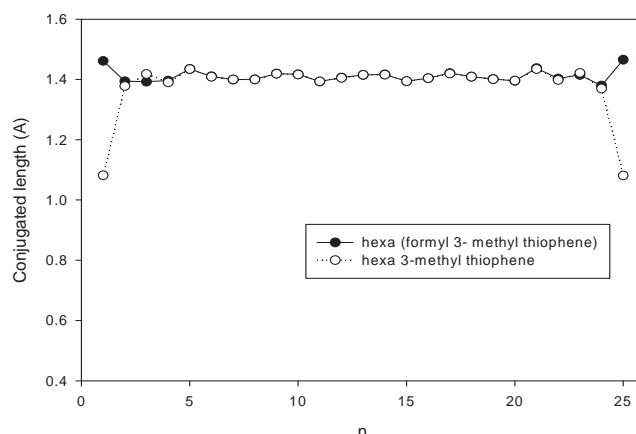


Fig1. Variation of the bond lengths (Å) in hexa (3-methylthiophene) and hexa (formyl 3-methylthiophene) with growing the length of chain at B3LYP/6-31G**.

Charge distribution for oligo(formyl 3-methylthiophene) calculated. It is obvious that equality of electrical charges on similar positions vary with attachment methyl to ring of thiophene. Electrical charge is more on α position of heteroatom ring (α position near to the substituent). Comparison the values of the electrical charge with the results related to calculations 3- methylthiophenes (without formyl group) indicate that in present end-capped formyl the distribution of electrical charge is less on all studied positions of the polymer chain. Consider of electrical energies of oligo (formyl 3-methylthiophene) indicate a clear reduction in comparison of 3-methylthiophene. And about HLGs, however some fluctuations observed, but a decreasing manner has demonstrated in values.

Conclusions:

Our calculations have shown when end capped add to oligo (3-methylthiophenes) all properties improve. Formyl as an end capped reduces electrical charge distribution for 3-methylthiophenes. The HLGs decrease and it reveals conductivity rise absolutely. Reduction of electrical energies makes an enhancement in stability.



References :

- [1]. H. Meng, J. Zheng, A. J. Lovinger, B. Wang, P. Gregory Van Patten, Z. Bao, *Chem. Mater.*, Vol. 15, No. 9, 2003.
- [2]. B. Yin, C. Jiang, Y. Wang, M. La, P. Lu, W. Deng, *Synthetic Metals* 160 (2010) 432.

15th Physical Chemistry Conference



ONIOM Calculation on the Interaction between TTA Derivatives and Linear–Dendritic Copolymers

N. Madadi Mahani^{*} and M. Oftadeh

Chemistry Department, Payame Noor University, 19395-4697, Tehran, I. R. of IRAN

Email: nmmadady@gmail.com

Keywords: ONIOM, Copolymer, anti-HIV drug, Interaction.

Introduction:

The ONIOM (our own n-layered integrated molecular orbital and molecular mechanics) hybrid method, which combines a quantum mechanical (QM) method with the molecular mechanical (MM) method, is one of the powerful methods that allow calculating large molecular systems [1] with the accuracy afforded for smaller molecular systems. The reliability of the ONIOM method has been well established by the Morokuma group and is increasingly adopted as an efficient approach beneficial to many areas of chemistry [2]. In the ONIOM2 approach, the system is divided into two layers, a small part of which, such as the drug and the reacting amino acids in the binding site of an enzyme, is treated at a high quantum chemical level, whereas the large surrounding region is modeled using a lower level of calculations[3]. Among the representatives of the non-nucleosides reverse transcriptase , NNRTIs, 2-(4- (2,4-dichlorophenyl)-1,2,3-thiadiazol-5-ylthio)-N-acetamide (TTA), has interesting structure and exhibit significant anti-HIV-1 activity A series of TTA derivatives have been synthesized and evaluated as potent inhibitors of HIV-1[4]. Linear–dendritic copolymers containing hyper branched poly (citric acid) and linear poly(ethylene glycol) blocks (PCA–PEG–PCA) are promising nonmaterial to use in nanomedicine[5]. Thus, to investigate their potential application in biological systems (especially for drug delivery), quantum chemical calculations and a two layered ONIOM2 method [3] were applied to study the nature of particular interactions between TTA derivatives and the PCA-PEG-PCA copolymers.

Computational Section:

In the present study, we perform two-layer ONIOM calculations to simulate the interaction between TTA derivatives as anti-HIV drug and the Linear–dendritic copolymers. All the



calculations were performed with the Gaussian 03 series of program with ONIOM2 (B3LYP/6-31G: UFF) method.

Results & discussion:

Binding energy (BE) analysis of these complexes allowed the fundamental features of the drug- the Linear-dendritic copolymers interactions to be assessed based on ONIOM2 method. Based on the obtained results, the binding energies of the optimal configuration of between TTA derivatives as anti-HIV drug and the Linear-dendritic copolymers are summarized in Table 1. The ONIOM2 calculation of the complex shows that they have weak interaction that these interactions contain hydrogen bond and van der Waals interaction. The results indicated clearly that these complexes have relatively low stability and so PCA-PEG-PCA copolymers can use to as drug delivery.

Table 1: The Binding energies TTA derivatives and PCA-PEG-PCA copolymer
With ONIOM2 (B3LYP/6-31G: UFF) method

R	Binding Energy (kcal/mol)
H	3.14917191
Ph	3.22344912
PhF	3.527793549
PhCl	3.49952571
PhBr	5.54927411
PhOH	3.36444034
PhNO ₂	5.006351212

References:

- [1] T. Vreven, K. Morokuma, *J. Comput. Chem.* 21 (2000) 1419.
- [2] K. Morokuma, *Bull. Korean Chem. Soc.* 24 (2003) 797.
- [3] Y. Z. Xiong, P.Y. Chen, *J. Mol. Model* 14(2008) 1083.
- [4] P. Zhan, X. Liu, Y. Cao, Y. Wang, C. Pannecouque, E. De Clercq, *Bioorg. & Med. Chem. Lett.* 18 (2008) 5368.
- [5] A. Tavakoli Naeini, M. Adeli, M. Vossoughi, *Eur. Polym. J.* 46 (2010) 165.



DFT Study stabilities and EPR of the Copper(II)hydrogenmalonate dihydrate complex

N. Noorani^{*a}, H. Rahemi^b

^a Department of Chemistry, Payame Noor University, P.O. Box 19395-3697 Tehran, Iran

Email:nnorani1@yahoo.com

^b Department of Chemistry, Nazhand Institute of High Educations, 57159-165, Iran

Key words: Copper(II)hydrogenmalonate dihydrate complex, DFT, EPR, NMR/GIAO

Introduction:

EPR spectroscopy represents one of the most powerful experimental methods for investigating electronic and structural features of systems containing unpaired electrons, such as radicals, coordination compounds and paramagnetic sites in solids [1, 2]. Since, the Copper(II)hydrogenmalonate dihydrate complex, $[\text{Cu}(\text{C}_3\text{H}_2\text{O}_4) \times 2\text{H}_2\text{O}]^{+2}$, has the d^9 configuration, it possesses an unpaired electron, and can interact with an applied magnetic field, making it EPR active. Therefore, our other principal goal will be studying changes of the EPR g tensor parameters in the 4.2–295 K temperature range [3] using the available solid state bond lengths and bond angles of the complex.

Methods:

All calculations were carried out at the level of density functional theory (DFT) using Gaussian 03 package of program. All structures were fully optimized with the Gaussian 03W program at the B3LYP/6-311G, 6-31G**, BWP91/6-31G** levels. The optimized structural parameters are saved for the next step of calculations. After the optimization, g values were calculated using the NMR/GIAO method [4,5].

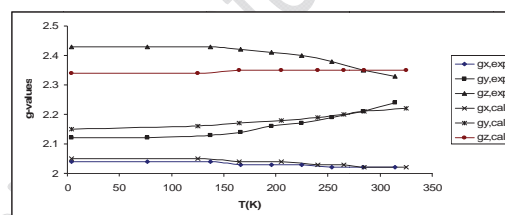
Result and discussion:

Geometry optimization of the Copper(II)hydrogenmalonate dihydrate complex is carried out at B3LYP/6-31G** and BPW91/6-31G** levels of calculations, which provide a chance to compare two basic methods B3LYP/6-31G** and BPW91/6-31G** with inclusion of

polarization in the basis sets. Bond angles and bond lengths were calculated in the gas phase; therefore it is expected that there will be a difference between experimental and calculated values. The B3LYP/6-31G** level of calculation provides a better agreement to corresponding experimental values. However, generally we expect by increasing the size of basis sets to approach the experimental values, but the level of calculation has a major effect in calculation. The g-tensor calculation was performed by using of NMR/GIAO option. The X-ray data in the temperature range of 4.2–295 K is available, therefore there is a chance to use solid state experimental geometry data to calculate g values and inspect for possible phase transitions. We have used the temperature experimental values in Fig 1. (B). (see below).



(A)



(B)

Fig. 1 (A) The B3LYP/6-31G** optimized structure of the CuHM, (B) The temperature dependence of the g-values.

Conclusions:

The structural optimization of Copper(II) hydrogenmalonate dihydrate complex has been carried out using B3LYP/6-31G** and BPW91/6-31G level of calculations. Reasonable correlations between calculated and experimental determined values are obtained when the g tensor components are calculated using these geometries with a B3LYP/6-31G** approach, a good correlation between the experimental and calculated values is only obtained for the lowest g-value. This demonstrates that the temperature dependent structure and g-values of this complex are more complicated and we are pursuing additional structural and EPR measurements on this system.

Reference:

- [1] N.M. Atherton, *Electron spin resonance, theory and applications*, Wiley, Chichester, 1973.
- [2] A. Abragam, B. Bleaney, *Electron paramagnetic resonance of transition metal ions*, Clarendon, Oxford, 1970.



- [3] A.T.H.LENSTRA, O.N.KATAEVA, *Acta Cryst. B*, 57 ,497,2001.
- [4] J.A.Tossell, *Chem Phys Lett*, 303,435–440,1999.
- [5] J.A.Kintop, W.V.M.Machado, M.Franco, H.E.Toma, *Chem Phys Lett* 309 ,90–94,1990.

15th Physical Chemistry Conference

DFT Study of Hydrogen-bonding affects on ^{17}O and ^2H Electric Field Gradient Tensors of of the bis- α -amino acid (S, S)-1 molecule

N. Noorani^{*a}, R. Eisavi^b

^{a,b}Department of Chemistry, Payame Noor University, P.O. Box 19395-3697 Tehran, Iran

Email:nnorani1@yahoo.com

Key words: bis- α -amino acid (S, S)-1, DFT, EFG, NQR

Introduction:

The electric field gradient (EFG) tensors arisen at the sites of quadrupole nuclei are important physical parameters to investigate the structural properties of molecules [1]. The high level quantum mechanics calculations yield the EFG tensors in principal axis system, PAS, which can be converted to NQR measurable parameters: nuclear quadrupole coupling constant (C_Q), and asymmetry parameter (η_Q). Present work calculates NQR tensors (EFG) was also performed on the open (C–H...O=S) and native (C–H...O=C) conformers of bis- α -amino acid (S,S)-1 molecule to systematically investigate the HB effects on the ^{17}O , ^2H EFG tensors.

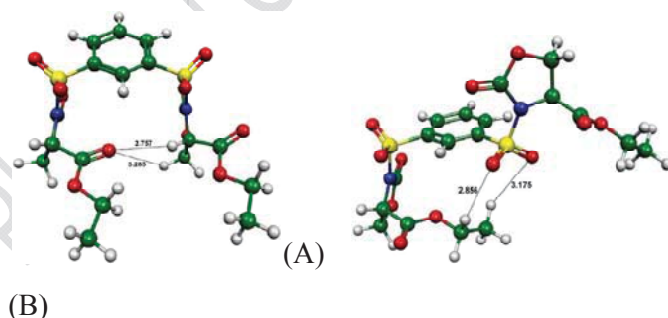


Fig. 1 Optimised structure of an isolated bis- α -amino acid (S, S)-1 molecule in its native conformation. Hydrogen bonding (A) between C–H and O=C and (B) between C–H and O=C are shown by a black dotted line.

Methods:

Quantum chemical calculations were carried out at the level of DFT using Gaussian 03 package of program. B3LYP exchange-functional method and 6-311++G* standard basis sets

were employed in the EFG and CS tensors calculations. The quantum chemical calculations were performed on the geometrical optimized models to evaluate the ^{17}O , and ^2H nuclei EFG tensors. The EFG tensors are calculated [2] by equation 1 and 2.

$$C_Q (\text{MHz}) = e^2 Q q_{zz} h^{-1} \quad (1)$$

$$\eta_Q = \left| \frac{q_{xx} - q_{yy}}{q_{zz}} \right| \quad (2)$$

Result and discussion:

The difference in energy between the open and native conformers provides an estimation of the strength of the $\text{C}(\alpha)\text{--H}\dots\text{O}=\text{C}$ hydrogen bond. At our level of theory, the native conformer is found to be $16.94 \text{ kJ mol}^{-1}$ more stable than the open conformation. We performed a computational work to study HB properties in the bis- α -amino acid (S,S)-1 molecule by evaluation of NQR parameters. Hydrogen bonding (HB) interactions in the bis- α -amino acid (S,S)-1 molecule contributes to two HB types, $\text{C}(\alpha)\text{--H}\dots\text{O}=\text{C}$ and $\text{C}(\alpha)\text{--H}\dots\text{O}=\text{S}$, Fig. 1. We observe the formation of two weak $\text{C}(\alpha)\text{--H}\dots\text{O}=\text{S}$ interactions between the ethyl group of one chain and the SO_2 group of the other. EFG tensors at O_{11} and H_3 nuclei are influenced by HB. However, It was also shown that hydrogen bonding interaction has a significant influence on $C_{(Q)}$ and $\eta_{(Q)}$ values.

Conclusion:

We performed a computational work to study HB properties in crystalline the bis- α -amino acid (S, S)-1 molecule. To this aim, the EFG tensors at the sites of ^{17}O , ^{14}N and ^2H nuclei. The EFG tensors are more sensitive to HB effects rather than the CS tensors.

Reference:

- [1] M.A. Rafiee, N.L. Hadipour, H. Naderi-mannesh, J. Comp. Aid. Molec. Des. 18 ,215–220,2004.
- [2] P.Pyykko , Mol Phys 99:1617–1629,2001.



Protonation of Caffeine; Theoretical and Experimental Study

H. Bahrami, M. Tabrizchi* and H. Farrokhpour

Department of Chemistry, Isfahan University of Technology, Isfahan, Iran

(email: m-tabriz@cc.iut.ac.ir)

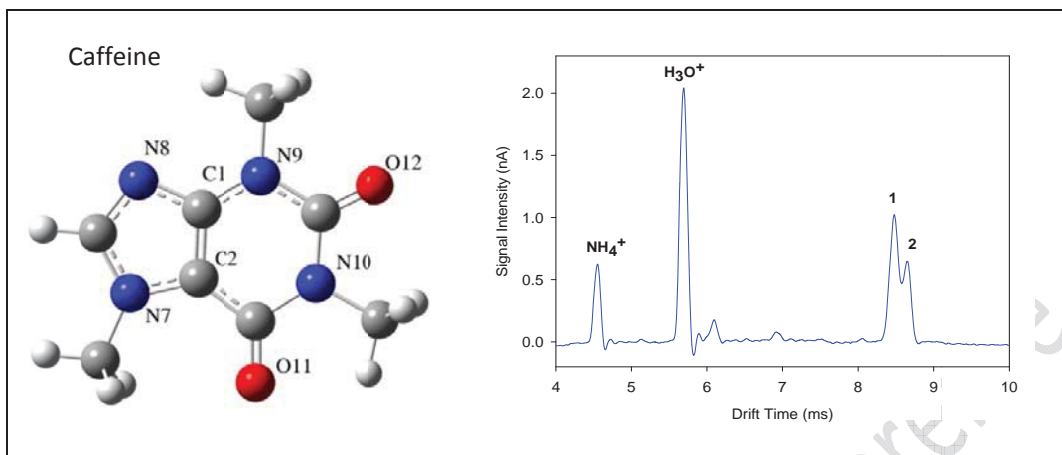
Keywords: thermodynamic, calculation, proton affinity, ion mobility spectrometry,

Introduction:

Caffeine or trimethylxanthine is a central nervous system and metabolic stimulant [1] which is widely consumed as tea, coffee and additive in drinks. The detection and measurement of caffeine have attracted the interest of numerous researchers. Mass spectrometric analysis of caffeine with corona discharge ionization source showed only one major peak at m/z 195 corresponding to MH^+ ion [2]. However, our experimental studies using an ion mobility spectrometer (IMS) with corona discharge as ionization source showed that the caffeine spectrum included two distinct product ion peaks. Here, we report a joint theoretical and experimental investigation of caffeine related ions. Considering theoretical calculation and experimental evidences we conclude that there is more than one stable protonated caffeine which are not distinguishable in mass spectrometer, but separated in IMS.

Experimental & Method:

The IMS used in this study was constructed in our laboratory at Isfahan University of Technology. Protonated caffeine was produced via reaction between caffeine vapor and gas phase H_3O^+ or NH_4^+ ions. The theoretical calculation was carried out with the GAUSSIAN 09 program. The theoretical results were based on density functional theory (DFT) calculations.



Chemical structure and ion mobility spectrum of caffeine

Experimental Results:

Ion mobility spectrum of caffeine shows two distinct peaks for caffeine. As the major ionization scheme in corona discharge (CD) is protonation of the analyte, one of these two peaks is well assigned to MH^+ . The second peak could be either M^+ or a fragment ion. Mass spectrometry studies showed that caffeine don't dissociate in CD ionization source. In addition no M^+ peak appeared on mass spectra of caffeine using CD ionization. Hence, the only option for the second peak remains to be protonated caffeine but from a different site.

Theoretical Results:

Protonation of eight different sites in caffeine molecule were examined based on three methods of density functional theory (DFT) including B3LYP, CAM-B3LYP and wB97X with the 6-311++G** basis set. Standard quantum chemical geometry optimizations (minimizing energy) were performed for selection of most stable structures. The electronic and Gibbs free energies of caffeine and its protonated isomers were obtained. Theoretical results show that Nitrogen 8 protonated isomer (N8H), is the most stable one. The next stable isomers, O11H and O12H, are about 5 kcal/mol above the N8 protonated caffeine. The remaining isomers, N7, N9 and N10, are all quite higher in energy and can be hardly detected in the gas phase. Therefore, three most probable sites for protonation of caffeine with CD ionization is Nitrogen 8 and Oxygen 11 and 12 of carbonyl groups. The two latest configuration are more less similar but different from that of N8. Hence, the two peaks observed in ion mobility spectra of caffeine with CD ionization source could be assigned to



N8 and O-protonated isomers. More experimental and theoretical evidences were observed to back this assignment.

Conclusion:

Caffeine has three different sites to form stable protonated molecule in gas phase. Since the corresponding ions are iso-mass, they are not separated in mass spectrometry. However, different shapes cause them to be separated in IMS. Hence, IMS can be used to measure proton affinity from different sites.

References:

- [1] Nehlig, A; Daval, JL; Debry, G. Caffeine and the central nervous system: mechanisms of action, biochemical, metabolic and psychostimulant effects, *Brain Research Reviews*, 1992, 17 (2) 139–70.
- [2] Iulia M. Lazar and Milton L. Lee, Design and Optimization of a Corona Discharge Ion Source for Supercritical Fluid Chromatography Time-of-Flight Mass Spectrometry, *Anal. Chem.*, 1996, 68 (11), pp 1924–1932.



Chalcogen-Chalcogen Interaction; an Electron Density Analysis

M. Lesani and K. Eskandari*

School of Chemistry, Damghan University, Damghan, Iran

(Email: mina_lesani@hotmail.com)

Key words: Chemical bond, Chalcogen-Chalcogen Interaction, QTAIM, IQA.

Introduction:

In the past decade, the Theory of Atoms in Molecules became widely recognized for its utility in the analysis of chemical bonding. Based on Professor Bader's Opinion, existence of a bond path (BP) between a pair of atoms, is regarded as the adequate condition for existence of a chemical bond between them [1]. Thus, can we say that existence of a BP always indicates a bonding Interaction? The answer to this question perhaps is clear for known bonds including ionic, van der Waals and Hydrogen bonds. Surely BP is a strong and useful concept to describe the formation of these kinds of bond, but this is not the whole story. On the other hand, Cioslowski and co-workers claimed that the existence of a BP between a pair of atoms should be interpreted as either bonding or nonbonding, attractive or repulsive interaction [2].

Methods:

Using the G03 program package, structures were fully optimized at MP2 theory level with 6-311++G(d,p) 6d basis functions. We analyzed the bonding characteristics by Bader's "Quantum Theory of Atoms in Molecules" (QTAIM).

Result and Discussion:

In this study, Chalcogen-Chalcogen interactions, wherein a bond path links a pair of chalcogen atoms have been studied in some compounds; To find an answer for the question: Do Chalcogen-Chalcogen BPs indicate a bonding interaction?

In addition, Bader's "Quantum Theory of Atoms in Molecules" (QTAIM) [1] has been used to describe the nature of chalcogen-chalcogen interactions in the studied molecules.



In all molecules a BCP and BP was seen between two chalcogen atoms. Moreover the values of ρ_b , $\nabla^2\rho_b$, V_{BCP} , G_{BCP} and H_{BCP} showed that we can classify these interactions as closed shell interactions.

Special systems were designed including O-O and S-S interactions to investigate QTAIM calculations and IQA energy decomposition analysis [3]. Based on energy components of Chalcogen atoms and potentials $V_{\text{ne}}^{A,\text{mol}}$, $V_{\text{en}}^{A,\text{mol}}$, $V_{\text{ee}}^{A,\text{mol}}$ and $V_{\text{nn}}^{A,\text{mol}}$, existence of O-O interaction was caused a net repulsion on the interacting Oxygen atom, While in direct contrast, in the other system existence of a BP caused a net attraction on the Sulfur atom. This means in case of Oxygen, the BP indicates a non-bonding interaction whereas in sulfur containing molecule a bonding interaction can be followed.

Conclusion:

Intra-molecular chalcogen-chalcogen interactions have been studied. QTAIM analysis of several molecules, which indicates a BP between two chalcogens in their molecular graphs, shows that all of these interactions can be categorized as closed shell interaction. Furthermore, an IQA energy decomposition analysis has been carried out for oxygen and sulfur atoms, to answer this question: "Does existence of a bond path *always* indicate a chemical bond?" considering all of attractive and repulsive potentials for oxygen atom reveal that sometimes existence of a bond path is accompanied by a net repulsive interaction. This means that, in contrast to Bader's statement, the existence of a bond path can not be *always* regarded as a chemical bond.

References:

- [1] Bader, R. W. F. (1990). *Atoms in Molecules, A Quantum Theory*. New York: OUP.
- [2] Cioslowski, J. (1990). "Two isomers of the Li₂C₂O₂ molecule: an ab initio study." *J. Am. Chem. Soc.*, Vol. 112, pp. 6536.
- [3] Blanco, M. A. Martin Pendas, A. Francisco. E. (2005). "Interacting Quantum Atoms: A Correlated Energy Decomposition Scheme Based on The Quantum Theory of Atoms in Molecules." *J. Chem. Theory Comput.*, Vol. 1, p. 1096.



Calculation of Rovibronic Transition Intensities for Diatomic Molecules

Ehsan Gharib Nezhad and Alireza Shayesteh

School of Chemistry, College of Science, University of Tehran, Tehran 14176, Iran

Email: shayesteh@khayam.ut.ac.ir

Key words: Line Intensities, Einstein A coefficient, MgH, Astrochemistry

Introduction:

Stars having remarkable emission lines in the optical spectra are called emission-line stars and widely distributed on the Hertzsprung-Russell diagram including various stellar types.¹ In addition to line positions, knowledge of Einstein A coefficients for rovibronic transitions has important applications in astrophysics.² Experimentally, Einstein A coefficients can be determined indirectly via lifetime measurement; however, this lifetime is related to the rate of radiative decay of an excited state to all lower energy levels.

Magnesium hydride is an important molecule in different astrophysically environments. Lines of the $A^2\Pi \rightarrow X^2\Sigma^+$ transition have been detected in different stellar regions such as the solar photosphere,³ the spectra of sunspot,⁴ nearby L dwarfs,⁵ and late-type stars.⁶ In addition, the $B'^2\Sigma^+ \rightarrow X^2\Sigma^+$ bands have been detected in sunspot umbral spectra.⁷

Theory:

Line intensities of rovibronic transitions are proportional to Einstein A coefficients which directly depend on transition wavenumber $\tilde{\nu}$ (in cm^{-1}), the Hönl-London factor $S_{J''}^{\Delta J}$, and the dipole moment operator $\mu(r)$ in Debye which is a function of internuclear distance r .

$$A_{J' \rightarrow J''} = 3.1361861 \times 10^{-7} \tilde{\nu}^3 \frac{S_{J''}^{\Delta J}}{2J' + 1} \left| \langle \psi'_{v'J'}(r) | \mathcal{R}(r) | \psi''_{v''J''}(r) \rangle \right|^2 \quad (1)$$

$$\left[M_{v''J''}^{v'J'} \right]^2 = \left| \langle \psi'_{v'J'}(r) | \mathcal{R}(r) | \psi''_{v''J''}(r) \rangle \right|^2 \quad (2)$$

Where $R(r)$ is the electronic transition dipole moment in Debye and can be written as:

$$R(r) = \langle \psi'_{el} | \mu(r) | \psi''_{el} \rangle \quad (3)$$

Electronic dipole moments $\mathcal{R}(r)$ can be computed theoretically from high level ab initio calculations.⁸ Using the matrix elements of dipole moment operator $\mu(r)$ in various internuclear distance, $[M_{v''j''}^{v'j'}]^2$ were calculated numerically by program LEVEL.⁹ This program uses an effective Hamiltonian in which rovibrational levels can be calculated numerically. If one uses Condon's approximation, Einstein A coefficients would depend on Frank-Condon factors $q_{v'-v''}$, defined by eq. 4.¹⁰ However, we do not make that approximation in program LEVEL, and use Eqs. (1) to (3) instead.

$$q_{v'-v''} = |\langle v' | v'' \rangle|^2 \quad (4)$$

The $A^2\Pi$ and $B'^2\Sigma^+$ excited states of MgH are close to each other, and there are extensive perturbations between them. These include spin-orbit and rotational perturbations that mix their wavefunctions. The program PGOPHER¹¹ can simulate and fit rovibronic lines with the aid of spectroscopic constants including rotational and spin-orbit constants.

Result and discussion:

Because of spin-orbit coupling, we expect 12 branches for each vibronic transition of the $A^2\Pi \rightarrow X^2\Sigma^+$ system with various intensities. For example, Table 1 shows that Einstein A coefficients of the R_{22} branch of the (1-0) band depend significantly on the total angular momentum quantum number J .

Table 1. Einstein A coefficients of R_{22} electronic transition band of $A^2\Pi \rightarrow X^2\Sigma^+$

$J'' \ v'v''$ energy $q_{v'-v''} [M_{v''j''}^{v'j'}]^2 \mathcal{S}_{J''}^A A(\text{calculated}) A(\text{PGopher})$									
R	0.5	1	5	353161.0000	0.121971000	-0.861079	16413.017	385553.230	397456.545
R	1.5	1	5	424416.0000	0.122034000	-0.861648	16413.998	429035.749	442267.975
R	2.5	1	5	454789.0000	0.121952000	-0.861980	16410.7425	450566.558	464440.244
R	3.5	1	5	471048.0000	0.121723000	-0.862064	16403.2785	462898.031	477118.363
R	4.5	1	5	480475.0000	0.121343000	-0.861877	16391.6151	470261.142	484665.203
R	5.5	1	5	485853.0000	0.120804000	-0.861390	16375.7781	474452.383	488934.105
R	6.5	1	5	488454.0000	0.120099000	-0.860561	16355.7986	476345.086	490825.702
R	7.5	1	5	488927.0000	0.119215000	-0.859340	16331.7236	476402.865	490817.641
R	8.5	1	5	487618.0000	0.118141000	-0.857662	16303.5965	474873.601	489166.955
R	9.5	1	5	484713.0000	0.116861000	-0.855450	16271.4773	471887.701	486010.635
R	10.5	1	5	480297.0000	0.115356000	-0.852609	16235.4418	467498.889	481405.439
R	11.5	1	5	474396.0000	0.113606000	-0.849030	16195.4646	461705.232	475350.441



R	12.5	1	5	466991.0000	0.111586000	-0.844581	16152.0176	454506.935	467849.043
R	13.5	1	5	458029.0000	0.109270000	-0.839106	16103.7042	445717.391	458711.969
R	14.5	1	5	447434.0000	0.106628000	-0.832426	16053.1082	435463.959	448071.637
R	15.5	1	5	435107.0000	0.103626000	-0.824325	15998.6709	423502.043	435681.780
R	16.5	1	5	420932.0000	0.100230000	-0.814554	15940.8175	409740.510	421450.019
R	17.5	1	5	404781.0000	0.096400400	-0.802820	15879.6988	394051.609	405248.216
R	18.5	1	5	386519.0000	0.092097200	-0.788776	15815.4635	376295.993	386940.567
R	19.5	1	5	366006.0000	0.087279600	-0.772019	15748.2602	356336.343	366385.678
R	20.5	1	5	343114.0000	0.081908600	-0.752071	15678.2533	334039.883	343454.630
R	21.5	1	5	317733.0000	0.075949100	-0.728371	15605.6235	309296.623	318036.809
R	22.5	1	5	289795.0000	0.069375400	-0.700257	15530.5658	282036.425	290063.636
R	23.5	1	5	259299.0000	0.062177300	-0.666944	15453.2956	252255.115	259533.756
R	24.5	1	5	226353.0000	0.054370400	-0.627505	15374.2721	220067.917	226564.712
R	25.5	1	5	191230.0000	0.046010200	-0.580836	15292.804	185704.470	191389.04
R	26.5	1	5	154455.0000	0.037213900	-0.525628	15210.3652	149734.680	154582.798
R	27.5	1	5	116917.0000	0.028190400	-0.460313	15126.7334	113021.386	117012.603
R	28.5	1	5	80047.1000	0.019285700	-0.383020	15042.2945	76994.154	80111.865
R	29.5	1	5	46064.1000	0.011047600	-0.291505	14957.4494	43870.705	46101.026
R	30.5	1	5	18329.8000	0.004321210	-0.183069	14872.6609	17018.765	18344.379

Conclusion:

Keeping the astrophysical importance of rovibronic intensities in mind, we have Einstein A coefficients of MgH for calculated the $A^2\Pi \rightarrow X^2\Sigma^+$ and $B'^2\Sigma^+ \rightarrow X^2\Sigma^+$ systems.

References:

- [1] Kogure, T.; Leung, K.-C., The Astrophysics of Emission-Line Stars. 1 edition ed.; Springer; 2007.
- [2] Bernath, P. F., Molecular astronomy of cool stars and sub-stellar objects. *International Reviews in Physical Chemistry* **2009**, 28 (4), 681-709.
- [3] Grevesse, N.; Sauval, A. J., A Study of Molecular Lines in the Solar Photospheric Spectrum. *Astronomy and Astrophysics* **1973**, 27, 29.
- [4] Sotirovski, P., Table of solar diatomic molecular lines spectral range 4900 - 6441 Å. *Astronomy and Astrophysics Supplement* **1972**, 6, 85.



- [5] Reid, I. N.; KIRKPATRICK, J. D.; GIZIS, J. E.; DAHN, C. C.; MONET, D. G.; WILLIAMS, R. J.; LIEBERT, J.; BURGASSER, A. J., FOUR NEARBY L DWARFS. *The Astrophysical Journal* **2000**,119, 369-377.
- [6] Boesgaard, A. M., Isotopes of Magnesium in Stellar Atmospheres. *Astrophysical Journal* **1968**,154 (185), 185.
- [7] Wallace, L.; Livingston, W. C.; Bernath, P. F.; Ram, R. S., An atlas of the sunspot umbral spectrum in the red and infrared from 8900 to 15,050 cm⁻¹ (6642 to 11,230 [angstroms]), revised. *Tucson: National Solar Observatory* **1999**,NSO Technical Report #99-001.
- [8] Saxon, R. P.; Kirby, K.; Liu, B., Ab initio configuration interaction study of the low-lying electronic states of MgH. *The Journal of Chemical Physics* **1978**,69 (12), 5301-5309.
- [9] Le Roy, R. J. *LEVEL 8.0* Chemical Physics Research Report: University of Waterloo, 2007.
- [10] Bernath, P. F., *Spectra of Atoms and Molecules*. Oxford University Press: 2005.
- [11] Western, C. M. *PGOPHER, a Program for Simulating Rotational Structure*, University of Bristol: 2010.



Quantum mechanical study on the mechanism and kinetics of the hydrolysis of Organopalladium Complex $[\text{Pd}(\text{CNN})\text{P}(\text{OMe})_3]^+$

A. Morsali^{a*}, S. A. Beyramabadi^a and S. H. Vahidi

^a Department of Chemistry, Mashhad Branch, Islamic Azad University, Mashhad, Iran

(Email: almorsali@yahoo.com)

Keywords: hydrolysis, Kinetics, Mechanism, Palladium, Density functional theory

Introduction:

Garcia et al. investigated the hydrolysis of Organopalladium Complex $[\text{Pd}(\text{CNN})\text{P}(\text{OMe})_3]^+$ in acidity media experimentally and reported valuable kinetic data. In this work, we investigated this mechanism using the quantum mechanical approach. More specifically, for the rate determining step, being not very clear experimentally, a mechanism was proposed which is compatible with experimental evidence.

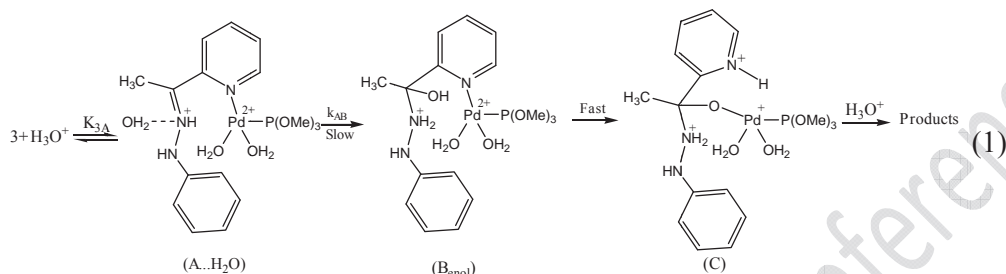
Computational details:

All of the present calculations have been performed with the B3LYP [2] hybrid density functional level using the G09 package. The 6-311+G(d,p) basis set was employed except for Pd atom, in which the LANL2DZ [3] basis set was used with including effective core potential functions. The gas phase optimized geometries used to apply the solvent effects, where the valuable PCM [4] model was employed.

Results and discussion:

We proposed the following mechanism (Eq. (1)) for the rate-determining step which is compatible with experimental evidence. In this mechanism, a fast equilibrium step (with equilibrium constant K_{3A}) will result in the formation of complex $\text{A} \dots \text{H}_2\text{O}$ which will be converted into enol form of B during a slow process. Thereafter, during a fast reaction (pseudo enol-keto tautomerization), form C is created which in the continuation of the process will be converted into reaction products. Considering reactant $\text{A} \dots \text{H}_2\text{O}$ and product $B_{\text{enol}}^{\text{Cis}}$, a transition state is obtained which we call TS_{AB}^{Cis} . Figure 1 presents the optimized

structures of $A \cdots H_2O$, B_{enol}^{Cis} and TS_{AB}^{Cis} . Using PCM model, the values of E_a , ΔH^\ddagger and ΔG^\ddagger (without thermal correction for G) are 106.85, 96.88 and 108.26 kJ/mol, respectively, having good consistency with experimental values ($\Delta H_{exp}^\ddagger = 90 \pm 6 \text{ kJ.mol}^{-1}$, $\Delta G_{exp}^\ddagger = 110.8 \pm 11 \text{ kJ.mol}^{-1}$).



Conclusion:

Using quantum mechanical method, hydrolysis of Organopalladium Complex $[Pd(CNN)P(OMe)_3]^+$ was investigated and ultimately a model was presented in which B_{enol}^{Cis} form is produced in the rate determining step and in continuation is converted into products.

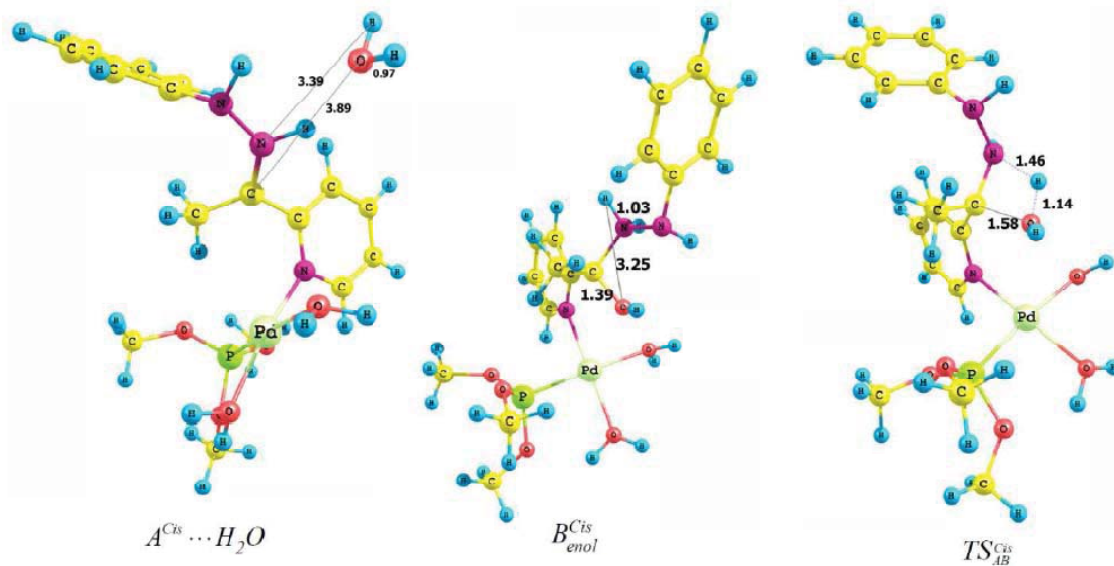


Fig 1. Optimized structure of the $A \cdots H_2O$, B_{enol}^{Cis} and TS_{AB}^{Cis} .

References:

- [1] B. García, F.J. Hoyuelos, S. Ibeas, M.S. Muñoz, I. Peñacoba, J.M. Leal, J. Phys. Chem. A 113 (2009) 911.



- [2] A.D. Becke, Phys. Rev. A, 38 (1988) 3098.
[3] P.J. Hay, W.R. Wadt, J. Chem. Phys. 82 (1985) 299.
[4] S. Miertus, E. Scrocco, J. Tomasi, Chem. Phys. 55 (1981) 117.

15th Physical Chemistry Conference



Theoretical Approaches Of Structure and Conformation Of α , β and γ Cyclodextrin

Sh. Rafiei^{a,c*}, M. Oftadeh^b, H. Seyedoff^a

^aChemistry department, Imam Khomeini International University, Qazvin, Iran

^b Payam- Noor University, Esfahan, Iran,

^c Payam- Noor University, Tehran, Iran,

shahnaz22rafiei@yahoo.com

Abstract:

Ab-initio calculations for the optimized bond length in family of CDs (α , β , γ) will serve to illustrate the effect of larger basis set. Here are the predicted value for several medium and large basis set. The optimization from the MP4/6-311++G(d,p) calculation was chosen as the best optimized geometry because its bond length was closest to the crystalline bond length for β -CD. The experimental bond length, for example (C_3 - C_4), in β -CD is 1.519 Å. Both 6-31G(d,p) and 6-311++G(d,p) basis set (polarized and diffused) are needed to produce a very accurate structure for this molecule.

The potential energy as a function of bond length has the same form for all of the basis sets. As the number of functions in the basis set increases, the energy decreases, which agrees with the variational principle.

Keywords: Cyclodextrin; Inclusion Complex; basis sets; Interaction Scheme; PM4; HF.

Introduction:

Generally, there are three natural cyclodextrins (CDs), α -, β -, and γ -CDs, whose molecular structures contain six, seven, and eight α -1, 4-linked D-glucopyranose as shown in Fig. 1, respectively. [1] These natural structures are characterized as wreath-shaped truncated cones with hydrophobic interior and hydrophilic exterior and have one narrow side (the primary hydroxyl group side) and one wide side (the secondary hydroxyl group side) in their cavities. The amphiphilic molecular structures of these CDs are easy to produce inclusion complexes through interaction with a lot of organic, inorganic, and biological compounds,[2-4] and the

inclusion complexes can be further modified by other small guest molecules, and thus introduce many novel physicochemical properties, particularly their water solubility and solution stability.[5–7] A basis set is the mathematical description of the orbital within a system used to perform the theoretical calculation. Larger basis set more accurately approximate the orbital by imposing fewer restriction on the location of the electron in space. Standard basis set for electronic structure calculations use linear combination of Gaussian function to form the orbital. Gaussian offers a wide range of pre-defined basis set which may be classified by the number and types of basis functions that they contain[3-9]. In this paper, bond length and potential energy surface (PES) in family of CDs (α , β , γ) were investigated employing a series of basis set such as: 6-31G(d,p) and 6-311G(3df,3pd) and 6-311++G(3df,3pd) has been used. Aim of this study-investigation of basis set effect on bond length and potential energy surface(PES) of CDs system – finding the appropriate basis set and method for calculation bond length and PES methodology. In this work, all quantum chemical calculation were performed with the Gaussian 98 program package. The single point energy calculation has been performed at the restricted Hartree-Fock theory, so the effect of basis set on the bond length and PES was evaluated.

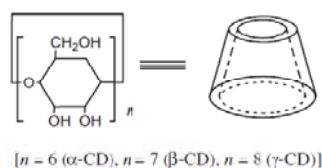


Figure 1. The structures of cyclodextrins

Result and discussion:

The CDs have been calculated by molecular mechanics (MM),[6-8] molecular dynamics (MD),[8]and Monte Carlo simulations (MC),[9] together with the semi-empirical CNDO,[10] AM1, and PM3 methods previously.[11] Because the PM3 method could consider the interactions between non bonded atoms (e.g. hydrogen bond and steric effects)[12] and has high computational efficiency in calculating the CD systems, it is selected to study the interaction of β -CD with Ace and the stability of the inclusion complex in our work. Recently, ab initio calculation at the level of Hartree-Fock (HF) and Density Function Theory (DFT) are also applied in CD chemistry to calculate the single point energy[11] and



proved to be very successful. Because DFT method could consider the electron correlation, its calculations are much more precise than the other methods. Thus, the DFT methods at the basis-set 6-31G* are also used here for higher precision of energy calculations. The initial structure of β -CD was built with the CS Chem3D Ultra (Version 8.0) from the crystal structure,[12] and its full optimization was done with PM3 method without imposing any symmetrical restrictions. Harmonic frequency analysis was used to ensure that the located stationary point was the true minima. The experimental bond length for the CDs for example (C₃-C₄) β -CD beta cyclodextrin molecule is 1.519 Å [1]. Experimental value and predicted values for several medium and large basis set is given in Table 1. Using the 6-31G(d) set, including diffuse functions on the hydrogen atom, improves the result over that obtained with diffuse function only on the fluorine atom, although the best result with this basis set is obtained with no diffuse function at all. All of the geometries predicted with the 6-31G(d,p) basis set are quite accurate. Adding two sets of diffuse functions yields a more accurate structure. However adding additional polarization functions does not significantly affect the result 6-311++G(d,p) thus appears to achieve the basis set limit for this model chemistry. The basis set agreement with the experimental bond length is achieved by 6-31G(d,p) basis set. So the most appropriate basis set finding the PES of the CDs system will be calculated by 6-31G(d,p) basis set at MP4 level of theory. It should be said that the β -CD and B3LYP methods are more accurate, but they are so time consuming and expensive[2]. All the calculations were performed with the GAUSSIAN 1998 software package.[11]



Table 1. The bond lengths, bond angles, and dihedral angles of the β -CD crystalline and the PM3-optimized β -CD.

	β -CD Crystalline	β -CD optimized	Difference
Bond lengths (°Å)			
C1–C2	1.519	1.558	0.039
C2–C3	1.530	1.552	0.022
C3–C4	1.520	1.558	0.038
C4–C5	1.529	1.554	0.025
C5–C6	1.523	1.546	0.023
O5–C1	1.398	1.401	0.003
Band angles (deg)			
C1–C2–C3	109.94	109.91	–0.03
C2–C3–C4	109.18	108.75	–0.43
C3–C4–C5	111.06	109.86	–1.20
C4–C5–C6	113.63	113.45	–0.18
O6–C6–C5	110.37	114.14	3.77
O5–C1–C2	111.14	111.93	0.79
Dihedral angles (deg)			
C1–C2–C3–C4	–53.81	–55.74	–1.93
C2–C3–C4–C5	55.11	54.60	–0.51
C3–C4–C5–O5	–55.93	–52.21	3.72
C4–C5–O5–C1	59.29	53.29	–6.00
C5–O5–C1–C2	–60.10	–54.18	5.92
O5–C1–C2–C3	56.02	54.82	–1.20

Table 1. The optimized values of the bond length C₃–C₄(in Å) at MP4 method.

Bond lengthÅ	α -CD	β -CD	γ -CD
Exp.	1.519	1.519	1.519
Basis Set			
6-31G(d)	1.5504	1.5524	1.5534
6-31G(d,p)	1.5471	1.5492	1.5509
6-31+G,p(d)	1.5482	1.5765	1.5632
6-31++G(d,p)	1.5584	1.5665	1.5574
6-311G(d,p)	1.5624	1.5516	1.5416
6-311++G(d,p)	1.5461	1.5520	1.5562
6-311G(3df,3pd)	1.5616	1.5631	1.5494
6-311++G(3df,3pd)	1.5602	1.5643	1.5593



References:

- [1]. Szejtli J, Chem Rev 98:1743, 1998.
- [2]. Connors KA, Chem Rev 97:1325, 1997.
- [3]. Rekharsky MV, Inoue Y, Chem Rev 98:1875, 1998.
- [4]. Lipkowitz KB, Chem Rev 98:1829, 1998.
- [5]. Dordunoo SK, Burt M, Int J Pharm 133:191, 1996.
- [6]. Tommasini S, Raneri D, Ficarra R, Calabro ML, Stancanelli R, Ficarra P, J Pharm Biomed Anal 35:379, 2004.
- [7]. Lyng SMO, Passos M, Fontana D, Process Biochem 40:865, 2005.
- [8]. Vejrazka M, Micek R, Stipek S, Biochim Biophys Acta 1722:143, 2005.
- [9] K. Huber and G. Herzberg, "Molecular Spectra and Molecular Structure 4. Constants of Diatomic Molecules", Van Nostrand, Princeton (1979)
- [10] S. Kotochigova, J. Res. Natl. Inst. Stan. Technol. 103 (1998) 201
- [11] James B. Foresman & Elen Frisch, "Exploring Chemistry With Electronic Structure Methods", Gaussian, Inc. Pittsburgh, PA (1995)
- [12] J. of Molecu. Structur Theochem 796 (2006) 53



DFT study on the mechanism for formation of olefin complexes in the reaction between palladium(II) and maleic acid

N. Beyzaie ^{a*}, J. S. Emampour ^a, H. Eshtiagh-Hosseini ^a, A. Morsali ^b and S. A. Beyramabadi ^b

^bDepartment of Chemistry, Ferdowsi University of Mashhad, Mashhad 91779, Iran

^aDepartment of Chemistry, Mashhad Branch, Islamic Azad University, Mashhad, Iran

(Email: nbeyzaie@gmail.com)

Keywords: Olefin complexes, Mechanism, Palladium, Density functional theory

Introduction:

Complex formation between $Pd(H_2O)_4^{2+}$ and maleic acid has been studied at 25 °C and 2.00 M ionic strength in acidic aqueous solution [1]. The maleic acid molecule, having a cis configuration, may act as an ambidentate nucleophile through its two carboxylic groups as well as through its C=C double bond. This property helps to stabilize the reaction product. In this work, using the quantum mechanics, the mechanism of reaction between $Pd(H_2O)_4^{2+}$ and maleic acid was investigated.

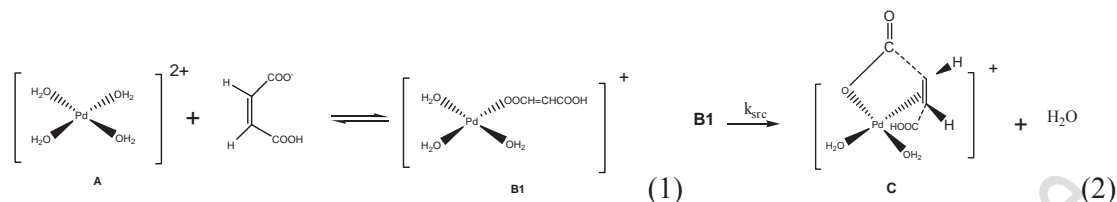
Computational details:

All of the present calculations have been performed with the B3LYP [2] hybrid density functional level using the G09 package. The 6-311+G(d,p) basis set was employed except for Pd atom, in which the LANL2DZ [3] basis set was used with including effective core potential functions. The gas phase optimized geometries used to apply the solvent effects, where the valuable PCM [4] model was employed.

Results and discussion:

The reaction between $Pd(H_2O)_4^{2+}$ with maleic acid and hydrogen maleate produces two intermediates which will be converted into final complex through three paths. The direct and dominant path is an intramolecular ring closure. The following mechanism (Eq.(1) and (2)) for the direct and dominant path was proposed which is compatible with experimental

evidence. In this mechanism, a fast equilibrium step will result in the formation of complex B₁ which will be converted into C and H₂O during a slow process.



The optimized structure of transition state obtained from step2 has been shown in Fig. 1. By taking Solvent effects into consideration, $\Delta G^\ddagger = 17.25 \text{ kcal/mol}$. The calculated value of ΔG^\ddagger (17.25 kcal mol⁻¹) for this path has a good consistency with the experimental value (17.6 kcal mol⁻¹). This shows that the model presented in this research is a suitable model for the rate determining step of urea hydrolysis catalyzed by palladium(II) complex.

Conclusion:

Using quantum mechanical method, the mechanism of reaction between $\text{Pd}(\text{H}_2\text{O})_4^{2+}$ and maleic was investigated and ultimately a model was presented in which B₁ complex is produced in the rate determining step and in continuation is converted into products.

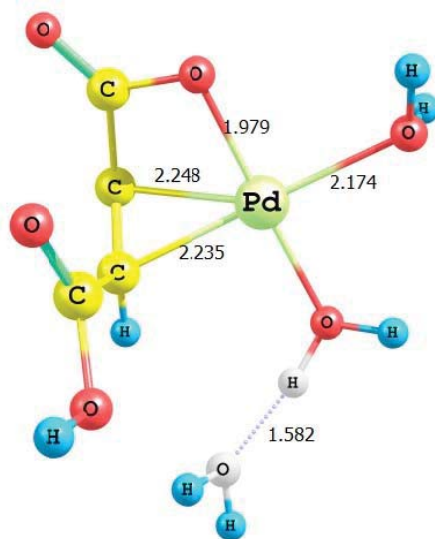


Fig 1. Optimized structure of the TS (step 2)

References:

- [1] T. Shi, L. I. Elding, Inorg. Chem. 37 (1998) 5544.



- [2] A.D. Becke, Phys. Rev. A, 38 (1988) 3098.
[3] P.J. Hay, W.R. Wadt, J. Chem. Phys. 82 (1985) 299.
[4] S. Miertus, E. Scrocco, J. Tomasi, Chem. Phys. 55 (1981) 117.

15th Physical Chemistry Conference

Experimental and Theoretical Study of Valence Photoelectron Spectrum of Proline Amino Acid

F. Fathi, H. Farrokhpour

Chemistry Department, Isfahan University of Technology, Isfahan, 84156-83111, Iran

fariman@ch.iut.ac.ir

Introduction:

The photoelectron spectroscopy of biological molecules such as amino acids and nucleotides in gas phase are very important because the intrinsic properties of amino acids, which are hidden in the complex medium of biological systems, can be understood. In this case, there is a probability that amino acids show properties which are not observable in the solution and provide scientific information which creates insight into the origin of physical and chemical properties of biological molecules. In this work, the valence photoelectron spectrum of proline in the gas phase has been investigated by He-I radiation (21.218 eV). Parallel to experiment, the *ab initio* calculations were performed to estimate the population ratio of proline conformers at the temperature of the experiment and calculate the photoelectron spectrum of each conformer. Fig. 1 shows the geometrical structures of the four most stable neutral conformers of the proline molecule in the gas phase.

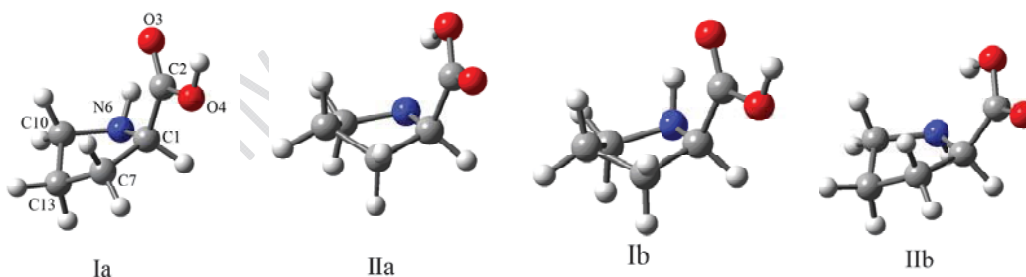


Fig. 1. four most stable conformers of proline

Method:

In this work the valence photoelectron spectrum of proline was recorded using a modern hemispherical electron analyzer (Scienta R4000) mounted in a vacuum chamber and coupled with a commercial noble gas resonance lamp (VSW Scientific Instrument) with helium (He-I: $h\nu = 21.21$ eV). After determining the suitable temperature (110 °C) by

quadruple mass spectrometry, for bringing the proline in to the gas phase, the photoelectron spectrum of L-proline (see figure 2) was recorded in the mentioned chamber. Among different conformers of proline, four lowest lying were selected for the theoretical calculations. Each structure was optimized at MP2/6-311++g** level of theory; Then the optimized geometries were used to separately calculate the energies of the vertical outer valence photoelectron spectra using symmetry adapted cluster/configuration interaction (SAC-CI) method based on single and double excitation operators (SD-R) with the same basis set [1, 2,3].

Results and Discussions:

Fig. 2 shows a comparison between the experimental (red trace) and theoretical spectrum (blue trace). It is evident that there is good agreement between experiment and theory both in position and the intensity of the vertical ionization bands. As it is seen in Fig. 2, all of the features in the experimental spectrum are predicted by theory. To obtain the theoretical spectrum, the Boltzmann weighted photoelectron spectra of proline conformers, calculated at SAC-CI level of theory, were summed.

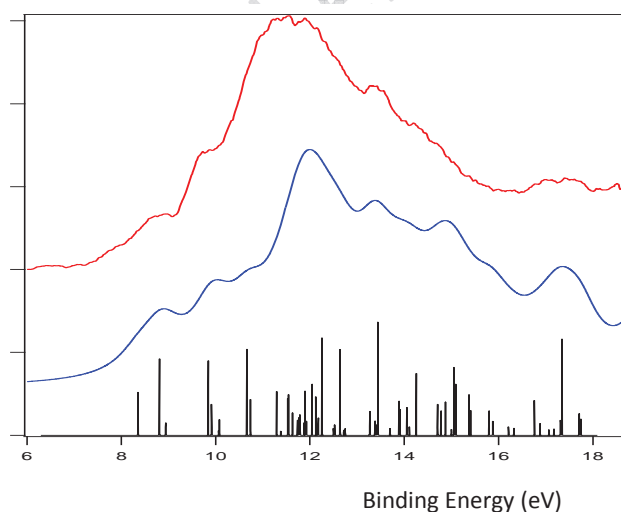


Fig. 2. Comparison between experimental (up red trace) and theoretical (middle blue trace) spectrum

Conclusion:

The valence photoelectron spectrum of L-proline was investigated experimentally and theoretically for the first time. Parallel to the experiment, high level and expensive *ab initio*



calculations at the SAC-CI level of theory is used to interpret and assign the features in the experimental spectrum.

References:

- [1] Nakatsuji, H.; Hirao, K. *J. Chem. Phys* 1978, 68, 2053.
- [2] Nakatsuji, H. *Chem. Phys. Lett* 1978, 59, 362.
- [3] Nakatsuji, H. *Chem. Phys. Lett* 1979, 67, 329.

15th Physical Chemistry Conference



Intramolecular Hydrogen Bonding in 5-Nitrosalicylaldehyde: Infrared Spectrum and Quantum Chemical Calculations

F. Taherian, Z. Moosavi-Tekyeh^{a*}, M. Bakherad^a

^aChemistry Department, Shahrood University of Technology, Semnan, Iran

Email: zmoosavi@gmail.com

Key words: 5-Nitrosalicylaldehyde, Intramolecular hydrogen bond, Infrared spectra, DFT

Introduction:

The experimental vibrational spectra and the advent of density functional methods (DFT) have been the effective tools for investigation of the strength of intramolecular hydrogen bond (IMHB). So, in this study, we used vibrational spectra and theoretical calculations for describing the strength of intramolecular hydrogen bonding of 5-nitrosaldehyde (5NSA) and comparing it with that in salicylaldehyde (SA). These compounds with IMHB can be candidate for molecular switches.

Materials and methods:

Geometry of 5NSA, is fully optimized with hybrid density functional B3LYP [1,2] using 6-31G**, 6-311G**, and 6-311++G** basis sets. Frequencies and ¹HNMR calculations with the GIAO approach were performed at B3LYP level of theory using 6-311G** and 6-311++G** basis sets.

Apparatus:

5NSA was purchased from Alfa Aesar company. The ¹HNMR spectrum was recorded with a Bruker DRX-500 FTNMR spectrometer at 500 MHz frequency using solution in CDCl₃ at 25°C. IR data for the studied molecule in the CH₂Cl₂ solution were recorded on a Fourier Transform Bomem MB-154 spectrometer, at room temperature. All calculations were performed using Gaussian 03W package program version B05.

Result and discussion:

The structures and the atom numbering of 5NSA is shown in Fig. 1. The selected geometrical parameters of 5NSA along with the reported experimental structural parameters are compared in Table 1. In all calculations for 5NSA the NO₂ group lies in the plane of enol ring. As it is obvious from data, the main effect of NO₂ substitution is shortening of the O···O distance and lengthening of the O–H bond length in comparison with that values for SA. The calculated O···O and O–H distances in 5NSA are 0.01–0.012 and 0.002–0.003 Å, respectively, shorter and longer than those in SA with all calculation. The NMR proton chemical shifts of 5NSA and SA are 12.07 and 11.05 ppm at B3LYP/6-311++G**, respectively. The IR spectrum of 5NSA in CH₂Cl₂ in 3500–2000 cm^{–1} region, exhibits a broad band with several sharp bands in this region. The frequency of this broad band is about 3110 cm^{–1} is assigned to OH stretching in 5NSA, the corresponding band in SA appears at 3200 cm^{–1}[3]. Upon deuteration, the □OH band in 5NSA disappears and a new band appears at about 2330 cm^{–1}, (□OD), for SA the analogous band appears at 2367 cm^{–1}.

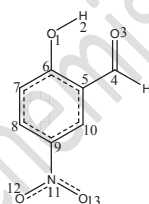


Fig.1

Table 1. The selected geometrical parameters and the stretching modes of 5NSA and SA calculated at the B3LYP.

Distance(Å)	5NSA				SA			
	6-31G**	6-311G**	6-311++G**	Exp.[4]	6-31G**	6-311G**	6-311++G**	Exp.[3]
O–H	0.992	0.987	0.986	0.937	0.990	0.984	0.984	-
O···O	2.609	2.623	2.629	2.613	2.621	2.633	2.639	-
H···O	1.718	1.744	1.755	1.728	1.730	1.753	1.764	-
Frequencies(cm ^{–1})	This work							
□OH	3317	3372	3382	3110	3359	3407	3415	3200
□OD	2419	2459	2466	2330	2449	2483	2490	2367

Conclusion:

In this study has tried to analyze the vibrational spectra of 5NSA between calculated frequencies with the experimental results. From the OH stretching mode and proton chemical



shift a stronger intramolecular hydrogen bond in 5NSA than that in SA was concluded. Although the electron withdrawing effect of NO₂ group decreases the strength of the bond, conjugation effects increases the hydrogen bond strength compared with SA.

References:

- [1] A.D. Becke, *J. Chem. Phys.* 98 (1993) 5648.
- [2] C. Lee, W. Yang, R.G. Parr, *Phys. Rev. B* 37 (1988) 785.
- [3] M. Berthelot, C. Laurence, D. Foucher and R. W. Taft, *J. Phys. Org. Chem.* 9 (1996) 255.
- [4] H. Tanak, M. Macit, M. Yavuza, S. Isıka, *Acta Cryst E.* 65 (2009) o3056.



Meta-stable excited states of Cl_2^{2-}

H. Sabzyan, Z. Nourisafa, E. Keshavarz

Department of Chemistry, University of Isfahan, Isfahan, 81746-73441, I.R. Iran

Email: sabzyan@sci.ui.ac.ir; z.nourisafa@sci.ui.ac.ir; elkeshavarz5@sci.ui.ac.ir

Keywords: Potential energy curves, Diatomic dianion, Repulsive Coulomb barrier.

Introduction:

Most of the small dianions are unstable in the gas phase, but in the electron impact experiments carried out on some diatomic anions, such as C_2^- and Cl_2^- , resonance structures have been reported that can be considered as a sign of the formation of excited state diatomic dianions [1,2]. The threshold behavior of the cross section and formation of doubly charged negative ions (dianions) as a result of the temporary capture of the incident electron by the singly charged negative ion, are two interesting aspects of such a collision system. No information has been available to date on the properties and potential characteristics of Cl_2^{2-} . In addition, diatomic dianions such as Cl_2^{2-} are of considerable intrinsic interest to physicists due to correlation between their outer space electrons [2]. To investigate the probability of the formation of Cl_2^{2-} during the electron impact experiment and its contribution to the etching process of semiconductors by the chlorine gas, the ground state potential energy curves of Cl_2 , Cl_2^- and Cl_2^{2-} species are calculated.

Computational methods:

Ab initio calculation of the ground and excited states potential energy curves (PECs) are carried out respectively at QCISD(T) and CIS level of theory with the aug-cc-pVQZ basis set. Rovibrational levels and Franck-Condon factors (FCFs) of possible transitions between PECs have been calculated using LEVEL8 program coded by LeRoy [3].

Results and discussion:

The ground state $X\ ^1\Sigma_g$ and four of the excited states of Cl_2^{2-} are purely repulsive and the lowest singlet $A\ ^1\Sigma_g$ and the lowest triplet $a\ ^3\Sigma_g$ states are meta-stable, having respectively

12 and 9 vibrational levels for the $[^{35}\text{Cl}^{35}\text{Cl}]^{2-}$ isotopomer. The characteristics of the $X^2\Sigma_g(\text{Cl}_2^-)$, $X^1\Sigma_g(\text{Cl}_2^-)$ and $a^3\Sigma_g(\text{Cl}_2^-)$ PECs are calculated and listed in Table 1. Values of the FCFs calculated for the $a^3\Sigma_g \text{Cl}_2 \rightarrow a^3\Sigma_g \text{Cl}_2^{2-}$, $X^1\Sigma_g \text{Cl}_2 \rightarrow A^1\Sigma_g \text{Cl}_2^{2-}$ and $X^1\Sigma_g \text{Cl}_2^- \rightarrow a^3\Sigma_g \text{Cl}_2^{2-}$ transitions are so large that the Cl_2^{2-} dianion can be predicted to produced in its excited states in the electron impact experiments on the $a^3\Sigma_g \text{Cl}_2$ and $X^2\Sigma_g \text{Cl}_2^-$ states. Furthermore, contribution of the centrifugal kinetic potential to the features of the $A^1\Sigma_g \text{Cl}_2^{2-}$ and $a^3\Sigma_g \text{Cl}_2^{2-}$ PECs are considered analytically for the rotational states $j=0-50$. By increasing j from 0 to 50, for the $A^1\Sigma_g \text{Cl}_2^{2-}$ state, the well depth changes from 1648.288 cm^{-1} to 1495.490 cm^{-1} , the barrier height changes from 1648.288 cm^{-1} to 1798.179 cm^{-1} and the width of the potential well (at barrier) decreases from 1.5155 \AA to 1.4629 \AA . The $a^3\Sigma_g \text{Cl}_2^{2-}$ PEC show similar behavior but with different scales; the well depth changes from 1403.835 cm^{-1} to 1252.683 cm^{-1} and the barrier height changes from 1403.835 cm^{-1} to 1593.889 cm^{-1} .

Table 1: Calculated equilibrium distances R_e (in \AA) and the well depth D_e (in eV) and the corresponding v_{max} and j_{max} obtained for the bound metastable electronic states of Cl_2 , Cl_2^- and Cl_2^{2-} .

	$^1\Sigma_g(\text{Cl}_2)$		$^3\Sigma_g(\text{Cl}_2)$		$^2\Sigma_g(\text{Cl}_2^-)$		$^1\Sigma_g(\text{Cl}_2^{2-})$		$^3\Sigma_g(\text{Cl}_2^{2-})$	
$R_e (\text{\AA})$	2.0040		2.4120		2.5859		2.8280		2.5972	
$D_e (\text{eV})$	2.36479		0.52528		1.60831		0.20436		0.17351	
$^{35}\text{Cl}-^{35}\text{Cl}$	v_{max}	j_{max}	v_{max}	j_{max}	v_{max}	j_{max}	v_{max}	j_{max}	v_{max}	j_{max}
	47	37	19	20	101	15	11	32	8	54

Conclusion:

Based on the analysis of the results obtained in this work, it can be predicted that formation of the Cl_2^{2-} dianion via an electron impact process initiating from the ground state Cl_2 and Cl_2^- is possible. Furthermore the $a^3\Sigma_g \text{Cl}_2^{2-}$ and $A^1\Sigma_g \text{Cl}_2^{2-}$ states of Cl_2^{2-} are metastable with $R_e=2.5972 \text{ \AA}$ and $R_e=2.8280 \text{ \AA}$ and $D_e=0.17351 \text{ eV}$ and $D_e=0.20436 \text{ eV}$ suiting 9 and 12 vibrational states, respectively.



References:

- [1] Pedersen, H. B. et al. Phys. Rev. Lett. 81, 24, 5302 (1998).
- [2] Collins, G. F. et al. H. Phys. Rev. A 72, 042708 (2005).
- [3] Le Roy, R. J. Level 8.0, see <http://leroy.uwaterloo.ca/programs/>.

15th Physical Chemistry Conference



Spectroscopic constants and molecular properties of OBr^- and OCl^-

H. Sabzyan, Z. Noorisafa

Department of Chemistry, University of Isfahan, Isfahan, 81746-73441, I.R. Iran

sabzyan@sci.ui.ac.ir; z.nourisafa@sci.ui.ac.ir

Keywords: Potential energy curves, Diatomic anion, Spectroscopic properties, OBr^- , OCl^-

Introduction:

There are a few reports on the experimental attempt towards determination of spectroscopic constants and molecular properties of diatomic anions [1,2]. In this study, we have studied the electronic structure, properties, and spectroscopic constants of two diatomic anions of astrophysical [3] and laboratory interest.

Computational methods:

Ab initio calculation of the ground states potential energy curves (PEC) of OBr^- and OCl^- are carried out at the QCISD(T) level of theory with the aug-cc-pVQZ basis set. Rovibrational levels and spectroscopic properties have been calculated based on these PECs using LEVEL8 program coded by LeRoy [4].

Results and discussion:

The calculated PECs, presented in Fig. 1, shows that $X^1\Sigma$ and $a^3\Sigma$ electronic states of OBr^- , and the $X^2\Sigma$ state of OBr are attractive with potential depths of $D_e = 2.68604\text{ eV}$, $D_e = 0.41404\text{ eV}$ and $D_e = 2.55485\text{ eV}$, respectively. The OCl^- diatomic anion in both $X^1\Sigma$ ($D_e = 3.69322\text{ eV}$) and $a^3\Sigma$ ($D_e = 0.36857\text{ eV}$) electronic states are more stable than its neutral diatomic anion in its ground state ($D_e = 2.69320\text{ eV}$), and their ionization energies are 2.28556 eV and 1.28468 eV , respectively. Similar calculations, carried out on OF^- , at QCISD(T)/aug-cc-pVQZ level of theory, failed due to drastic fluctuations in its PECs. The spectroscopic constants and molecular properties of the anionic OBr^- and OCl^- species (in

the $X^1\Sigma$ and $a^3\Sigma$ states) and their neutral molecules (in the $X^2\Sigma$ state) are summarized in Table 1.

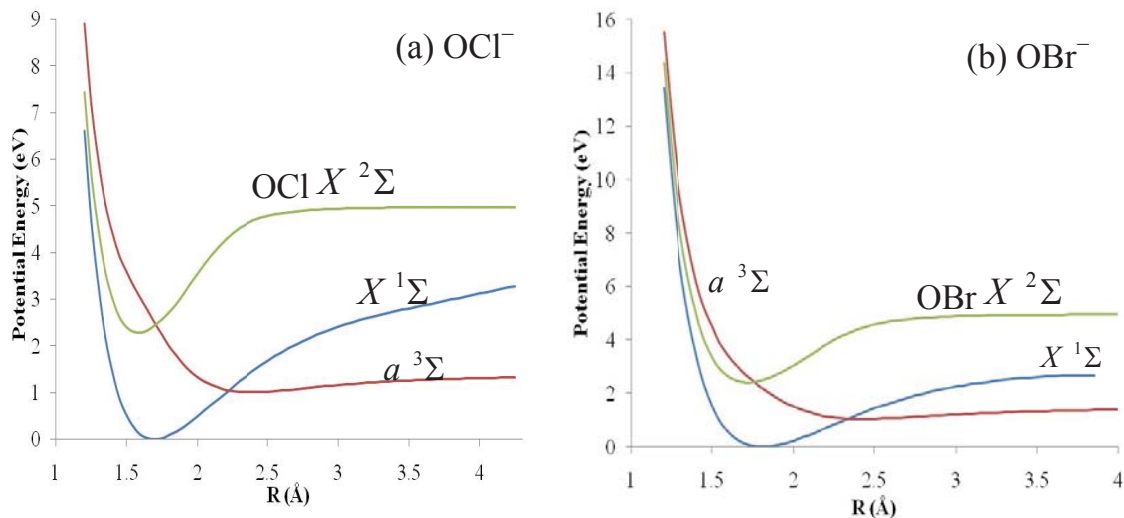


Figure 1: Potential energy curves of the $X^1\Sigma$ and $a^3\Sigma$ states of the anionic diatomics OCl^- (a) and OBr^- (b). The PECs of the ground state ($X^2\Sigma$) neutral molecules are also given for comparison.

Table 1: Calculated equilibrium distances R_e (in Å) and the well depth D_e (in eV), and the corresponding spectroscopic properties obtained for the ground and the first triplet electronic states of OBr^- and OCl^- at QCISD(T)/aug-cc-pVQZ level of theory.

Spectroscopic Parameter	OBr^- $X^1\Sigma$	OBr^- $a^3\Sigma$	OBr $X^2\Sigma$	OCl^- $X^1\Sigma$	OCl^- $a^3\Sigma$	OCl $X^2\Sigma$
R_e (Å)	1.8070	2.4300	1.7190	1.6950	2.3840	1.5830
D_e (eV)	2.68604	0.41404	2.55485	3.69322	0.36857	2.69320
ω_e (cm ⁻¹)	-403.797	-149.345	-486.424	-441.711	-157.312	-512.533
$\omega_e X_e$ (cm ⁻¹)	978.997	362.682	1179.632	1070.962	382.246	1242.746
$\omega_e Y_e$ (cm ⁻¹)	-365.661	-136.515	-441.167	-400.087	-144.260	-464.387
B_e (cm ⁻¹)	0.387	0.214	0.428	0.532	0.270	0.505
α_e (10 ⁻³ cm ⁻¹)	3.561	3.798	3.972	5.321	5.927	4.427
D (10 ⁻⁷ cm ⁻¹)	6.409	7.684	5.919	13.90	13.65	8.802
β_e (10 ⁻⁹ cm ⁻¹)	-1.186	34.89	14.88	-7.033	79.75	5.328
ν_e (0 → 1) (cm ⁻¹)	594.3412	217.6635	715.0503	649.9843	228.5141	753.9620
ν_e (1 → 2) (cm ⁻¹)	586.9296	209.2450	704.6288	641.4369	217.7093	743.4829



Ionization energy (eV)	2.41646	1.36404	–	2.28556	1.28468	–
------------------------	---------	---------	---	---------	---------	---

References:

- [1] S. Midda, A. K. Das, Intern. j. Quant. Chem. 98 (2004) 447.
[2] S. Midda, A. K. Das, THEOCHEM 713 (2005) 101.
[3] R. P. Turco, J. Geophys. Res. 82 (1977) 3585.
[4] Le Roy, R. J. Level 8.0, see <http://leroy.uwaterloo.ca/programs/>.

15th Physical Chemistry Conference



Prediction of gas chromatography retention of alcohols based on quantum chemical parameters

A. Morsali^a, M. M. Heravi^a, E. Amin^a and A. Mansoorinasab^{* a}

^aDepartment of Chemistry, Mashhad Branch, Islamic Azad University, Mashhad, Iran

(Email: chemquantum@yahoo.com)

Keywords: Gas chromatography, Retention time, Quantitative structure-retention relationship, Density functional theory

Introduction:

Quantitative structure-retention relationship (QSRR) [1-2] models for the gas chromatography retention times of alcohols on DB-624, DB-wax and DB-1 have been developed. Using multiple linear regression method, the correlation between retention time and structural parameters was obtained.

Computational details:

Structural parameters have been obtained using quantum mechanical calculations. The following parameters have been considered: dipole moments (μ), molecular volumes (V), molecular radius (r), the lowest unoccupied molecular orbital (LUMO), the highest occupied molecular orbital (HOMO), Müllicken charges (Q) and Müllicken negative charges with hydrogens summed into heavy atoms in molecule (QH). All calculations were performed with the B3LYP hybrid density functional level [3] using the Gaussian 03 program [4]. Geometries of Alcohols were optimized at 6-311+G(d,p) basis sets. The calculated frequencies have no imaginary vibrational frequency, indicating that the optimized geometries are reasonable and reliable. In this work, linear method has been used. The relation between retention time and structural parameters is established by the following multi-linear form:

$$t = a_0 + a_1 p_1 + a_2 p_2 + \dots + a_n p_n \quad (1)$$

where t is retention time and $p_1, p_1 \dots p_1$ are structural parameters. The intercept (a_o) and the regression coefficients ($a_1, a_2 \dots a_n$) were determined using least square method. Sigmaplot software has been used for this purpose.

Results and discussion:

Molecular volume and molecular radius control retention time by affecting on rate of mass transfer. Dipole moment is important in the interaction of the molecules with polar and apolar stationary phases. Each increase in polarity of the stationary phase causes a parallel increase in the role of dipole moment. Q and Q_H play an important role in van der Waals interactions between molecules. HOMO as an electron donor and LUMO as an electron acceptor are specifically effective in chemical reactions.

Using Eq. (1), the intercept (a_o) and the regression coefficients ($a_1, a_2 \dots a_n$) were obtained. These coefficients were presented in Table 1. Correlation coefficient (R) and square of correlation coefficient (R^2) for this fitting were obtained 0.9921 and 0.9910, respectively, being very appropriate for prediction of retention times of alcohols. Subsequently, DB-wax (Polyethylene Glycol) and DB-1 (Dimethylpolysiloxane) columns were considered for testing the presented model.

Conclusion:

In this work, structural parameters have been obtained using quantum mechanical approach. Each parameter is somehow effective in retention time. Using multiple linear regression method, the correlation between retention time and structural parameters was obtained. The appropriate correlation obtained in connection with different columns shows the efficiency of the applied model for prediction of retention times of alcohols.

Table 1. The intercept (a_o), the regression coefficients ($a_1, a_2 \dots$) and correlation coefficient (R)

column	a_o	$a_1(V)$	$a_2(r)$	$a_3(\mu)$	$a_4(Q)$	$a_5(Q_H)$	$a_6(HOMO)$	$a_7(LUMO)$	R
DB-64	-136.96	10.94	-3.17	-14.97	6.15	11.84	40.59	-0.5766	0.9921
DB-1	-77.21	9.12	-4.03	-15.36	8.06	-5.42	19.74	-0.2855	0.9911
DB-wax	-55.71	18.12	-3.36	-15.29	2.74	15.49	9.480	-0.1472	0.9900



References:

- [1] T. Kortvelyesi, M.Gorgenyi, K. Heberger, *Anal. Chim. Acta* 428 (2001) 73.
- [2] T. Woloszyn, P. Jurs, *Anal. Chem.* 64 (1992) 3059.
- [3] A. D. Becke, *J. Chem. Phys.* 98(1993) 5648.
- [4] M.J. Frisch, et al. *Gaussian 03*, Revision 6.0; Gaussian, Inc.: Pittsburgh PA, 2003.

15th Physical Chemistry Conference



Interaction of Potassium ion with Amino Acids(alanine) as Building block of Proteins: A DFT and HF study

Kh.Yarijoo*, f.parvinzadeh

Islamic Azad University,yasooj .Iran

Email:khyarijoo@yahoo.com

Keywords:amino acids,biological systems,DFT, HF method,IR spectrum and NMR

Introduction:

The metal ions have important roles in structure and function of proteins and other biomolecules [1]. The role of metals as cofactor is greatly magnified in activation of enzyme [2,3]. understanding the mechanism of activation inhibition and other reaction, in which the metal ions have a critical role, is achieved by clarifying the interaction of protein sequences and the metal ions. The amino acid cations are undoubtedly much abundant ions in biological systems. They act as which bind weakly to organic are ideally suited in generating ionic gradients across membranes and for the maintenance of osmotic balance .on the other hand the Potassium ion as metal ion have an important application as anti mania drug for the depression disease . Study of the interactions between Potassium ion with biological molecule may be inaccessible because of the complexity of the biomolecules. it seems that the first estimation of these interactions can be obtained by studying the interaction of the metal(Potassium) ions with the simple molecule such as alcohol, amide, amine and other molecules containing functional group resemble to functional group exist in biomolecules. As a result extended research was done to understand the nature of Potassium ion interaction with small organic systems .linear 1-4 carbon alcohols .substituted acetophenones [3] formaldehyde . This research deals with the Potassium ion bond dimer of some substituted ketones and study the effects of the group's nature on structure, stability and heat of formation of them. This could be considered as beginning to understanding the interaction of metal ion on small organic molecules as an estimation of biological systems.

Materials and methods:

The structure of each species in this research include; Amino Acids, Potassium ion attached to Amino Acids and Potassium ion bonded dimer of them were optimized by DFT, HF

method, 6-311++G** basis set and gaussian2003 package. Energy parameters, IR spectrum and NMR of each species were calculated by using same method and basis set described previously.

Results and Discussion :

1. Structure and Stability of Species: Structure of each substituted Amino Acid, Potassium ion complex and Potassium ion bonded dimer of them were optimized by method and basis sets mentioned previously in two conformations. The stability of the Potassium bond dimers were estimated by considering the IR spectrum of them. In Fig., the structure of Potassium ion bonded dimer of Amino Acids which $R_1=H$ and $R_2=NH_2$ in two forms and IR spectrum of them are shown.

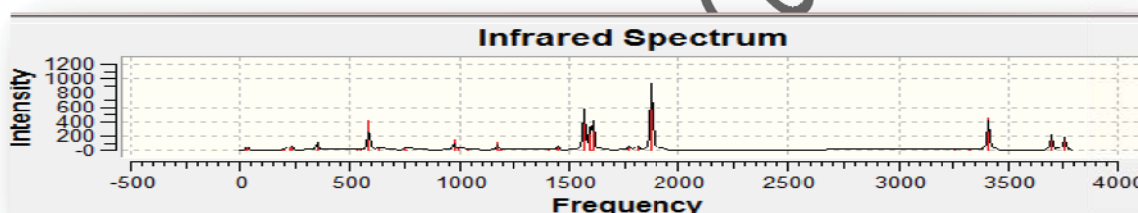


Fig.1 the structure IR Spectrum of them in which $R_1=H$ and $R_2=NH_2$

2. K-O Bond length and enthalpy of formation of each Potassiumion bonded dimer

In this section the K-O bond length which show the strength of the K-O bond were calculated for each substituted Potassium ion bonded dimer. The s factor defines as Eq.1; show the reduction of charge of Potassium ion as the result of dimerization. In Fig. the result of K-O bond length versus s factor is shown. In **Error! Reference source not found.**, the enthalpy of formation of Potassium ion bonded dimer of substituted Amino Acids versus s factor is shown.

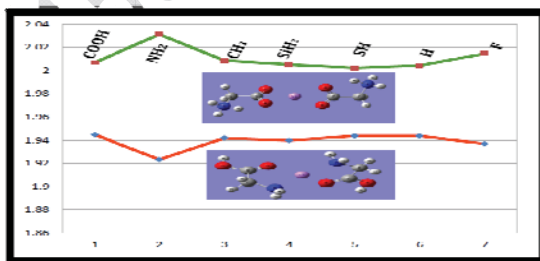


Fig.2 K-O bond length of Potassium ion bonded dimer of substituted Amino Acids versus s factor

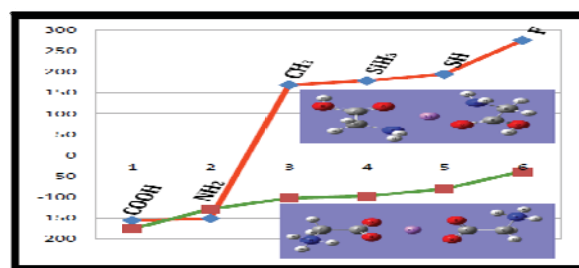


Fig.3 Enthalpy of formation of Potassium ion bonded dimer of substituted Amino Acids versus s factor



Conclusion :

The energy parameters of them were analyzed by same method and show that each parameter such as electron releasing or withdrawing properties of substitutions reduced positive charge on potassium ion, makes the dimer more stable.

References:

- [1] Hille R., Chem. Rev., 1996, 96, p.2757
- [2] R.B. Davies and E.P. Abraham, Biochem. J., (1974) 143, p.129
- [3] S. Karlin, M. Zuker, L. Brocchieri, J. Mol. Biol. 239 (2006) 227

15th Physical Chemistry Conference



Interaction of Potassium ion with Amino Acids and the net charge on the carbonyl of the free bases: A DFT study

*Kh. Yarijoo f. parvinzadeh,

Islamic Azad University, yasooj .Iran

Email: khyarijoo@yahoo.com

Keywords: Potassium Ion, Potassium Ion Bonded Dimer, Amino Acids, Na⁺/K⁺ pump

Introduction:

The metal ions have important roles in structure and function of proteins and other biomolecules [1]. The role of metals as cofactor is greatly magnified in activation of enzyme [2,3]. Understanding the mechanism of activation, inhibition and other reactions, in which the metal ions have a critical role, are achieved by clarifying the interaction of metal ions with protein sequence. The alkali metal cations, specially sodium and potassium are undoubtedly much abundant ions in biological systems. The nervous system function seriously depends on the activity of the Na⁺/K⁺ pump, the transporter responsible for maintaining steep Na⁺ and K⁺ gradients across the neuron plasma membrane. Study of the interaction between potassium ion and biosystems may be unreachable because of the complexity of the biomolecules. It seems that the first estimation of these interactions can be obtained by studying the interaction of the metal ions with the simple molecule such as alcohol, amide, amine and other molecules containing functional groups that resemble functional groups that exist in biomolecules. In this manner, extended research was done to understand the nature of the interactions [4,5]. In this research the interaction of potassium ion with amino acids as building blocks of proteins was studied. This research can be considered as a starting point in finding the interaction of potassium ion with proteins.

Materials and methods:

Amino acids are building blocks of proteins in which have amine (NH₂) and carboxylic acid group attached to a single carbon. There are two forms of amino acids; neutral and ionic forms. The properties of them are changed from electron withdrawing groups to electron

releasing groups. study the interaction of potassium ion with substituted Amino Acids. The structure of each species in this research include; Amino Acids, potassium ion attached to Amino Acids and potassium ion bonded dimer of them were optimized by DFT method, 6-311++G** basis set and gaussian2003 package. Energy parameters, IR spectrum and NMR of each species were calculated by using same method and basis set described previously The potassium ion bond length to oxygen or nitrogen shows the strength of it.

Results and discussion

1. Structure and stability of Amino Acids, potassiumion bonded to Amino Acids and potassium ion bondeddimer of them:

Structure of all species such as Amino Acids, potassiumion bonded to Amino Acids and potassium ion bondeddimer of them was calculated.

2. Potassium ion bond strength and enthalpy of formation for potassium bonded dimer of Amino Acids:

The potassium ion parametrs(η) versus δ factor. Decrease in potassium positive charge or δ factor can be defined as Eq.1

$$\sigma = \text{charge of isolated } K^+ - \text{charge of } K^+ \text{ in dimer}$$

$$\eta = \frac{LOMO - HOMO}{2}$$

the bond length of K^+ to Oxygen or Nitrogen versus decrease in potassium charge or(δ)factor is plotted. In

Fig.1, plot of the parametrs(η) of formation for the different dimers versus (η)factor is shown.

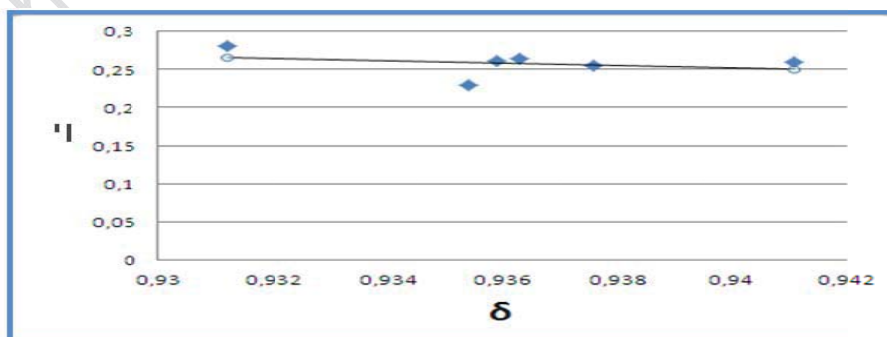


Fig.1 parametrs(η)of the different dimers versus (δ) factor



when the charge in central potassium ion in dimer decreases (higher δ factor) the strength of potassium bond to amino acids is strengthened and the parameters (η) of formation of dimer increases.

Conclusion:

The structure and stability of potassium ion bonded dimers of different substituted amino acids which resembled the interaction of potassium ion with proteins, were calculated by ab initio calculations. The energy parameters of them were analyzed by same method and show that each parameter such as electron releasing or withdrawing properties of substitutions reduced positive charge on potassium ion, makes the dimer more stable.

References:

- [1] Crichton R. R., Biological Inorganic Chemistry an Introduction, Elsevier, 1st edition. 2008
- [2] Cowan J. A., Chem. Rev. 1998, 98, p.1067
- [3] Hille R., Chem. Rev., 1996, 96, p.2757
- [4] Amtmann A, Blatt M.R., (2009) Regulation of macronutrient transport. New Phytol 181:35–52



Influence of structural features on ion mobility spectra of Substituted Benzaldehyde isomers at atmospheric pressure and different temperature

A. Abedi*¹, M. Azadi²

*¹ Department of Science, Islamic Azad University, Shahreza Branch, Shahreza, Iran, abedi@iaush.ac.ir

² maryam.azadi2000@yahoo.com

Key words: Ion mobility spectrometry, Structural Isomer, Substituted benzaldehyde Isomers, Temperature Dependence.

Introduction:

The term ion mobility spectrometry (IMS) refers to the principle methods and instrumentation for characterizing chemical substances on the basis of velocity of gas-phase ions in an electric field [1]. Usually recognizing of isomeric compounds from each other is difficult and needs special and expensive laboratory devices [1, 5]. IMS permits the rapid and simple determination of these compounds. This instrument works at atmospheric pressure therefore the experiments are done very simple with this method in compare with other instruments such as mass spectrometry. The aim of this work is identification of some benzaldehyde substituted isomers by ion mobility spectrometry and investigation the temperature and the drift gas composition on ion mobility spectra of these compounds in order to find the optimum condition for identification of them from each other by ion mobility spectrometry.

Materials and methods:

The isomeric compounds that were investigated in this research are ortho, meta and para isomers of hydroxy benzaldehyde and nitro benzaldehyde. These materials were synthesized by Merck Company. The drift and carrier gas were nitrogen and argon. The temperature was changed from 30°C to 200°C and the follow rates of carrier and drift gas were 250 and 500 ml/min respectively.



Apparatus :

The IMS apparatus with the continuous corona discharge as ionization source has been used. Corona discharge source is constructed from a stainless steel needle and an aluminum ring in front of it. The IMS cell has been made from 16 aluminum rings that were separated from each other by non-conductive Teflon sheets. The aluminum rings are connected to each other by a series of resistors in order to form a uniform electric field.

Result and Discussion:

Ion mobility is influenced by the molecular mass of analyt and their collision cross-section in addition to the operational parameters such as temperature, drift gas composition and electric field. Therefore, ions with different mass and structure attain different drift velocities, providing a basis for the separation of ions in IMS analyzers. We investigated and compared isomeric compounds, that they have an identical molecular weight but different structures therefore it enables the mass effects to be ruled out and allows the structural effects to be examined. It is expected these processes lead to differences in the ion mobility spectra of different isomeric compounds. These differences can be caused either by various processes of ion formation at atmospheric pressure or during the motion of ions through the drift.

The effects of temperature and drift gas composition on mobility spectra of these isomeric compounds also were investigated. Figure 1 shows the ion mobility spectra of 4-hydroxi benzaldehyde at different temperatures in N₂. At low temperatures in addition of the molecular ion peak the dimmer ion peaks were appeared at high drift time. By increasing the temperature the intensity of dimmer ion peaks decrease and it was disappeared at 100 °C therefore the spectrum becomes more clear. The intensity of dimmer peaks also is dependent on the sample concentration. Figure 2 shows the ion mobility spectra of different isomers of hydroxi benzaldehyde at 150 °C in N₂. The ion mobility spectra of ortho, meta and para hydroxi benzaldehyde isomers have different ion pattern that related to different ion products with different mobility that is probably related to different collision cross-section of ion-neutral molecules because of different size and shape of products. Ortho isomer didn't have dimer ions peak even at low temperature. It could be related to the formation of inter molecular hydrogen bound. The ion mobility spectra have the same ion pattern in Ar such as in N₂.

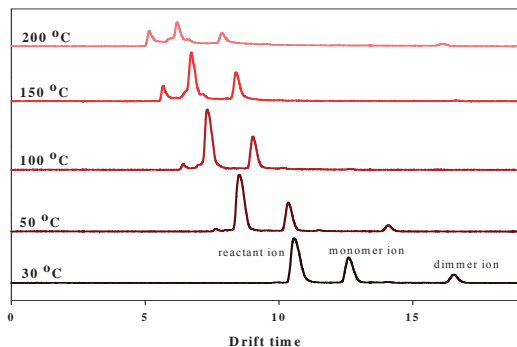


Figure 1: Ion mobility spectra of 3-Hydroxybenzaldehyde at different temperature

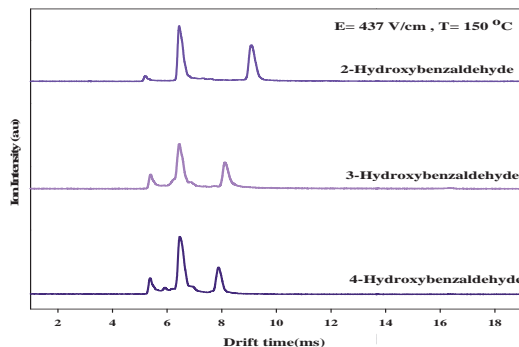


Figure 2: Ion mobility spectra of hydroxybenzaldehyde isomers in N₂.

Conclusion:

In this research ion mobility spectrometer with corona discharge ionization source was applied for detection of several benzaldehyde substituted isomers at atmospheric pressure. The result showed the isomeric compounds had different ion mobility spectrum that arise from different structure and different ion products. IMS can be introduced as a sensitive and selective method for identification of these compounds.

References:

- [1] G.A.Eiceman, Z.Karpas; " Ion Mobility Spectrometry" CRC Press, Boca Raton, 2005.
- [2] H.Borsdorf, T. Mayer; Int. J. Ion Mobil. Spec; 2010, **13**, 103–108.
- [3] S.Larissa, J. McLean; Phys. Chem.; 2011, **13**, 2196–2205.
- [4] H.Borsdorf; Int. J. Ion Mobil. Spec; 2008, **11**, 27–33.
- [5] H. Borsdorf; J. Am. Soc. Mass Spectrom; 2002, **13**, 1078–1087.



Three-particle quantum scattering via separable potentials: Application to statistical mechanics

V. Moheb Maleki and A. Maghari

Department of Physical Chemistry, College of Science, University of Tehran, Tehran, Iran

E-mail: vahdat_mohebmaleki@yahoo.com

Abstract:

In the present work, we have calculated three-body system transition matrices in the presence of a non-local separable potential and any other scattering properties such as poles of transition matrix, phase shift, cross sections, time delay, cross sections and collision integrals. Analytical expressions for some equilibrium thermodynamics properties, such as the Helmholtz free energy and heat capacities as well as some non-equilibrium thermophysical properties, such as collision cross sections and transport collision integrals have been studied.

Keywords: Faddeev equation, Three-body scattering, thermophysical properties

Introduction:

From the Faddeev point of view, in a three-body system there are three different two-body subsystems. The idea is to sum up the pair forces in each two-body subsystem to infinite order, and then in a second step among all three particles. The approach based on the direct use of the Lippmann-Schwinger equation is found to be inapplicable in this case. In fact, it can be shown that even for a two-particle system the Lippmann-Schwinger equation does not have unique solution, if we take in to account the motion of the center of mass of the system. A similar indeterminacy in the solution of the Lippmann-Schwinger equations is also found for systems consisting of three or more particles. In recent works, the scattering properties of a two-body system with zero and non-zero angular momentum via a separable potential of rank 2 was calculated and then applied to obtain the equilibrium statistical mechanical properties of fluids. A generalized formulation for the partial-wave scattering wavefunction and its properties, such as the phase shift and time delay, subjected to the potential scattering in a given partial-wave form factor with arbitrary angular momentum has recently been

developed. Our generalization also allows for the calculation of the non-equilibrium thermodynamic properties as well as equilibrium thermodynamic properties. In this work our previous results of three-body scattering properties have been used in the framework of quantum statistical mechanics and of the corresponding kinetic theory to calculate the equilibrium and non-equilibrium thermophysical properties.

The Faddeev Method:

The indeterminacy of the Lippmann-Schwinger equations can be removed by means of an appropriate rearrangement of the equations; the equations obtained as the result of such a rearrangement are usually called Faddeev equations. We now adopt the following notation and conventions for a system of three non-relativistic spinless particles: Let the initial state consist of particle 1 impinging on a bound state of 2 and 3. The split-up of the hamiltonian corresponding to this arrangement is

$$\begin{aligned} H &= H_1 + H'_1 \\ H_1 &= H_0 + V_{23} \quad H'_1 = V_{12} + V_{13} \end{aligned} \quad (1)$$

The Green function of the simple hamiltonian H_1 is given by

$$g_1(E) = (E - H_0 - V_{23})^{-1} \quad (2)$$

The T operator appropriate to the description of collision in which the final arrangement is again 1(2,3) is called T_{11} . The \mathbf{T} matrix is obtained from it by taking matrix elements between eigenstates of H_1 . Its equation is

$$T_{11} = H'_1 + H'_1 g_1^+ T_{11} = V_{12} + V_{13} + (V_{12} + V_{13}) g_1^+ T_{11} \quad (3)$$

T operators appropriate to rearrangements in which the final state is 2(1,3) or 3(1,2) are called T_{21} and T_{31} , respectively. They can be obtained from T_{11} by the equations

$$\begin{aligned} T_{21} &= H'_2 + H'_2 g_1^+ T_{11} = V_{23} + V_{21} + (V_{23} + V_{21}) g_1^+ T_{11} \\ T_{31} &= H'_3 + H'_3 g_1^+ T_{11} = V_{31} + V_{32} + (V_{31} + V_{32}) g_1^+ T_{11} \end{aligned} \quad (4)$$

Results and discussion:

In this work the analytical expression that we obtained for T_{11} is as follow:

$$\begin{aligned} &\langle p_r, p_{23} | T_{11} | p'_r, p'_{23} \rangle \\ &= \sum_{j=2}^3 \sum_{n,m,k=1}^2 \gamma_{nm}^{1j} v_k^{1j} \chi_k^{1j}(p_r, p_{23}) \chi_k^{1j}(p_r, p_{23})^* \langle \chi_n^{1j} | \chi_m^{1j} \rangle \langle \chi_k^{1j} | \Lambda^{-1} | \chi_n^{1j} \rangle \end{aligned} \quad (5)$$

where γ_{nm}^{1j} are coefficients which can be found by applying the separable potential model, v_k^{1j} is the attractive (or repulsive) coupling strength and $\chi_k^{1j}(p_r, p_{23})$ is the state of the system with angular momentum quantum number l , which is a real number in the unitary case. Analytical expression for $\chi_k^{1j}(p_r, p_{23})$, $\langle \chi_n^{1j} | \chi_m^{1j} \rangle$ and $\langle \chi_k^{1j} | \Lambda^{-1} | \chi_n^{1j} \rangle$ are as follow:

$$\chi_k^{1j}(p_r, p_{23}) = \frac{2^{2l} l! (2l+1) (a_k^{1j} a_k^{23})^{\frac{2l+1}{2}}}{\pi^{\frac{3}{2}} \Gamma(l+\frac{1}{2})} \frac{p_r^l p_{23}^l P_l(\cos\theta_{pr}) P_l(\cos\theta_{p23})}{[(a_k^{1j})^2 + p_r^2]^{l+1} [(a_k^{23})^2 + p_{23}^2]^{l+1}} \quad (6)$$

$$\langle \chi_n^{1j} | \chi_m^{1j} \rangle = \frac{1}{\pi} \left[\frac{\pi 2^{l+1} l! (2l-1)!!}{\Gamma(l+\frac{1}{2})} \right]^2 \frac{(a_n^{1j} a_m^{1j} a_n^{23} a_m^{23})^{l+\frac{1}{2}}}{(a_m^{1j} + a_n^{1j})^{2l+1} (a_m^{23} + a_n^{23})^{2l+1}} \quad (7)$$

$$\langle \chi_k^{1j} | \Lambda^{-1} | \chi_n^{1j} \rangle = \frac{4(a_m^{1j} a_n^{1j} a_m^{23} a_n^{23})^{\frac{1}{2}}}{(a_m^{23} + a_n^{23})} \frac{a_m^{1j} [(a_n^{23} + 2i\omega_n)\omega_n + a_m^{23}(\omega_n - 2ia_n^{23})]}{[(a_m^{1j})^2 - (a_n^{1j})^2] [(a_m^{23})^2 + \omega_m^2] [(a_n^{23})^2 + \omega_n^2]} \quad (8)$$

where $\Gamma(l + \frac{1}{2})$ is the gamma function and $\omega_n = \sqrt{q^2 + (a_n^{1j})^2}$ and $\omega_n = \sqrt{q^2 + (a_n^{1j})^2}$.

Moreover, the obtained expressions are applied to obtain the scattering and thermodynamics properties of three-body systems from the three-body potential model in the Faddeev approximation. The potential parameters are adjusted to fit the two-body phase shift data and then applied to calculate the third virial coefficients of some appropriate systems. By calculating these scattering properties we have extended our previous work for obtaining the analytic expressions for both equilibrium and non-equilibrium thermophysical properties of fluids at moderately densities.

References:

- [1] Maghari, A. and Dargahi, M., *J. Phys. A: Math. Theor.* **41** (2008) 275306
- [2] Maghari, A. and Tahmasbi, N., *Physica A* **382** (2007) 537
- [3] Maghari, A. and Tahmasbi, N. *J. Phys. A: Math. Gen.* **38** (2005) 4469
- [4] Newton R G., *Scattering Theory of Waves and Particles* (New York: McGraw-Hill), 1966
- [5] Phillips, A.C., *Phys. Rev.* **142** (1966) 985
- [6] Ueta, K., Miyake, H. and Bund, G.W., *Phys. Rev.* **59C** (1999) 1806.

Laser Mass Spectrometry of Alkali-Earth Halides

M. Mirian, M. Tabrizchi, F. Abyar, H. Farrokhpour

Email: mmirian66@yahoo.com

Department of Chemistry, Isfahan University of Technology, Isfahan, Iran, 84156-83111

Keywords: Time-of flight, Alkali-Earth Halides, Isotope pattern, Detection devices.

Introduction:

Time of flight (TOF) mass spectrometry is one of the most important analyzing techniques which works based on acceleration and separation of ions in vacuum. The advantage of TOF instrument is that it can readily reach mass resolving power ($m/\Delta m$) of 1000–10000 with very high efficiency compared to other detection devices including magnetic sectors, quadrupole and ion traps. In this work, mass spectra of earth alkali halides including MgCl_2 , CaCl_2 , SrCl_2 and BaCl_2 ; and their mixtures have been recorded using a laser ionization technique and a home made TOF mass spectrometer. The spectra were assigned and the effects of the laser intensity and acceleration voltages on the spectra were investigated.

Experimental:

The TOF mass spectrometer, constructed in the Isfahan University of Technology, is schematically shown in Fig.1. The solid sample coated on the repeller of the accelerator and was irradiate by laser light. The produced ions accelerated in region A and fly in a field free region. The ions are separate based on the mass to charge ratio (m/z). The chamber was under high vacuum (10^{-7} mbar).

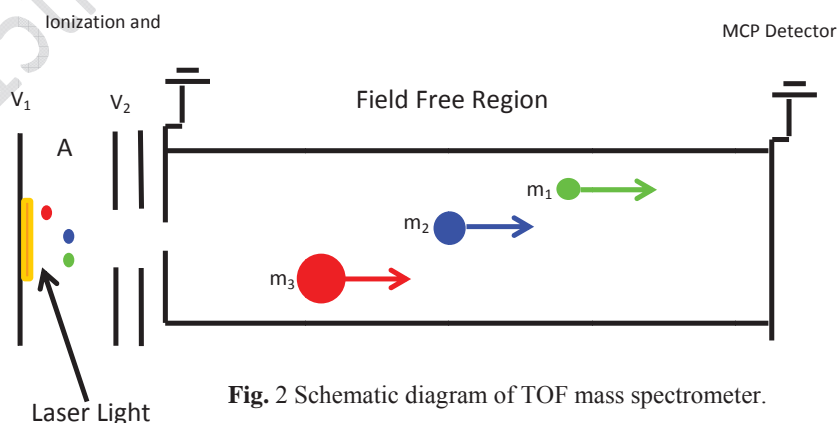


Fig. 2 Schematic diagram of TOF mass spectrometer.

Result and discussion:

Fig. 2 and 3 shows the recorded TOF spectra of SrCl_2 and BaCl_2 , respectively. Molecular ion patterns were used for assignment. Ba and Cl have five and two stable isotopes, respectively. This makes several types of BaCl^+ ion. To simulate the mass pattern of BaCl , the relative population of each isotope was calculated based on the natural abundances of each atom. The solid lines in Fig. 2 show the simulated pattern of the recorded spectrum related to Ba isotopes and the different combinations of BaCl . Fig.3 also demonstrates the TOF spectrum of SrCl . Sr^+ and SrCl^+ ions are evident in the spectrum.

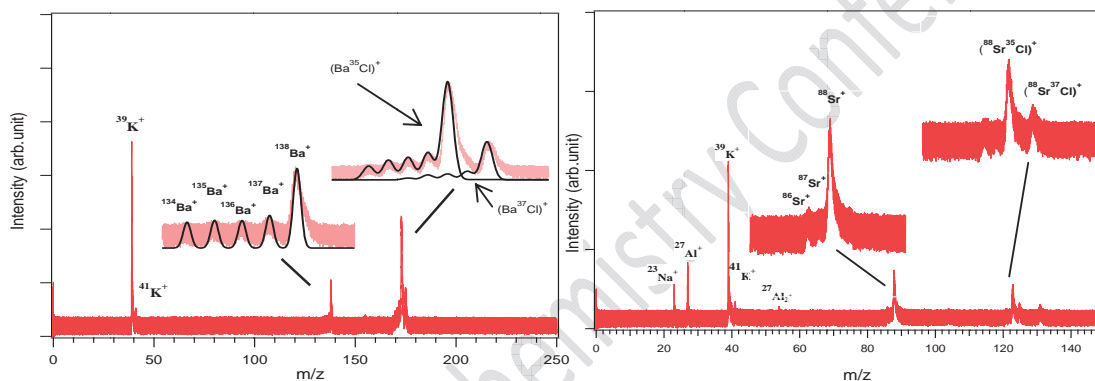


Fig.2 &3. TOF spectra of BaCl_2 and SrCl_2 .

Conclusions:

Time-of-flight mass spectra of CaCl_2 and SrCl_2 have been recorded using laser as ionization source. The spectra includes AE^+ and AEX^+ where AE and X stands for alkali earth and halide, respectively. The simulated isotope pattern confirms the mass assignment.

References:

- [1] M. Tabrizchi, Construction of a laser ionization time-of-flight mass spectrometer, Iranian Patent No. 73361, 2012.
- [2] M.Yildirima, O.Siseb, M.Doganb, H.S. Kilic, Designing multi-field linear time-of-flight mass spectrometers with higher-order space focusing, J. Mass Spectrom. 2010; 291:1–12.



The effect of phenyl substitutions on the structure and metal- ligand bond strength of copper acetylacetonate. A DFT study.

Mohammad Vakili, Mahnoosh Hakimi Tabar*, Ali Reza Berenji, Raheleh Afzali

Department of Chemistry, Ferdowsi University of Mashhad, Mashhad 91779, Iran

(Email: mhakimitabar@yahoo.com)

Keywords: Cu complexes, DFT, β -diketones, Complex stability.

Introduction:

β -diketones are important organic reagents and were found to be useful chelating ligands. The investigation on the structures and properties of metal β -diketonates is of significant importance because of a variety of potential applications [1, 2]. The most studies on metal complexes of β -diketones have been carried out on complexes of acetylacetone (AA) and their properties. However, there are only few studies on metal complexes of benzoylacetone (BA) and dibenzoylmethane (DBM) and their properties, especially their stabilities.

The aim of the present work is to investigate the effect of phenyl substitutions (instead of the methyl groups in the β position of AA) on the structure and metal-ligand bond strength of copper acetylacetonate using density functional theory (DFT). Hence, the structure of $\text{Cu}(\text{AA})_2$, $\text{Cu}(\text{BA})_2$, and $\text{Cu}(\text{DBM})_2$ are optimized and the structural parameters are compared.

Method of analysis:

All computations on the structure and vibrational spectra of the complexes were performed using Gaussian 03 at the B3LYP/6-311G* level. The assignment of the calculated wavenumbers is aided by the animation option of the GaussView 5 graphical interface for the Gaussian program, which gives a visual presentation of the shape of the vibrational modes.

Results and discussion

According to the theoretical calculations, two configurations are possible for $\text{Cu}(\text{BA})_2$, cis and trans ones. The trans configuration is considerably more stable than the cis one (about 0.3 kcal mol⁻¹) in the gas phase.

The fully optimized geometrical parameters of Cu(AA)₂, Cu(DBM)₂, and cis and trans conformers of Cu(BA)₂ are listed in Table 1. Upon substitution of phenyl group in β -position, the Cu-O bond lengths and O...O distance in Cu(BA)₂ and Cu(DBM)₂ decrease in comparison with those of Cu(AA)₂. Thus, the stability of the complexes of Cu follows this order: Cu(DBM)₂ > Cu(BA)₂ > Cu(AA)₂ which is in agreement with the literature [3]. It is noteworthy to say that the C-O bond lengths increase by addition of phenyl group.

The calculated Cu-O symmetric stretching (A species) is a good criterion to evaluate the stability of these complexes. This vibrational mode was predicted to observe at 450, 555, and 573 cm⁻¹ in Cu(AA)₂, Cu(BA)₂, and Cu(DBM)₂, respectively. Therefore, the mentioned stability order can be confirmed once more.

Table 1. The calculated bond lengths for the mentioned Cu complexes. ^a

Bond lengths	Cu(AA) ₂	Cu(BA) ₂		Cu(DBM) ₂
		Cis	Trans	
Cu-O(Ph)	1.925	1.923	1.920	1.919
Cu-O(Me)	1.925	1.922	1.923	1.919
C-O(Ph)	1.270	1.274	1.274	1.275
C-O(Me)	1.270	1.271	1.272	1.275
O...O	2.769	2.760	2.760	2.754

^a, The words in parentheses indicate the adjacent functional groups in the ligands.

Conclusions

The calculated bond lengths of Cu-O and O...O are shorter in Cu(DBM)₂ than the corresponding ones in Cu(AA)₂ and Cu(BA)₂. The Cu-O symmetric stretching frequency is higher in Cu(DBM)₂ than Cu(AA)₂ and Cu(BA)₂. Therefore, the resonance and also stability of Cu(DBM)₂ is increased in comparison with Cu(BA)₂ and Cu(AA)₂.

References

- [1] H. H. Murray, Appl. Clay Sci. 17 (2000) 207.
- [2] J. Guzman, B. C. Gates, Angew. Chem., Int. Ed. 42 (2003) 690.
- [3] K. Nakamoto, Y. Morimoto, A. E. Martell, J. Phys. Chem. 66 (1962) 346.



DFT study on the mechanism of the Formation of Monodentate Acetate Complex of Palladium(II)

A. Morsali^a, S. A. Beyramabadi^a and F. Rezazadeh^{* a}

^a Department of Chemistry, Mashhad Branch, Islamic Azad University, Mashhad, Iran

(Email: faeze.rezazade@yahoo.com)

Keywords: Monodentate Acetate Complex, Mechanism, Palladium, Density functional theory

Introduction:

There are few investigations of reactions between square planar Pd(II) centers and carboxylic acids/carboxylates in aqueous solution. Shi and Elding [1] described studies of equilibria and kinetics for complex formation between $[Pd(H_2O)_4]^{2+}$ and acetic, propionic, and glycolic acids, with the aim to elucidate the reaction mechanism. Kinetics and equilibria for reversible formation of 1:1 monodentate complexes between $[Pd(H_2O)_4]^{2+}$ and acetic, propionic, and glycolic acid (RCOOH) according to the equation (1) were studied as a function of temperature and pressure in an aqueous medium [1]:



In this work, the mechanism of the Formation of Monodentate Acetate Complex of Palladium(II) has been studied using density functional methods..

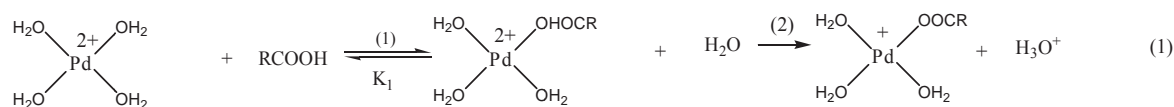
Computational details:

All of the present calculations have been performed with the B3LYP [2] hybrid density functional level using the G09 package. The 6-311+G(d,p) basis set was employed except for Pd atom, in which the LANL2DZ [3] basis set was used with including effective core potential functions. The gas phase optimized geometries used to apply the solvent effects, where the valuable PCM [4] model was employed.

Results and discussion:

The following mechanism (Eq.(1)) for the Formation of Monodentate Acetate Complex of Palladium(II) was proposed which is compatible with experimental evidence. In this

mechanism, a fast equilibrium step (with equilibrium constant K_1) will result in the formation of complex $[Pd(H_2O)_3OHOCR]^{2+}$ which will be converted into $[Pd(H_2O)_3OOCR]^+$ and $[H_3O]^+$ during a slow process.



The optimized structure of transition state obtained from step2 has been shown in Fig. 1. By taking Solvent effects into consideration, $E_a = 15.8 \text{ kcal/mol}$. This shows that the model presented in this research is a suitable model for the Formation of Monodentate Acetate Complex of Palladium(II).

Conclusion:

Using quantum mechanical method, mechanism of the Formation of Monodentate Acetate Complex of Palladium(II) was investigated and ultimately a model was presented in which $[Pd(H_2O)_3OHOCR]^{2+}$ form is produced in the rate determining step and in continuation is converted into products.

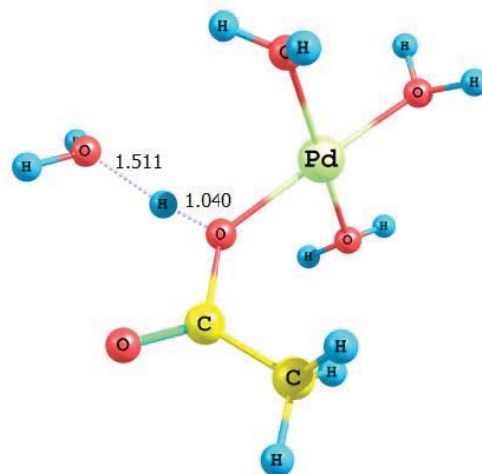


Fig 1. Optimized structure of the TS (step 2)

References:

- [1] T. Shi, L. I. Lars, Inorg. Chem. 35 (1996) 735.
- [2] A.D. Becke, Phys. Rev. A, 38 (1988) 3098.



- [3] P.J. Hay, W.R. Wadt, J. Chem. Phys. 82 (1985) 299.
[4] S. Miertus, E. Scrocco, J. Tomasi, Chem. Phys. 55 (1981) 117.

15th Physical Chemistry Conference



Considering the one-electron density of hydrogen ion molecule within the context of the Hooke – Calogero model

H.R. Jouypazadeh

Department of chemistry, Faculty of science, ShahidBeheshti University, Tehran, Iran

Email: hamidrezair2021@iran.ir

Keyword: Hooke–Calogero model, Electronic density, Calmped nucleus approximate, QTAIM

Introduction:

The Schrödinger equation for most N – body systems is not usually solvable by analytical techniques. This obstacle can be partly circumvented by studying *model* systems. Hooke – Calogero model provides an analytical solution for non – adiabatic Schrödinger equation of hydrogen molecule as well as hydrogen ion molecule. So, if this model is similar enough to real molecule, it will be a suitable model for researches to probe the traits behind the clamped nucleus approximation. The aim of considering this model in the present work is to study the compatibility this model with real molecule for the development of the quantum theory of atom in molecule (QTAIM). For this purpose, one-electron density of the molecules produced within the context of this model must be similar to the one-electron density produced within the coulombic model.

Hydrogen ion molecule in Hooke – Calogero model:

In the Hooke – Calogero model, a harmonic potential replaces the electron – nuclear interaction and an inverse square potential substitutes the nuclear – nuclear interaction [1]. In this model, Hamiltonian for ion molecule hydrogen is:

$$H = -\frac{1}{2M}\nabla_{R_A}^2 - \frac{1}{2M}\nabla_{R_B}^2 - \frac{1}{2}\nabla_r^2 + \frac{1}{|R_A - R_B|^2} + \frac{\omega^2}{2}(r - R_A)^2 + \frac{\omega^2}{2}(r - R_B)^2 \quad (1)$$

Where r represents the coordinate of the electron and R_A and R_B represent the coordinates of the nuclei and M represents the mass of each nucleus. By applying the following coordinate transformation on the equation 1, equation 2 is derived.

$$P = \frac{r + MR_A + MR_B}{M_T}, R = R_A - R_B, Q = r - \frac{R_A + R_B}{2}$$

$$H = -\frac{\nabla_P^2}{2(2M + 1)} - \frac{\nabla_R^2}{M} - \frac{(2M + 1)}{4M}\nabla_Q^2 + \frac{1}{R^2} + \frac{R^2\omega^2}{4} + Q^2\omega^2 \quad (2)$$

The one-electron density is usually considered within the clamped nucleus approximation. So, by applying $M \rightarrow \infty$ in equation 2, electronic Hamiltonian within the clamped nucleus framework is obtained:

$$H_{elec} = -\frac{1}{2}\nabla_Q^2 + \frac{1}{R^2} + \frac{R^2\omega^2}{4} + Q^2\omega^2 \quad (3)$$

Eigenfunctions of equation 3 are [2]:

$$\Psi(Q, \theta, \phi) = \psi_{n_Q, l_Q}(Q) Y_{l_Q, m_Q}(\theta_Q, \phi_Q)$$

$$\psi_{n_Q, l_Q}(Q) = N Q^{l_Q} \text{Exp}\left(-\sqrt{\frac{M}{2M+1}}\omega Q^2\right) B\left(-n_Q, l_Q + \frac{3}{2}, 2\sqrt{\frac{M}{2M+1}}\omega Q^2\right) \quad (4)$$

Where $B(a, b, z)$ is the Kummer confluent hypergeometric function ${}_1F_1(a, b, z)$ and N is Normalization coefficient and $\omega = \sqrt{2}/4$.

Results and discussion:

For the hydrogen ion molecule, one-electron density is calculated from the following equation:

$$\rho_e = |\Psi_{el}(\vec{Q})|^2 = |\Psi(Q, \theta_Q, \phi_Q)|^2 = |\Psi(x, y, z)|^2 \quad (5)$$

In the following figure, the one-electron density of hydrogen ion molecule in Hooke – Calogero model is depicted.

According to this figure, maximum probability of the presence of the electron in Hooke – Calogero model is located at the geometric center of nuclei, but in coulombic model it is located on nuclei. The origin of this difference is the difference between electron – nucleus interaction in Hooke – Calogero model and coulombic model. In Hooke – Calogero model the minimum of potential energy is located at the geometric center of nuclei, but in coulombic model, two potential wells are located on the nuclei.

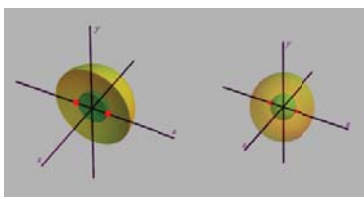


Figure 1: electronic density of hydrogen ion molecule in Hooke – Calogero model (The red dot and green iso-surface represent the nuclei and more dense surface respectively)



Conclusion :

These calculations have been performed also on H_2 and H_3^+ and the results were similar. According to these calculations, one-electron density of the molecules produced with the frame of the Hooke – Calogero model is similar to the one-electron density of atoms in coulombic model. So, this model is not suitable for the development of QTAIM at non – adiabatic state since in this model, the identity of atoms in molecules is not recognized.

References:

- [1] Lopez, X.; Ugalde, J.M.; Ludeña, E.V., *Eur. Phys. J. D***2006**, 37, 351
- [2] Lopez, X.; Ugalde, J.M.; Ludeña, E.V., *J. Chem. Phys.* **2005**, 123, 024102



Interaction between stretching and bending modes in Naphthazarin hydrogen bond

F. Afshar-Qahremani, M. Zahedi-Tabrizi*

Department of chemistry, Alzahra University, Tehran, Iran

Email: zahedi@alzahra.ac.ir

Keywords: Naphthazarin, proton transfer, potential function, tunneling frequency.

Introduction:

Tunneling has been successfully used to explain the fast rates of exchange in certain inter- and intramolecular proton transfers. To treat proton tunneling in bent hydrogen-bonded systems, we have developed a simple and practical method, in which a two-dimensional potential energy surface (PES) function was able to describe the motion of the hydrogen atom successfully. This potential energy surface function couples OH stretching and in-plane bending modes.

We apply this method to study the proton potential function in naphthazarin (NZ), a β -dicarbonyl compound which has peculiar symmetry properties insofar as its molecular symmetry depends on the positions of two mobile protons in intramolecular hydrogen bonds. In the following, we will assess the performance of our simple method in predicting the proton tunneling, O-H/ O-D stretching and in-plane bending frequencies for NZ [1-4].

Method of calculations:

All calculations were performed using Gaussian 03W. To explore two-dimensional proton tunneling we varied the OH distance in NZ from 0.8 to 1.3 Å and COH angle from 5° to 42°. We have calculated the energies at B3LYP/6-31G**, B3LYP/6-311G**, G96LYP/6-31G*, and MP2/6-31G* levels. A two dimensional potential energy surface which couples OH stretching with in plane bending has been calculated for a fixed skeleton geometry. The obtained potential functions have been fitted in a symmetric two dimensional double minimum potential. The obtained Hamiltonian matrix, then, was diagonalized. This potential



energy function is used for calculation the tunneling splitting, OH stretching and in plane bending frequencies.

Results and discussion:

With decrease of range of mobility of proton, the tunneling splitting must increase. Also, the tunneling velocities must decrease with increasing of mass of tunneling particle. In the protocol, the tunneling splitting of 6.4 and 0.3 cm^{-1} was obtained for light and deuterated NZ respectively for potential energies of higher of 6000 cm^{-1} . These results are in excellent agreement with articles related to searching about tunneling [5]. Calculations showed that the eigenvalues were independent of the choice of the origin of expansion located in large regions in the X and Y axis. Therefore we have selected the origin of the coordinate system. The size effect of the matrix on the energy levels was examined also. After testing the convergence we found that a 30×20 matrix was big enough for the best convergence of the lower energy levels.

Conclusion:

A simple and practical two-dimensional potential function was applied to calculate the hydrogen-bond transition frequencies in NZ. In this method, ab initio programs were used to generate a two dimensional potential energy surface, which correctly predicted the equilibrium molecular geometries. This potential function, which couples the O-H stretching to the in-plane bending motion, was then employed to calculate the O-H/O-D vibrational energy levels. For NZ, this method predicted the proton tunneling, O-H/O-D stretching and in-plane bending frequencies all in excellent agreement with theoretical data. A Barrier height about 35.6 kJ/mol was calculated for the intramolecular hydrogen bond in NZ.

Reference:

- [1] J. R. De La Vega, J. Acc. Chem. 15 (1982) 185-191.
- [2] S. F. Tayyari, M. Zahedi-Tabrizi, H. Rahemi, H.A. Mirshahi, J.S. Emampour, M. Rajabi, F. Milani-Nejad, J. Mol. Struct. (Theochem) 730 (2005) 17-21.
- [3] S. F. Tayyari, M. Zahedi-Tabrizi, H. Azizi-toupkanloo, S.S. Hepperle, Y.A. Wang, J. Chem. Phys. 368 (2010) 62-65.



- [4] S. Bratan, F. Strohbusch, J. Mol. Struct. 61 (1980) 409-414.
- [5] M. Zahedi-Tabrizi, S. F. Tayyari, F. Tayyari, M. Behforouz, J. Spectrochim. Acta Part A 60 (2004) 111-120.

15th Physical Chemistry Conference



Hydrophilic gel composition effect on the molecular association and spectroscopic behavior of Methylen blue

F. Khadem kalan ^{a*}, H. Nikoofard ^a, M. S. Zakerhamidi ^b

^aFaculty of Chemistry, Shahrood University of Technology, Shahrood, Iran

^bResearch Institute for Applied Physics and Astronomy, University of Tabriz, Tabriz, Iran

(Email: Khadem.fatemeh@gmail.com)

Key words: Methylen blue, Polyacrylamide hydrogel, Dye aggregation, Exciton theory

Introduction:

Ionic dyes such as MB can easily form aggregates in solution that this aggregation leads to a strong coupling of the molecular transition dipoles. Exist electrostatic interaction between molecular transition dipoles of the chromophores split energy levels of the excited states of the dye molecules [1-2]. This study is intended to provide the information about the effect of the PAAM structural composition on the guest–host interactions and aggregative properties of MB in binary hydrogel solvent systems by means of the exciton theory.

Materials and methods:

Acrylamide(97%), *N,N*-methylenebisacrylamide($\geq 98\%$), *N,N,N,N*-etramethylethylenediamine ($\geq 99\%$) (TEMED) and ammonium persulfate ($\geq 98\%$) (APS) were used for synthesizing polyacrylamide gels with compositional 20% (Polyacrylamide/Water (w/w)). The MB dye was procured from Exciton and used without further purification. The dye-loaded hydrogel was prepared by soaking the hydrogel host in aqueous solutions of MB dye with known concentration for various durations of time (1 min to 10 hours) at 22 °C.

Apparatus:

Double beam Shimadzu UV-2450 Scan UV–Visible spectrophotometer was used for recording the absorption spectra over a wavelength range between 300 to 800 nm.

Results and discussion:

The host nature can strongly influence the position and relative intensity of the doublet absorption bands. The shape variation of the dye optical spectrum might be controlled by distinct phenomena such as solvent–solute and solute-solute interactions [3].

MB is a cationic dye and typically possesses a doublet bands, i.e. a maximum (λ_{max}) and a shoulder ($\lambda_{\text{shoulder}}$). Absorption spectra of aqueous solution of MB ($5 \times 10^{-5}\text{M}$) and hydrogel host were investigated and compared in Fig. 1. As it can be seen from Fig. 1, a slight red shift (4 nm) the monomer absorption wavelength of MB dye-loaded hydrogel 20% may be due to the similar interactions between the MB molecules with the two host systems (i.e. water and hydrogel). The presence of the dimethyl groups in MB prevents or at least decrease the ability of H-bonds formation between MB and free water molecules in the hydrophilic gel matrix.

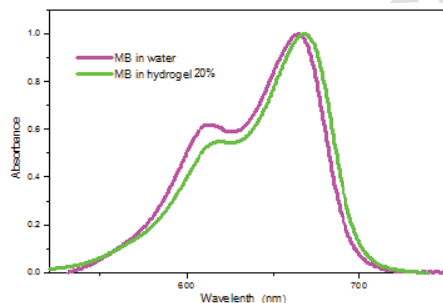


Fig. 1. Visible absorption spectra of MB ($5 \times 10^{-5}\text{M}$) in aqueous solution and hydrogel 20%

Absorption spectra of aggregated dye molecules usually show large differences when compared to the individual molecules. By using Kasha exciton theory in its developed form the angle between the transition dipoles of chromophores for the MB in water and in hydrogel 20% in different soaking times were obtained. These data show that MB in aqueous solution and hydrogel clearly shows H-aggregation. α angle in aqueous solution show lower amount than hydrogel with rising of soaking time.

Conclusions:

The obtained excitonic parameters explain that in the initial soaking time MB molecules interact with hydrogel active functional groups in polymeric chain and freezing water molecules in hydrogel pores. Via increasing this time MB molecules interact with free water



of hydrogel pores. In other words, inter-monomeric interaction energy of MB in hydrogel media is higher than aqueous solution.

References:

- [1] M. Kasha, H.R. Rawls, M.A. El-Bayoumi, *Pure Appl. Chem.* 11 (1965) 371–392.
- [2] A. Ghanadzadeh Gilani, H. Tajalli, M.S. Zakerhamidi, *J. Mol. Liquid.* 143 (2008) 81-88.
- [3] C.S. Oliveira, K.P. Branco, M.S. Baptista, G.L. Indig, *Spectrochim. Acta A* 58 (2002) 2971–2982.



Proton Transfer in X-Anilide–HF: Can the Substituents in Para Position of Anilide ion Influence the $\text{N}^-\cdots\text{H}-\text{F} \rightarrow \text{N}-\text{H}\cdots\text{F}^-$ Switching

H. Roohi ^{*a}, K. Roshan ^b

Department of Chemistry, Faculty of Science, University of Guilan, Rasht, Iran

Email: java6633@yahoo.com

Key words: quantum chemistry, anilide, proton transfer, H-bonding, AIM, NBO

Introduction:

H-bonding is one of the most important kinds of interactions. The presence of such interactions is significant for biologically important systems and materials science [1-3]. The proton transfer (PT) phenomenon is a crucial event in the chemical and biological sciences. They include intramolecular proton transfer of aromatic compounds in the excited state, excited-state intermolecular proton transfer in a hydrogen-bonded complex, and also excited-state proton transfer of various photoacids to solvent [4-6].

Methods:

The geometries of all complexes were optimized using B3LYP and MP2 methods in conjunction with the 6-31++G(d,p), 6-31++G(2d,2p) and 6-311++G(2d,2p) basis sets. The B3LYP calculated vibrational frequencies have been used to characterize stationary points and calculation of zero-point vibrational energies (ZPVE). The vibrational frequencies were calculated without scaling. All calculations were performed using the Gaussian 98 program package.

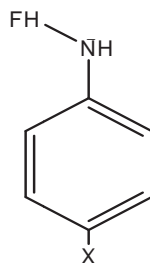
Results and discussion:

In the present work, a detailed analysis of PT between HF and anilide ion (**An**) are performed in complexes **X-anilide–HF** (X = H, Me, CHO, CN, NO, F, NO₂, OH and OMe) (**Scheme 1**). The effect of substituent in para position of anilide on the $\text{HN}^-\cdots\text{H}-\text{F} \rightarrow \text{N}-\text{H}\cdots\text{F}^-$ proton transfer switching in **X-An–HF** (X = H, Me, CHO, CN, NO, F, NO₂, OH and OMe) complexes were investigated by means of quantum chemical methods. Our results revealed

that the geometry and electronic structure of the anilide ion were very sensitive to both substituent and H-bonding effects. The changes in H-bond strength due to variation of substituent in para position of anilide were well accompanied by change in binding energy (BE), structural parameter, electron density, natural charge and charge transfer. For X = H, Me, CHO, CN, NO, F and NO₂ substituents, our results at MP2/6-311++G(2d,2p) level showed that the minimum-energy structures for these substituents correspond to the **X-An...HF** complexes without proton transfer occurring. For electro-donating substituents OH and OME, proton is transferred from HF to anilide ion and the minimum energy structures correspond to X-PhNH₂...F⁻ complexes.

Table 1. BEs calculated at two L1 (B3LYP/6-311++G(2d,2p)) and L2 (MP2/6-311++G(2d,2p)) levels.

		H	CHO	CN	F	ME	NO	NO ₂	OH	OME
ΔE_{elec}		-	-	-	-	-	-	-	-	-
	L1	141.6	116.3	119.5	141.3	143.2	108.9	109.7	147.7	146.8
		-	-	-	-	-	-	-	-	-
	L2	131.7	111.8	115.5	132.1	132.7	104.4	106.8	137.9	136.6
$\Delta E_{\text{elec}}^{\text{BSSE}}$		-	-	-	-	-	-	-	-	-
	L1	140.9	115.6	118.8	140.6	142.4	108.3	109.1	146.9	146.0
		-	-	-	-	-	-	-	-	-
	L2	129.0	109.4	113.2	129.2	129.9	102.1	104.5	134.0	132.7
$\Delta E_{\text{ZPE}}^{\text{BSSE}}$		-	-	-	-	-	-	-	-	-
	L1	131.7	107.1	109.6	130.9	127.0	-95.6	-96.6	131.8	125.6
		-	-	-	-	-	-	-	-	-
	L2	119.8	-98.5	105.7	119.6	114.5	-89.4	-92.0	118.8	115.6



X = (H, Me, CHO, CN, NO,

Scheme 1

The results in Table 1 show that the BE for electron donating substituents is greater than electron accepting ones and is smallest for strong electron accepting groups.



Conclusions:

The results at MP2/6-311++G(2d,2p) level show that the **X-An** (X = H, Me, CHO, CN, NO, F and NO₂) ions with HF form H-bonded complexes **X-An-HF** without proton transfer. For (X = OH and OMe), the proton is transferred from HF to anilide ion.

References:

- [1] E.A. Meyer, R. K Castellano, F. Diederich, *Angew. Chem. Int. Ed.* 42 (2003) 1210–1250.
- [2] K. Biratha. *Cryst. Eng. Commun.* 5 (2003) 374–384.
- [3] S. Kitagawa, K. Uemura, *Chem. Soc. ReV.* 34 (2005) 109–119.
- [4] Y. Podolyan, L. Gorb, J. Leszczynski, *J. Phys. Chem. A* 106 (2002) 12103–12109.
- [5] X. Hu, H. Li, W. Liang, S. Han, *J. Phys. Chem. B* 108 (2004) 12999–13007.
- [6] D. S. Ahn, S. Lee, B. Kim, *Chem. Phys. Lett.* 390 (2004) 384–388.



Theoretical investigation of phenyl group effect as an end-substitution on electronic properties of oligothiophenes

Hossein Nikoofard, Mohamad Gholami *

Faculty of Chemistry, Shahrood University of Technology, Shahrood, Iran

Email: s.gh_1985@yahoo.com

Key words: DFT, End-substitution, Electronic properties, Oligothiophenes

Introduction:

Oligothiophenes have received great attention over the past few years for their potential use in a variety of devices, including nonlinear optics, Schottky diodes, organic light-emitting diodes (OLEDs), and thin-film field-effect transistors (FETs) [1]. One approach to develop a higher performance of oligothiophenes is the introduction of substituent at specific position of monomer ring. The other approach is to cap both ends of the thiophene chain by the substitution groups. The capped-oligothiophenes have a well-defined molecular size and a high chemical stability. Recently, it has found that phenyl-capped oligothiophenes (PnT, where n is number of thiophene ring) have novel light-emitting properties [2]. In this work we investigated the electronic properties of phenyl-capped oligothiophene including HOMO-LUMO gap, first excitation energy, charge distribution, ionization potential and electron affinity.

Computational methodes:

All hybrid DFT calculations were carried out using Gaussian 09 program package. The geometry of oligothiophenes and phenyl-capped oligothiophenes and their ionic species were optimized at the B3LYP/6-31G(d,p) levels of theory. The excitation energies were calculated by means of time-dependent DFT calculations at the B3LYP/6-31G(d,p) levels of theory.

Result and discussion:

Results show an improvement for electronic propertise of oligothiophenes capped by phenyl groups. It's observed that the phenyl-capped oligothiophenes indicate narrow HOMO-LUMO

gap comparison with corresponding oligothiophenes. It's also found a red shift in simulated absorption spectra of oligothiophenes capped by phenyl group. In this way, simulated absorption spectra of hexathiophene and phenyl-capped hexathiophene is compared in fig 1. Charge carrier injection rate results show an increasing in the rate of charge injection for phenyl-capped oligothiophenes. Ionization potential and electron affinity result indicate a decreasing in phenyl-capped oligothiophenes which improved the degree of charge extraction (hole or electron). Investigation of mulliken charge of each ring for neutral and ionic species show larger inter-ring charge separation in phenyl-capped oligothiophenes which indicating that a large dipole moment is locally generated. It is found that the oligothiophenes show better π -conjugation after closing the end sides of polymer chain with phenyl groups.

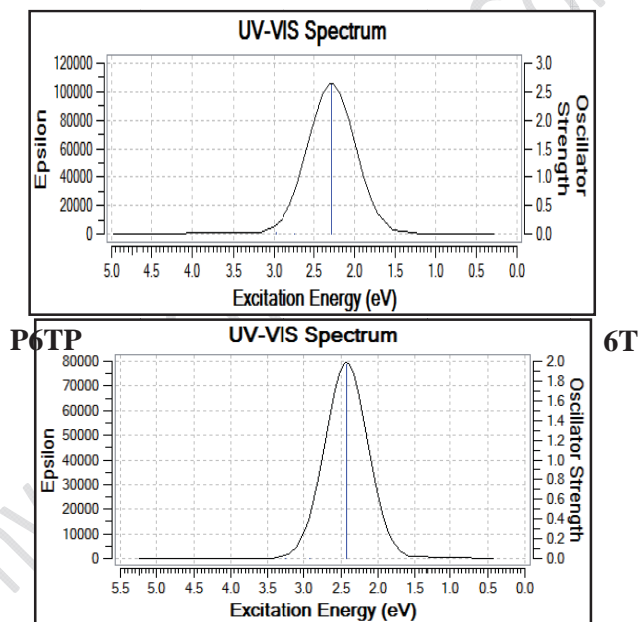


Fig 1. Simulated absorption spectra of the hexathiophene(6T) and the phenyl-capped hexathiophene(P6TP).

Conclusion:

It is found that the phenyl groups as end-substitutions effect on the geometry, the excitation states, the electron conjugation, the conducting type (p- or n-type), and the inter-chain charge carrier hoping channels of oligothiophenes. DFT studies show an improvement in electronic properties of oligothiophene capped by phenyl.



Refrence:

- [1] Juan Casado et al; " Multidisciplinary Physicochemical Analysis of Oligothiophenes End-Capped by Nitriles: Electrochemistry, UV-Vis-Near-IR, IR, and Raman Spectroscopies and Quantum Chemistry" *Journal of Physical Chemistry B* 109 (2005) 10115-10125.
- [2] H. Tachikawa et al; "A DFT and direct MO dynamics study on the structures and electronic states of phenyl-capped terthiophene" *Journal of Organometallic Chemistry* 690 (2005) 2895–2904.

15th Physical Chemistry Conference



A DFT study on structural properties of phenyl-capped oligothiophenes

Hosein Nikoofard, Mohamad.Gholami*

Faculty of Chemistry, Shahrood University of Technology, Shahrood, Iran

Email: s.gh_1985@yahoo.com

Key words: DFT, Structural properties, Phenyl-capped, Oligothiophenes

Introduction:

One of important structural factors related to the extension of the π -conjugation of a polymeric system is the chain planarity which can be reflect by the tortional angles and alternation of single and double bonds along the polymer chain which can be indicate by bond alternation parameter or quinoid parameter. In this work, we investigate the structural properties for some oligothiophenes with and without phenyl-capped group using DFT calculations. Effective dihedral angles, bonds length of carbon backbone in π -conjugated system, bond alternation parameter and quinoid parameter is obtained in this work.

Computational methodes:

Density functional theory (DFT) [1] as implemented in Gaussian 09 program has been employed to optimize the geometry of oligomers. The geometry optimizations are carried out at the B3LYP/6-31G(d,p) level of theory without symmetry restriction for neutral, cationic and anionic species of each oligomer.

Result and discussion:

Structural properties relating with π -conjugation of polymeric system as effective dihedral angles, bonds length of carbon backbone in π -conjugated system, bond alternation parameter [2] and quinoid parameter [3] for oligothiophene and phenyl-capped oligothiophene is calculated. Structure of Hexathiophene and Phenyl-capped Hexathiophene and their summary name is shown in Fig 1 as example. Results show decrease of torsional angles in oligothiophenes capped with phenyl group. also it's observed singlet and doublet bonds length of carbon backbone in π -conjugated system approach to each other after closing end

side of oligothiophenes by phenyl group which cause decrease of bond alternation parameter and quinoid parameter. All parameters studied for cationic and anionic species too.

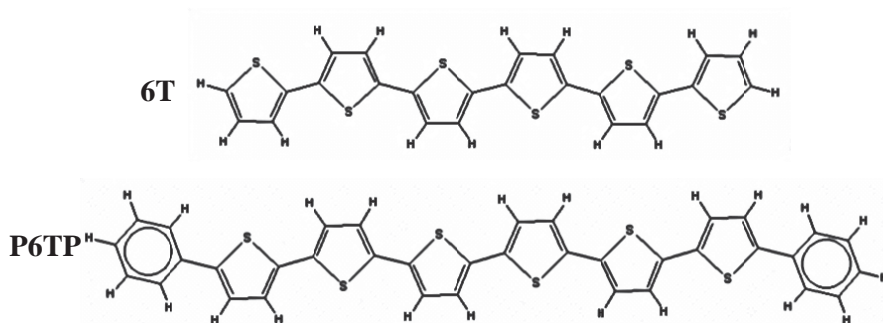


Fig 1. Structures and summary names of the hexathiophene(6T) and phenyl-capped hexathiophene(P6TP)

Conclusion:

It is found that phenyl group as a end-substitution effected on structural properties of oligothiophenes and improved the structural properties which effect on π -conjugation. It is observed that the ionic species indicate almost pure planar structure, and low bond alternation parameter and quinoid parameter as expected, because it is known in conductive polymers conduction occur after doping which radical cationic or radical anionic species of polymers is formed.

Reference:

- [1] Parr RG, Yang W; "Density-functional theory of atoms and molecules"; Oxford University Press, New York (1989).
- [2] Gui-Ling Zhang and et al; "End-substitution effect on the geometry and electronic structure of oligoheterocyclics"; Theor Chem Account (2008) 121:109–122.
- [3] Omrani A, Sabzyan H; "Theoretical study of chloropyrroles as monomers for new conductive Polymers"; J Polymers. J Phys Chem A (2005) 109:8874-8879.



Absorption Spectrum of SO₂ Molecule: Including S₁–S₂ Vibronic Coupling

M. Mansoori Kermani^{*}, M. Dehestani

Department of Chemistry, Shahid Bahonar University of Kerman, Kerman, Iran.

E-mail: mansoori.2002@yahoo.com

Keywords: Vibronic coupling, Time correlation theory, Absorption spectrum, SO₂ molecule

Introduction:

In this work, we present a model Hamiltonian including three vibrational modes of sulfur dioxide molecule and determine the potential energy surfaces of the lowest two excited states S₁[¹A₂] and S₂[¹B₁], which are strongly coupled to each other [1]. The leading coefficients of the Taylor expansion of the diabatic potential-energy surfaces in terms of ground-state normal coordinates at the reference geometry have been obtained [2] at the CIS/6-311++G(3df, 3pd) level. The gas phase absorption spectrum of SO₂ molecule has been calculated in the 2400–3400 Å regions using the time correlation theory, including vibronic coupling. The absorption spectrum is in acceptable agreement with the experimental spectrum. As is well known the symmetry of SO₂ molecule is C_{2v}. It has three normal modes, in which, symmetry stretching and bending are classified into a₁ and anti symmetry stretching into b₂. The optimized geometric parameters, the calculated electronic transition energies and their oscillator strengths for the ¹A₂ and ¹B₁ states of SO₂ are calculated. For both electronic states, the computed bond lengths and angles seems to be highly consistent and reliable results can be obtained with SAC-CI/DGDZVP level. The adiabatic vibrational frequencies calculated at various levels of theory for the 2 ¹A₁ and 1 ¹B₁ states. The vibrational frequencies calculated of the ¹A₂ and ¹B₁ states give the best agreement with experimental values. For the purpose of obtaining correct estimates of the multidimensional time domain integrals and absorption cross sections, the theoretical method should be selected from the viewpoint of whether it can provide sufficiently correct analytic gradients and second derivatives of excited adiabatic potential energy surfaces (¹A₂ and ¹B₁) at the ground state.



Result and discussion:

The comparison of the experimental spectrum with calculated spectrum in the present work shows that the computed absorption spectrum is almost identical to the experimental spectrum and one can observe relatively good performance of our vibronic method. The calculated vibronic fine structure of the spectrum is qualitatively correct, but not yet quantitatively satisfactory. A more accurate calculation of the spectrum fine structure seems to require a description of the multidimensional diabatic S_1 and S_2 surfaces beyond the harmonic approximation. Clearly, anharmonicity should be incorporated into the model for computing Franck Condon factors in order to achieve better agreement between simulation and observation.

Conclusion:

In this work, the theoretical investigation contained the optimized parameters and vibrational frequencies of ground and two excited states of SO_2 molecule. With attention to the vibronic coupling between 1A_2 and 1B_1 states, the absorption spectrum of this molecule using the time correlation theory and displaced distorted rotated harmonic oscillator model were calculated. In the present work, to explore the effects of vibronic coupling of the 1A_2 and 1B_1 states of SO_2 on the absorption spectrum, we have applied a vibronic coupling model based on the Taylor expansion of the diabatic potentials in terms of normal coordinate at the reference geometry (ground electronic state) and taking into account all three normal modes. The elements of J and D matrices were obtained, also molecular dynamics of SO_2 molecule in excitation to the 1A_2 and 1B_1 states, using its entire modes were calculated. There were no previous studies and thus calculations have been performed for the first time.

References:

- [1] M. Dehestani, M. Mansoori Kermani, *Comp. Theo. Chem.* 978 (2011) 1-6.
- [2] A. Raab, G. A. Worth, H. D. Meyer, L.S. Cederbaum, *J. Chem. Phys.* 110 (1999) 936–946.

Conformational analysis of Cysteine side chain for HCO-L-Cys-L-Ala-NH₂ protected dipeptide. A DFT study

Behzad Chshkandi, Seyed Javad Hossini, Mehdi Mohseni

Department of Chemistry, Shahrood Branch, Islamic Azad University, Shahrood, Iran

Corresponding author Email: Mehdi.Mohseni66@gmail.com

Key words: Cysteine, Dipeptide, Dihedral Angle, DFT.

Introduction:

The aim of this study is to investigate the role of Cysteine side chain on the stability of L-Cys-L-Ala protected dipeptide (see Fig 1). The 20 naturally occurring amino acids can occur both in the L- and D-enantiomeric configuration [1]. As of yet, the process of protein folding is not fully understood. A typical protein has such a multitude of possible conformations that it can occupy simple counting argument of Levinthal [2]. Dipeptide models are increasingly used in peptide folding studies as they of typical triamide conformations [3] folding has received intense study due to its fundamental importance in living organisms, the growing availability of protein sequences, and the increasing recognition that some diseases are a result misfolded proteins [4].

X = 3-4-20-21

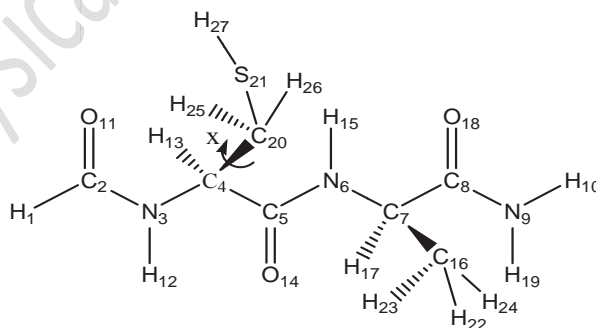


Fig. 1. Schematic diagram with torsional angle definitions for HCO-L-Cys-L-Ala-NH₂

Computational Method:

The Cysteine side chain dihedral angle (χ) rotated around $N_3-C_4-C_{20}-S_{21}$ atoms, ($-C_4-C_{20}-$) was changed at 30° intervals from 0° to 360° by using DFT geometry optimization



calculations at the B₃LYP/6-31G (d) level of theory and we determined three more stable structure among 12 optimized conformations. All of calculations performed by using Gaussian09 program.

Result and Discussion:

In this research we found three more stable states in the 300°, 180° and 60° that they known at this title: negative gauche(g^-), anti and positive gauche(g^+) State, Respectively. The results show that for HCO-L-Cys-L-Ala the energies of three minima gauche(-), anti, gauche(+) states are -666894.34, -666894.27, -666892.40 kcal mol⁻¹ respectively, Among three states gauche(-) has the highest stability.

References:

- [1] M.A. Sahai, S. Lovas, G.A. Chass, B. Penke, I.G. Csizmadia, J. Mol. Struct. (THEOCHEM), in this issue.
- [2] C.J. Levinthal, Chim. Phys. 65 (1968) 44.
- [3] A. Perczel, M.A. McAllister, P. Csa'zsa'r, I.G. Csizmadia, J. Am.
- [4] C.M. Dobson, Trends Biochem. Sci. 24 (1999) 329.

Conformational analysis of Cysteine side chain for HCO-D-Cys-D-Ala-NH₂ protected dipeptide. A DFT study

Behzad Chshkandi, Seyed Javad Hossini, Mehdi Mohseni

Department of Chemistry, Shahrood Branch, Islamic Azad University, Shahrood, Iran

Corresponding author Email: Mehdi.Mohseni66@gmail.com

Key words: Cysteine, Dipeptide, Dihedral Angle, DFT.

Introduction:

The aim of this study is to investigate the role of Cysteine side chain on the stability of D-Cys-D-Ala protected dipeptide (see Fig 1). The 20 naturally occurring amino acids can occur both in the L- and D-enantiomeric configuration [1]. As of yet, the process of protein folding is not fully understood. A typical protein has such a multitude of possible conformations that it can occupy simple counting argument of Levinthal [2]. Dipeptide models are increasingly used in peptide folding studies as they of typical triamide conformations [3] folding has received intense study due to its fundamental importance in living organisms, the growing availability of protein sequences, and the increasing recognition that some diseases are a result misfolded proteins [4].

X=3-4-20-21

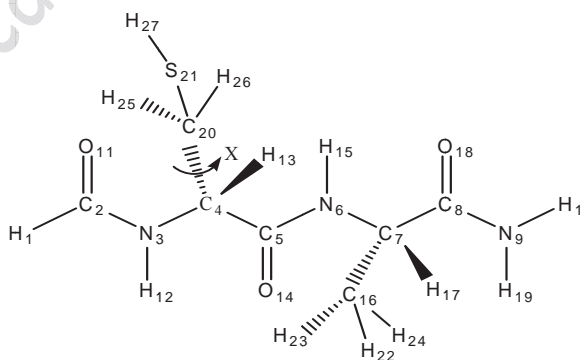


Fig. 1. Schematic diagram with torsional angle definitions for HCO-D-Cys-D-Ala-NH₂

Computational Method:

The Cysteine side chain dihedral angle (χ) rotated around N_3 - C_4 - C_{20} - S_{21} atoms, ($-C_4$ - C_{20} -) was changed at 30° intervals from 0° to 360° by using DFT geometry optimization



calculations at the B₃LYP/6-31G (d) level of theory and we determined three more stable structure among 12 optimized conformations. All of calculations performed by using Gaussian09 program.

Result and Discussion:

In this research we found three more stable states in the 300°, 180° and 60° that they known at this title: negative gauche(g^-), anti and positive gauche(g^+) State, Respectively. The results show that for HCO-D-Cys-D-Ala the energies of three minima gauche(+), anti, gauche(-) states are -666894.34, -666894.27, -666892.40 kcal mol⁻¹ respectively, Among three states gauche(+) has the highest stability.

References:

- [1] M.A. Sahai, S. Lovas, G.A. Chass, B. Penke, I.G. Csizmadia, J. Mol. Struct. (THEOCHEM), in this issue.
- [2] C.J. Levinthal, Chim. Phys. 65 (1968) 44.
- [3] A. Perczel, M.A. McAllister, P. Csa'zsa'r, I.G. Csizmadia, J. Am.
- [4] C.M. Dobson, Trends Biochem. Sci. 24 (1999) 329.



Potential energy curves of the $^3\Sigma^+$ and $^1\Delta$ states of the HCl^{2+} dication

Hassan Sabzyan*, Elham Keshavarz

Department of Chemistry, University of Isfahan, Isfahan 81746-73441, I. R. Iran

Email: sabzyan@sci.ui.ac.ir

Keywords: Dication, HCl^{2+} , Potential energy curve, Ghost atom, Spectroscopic constants

Introduction:

The HCl^{2+} dication has been studied both experimentally and theoretically, but only some of these studies have vibrational resolution. The potential energy curves of this dication have been calculated by multi-reference configuration interaction (MRCI) method to find the supported vibrational levels of some metastable electronic states [1,2]. Spectroscopic constants of some electronic states of HCl^{2+} dication have been obtained by polynomial fitting of MRCI potential energy curves [1,3]. In an Auger spectroscopic study of HCl molecule, some of its vibronic levels could be assigned [4]. Also double photoionization of HCl studied by threshold photoelectrons coincidence (TPEsCO) method, has revealed peaks corresponding to the vibronic levels of dication [5]. The DFT methods have been applied successfully for investigation of a large number of molecules. The well-known B3LYP functional has kept its fame beyond lots of newly designed functional, among which the HSE06 is chosen in this paper based on its previous use for some diatomics and its appropriate range of application [6]. In the present study, abilities of these two density functionals in the prediction of potential energy curves and the corresponding spectroscopic characteristics have been evaluated by comparison to available experimental data. Also the effect of the presence of ghost atom and its position on the calculated constants and vibrational level energies of the first singlet and triplet states of the HCl^{2+} dication has been investigated.

Method of calculations:

The large basis set 6-311g(3df,3pd) has been used without any diffuse function. The Li ghost atom has been considered once in a fixed distance of 0.5 Å from the H nucleus and once in the middle of the HCl bond. The interaction energy of the lowest singlet and triplet

states are calculated over a range of inter-nuclear distance, and their BSSEs are corrected using Counterpoise method. The potential energy curves obtained in each step is fed into the LEVEL8 program of LeRoy [7], to calculate energies of the bound vibrational levels. The spectroscopic constants have been obtained by polynomial fitting.

Results and discussion:

The calculated parameters of the $^3\Sigma^+$ and $^1\Delta$ states of the HCl^{2+} dication are reported in Table 1. Results show that, with both functionals, insertion of a ghost atom decreases the deviation of the calculated values from the experimental data. This effect is expected because by insertion of the ghost atom the wavefunctions and the interactions are described more accurately. Results obtained with the two positions of the ghost atom show no considerable difference. Apparently, the B3LYP functional gives better agreement with experimental results.

Table 1. Vibrational energies (in eV) and spectroscopic constants of the $^3\Sigma^+$ state of the HCl^{2+} dication.

Methods:	Exp. ⁵ (1994)	MRCI ³ (1987)	MRCI ¹ (1988)	HSE06				B3LYP			
				Without Li	HLi fixed	Li mid	LiCl fixed	Without Li	HLi fixed	Li mid	LiCl fixed
³ Σ ⁺ State											
E (v = 0)	0.0	0.0	0.0	0.0	0.0	0.0	0.0	0.0	0.0	0.0	0.0
E (v = 1)	0.17	0.207	0.18	0.180	0.178	0.174	0.175	0.172	0.169	0.165	0.166
E (v = 2)	0.23	0.388	0.33	0.330	0.324	0.315	0.316	0.311	0.304	0.294	0.294
R _e (Å)	1.39	1.430	1.46	1.464	1.47	1.47	1.47	1.474	1.48	1.48	1.48
ω _e (cm ⁻¹)	1581	1891	1758	1707	1763	1664	1701	1661	1642	1668	1655
ω _e χ _e (cm ⁻¹)	89	109	129	126	164	132	143	135.5	138.5	136	156
¹ Δ State											
E (v = 0)	0.0	0.0	0.0	0.0	0.0	0.0	0.0	0.0	0.0	0.0	0.0
E (v = 1)	0.17	0.207	0.18	0.178	0.173	0.170	0.172	0.170	0.165	0.163	0.163
E (v = 2)	0.23	0.384	0.34	0.322	0.312	0.305	0.305	0.303	0.293	0.286	0.285
R _e (Å)	1.44	1.429	1.46	1.468	1.47	1.48	1.46	1.477	1.48	1.48	1.47
ω _e (cm ⁻¹)	1468	1922	1797	1703	1668	1654	1698	1661	1622	1628	1657
ω _e χ _e (cm ⁻¹)	48	125	136	135.5	136	141.5	155.5	146	147	158	169.5

References:

- [1] A. Banichevich et al., Chem. Phys. 121 (1988) 351-359.
- [2] F.R. Bennett et al., Chem. Phys. Lett. 251 (1996) 405-412.
- [3] B.J. Olsson et al., J. Phys. B: At. Mol. Phys. 20 (1987) L137-L141.



- [4] S. Svensson et al., Phys. Rev. A 40 (1989) 4369-4377.
- [5] A.G. McConkey et al., J. Phys. B: At. Mol. Opt. Phys. 27 (1994) 271-282.
- [6] T.M. Henderson et al., J. Chem. Phys. 131 (2009) 044108.
- [7] R.J. LeRoy, LEVEL, University of Waterloo Chemical Physics Research Report, CP-555R, 1996.

15th Physical Chemistry Conference



Determination of the potential energy curves of diatomic bound electronic states using the energy- consistent method

H. R. Naeij^{*}, R. Islampour

Faculty of chemistry, Kharazmi (Tarbiat Moallem) University, Tehran, Iran

Email: Naeijhamidreza@yahoo.com

Keywords: Potential function, Potential curves, Diatomic bound electronic states, RKR data.

Introduction:

Knowledge of an accurate potential energy curve (PEC) and the vibrational structure of diatomic molecules is important for evaluation of the spectroscopic constants and requiring in studies such as vibrational excitations of electron-molecule collision. Much works have been done for investigation the PEC since the early Morse potential (1929) up to the lately full configuration-interaction (CI) calculations and experimental studies using threshold photoelectron spectroscopy. In this study, the so-called energy-consistent method (ECM) has been employed to accurately parameterize some of proposed analytical potential energy functions for the bound electronic states of diatomic molecules.

Energy- consistent method (ECM):

As it has been suggested by Murrell and Sorbie the extended Rydberg (ER) potential function of diatomic molecules is: [3]

$$V(R) = -D_e(1 + a_1x + a_2x^2 + a_3x^3) \exp(-a_1x) \quad (1)$$

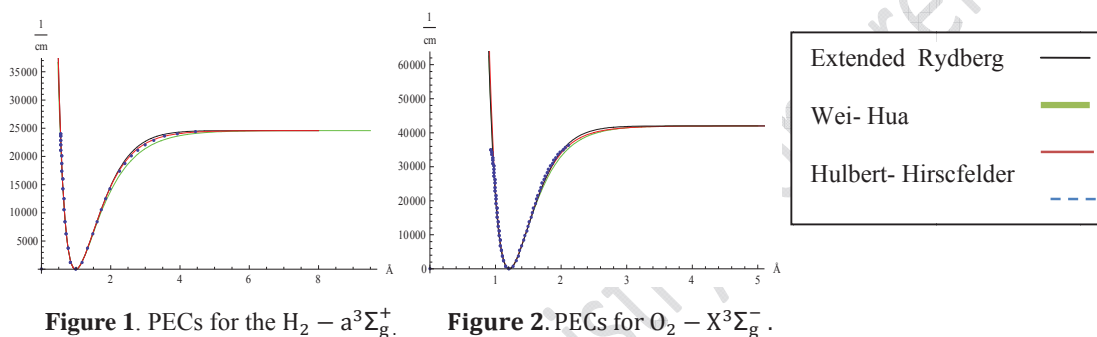
with $x = R - R_e$, where R is internuclear distance. The ECM based on ER potential is stated as following:

- Relationships between the potential coefficients (a_1, a_2, a_3) and the force constants (f_2, f_3, f_4) are determined and perturbation theory is used for determining the relationship between the force constants and the spectroscopic constants.
- The experimental values of molecular dissociation energy (D_e), equilibrium internuclear distance (R_e), reduced mass (μ), molecular vibrational and rotational constants ($\omega_e, \omega_e x_e, \alpha_e, B_e$) used for determining the potential coefficients.

- (c) The radial Schrodinger equation (RSE) is solved numerically using the Numerov method for the ER parameterized potential.
- (d) The vibrational energies of the RSE are compared with the RKR data available for diatomic bound electronic states.

Results and discussion:

As examples, figures (1) and (2) compares the potential energy curves (PEC) obtained by ECM with the empirical curves of RKR.



Investigation of the PECs shows that in the lower vibrational levels excellent convergence exists between the curves of ECM potentials and RKR curves. In the all diatomic electronic states studied by ECM, the convergence between the curves decreases slowly in the asymptotic region. The same trend is observed in the vibrational energies obtained by ECM.

Conclusion:

Although the ECM was performed only with the ER potential but this work shows Wei-Hua and Hulbert- Hirschfelder potentials can be also parameterized by this method. ECM can parameterize the potentials in which the number of parameters is high. For the potentials in which the number of parameters is low, the relationship between parameters, force constants and spectroscopic constants can be determined without using the perturbation theory. The numerical results for several electronic states of H_2 and O_2 molecules show that the ECM data are in very good agreement with the known RKR data. The suggested ECM provides an efficient alternative to quickly calculate the accurate potential curves, thereby, the correct vibrational eigenvalues and eigenfunctions of a diatomic system.



References:

- [1] J. L. Dunham, *Phys. Rev.* **41**, 721 (1932).
- [2] H. M. Hulbert and J.O. Hirschfelder, *J. Chem. Phys.* **35**, 1901 (1961).
- [3] J. N. Murrell and K. Sorbie, *J. Chem. Soc. Faraday, Trans. 2.* **70**, 1552 (1974).
- [4] W. Sun and H. Feng, *J. Phys.* **32**, 5109 (1999).

15th Physical Chemistry Conference



Self-association of thiazine dyes in aqueous and aqueous urea solutions

A. Ghanadzadeh Gilani*, T. Ghorbanpour

Department of Chemistry, University of Guilan, Rasht, Iran

Email: tghorbanpour@yahoo.com

Keywords: Azure A, Thionine, Thiazine dyes, Dye aggregation, Exciton theory

Introduction:

The molecular association of ionic dyes in solutions due to the strongly attractive electrostatic forces is a well-known phenomenon [1,2]. The presence of aggregates in the dye solutions may influence considerably in their photo-physical behavior. The strength of the molecular association depends on the several factors including the dye concentration and structure, temperature, pressure, solvent and other factors [3,4]. The structure of the aggregates has been studied by applying exciton theory to the analysis of the absorption spectra [5]. The dye aggregation leads to a strong coupling of the molecular transition dipoles, resulting in excitonic absorption band, which is considerably different from the absorption of the monomeric species. Thiazine dyes such as Azure A and Thionine are an important group of organic compounds which have a variety of industrial and scientific applications [6]. The photo-physical properties of this group of dyes have been demonstrated by several authors [7]. In this report, we describe the effects of concentration on the spectral data and aggregative properties of Azure A and Thionine in aqueous and aqueous urea solutions.

Materials and method:

Azure A chloride, AA, and Thionine acetate, Th, were of analytical grade and obtained from Sigma-Aldrich and Merck, respectively. Urea (CON_2H_4) was obtained from Merck. The absorption spectra of the dyes were recorded on a Cary UV-Vis double-beam spectrophotometer (Model 100) at room temperature. The thermostated sample holders were a series of rectangular cell with 1–10 mm path lengths.

Results and discussion:

The investigated thiazine dyes typically possess a doublet band, i.e. a maximum (λ_{max}) and a shoulder ($\lambda_{shoulder}$) in their optical absorption spectra. The absorption spectra of the



investigated dyes in aqueous solutions and aqueous urea solutions at 12 different concentrations ranging from 1×10^{-6} to 1×10^{-3} M were recorded at room temperature. The absorption spectrum of AA and Th in water shows an intense band at 630 and 596 nm which is neighbored by a shoulder at nearly 584 and 558 nm, respectively. These dyes form dimer in concentrated aqueous solutions. In this research, the absorption spectra and the aggregate formation of AA and Th in aqueous solutions of urea (0.4 and 0.8 M) were also investigated. Some spectral data are achieved. In two cases, the spectral data show that the extent of dye aggregation decreases in aqueous urea solutions.

Conclusions:

AA and Th in aqueous solutions appear to exist almost in their monomeric form at concentrations below 5×10^{-5} M and 8×10^{-5} M. The development of shoulder at shorter wavelength in the absorption spectra of the dyes in solutions could be attributed to the dimer formation. The excitonic parameters (θ , U , K_d , R) of the dyes in aqueous and aqueous urea solutions were evaluated and compared.

References:

- [1] A. Ghanadzadeh, A. Zeini, A. Kashef, M. Moghadam, J. Mol. Liquids 138 (2008) 100.
- [2] J. Georges, Spectrochim. Acta 51A (1995) 985.
- [3] L. Antonov, G. Gergov, V. Petrov, M. Kubista, J. Nygren, Talanta 49 (1999) 99.
- [4] A. Ghanadzadeh, H. Tajalli, P. Zirack, J. Shirdel, Spectrochim. Acta 60A (2004) 2925.
- [5] M. Kasha, H.R. Rawls, A. El-Bayoumi, Pure Appl. Chem. 11 (1965) 371.
- [6] A. Ghanadzadeh, M.A. Zanjanchi, R. Tibandpay, J. Mol. Struct. 616 (2002) 167.
- [7] K. Patil, R. Pawar, P. Talap, Phys. Chem. Chem. Phys. 2 (2000) 4313.



Analysis of vibronic structure in electronic spectra of large polyatomic molecules

M. Miralinaghi^{a*}, A. Khavaninzadeh^b, and R. Islampour^b

^a Department of Chemistry, Varamin-Pishva Branch, Islamic Azad University, Varamin, Iran

^b Department of Chemistry, Tarbiat Moallem University, 49 Mofateh Avenue, Tehran, Iran

Email: m_miralinaghi@iauvaramin.ac.ir, msmiralinaghi@gmail.com

Key words: Fluorescence excitation spectrum, Herzberg-Teller model, linear polyenes

Introduction:

The highly versatile role of linear polyenes in several important biological processes, such as vision, photosynthesis, and also their usefulness as computationally tractable models for more complex chromophores, retinal and carotenoids make them as intriguing subject of experimental and theoretical investigations. Optical experiments have established that (*all-trans*-) linear polyenes with four or more conjugated double bonds have a dark 2^1A_g state between the 1^1A_g ground state and dipole allowed 1^1B_u excited state.

One- and two- photon fluorescence excitation spectra for the lowest energy singlet transition $1^1A_g \rightarrow 2^1A_g$ of *all-trans*-1,3,5,7-octatetraene (hereafter, simply referred to as "octatetraene") in *n*-octane host crystal at 4.2 K [1] and in He free-jet expansions [2], as well as its He free-jet fluorescence spectrum [2] have been measured and vibrationally analyzed. The one-photon spectrum exhibits the features of a forbidden transition. The $0-0'$ band is absent and most of intensity is distributed among the bands which are progressions in Franck-Condon active totally symmetric a_g modes built on several $0-1'$ false origins due to non-totally symmetric b_u Herzberg-Teller promoting modes. The two-photon spectrum is electronically allowed and the progressions in a_g modes are built in usual way on the $0-0'$ true origin. The $2^1A_g \rightarrow 1^1A_g$ fluorescence spectrum is a good mirror image of the two-photon absorption.

Theory:

In this study we present the general approach for the computation of vibronically resolved optical spectra of large molecules, including both the Duschinsky rotation and the effect of

finite temperature in the framework of time domain correlation function and Franck-Condon simulation, to deal with the more general case of the Herzberg-Teller model, where also the linear dependence of transition dipole moment on the nuclear coordinates is taken into account. This generalization allows us to investigate vibronically allowed as well as forbidden transitions by far extending the range of application of the method. The effectiveness of the method is illustrated by computing the fluorescence excitation spectrum for $2^1A_g \rightarrow 1^1A_g$ symmetry-forbidden transition of octatetraene at zero temperature in harmonic approximation.

Results and discussion:

The one-photon $2^1A_g \rightarrow 1^1A_g$ spectrum of octatetraene is electric-dipole forbidden. The transition moments of $2^1A_g \leftrightarrow 1^1A_g$ spectra are derived from vibronic coupling between 2^1A_g and 1^1B_u states via b_u in-plane vibrations. Therefore, the one-photon spectrum is built on b_u Herzberg-Teller promoting modes, which are origins of progressions in a_g in-plane modes[2].

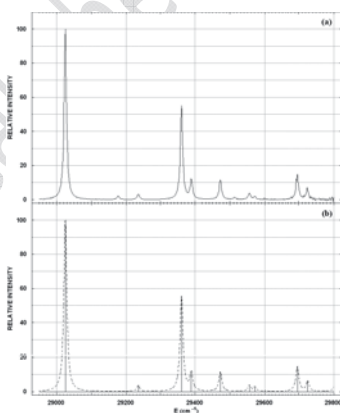


Figure1. Fluorescence excitation spectrum of octatetraene from 2^1A_g to 1^1A_g transition.

- (a) calculated spectrum by using of time-correlation formalism for displaced-distorted model ;
- (b) FC simulated spectrum for displaced-distorted-rotated model.

Figures 1a and 1b show that calculated fluorescence excitation spectrum related to the $2^1A_g \rightarrow 1^1A_g$ symmetry-forbidden electronic transition for octatetraene by making use of time correlation formalism and Franck-Condon (FC) simulation, respectively. The effects of



normal mode rotations on the spectra have been investigated in the simulated spectral profile in figure 1b. The calculated spectra are in good agreement with experimental data [2].

Conclusion:

The presented general approach for calculating the non-Condon vibronic structure observed in electronic absorption spectra of large organic polyatomic molecules has been successfully applied for the $2^1A_g \rightarrow 1^1A_g$ symmetry-forbidden transition in octatetraene.

References:

- [1] Granville, M. F.; Holtom, G. R.; Kohler, B. E. *J. Chem. Phys.* **1980**, 72, 4671-4675.
- [2] Petek, H.; Bell, A. J.; Choi, Y. S.; Yoshihara, K.; Tounge, B. A.; Christensen, R. L. *J. Chem. Phys.* **1993**, 98, 3777-3794.



Excited state electric dipole moment of thiazine dyes: A comparative study

A. Ghanadzadeh Gilani *, M. Salmanpour

Department of Chemistry, Faculty of Science, University of Guilan, Rasht, Iran

Email: m.salmanpour@gamil.com

Abstract:

A quantitative study of the solvent effect on the photophysical properties of two cationic thiazine dyes, Methylene blue, Thionine was carefully carried out at room temperature. The electronic absorption and emission spectra of the dyes were recorded in various organic solvents with different polarity at room temperature. The ground state and the excited state dipole moments of the dyes were estimated from solvatochromic shifts of absorption and fluorescence spectra. The solvent dependent spectral shifts in absorption and fluorescence spectra were analyzed by the Kamlet-Taft parameters.

Materials and methods:

MB Chloride and Thionine Acetate were obtained from Merck. All the organic solvents with high purity were purchased from Merck.

The absorption spectra of the dyes were recorded on a double beam Cary UV-Visible spectrophotometer (Model 100) over a wavelength range 400–800 nm. Fluorescence of the dye solutions was studied with a JASCO FP-6200 with standard Quartz cuvettes. The uncertainty in the measured wavelength of absorption and fluorescence maxima is ± 0.1 nm and ± 1 nm, respectively. The dye concentrations were chosen to be 1×10^{-5} M for all the organic solvents.

Results and discussion:

Absorption bands of these dyes in visible region (600-670 nm) are due to the $\pi^* \leftarrow n$ transition associated with the presence of a $C=S$ chromophore group in these dyes. Only small shifts of the absorption band maxima of dyes were observed, when varying the polarity of the solvent.



The fluorescence excitation spectra are generally located at wavelengths close to the absorption spectra of the dyes. the fluorescence emission of MB was slightly red-shift upon increasing the solvent polarity, whereas in the case of Thionine , no significant shifts was noticed upon changing the solvent polarity.

For evaluating the role of solvents in the determined spectral variation of the dyes, Kamlet-Abboud - Taft (KAT)) multi-parameter scales were used .

$$A=A_0+n\alpha+m\beta+s(\pi^*+\sigma) \quad (1)$$

In these relations, A is maximum wave number , A_0 is intercept , σ is a scale of solvent hydrogen-bond donor (HBD) acidities, σ^* scale of solvent hydrogen-bond acceptor (HBA) basicities, π^* scale of solvent dipolarity-polarizability using UV/Vis spectral data of solvatochromic compounds.

Conclusion:

The absorption and emission spectra of MB and Thionine in different media were studied. The solvatochromic method was used to determine the ground and excited state dipole moments.

References:

- [1] A. Ghanadzadeh Gilani, H. Tajalli, M.S. Zakerhamidi, Molecular Liquids 143 (2008) 81–88.
- [2] Martina Havelcova, Pavel Kuba, Irena Neřmcova, Dyes and Pigments 44 (2000) 49-54.
- [3] C. PAmcANYrt and C. BONIFACE, J. J. AAnoN and M. MAAF, Spmrochimica Arm, Vol. 49A. No. 12. pp. 1715-1725.



Altered Luminescence Efficiency of Cadmium Sulphide Quantum Particles via co-doping Ni_xZn_y ions

F. Bozorg Bigdeli^a, M. Yousefi^a, A.A. Khosravi^b, S.M. Taheri Otaqsara^c, M.S. Abdikhani^a

^aFaculty of science, Islamic Azad University, Shahr-Rey Branch, Tehran, Iran

^bDepartment of Physics, Shahed University, Tehran, Iran

^cScience Research and Technology Center, Jihad Organization, Tehran, Iran

faezehbigdeli@gmail.com

Introduction:

Nanosized semiconductor materials have drawn significant attention due to their unique optical and chemical properties originating from the quantum confinement effect [1,2]. Doped materials show different type of luminescence properties which are strongly depended on the type of dopant ions. These dopant impurities play an important role in changing the electronic structure and transition probabilities of the host material [3]. In this work, we report the synthesis of single/double impurity (Ni:Zn) doped CdS quantum dots at ambient temperature by wet-chemical method. Doped $\text{Cd}_{1-x-y}\text{Ni}_x\text{Zn}_y\text{S}$ Q-dots were synthesized by the procedure reported in our previously work [4-6].

Results and Discussion:

The absorption edge of bulk CdS is at 515 nm [4]. UV-vis of doped and co-doped CdS is shown in Fig. 1 (left graph). The excitonic transition red-shifts and becomes less prominent on doping. The red shift indicates the formation of larger particles on doping. Furthermore, for calculating the direct band gap value $(\alpha h\nu)^2$ as a function of $h\nu$ is plotted and it is shown in Fig. 1 (right graph). From the value of band gap shift and using Brus model [1] the size of nanoparticles have been calculated and those are shown in inset Fig. 1 (right graph).

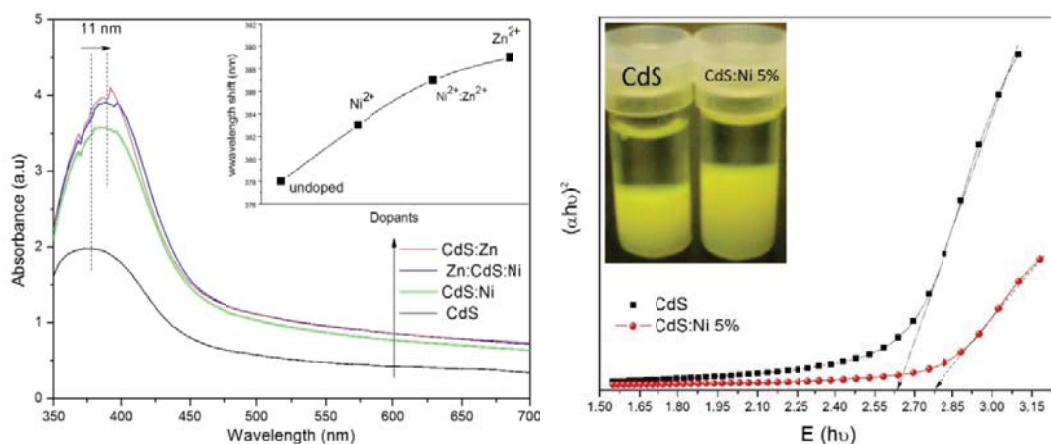


Fig. 1. (Left): UV-visible spectra of $\text{Cd}_{1-x-y}\text{Ni}_x\text{Zn}_y\text{S}$ Q-dots; (right): Profiles of $(\alpha h\nu)^2$ versus $h\nu$.

The room temperature PL spectra obtained at 280 nm excitation of un/co-doped CdS nanoparticles are shown in Fig.2. A strong band located at 488 nm (blue emission) and weaker band at 530 nm (green emission) were observed. The blue-green emission band can be attributed to the radiative transition of through the defect state. Defect states can be attributed to the presence of anion vacancies [7]. The PL emission does not show any shifting on doping, but the luminescence emission intensity (LEI) of samples varies on increasing of impurity molar ratios. The LEI of $\text{Cd}_{1-x-y}\text{Ni}_x\text{Zn}_y\text{S}$ nanoparticles is about 3 times larger than that of undoped CdS nanoparticles.

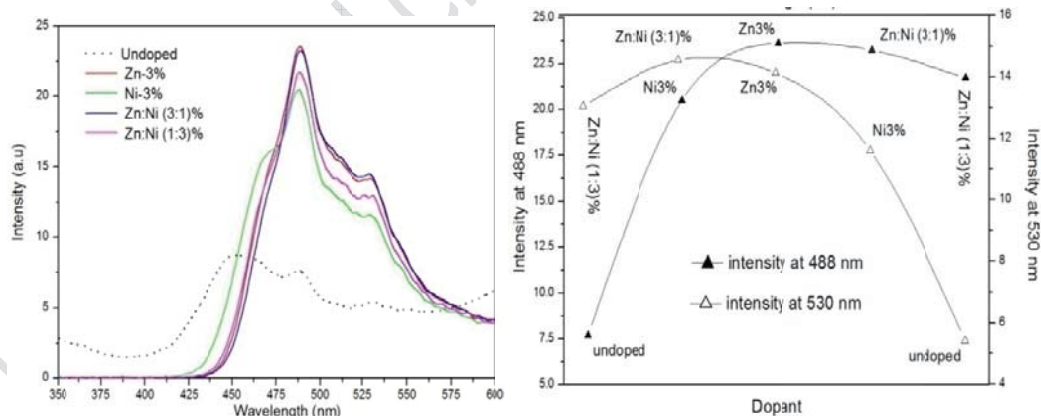


Fig. 2. (left): PL spectra of $\text{Cd}_{1-x-y}\text{Ni}_x\text{Zn}_y\text{S}$ Q-dots; (right): Profiles of relative intensity on various dopant.

Conclusions:

Ni_xZn_y co-doped CdS nanoparticles are successfully synthesized by wet-chemical method. The action of single/double doping is studied using UV-Vis spectra of CdS nanoparticles.



The blue-green emission band can be related to the radiative transition via defect state. In contrast to single-ion doped crystals, co-doped material exhibits high luminescence emission intensity in PL spectrum.

References

- [1] L. E. BRUS, J. Chem. Phys. 79 (1983) 5566.
- [2] A. A. Khosravi, M. Kundu, L. Jatwa, S. K. Deshpande, Appl. Phys. Lett, 67 (18) 1995.
- [3] M. Mall, L. Kumar, J. Lumines, doi:10.1016/j.jlumin.2009.11.012.
- [4] S. M. Taheri, M. H. Yousefi, A.A. Khosravi, Braz. J. Phys, 40 (2010) 301.
- [5] M. Yousefi, A.A. Khosravi, K. Rahimi, A. Nazesh, Eur. Phys. Appl. Phys, 45 (2009) 10602.
- [6] A. A. Khosravi, M. Kundu, S. Deshpanda, S.K. Kulkarni, Appl. Phys. Lett, 67 (1995) 2702.
- [7] C. Unni, D. Philip, S.L. Smitha, Spectrochimica Acta Part A, 72 (2009) 827.



Quantum mechanical study on the mechanism of nucleophilic substitution reaction of α -Chlorododecyl Carboxylate with trimethylamin

A. Morsali^a, M. M. Heravi^a and H. Hasheminasl^{* a}

^aDepartment of Chemistry, Mashhad Branch, Islamic Azad University, Mashhad, Iran
(Email: helenahasheminasl@yahoo.com)

Keywords: Nucleophilic substitution, Mechanism, α -Chlorododecyl carboxylate, Density functional theory

Introduction:

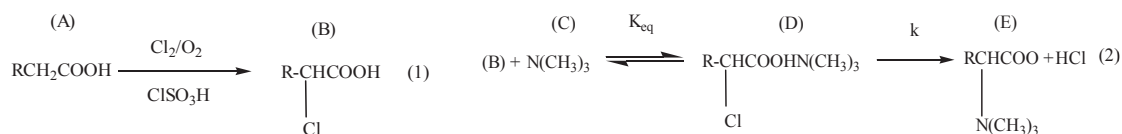
The nucleophilic substitution reaction is among the most popular approaches in organic chemistry. A nucleophilic substitution reaction was developed to synthesize the zwitterionic surfactant using a renewable natural fatty acid rather than a petroleum derivative as the raw material. The kinetics and mechanism of the nucleophilic substitution reaction of α -chlorododecyl carboxylate with trimethylamine were investigated in protic and dipolar aprotic solvents including water, ethanol and N, N-dimethyl formamide[1]. The rate equations were derived using initial rates and the activation parameters in different solvents were determined empirically and compared with each other to obtain important information about the reaction mechanism [1]. In this work, the mechanism of nucleophilic substitution reaction of α -Chlorododecyl Carboxylate with trimethylamin has been studied using density functional methods.

Computational details:

All of the present calculations have been performed with the B3LYP [2] hybrid density functional level using the G09 package. The 6-311+G(d,p) basis set was employed. The gas phase optimized geometries used to apply the solvent effects, where the valuable PCM [4] model was employed.

Results and discussion:

The following mechanism (Eqs.(1 and 2)) for the rate-determining step was proposed which is compatible with experimental evidence.



In this mechanism, a fast equilibrium step (with equilibrium constant K_{eq}) will result in the formation of D which will be converted into E and HCl during a slow process. The optimized structure of transition state obtained from step2 has been shown in Fig. 1. The optimized structure of transition state obtained from step2 (D to E) has been shown in Fig. 1. By taking Solvent effects into consideration, $E_a = 79.65 \text{ kcal/mol}$ ($E_a(\text{exp}) = 74.18 \text{ kcal/mol}$). This shows that the model presented in this research is a suitable model for this reaction.

Conclusion:

The kinetics and mechanism of the nucleophilic substitution reaction of α -chlorododecyl carboxylate with trimethylamine were investigated in water using quantum mechanical approach. The reaction between α -chlorododecyl carboxylate and trimethyl amin produces trimethylamin α -chlorododecyl carboxylate (structure D) which will be converted into final products. The activation energy (E_a) has been calculated and compared with experimental data. The calculated value of activation energy has a good consistency with the experimental value.

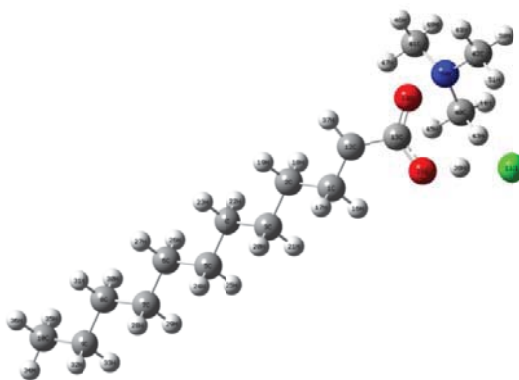


Fig 1. Optimized structure of the TS (step 2).

References:

- [1] Z. Wang, S. Zhang, Y. Fang, H. Yang, L. Qi, J. Surfact. Deterg. 13 (2010) 361.
- [2] A.D. Becke, Phys. Rev. A 38 (1988) 3098.
- [3] S. Miertus, E. Scrocco, J. Tomasi, Chem. Phys. 55 (1981) 117.



Nucleus-independent chemical shift (NICS) profiles in aromaticity and reactivity patterns of Ferrocene complexes

M.Nouraliei^{a, b}, S.Bagherzadeh^{a, b}, A.Askarizadegan^{a, b}, S.Naghbi^{a, b}, A.Amiri^{*a}

^aDepartment of Chemistry, Islamic Azad University, Center Tehran Branch, Tehran, Iran

^bYoung Researchers Club, Central Tehran Branch, Islamic Azad University, Tehran, Iran

Email: afsaaamiri@gmail.com

Keywords: Ferrocene, DFT, HF, aromaticity, independent chemical shift (NICS)

Introduction:

Since the discovery of Ferrocene $\text{Fe}(\text{C}_5\text{H}_5)_2$ in 1951 this molecule and a great variety of its derivatives have been used for many different purposes, [1]. Various quantitative measures, which evaluate aromaticity are available and they can be classified as geometric, energetic and magnetic criteria, and reactivity based descriptors [2–4]. Exaltation of magnetic susceptibilities and proton chemical shifts are based on the magnetic criterion. Nucleus independent chemical shift (NICS) values have been extensively used to evaluate aromaticity [4, 5].

Materials and methods:

Several ab-initio computational studies have been reported for Ferrocene (and other metallocenes as well). In This research study the geometry of the system has been fully optimized with the hybrid DFT and HF by GAUSSIAN 03 programs on a Pentium-PC computer with 3600 MHz processor [6]. The NICS values calculated at the center of the rings (NICS(0)) and 0.5 Å above the rings (NICS(1)) obtained using the gauge invariant atomic orbital GIAO procedure at the B3LYP/6-31G** and HF/6-31G**.



Result and discussion:

The computation predicted that their most stable structures are in D_{5h} and D_{5d} symmetry. The predicted B3LYP energy differences ($D_{5h}-D_{5d}$) for is 0.75 kcal/mol. The Ferrocene structure were optimized at the B3LYP/6-31G** level of calculation. The normal modes of

the imaginary frequencies correspond to the out-of-plane distortion of the H attached to the heteroatom. NICS calculations at the center of the rings were performed on all the systems using the gauge invariant atomic orbital (GIAO) approach at the HF/6-31G** level. The results have

been reported in the table.1.

Table.1 DFT-calculated nuclear independent chemical shifts (NICS) values in ppm

structure ring up	dummy atom number	Distance to hetrocycle center	NICS values(ppm)	structure ring down	No of dummy atom	Distance to hetrocycle center	NICS values(ppm)
	3	1.00	-17.7157		3	1.00	-17.7308
	2	0.50	-30.8632		2	0.50	-30.8825
	1	0.0	-46.0942		1	0.0	-46.1002

Conclusion:

DFT studies have been shown to describe various properties of these molecules satisfactorily with a fraction of computational cost. On the B3LYP/6-31G** level the D5h conformation of Ferrocene is slightly more stable than the D5d conformation, although the barrier of rotation is extremely small ($-0.12 \text{ kcal mol}^{-1}$). NISC analysis in DFT and HF levels with three virtual atoms (Bq) at 0.5 Å up to the molecular surface have been carried out. The B3LYP/6-31G** results have been shown that aromatic stability of ring up, at the atomic distance of 0.0 Å to the value of -46.0942 ppm is in the ring down with a distance of 0.0 Å to the value of -46.1002 ppm. The HF/6-31G** calculation of aromatic stability of rings up the atomic distances of 1.0 Å to the value of 8.2626 ppm is in the ring Down with a distance of 1.0 Å to the value of 8.2701ppm.

References:

- [1] (a) T.J. Kealy, P.L. Pauson, Nature (London) 168 (1951) 1039; (b) R.B. Woodward, M. Rosenblum, M.C. Whiting, J. Am.Chem. Soc. 74 (1952) 3458; (c) G. Wilkinson, J. Organomet. Chem. 100 (1975) 273; (d) P.L. Pauson, Pure Appl. Chem. 49 (1977) 839. (d)



D.W. Bruce, in: D.W. Bruce, D. O'Hare (Eds.), *Inorganic Materials*, second ed., Wiley, Chichester, 1996; (e) A.P. Polishchuk, T.M. Timofeeva, Russ.

[2] *Chem. Rev.* 101 (5) (2001).

[3] V. Minkin, B. Simkin, M. Glukhotsev, *Aromaticity and Antiaromaticity; Electronic and Structural Aspects*, Wiley, New York, 1994.

[4] M.K. Cyranski, T.M. Krygowski, A.R. Katritzky, P.v.R. Schleyer, *J. Org. Chem.* 67 (2002) 1333.

[5] U.D. Priyakumar, G.N. Sastry, *J. Am. Chem. Soc.* 122 (2000) 11173.

[6] M. j. Frisch et al. *GAUSSIAN 03*, Revision C. 01, Gaussian Inc., Wallingford, CT, 2004.



Molecular structure and Spectroscopic analysis (FT-IR, UV-VIS, ¹H NMR) of Ciprofloxacin via Quantum liquid DFT calculation

Afsaneh Amiri^{1*}, Saman Naghibi^{1,2}, Milad Nouralie^{1,2}, Simin Tadayon¹

¹Department of Chemistry, Islamic Azad University, Central Tehran Branch, Tehran, Iran.

²Young Researchers Club, Central Tehran Branch, Islamic Azad University, Tehran, Iran.

Email: afsaamiri@gmail.com

Keywords: Ciprofloxacin, Spectroscopic analysis, B3LYP, DFT, FT-IR, UV-VIS, ¹H NMR.

Introduction:

Ciprofloxacin (C₁₇H₁₈FN₃O₃, 1-cyclopropyl-6-fluoro-1,4-dihydro-4-oxo-7-(1-piperazinyl)-3-quinoline carboxylic acid) is a synthetic antibiotic of the Fluoroquinolone drug class [1- 3]. It is a second-generation fluoroquinolone antibacterial. It removes bacteria by interfering with the enzymes that cause DNA to rewind after being copied, which stops synthesis of DNA and of protein. In this research study, the formation potential Molecular structure, Spectroscopic analysis (FTIR, UV-VIS, NMR) of Ciprofloxacin have been investigated by DFT calculation.

Material and Methods:

The geometry of the system has been fully optimized with the hybrid DFT and HF. DFT and HF calculations were performed with the GAUSSIAN 03W programs on a Pentium-PC computer with 3600 MHz processor [4]. To verify that the concluding structure wasn't in the local minimum point, the normal mode frequency calculation was carried out for the optimized molecules. The Spectroscopic analysis (FT-IR, UV-VIS, NMR) of the molecule in the liquid phase, were carried by using the Onsager SCRF method at the B3LYP/6-311+G**.

Result and Discussion:

Computational calculations of Ciprofloxacin have been carried out using the Becke-3-Lee-Yang-Parr density (B3LYP) functional methods with 6-311+G (d, p) basis set. The geometry optimization and fundamental frequencies of the most stable configuration have been

calculated. The FTIR spectra of the compound have been recorded and compared to the calculated frequency values. The ^1H NMR chemical shifts have been calculated using the gauge-independent atomic orbital approach. (Fig.1-3)

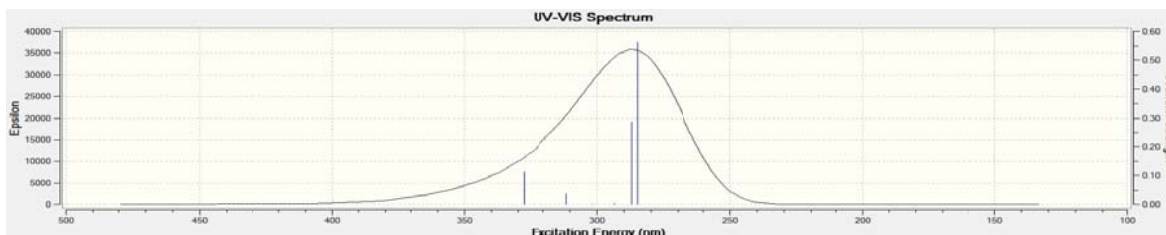


Fig. 1. Theoretical UV spectra of Ciprofloxacin of Fluoroquinolone derivatives

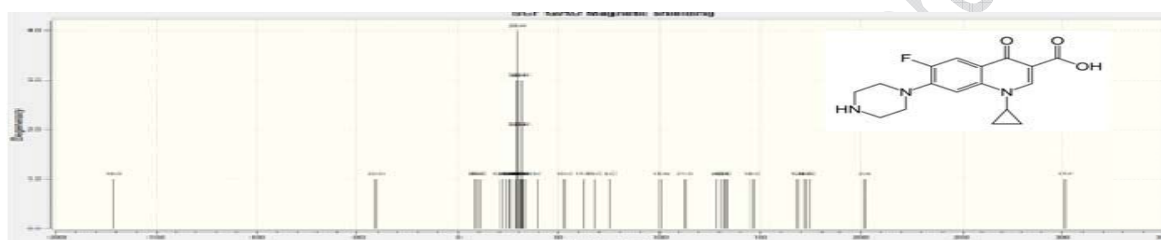


Fig. 2. Theoretical spectra of ^1H NMR Ciprofloxacin of Fluoroquinolone derivatives

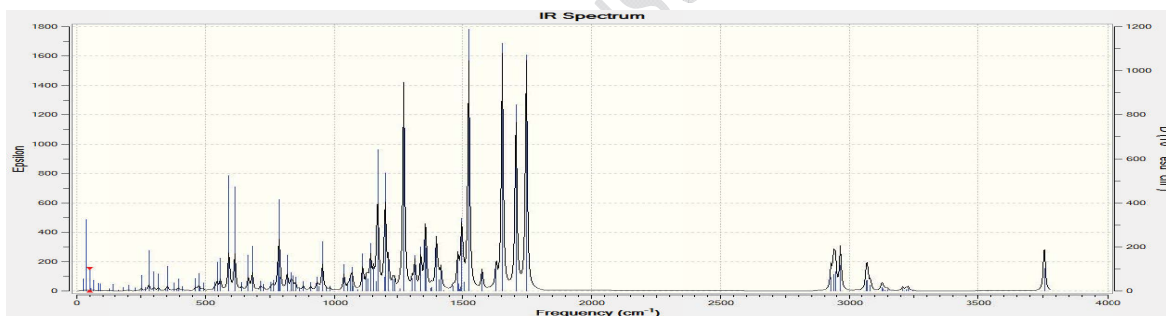


Fig. 3. Theoretical spectra of FT-IR Ciprofloxacin of Fluoroquinolone derivatives

Conclusion:

The calculated parameters were compared to experimental characteristic of Ciprofloxacin. Respectively good correlation in the range is 0.9005- 0.9878 between experimental and theoretical spectra was noted.

References:

- [1] Nelson, JM.; Chiller, TM.; Powers, JH.; Angulo, FJ. (Apr 2007). "Fluoroquinolone-resistant *Campylobacter* species and the withdrawal of fluoroquinolones from use in poultry: a public health success story.". *Clin Infect Dis* **44** (7): 977–980.



- [2] Kawahara, S. (Dec 1998). "[Chemotherapeutic agents under study]". *Nippon Rinsho* **56** (12): 3096–3099.
- [3] "Ciprofloxacin-Hydrochloride". *The American Society of Health-System Pharmacists*.
<http://www.drugs.com/monograph/ciprofloxacin-hydrochloride.html>. Retrieved 3 April 2011.
- [4] M. j. Frisch et al. *GAUSSIAN 03*, Revision C. 01, Gaussian Inc., Wallingford. CT, 2004.

15th Physical Chemistry Conference



DFT prediction on pK_a of L-dopa in an aqueous solution

Reza Behjatmanesh-Ardakani^a, Fatemeh Sajedi-Moghadam^{a,*}

^a Chemistry Department, Payame Noor University, 19395-4697 Tehran, I.R. of Iran

E-mail: fsajedi@ymail.com

Key words: L-dopa, acidity constant, DFT, hydrogen bonding

Abstract:

Levedopa (3,4-dihydroxyphenylalanine, L-dopa) [1] is a very important compound that is considered for Parkinson's disease in parts of brain. Predicting properties of L-dopa is an interesting subject of research. Several methods have been developed for predicting properties of compounds such as QSPR [2], QSAR [3], and ab initio/DFT methods [4]. Quantum mechanical methods have been previously used to investigate and to predict acidity constants of different acids or bases [5]. In this paper, by means of DFT method, acidity constant of L-dopa is predicted.

Geometry of each compound was fully optimized at B3LYP/6-31++G(d,p), and B3LYP/6-311++G(d,p) levels of theory [6]. Total free energy of each compound in water was calculated using CPCM and SMD models at the HF/6-31G and HF/6-31G(d,p) levels of theory to evaluate pK_a values. All of the theoretical calculations were carried out with the Gaussian 2009 suite of programs, and molecules were drawn by GaussView 5.0 program. Comparing the results, one can find out that increasing the basis set of theory yields a significant improvement in the calculated pK_a values. Data show significant effects hydrogen bonding in CPCM model

References:

- [1] Xiaofeng Chen, Jiyong Zhang, Honglin Zhai, Xingguo Chen, Zhide Hu. 92 (2005) 381-386.
- [2] Gupta, S. P. Chem. Rev. 91 (1991) 1109.
- [3] Gupta, S. P. Chem. Rev. 87 (1987) 1183.



- [4] J. Baker.” An algorithm for the location of transition- states”. J.Com.Chem, 7 (1986) 385-950.
- [5] R. Behjatmanesh- Ardakani, M. A. Karimi, A. Ebady. 910 (2009) 99-103.
- [6] A. D. Becke, J. Chem. Phys. 98 (1993) 5684.

15th Physical Chemistry Conference

Laser Mass Spectrometry of Alkali-Earth Halides

M. Mirian, M. Tabrizchi, F. Abyar, H. Farrokhpour

Department of Chemistry, Isfahan University of Technology, Isfahan, Iran, 84156-83111

Email: mmirian66@yahoo.com

Keywords: Time-of flight, Alkali-Earth Halides, Isotope pattern, Detection devices.

Introduction:

Time of flight (TOF) mass spectrometry is one of the most important analyzing techniques which works based on acceleration and separation of ions in vacuum. The advantage of TOF instrument is that it can readily reach mass resolving power ($m/\Delta m$) of 1000–10000 with very high efficiency compared to other detection devices including magnetic sectors, quadrupole and ion traps. In this work, mass spectra of earth alkali halides including MgCl_2 , CaCl_2 , SrCl_2 and BaCl_2 ; and their mixtures have been recorded using a laser ionization technique and a home made TOF mass spectrometer. The spectra were assigned and the effects of the laser intensity and acceleration voltages on the spectra were investigated.

Experimental:

The TOF mass spectrometer, constructed in the Isfahan University of Technology, is schematically shown in Fig.1. The solid sample coated on the repeller of the accelerator and was irradiate by laser light. The produced ions accelerated in region A and fly in a field free region. The ions are separate based on the mass to charge ratio (m/z). The chamber was under high vacuum (10^{-7} mbar).

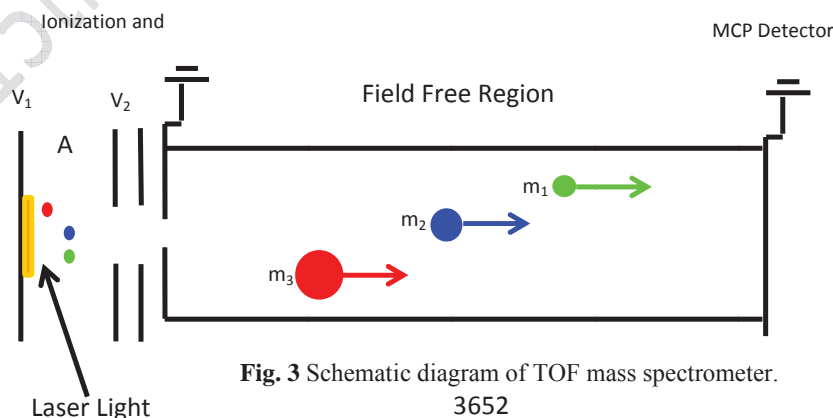


Fig. 3 Schematic diagram of TOF mass spectrometer.

Result and discussion:

Fig. 2 and 3 shows the recorded TOF spectra of SrCl_2 and BaCl_2 , respectively. Molecular ion patterns were used for assignment. Ba and Cl have five and two stable isotopes, respectively. This makes several types of BaCl^+ ion. To simulate the mass pattern of BaCl , the relative population of each isotope was calculated based on the natural abundances of each atom. The solid lines in Fig. 2 show the simulated pattern of the recorded spectrum related to Ba isotopes and the different combinations of BaCl . Fig.3 also demonstrates the TOF spectrum of SrCl . Sr^+ and SrCl^+ ions are evident in the spectrum.

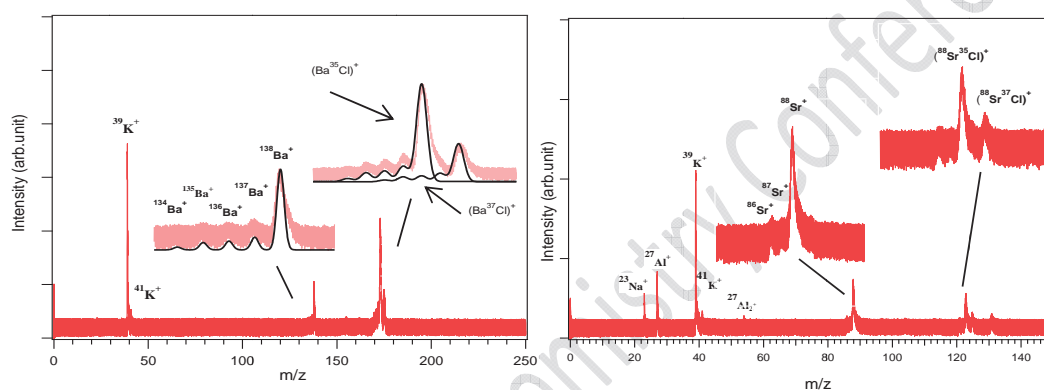


Fig.2 &3. TOF spectra of BaCl_2 and SrCl_2 .

Conclusions:

Time-of-flight mass spectra of CaCl_2 and SrCl_2 have been recorded using laser as ionization source. The spectra includes AE^+ and AEX^+ where AE and X stands for alkali earth and halide, respectively. The simulated isotope pattern confirms the mass assignment.

References:

- [1] M. Tabrizchi, Construction of a laser ionization time-of-flight mass spectrometer, Iranian Patent No. 73361, 2012.
- [2] M.Yildirima, O.Siseb, M.Doganb, H.S. Kilic, Designing multi-field linear time-of-flight mass spectrometers with higher-order space focusing, J. Mass Spectrom. 2010; 291:1–12.



Calculation of Decay Rate Constants of $2^1A_g \rightarrow 1^1A_g$ Internal Conversion in *trans,trans*-1,3,5,7-Octatetraene

A. Khavaninzadeh ^{*a}, M. Miralinaghi ^b, and R. Islampour ^a

^a Department of Chemistry, Tarbiat Moallem University, 49 Mofateh Avenue, Tehran, Iran

^b Department of Chemistry, Varamin-Pishva Branch, Islamic Azad University, Varamin, Iran

Email: a_khavaninzadeh@yahoo.com

Key words: *all-trans*-1,3,5,7-Octatetraene, Internal Conversion, Dipole forbidden transition.

Introduction:

The first excited state of linear (*all-trans*-)polyenes with four or more double bonds is the covalent 2^1A_g electronic state in which transition from the ground state 1^1A_g to that is dipole forbidden to first order. The 0–0' band is absent and most of intensity is distributed among the bands which are progressions in Franck-Condon active totally symmetric a_g modes built on several 0–1' false origins due to nontotally symmetric b_u Herzberg-Teller promoting modes.

It is our aim of this paper to calculate decay rate constant of $2^1A_g \rightarrow 1^1A_g$ internal conversion of *trans,trans*-1,3,5,7-octatetraene using theoretical expressions developed in the previous works [1]. In addition, the vibrational normal modes which have the highest contributions to this process are investigated.

Theory:

It has been previously shown that [2] the internal conversion decay rate constants between two adiabatic displaced-distorted-rotated potential energy surfaces, by including all vibrational modes, can be written as

$$k_{IC}(\Omega_{ab}, T) = \int_{-\infty}^{\infty} dt \exp(i\Omega_{ab}t) G(t) \quad (1)$$

with

$$G(t) = 2^N \left[h(t) \left(\det \Gamma'^{-1} \Gamma^{-1} \mathbf{T}' \mathbf{T} \mathbf{W}_1 \mathbf{W}_2 \right)^{-1/2} \exp(-\mathbf{D}^T \mathbf{W}_3^{-1} \mathbf{D}) \right]_{\Gamma_p} \times \prod_{j \neq p} \left[\left(\det \Gamma'^{-1} \Gamma^{-1} \mathbf{T}' \mathbf{T} \mathbf{W}_1 \mathbf{W}_2 \right)^{-1/2} \exp(-\mathbf{D}^T \mathbf{W}_3^{-1} \mathbf{D}) \right]_{\Gamma_j} \quad (2a)$$

$$h(t) = \frac{1}{2} \mathbf{R}^\dagger (-\mathbf{W}_3^{-1} + \mathbf{W}_4^{-1}) \mathbf{R} + (\mathbf{R}^\dagger \mathbf{W}_3^{-1} \mathbf{D}) (\mathbf{D}^T \mathbf{W}_3^{-1} \mathbf{R}) \quad (2b)$$

where the first bracket on the right hand side of equation (2a) corresponds to the promoting modes, those induce the non-radiative transitions, and the next brackets to the accepting modes, those act as sinks for the electronic energy. The dimensions of the symmetric matrices \mathbf{W}_1 , \mathbf{W}_2 , \mathbf{W}_3 , \mathbf{W}_4 and diagonal matrices $\mathbf{\Gamma}'$, $\mathbf{\Gamma}$, \mathbf{T}' , and \mathbf{T} (all defined in reference 1) are determined by the number of the vibrational modes which have the same symmetry species. In equation (2b) \mathbf{R} is the column vector of the nonadiabatic coupling matrix elements $R_p = -i\hbar \langle \Phi_a | \partial / \partial Q_p | \Phi_b \rangle_0$ in the Condon approximation, where $\langle \dots \rangle_0$ means the value of the matrix elements in the vicinity of some reference configuration. Equations (2a,b) have been used to estimate the decay rate constant of $2^1A_g \rightarrow 1^1A_g$ internal conversion in octatetraene molecule.

Results and discussion:

2^1A_g and 1^1A_g electronic states are vibronically coupled by the a_g normal modes ν_6 and ν_{12} . However, ν_6 is more effective than ν_{12} due to its higher frequency, significantly larger displacement parameter, and larger nonadiabatic coupling constant.

Our calculations show that in the low temperature limit $2^1A_g \rightarrow 1^1A_g$ internal conversion takes place on a 2 μ s time scale under the isolated conditions. The temperature dependence of τ_{IC} has been also investigated. τ_{IC} remains almost constant at a value of $\sim 0.3 \mu$ s up to 490 K. This may be considered as an indication that the decrease in $2^1A_g \rightarrow 1^1A_g$ fluorescence lifetime with increasing temperature is due to another radiationless process, as *trans* \rightarrow *cis* isomerization in the 2^1A_g excited electronic state [3, 4].

Conclusion:

The decay time constants obtained in the present work for the $2^1A_g \rightarrow 1^1A_g$ internal conversion under isolated conditions are in reasonable agreement with the observed and calculated decay time constants. The distortions of the normal modes considerably reduce the decay rate constant of this transition. It has been also explored that a 3-displaced mode model



consisting of the three totally symmetric promoting modes ν_6 , ν_{12} and ν_{16} , which have the highest Huang-Rhys factors can approximately produce the observed decay time constant for this process.

References:

- [1] Islampour, R.; Miralinaghi, M. *J. Phys. Chem. A*, 2007, **111**, 9454-9462 ; Islampour, R.; Miralinaghi, M. *J. Phys. Chem. A*, 2009, **113**, 2340-2349.
- [2] Islampour, R.; Miralinaghi, M. ; Khavaninzadeh, A. *J. Phys. Chem. A*, 2011, **115**, 8860-8869.
- [3] Ackerman, J. R.; Kohler, B. E.; Huppert, D.; Rentzepis, P. M. *J. Chem. Phys.* 1982, **77**, 3967-3973.
- [4] Garavelli, M.; Celani, P.; Yamamoto, N.; Bernardi, F.; Robb, M. A.; Olivucci, M. *J. Am. Chem. Soc.* 1996, **118**, 11656-11657.



Dynamic NMR of Ranitidine: An Empirical and Computational Study

S. M. Ghoreishi^a, M. Taffazoli*^a

^aDepartment of chemistry, Sharif university of technology, Tehran, Iran

Email: tafazzoli@sharif.edu

Keyword: Ranitidine, DNMR, Gaussian, DFT

Abstract:

In this work we have studied conformation of ranitidine by dynamic nuclear magnetic resonance spectroscopy (DNMR) in four different solvents: chloroform, acetone, dimethylsulfoxide, and deuteriumoxide. Ranitidine has three tautomeric forms of enamine, nitoic acid, and imine, but its stable structure is enamine. Temperature dependent ¹HNMR spectra of ranitidine which achieved at 500MHz were consistent with the following free activation of energies ΔG^\ddagger (kcal mol⁻¹): chloroform = 16.2; acetone = 15.4; dimethylsulfoxide = 15.1. The experimental results were confirmed by DFT theoretical calculations at the B3LYP/6-311++G (d, p) level of theory. It was also proved that ranitidine has the form of imine in deuteriumoxide, while in the three other solvents, acetone, chloroform, and dimethylsulfoxide, has the enamine form.



Influence of $\text{Cu}^{+2}:\text{Mn}^{+2}$ co-doping ZnS Nanoparticles on Light Emission Efficiency

M.S. Abdikhani^a, A.A. Khosravi^b, S.M. Taheri Otaqsara^c, F. Bozorg Bigdeli^a, M. Yousefi^a

^aFaculty of science, Islamic Azad University, Shahr-Rey Branch, Tehran, Iran

^bDepartment of Physics, Shahed University, Tehran, Iran

^c Science Research and Technology Center, Jihad Organization, Tehran, Iran

m_abdikhani@yahoo.com

Introduction:

Colloidal luminescent semiconductor nanocrystals (NCs), also known as quantum dots (Q-dots), have attracted considerable attention due to their significant potential application [1]. Quantum size effects (QSE) associated with the low dimensionality lead to several remarkable modifications in the physical properties of materials [2,3]. Co-doped ZnS NPs were synthesized by the procedure reported in our previously work [4,5]. Here, we report the results of our study on the PL characterization of $\text{Cu}^{+2}\text{-Mn}^{+2}$ co-doped ZnS Q-dots.

Results and Discussion :

Fig. 1 shows the absorption spectra of doped and co-doped CdS nanoparticles. On doping, absorption spectra shoulder is red shift from 278 nm to 285(283) nm for Cu (Mn:Cu), respectively. Furthermore, for calculating the direct band gap value $(\alpha h\nu)^2$ as a function of $h\nu$ is plotted and it is shown in Fig. 1 (right graph). From the value of band gap shift and using Brus model [6] the size of nanoparticles have been calculated and those are shown in Fig. 2 (right graph). The band gap of the semiconductor becomes lower with increasing particle size (Fig. 2), and is indicated by an absorption shift to higher wavelengths. Photoluminescence spectra of un/co-doped ZnS nanoparticles are shown in Fig.3.

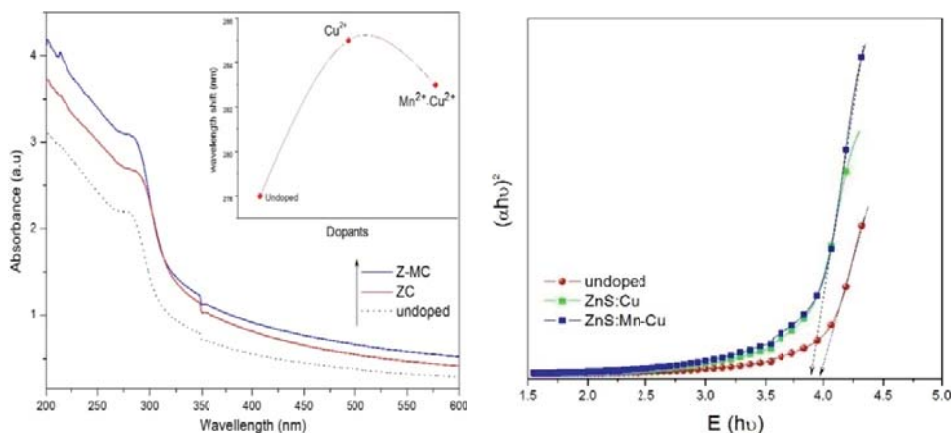


Fig. 1. (Left): UV-visible spectra of $\text{Cd}_{1-x-y}\text{Ni}_x\text{Zn}_y\text{S}$ Q-dots; (right): Profiles of $(\alpha h\nu)^2$ versus $h\nu$.

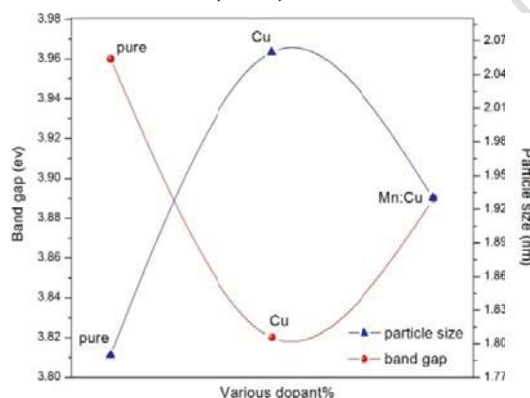


Fig. 2. Band gap and particle size versus various dopant percentage.

A broad band located at 424 nm was observed which the blue emission band can be attributed to the radiative transition of through the defect state. Defect states can be attributed to the presence of anion vacancies [7]. The luminescence emission intensity (LEI) of samples varies on increasing of impurity molar ratios. The LEI of un-doped CdS nanoparticles is about 1.3 times larger than that of ZnS:CuMn (0.5:1.5) nanoparticles.

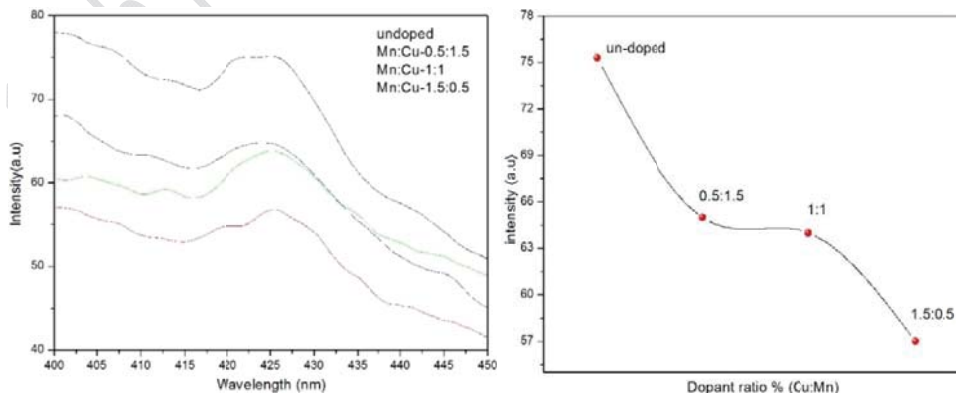


Fig. 3. (Left): PL spectra of $\text{Zn}_{1-x-y}\text{Cu}_x\text{Mn}_y\text{S}$ NPs; (right): Profiles of relative intensity on various dopant.



Conclusions :

Cu_xMn_y co-doped ZnS nanoparticles are successfully synthesized by wet-chemical method. The action of single/double doping is studied using UV-Vis spectra of ZnS nanoparticles. The 425 nm emission band can be related to the radiative transition via defect state. In contrast to un-doped crystals, co-doped material exhibits low luminescence emission intensity in PL spectrum.

References :

- [1] X. Duan, Y. Huang, *et.al.* Nature, 421(2003) 241.
- [2] Y. Kayanuma, Phys. Rev. B 38(1988) 9797.
- [3] P. Nandakumar, C. Vijatan, Y. V. Murati, Opt. Commun. Am, 185(2000) 457.
- [4] A. A. Khosravi, M. Kundu, *et.al.*, Appl. Phys. Lett, 67 1995 (18).
- [5] S. M. Taheri, M. H. Yousefi, A.A. Khosravi, Braz. J. Phys, 40 (2010) 301.
- [6] L. E. BRUS, J. Chem. Phys. 79 (1983) 5566.
- [7] C. Unni, D. Philip, S.L. Smitha, Spectrochimica Acta Part A, 72 (2009) 827.



Spectrophotometry studies on the interaction of new complex, tribromo phenanthridine aurum (III), with calf thymus DNA

Sasan Moradi ^a, Davood Ajloo ^{a,b}, Taghi Lashkarbolouki ^b, Robabeh Alizadeh ^a, Mina Evini^c

^a School of Chemistry, Damghan University, Damghan, Iran.

^b Institute of Biological Science, Damghan University, Damghan, Iran

^c Institute of Biochemistry and Biophysics, University of Tehran, Tehran, Iran

Email: sasan9xp@yahoo.com, ajloo@du.ac.ir

Keywords: Calf-thymus DNA, (phend) Br₃-Au (III), Interaction, Spectroscopy

Introduction:

Nucleic acids play an important role in biological systems and carry out a broad range of biological functions. Increasing interest is being shown in DNA because of their application in various type of therapy [1]. The biological function of DNA is often dependent on interactions with different moieties such as metal ions [2, 3]. DNA structure can undergo conformational changes due to ligand binding. Metal ions are important cofactors in DNA structures and function, facilitating the double helical structure stabilization and catalysis [4]. Also the extent of hydration of cations bound to DNA is a key parameter in the energies of the binding process as well as a relevant issue in the catalytic roles and structural effects of bound ions. An understanding of the factors involved in metal ion–DNA interaction is thus of considerable importance.

Methods:

Absorption titration was carried out in a quartz cell by adding increased amounts of CT-DNA to a solution of Au(III) of a fixed concentration, and recorded the UV-Vis spectrum after each addition. The viscosity experiments conducted at 298.15 K on ostwald viscometer. An appropriated amount of (Phend)Br₃-Au(III) was added at certain $r_1 = ([\text{complex}]/[\text{DNA}])$ and flow time was measured. At emission measurement the excitation wavelength was fixed and the emission range was adjusted before measurements. All measurements were made at 298.15 K in a thermostated cuvette holder with entrance and exit slit widths of 5 nm.



Emission titration experiments were performed at a fixed concentration of the metal complex (46 μ M) to which increasing amounts of CT-DNA. The emission enhancement factors were measured by comparing the intensities at 376 nm in the absence and presence of CT-DNA. DNA melting experiment of CT-DNA and DNA-Au(III) complex were performed by monitoring absorbance intensities at different temperature.

Result and discussion:

In absorption spectral studies the spectra indicate that there are some interactions between the complex and DNA. And exhibit hypochromism at 250 nm. Also the intrinsic binding constant K_b obtained is approximately 1.75×10^8 . Emission Studies showed that upon addition of CT-DNA, the emission intensity of the complex decreases relative to the intensity of complex alone. The interaction of (Phend)Br₃-Au(III) with DNA cause increase in T_m of (Phend)Br₃-Au(III), the result revealed that binding mode of (Phend)Br₃-Au(III) is intercalation. When a metal complex intercalate between the base pairs of DNA, length of DNA increases which lead to the increase in viscosity. This experiment showed that the viscosity of the DNA-bound complex increase with the increase in the concentration of the complex.

Conclusion:

In this study we have attempted to unravel the DNA interaction with the tribromo phenanthridine Au(III) complex. The binding behavior of this complex with DNA was characterized by absorption titration, DNA melting technique, fluorescence and viscosity measurements. The experimental results indicate that the complex binds to DNA by an intercalative mode.

References:

- [1] L. Stryer, Biochemistry, W.H. Freeman and Company, San Francisco, CA; 1994.
- [2] L.H. Hurley, Nat; Rev. Cancer; 2, 188–194, 2002.
- [3] H. Mansouri-Torshizi, M. Islami-Moghaddam, A. Divsalar, A.A. Saboury; Bioorg Med. Chem; 16, 9616–9620, 2008.
- [4] G.L. Eichhorn; Advances in Inorganic Biochemistry; 3, 2, 1981.



Vibrational Assignment and Density Functional Theory Calculations of N-salicylideneaniline

N. Dastani, Z. Moosavi-Tekyeh^{a*}, Z. Kalantar^a

^aChemistry Department, Shahrood University of Technology, Semnan, Iran

Email: ztmoosavi@gmail.com

Key words: 5-Nitrosalicylaldehyde, Intramolecular hydrogen bond, Infrared spectra, DFT

Introduction:

Much attention has been directed, from both experimental and theoretical viewpoints, toward intramolecular molecular hydrogen bonded molecules (IMHB). ESIPT is a very simple chemical process readily accessible for both accurate measurement and quantitative theoretical analysis. The study of the strength of IMHB facilitates understanding chemical and biochemical processes at the molecular level. The experimental IR and ¹HNMR spectra and theoretical calculation, especially DFT methods, have provided a cost effective means to obtain accurate vibrational and chemical shift data of this type of systems containing a strong IMHB. In this research, we used these tools for determining the strength of intramolecular hydrogen bonding of N-salicylideneaniline (SAn) and comparing it with that in ortho-2-iminomethyl-phenol (2IMP) and 2-methyl-iminomethyl-phenol(2MIMP). These compounds are called as Schiff bases and have a wide variety of applications in biological and analytical chemistry.

Materials and methods:

SAn were prepared by refluxing equimolar quantity of salicylaldehyde and aniline in ethanol medium for about three hours. Then mixture was filtered and recrystallised from ethanol to obtain solid Schiff base. The ¹HNMR spectrum was recorded with a Bruker DRX-500 FTNMR spectrometer at 500 MHz frequency using solution in CDCl₃ at 25°C. IR data for the studied molecule in the CCl₄ solution were recorded on a Fourier Transform Bomem MB-154 spectrometer, at room temperature. Geometry of SAn, is fully optimized with hybrid density functional B3LYP [1,2] using 6-31G, and 6-311++G** basis sets. Frequencies and

¹HNMR calculations with the GIAO approach were performed at B3LYP/6-311++G** basis sets. All calculations were performed using Gaussian 03W package program version B05.

Result and discussion:

The structures of SAn is shown in Fig. 1. The selected parameters along with the reported experimental parameters of SAn and 2IMP and 2MIMP are compared in Table 1. The full optimization of SAn shows it has a non-planar structure. As it is obvious from data, the O...N distance and O-H bond length in comparison with that values for 2IMP and 2MIMP. The calculated O...N and O-H distances in SAn are 2.636 and 0.993 Å, respectively, longer and shorter than those in 2IMP and 2MIMP with all calculation. The NMR proton chemical shifts of SAn, 2IMP and 2MIMP are 12.86, 12.99 and 12.79 ppm at B3LYP/6-311++G**, respectively. the OH band in SAn, 2IMP and 2MIMP disappears at about 3220, 3200 and 3160 cm⁻¹, respectively.

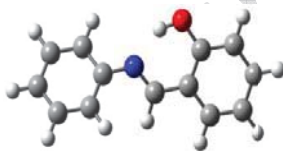


Fig.1

Table 1. The selected distances, the stretching modes and chemical shift of SAn and 2IMP calculated at the B3LYP.

parameters	SAn			2IMP		2MIMP	
	6-31G**	6-311++G**	Exp.	6-31G**	6-311++G**	6-31G**	6-311++G**
R(O-H)(Å)	0.998	0.993	-	0.999	0.994	1.00154	0.99591
R(O...N)	2.622	2.636	-	2.601	2.618	2.60803	2.62431
R(H...N)	1.721	1.746	-	1.700	1.729	1.70015	1.72768
νOH (cm ⁻¹)	3169	3220	2910	-	3200	3101.57	3160.44
νOD	2419	2466	2150	2294	2332	-	-
δ (ppm)	13.27	12.86	13.26	13.30	12.99	13.38	12.79

Conclusion:

In this study has tried to analyze the vibrational spectra of SAn between calculated frequencies with the experimental results. From the OH stretching mode and proton chemical shift and νOH a stronger intramolecular hydrogen bond in 2MIMP than that in 2IMP and



SAn was concluded.

References:

- [1] A.D. Becke, *J. Chem. Phys.* 98 (1993) 5648.
- [2] C. Lee, W. Yang, R.G. Parr, *Phys. Rev. B* 37 (1988) 785.

15th Physical Chemistry Conference

Simulation of photoelectron spectrum of $\text{CH}_3\text{CH}_2\text{OO}^\cdot$

^aM. Dehestani*, ^bF. Farsinia

^aDepartment of Chemistry, Shahid Bahonar University of Kerman, Kerman, Iran.

^bDepartment of Chemistry, Payame Noor University of Kerman, Kerman, Iran.

E-mail: dehestani2002@yahoo.com

Keywords: Photoelectron spectrum, Multidimensional Franck-Condon integral, Methyl peroxy radical,

Introduction:

A theoretical method described by Islampour and *et.al.* [J. Mol. Spectrosc. 194, 179 (1999)] is used to calculate multidimensional Franck-Condon factors that arise in simulation of photoelectron spectra of peroxy anions $\text{CH}_3\text{CH}_2\text{OO}^\cdot$. The Franck-Condon coefficients have been evaluated for the cases in which electronic transitions take place between displaced-distorted-rotated harmonic potential energy surfaces. Different methods [1-2] have been proposed to calculate multidimensional Franck-Condon integrals. We choose a new closed form expression for the Franck-Condon integrals for overlap between arbitrary multidimensional harmonic oscillators by employing the generating functions method [3]. The calculations lead to deduction of the some general rules whereby an arbitrary multidimensional Franck-Condon integral can be expressed as sums of products of the Hermite polynomials as following:

$$\begin{aligned} \langle \nu_1'' \nu_2'' 0_3'' \dots 0_N'' | \nu_1' \nu_2' 0_3' \dots 0_N' \rangle &= \langle 0_1'' \dots 0_N'' | 0_1' \dots 0_N' \rangle \times \prod_{j=1}^2 (-1)^{\nu_j''} (\nu_j''! \nu_j'!)^{1/2} \sum_{k_1=0}^{\nu_1''} \dots \sum_{k_6=0}^{\nu_6''} \frac{(-\beta_{12})^{k_1}}{k_1!} \frac{(-2R_{11})^{k_2}}{k_2!} \\ &\times \frac{(-2R_{12})^{k_3}}{k_3!} \frac{(-2R_{21})^{k_4}}{k_4!} \frac{(-2R_{22})^{k_5}}{k_5!} \frac{(-\alpha_{12})^{k_6}}{k_6!} \times \left\{ \frac{(\beta_{11}/2)^{(\nu_1''-k_1-k_2-k_3)/2}}{(\nu_1''-k_1-k_2-k_3)!} H_{\nu_1''-k_1-k_2-k_3} [\beta_{11}^{-1/2} (R\delta)_1] \right\} \\ &\times \left\{ \frac{(\beta_{22}/2)^{(\nu_2''-k_1-k_4-k_5)/2}}{(\nu_2''-k_1-k_4-k_5)!} H_{\nu_2''-k_1-k_4-k_5} [\beta_{22}^{-1/2} (R\delta)_2] \right\} \\ &\times \left\{ \frac{(\alpha_{11}/2)^{(\nu_1'-k_2-k_4-k_6)/2}}{(\nu_1'-k_2-k_4-k_6)!} H_{\nu_1'-k_2-k_4-k_6} \{\alpha_{11}^{-1/2} [(E-P)\delta]_1\} \right\} \\ &\times \left\{ \frac{(\alpha_{22}/2)^{(\nu_2'-k_3-k_5-k_6)/2}}{(\nu_2'-k_3-k_5-k_6)!} H_{\nu_2'-k_3-k_5-k_6} \{\alpha_{22}^{-1/2} [(E-P)\delta]_2\} \right\} \end{aligned} \quad (1)$$

Where ν'' and ν' refer to vibrational quantum numbers the two electronic states, $\delta = \Gamma^{1/2} \mathbf{D}$ is the N -dimensional vector of reduced displacements $\{\gamma^{1/2} D_j\}$, and Γ is an $N \times N$ diagonal

matrix of the reduced frequency ω_j/\hbar , \mathbf{E} is an $N \times N$ unit matrix, and $N \times N$ symmetric matrices \mathbf{P} and \mathbf{Q} and the $N \times N$ matrix \mathbf{R} are defined by

$$\mathbf{Q} = \mathbf{\Gamma}^{n1/2} \mathbf{G}^{-1} \mathbf{\Gamma}^{p1/2} \mathbf{J} \mathbf{G}^{-1} \mathbf{J}^\dagger \mathbf{\Gamma}^{r1/2}, \quad \mathbf{R} = \mathbf{\Gamma}^{n1/2} \mathbf{G}^{-1} \mathbf{J}^\dagger \mathbf{\Gamma}^{r1/2}, \quad \mathbf{G} = \mathbf{\Gamma}^n + \mathbf{J}^\dagger \mathbf{\Gamma}^r \mathbf{J},$$

$$\alpha_{ij} = (\mathbf{E} - 2\mathbf{P})_{ij}, \quad \beta_{ij} = (\mathbf{E} - 2\mathbf{Q})_{ij}$$

and $\langle 0''_1 \dots 0''_N | 0'_1 \dots 0'_N \rangle = (\det \mathbf{\Gamma}^{n1/2} \mathbf{\Gamma}^{r1/2} \mathbf{Q})^{1/2} 2^{N/2} \exp \left[-\frac{1}{2} \boldsymbol{\delta}^\dagger (\mathbf{E} - \mathbf{P}) \boldsymbol{\delta} \right]$

Computational Method:

Complete geometry optimization and vibrational frequency computations were carried out at the QCISD/6-311+G (d, p) level, for the X^2A'' state of $\text{CH}_3\text{CH}_2\text{OO}$ and for the X^2A' state of the negative ion $\text{CH}_3\text{CH}_2\text{OO}^-$. To stimulate the photoelectron spectra, one needs to evaluate vibrational overlap integrals. Since bond lengths, angles, and force constants for the neutral and anion are not the same, normal coordinates of neutral (\mathbf{Q}') can be expressed as a linear combination of the normal modes of the anion (\mathbf{Q}'') as $\mathbf{Q}' = \mathbf{J}\mathbf{Q}'' + \mathbf{D}$ where \mathbf{J} and \mathbf{D} are the Duschinsky rotation matrix, and the N-dimensional column vector of the changes in the nuclear equilibrium positions from the anion to the neutral electronic state, respectively. The \mathbf{J} and \mathbf{D} matrices should be determined before one can evaluate Franck-Condon integrals.

Result and Discussion:

All of the calculations for simulations of the spectra were performed using Mathematica programs. Figure 1 compares the calculated photoelectron spectrum of $\text{CH}_3\text{CH}_2\text{OO}^-$ with experimental spectrum of Blankspy *et al.* [4].

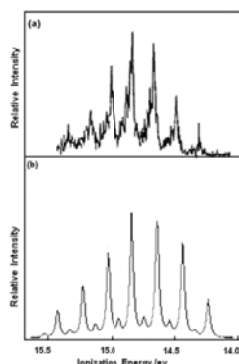


Figure 1: (a) Experimental photoelectron spectrum of $\text{CH}_3\text{CH}_2\text{OO}^-$ (Ref. [4]), (b) Simulated photoelectron spectrum.



Conclusion:

The difference in the O-O bond length of anion and neutral explains the presence of progression in the O-O stretch, and the difference in the bond length hints at the possibility of C-O-O bending vibration. The comparison of the experimental spectrum [4] with simulated spectrum in the present work shows that the spectrum calculated is in good agreement with experiment.

References:

- [1] V. Doktorov, I. A. Malkin, and V. I. Manko, *J. Mol. Spectrosc.* **56** (1975) 1.
- [2] H. Kupka, P.H. Cribb, *J. Chem. Phys.* **85** (1986) 1303.
- [3] R. Islampour, M. Dehestani, S. H. Lin, *J. Mol. Spectrosc.* **194** (1999) 179.
- [4] S. J. Blanksby, T. M. Ramond, G. E. Davico, M. R. Nimlos, S. Kato, V. M. Bierbaum, W. C. Lineberger, G. B. Ellison, and M. Okumura, *J. Am. Chem. Soc.* **123** (2001) 9585.



Red-shifting and Blue-shifting Halogen Bonds; a QTAIM Study

Y. Jalalian and K. Eskandari,

School of Chemistry, Damghan University, Damghan, 36716-41167, Iran.

eskandari@du.ac.ir

Keywords: Halogen Bond, QTAIM, Atomic Multipole Moment

Introduction:

Generally, the formation of halogen bonds is always connected with the red-shifting and blue-shifting [1]. In red-shifting the $A-X$ bond in the complex $A-X \cdots N$ is longer and has a lower vibrational frequency than in isolated $A-X$. In blue-shifting the $A-X$ bond length decreases and its vibrational frequency increases. In recent years, numerous studies devoted to finding the origin of $A-X$ bond length changes in halogen bonded complexes. Wang and Hobza showed that although red-shifting is caused by charge transfer, in blue-shifting halogen bonds the charge transfer is only of minor importance and it is the electrostatic interactions that cause the $A-X$ bond contraction [2]. In the current work, we used atomic monopole and dipole moments, derived from quantum theory of atoms in molecules (QTAIM) [3], to find differences between red-shifting and blue-shifting halogen bonds.

Materials and methods:

The geometries and electronic wavefunctions of the isolated molecules and their complexes have been fully optimized at the MP2/aug-cc-PVDZ level of theory using *Gaussian 09* program. Bader's QTAIM was used to evaluate atomic electrostatic moments. Integration over atomic basins was carried out using standard mode of AIMAll program.

Results and discussion:

Red-shifting and blue-shifting halogen bonded complexes formed between some Lewis bases (NH_3 , Br^- , Cl^- and F^-) and bromine in H_3C-Br and F_3C-Br have been considered. The values of $C-Br$ bond length changes (Δr) have been listed in Table 1. The positive and negative values of Δr correspond to red-shifting and blue-shifting halogen bonds,

respectively. In addition, the values of atomic charges and dipole moments of carbon and bromine (in $C - Br$ bond) before and after complexation have been also collected in Table 1. As indicated, in the complexes of $H_3C - Br$ the absolute values of charges of bromine and carbon and also dipoles of bromine decrease in compare to isolated $H_3C - Br$ molecule. In the case of $F_3C - Br$ complexes, the absolute values of charges of bromine and dipoles of carbon increase while, charges of carbon and dipoles of bromine decrease.

Table 1. Bond length changes (in Angstrom), atomic charges and atomic dipoles (in a.u.) of Br and C in the studied complexes.

	Δr	$q(Br)$	$q(C)$	$\mu(Br)$	$\mu(C)$
CH_3Br	--	-0.138	0.052	-0.376	-0.002
$CH_3Br - NH_3$	0.0008	-0.103	0.044	-0.269	-0.036
$CH_3Br - Br^-$	0.0066	-0.046	0.037	-0.186	-0.104
$CH_3Br - Cl^-$	0.0094	-0.032	0.035	-0.147	-0.115
$CH_3Br - F^-$	0.0324	0.037	0.012	0.061	-0.194
CF_3Br		0.057	1.768	-0.397	-0.816
$CF_3Br - NH_3$	-0.0026	0.106	1.706	-0.296	-0.876
$CF_3Br - Br^-$	-0.0014	0.164	1.593	-0.227	-0.985
$CF_3Br - Cl^-$	-0.0006	0.183	1.581	-0.180	-1.004
$CF_3Br - F^-$	0.0215	0.256	1.498	0.068	-1.093

Conclusions

Clearly, the bond length of $C - Br$ in isolated molecules and related halogen bonded complexes is determined by a competition between attractive and repulsive forces. In electrostatics point of view, these forces are monopole-monopole and dipole-dipole interactions. In $H_3C - Br$ and its complexes (with the exception of $H_3C - Br \cdots F^-$) there are attractive monopole-monopole and attractive dipole-dipole interactions between carbon and bromine atoms, however, these forces in the complexes are smaller than those of isolated molecule. Therefore, an increase in the bond length of $C - Br$ is expected in these complexes. On the other hand, in $F_3C - Br$ and its complexes there are repulsive monopole-monopole but attractive dipole-dipole interactions. Both of them decrease upon complex formation, however, the dipole-dipole interaction is of minor importance and reduction of repulsive monopole-monopole interaction is mainly responsible for $C - Br$ bond contraction.



References

- [1] W. Z. Wang, N. B. Wong, W. X. Zheng, A. M. Tian, *J. Phys. Chem. A* 108 (2004) 1799.
- [2] W. Wang, P. Hobza, *J. Phys. Chem. A*, 112 (2008) 4114.
- [3] R.F.W. Bader, *Atoms in Molecules. A Quantum Theory*, Oxford University Press, Oxford, 1990.

15th Physical Chemistry Conference



Schrödinger Equation under a q-Deformed Morse plus Coulomb Interaction

S. Zarrinkamar^{1*}, A. A. Rajabi¹ and H. Hassanabadi¹

¹Physics Department, Shahrood University of Technology, P.O.Box 3619995161-316 Shahrood, Iran

Email: zarrinkamar.s@gmail.com

Abstract:

Due to successful phenomenological outcomes of Morse and Coulomb interactions in physics and chemistry, we solve the nonrelativistic Schrödinger equation under these potentials via the quasi-exact ansatz technique. For the sake of generality, we consider the problem in the D-dimensional space.

Keywords: Schrödinger equation, q-deformed Morse potential, Coulomb potential, Ansatz solution.

Introduction:

The most essential ingredient in theoretical quantum chemistry is probably solving the Schrödinger equation under a desired interaction. This, in many cases, is not an easy task and we often have to use numerical techniques which are often time-consuming and rather vague in comparison with their analytical counterparts. On the other hand, exact analytical techniques of quantum mechanics such as factorization technique, supersymmetry quantum mechanics (SUSQM) and Nikiforov-Uvarov (NU) do not work in all cases [1-4]. One economical way in such cases is the quasi-analytical ansatz technique. Here, we intend to solve the Schrödinger equation under a Morse interaction modified with a Coulomb term which have successfully accounted for many observed phenomena in chemistry [5].

The Schrodinger equation in D-dimensions :

The radial Schrödinger equation as [1]

$$\left[\frac{d^2}{dr^2} - \frac{2\mu}{\hbar^2} V(r) - \frac{(D+2l-1)(D+2l-3)}{4r^2} + \frac{2\mu E_{n,l}}{\hbar^2} \right] R_{n,l}(r) = 0, \quad (1)$$

Where $\hbar, \mu, V(r), D, l, E_{n,l}$ and $R_{n,l}(r)$ respectively stand for the Planck constant, reduced mass, potential, dimension of space, orbital quantum number, energy and the wavefunction. Here, to provide a more general result, we consider the q-deformed Morse potential [5]

$$V(r) = D_e \exp(-2a(r-r_e)) - 2qD_e \exp(-a(r-r_e)) + q^2 D_e, \quad (2)$$

where D_e, a, q and r_e respectively represent the depth of the well, range of the potential, deformation parameter and the equilibrium intermolecular distance. To be able to solve the problem we expand it up to fourth orders to have a polynomial which contains all terms from quartic to inverse square one.

The Ansatz Solution:

We propose an ansatz solution of the form

$$R_n(x) = f_n(x) \exp(g_n(x)) \quad (3-1)$$

$$f_n(x) = \begin{cases} 1, & \text{if } n=0 \\ \prod_{i=1}^n (x - \alpha_i^n), & \text{if } n \geq 1 \end{cases} \quad (3-2)$$

Let us consider the nodless state. After some algebra, The solution to our Riccati equation is

$$g(x) = \alpha x^3 + \beta x^2 + \gamma x + \delta \ln x. \quad (4)$$

Substituting the latter in Eq. (2) and equating the corresponding powers on both sides, we find

$$\begin{aligned} \left(\frac{2\mu a^2}{\hbar^2} (D_e e^{2ar_e} - 2qD_e e^{ar_e} + q^2 D_e) + \frac{2\mu E_{n,l} a^2}{\hbar^2} \right) &= \gamma^2 + 2\beta, \frac{2\mu a^2}{\hbar^2} (2D_e e^{2ar_e} - qD_e e^{ar_e}) = 6\alpha\delta + 4\beta\gamma + 4\beta\delta + 6\alpha, \\ \frac{2\mu a^2}{\hbar^2} (2D_e e^{2ar_e} - qD_e e^{ar_e}) &= 4\beta^2 + 6\alpha\gamma, \frac{2\mu a^2}{\hbar^2} \left(\frac{4D_e e^{2ar_e}}{3} - \frac{qD_e e^{ar_e}}{3} \right) = 12\alpha\beta, \\ \frac{2\mu a^2}{\hbar^2} \left(\frac{2D_e e^{2ar_e}}{3} - \frac{qD_e e^{ar_e}}{12} \right) &= 9\alpha^2, \frac{2\mu a^2 C}{\hbar^2} = 2\gamma\delta, \frac{\mu a^4 (D+2l-1)(D+2l-3)}{2\hbar^2} = \delta^2 - \delta, \end{aligned} \quad (5)$$

which simply determine the solution. The interested reader may find instructive points on ansatz technique in [6-9].



Conclusion:

Although we only performed the first step, the higher nodes can be systematically obtained via choosing $f_n(x)$ as $(z - \alpha_1^1)$, $(x - \alpha_1^2)(x - \alpha_2^2)$ for the first node, second node, etc. Our results can be used in spectroscopy of atoms and after proper fits done.

References:

- [1] Sh. H. dong; Wave Equations in High Dimensions, ISBN 978-94-007-1916-3, Springer, Netherlands (2011).
- [2] S. Zarrinkamar, A. A. Rajabi and H. Hassanabadi, Ann. Phys. 325, 2522 (2010).
- [3] H. Hassanabadi, B. H. Yazaloo, S. Zarrinkamar and M. Solaimani, Int. J. Quant. Chem. (2012); DOI: 10.1002/qua.24064.
- [4] W. Ch. Qiang and Sh. H. Dong, Int. J. Quan. Chem. 110 (2010) 2342.
- [5] C.S. Jia et al., Phys. Lett. A 311 (2003) 115.
- [6] S. Hassanabadi, A. A. Rajabi and S. Zarrinkamar, Mod. Phys. Lett. A27 (2012) 1250057.
- [7] H. Hassanabadi, H. Rahimov and S. Zarrinkamar, Ann. Phys. (Berlin) 523 (2011) 566.
- [8] D. Agboola and Y. Zhang, J. Math. Phys. 53 (2012) 042101.
- [9] H. Hassanabadi, B. H. Yazarloo, S. Zarrinkamar and A. A. Rajabi, Phys. Rev. C 84 (2011) 064003.



The Exponential Potential within a Semi-relativistic Two-Body formulation via Nikiforov-Uvarov Technique

S. Zarrinkamar^{*1}, A. A. Rajabi¹ and H. Hassanabadi¹

¹Physics Department, Shahrood University of Technology, Shahrood, Iran

zarrinkamar.s@gmail.com

Abstract

We solve the two-body spinless Salpeter equation (in fact the Schrödinger equation with a relativistic correction) under an exponential interaction via a Pekeris-type approximation and the Nikiforov-Uvarov technique.

KeyWords: Two-body system, Semirelativistic equation, Exponential interaction, Nikiforov-Uvarov technique.

Introduction:

We frequently face two-body systems from diatomic molecules in chemistry and excitons in atomic physics to mesons in particle physics. Here we solve the two-body spinless Salpeter equation (SSE from short) under an exponential interaction $V(r) = v_0 e^{-a(r-r_0)}$ which is a successful phenomenological interaction in various fields. In simple words, SSE is a generalization of the nonrelativistic Schrödinger equation to the relativistic regime. Within this equation, the time dependence as well as the spin degrees of freedom are neglected. This equation is nonlocal and we ought to use approximate schemes in dealing with it [1,2,3,4,5,6,7].

The Two-Body-Hamiltonian:

The SSE for two particles for a spherically symmetric potential is [1,2,3]

$$\left[\sum_{i=1,2} \sqrt{\nabla^2 + m_i^2} + V(r) - M \right] \chi(r) = 0, \quad \mu = \frac{m_1 m_2}{m_1 + m_2}, \quad \eta = \mu \left(\frac{m_1 m_2}{m_1 m_2 - 3\mu^2} \right)^{1/3} \quad (1)$$



After some solve cumbersome algebra, Eq. (1) with an acceptable approximation appears as [2,3]

$$\left[\frac{-\hbar^2}{2\mu} \frac{d^2}{dr^2} + \frac{l(l+1)\hbar^2}{2\mu r^2} + W_{nl}(r) - \frac{W_{nl}^2(r)}{2\tilde{m}} \right] \psi_{nl}(r) = 0, \quad \text{with}$$

$$W_{nl}(r) = V(r) - E_{nl}(r), \quad \tilde{m} = \eta^3 / \mu^2 = (m_1 m_2 \mu) / (m_1 m_2 - 3\mu^2). \quad (2)$$

After inserting the interaction, we introduce the following Pekeris-type approximation [4],

$$\frac{1}{r^2} \approx (C_0 + C_1 e^{-\alpha x} + C_2 e^{-2\alpha x}), \quad \text{with}$$

$$x = \frac{r-r_0}{r_0}, \quad \alpha = ar_0, \quad C_0 = \frac{1}{r_0^2} \left(1 - \frac{3}{\alpha} + \frac{3}{\alpha^2} \right), \quad C_1 = \frac{1}{1r_0^2} \left(\frac{4}{\alpha} - \frac{6}{\alpha^2} \right), \quad C_2 = \frac{1}{r_0^2} \left(\frac{-1}{\alpha} + \frac{3}{\alpha^2} \right). \quad (3)$$

The Parametric Nikiforov-Uvarov (NU) Technique:

The NU technique is based on the idea of transforming an ordinary second-order differential equation into the hypergeometric form. In its more user friendly way, solves

$$\left\{ \frac{d^2}{ds^2} + \frac{\alpha_1 - \alpha_2 s}{s(1 - \alpha_3 s)} \frac{d}{ds} + \frac{1}{[s(1 - \alpha_3 s)]^2} [-\xi_1 s^2 + \xi_2 s - \xi_3] \right\} \psi_n(s) = 0. \quad (4)$$

According to the parametric NU method, the eigen functions are [13]

$$\psi_n(s) = s^{\alpha_{12}} (1 - \alpha_3 s)^{-\frac{\alpha_{13}}{\alpha_3}} P_n^{(\alpha_{10}-1, \frac{\alpha_{11}}{\alpha_3} - \alpha_{10}-1)}(1 - 2\alpha_3 s), \quad (5)$$

where P is the Jacobi polynomial and the eigenenergies satisfy

$$\alpha_2 n - (2n+1)\alpha_5 + (2n+1)(\sqrt{\alpha_9} + \alpha_3 \sqrt{\alpha_8}) + n(n-1)\alpha_3 + \alpha_7 + 2\alpha_3 \alpha_8 + 2\sqrt{\alpha_8 \alpha_9} = 0, \quad (6)$$

where

$$\alpha_4 = \frac{1}{2}(1 - \alpha_1), \quad \alpha_5 = \frac{1}{2}(\alpha_2 - 2\alpha_3), \quad \alpha_6 = \alpha_5^2 + \xi_1, \quad \alpha_7 = 2\alpha_4 \alpha_5 - \xi_2, \quad \alpha_8 = \alpha_4^2 + \xi_3, \quad \alpha_9 = \alpha_3 \alpha_7 + \alpha_5^2 \alpha_8 + \alpha_6,$$

$$\alpha_{10} = \alpha_1 + 2\alpha_4 + 2\sqrt{\alpha_8}, \quad \alpha_{11} = \alpha_2 - 2\alpha_5 + 2(\sqrt{\alpha_9} + \alpha_3 \sqrt{\alpha_8}), \quad \alpha_{12} = \alpha_4 + \sqrt{\alpha_8}, \quad \alpha_{13} = \alpha_5 - (\sqrt{\alpha_9} + \alpha_3 \sqrt{\alpha_8}). \quad (7)$$

If $\alpha_3 = 0$, the wave function includes Laguerre function and $\psi(s) = s^{\alpha_{12}} e^{\alpha_{13}s} L_n^{\alpha_{10}-1}(\alpha_{11}s)$. After

substituting the exponential term and the approximation (3) in Eq. (1), changing the independent variable as $s = e^{-\alpha x}$ and making a comparison with Eq. (3), from (5) and (6) we have



$$\psi(s) = s^{-\frac{1}{2} + \sqrt{\frac{1}{a^2} \left(C_1 l(l+1) + \frac{2\mu v_0}{\hbar^2} + \frac{2v_0 E_{nl} \mu}{\tilde{m} \hbar^2} \right)}} e^{-s \sqrt{\frac{\mu v_0^2}{\tilde{m} \hbar^2} + C_2 l(l+1)}} L_n^{\alpha_{10}-1} \left(2 \sqrt{\frac{1}{a^2} \left(-C_0 l(l+1) + \frac{2\mu E_{nl}}{\hbar^2} + \frac{\mu E_{nl}^2}{\tilde{m} \hbar^2} \right)} s \right). \quad (8)$$

and the energy satisfies

$$(2n+1) \sqrt{\frac{1}{a^2} \left(-\frac{\mu v_0^2}{\tilde{m} \hbar^2} + C_2 l(l+1) \right)} - \frac{1}{a^2} \left(C_1 l(l+1) + \frac{2\mu v_0}{\hbar^2} + \frac{2v_0 E_{nl} \mu}{\tilde{m} \hbar^2} \right) + \frac{2}{a^2} \sqrt{\left(\frac{\mu v_0^2}{\tilde{m} \hbar^2} - C_2 l(l+1) \right) \left(-C_0 l(l+1) + \frac{2\mu E_{nl}}{\hbar^2} + \frac{\mu E_{nl}^2}{\tilde{m} \hbar^2} \right)} = 0, \quad (9)$$

Conclusion:

We see that the Pekeris approximation and the NU technique can provide us with invaluable source of knowledge in quantum chemistry and physics. In particular, we could give arbitrary-state solutions of the two-body Hamiltonian under an exponential interaction. The results can be directly applied to a two-body system after requisite fits done.

References:

- [1] W. Lucha and F. F. Schöberl, J. Phys. A 40 (2007) 6183-6192.
- [2] R. Hall and W. Lucha, J. Phys. A: Math. Theor. 41 (2008) 355202.
- [3] S. M. Ikhdair and R. Sever, Int. J. Mod. Phys. E 17 (2008) 1107.
- [4] C. Berkdemir, Nuclear Physics A 770 (2006) 32-39.
- [5] C. Tezcan and R. Sever, Int. J. Theor. Phys. 48 (2009) 337.
- [6] S. Hassanabadi, A. A. Rajabi and S. Zarrinkamar, Mod. Phys. Lett. A 27 (2012) 1250057.
- [7] S. Zarrinkamar, A. A. Rajabi, H. Hassanabadi and H. Rahimov, Phys. Scr. 84 (2011) 065008.



Spectral studies on the binding of cationic Zn(II) tetrapyridinoporphyrazine to calf thymus DNA and oligonucleotide

H. Dezhmpanah^{a*}, B. Ghalami^a and S. Feyzolahjani^a

^a Department of Chemistry, Faculty of Science, University of Guilan P.O. Box 1914, Rasht 0098, Iran. (*e-mail: h.dpanah@guilan.ac.ir)

Introduction

Cationic tetraazaporphirins, or porphyrazines, represent an alternative and highly under developed class of cationic porphyrinic compounds. Microcycles based on the porphyrazine core, including phthalocyanins, but the replacement of the meso methylene carbons of porphyrins with nitrogen in porphyrazines creates profound differences [2]. For example, porphyrazines absorb more strongly at longer wavelengths a critical feature in biological and medical applications [1].

The present work was undertaken to determine the equilibrium binding processes of N, N', N'', N''' tetramethyltetra-3,4-pyridinoporphyrazinato zinc(II) [Zn(tmtppa)] to calf thymus DNA (ct DNA) and characterized binding target by using of synthetic nucleotide G-C, A-T. In this way binding constants, binding modes, the values of the Stern-Volmer constant (K_{SV}) and the rate constants for the quenching (k_q) were determined by using optical absorption and fluorescence spectroscopy.

Methods:

[Zn (tmtppa)] was prepared and purified according to literature methods [2]. The stock solution of porphyrazine complex (5.3×10^{-4} M) was prepared in 5 mM phosphate buffer, pH 7.2 and stored in the dark at 5–10 °C. All experiments were run in phosphate buffer of pH 7.2. Aqueous solution of [Zn(tmtppa)] (1.54×10^{-5} M) was titrated by adding appropriate volume concentrated solutions of ct-DNA and synthetic nucleotide G-C, A-T, respectively. The absorbance was measured on the double beam absorbance spectrophotometer Cary 100 scan UV-vis-NIR after stirring for 30 min at 25 °C. Emission spectra of Ethidium bromide (EB) bound to DNA in the absence and presence of the [Zn (tmtppa)] was recorded on a spectrofluorimeter Shimadzu model RF-5000. In a typical experiment, titration of a mixed

DNA and EB solution with porphyrazine in phosphate buffer was performed by stepwise addition of porphyrazine solution in the same buffer directly to the cuvette.

Results and discussion:

The results of a titration experiment involving [Zn(tmtppa)] with ct-DNA and synthetic nucleotide G-C are shown in Figs. 1A and B. The absorption spectrum of [Zn(tmtppa)] displays a Q band at 686 nm. A considerable hypochromicity without any moderate shift in the Q band of porphyrazine is caused by its interaction with the ct-DNA surface as a typical external groove binder. In other words, this complex is inhibited from intercalation and externally binds. The large hypochromicity suggests that the porphyrazine π electrons are perturbed considerably upon binding to ct-DNA. The changes in absorbance of the Q band upon addition of DNA were monitored at the maximum of the Q band. The apparent binding constant of [Zn(tmtppa)] was calculated to be $2.5 \times 10^5 \text{ M}^{-1}$.

The fluorescence quenching curve of EB bound to DNA by the porphyrazine was drowning. The quenching plot illustrates that the quenching of EB bound to DNA by the porphyrazine is in good agreement with the linear Stern–Volmer equation, which also proves that the porphyrazine bind to DNA. Uv- Vis and fluorescence measurements show that porphyrazine [Zn(tmtppa)] interacted with G-C base pairs and have high selectivity for GC-rich DNA sequences.

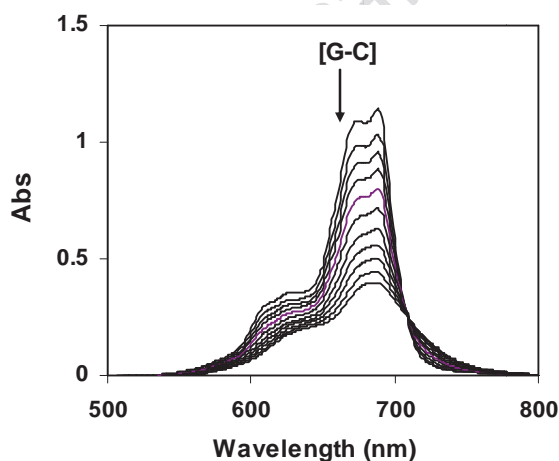


Fig2. The UV-vis spectra of [Zn(tmtppa)] 15.4 μ M in the presence of various nucleotide G-C concentrations (0 \rightarrow 9.64 μ M) at the buffer solutions .

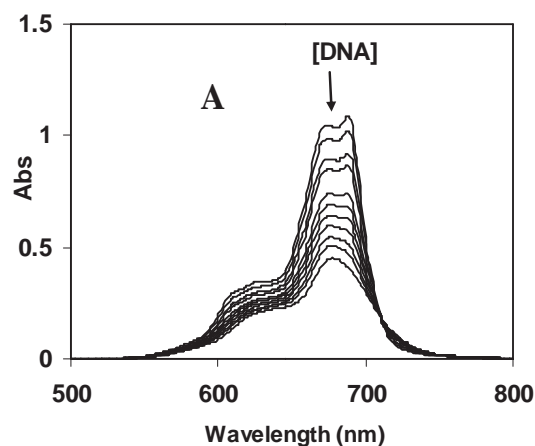


Fig1. The UV-vis spectra of [Zn(tmtppa)] 15.4 μ M in the presence of various DNA concentrations(0 \rightarrow 18.23 μ M) at the buffer solutions .



References

- [1] Paul, P. Kumar, G. S. *Journal of Hazardous Materials* **2010**, 184: 620–626.
- [2] Bordbar, A. K. Dezhampanah, H., Asadi, M., Safaei, E., Sohrabi, N. and Khodadost, Y. *J. Porphyrins Phthalocyanines* **2007**, 11: 556–565.

15th Physical Chemistry Conference



Study of multi-nucleon systems in the hyper central approach

Asadolah Tavakolinezhad^a, Zahra Ghalenovi^{a*} and Ali Akbar Rajabi^a

^a Physics Department, Shahrood University of Technology, Shahrood, Iran

*Email: z_ghalenovi@shahroodut.ac.ir

Key words: Multi-nucleon systems, Schrodinger equation, Hyper central model, Cornell potential, Variational method, Spin dependent potential.

Introduction:

The investigation of nucleus structure is of great interest at the atomic scale [1, 2]. There is renewed interest both experimentally and theoretically in the static properties of multi-nucleon systems. The coulomb-plus-linear potential $V(x) = -a/x + bx$, also known as the Cornell potential [3, 4], has received a great deal of attention both in atomic and molecular physics where it represents a radial Stark effect in hydrogen.

The purpose of this paper is to obtain the energy eigenvalues and wave function of systems containing few nucleons in the hyper central model [5, 6] by using the variational approach and introduce a way to calculate the mass, magnetic moment and charge radius of the system.

Methods:

A variational solution of the radial Schrodinger equation wave function for the considered potential, $V(x) = -a/x + bx$ is introduced, where a and b are constants. The Schrodinger equation for N-nucleon systems in the hyper central model is as [5, 6]

$$\left[\frac{d^2}{dx^2} + \frac{D-1}{x} \frac{d}{dx} - \frac{\gamma(\gamma+D-2)}{x^2} \right] \psi_\gamma(x) = -2m[E_\gamma - V(x)] \psi_\gamma(x) \quad (1)$$

Where $\psi_\gamma(x)$, E_γ , x , m , D and γ are the wave function, energy eigenvalues, hyper radius, reduced mass, dimension ($D=3N-3$ for $N>1$) and angular quantum number respectively. We investigate the ground state of the system for $\gamma=0$.

Results and discussion:

Now by solving the Schrodinger equation we can obtain the eigenvalues energy and eigenfunctions of the system.



For example the results for “three nucleons system” is as following

$$\psi_{\gamma}(x) = 2\sqrt{2}p^3x^{5/2}e^{-p^2x^2}, \quad E(p) = \langle \chi | H | \chi \rangle = 3p^2 - a \cdot \frac{3}{4} \cdot \sqrt{\frac{\pi}{2}} \cdot p + b \cdot \frac{15}{16} \cdot \sqrt{\frac{\pi}{2}} \cdot p^{-1}. \quad (3)$$

Where p is the variational parameter. Now by using the condition $dE/dp|_{p=p_0} = 0$, the value of p_0 is found. Finally a perturbative spin-dependent energy is introduced. Then the mass, magnetic moment and charge radius of multi-nucleon system are discussed.

Conclusion:

In this paper we solve the Schrodinger equation by using the variational method in the hyper central approach and obtain the ground state wave function as well as the corresponding eigenvalues of energy of N nucleons system. Finally static properties of the system are considered.

References:

- [1]P. Van. Isacker; “Dynamical symmetries in the structure of nuclei”; Rep. Prog. Phys. 62 1661; 1999.
- [2]S. Typel; “Pseudospin, supersymmetry and the shell structure of atomic nuclei”; arXiv: 0802.0929v2 [nucl-th]; 2008.
- [3]G. Plante and A. F. Antippa; “Analytic solution of the Schrödinger equation for the Coulomb-plus-linear potential. I. The wave functions”; J. Math. Phys. 46 062108; 2005.
- [4]I. M. Narodetskii and M. A. Trusov; “The heavy baryons in the nonperturbative string approach”; arXiv: hep-ph/0104019v2; 2001.
- [5]B. Patel and etal; “Masses and magnetic moments of heavy baryons in the hyper central model”; J. Phys. G: Nucl. Part. Phys. 35 065001; 2008.
- [6]H. Hassanabadi and etal; “Spectrum of baryons and spin-isospin dependence”. Mod. Phys Lett A; 23 7 527-537; 2008.



Study of two-body systems in the Yukawa potential

Zahra Ghalenovi ^{a*}, Ali Akbar Rajabi ^a and Asadollah Tavakolinezhad ^b

^a Physics Department, Shahrood University of Technology, Shahrood, Iran

^b Physics Department, Shahrood University of Technology, Shahrood, Iran

*Email: z_ghalenovi@shahroodut.ac.ir

Key words: Schrodinger equation, Yukawa potential, Energy eigenvalues, Two-body system.

Introduction:

Different versions of model have been recently proposed in order to describe the structure of two-body systems such as diatomic molecules, deuterium nucleus, mesons and et cetera [1-3]. These systems are usually described well, although the various models are quite different. The investigation of two-body systems is of great interest in understanding the dynamics of diatomic molecules. The purpose of this paper is to calculate the energy eigenvalues and wave function of systems containing two particles in the non-relativistic model and introduce a way to calculate the mass, magnetic moment and charge radius of the system. The potential is assumed to be in the form of the Yukawa term. Schrodinger equation is solved by ansatz method analytically. Many models were have used this method to consider many-body systems [4-5], but there is not any work to solve the equation with Yukawa potential by using this method.

Methods:

An analytical solution of the radial Schrodinger equation wave function for the potential $V(x)$ is introduced. The present method can easily be applied to a two-body problem. The Schrodinger equation is as

$$\left[\frac{d^2}{dx^2} + \frac{2}{x} \frac{d}{dx} - \frac{\gamma(\gamma+1)}{x^2} \right] \psi_\gamma(x) = -2m[E_\gamma - V(x)] \psi_\gamma(x) \quad (1)$$



Where $\psi_\gamma(x)$, E_γ , x and γ are the wave function, energy eigenvalues, distance between two particles, and angular quantum number respectively. Where $V(x) = \frac{e^{-\alpha x}}{\alpha x}$ and m is the reduced mass. By an expansion method we transform the Yukawa potential to a combination of Coulombic, linear confining and harmonic oscillator terms.

Results and discussion:

Finally by solving the Schrodinger equation we can obtain the eigenvalues energy and eigenfunctions of the system as following

$$\psi_\gamma = N_\gamma x^{\frac{5}{2}} \varphi_\gamma = N_\gamma x^{\frac{5}{2}} \exp\left(-\frac{m\omega}{2}x^2 - \frac{2mc}{(2\gamma+5)}x\right), \quad E_\gamma = (2\gamma+6)\frac{\omega}{2} - \frac{2mc^2}{(2\gamma+5)^2}. \quad (3)$$

Where N_γ , ω and c are the normalization constant, frequency of the oscillator and coefficient of Coulombic term respectively. Now by using the results, perturbative spin-dependent energy and then the mass, magnetic moment and charge radius of two-body system are discussed[5, 6].

Conclusion:

In this paper we solve the Schrodinger equation by using the ansatz method analytically and obtain the ground state and excited state wave function as well as the corresponding eigenvalues of energy of two-body systems. Finally static properties of the system are considered. One can use this method to study the three particle systems.

References:

- [1] Z.L. Gasyna; "Solution of the Schrödinger Equation for a Diatomic Oscillator Using Linear Algebra"; *J. Chem. Educ.*; 85 6; 2008.
- [2] A. Heidari and et al; "Numerical solution of the heteronuclear diatomic Schrodinger equation using various empirical potential functions via the Numerov method"; *Int. Jour. App. Math. Mech.*, **7** (8), 38-55; 2011.
- [3] P. Rudra; "Time-dependent Schrödinger equation for a two-body system: Symmetry classes of central potentials"; *Phys. Rev. A* 41, 4042–4045; 1990.



- [4] A.A. Rajabi; "Spectrum of mesons and hyperfine dependence potentials". Iran. Jour. of Phys. Research; 6 2, 2006.
- [5] H. Hassanabadi and et al; "Quadratic and coulomb terms for the spectrum of a three-electron quantum dot". Few body Syst; 48, 53-58, 2010.
- [6] H. Hassanabadi and et al; "Spectrum of baryons and spin-isospin dependence". Mod. Phys Lett A; 23 7 527-537; 2008.

15th Physical Chemistry Conference



DFT Investigation of tautomerism in 6-flourothymine: Comparison between gas phase and solution

Behzad Chahkandi, Narges Bafekr Shirvan, Mehdi Nekoei

Department of Chemistry , Shahrood Branch, Islamic Azad University, Shahrood, IRAN

Email : nbafekr@gmail.com

Keywords: Tautomerism, 6-flourothymine, SCRF, Chloroform, B3LYP

Introduction:

Quantum calculations were carried out to determining structural parameters, energies and thermodynamic properties of various tautomers of 6-flourothymine (FT). FT can be presented by five tautomeric forms. All tautomers from 1, 3 hydrogen migration between N and O were optimized at the B3LYP/6-311++g** level of theory in gas phas and chloroform solvent. And also by using frequency calculation at the same level thermodynamic properties such as ΔE , ΔH , ΔG and equilibrium constant (K_{eq}) for five tautomerism reactions were determined. Studies of tautomerism phenomena have been valuable in many areas of chemistry a demonstrated by several reviews of experimental and theoretical studies in chemistry and biochemistry. [1]. Tautomeric equilibria of pyrimidine bases are of continuing interest both from the theoretical [2] and experimental [3] points of view, partly due tosuggestions that the presence of unusual tautomers may have important biological properties,such as mutagenesis. One hypothesis suggests that the frequency of mispairing in DNA andthus, mutagenesis is correlated with equilibrium constants for the keto-enol or amino \pm imino tautomerisation [4]. In the present work, a complete tautomery scheme between tautomers for FT (Fig. 1) were studied using B3LYP/6-311++G(d,p) level of theory. In addition, From the calculations, relative energies of different tautomers, and thermodynamic properties of tautomerism equilibrium in FT were obtained. Thence, the effects of solvent on the equilibrium have been investigated using chloroform as solvent and gas phase.

Theoretical Calculations:

All of the geometry optimizations were performed by density functional theory (DFT) which were implemented in the Gaussian 09W program package. The optimizations of all structures

and frequency calculations were carried out using at B3LYP/6-311++G(d,p) level of theory. All of calculations were performed using SCRF keyword with Tomasi's polarized continuum (PCM) model in chloroform solvent at temperature 298.15 K and pressure 1 atm.

Results and Discussion:

Five tautomers of FT presented in Fig.1. Thermodynamic properties such as Gibbs free energies, enthalpies and energies for all tautomers are shown in Tables 1 and 2. All equilibrium constant for tautomeric conversion were calculated using $\Delta G = -RT \ln K_{eq}$.

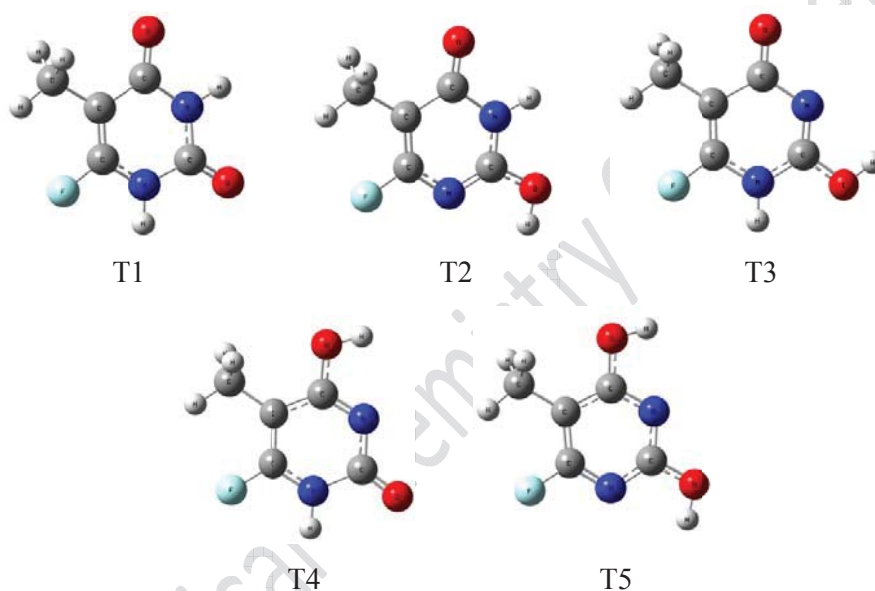


Fig. 1. Structure of various tautomers of FT.

The results in Table 1 show that the order of stability of five tautomers is $T_1 > T_2 > T_5 > T_4 > T_3$ in gas phase and chloroform. Tautomers T_1 and T_3 have the highest and lowest stability respectively in both phases, also all of tautomers have more stability in chloroform. The difference between Gibbs free energies of tautomers T_1 and T_2 , T_1 and T_3 , T_1 and T_4 , T_4 and T_5 , T_5 and T_2 are 6.72, 19.21, 12.63, -3.79, -2.09 and 7.13, 17.61, 11.91, -1.21, -3.56 kcal mol⁻¹ in gas phase and solution respectively.

Table1. Energies of all tautomers in gas phase and solution.

Tautomer	T ₁	T ₂	T ₃	T ₄	T ₅
Gas phase	-553.427103	-553.416833	-553.396579	-553.407455	-553.413672
Chloroform	-553.446384	-553.435205	-553.418485	-553.427644	-553.429597



Table2. Thermodynamic parameters of all tautomer in gas phase and solution.

	Gas				Chloroform			
	ΔE	ΔH	ΔG	K_{eq}	ΔE	ΔH	ΔG	K_{eq}
$T_1 \rightarrow T_2$	6.44	6.44	6.72	1.19×10^{-05}	7.01	6.92	7.13	5.68×10^{-06}
$T_1 \rightarrow T_3$	19.15	19.15	19.21	8.30×10^{-15}	17.51	17.52	17.61	1.23×10^{-13}
$T_1 \rightarrow T_4$	12.33	12.33	12.63	5.52×10^{-10}	11.76	11.67	11.91	1.86×10^{-09}
$T_4 \rightarrow T_5$	-3.90	-3.90	-3.79	5.99×10^{02}	-1.23	-1.27	-1.21	7.70×10^{00}
$T_5 \rightarrow T_2$	-1.98	-1.98	-2.09	3.40×10^{01}	-3.52	-3.48	-3.56	4.07×10^{02}

Therefore, the values of equilibrium constant (calculated from Gibbs free energies) for converting tautomer T_1 to T_2 , T_1 to T_3 , T_1 to T_4 , T_4 to T_5 and T_5 to T_2 are (1.19×10^{-05} , 8.30×10^{-15} , 5.52×10^{-10} , 5.99×10^{02} , 3.40×10^{01}) and (5.68×10^{-06} , 1.23×10^{-13} , 1.86×10^{-09} , 7.70×10^{00} , 4.07×10^{02}) in gas phase and chloroform respectively. The results show that the highest equilibrium constant is for tautomeric conversion T_4 to T_5 and T_5 to T_2 in gas phase and chloroform respectively (Table 2).

Conclusion:

The results of the present work obtained using DFT optimization and frequency calculations at the B3LYP/6-311++G(d,p) level of theory on 6-fluorothymine indicating that:

- 1- The order of stability of five tautomers is $T_1 > T_2 > T_5 > T_4 > T_3$ in gas phase and chloroform .
- 2- All of tautomers have more stability in chloroform.
- 3- The highest equilibrium constant is for tautomeric conversion T_4 to T_5 in gas phase but in chloroform T_5 to T_2 reaction has the highest equilibrium constant.

References:

- [1] A.R. Katritzky, J.M. Lagowski, Adv. Heterocycl. Chem. 1(1963) 2.
- [2] N. Bodor, J.S.M. Dewar, A.J. Harget, J. Am. Chem. Soc. 118(1996) 6811.) (1998) 989.
- [3] M. Orozco, B. Hernandez, F.J. Luque, J. Phys. Chem. B 102(1998) 5228.
- [4] M.D. Topal, J.R. Fresco, Nature (London) 263 (1976) 285.



DFT Investigation of transition state of tautomerism in 6-fluorothymine in chloroform solvent

Behzad Chahkandi, Narges Bafekr Shirvan, Mehdi Nekoei

Department of Chemistry, Shahrood Branch, Islamic Azad University, Shahrood, IRAN

Email : nbafekr@gmail.com

Keywords: Tautomerism, 6-fluorothymine, SCRF, Chloroform, B3LYP, TS

Introduction

Quantum calculations were carried out to determine structural parameters, energies and thermodynamic properties of transition state (TS) of various tautomers of 6-fluorothymine (FT). FT can be presented by five TS forms. All TS from 1, 3 hydrogen migration between N and O were optimized at the B3LYP/6-311++g** level of theory in chloroform solvent. And also by using frequency calculation at the same level thermodynamic properties such as ΔE^{++} , ΔH^{++} , ΔG^{++} and rates constant (K_{rat}) for five tautomerism reactions were determined. Studies of tautomerism phenomena have been valuable in many areas of chemistry as demonstrated by several reviews of experimental and theoretical studies in chemistry and biochemistry. [1]. Notable studies have been performed on thymine tautomers such as The structures and the relative energies of six possible tautomers of the thymine base have been studied by density functional theory (DFT) using the B3LYP and BP86 functionals. The keto-thymine (T1) is predicted to be the most stable thymine tautomer, which is consistent with the other theoretical results and experimental data. T1 has the largest ionization potential and the lowest proton affinity among all the considered thymine tautomers [2]. Tautomerism of thymine on gold and silver nanoparticle surfaces has been comparatively analyzed means of surface-enhanced Raman scattering (SERS). The N3-deprotonated tautomer was predicted to be more favorable on Au than on Ag the DFT calculation as consistent with our SERS spectra. [3] In the present work, a complete TS scheme for tautomers for FT (Fig. 1) were studied using B3LYP/6-311++G(d,p) level of theory. In addition, From the calculations, thermodynamic properties of TS of tautomerism equilibrium in FT were obtained. Thence, the effects of solvent on the TS of equilibrium have been investigated using chloroform as solvent.

Theoretical Calculations:

All of the geometry optimizations were performed by density functional theory (DFT) which were implemented in the Gaussian 09W program package. The optimizations of all structures and frequency calculations were carried out using at B3LYP/6-311++G(d,p) level of theory. All of calculations were performed using SCRF keyword with Tomasi's polarized continuum (PCM) model in chloroform solvent at temperature 298.15 K and pressure 1 atm.

Results and Discussion:

Five TS of FT presented in Fig.1. Thermodynamic properties such as Gibbs free energies, enthalpies and energies for all TS are shown in Tables 1 and 2. All rate constant for tautomeric conversion were calculated using. $K_{\text{rate}} = k_B T / hc^0 e^{-\Delta G^{\ddagger} / RT}$

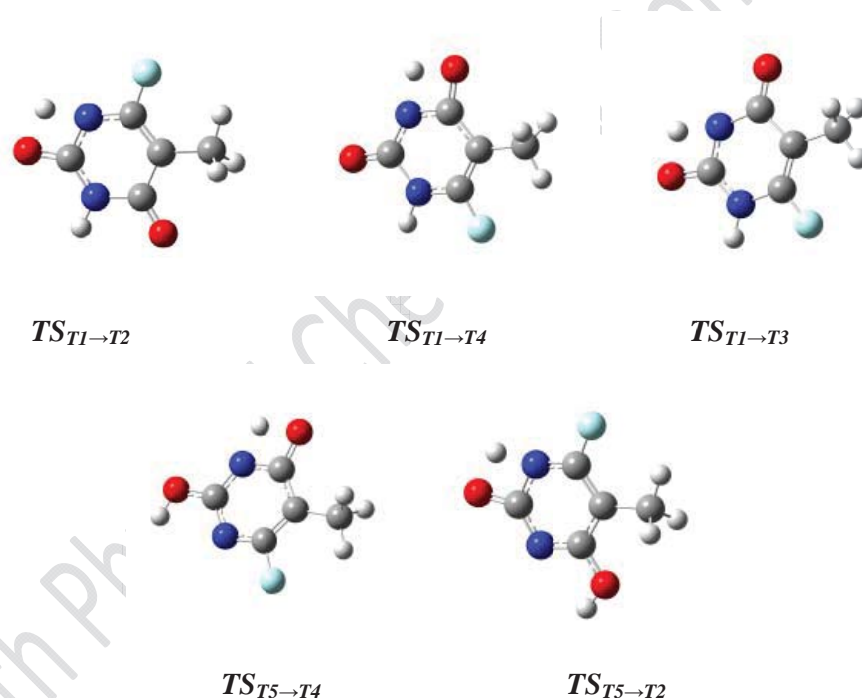


Fig. 1. Structure of various TS of FT.

The results in Table 1 show that the order of stability of five TS is $TS_{T1 \rightarrow T4} > TS_{T1 \rightarrow T2} > TS_{T5 \rightarrow T2} > TS_{T1 \rightarrow T3} > TS_{T4 \rightarrow T5}$. $TS_{T1 \rightarrow T4}$ and $TS_{T4 \rightarrow T5}$ have the highest and lowest stability respectively in solvent. The difference between Gibbs free energies TS of tautomers T_1 to T_2 , T_1 to T_3 , T_1 to T_4 , T_4 to T_5 , T_5 to T_2 are 43.02, 48.40, 41.80, 36.76, 34.09 kcal mol⁻¹ in solution respectively.



Table1. Energies TS of all tautomers chloroform solution.

TS	TS _{T1→T2}	TS _{T1→T3}	TS _{T1→T4}	TS _{T4→T5}	TS _{T5→T2}
E _{TS}	-553.369267	-553.360983	-553.371076	-553.360596	-553.366054

Table2. Thermodynamic parameters TS of all tautomer chloroform solution.

	ΔE^{++}	ΔH^{++}	ΔG^{++}	K _{rat}
T ₁ →T ₂	42.84	42.84	43.02	1.82×10 ⁻¹⁹
T ₁ →T ₃	48.04	48.04	48.40	2.07×10 ⁻²³
T ₁ →T ₄	41.71	41.71	41.80	1.42×10 ⁻¹⁸
T ₄ →T ₅	36.61	36.61	36.76	7.05×10 ⁻²⁷
T ₅ →T ₂	34.45	34.45	34.09	6.38×10 ⁻²⁵

Therefore, the values of rate constant (calculated from Gibbs free energies) for converting tautomer T₁ to T₂, T₁ to T₃, T₁ to T₄, T₄ to T₅ and T₅ to T₂ are (1.82×10⁻¹⁹, 2.07×10⁻²³, 1.42×10⁻¹⁸, 7.05×10⁻²⁷, 6.38×10⁻²⁵) chloroform respectively. The results show that the highest rate constant is for tautomeric conversion T₁ to T₄ chloroform respectively (Table 2).

Conclusion:

The results of the present work obtained using DFT optimization and frequency calculations at the B3LYP/6-311++G(d,p) level of theory on 6-fluorothymine indicating that:

- 4- The order of stability of five TS is TS_{T1→T4}> TS_{T1→T2}> TS_{T5→T2}> TS_{T1→T3}> TS_{T4→T5} in chloroform .
- 5- The highest and lowest rate constant is for tautomeric conversion T₁ to T₄ and T₄toT₅
- 6- . tautomers T₁to T₄ and T₄ to T₅ have the lowest and highest stability respectively in chloroform solvent.

References:

- [1] A.R. Katritzky, J.M. Lagowski, Adv. Heterocycl. Chem. 1(1963) 2.
- [2] Dongsheng Jiao,^a Hongyan Wang,^b Yanlan Zhang,^a Yu Tang^a 18 December 2008.
- [3] Kwang-Hwi CHO, Jaebum CHoo, sang-Woo Joo. 2005



Photoelectron spectra of Oxyacids of Nitrogen in Gas phase and Solution

Z. Rezaie arjmand^a, H. Farrokhpour^b, M. Vahepour^a

^aDepartment of Chemistry, University of Zanjan, Zanjan, Iran

^bChemistry Department, Isfahan University of Technology, Isfahan, Iran, 84156-83111

Email: fr.rezae@gmail.com

Key Words: Ionization, Photoelectron Spectroscopy, SAC-CI, Oxyacids of Nitrogen

Introduction:

Oxyacids of Nitrogen such as Nitrous acid (HNO₂), Nitric acid (HNO₃) and pernitric acid (HNO₄) are important in atmospheric chemistry. For example, in the troposphere, nitric acid produces acidic rain. These inorganic acids can be decomposed to NO, NO₂, NO₃; and radicals including OH, O₂H. These species are important in photochemical cycles responsible for ozone formation. Because of the importance of these molecules in atmospheric chemistry, extensive experimental works have been carried out on the spectroscopy of Oxyacids of Nitrogen. In this work the photoelectron, UV and IR spectra of these compounds are calculated, in the gas phase and solution, using high level correlative computational methods and then compared with the experimental data. In addition, the validity of Koopmans theorem was investigated for the considered molecules using the calculated photoelectron spectra..

Method:

The geometry of the considered molecules were optimized at the B3LYP/6-311++G(2d,2p) level of theory. The optimized geometries, obtained at the DFT level of theory, were re-optimized using coupled cluster singles and doubles (CCSD) level of theory with the same basis set. The symmetry adapted cluster/configuration interaction (SAC-CI) method based on single and double excitation operators (SD-R) with the 6-311++G(2d,2p) basis set was used for calculating the UV and Photoelectron spectra of Nitrogen oxyacids in the gas phase and solution [1]. The SAC-CI SD-R method is based on the spin and space symmetry-adapted formalism of the cluster expansion method. The inner orbital (1s) of O and N was excluded from the SAC-CI calculations, and frozen core approximation was used. The threshold for the

selection of double excitation operators for SAC-CI calculations were set on the highest recommended level (level three). All of the calculations were performed using G09 software.

Result and discussion:

Typically, table 1 reports the vertical ionization energies and their ionization cross sections for HNO₃ molecule in the gas phase. The monopole approximation was used for calculating the ionization cross sections. As seen, the wave function of the ionized states strictly composed of one one-electron ionization determinant except the last ionization state which is a shake up process. Fig. 1 shows the calculated photoelectron spectrum of HNO₃ molecule in the gas phase up to 22eV binding energy and compares it with the experimental spectrum [2]. As shown, there is a good agreement between the theory and experiment. The photoelectron spectrum of each Oxyacid was produced by convoluting the discrete photoelectron bands with Gaussian distribution function and the same Gaussian width (300 meV; full width at the half maximum) was considered for each band.

Table 1: Calculated ionization potential (IP), monopole intensities and the main configurations of the ionized states of HNO₃ at the SAC-CI SD-R level of theory and using 6-311++G(2d,2p) basis set.

Ionization state number	Ionization Energy	Intensity	Main Configuration
1	12.417	0.91954	0.95(15)
2	12.695	0.92943	-0.96(16)
3	13.135	0.91760	0.94(14)
4	13.831	0.90501	0.95(13)
5	17.280	0.92790	-0.96(12)
6	19.081	0.89466	-0.94(11)
7	19.229	0.79163	0.88(10)
8	20.234	0.88456	0.92(9)
9	22.738	0.0022	-0.91(15, 16→18)

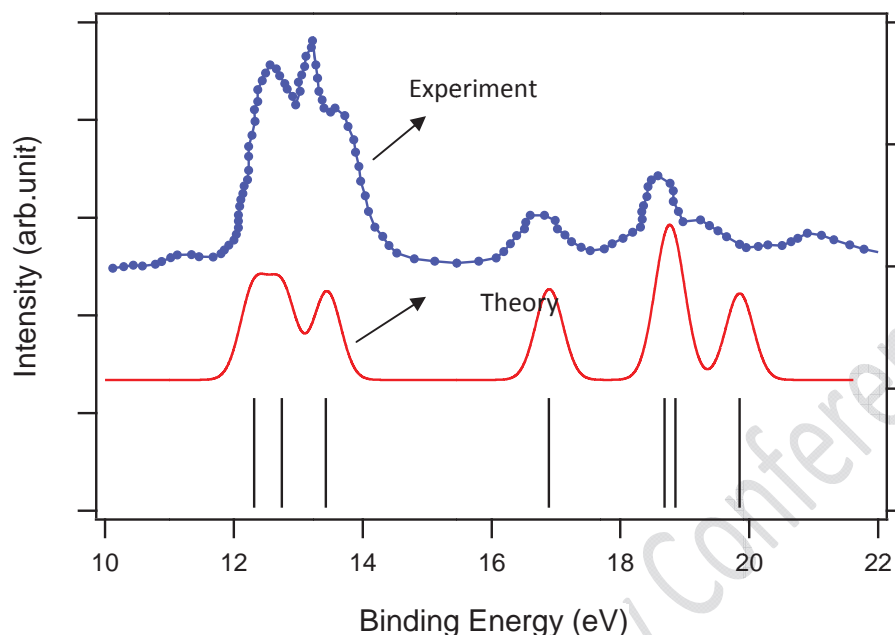


Fig. 1. Comparison of the experimental He-I Valence photoelectron spectrum of HNO_3 [], (dotted blue trace) with the spectrum calculated in this work (solid red trace). The vertical lines show the position of the ionization bands.

Conclusion:

The valence photoelectron spectra of Oxyacids of Nitrogen, in the gas phase and solution, are studied theoretically in the present work. High level *ab initio* calculations were used to calculate and to assign the photoelectron spectra. For this purpose, the SAC-CI SD-R method was applied for calculating the photoelectron bands of each Oxyacid. The calculated photoelectron spectra confirm the corresponding experimental spectra in the literature.

References:

- [1] R. Fukuda, H. Nakatsuji, *J. Chem. Phys.* 94105,128, 2008.
- [2] D. R. Lloyd, P. J. Robert, *J. Chem.Soc. Faraday. Trans.* 496, 71, 1975.



A novel view of the interaction between PLGA-PEG-PLGA with HSA synchronous fluorescence spectroscopy method

M. Ahmadi-Khalkhali^{1*}, M. Pirouzi¹, M. R. Saberi², J. Chamani¹

1. Department of Biology, Faculty of Sciences, Mashhad Branch, Islamic Azad University, Mashhad, Iran

2. Department of Medical Chemistry, School of Pharmacy, Mashhad University of Medical Sciences, Mashhad, Iran

Maral.ahmadi65@yahoo.com

Abstract:

In the present work, we studied the interaction between PLGA-PEG-PLGA with HSA. Here we get that HSA modification by PLGA-PEG-PLGA using synchronous fluorescence spectroscopy methods, PLGA-PEG-PLGA is a polymer with molecular weight of 11011 kDa. HSA has molar mass of 66.5 kDa, HSA is a principal extra cellular protein with a high concentration in blood plasma and a carrier of many drugs to deferent molecular targets. The conformation of HSA was discussed by synchronous fluorescence techniques. The synchronous spectra indicated that the structures of Tyr and Trp residues environments were altered the physiological function of HSA were affected by 0.

Keyword: Polymer PLGA-PEG-PLGA, Human serum albumin, Fluorescence spectroscopy

Introduction:

Studies on the interaction of PLGA-PEG-PLGA to HSA are of great importance in biological biomedical and pharmaceutical sciences. Among investigated proteins, a special attention was paid to human serum albumin (HAS), the principal extracellular protein in the blood plasma. Its main physiological function consists in the storage and transportation of a wide range of endogenous and exogenous compounds.

Materials and methods:

The fluorescence spectra were record on F-2500 (Hitachi, Japan) with a 150 W Xenon lamp, a 1.0-cm quartz cell and a thermostat bath. HSA solution was 15×10^{-4} mM for fluorescence

were prepared in phosphate buffer (pH 7.4) and equilibrated over night. PLGA-PEG-PLGA was 9.08×10^{-5} . Synchronous fluorescence were obtained using $\Delta\lambda = 15$ (Tyr excitation) and $\Delta\lambda = 60$ nm (Trp excitation), where $\Delta\lambda = \lambda_{em} - \lambda_{ex}$. All solution were stored in refrigerator at 4°C in dark.

Results and discussion:

The explor the structural change of HSA by addition of PLGA-PEG-PLGA, we measured synchronous fluorescence spectra of HSA (Fig. 1) with various amounts of PLGA-PEH-PLGA. Synchronous fluorescence spectroscopy technique was introduced by Lloyd in 1971 [1]. The synchronous fluorescence spectroscopy give information about the molecular environment in a vicinity of the chromospheres molecules and has several advantages, such as sensitivity, spectral simplification, spectral bandwidth reduction and avoiding different perturbing effect [2]. Yuan et al. [3] suggested a useful method to study the environment of amino acid residues by measuring the possible shift in wavelength emission maximum MAX, the shift in position of emission maximum is corresponding to the change of polarity around the chromospheres molecule. When the D value ($\Delta\lambda$) between excitation wavelength and emission wavelength were stabilized at 15 nm or 60 nm, the synchronous fluorescence gives the characteristic information of tyrosine or tryptophan residues. It was apparent from Fig. 1 the emission maximum of tyrosine residues did significant blue shift tryptophan residue did quenching and which indicated that the conformation of HSA was changed. The polarity around the tyrosine residue was decreased and hydrophobicity was increased [4].

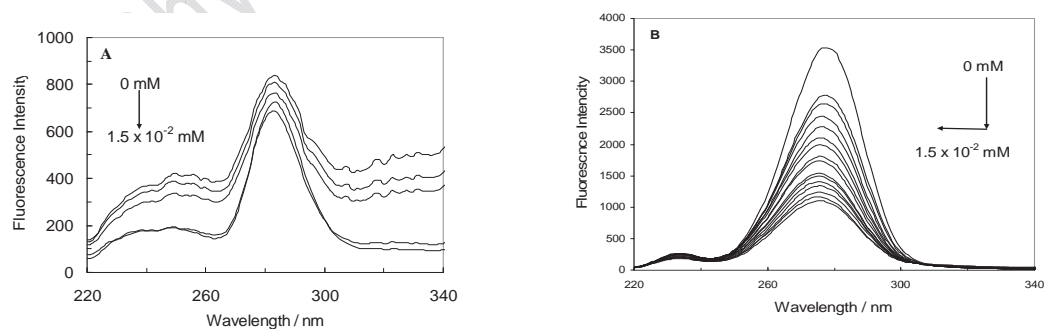


Fig. 1. Synchronous fluorescence spectrum of HAS($T = K$, $Ph = 7.40$). $c(HAS) = 1.5 \times 10^{-2}$ mM; $c(PLGA-PEG-PLGA)/(mM)$, from up to down: 0 to 1.5×10^{-2} mM respectively. (A) $\Delta\lambda = 15$ nm and (B) $\Delta\lambda = 60$ nm.



Conclusion:

In this work spectroscopic studied on the interaction of PLGA-PEG-PLGA with HAS using synchronous fluorescence. It was showed that the fluorescence of HSA has been quenched while reaction with PLGA-PEG-PLGA. The quenching belonged to static fluorescence quenching. Synchronous fluorescence was showed that the structures of these Tyr and Try residues environments were alternate by PLGA-PEG-PLGA. Studies on the interaction of drugs with protein are of great important in pharmacy and pharmacology.

References:

- [1] J.B.F. Lloyd, Nature 231 (1971) 64-65.
- [2] Y..J. Hu, Y.Liu, Z.B. Pi, S.S. Qu, Bioorg. Med. Chem. 13 (2005) 6609-6614.
- [3] T. Yuan, A.M. Weljie, H.J. Vogel, Biochemistry 37(1998) 3187-3195.
- [4] B.Klajnert, M. Bryszewska, Bioelectrochemistry 55 (2002) 33-35

Quantum mechanical study on the mechanism of coordination of indole derivatives to Palladium (II) Ions in Complexes

A. Morsali^a, M. M. Heravi^a and M. Hoseinzadeh^{* a}

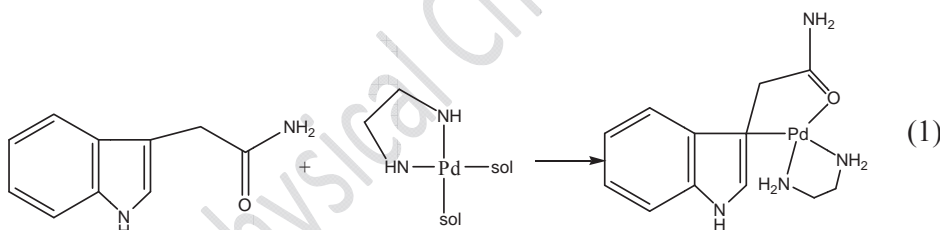
^a Faculty of Science, Department of Chemistry, Mashhad Branch, Islamic Azad University, Iran

(Email: mahlaho3inzade66@yahoo.com)

Keywords: Mechanism, indole derivatives, Density functional theory, Palladium (II) Ions

Introduction:

Binding of tryptophan residue to intrinsic metal ions in proteins is unknown, and very little is known about the coordinating abilities of indole. Indole-3-acetamide displaces the solvent ligands from $\text{cis}[\text{Pd}(\text{en})(\text{sol})_2]^{2+}$, in which sol is acetone or H_2O , in acetone solution and forms the complex $\text{cis}[\text{Pd}(\text{en})(\text{indole-3-acetamide})]^{2+}$ (3) of spiro structure, in which the new bidentate ligand coordinates to the Pt(II) atom via the C(3) atom of the indolyl group and the amide oxygen atom (Eq. (1)) [1]. In this work, we investigated this mechanism using the quantum mechanical approach.



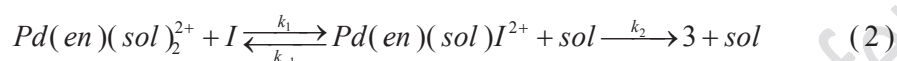
Computational details:

All of the present calculations have been performed with the B3LYP [2] hybrid density functional level using the G09 package. The 6-311++G(d,p) basis set was employed. The gas phase optimized geometries used to apply the solvent effects, where the valuable PCM [3] model was employed. We assumed that the change of the molecular geometry upon solvation has a negligible effect on the thermodynamic parameters. Thus, the optimized geometries calculated in gas phase were used. Basically, the optimized structures in solvent should be

used for frequency calculations, but to reduce computational cost, optimized structures in gas phase could be used as an approximation for this purpose.

Results and discussion:

The following mechanism (Eq. 2)) for coordination of indole derivatives to Palladium(II) Ions in Complexes was proposed [1]. In step k_2 , a fast equilibrium step (with equilibrium constant K_2) will result in the formation of complex $Pd(en)(sol)I^{2+}sol$ which will be converted into Products during a slow process.



The optimized structure of transition state (TS_2) obtained from step k_2 has been shown in Fig. 1. By taking Solvent (acetone) effects into consideration, $E_a = 19.7 kcal / mol$. This shows that the model presented in this research is a suitable model for the rate determining step of coordination of indole derivatives to Palladium(II) Ions in Complexes

Conclusion:

Using quantum mechanical method, coordination of indole derivatives to Palladium(II) Ions in Complexes was investigated and a model was presented in which an intermediate is produced in the fast equilibrium step ($Pd(en)(sol)I^{2+}sol$) and in continuation is converted into product in the rate determining step.

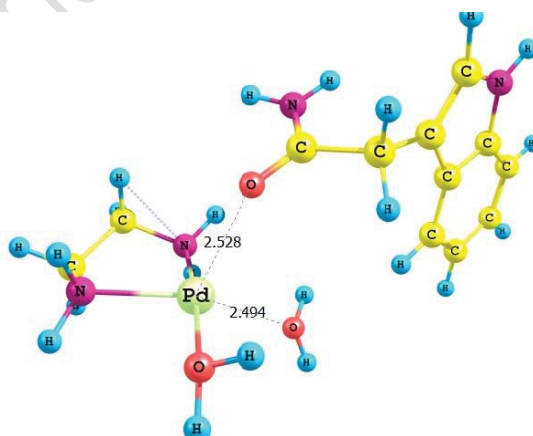


Fig 1. Optimized structure of the TS_2

References:



- [1] N. V. Kaminskaia, G. M. Ullmann, D. B. Fulton, N. M. Kostic, [Inorg. Chem., 39 (2000) 5004.
- [2] A.D. Becke, Phys. Rev. A, 38 (1988) 3098.
- [3] S. Miertus, E. Scrocco, J. Tomasi, Chem. Phys. 55 (1981) 117.

15th Physical Chemistry Conference



Novel furandicarboxylate derivatives as excellent fluorescence standards: spectroscopical and electrochemical study

K.Zargoosh^a, Y.Ghayeb^a, N.Aeineh^a, M.Qandalee^b, A.A.Miran Beigi^c

^aDepartment of Chemistry, Isfahan University of Technology, Isfahan 84156-83111, Iran

^bDepartment of Biology, Garmsar Branch, Islamic Azad University, Garmsar, Iran

^c Oil Refinery Research Division, Research Institute of Petroleum Industry, Tehran, Iran

E-mail : Aeinehneda@yahoo.com

Keywords: fluorescence standard; fluorescence quantum yield; chemiluminescence quantum yield; peroxyoxalate chemiluminescence; furan derivatives; cyclic voltammetry.

Introduction:

Frequent applications of luminescence dyes in different areas of research such as clinical, pharmaceutical, biochemical, organic light-emitting diodes (OLEDs), organic field effect transistors (OFETs) [1] have spurred the demand for preparation of novel standard luminescence materials. In addition most luminescence-based assays need calibration steps such as spectral correction of detectors, demonstration of day-to-day stability of signals, comparison of instrument- to- instrument performance and determination of wavelength accuracy. Standard luminescent chemicals have important roles in these calibration procedures [2]. In most cases, suitable chromophore-based standards for the calibration and performance validation of photoluminescence measuring systems and for the measurement of the important fluorometric quantities (e.g. fluorescence quantum yields of the fluorophores) should have several characteristics such as simple and unstructured emission spectra, moderate to high fluorescence quantum yield, stable chemical structure, low overlap between absorption and emission spectrum and resistance to photo-degradation. We found that novel furandicarboxylate derivatives synthesized in our laboratory [3] have all of the required criteria mentioned above for suitable fluorescence standards. Thus in this work, we report the main spectroscopical and electrochemical properties of the novel furandicarboxylate derivatives as potential fluorescence standards. Their outstanding characteristics make them



preferable alternatives to the well-known and widely used fluorescence standards such as luminol and anthracene.

Materials and method:

Six novel furandicarboxylate derivatives were synthesized in our laboratory [3]. In the CL measurements, appropriate volumes of the stock solutions of imidazole, fluorophore and Bis(2,4,6-trichlorophenyl)oxalate (TCPO) were added to the glass cell respectively, completed with acetonitrile to obtain a fix volume. The CL reaction was initiated by rapid injection of the H₂O₂ solution.

Apparatus:

Chemiluminescence measurements (intensity versus time) were carried out on a Safa luminometer (Safa Electronic, Isfahan, Iran) equipped with a photomultiplier. Steady-state fluorescence spectra were recorded on a PerkinElmer, Ls50B spectrofluorimeter instrument. The cyclic voltammetric experiments were performed on an Autolab model 302N modular potentiostat (Metrohm, Switzerland).

Results and discussion:

Based on the fluorescence and CL quantum yield measurements, we understand that presence of the cyclohexyl and ethenyl substituents in the molecular structures of the studied fluorophores can significantly enhance the rigidity of the fluorophore structures and hence, enhance the fluorescence quantum yields of the fluorophores. On the other hand steric hindrances of the tert-butyl substituents can reduce the chemiluminescence quantum yields of the studied fluorophores. In addition cyclic voltammetric measurements show that presence of biphenyl-ethenyl substituents on the furan ring can improve the kinetic of the electron transfer and result in the reversible oxidation of the fluorophores.

Conclusion:

excellent stability, moderate chemiluminescence quantum yield, high fluorescence quantum yield and simple and unstructured emission spectra of the furandicarboxylate derivatives make them suitable alternatives to the well-known and widely used fluorescence standards



for instrumental calibrations and spectroscopical measurements. In addition, presence of amine and carboxylate substituents in the chemical structure of these derivatives makes them suitable substrates for synthesis of fluorescent biomarkers.

References:

- [1] L.R. Dalton, P.A. Sullivan, Chem. Rev. 110 (2009) 25–55.
- [2] S.A. Wise, L.C. Sander, W.E. May, J. Chromatogr. 642 (1993) 329-349.
- [3] S. Asghari, M. Qandalee, Acta.Chim. Solv.54 (2007) 638-641.

15th Physical Chemistry Conference



Vibrational assignment and structure of Vanadyl acetylacetonate: A density functional theoretical study

M. Vakili^a, F. Bagheryan^{a*}, A.-R. Nekoei^b

^a Department Of Chemistry, Ferdowsi University Of Mashhad , Mashhad, Iran

^b Department of Chemistry, Shiraz University of Technology, Shiraz 71555-313, Iran

Email: Bagheryanfatemeh@yahoo.com

Keywords: Vanadyl bis acetylacetonate; Density Functional Theory; Vibrational analysis, oxobis(2,4-pentanedionato)vanadium(IV)

Introduction:

β -diketones have a wide range of applications, which make attention in science. Vanadyl acetylacetonate (known as dipivaloylmethane), $(VO(AA)_2)$, is used in organic chemistry as a reagent in the epoxidation of allylic alcohols. $VO(AA)_2$ also exhibits insulin mimetic properties. The aim of present study is to compare the theoretical and experimental results on structure and vibrational analysis of $VO(AA)_2$.

Method of analysis :

The Geometries and vibrational frequencies calculations of the $VO(AA)_2$ were performed using GAUSSIAN 09 with B3LYP using 6-311G(d) basis set.

Results and discussion :

The structure and the atomic numbering of $VO(AA)_2$ is shown in Fig. 1. The full optimized geometrical parameters of $VO(AA)_2$ along with its reported experimental parameters [1] are compared in Table 1. According to this table1, the V=O, C=O, and V-O bond lengths and OVO, COV bond angles in $VO(AA)_2$ are in excellent agreement with the results of the experimental structures nearly in the experimental error range.

According to C_{2v} symmetry for the $VO(AA)_2$ complex, the 84 vibrational modes can be classified among the symmetry species: $\Gamma_{vib} = 23A_1 + 19A_2 + 20B_1 + 22B_2$. A part of calculated harmonic vibrational band frequencies and their approximate assignments of



VO(AA)₂, along with the observed infrared and Raman frequencies are listed in Table 2. According to our assignment, the weak Raman bands at 3092, 3005 and 2978 cm⁻¹ and the strong IR band at 2927 cm⁻¹ assigned to νCH_α, νaCH₃, and νsCH₃, respectively, which are in agreement with Vlckova results [2]. The δCH_α, νV=O, δCH_α, and out of plane ring deformation (Γ) modes appear at 1188, 990, 799-789, and 688cm⁻¹, respectively. The bands at 1560 and 1525cm⁻¹ in Raman spectrum according to our calculations attributed to νsC-O and νaC-C-C, which the later coupled with δCH_α, while these bands are assigned to νC-O and the later to νC-C-C by Vlckova. The band at 1032cm⁻¹ in Raman spectrum attributed to ρCH₃, which coupled with δC-C-C, while assigned by Vlckova only to ρCH₃. The bands at 660, 480, and 462 cm⁻¹ are attributed to νsVO, upon our assignments the bands at 480 and 462 cm⁻¹ are in agreement with Vlckova results, while Vlckova assigned the first band to δ(ring).

Table 1. Selected geometrical parameters of VO(AA)₂ calculated at B3LYP/6-311G*, in comparison with experimental geometry.

Bond distances(Å)	Theoretical	Exp.
V=O(30)	1.564	1.586(15)
V-O(2)	1.993	1.968(14)
V-O(3)	1.993	1.964(13)
V-O(4)	1.993	1.967(13)
V-O(5)	1.993	1.973(13)
C(6)=O(2)	1.275	1.274(2)
C(7)=O(3)	1.275	1.270(2)
C(8)=O(4)	1.275	1.280(2)
C(9)=O(5)	1.275	1.273(2)
C6-C10/ C7-C10	1.401	
C8-C11/ C9-C11	1.401	
C-Me	1.507	
Angles (°)		
O(30)-V-O(4)	106.74	104.75(7)
O(30)-V-O(2)	106.74	107.16(8)
O(4)-V-O(5)	85.92	87.17(6)
O(4)-V-O(2)	84.56	83.90(6)
C(7)-O(3)-V	129.75	128.96(11)
C(9)-O(5)-V	129.75	128.78(11)
O(4)-V-O(3)	146.51	150.23(6)

Table2. Fundamental band assignment of VO(AA)₂. Frequencies are in cm⁻¹ and intensities are relative.

Sym.	Theo.	Exp.		Assignment	
	freq	IR	R	this work	[2]
A1	3210		3092(vw)	νsCH _α	νC-H
B2	3210	3100(br)	3092	νaCH _α	νC-H
A1	3134	3000	3005	νaCH ₃	νaCH ₃
B1	3101		2978(w)	νaCH ₃	νaCH ₃
A1	3045		2927(s)	νsCH ₃	νsCH ₃
A1	1640	1587(sh)		νsC-O	νC-O
B2	1616	1556(s)	1560(vw)	νsC-O	νC-O
B1	1568	1524(vs)		νaC-C-C, δCH _α	νC-C-C
A2	1566		1525(w)	νaC-C-C, δCH _α	νC-C-C
B1	1226	1188(w)		δCH _α	δC-H
A1	1120	995(s)	990(vs)	νV=O	νV=O
A1	1058	1020(m)	1032(mw)	ρCH ₃ , δCCC	ρCH ₃
A1	973		945(m)	δC-C-C, ρCH ₃	νC-CH ₃
A2	948		825(w)	νaC-CH ₃ , Δ	νC-CH ₃
A1	794	799(w)		γCH _α	γCH _α
B2	794	789(w)		γCH _α	γCH _α
A1	688		688(m)	Γ(ring)	δ(ring)
A1	676		660(w)	νsVO(i.p)	δ(ring)
B2	674	658(vw)		νsVO(o.p)	δ(ring)
B2	485	483(vs)	480(sh)	νsVO (o.p)	ν(VO4)
A1	460	465(sh)	462(vs)	νsVO (i.p)	ν(VO4)

Fig 1. Structure and the atomic numbering of VO(AA)₂.

References:

- [1] E.V.Fedorova, V.B. Rybakov, V.M. Senyavin, A.V.Anisimov, and L.A.Aslanov, crystallography reports. 50(2005) 224.
- [2] B. Vlckova, B. Strauch, M. Horak, Collection Czechoslovak Chem. Commun. 52(1987)686.



Molecular structure and intramolecular hydrogen bonding of 4-phenylamino-3-penten-2-one and its para substitutions. A DFT study

M. Vakili, M. Bayatmokhtari*, R. Afzali

Department of Chemistry, Ferdowsi University of Mashhad, Iran

E-mail: zbayatmokhtari@yahoo.com

Keyword: 4-phenylamino-3-penten-2-one; Intramolecular Hydrogen bond strength; 4-amino-3-penten-2-one; Density functional Theory,

Introduction:

α,β -unsaturated- β -ketoamines are capable of forming an N-H...O asymmetric intramolecular hydrogen bond [2]. The 4-amino-3-penten-2-one (APO) has an N-H...O intramolecular hydrogen bond. Furthermore this compound is capable of forming tautomeric equilibria between ketoamines, ketoimine, and enolimine (See Fig. 1). APO has been studied experimentally and theoretically by DFT calculations. The results of the calculations show that APO has a relatively strong intramolecular hydrogen bond with a N...O distance of 2.658 Å [1].

The goal of this work is to investigate the relative energies of tautomers, structure and Intramolecular hydrogen bond (IHB) strength of 4-phenylamino-3-penten-2-one (PhAPO) and its para substitutions by means of DFT calculation and comparison of their IHB strength with APO.

Method of analysis:

All possible ketoamines, ketoimine, and enolimine tautomers of 4-phenylamino-3-penten-2-one and its para substitutions were fully optimized at the B3LYP with different basis sets, using Gaussian 09W software package.

Results and discussion:

According to our calculations, the hydrogen atoms of the methyl groups in ketoamine, ketoimine are eclipsed and at enolimine are staggered. Among all of them, only ketoamine is the most stable one. These results are in consistent with their para substitutions. The relative

stabilities of the ketoimine and enolimine forms are in the range of 4.8–10.3 kcal/mol calculated at B3LYP/6-31G**, with respect to the most stable ketoamine form.

The selected fully optimized geometrical parameters of ketoamine tautomer for APO and 4-phenylamino-3-penten-2-one and its para substitutions, calculated at the B3LYP/6-311++G** level, are given in Table 1. According to the results of Table 1, The O-H and N...O decrease in PhAPO and its substitutions, in comparison with APO, whereas the N-H and C=O increase. Also the NHO bond angle increase in PhAPO and its substitutions, in relative to APO. Upon our expectation the N-H chemical shift of APO is less than that of PhAPO, the experimental NMR proton chemical shift of the N-H in APO is 9.7 ppm [2], which is considerably lower than the corresponding value for PhAPO (12.45 ppm) [3]. In the case of the other substitutions ¹HNMR chemical shift for N-H is about 12.4 ppm, which is agreement with their N...O distances and NHO bond angles.

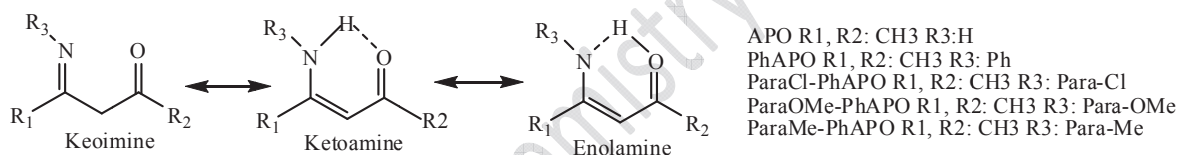


Fig1: Tautomerization equilibria in APO and derivatives

Conclusion:

The theoretical and the ¹HNMR chemical shift for N-H indicate that IHB strength in PhAPO and its substitutions is stronger than in APO. Also, the mentioned results show, by adding the substitutions on the para position of phenyl ring there is no significant deviations on the IHB strength.

Table 1. Comparison of theoretical geometric parameters of *p*-ClPhAPO, *p*-MePhAPO, *p*-OMePhAPO and APO at B3LYP/6-311++G** level of theory

	APO	PhAPO	<i>p</i> -Cl PhAPO	<i>p</i> -Me PhAPO	<i>p</i> -OMe PhAPO
C=C (Å)	1.377	1.384	1.382	1.385	1.385
C-C (Å)	1.443	1.438	1.441	1.437	1.437
N-C (Å)	1.348	1.356	1.358	1.354	1.353
C-O (Å)	1.242	1.246	1.245	1.264	1.247
O-H	1.890	1.773	1.773	1.777	1.782
N...O (Å)	2.669	2.645	2.646	2.647	2.647
<NHO	130.75	139.9	139.9	139.7	139.1



References:

- [1] H. Raissi, M. Bakavol, I. Jimenez-Fabian, J. Tajabadi, E. Mdoshfeghi, A. F. Jalbout, *Mol. Struct.* 847 (2007) 47-51.
- [2] S. F. Tayyari, H. Raissi, F. Tayyari, *Spectrochimica Acta Part A* 58 (2002) 1681-1695.
- [3] E. Safaee, M.Sc Thesis, Ferdowsi University of Mashhad (2011).

15th Physical Chemistry Conference



Structural and Spectroscopic (NMR, IR, and UV) analysis of Lemofloxacin via DFT quantum chemical studies

Afsaneh Amiri^{1*}, Sara Moghimi², Sanaz JavanshiriVaziri², Simin Tadayon¹

¹Department of Chemistry, Islamic Azad University, Central Tehran Branch, Tehran, Iran.

²Department of Chemistry, Islamic Azad University, North Tehran Branch, Tehran, Iran.

Email: afsaamiri@gmail.com

Keywords: Lemoofloxacin, Specteroscopic analysis, B3LYP, DFT, FT-IR, UV-VIS, ¹H NMR.

Introduction:

Lomefloxacin (1-ethyl-6,8-difluoro- 7-(3-methylpiperazin-1-yl)- 4-oxo-quinoline-3-carboxylic acid,) , Lomefloxacin (LMF) is a synthetic, broad-spectrum fluoroquinolone antibacterial agent. It was active against a wide variety of aerobic gram-negative and gram-positive bacteria like norfloxacin [1]. Lomefloxacin is one representative of the quinolone family. In general, quinolones can form supramolecules with other compounds through charge transfer complex formation [2, 3]. In this research study, the formation potential Molecular structure, Specteroscopic analysis (FTIR, UV-VIS, NMR) of Lemofloxacin have been investigated by DFT calculation.

Material and Methods:

The geometry of the system has been fully optimized with the hybrid DFT and HF. DFT and HF calculations were performed with the GAUSSIAN 03W programs on a Pentium-PC computer with 3600 MHz processor [4]. To verify that the concluding structure wasn't in the local minimum point, the normal mode frequency calculation was carried out for the optimized molecules. The Specteroscopic analysis (FT-IR, UV-VIS, NMR) of the molecule in the liquid phase, were carried by using the Onsager SCRF method at the B3LYP/6-311+G**.

Result and Discussion:

Computational calculations of Ciprofloxacin have been carried out using the Becke-3-Lee–Yang–Parr density (B3LYP) functional methods with 6-311+G (d, p) basis set. The geometry

optimization and fundamental frequencies of the most stable configuration have been calculated. The FTIR spectra of the compound have been recorded and compared to the calculated frequency values. The ^1H NMR chemical shifts have been calculated using the gauge-independent atomic orbital approach. (Fig.1-3)

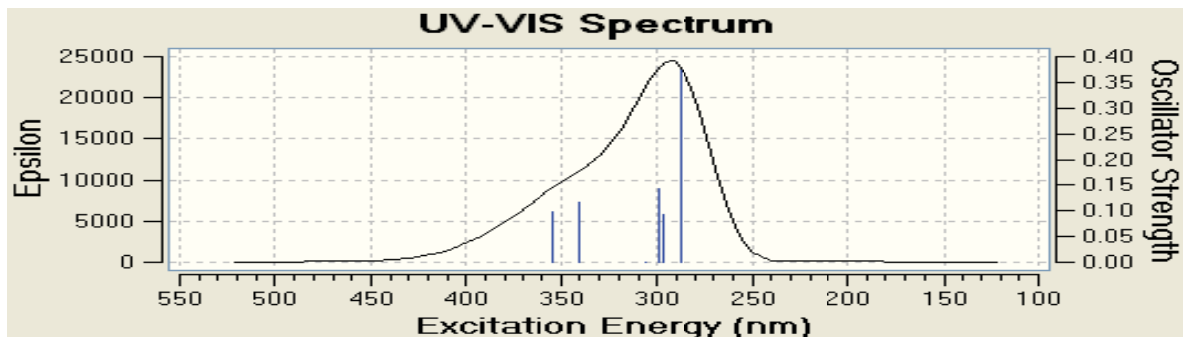


Fig.1. Theoretical UV spectra of Lemofloxacin derivatives

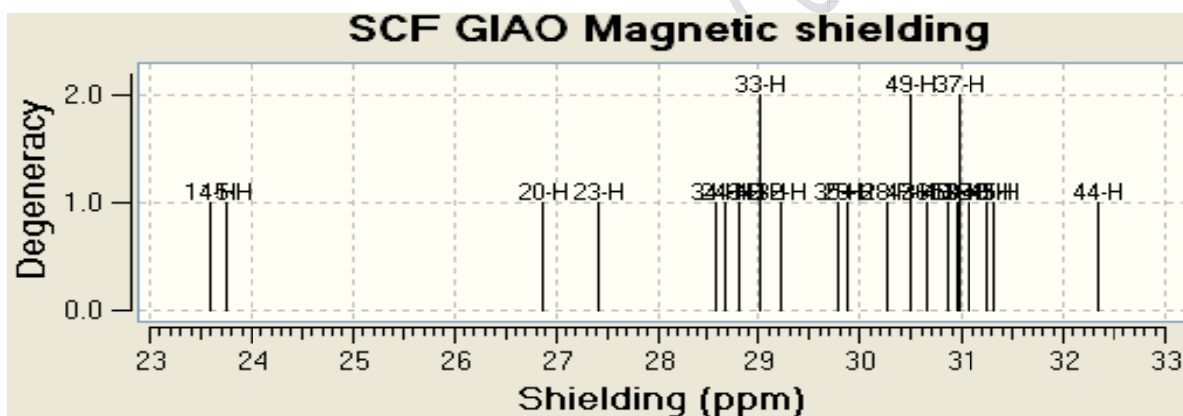


Fig.2. Theoretical spectra of ^1H NMR Lemofloxacin of Fluoroquinolone derivatives

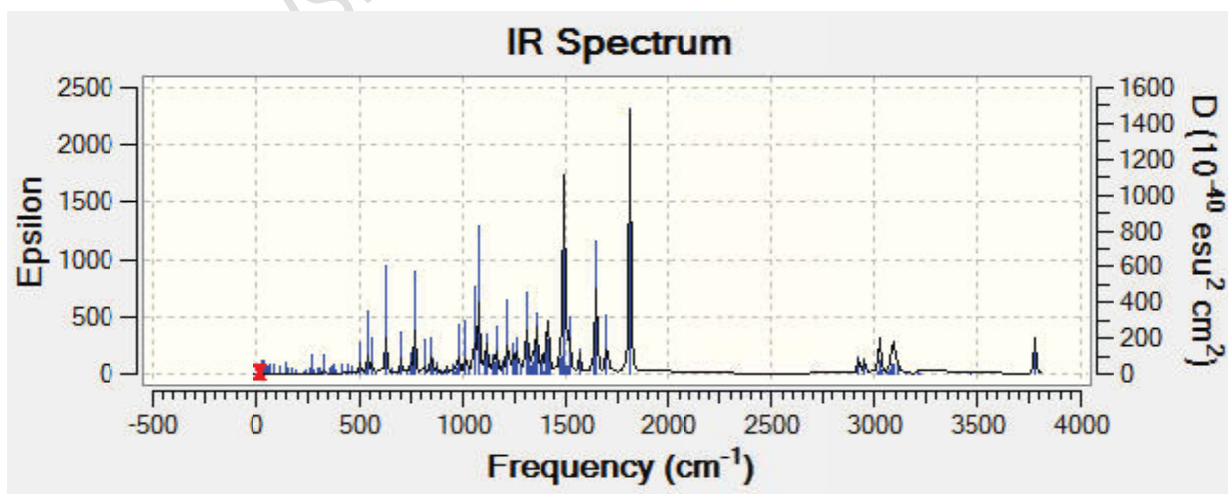


Fig. 3. Theoretical spectra of FT-IR Lemofloxacin of Fluoroquinolone derivatives



Conclusion:

But there are no reports about crystal structures of LMF or forming supramolecules with other organic molecules. Our interest has been directed toward the synthesis of a metal complex based on LMF. The asymmetric unit of the title compound consists of one LMF, one half of 1,4 benzenedicarboxylic acid and one water molecule. The structure has extensive intermolecular and intramolecular hydrogen bonds that consolidate a three-dimensional network. The calculated parameters were compared to experimental characteristic of Ciprofloxacin. Respectively good correlation in the range is 0.9005- 0.9878 between experimental and theoretical spectra was noted.

References:

- [1] Gao, F.; Yang, P.; Xie, J.; Wang, H J. *Inorg. Biochem.* **60** (1995) 61-67.
- [2] Chen, Z.-F.; Xiong, R.-G.; Zhang, J.; Chen, X.-T.; Xue, Z.-L.; You, X.-Z. *Inorg. Chem.* **40** (2001) 4075- 4077.
- [3] Chen, Z.-F.; Xiong, R.-G.; Zuo, J.-L.; Guo, Z.-J.; You, X.-Z.; Fun, H.-K.: *J. Chem. Soc., Dalton Trans.* (2000) 4013-4014.
- [4] M. j. Frisch et al. *GAUSSIAN 03*, Revision C. 01, Gaussian Inc., Wallingford. CT, 2004.



Tautomerization in imide compounds; DFT and NBO studies

A-R.Nekoei*, N. Zakerabbasali, S. Behrouz

Department of Chemistry, Shiraz University of Technology, Shiraz 71557-313, Iran

Email: nekoei@sutech.ac.ir

Keywords: Imide, Imidic acid, Tautomerization, Structure, Intramolecular hydrogen bonding

Introduction:

Imide compounds are similar to amides ($R-CO-NH-R'$), but have an extra acyl group bounded to nitrogen atom. They have lots of applications; for instance, imides are best known as components of high-strength polymers used to make "space suits". Amide molecules, like ketones, show a tautomerism in which their tautomeric form is called imidic acid. From the structural point of view, except that N atom is replaced for the C atom in α position, imides are similar to β -diketones and capable to form an intramolecular hydrogen bonding (IHB) in their imidic acid forms. In this paper structure of imide tautomers, their relative stability and tautomerism have been theoretically investigated by means of DFT and NBO calculations. For more clear comprehension, the results have been compared with the similar substituted β -diketones.

Method of analysis :

All calculations have been performed using GAUSSIAN 03 and NBO 5.0 program packages. The modern density functional theory (DFT) at B3LYP level using 6-31G** and 6-311G** basis sets has been applied for calculations.

Results and discussion:

All possible tautomers for three symmetric molecules of imide category with different substitution R groups (see Figure 1) were fully optimized at B3LYP/6-31G** and B3LYP/6-311G** levels of theory. According to the results of DFT calculations, all studied imides are more stable than their corresponding imidic acids, which is in good agreement with less reactivity of the imides compared to the imidic acids. Although cis-enol forms of β -diketones are generally more stable than their corresponding keto forms, imidic acids (with even a planar chelated ring) are not more stable than their corresponding imides. The chelated rings

of imidic acid forms, like enol forms of β -diketones, are completely planar and their IHB is of type the resonance assisted hydrogen bond (RAHB). According to the results of charge transfer in NBO analysis, the electron delocalization in the chelated ring of the cis-enol forms of β -diketones is much higher than that in the similar imidic acids. Therefore, the IHB in the enol forms of β -diketones is more assisted by resonance than that in imidic acid forms of imide compounds. Although the geometrical parameters for formation of IHB in imidic acids seem to be better than those in the enol form of β -diketones (Table 1), stronger RAHB is the reason for better enol forms of β -diketones compared to imidic acid forms of imides. Also, the NBO analyses indicate that the imide forms are in the better situation than the keto forms of β -diketones. There are some kinds of favorable charge transfer in imides that are absent in the keto forms of β -diketones, for instance, between the lone pair of N (as donor) and the C=O bonds (as acceptor). This is a confirmation for existence of another resonance form of imides, in which the N and O atoms are respectively positive and negative, in the best agreement with the natural charge analyses. Also it has been shown that the atom N prefers to have simple bonds (pyramidal structure) despite double bond. All these reasons show that the imide forms are more stable (less reactive) than the imidic acid forms. Also substitutions at R position have a very important effect on stability of each form and therefore could affect the tautomerism in imide compounds, which are investigated in detailed.

Conclusion:

Imide forms are more stable than the imidic acid forms, because of the higher total bond energies, and also having an extra resonance form. The relatively strong IHB in the imidic acid forms could not make these forms to predominate, because the electron delocalization in their chelated rings is much less than corresponding values in the enol forms of similar β -diketones.

Table 1: Some calculated parameters related to IHB strength for similar R substituted Acetylacetone (AA) and imide2.

Bond distance(Å)	AA	2
O...O	2.541	2.501
O...H	1.627	1.604
O-H	1.003	1.005
Angle(°)		
OHO	149.1	146.2
OCCO	0.0	0.0
E _{IHB} (kcal/mol)	16.55	16.14

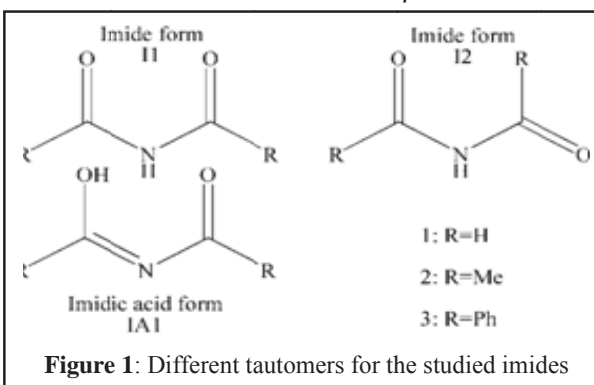


Figure 1: Different tautomers for the studied imides



References:

- [1] J. March “Advanced Organic Chemistry”, Part 1, 4thEd., John Wiley&Sons, Singapore, 2005
- [2] M. A. Fox and J. K. whitesell, “Organic Chemistry”, 3rd Ed., Janes& Bartlett, London, 2004.
- [3] S. F. Tayyari, J. S. Emampour, M. Vakili, A. R. Nekoei, H. Eshghi, S. Salemi, M. Hassanpour, *J. Mol. Struct.* 794, 204-214, 2006.

15th Physical Chemistry Conference



Structure, tautomerism and intramolecular hydrogen bonding of β -ketosulfoxide compounds

A-R.Nekoei*, N. Zakerabbasali, S. Behrouz

Department of Chemistry, Shiraz University of Technology, Shiraz 71557-313, Iran

Email: nekoei@sutech.ac.ir

Keywords: β -Keto sulfoxide, Tautomerism, Molecular structure, Intramolecular hydrogenbonding, DFT, NBO

Introduction:

Many studies have been done on molecular structure of β -diketone(BDK) conformations and the strength of their intramolecular hydrogen bonding (IHB)by theoretical and experimental methods. β -keto sulfoxides (α -sulfinyl ketones), hereafter BKS, also have keto-enoltautomerization and exhibit the IHB in their enol forms. The only difference between BDK andBKS compounds with similar functional groups refers to the sulfur atom.Due to the special characterizations of the sulfur,BKS compounds have particular properties,which affect the tautomeric equilibrium and stability of different conformers. The present paper is an investigation on the molecular structure and relative stability of different tautomers of BKS compounds, and a comparison between their tautomerization and that inBDK compounds.

Method of analysis:

All quantum calculations have been carried out by GUASSIAN 03W and NBO 5.0 program packages applying B3LYP level of DFT method, using 6-31G** and 6-311G** basis sets.

Results and discussion:

All possible conformations for keto and enol tautomers of three different substituted BKS molecules have been investigated. Figure 1 shows the four most important tautomers of target BKS molecules. The B3LYP calculations for all studied compounds show that the E2 enol conformers are not stable and turn into E1 forms under optimization. Also, the relative

stabilities for different tautomers of the target molecules calculated at both B3LYP/6-31G^{**} and B3LYP/6-311G^{**} levels of theory, confirms that the keto forms are more stable even than the cis-enol forms. The NBO analyses (Table 1) show that the negative charge on the atom O linked to the atom S is very high (due to an additional lone pair) and S-O bond order is about 1.26, confirming $ap\pi-d\pi$ bonding between S and O atoms. Therefore these molecules have two canonical forms but the bond is nevertheless localized, despite the resonance. The reason for more stability of the keto forms, compared to the enol tautomers, could be explained by the total bond energies. In the case of BDK, the cis-enol forms are generally more stable due to the strong resonance assisted IHB. In BKS molecules, the chelated ring in the cis-enol (E1) forms is not planar, so the IHB is not strong enough to dominate the bond energies. It is confirmed by comparing some geometrical parameters related to the IHB strength given in Table 2. All DFT and NBO analyses show that different R substitutions have different important effects on the structure, the IHB strength and the stability of the conformers, in such a way that even an enol form of a BKS could be more stable than its keto forms. In this study, all these effects are investigated in detail.

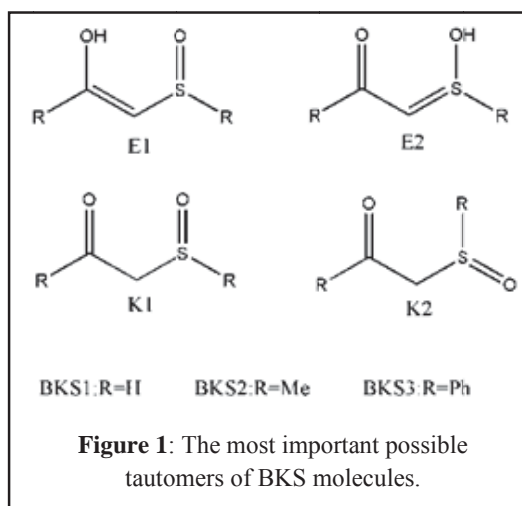
Conclusion:

The DFT calculations show that, despite of BDKs, the keto tautomers of BKS molecules are the predominated forms. The NBO results indicate that this is due to non-planar chelated ring, less strong IHB and less electron delocalization in the chelated ring in their cis-enol forms, compared to those in the same forms of the similar BDK.

Table 1: Some NBO results for two similar molecules of BDK (dibenzoylmethane, DBM) and BKS compounds.

	Bond order				Natural charge			
	C-O	C-S	S-O	S-C	C _α	S	O(linked C)	O(linked S)
DBM	1.77	0.98			-		-0.55	
					0.57			
BKS3	1.77	0.99	1.26	0.87	-	1.21	-0.55	-0.94
					0.63			

	Bond distance(Å)			Bond angle(°)			E _{IHB}
	O...O	O...H	O-H	OHO	OCCO	OCSO	
DBM	2.500	1.569	1.010	150.9	0.0		17.06
BKS3	2.593	1.655	0.997	154.9		14.8	12.56





References:

- [1] K.-L. Han, G.-J. Zhao, "Hydrogen Bonding and Transfer in the Excited State", Vol.I, John Wiley & Sons, UK, 2011.
- [2] J. March "Advanced Organic Chemistry", Part 1, 4th Ed., John Wiley & Sons, Singapore, 2005.
- [3] S. F. Tayyari, J. S. Emampour, M. Vakili, A. R. Nekoei, H. Eshghi, S. Salemi, M. Hassanpour, *J. Mol. Struct.* 794, 204-214, 2006.

15th Physical Chemistry Conference

Determination of Dunham constants and potential energy curves for InH from combined analysis of UV/visible and infrared spectra

E. Ghazizadeh and A. Shayesteh*

School of Chemistry, College of Science, University of Tehran, Tehran, Iran

E-mail: shayesteh@khayam.ut.ac.ir

Keywords: Electronic spectroscopy, Dunham constants, Potential energy curves

Introduction:

Spectroscopic investigations on InH began in 1938, and so far, several electronic transitions involving the $X^1\Sigma^+$ ground state and the low-lying excited states have been observed [1-4]. The $a^3\Pi_0 \rightarrow X^1\Sigma^+$, $a^3\Pi_1 \rightarrow X^1\Sigma^+$ and $A^1\Pi \rightarrow X^1\Sigma^+$ transitions appear near 16200, 16800 and 22000 cm^{-1} , respectively.

Data analysis and results:

We used the experimental data listed in Tables 1 and 2, and determined spectroscopic constants for the $X^1\Sigma^+$, $a^3\Pi_0$ and $a^3\Pi_1$ states of InH by least-squares fitting.

Table 1. Electronic transitions of InH

Transition	v' range	v'' range	Ref.
$a^3\Pi_0 \rightarrow X^1\Sigma^+$	0 to 3	0 to 4	[1]
$a^3\Pi_1 \rightarrow X^1\Sigma^+$	0 to 3	0 to 3	[1,2]

Table 2. Vibration-rotation bands of InH

Electronic state	Infrared bands	Ref.
$X^1\Sigma^+$	$v = 1 \rightarrow 0$	[3,4]
	$v = 2 \rightarrow 1$	
	$v = 3 \rightarrow 2$	
	$v = 4 \rightarrow 3$	
	$v = 5 \rightarrow 4$	

All the observed transition wavenumbers were fitted using the Dunham expression:

$$E(v, J) = \sum_{m=0} \sum_{l=0} Y_{l,m} (v + \frac{1}{2})^l (J(J+1) - \Lambda^2)^m$$

The preliminary equilibrium molecular constants for the low-lying electronic states of InH are listed in Table 3.

Table 3. Preliminary equilibrium molecular constants for InH (in cm⁻¹)

State	T_e	ω_e	$\omega_e x_e$	B_e	α_e
$X^1\Sigma^+$	0	1475.417(1)	25.145(1)	4.996104(9)	0.145319(5)
$a^3\Pi_0$	16277.68 (14)	1458.94(27)	61.13(15)	5.346(2)	0.2796(3)
$a^3\Pi_1$	16947.30(10)	1413.48(29)	42.48(19)	5.478(4)	0.47(1)

The Dunham coefficients $Y_{l,0}$ and $Y_{l,1}$ have been used to determine the RKR potential energy curves for the $X^1\Sigma^+$ ground state and the low-lying excited states of InH molecule. In the next step, potential energy parameters were determined accurately by fitting to all the data using the direct-potential-fit (DPF) [5] approach for $X^1\Sigma^+$ and $a^1\Pi$ states of InH. As a result of fitting the potential energy parameters and the Born-Oppenheimer Breakdown (BOB) correction parameters, the potential energy curves have been determined for the $X^1\Sigma^+$, $a^3\Pi_0$ and $a^3\Pi_1$ states of InH (see Fig 1).

In addition, the equilibrium internuclear distances (r_e) and the equilibrium dissociation energy (D_e) for $X^1\Sigma^+$ and $a^1\Pi$ states of InH have been determined accurately.

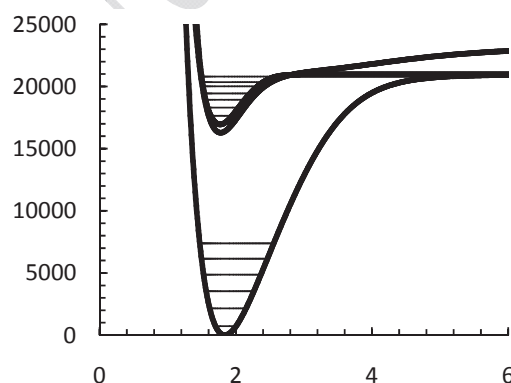


Fig. 1. potential energy functions determined for the $X^1\Sigma^+$ and $a^1\Pi$ states of InH.

References

- [1]. M. L. Ginter, J. Mol. Spectrosc. 11, 301 (1963).
- [2]. H. Neuhaus, Z. Phys. 152, 402 (1958).



- [3]. J. B. White, M. Dulick. And P. F. Bernath, J. Mol. Spectrosc. 169, 410-420 (1995).
- [4]. F. Ito, T. Nakanaga, H. Takeo, K. Essig, and H. Jones, J. Mole. Spectrosc. 169, 421-426 (1995).
- [5]. R. J. Le Roy and Y. Huang, J. Mol. Struct.: THEOCHEM 591, 175 (2002).

15th Physical Chemistry Conference



Surface Chemistry

15th Physical Chemistry Conference



The study of mixed micellization of Hyamine and Triton X-100 in water-buthanol mixtures

Zahra.felegari^{a*}

^{a*}Department of Chemistry, Faculty of Basic science, Science and research branch of Islamic azad university, Tehran, Iran. (Zahra.felegari@gmail.com)

Keywords: Mixed micelle, Synergism, Surfactant, Surface tension, Potentiometry

Introduction:

Surfactants are often mixed in water and surfactant mixtures often exhibit features deviating significantly from individual surfactants. To maximize beneficial effects of mixtures over individual surfactants, it is helpful to understand the interactions among surfactants in the mixtures. Surfactants have natural polydispersity in length when they are produced with chain polymerization; therefore, obtaining a pure system requires additional processing and can be more expensive to produce [1-3]. The micelle formation in an aqueous solution is known to be affected by organic additives, and there have been many investigations concerning the effect of organic additives on the cmc of individual surfactant. In this research, we studied the synergistic effect between cationic surfactant (Hyamine) and non-ionic surfactant (Triton X-100) in water/ethanol and water/buthanol mixtures at different percentage of alcohol. Surfactants can either be anionic, cationic, ampholytic (both anionic and cationic), or non-ionic. The type of drug dissolved and the conditions of the target site will dictate the type of surfactant used to carry the medicine. The concentration of the micelle largely influences its properties. There is a finite range in which the micelle will provide maximum utility[2-4]. This critical micelle concentration (cmc) will determine the effectiveness of the delivery. The composition of the surfactant, the target site in the body, and the type of drug to be delivered must be considered in determining the cmc.

Method:

We used potentiometry and surface tension technique. The ion selective electrode sensitive to Hyamine was used for the measurement of the free concentration of surfactant ion in

equilibrium with micelles at different condition. In surface tension used automatic tensiometer for determination of surfactant solution and the ring method were done.

Result:

In the absence of any significant net interaction between surfactant types the ideal theory predicts the cmc of mixture as following:

$$\frac{1}{cmc} = \sum_i \frac{y_i}{\gamma_i^m cmc_i}$$

Where y_1 is the solution mole fraction of the surfactant 1 with critical concentration cmc_1 and cmc_2 . The ideal mixing theory has been successful in explaining the properties of mixtures composed of surfactants with similar chemical structures. In this work the individual surfactant interact and more elaborate analysis is required to gain molecular insight.

Analyzed by using a regular solution theory which introduces an interaction parameter to characterize the interactions between the two surfactant species in the mixed micelle. Interaction parameter is related to the activity coefficients of the surfactants within the micelle by:

$$\gamma_1 = \exp \beta (1 - x_1)^2 \quad \gamma_2 = \exp \beta x_1^2$$

X_1 is the mole fraction of the surfactant 1 in the mixed micelle. The interaction parameter, β , can be evaluated from the following equation:

$$\beta = \frac{\ln(cmc * y_1 / cmc_1 x_1)}{(1 - x_1)^2}$$

The results showed that β (the interaction parameter) is a composite dependent parameter. The additive (alcohol) behaves as co-surfactant at low concentrations and causes a decrease in cmc while behaves as co-solvent at higher concentrations and cause an increase in cmc by decreasing in hydrophobicity of solvent. The excess free energy of mixed micellization as a function of system composition shows a non-symmetric shape, which is contrary to Regular Solution Theory[3-5].



Conclusion:

Recently, Rosen has proposed a new approach for determination of maximum synergism in mixed micelle formation. According to Rosen approach, the maximum synergism is occur at $x_1=y_1$ (x_1 = molar fraction of surfactant in mixed micelle, y_1 molar fraction of surfactant in solution) . Plot of evaluated x_1 versus y_1 shows a curve that its intersection with the line $x_1 = y_1$ gives the maximum synergism. the observed maximum synergism were obtained from $x_1=0.25$ to $x_1=0.35$ at different concentration of butanol.

References:

- [1] Shimizu, S., Augusto, P., Pries, R., Watson, L. and Sexid, E., 2004, "Thermodynamics of micellization of cationic surfactants in aqueous solutions: consequences of the presence of the 2-acylaminoethyl moiety in the surfactant head group", Colloid Polym. Sci., Vol. 282: 1026-1032.
- [2] Gharibi, H., Javadian, A. S., Hashemianzadeh, A. M., 2004, "Investigation of interaction of cationic surfactant with HSA in the presence of alcohols using PFG-NMR and potentiometric technique Colloids and Surfaces A", Physicochem. Eng. Vol. 232, pp. 77-86.
- [3] Bhattacharyya, K., Das, C., 2003, "Modeling the Variation of Surfactant Tension with Composition for Binary Liquid Mixtures", Chem. Phys. Letters, Vol. 374:676-683.
- [4] Azizian, S., Hemmati, M., 2003, "Surface Tension of Binary Mixtures of Ethanol + Ethylene Glycol from 20° C to 50° C", J. Chem. Eng. Data., Vol. 48: 662-663.
- [5] Pellicer, J., Garcia, V., 2003, "On the Experimental Values of The Water Surface Tension Used in Some Textbooks", Am. J. Phys., Vol. 70: 705-709.



Equilibrium biosorption isotherm for neutral red on persimmon leaf

Ghazaleh Koutchakzadeh

Department of chemistry , Science Faculty , Islamic Azad University ,Khorramabad Branch , Khorramabad ,
Iran

Email:gh_kouchakzadeh@yahoo.com.

Keywords : Biosorption , Neutral red , Persimmon leaf , Langmuir isotherm

Introduction:

Dyes are widely used in industries such as textile, rubber, plastic, cosmetic etc. [1]. Dyes released by a wide variety of sources, and have adverse effects on living organisms [2]. Different methods have been applied for purification purposes including mechanical, physical, chemical and biological [3]. Adsorption process is one of the effective methods for removal of dyes from wastewater.

Since one of the best and cheapest adsorbents is tree leaves, we used an inexpensive adsorbent such as persimmon leaf. The goal of present work was to test the ability of persimmon leaf for biosorption of neutral red from aqueous solutions. Adsorption equilibrium data were correlated with the Langmuir and Freundlich isotherms.

Materials and Methods:

Neutral red was purchased from Merck. The concentration of neutral red solution was 20 to 45 mg/l. The concentration of colouring matter in each sample was determined by calibration plots drawn by recording the absorbance of dye at different concentrations. All measurements were made at λ_{max} (490 nm) on a JENWAY UV-Vis spectrophotometer (model 6505).

Persimmon leaf as adsorbent produced from local trees. Persimmon leaves were washed with double distilled water and dried, then ground to get powder.

Result and Discussion:

The results of biosorption showed uptake of dye increased quickly until 10 min, then the change became slow. Then, suitable persimmon leaf dose was determined 0.1 g adsorbent in

20 ml dye solution. After determining adsorbent dose and biosorption time, we studied removal dye in different concentrations, Then equilibrium data were corresponded with the Langmuir and Freundlich isotherms.

The isotherms fit the Langmuire equation (1) and Freundlich equation (2) .

$$\frac{1}{q_e} = \frac{1}{qb} \left(\frac{1}{C_e} \right) + \frac{1}{q} \quad (1)$$

$$\log q_e = \log K_f + \frac{1}{n} \log C_e \quad (2)$$

Where C_e is the equilibrium concentration of the adsorbate (mgL^{-1}), q_e is the amount of adsorbate adsorbed per unite mass of adsorbent (mgg^{-1}), q and b are Langmuir constants related to adsorption capacity and rate of adsorption, respectively and K_f and n are the Freundlich constants [4].

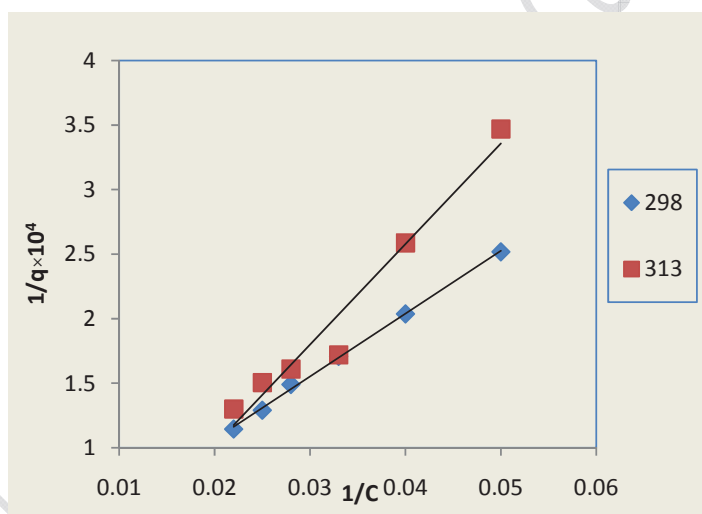


Figure 1. Plot of $1/q_e$ vs. $1/C$ neutral red (Langmuir equation)

Conclusion:

Persimmon leaf is able to adsorb neutral red from aqueous solutions very well, for example, dye removal efficiency at the initial dye concentration of 30 mg/l was calculated 94% after about 10 min. The experimental data were corresponded with Langmuir and Freundlich isotherms, thus standard deviation correlation coefficient for fitting the Langmuir equation were better than Freundlich equation. In this study, adsorption decreased with increasing temperature, thus this process may be exothermic.



References

- [1] S. Saiful Azhar and et al. "Dye Removal from Aqueous Solution by using Adsorption on Treated Sugarcane Bagasse"; American J.of Applied Sciences, 2(2005),1499-1503.
- [2] Y. M. Slokar,M.Le Marechal, " dye pigment" 37 (1998) 335-356.
- [3] M. abbasi, N. Razzaghi Asl, J. Hazard. Mater. 153 (2008) 942-947.
- [4] Han,R. et al. "Equilibrium biosorption isotherm for lead ion on chaff"; J. Hazardous Materials,B125(2005),266-271.

15th Physical Chemistry Conference



Study of surface molar area of component in organic binary mixtures

E. Ghasemian*, E. Karegar, R. Zobeidi

Faculty of Science, Ilam University, Ilam, Iran

Email: Eghasemian@ymail.com

Abstract:

Surface tension is a physical property that examines theoretical and experimental. More theories that used for calculation of surface tension; use the value of the molar surface area of the compounds as input data. So long as the molar surface area can be calculated from different models, it is the mean source of error to apply these theoretical models. In the present work, partial surface molar areas in binary organic mixtures using experimental density of solution were calculated and variations of partial surface molar area versus composition were studied.

Keywords: surface molar area, organic binary mixtures, surface tension, density

Introduction:

Surface tension is one of the most useful thermophysical properties that have been widely used to characterize surfaces of liquids in chemistry and chemical engineering areas such as the manufacturing of plastics, coatings, textiles and films. Surface tension is defined as the energy needed in bringing a liquid molecule to the surface for formation and maintaining the surface area in equilibrium, which is represented by surface free energy per unit surface area in thermodynamics [1,2]. In the present work, partial surface molar area in binary organic mixtures using experimental density of solution was calculated and variations of partial surface molar area versus composition were studied.

Results and discussion:

In this study three equations with our new method have been used to calculate of surface molar area and partial surface area. In our method, partial molar volume is important and necessary parameter to calculate partial surface molar area. Application of different equation to calculate surface molar area.



We tested the HSIS theory [3], which is based in Guggenheim's ideal solution equation [4]. It assumes that, the bulk liquid and the surface layer, form ideal solutions and it must be applied when the size of the molecules in the mixture is similar. Also HSEG[5] and sprow-prousnits[6] model have been used to prediction of surface tension based on our new method to calculate surface molar area. In next view we are going to extrapolate surface molar area from experimental surface tension data.

References:

- [1] C. A. Miller and P. Neogi, Interfacial phenomena: equilibrium and dynamic effects, Marcel Dekker, Inc., New York (1985).
- [2] J. Lykema, G. J. Fleer, J. M. Kleijn, F. A. M. Leermakers, W. Norde and T. Van Vliet, Fundamentals of interface and colloid science, volume III: Liquid-fluid interfaces, Academic Press (2000).
- [3] J.H. Hildebrand, R.L. Scott, Solubility of Nonelectrolytes, Reinhold Pub. Corp., New York, 1950.
- [4] E.A. Guggenheim, Mixtures, Oxford University Press, London, 1950, Chapter 9.
- [5] R.L. Schmidt, J.C. Randall, H.L. Clever, J. Phys. Chem. 70 (1966) 3912–3916.



Applying a new correction in Jouyban-Acree model to prediction of organic binary mixtures surface tension

E. Ghasemian*

Faculty of Science, Ilam University, Ilam, Iran

Email: E.ghasemian@ymail.com

Abstract:

In this research the basic solution model, i.e. the combined nearly ideal binary solvent-Redlich-Kister equation by Acree was used to prediction of surface tension on some organic binary mixtures by applying new correction. In this new correction, we calculate activity of components using UNIFAC equation and combined with Jouyban-Acree model. The accuracy of the model was evaluated by calculation mean relative standard error (MRSD).

Keywords: surface tension, organic binary mixtures, Jouyban-Acree model, activity

Introduction:

Surface tensions of liquid mixtures are important physicochemical properties which affect mass and heat transfer in solutions. The mass and heat transfer in solutions influence many and availability of the related data should be helpful in designing and engineering of such processes. However, in most of the cases different blends of solvents are used. It has been observed that physicochemical properties in mixture of solvents show deviation from ideal mixing. Thus, finding a suitable blend of solvents for a desired amount of physicochemical property requires some experimental determinations or accurate models. One of the most accurate mathematical models for the correlation of physicochemical properties in a mixture of solvents is the Jouyban-Acree model [1-4]. But in this research the Jouyban-Acree model was used to prediction of surface tension on some organic binary mixtures by applying new correction. In this new correction, we calculate activity of components using UNIFAC equation and combined with Jouyban-Acree model. The accuracy of the model was evaluated by calculation mean relative standard error (MRSD).

Results and discussion:

In the present work, we used reported experimental surface tensions for Surface tension of binary mixtures of alkyl acetates (butyl, pentyl, hexyl) with polar solvents (1,4-dioxane, DMF), nonpolar solvents (benzene, toluene, heptane) and protic solvents (methanol, ethanol, propanol, 2-propanol). Then we carried out comparisons between experimental surface tension and predicted surface tension from Jouyban-Acree model equation. We used the UNIFAC theory to calculate of the activity coefficients for the components in both the bulk and interface and replaced activity of component(eq.2) instead of mole fraction as shown as following equations.

$$\ln \sigma = x_1 \ln \sigma_1 + x_2 \ln \sigma_2 + J_0 \left[\frac{x_1 \cdot x_2}{T} \right] + J_1 \left[\frac{x_1 \cdot x_2 \cdot (x_1 - x_2)}{T} \right] + J_2 \left[\frac{x_1 \cdot x_2 \cdot (x_1 - x_2)^2}{T} \right] \quad (1)$$

$$\ln \sigma = x_1 \ln \sigma_1 + x_2 \ln \sigma_2 + \left[\frac{a_1 \cdot a_2}{T} \right] + \left[\frac{a_1 \cdot a_2 \cdot (a_1 - a_2)}{T} \right] + \left[\frac{a_1 \cdot a_2 \cdot (a_1 - a_2)^2}{T} \right] \quad (2)$$

calculated values of MRSD, has been shown that the proposed method can be apply to estimate the surface tension for the binary systems studied in this work.

References:

- [1] A. Jouyban, A. Fathi-Azarbayjani, M. Khoubnasabjafari and W. E. Acree Jr., Indian J. Chem.-A, 44, 1553 (2005).
- [2] A. Jouyban, M. Khoubnasabjafari, Z. Vaez-Gharamaleki, Z. Fekari and W. E. Acree Jr., Chem. Pharm. Bull., 53, 519 (2005).
- [3] A. Jouyban, A. Fathi-Azarbayjani and W. E. Acree Jr., Chem. Pharm. Bull., 52, 1219 (2004).
- [4] A. Jouyban, A. F. Azarbayjani, M. Barzegar-Jalali and W. E. Acree Jr., Pharmazie, 59, 937 (2004).
- [5] Gmehling, J., Li, J., Schiller, M., Ind. Eng. Chem. Res., 32, 178(1993).
- [6] Amir Abbas Rafati *, Ensieh Ghasemian, J. Colloid Interface Sci. 328 (2008) 385–3907.
- [7] Amir Abbas Rafati *, Ensieh Ghasemian, J. Chem. Thermodynamics 41 (2009) 386–391
- [8] Amir Abbas Rafati,* Ensieh Ghasemian, and Hossein Iloukhani, J. Chem. Eng. Data 2008, 53, 1944–1949



Study of thermodynamic dye removal from solutions by using biosorbent

Zeinab Pourghobadi^{*a}, Roghiyeh pourghobadi^b

^aDepartment of Chemistry, Faculty of Science, Branch Khorramabad, Islamic Azad University, Khorramabad, Iran

^bEducation Organization, Khorramabad, Lorestan, Iran

Email: zpourghobadi@gmail.com

Keywords: Adsorption, Longmirisotherm, Acid orange 7, Removal, Thermodynamic, Biosorbent

Introduction:

Dyes are one of the major constituents of the wastewater produced from dye stuff manufacture and some similar industries, which poses a severe threat to the surrounding ecosystem because many of the dyes are extremely toxic (1-3). There are a lot of ways that dyes and pigments removal from solution. In this research, the suitability of the *Platanus* for Acid orange 7 adsorption was assessed.

Materials and Methods:

In the equilibrium adsorption experiment, 0.6 g of adsorbents were added into 50 ml of dyes aqueous solutions with different concentrations. Then, the samples were placed in shaker for 90 min to reach equilibrium. The final concentration of dye in the solution was analyzed by the UV-Vis spectrophotometer at 492 nm. The adsorption capacity at equilibrium, $q_e = (C_0 - C_e)V/M$ where C_0 and C_e (mg L^{-1}) are the liquid-phase concentrations of dye at initial and equilibrium, respectively. V is the volume of the solution (L) and W is the mass of dry adsorbent used (g).

Dye solution preparation:

Solution of Acid orange 7 was prepared in double distilled water. Its concentration was determined by using absorbance values measured before and after the treatment, at 492 nm with JENWAY UV-Vis spectrophotometer (Model 6505).

Results and Discussions:

We investigated effect of pH and amount of adsorbent for removal dye from solution. The adsorption of dye was increased at 2-10 pHs then it was constant in 3-5 pHs but decreased in 5-10 pHs. the adsorption of acid orange7 was optimum at the pH = 5 for all studies. Then we investigated amount of adsorbent. As the adsorbent dose increases, available sites for dye molecules also increase and consequently better adsorption takes place. We studied amount of 0.2-1g of adsorbent in 60 mg L⁻¹ dye solution. the maximum adsorption was at 0.6g adsorbent mass for removal dye from solution.

Conclusion:

The present study shows that Platanus is an effective adsorbent for removal dye solution. The optimum PH for adsorption was found to be up 5. The adsorption isotherm of Acid orange7, was fitted by Langmuir model.

biosorbent	$\frac{T}{K}$	K	R ²	ΔG° Jmol ⁻¹	ΔH° Jmol ⁻¹	ΔS° Jmol ⁻¹ k ⁻¹
Platanus	298	6.43	0.955	-4610.89	49662.8	19.65

Table 1. Values of thermodynamic parameters for the adsorption acid orange 7 on Platanus

Where K is equilibrium constant, ΔH° is heat of adsorption, R is gas constant and T is temperature. From slope of equation, ΔH° in adsorption dye by Platanus was calculated 49.7KJ/mol. We can say the positive value of indicated the endothermic nature of the adsorption. The positive value of ΔS° showed the affinity of the Platanus for acid orange 7 and the increasing randomness at the solid-solution interface during the adsorption process. The negative values of ΔG° indicated the feasibility of the process and the spontaneous nature of the adsorption (Table.1).

Reference:

- [1] W. Yang, et al., "Colloids and surfaces A: Physicochem", Eng. Aspects 312 (2008) 118.
- [2] Han. R. et al., "Biosorption of copper and lead ions by waste beer yeast", Journal of Hazardous B 137. 1569-1576, 2006.



[3]N.A.Adesola and etal;"Isotherm and thermodynamic studies of biosorption of Cd(II) from solutions by maize leaf",International journal of physical sciences;Vol2(8) ,207-211,2007

15th Physical Chemistry Conference



Kinetic survey and thermodynamic modeling of reduction COD sewer by adsorbents: in methanol unit of Fanavaran petrochemical company

Z. Saadati^{a,*}, S. Mashaiekh^a

^a Department of Chemistry, Islamic Azad University, Omidiyeh Branch, Omidiyeh, Iran

Email : zohrehsaadati@gmail.com

Key words: Adsorption; Activated carbons; COD removal; Wastewater treatment; Rice husk

Introduction:

Adsorption technology is currently being used extensively for the removal of organic and inorganic micro pollutants from aqueous solutions. Petrochemical industries generate large quantities of wastewater, which are very toxic and difficult to be disposed by physical, chemical and microbiological methods. Petrochemical wastewater is characterized by high chemical oxygen demand (COD is resistant to conventional wastewater treatment). Activated carbon has been widely used in wastewater treatment to remove organic and inorganic pollutants. Possessing high surface area, activated carbon frequently exhibits high removal efficiency for most dissolved compounds. Activated carbon is expensive; therefore, development of low cost alternative adsorbent has been the focus of recent research. A number of workers have used different materials as the adsorbent for the removal of different pollutants [1-2].

Materials and methods:

The pH of the test solutions was adjusted using reagent grade dilute sulfuric acid and sodium hydroxide. Rice husk was cleaned and thoroughly washed with distilled water and dried. It was treated with acetic acid and again washed with distilled water. COD was measured for both the wastewater and blank samples, and the two were compared. The oxygen demand in the blank sample was subtracted from the COD for the original sample to ensure a true measurement of organic matter. In the present investigations, COD (mg/L) was determined using the Eq. (1)



$$\text{COD} = \frac{(b-a) \times (N) \text{ of ferrous ammonium sulfate } (100) \times (8)}{\text{Volume (ml) of sample}} \quad (1)$$

Results and Discussion:

These studies had been carried out for pH range of 2.0 to 12. It was found that the extent of adsorption for adsorbents rice husk and activated carbon was higher in alkaline medium than acidic medium the maximum adsorption capacity for adsorbents rice husk and activated carbon was observed at pH 8. Rice husk and activated carbon were studied for different contact time with fixed adsorbents dose at fixed pH and temperature (25°C). Increase in time has significant effect on the adsorption of adsorbents.

The adsorptions of adsorbents were analyzed by models given by Langmuir and Freundlich. These isotherms are given as :

$$\frac{1}{q_e} = \frac{1}{Q_o} + \frac{1}{bQ_o C_e} \quad (2)$$

$$\text{Log } q_e = \text{log } K_f + (1/n) \text{ log } C_e \quad (3)$$

In order to evaluate the adsorption kinetics of adsorbents, two different kinetic models, the pseudo first order and the pseudo second order, were applied to the experimental data. A linear form of pseudo-first-order model was described by Lagergren [3] in the form:

$$\log(q_e - q_t) = \frac{\log q_e - k_1 t}{2.303} \quad (4)$$

Ho and McKay presented the pseudo-second-order kinetic equation [4] as

$$\frac{t}{q_t} = \frac{1}{k_2 q_e^2} + \frac{1}{q_e} t \quad (5)$$

Conclusions:

The adsorption data followed pseudo-first order kinetics for both adsorbents. Equilibrium isotherms were well described by the Freundlich equation. The present study suggests that rice husk is attractive low-cost natural adsorbents for removal of COD and other pollutants from industrial wastewaters.

Reference:

[1] Jain A K, Gupta V K, Bahtnagar A & Suhas, Utilization of industrial waste products as adsorbents for the removal of dyes, J Hazardous Mat, 101 (2003) 31-42.



- [2] Mohan D, Singh K P, Vinod K S. Wastewater treatment using low cost activated carbons derived from agricultural byproducts, *J Hazardous Mat* 152 (2008) 1045–1053.
- [3] S. Lagergren, Zurtheorie der sogenannten adsorption gelöster stoffe, *Kungliga Svenska Vetenskapsakad, Handl.* 24 (1898) 1–39.
- [4] Y.S. Ho, G. McKay, Pseudo-second-order model for sorption processes, *Process Biochem.* 34 (1999) 451–465.

15th Physical Chemistry Conference



Thermodynamic of the Co (II) adsorption onto silica aerogel-activated carbon nano composites from aqueous solutions

M. Shoogerdzadeh^a, Z. Saadati^{a,*}, M. Hosseiny

^a Department of chemistry, Islamic Azad University, omidiyeh Branch, omidiyeh, Iran

Email: zohrehsaadati@gmail.com

Key words: Co (II), Nano composite, isotherm, Adsorption, silica aerogel

Introduction:

The presence of heavy metals in aqueous solution beyond certain limit creates serious threat to the environment due to their non-degradability and toxicity. Cobalt is present in mining, electronics, metallurgical, electroplating and paint industries. Cobalt as a pollutant has many toxic effects such as imparting neurotoxicological disorders, genotoxicity, carcinogenicity, cardiomyopathy and bronchial asthma [1]. Nano composite in this study consists of two phases of silica aerogel and activated carbon. active carbon has high surface area, porous structure and functional group has been the most popular and widely used adsorbent in water treatment technology all over the world [2]. Aerogel is composed of a series of particles in the nanometer range in a network With three-dimensional arrangement and have covalent bonds together. This material is very porous and very large specific surface [3]. The objective of this study was to investigate the possible use of silica aerogel-activated carbon nano composites as an alternative adsorbent material for the removal of Co^{2+} cations from aqueous solutions.

Materials and methods:

1000 mg/l standard stock solutions prepared from $\text{Co}(\text{NO}_3)_2 \cdot 6\text{H}_2\text{O}$ salt in double distilled water. The pH of the solutions was adjusted using various concentrations of H_3BO_4 , $\text{C}_6\text{H}_8\text{O}_7$ and $\text{Na}_3\text{PO}_4 \cdot 12\text{H}_2\text{O}$. All the used chemicals were of Analytical grade. 20 mL $\text{Co}(\text{NO}_3)_2 \cdot 6\text{H}_2\text{O}$ solution (pH= 6) with known concentration was added to 0.1g adsorbent synthesized by hydrothermal method. The solution was stirred on a magnetic stirrer for 1.5 h. Then the solution was centrifuged, filtered and the filtrate absorbance was measured.

Apparatus:

pH measurements were made using a digital pH meter (ATC model GP 353). Absorbance measurements of metal ions were recorded using a Perkin-Elmer Spectrum model AAnalyst300

Result and discussion:

The adsorption isotherm data were analysed with Langmuir and Freundlich isotherms. Results obtained showed that the adsorption data fitted best to the Langmuir adsorption isotherm (Table 1).

Table 1. Langmuir, Freundlich and Temkin constants for adsorption of Co^{2+} onto nano composites

Langmuir adsorption isotherms constants		
Q_0 (mg/g)	K (L/mg)	R^2
0.804	0.653	0.989
Freundlich adsorption isotherms constants		
k_f (mg/g)	n	R^2
0.323	2.532	0.986
Temkin adsorption isotherms constants		
k_T (L mg^{-1})	B (J mol^{-1})	R^2
6.926	0.172	0.982

The temperature range used was from 35 to 65 °C. Adsorption increased with increase in temperature. Thermodynamic parameters, standard free energy change (ΔG°), enthalpy change (ΔH°) and entropy change (ΔS°) were calculated and are shown in Table 2. The adsorption process is endothermic in nature and negative values of ΔG° showed the spontaneous adsorption of Co (II) on the adsorbent.

Table 2. Thermodynamic parameters for the adsorption of Co(II)

T(K)	K_d	ΔG° (J/mol)	ΔH° (J/mol) ^o	ΔS° (J/mol K)
308	121.716	-12183.033		
323	168.098	-13587.018	16645.459	93.599
338	227.503	-14991.003		



Conclusion:

The silica aerogel-activated carbon nano composites were found to be suitable adsorbent for the removal of Co(II) from aqueous solution. The experimental data showed good fit to the Langmuir isotherm model. Thermodynamic investigations indicate that the adsorption reactions are spontaneous, endothermic and irreversible.

Reference:

- [1] K. Anoop Krishnan, T.S. Anirudhan., Kinetic and equilibrium modeling of cobalt(II) adsorption onto bagasse pith based sulphurised activated carbon. Chemical Engineering Journal 137 (2008) 257–264
- [2] Huang, L., Sun, Y.Y., Yang, T., Li., Adsorption behavior of Ni (II) on lotus stalks derived active carbon by phosphoric acid activation. Desalination 268 (2011) 12-19.
- [3] S. Marzouk, F. Rachdi, M. Fourati, J. Bouaziz, Synthesis and grafting of silica aerogels, Colloids and Surfaces A 234 (2004) 109-116.



Thermodynamic and kinetic study of adsorption Direct red 81 on sonchus arvensis

M.M.Heravie^{a*}, Z.Abbasiyoun^a, A.Morsaly^a, T.Ardalan^b

^a Department of chemistry, Faculty of sciences, Islamic Azad university, mashhad branch, Iran

^b Department of chemistry, Faculty of sciences, Islamic Azad university, mashhad, branch Iran, yang
reasercher club

Email: Abasion.zari@gmail.com

Key words: Direct dye, Sonchus, Adsorption, Kinetic, isotherm, Thermodynamic

Introduction:

The textile industry plays a part in the economy of several countries around the world. Dyeing is a fundamental operation during textile fiber processing. Disposal of this colored water into receiving water can be toxic to aquatic life and it is toxic for human. Adsorption has been found to be superior techniques for waste water treatment. This study investigates the use of activated carbon prepared from souchus arvensis as a local low cost, high efficiency, ecofriendly adsorbent and available in IRAN for the removal of direct red dye from aqueous solution. A series of experiments were conducted in a batch system to assess the effect of the system variables, ie. temperature, initial dye concentration, adsorbent dosage and contact time, model Langmuir and Freundlich isotherms, adsorption kinetic data and thermodynamic parameters were tested[1-3].

Material and methods:

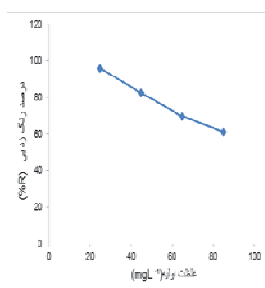
Direct red 81 dye, a product of germany sigma alderich company. A stock solution of 1000 mg/L were prepared by dissolving the required amount of dye in double distilled water. Working solutions of the desired concentrations were obtained by successive dilutions of the stock solution. The tools have been applied for adsorption thechnique were suitable. experiments were conducted in a batch system of VS-1907W and The concentration of the dye was determined using UV spectrophotometer by Perkin Elmer lambda 25. The formoula of adsorption:

$$\% \text{Removal of dye} = (C_0 - C_e) 100 / C_0$$

$$q_e = (C_0 - C_e) \cdot V / W$$

Result and discussion:

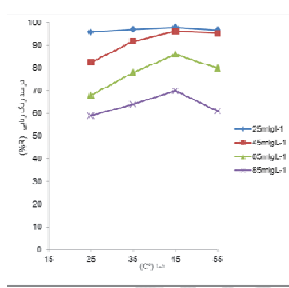
The results showed that the percentage of dye removal increased as the amount of adsorbent increased but it decreased with the increase in initial dye concentration¹ and solution temperature up 45° C. The Maximum dye decolorizing was 98% and It was observed at temperature of 45° C². The biosorption followed pseudo second order kinetic³, model langmuir⁴ was used to analyze the equilibrium data. In addition, various thermodynamic parameters have been calculated. The biosorption process was found to be spontaneous process.



1: $C_0 = 25, 45, 65, 85$

M=0/1 gr

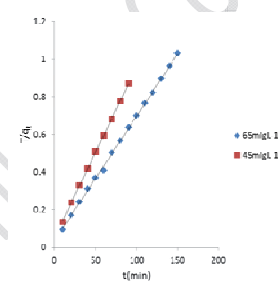
T: 25° C



2: $C_0 = 25, 45, 65, 85$

M=0/1 gr

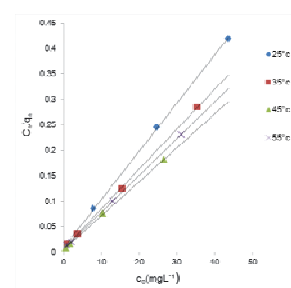
T: 25, 35, 45, 55 ° C



3: $C_0 = 45, 65$

M=0/1 gr

T: 25° C



4: $C_0 = 25, 45, 65, 85$

M=0/1 gr

T: 25, 35, 45, 55 ° C

Conclusion:

The experimental studies concludes that the activated carbon prepared from sonuchus fruit could be employed as low -cost, high potential and an effective adsorbent as alternatives to commercial activated carbon for the removal of direct red 81 from aqueous solution and for the removal of color, ingeneral.

References:

[1] A.Nevine Kamal; "Removal of direct blue-106 dye from aqueous solution using new activated carbons developed from pomegranate peel: adsorption and Kinetics"; Journal of Hazardous materials, 2008, HAZMAT-8908; No of Pages 11.



- [2] D.Suteu ; and D.Bilba: "Equilibrium and kinetic study of reactive dye Brilliant red HE-3B Adsorption by Activated charcoal . Actachim.slov.2005 ,52:73-79.
- [3] A.Nevine Kamal ; "removal of reactive dye from aqueous solutions by adsorption on to activated carbons prepared from sugarcane bagasse pith"; De salination 223(2008)152-161

15th Physical Chemistry Conference



Preparation of Poly Phosphoric Acid Impregnated on Silica Gel (PPA-SiO₂) and study of its activity for the Synthesis of 1,2,4,5-Tetrasubstituted Imidazoles

P. Vahedian^a, M. Khoddadi^b

^aDepartment of Chemistry, Qaemshahr Branch, Islamic Azad University, Qaemshahr, Iran, Email: ^bDepartment of Chemistry, Tonekabon Branch, Islamic Azad University, Tonekabon, Iran.

parisa.vahedian@gmail.com

Key words : Multicomponent reactions , tetrasubstituted imidazoles , poly phosphoric acid supported silicagel

Introduction:

Multi-component, one-pot reactions are highly important because of their wide range of application in pharmaceutical libraries for drug discovery. In five-membered heterocycles, imidazoles moiety is present in a wide range of naturally molecules and uses in preparation of fungicides, herbicides. [1-3] in recent years solid-supported reagent, such as silica gel supported acids, could be used as a multipurpose acid catalyst. [4-5] in this study we uses of PPA-SiO₂ as solid acid catalyst and use of microwave irradiation.

Method:

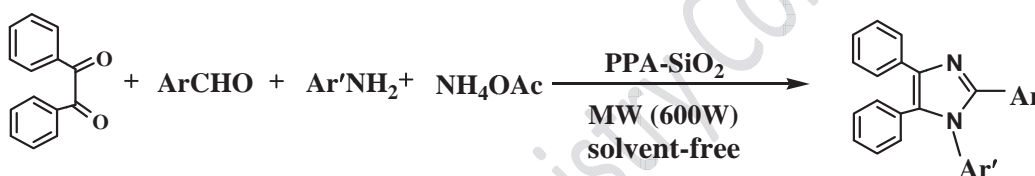
PPA-SiO₂ was prepared by the method similar to the Aoyama and coworkers [6] , PPA (2.1g) was charged in the round-bottom flask and CHCl₃ (100ml) was added. the mixture was stirred at 50°C for 1h, SiO₂ (200-400 mesh, 4.9g) was added to the solution and mixture was stored for another 1h. The CHCl₃ was removed with rotary evaporator and the resulting solid was dried in vacuum at r.t for 3h.

Results and discussion:

In this paper we decided to investigate the efficiency of PPA-SiO₂ as solid acid catalyst in the synthesis of 1,2,4,5- tetrasubstituted imidazoles under microwave irradiation conditions. To initiate our study, in order to optimize the reaction condition, the one-pot synthesis of 1,2,4,5-

tetraphenyl imidazole was used as a model reaction. the reaction was carried out by microwave irradiation a mixture of benzil, benzaldehyde, aniline and ammonium acetate under various amount of PPA-SiO₂ as catalyst under solvent-free and microwave irradiation condition at 600w. PPA-SiO₂ carried the reaction out by adsorption and the catalyst is necessary for the reaction, increasing the amount of the catalyst, increased the yield of the product. The optimal amount of PPA-SiO₂ was 10 mg, after this, increasing the catalyst did not increase the yield noticeably .

The reusability of the catalyst was checked by the same model reaction under optimized conditions. After completion of the reaction, the catalyst was filtered under hot condition, washed ethanol, dried and reused for the same reaction process. the catalyst could be reused at least four times with only slight reduction in the catalyst activity of the catalyst.



Conclusion:

In summary, we have successfully developed a very simple, mild and efficient methodology For the preparation of a wide variety of tetrasubstituted imidazoles through one-pot multicomponent reaction of benzil, aromatic aldehyde, primary amines and ammonium acetate employing PPA-SiO₂ as the recyclable solid acid catalyst under solvent-free and microwave irradiation condition for the first time. Other advantages of this protocol are high yields, short reaction time , easy work-up and omitting any volatile and hazardous organic solvents.

References:

- [1] Sunderhous J. D., Martin S. F. *Chem. Eur. J.*, 15: 1300 (2009)
- [2] Caddick S., *tetrahedron*, 51: 10403 (1995).
- [3] Lewis J. R., *Na. Prod. Rep.*, 29: 223 (2002).
- [4] A. Davoodnia, M. M. Heravi, Z. Safavi-Rad, N. Tavakoli-Hoseini, *synthetic Communications*, 40, 2588 (2010).



- [5] N. Montazeri, S. Khaksar, A. Nazari, S.S. Alavi, S.M.Vahdat, M. Tajbakhsh, J. Fluorine Chem., 132: 450 (2011)
- [6] T .Aoyama, T. Takido, M. Kodomari, Synlett., 13: 2307 (2004).

15th Physical Chemistry Conference



An experimental study on the surface properties of aqueous solutions of cyclic amino acids

M.H. Ghatee*, H. Ghazipour

Department of chemistry, Faculty of sciences, Shiraz university, 71454, Shiraz, Iran

Email:ghatee@susc.sc.ir

Keywords: Histidine aqueous solutions; Phenylalanine aqueous solutions; Amino acids; Temperature dependent surface tension; Capillary raise method; Surface entropy and energy

Introduction:

Surface tension of human-body protein as the biological fluid solution depends on the surface tension of its constituting components. Proteins are made of amino-acids and their properties and biological activities are determined by the nature and sequencing of amino-acids. The surface properties of these amino acids are important to the structure of proteins and their biological tasks. Thus, surface tension of aqueous solutions of proteinogenic amino acids [1] at the human body temperature range under liquid/vaper equilibrium is importantly must be known. In this paper, the surface tension of L-histidine and L-phenylalanine aqueous solutions are measured experimentally and temperature dependence of their surface thermodynamic properties at different solution concentrations are studied.

Materials and methods:

L-histidine (>99%, Merk) and L-phenylalanine (99%, Merk) were used without additional purification. Solutions were prepared using deionized water. The surface tension of aqueous solutions of histidine and phenylalanine solutions were measured by the capillary rise method [2] using a homemade capillary apparatus shown in Figure 1.

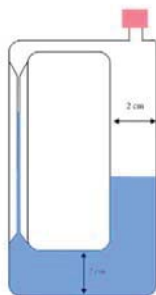


Figure 1. The apparatus for capillary rise measurement.

Results and Discussion:

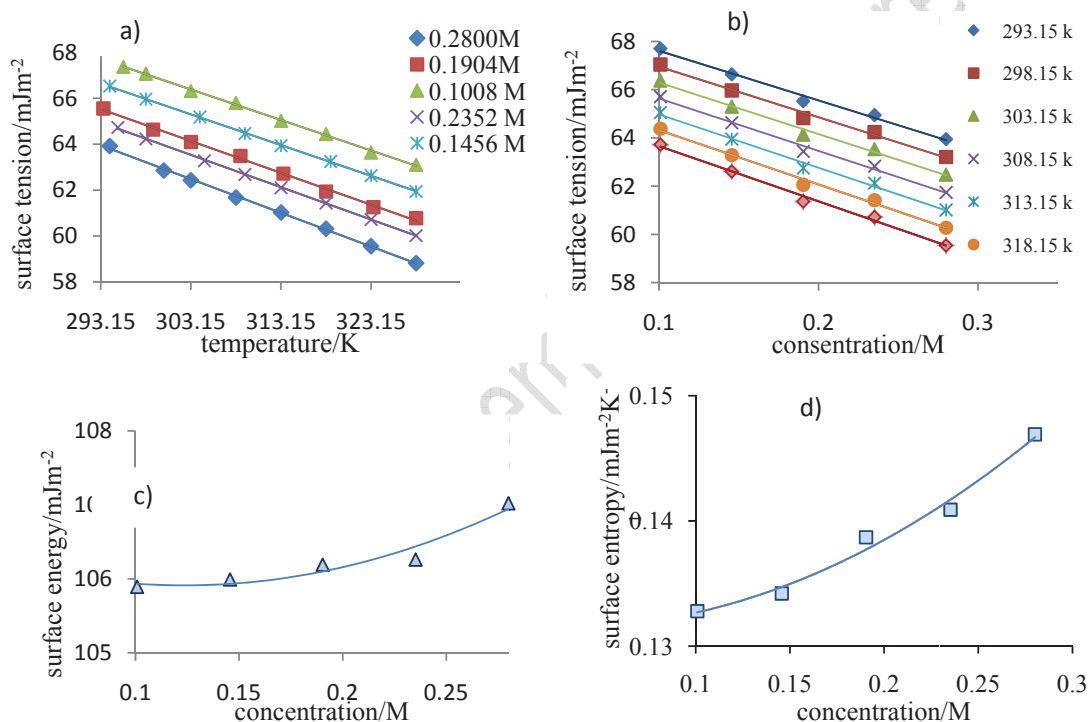


Figure 2. Histidine surface tension, (a) versus temperature, (b) versus concentration. Histidine, (c) surface energy, (d) surface entropy versus concentration.

Conclusions :

Surface tension of the aqueous solutions of histidine (in Figure 2) and phenylalanine as well (not shown) are decreased with concentration. So these amino acids can be treated as surfactants. Surface tension of aqueous solution of phenylalanine is less than histidine at the same concentration and temperature; this means that increase in the number of carbon atoms of the amino acid reduces the surface tension of the solution. Surface energy of both amino



acids decreases with increasing the concentration. Surface entropy of both amino acids increases with increasing concentration tending a maximum.

Reference:

- [1] A. Ambrogelly, S. Palioura, "Natural expansion of the genetic code"; Jan 2007.
- [2] M. H. Ghatee and A. R. Zolghadr, *Fluid Phase Equilibria*, 263 (2008) 168-175.

15th Physical Chemistry Conference



Calculation of surface tension, surface entropy, surface enthalpy, and surface excess concentration of organic binary mixtures

Z. Almasi^a, E. Ghasemian^{b*}

^aKhuzestan science and research branch, Islamic Azad university, Ahvaz, Iran

^bFaculty of Science, Ilam University, Ilam, Iran

Email: z.almasi1720@yahoo.com

Abstract:

Among lots of theoretical and experimental studying of surface tension of different solutions, a great part is related to surface tension and surface properties of organic binary mixtures. In this paper, surface tension, and surface mole fraction have been calculated using Sprow - Praunzitz equation of state and UNIFAC group contribution method.

Comparisons of the calculated surface tensions with experimental data show surface tension predictions are found to be extremely sensitive to the molar surface areas and difference in pure surface tension. In addition to find more information about surface structure of binary mixtures we focused on study of surface tension of mixtures by a generalized Langmuir model, surface entropy, surface enthalpy and surface excess concentration.

Keywords: organic binary mixtures, Surface tension, surface mole fraction, UNIFAC, Relative Gibbs adsorption.

Introduction:

A great part of theoretical and experimental studying of surface tension of solutions is related to surface tension and surface properties of organic binary mixtures and has received increasing attention in the different scientific research fields. Several theoretical approaches such as classical thermodynamic theories [1], gradient theory [2], perturbation theory [3], and parachor method [4], have been used to prediction of surface tension. In this study, to find more information about surface structure of binary mixtures, surface tension, surface entropy, surface enthalpy, surface mole fraction and surface excess concentration was calculated.



Result and discussion:

In this paper we calculated theoretical surface tension, surface mole fraction, surface activity, surface excess concentration, surface entropy and surface enthalpy have been calculated. We carried out comparisons between experimental surface tension and predicted surface tension. By considering calculated values of MRSD, it has been shown that the proposed method can be apply to estimate the surface tension for the binary systems studied in this work. Also values of surface excess concentration show the adsorption of solute on the surface and the addition of this species to solution causes a decreasing effect in surface tension of solution. For studied system surface entropy exhibited one minimum and surface enthalpies show a maximum and then decreases by increasing the solute concentrations.

Conclusion:

Thermodynamic properties of the surface of both systems show a complicated behavior. Analysis of the surface composition with the Gibbs adsorption isotherm and also with the extended Langmuir model shows that the surface of mixtures is enriched with component with lower surface tension. Theoretical method to calculate surface tension that used in this paper show application of real partial molar area affected results of prediction of surface tension.

References:

- [1] Nath, S.: Surface Tension of Nonideal Binary Liquid Mixtures as a Function of Composition. *J. Colloid Interface Sci.* 209, 116–122 (1999)
- [2] Pinerio, A., Brocos, P., Amigo, A., Fadrique, J. G.; Lemus, M. G. Extended Langmuir isotherm for binary liquid mixtures. *Langmuir*. 17, 4261-4266 (2001)
- [3] Toxvaerd, S.: Perturbation theory for non uniform fluids surface tension. *J. Chem. Phys.* 57, 4092-4096 (1972)
- [4] Allen, C., Watts, K. C., Ackman, R. G.: Predicting the surface tension of biodiesel fuels from their fatty acid composition. *J. Am. Oil. Chem. Soc.* 76, 317-323 (1999)



Application of the UNIFAC model for Estimation of Relative Gibbs Adsorption and thickness of the surface layer in the binary mixtures

K. Alizadeh^a, A. Bagheri^{b*}

^aDepartment of Chemistry, Science and Research Branch, Islamic Azad University, Khouzestan, Iran

^bDepartment of Physical Chemistry, Faculty of Chemistry, Semnan University, Semnan, Iran

Email: bagheri.alm@gmail.com

kolsoum.alizadeh@yahoo.com

Keywords: Surface tension, Adsorption, UNIFAC, Thickness, Binary mixture

Introduction:

Models for calculation of surface tensions are normally based on the assumption that the surface layer forms a separate phase with constant and uniform composition which is different from the composition of the adjacent vapor and liquid bulk phases.

In this paper, we used experimental values of surface tension for binary mixtures of organic acids (formic, acetic, propionic and butyric acid) with water in the temperature range from 293.15 K to 323.15 K. The activity coefficients in surface and bulk were evaluated using the UNIFAC group contribution model and then this coefficients is used to estimate the relative Gibbs adsorption and the thickness of surface layer. We compare these measurements with calculations of the lengths of molecules based on molecular modeling using Hyperchem software [1, 2].

Methods:

In a binary mixture, from the Gibbs equation, the relative adsorption of component 2, $\Gamma_{2,1}$, at the liquid–air interface is defined by

$$\Gamma_{2,1} = -\frac{1}{RT} \left(\frac{\partial \sigma}{\partial \ln a_2} \right) \quad (1)$$

where σ and $a_2 = \gamma_2 x_2$ are the surface tension of the solution and activity of component 2 in the mixture, respectively. The thickness of surface layer (t) has been calculated from the Panayiotou equation modified for liquid surfaces [2, 3]:

$$t = -\frac{1}{RT} \left(\frac{\partial \sigma}{\partial \ln a_2} \right) \left(\frac{\phi_2^s}{v_2} - \frac{\phi_1^s x_2^b}{v_1 x_1^b} \right)^{-1} \quad (2)$$

where ϕ_1^s and ϕ_2^s are the volume fraction of components 1 and 2 in the surface phase.

Result and discussion:

In all temperatures, $\Gamma_{2,1}$, increased with increasing the length of the organic acids chains (see Fig. 1). This trend is nonlinear and surface tension decreased rapidly with increasing organic acid concentration.

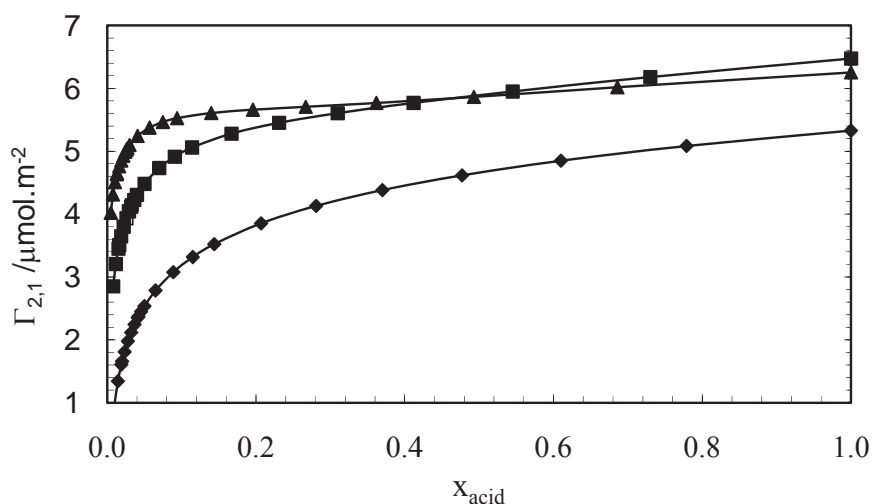


Fig. 1. Plot of change in Relative Gibbs Adsorption of the mol fraction in the binary mixtures at 303.15K:
(♦)Formic Acid/Water,(■)Acetic Acid/Water,(▲)Propionic Acid/Water.

The thickness of surface layer increased with decreasing the polarity of organic acids. From the molecular point of view, the thickness of surface layer is strongly dependent on the molecular interactions, molecular size, surface tension and temperature.

Conclusions:

The thickness of four miscible liquid–air surfaces has been calculated by combining relative Gibbs adsorption and UNIFAC model. As expected from the theory, the interfacial thickness is related to the activity coefficients of solutes and surface compositions. Our calculations



indicate that the thickness of surface layer is generally of the order of Angstrom and is affected by varying of composition.

References:

- [1] E. Alvarez, G. Vazquez, J. M. Navaza, J. Chem. Eng. Data. 42 (1997) 957-960.
- [2] A. A. Rafati, A. Bagheri, A. R. Khanchi, E. Ghasemian, M. Najafi, J. Colloid Interface Sci. 355 (2011) 252–258.
- [3] K. S. Birdi, C. G. Panayiotou, Handbook of Surface and Colloid Chemistry, second ed., CRC Press, 2003.



Self – Assembly in System of Lecithin and Nonionic Amphiphile from NMR Studies

S . Sadaghiani¹ , Sima Rezalou^{2,*}

¹Department of Chemistry, Payame Noor University, ourmia, IRAN

^{2,*} Department of Chemistry, Payame Noor University, Khoy, IRAN

Email: simarezalou@yahoo.com

Abstract:

The binary solution can solubilize variable quantities of lecithin depending on sample composition, the maximum amount being 10 wt % of lecithin. The self-diffusion coefficients of Triton X-100, $D(T)$, water, $D(W)$, and lecithin, $D(L)$ were measured with the Fourier transformed pulsed-gradient spin-echo (FT-PGSE) NMR technique. In the binary system, the $D(W)$ values decrease continuously with increasing surfactant concentration (0-80 wt % surfactant), whereas there is a sharp decrease of the $D(T)$ value until a minimum is reached, after which there is a slow increase in the diffusion coefficient of Triton X-100. The water diffusion data are analyzed with the cell diffusion model, and a constant hydration number, $n = 6$ (molecules of water per EO group), to be consistent with a water continuous structure up to at least 80 wt % Triton X-100 at 305 K. The surfactant diffusion data are used to show the formation of nonspherical normal micelles even in the very dilute region, and the micelles undergo size and/or shape changes with increased Triton X-100. The micellar growth is more pronounced if the system contains lecithin. The $D(T)$ and $D(L)$ values are used to obtain the Triton X-100 monomer concentration, which is approximately equal to the cmc of Triton X-100 in water.

Keywords : Triton X-100 , (FT-PGSE) NMR , lecithin

Introduction :

The nonionic surfactant Triton X-100 is a commercial polydisperse preparation of [p-(1,1,3,3,-tetramethylbutyl)-phenyl]poly(oxyethylene), containing an average number of 9.4 oxyethylene units per molecule.

The surfactant molecules undergo self-association in water forming micelles and liquid crystals.¹⁻⁴ Recently, NMR studies of liquid crystalline phases for the system Triton X-100 and hexagonal phases can incorporate Triton X-100 and lecithin.²³ For systems containing lecithin vesicles, addition of surfactant leads to a growth of vesicles at low surfactant/lecithin molar ratios, but at higher ratios, mixed micelles are found to form.²¹

Experimental Section :

The isotropic solution phase produced in the ternary system of soybean lecithin-water with TritonX-100 at 305K was chosen for study by NMR methods. The ternary phase diagram of the system was studied in detail.²³ At 305K TritonX-100 is miscible with water at all proportions and this solution phase can solubilize a maximum of 10wt% of lecithin in the water-rich part, whereas the solubility of lecithin in TritonX-100-rich solutions is somewhat less (~5%). About 10wt% of lecithin can be solubilized in neat TritonX-100. The isotropic solution phase of this system is in equilibrium with lamellar liquid crystalline phase through two- and three-phase heterogeneous regions.

NMR Self-Diffusion Measurement. The NMR self-diffusion studies were performed on a modified Jeol FX-60FT NMR instrument operating at 60 MHz for protons. External deuterium lock was used for all samples. The basic pulsed gradient spin-echo (PGSE) NMR experiment generates a spin-echo by a 90°-180° pulse sequence, with a magnetic field gradient G applied during a time δ in the form of two pulses separated by time Δ , one pulse before and one after the 180° pulse. Fourier transformation of the digitized second half of the echo separates the contributions to the echo from the different signals in the spectrum.

Results and Discussion :

1. We find that (from eqs 5-8) X_B and D_B cannot be separately determined from the data.
2. Almost identical theoretical curves can be generated (by adjusting D_B) for any X_B value by eqs 6 and 7 as shown in Figure 1.)
3. We also plotted D_B/D_0 of the TritonX-100-water system as a function of X_B in Figure 2.)
4. By assuming $X_B = 6$ and $D_B/D_0 = 1$ from eqs 6 and 7, one can find separately the obstruction effect as shown in Figure 3.

5. We have found that the X dependence of the macroscopic water diffusion coefficient in the Triton X-100 – water system can be quantitatively accounted for with constant (independent of X) values of X_B and D_B .

Self-Diffusion of Surfactant. The self-diffusion coefficient of Triton X-100 in water is found to decrease rapidly with increasing surfactant concentration until a minimum is reached, whereafter there is a slow increase in the self-diffusion coefficient toward the value for the neat liquid Triton X-100 (Figure 4).

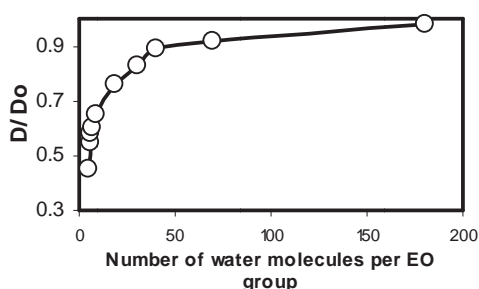


Figure 1. Relative self-diffusion coefficient of water vs the total number of water molecules per ethylene oxide group.

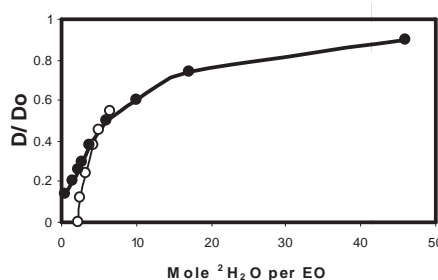


Figure 2. Relative self-diffusion coefficient of water at 305K vs the total number of water molecules per ethylene oxide group.

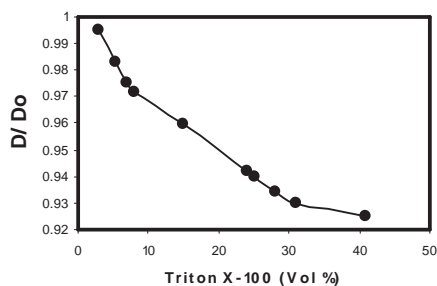


Figure 3. Obstruction factor $A (= D / D_o)$ plotted vs the obstructing volume at 305 K.

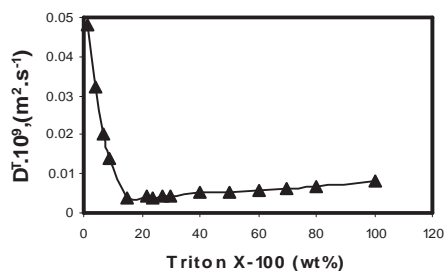


Figure 4. Self – diffusion coefficient of Triton X-100 in the binary system of Triton X-100 – water vs the weight percent of Triton X-100 at 305 K.



References:

- [1] Khan, A; in “Nuclear Magnetic Resonance” (G . A. Wwbb, Ed.) Specialist Periodical Report, Vol. 18, P,408. Royal Socirty of Chemistry, London, 2009.
- [2] Ekwall. P., in“Advance in Liquid Crystals. ” (G . H. Brown, Ed.), Vol. 1. Chap. 1. Academic Press London / New York, 1995.
- [3] Tiddy, G. J. T,. Phys. Rep. 57, 1 (2000)
- [4] Lindman, B., and Wennerstrom, H., Top. Curr. Chem.87, 1 (2000).
- [5] Fontell, K., Mandell, L., Lenhtinen. H., and Ekwall, P., Acta Polytech. Scand. 74, 1 (1988)
- [6] Lindman, B., J. Phys Chem. 88, 53 (2004).
- [7] Jonsson, B., AND Wennerstorm, H., J. Colloid Interface Sci. 80, 482 (2001).
- [8] Jonsson, B., Wennerstrom, H., Nilsson, P. G., and Linse, P., Colloid Polym. Sci.264, 77 (2006).
- [9] Jokela. P., Jonsson. B., and Khan, A., J. Phys. Chem, 91, 3291 (2007)
- [10] Jokela, P., Jonsson. B., Eichmuller, B., and Fontell. K., Langmuir 4. 187 (2008).
- [11] Jokela, P ., and Jonsson, B., J. Phys. Chem. 92, 1923 (2008).
- [12] Backstrom. K., Lindman, B., and Engstrom. S., Langmuir 4, 872 (2008).
- [13] Malmsten. M., and Lindman. B., Langmuir 5, 1105 (2009).
- [14] Jonsson , P., and Moseley, M. E., Chem. Scr. 15, 176 (200).
- [15] Stilbs, P ., and Moseley, M. E., Chem. Scr. 15,176(200).
- [16] Stilbs, P., Prog. Nucl. Magn. Reson. Spectrosc. 19, 1 (2007).



Phase Behavior and Phase Structure for Catanionic Surfactant Mixture: Dodecyltrimethylammonium Chloride-Sodium Nonanoate-Water System

S. Sadaghiani¹, Sima Rezalou^{2,*}

¹Department of Chemistry, Payame Noor University, ourmia, IRAN

^{2,*} Department of Chemistry, Payame Noor University, Khoy, IRAN

Email: simarezalou@yahoo.com

Abstract:

The phase behavior and phase structure of catanionic surfactant mixtures of DoTAC (dodecyltrimethylammonium chloride) and SN (sodium nonanoate) with water are studied by combined ²H NMR, SAXS, and microscopy techniques at 40 °C. The system forms a large isotropic micellar solution phase with excess water. As the concentration of total surfactant is increased, the solution phase coexists with different liquid crystalline phases-a lamellar phase at equimolar ratio of the two surfactants and hexagonal phases with excess DoTAC and excess SN. The lamellar and hexagonal liquid crystalline phases formed by the binary DoTAC system extensively swell with water on adding the anionic surfactant, and the swelling is more dramatic for the lamellar phase which extends to an equimolar ratio of the two surfactants. The mesophase of the short alkyl chain is incapable of solubilizing any substantial amounts of the long chain DoTAC molecules. SAXS data shows a decrease in bilayer thickness and an unchanged average area per polar group on adding SN into the lamellar phase. For the DoTAC-rich hexagonal phase, the diameter of the cylinder remains unchanged and the average area per polar headgroup is decreased in catanionic mixtures. The ²H NMR quadrupolar splitting values in the hexagonal liquid crystalline phase indicate that the polar headgroups are less extensively hydrated in catanionic mixtures compared to the hydration of the headgroups in the single surfactant systems. The ²H splitting value in the lamellar phase first decreases, going through a zero splitting value, and then the splitting increases again on a continuous decreasing of the total surfactant concentrations. Alkyl chain asymmetry is found to play a dominant role in the formation and stability of aggregates in catanionic surfactant mixtures.



Keywords : DoTAC (dodecyltrimethylammonium chloride) , SN (sodium nonanoate)

Introduction :

In recent years, the self-assembly processes of this type of surfactant in water have been under active study. Generally, it has been observed that, for $n^+ = n^- > 8$ where n^+ and n^- denote, respectively, the alkyl chain length of a cation and an anion in a catanionic surfactant, the surfactants are practically insoluble in water and the binary phase diagrams (composition vs temperature) are dominated by the formation of a lamellar liquid crystalline phase in the water-poor region of the catanionic surfactant-water system.² The chemical composition of the surfactant headgroups for the reported system has been found to have no strong effects on the phase behavior of the binary catanionic surfactant-water system.² However, the systems form only solution phases with catanionic pairs, $n^+ = n^- < 8$.³

Experimental Section :

Small Angle X-ray Scattering (SAXS) . The SAXS experiments were performed with a Kratky compact small angle system equipped with a positron sensitive detector containing 1024 channels of width 51.3 μm . The sample-to-detector distance was 277 mm, and Cu K α radiation of wavelength 1.54 \AA was used . The method allows measurements down to a scattering vector $q = 0.01 \text{ \AA}^{-1}$. The samples for the SAXS measurements were filled into a paste holder with thin mica windows. The temperature of the samples was controlled by using a Peltier element. The space between the sample and the detector was under vacuum during the measurements, in order to minimize scattering from the air.

Results and Discussion :

DoTAC-Rich Hexagonal Phase. Addition of sodium nonanoate to the hexagonal liquid crystalline phase formed by the binary DoTAC- $^2\text{H}_2\text{O}$ system leads to a considerable extension of the single phase toward high water content.

Lamellar Liquid Crystalline Phase. The swelling behavior of the lamellar phase formed in the water-poor part of the binary DoTAC- $^2\text{H}_2\text{O}$ system is the same as that for the hexagonal phase, but the extension of the phase with water is more dramatic, and the phase consists of equimolar amount of the two surfactant at its maximum stability.

²H NMR in Liquid Crystalline Phase. In the course of characterizing phases and determining phase boundaries, we have recorded ²H NMR spectra for a large number of samples in the different anisotropic liquid crystalline phases. For the lamellar phase we have measured $\Delta^2H = 3.9$ KHz at 8 wt% ²H₂O for the binary DoTAC-water system (Figure 1). Unlike the lamellar and SN-rich hexagonal phase, the DoTAC-rich hexagonal phase has a relatively wider stability range (Figure 2).

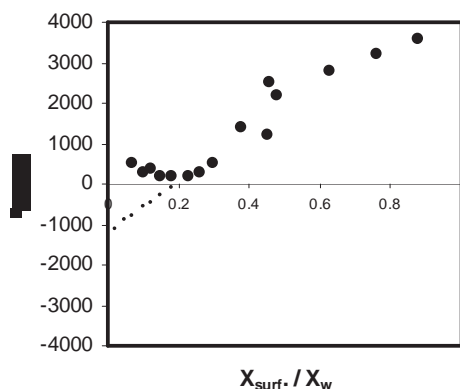


Figure 1. ²H NMR quadrupolar splitting value, Δ^2H , in the lamellar phase as a function of molar ratio between total surfactant and water, X_s / X_w , for the system DoTAC-SN-²H₂O at 40 °C

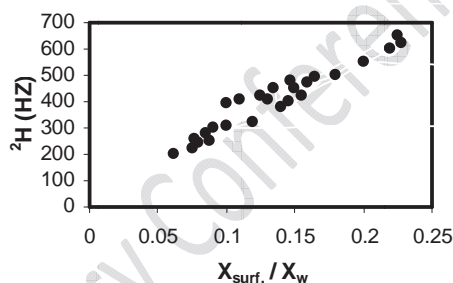
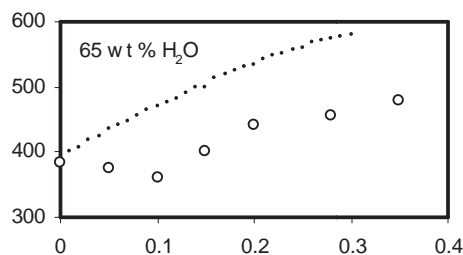
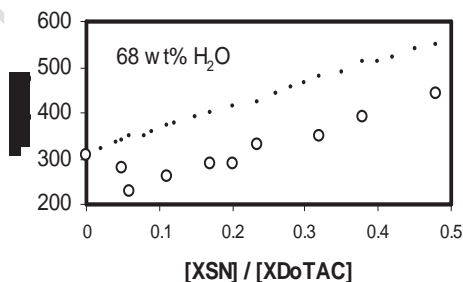


Figure 2. ²H NMR quadrupolar splitting value, Δ^2H , in the DoTAC-rich hexagonal phase as a function of molar ratio between total surfactant and water, X_s / X_w , for the system DoTAC-SN-²H₂O at 40 °C

The low splitting values measured (Figure 3) may be understood in term of reduced hydration per average headgroups. However, An increase of the Δ^2H values measured experimentally with increased C_8COO^- contents is a strong indication that the C_8COO^- molecules retain a higher degree of hydration in the mixed aggregates.



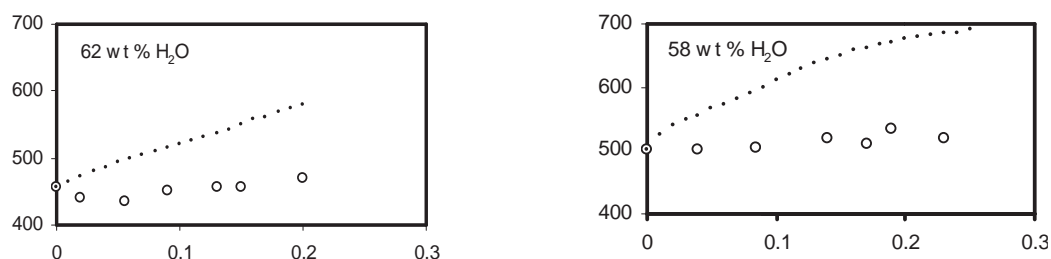


Figure 3. $^2\text{HNMR}$ quadrupolar splitting value, Δ^2H , in the DoTAC-rich hexagonal phase as a function of molar ratio between anionic and cationic surfactants, $X_{\text{SN}} / X_{\text{DoTAC}}$, at different constant wt % of water for the system DoTAC – SN – $^2\text{H}_2\text{O}$ at 40°C . Notations in the figures are as follows: (o) experimental, and (...) calculated splitting values.

References:

- [1] Khan, A; in "Nuclear Magnetic Resonance" (G. A. Webb, Ed.) Specialist Periodical Report, Vol. 18, P.408. Royal Society of Chemistry, London, 2009.
- [2] Ekwall, P., in "Advance in Liquid Crystals." (G. H. Brown, Ed.), Vol. 1. Chap. 1. Academic Press London / New York, 1995.
- [3] Tiddy, G. J. T., Phys. Rep. 57, 1 (2000)
- [4] Lindman, B., and Wennerstrom, H., Top. Curr. Chem. 87, 1 (2000).
- [5] Fontell, K., Mandell, L., Lenhinen, H., and Ekwall, P., Acta Polytech. Scand. 74, 1 (1988)
- [6] Lindman, B., J. Phys. Chem. 88, 53 (2004).
- [7] Jonsson, B., and Wennerstrom, H., J. Colloid Interface Sci. 80, 482 (2001).
- [8] Jonsson, B., Wennerstrom, H., Nilsson, P. G., and Linse, P., Colloid Polym. Sci. 264, 77 (2006).
- [9] Jokela, P., Jonsson, B., and Khan, A., J. Phys. Chem, 91, 3291 (2007)
- [10] Jokela, P., Jonsson, B., Eichmuller, B., and Fontell, K., Langmuir 4, 187 (2008).
- [11] Jokela, P., and Jonsson, B., J. Phys. Chem. 92, 1923 (2008).
- [12] Backstrom, K., Lindman, B., and Engstrom, S., Langmuir 4, 872 (2008).
- [13] Malmsten, M., and Lindman, B., Langmuir 5, 1105 (2009).
- [14] Jonsson, P., and Moseley, M. E., Chem. Scr. 15, 176 (200).
- [15] Stilbs, P., and Moseley, M. E., Chem. Scr. 15, 176 (200).
- [16] Stilbs, P., Prog. Nucl. Magn. Reson. Spectrosc. 19, 1 (2007).



The Kinetics & Thermodynamic Study on adsorption of ascorbic acid using SiO₂ and PPy/SiO₂ nanocomposite

S. M. Shademan^a, R. Ansari^{a*}, N. Alizade^a

^a Chemistry Department, Faculty of science, University of Guilan, Rasht, Iran

Email: ransari@guilan.ac.ir

Keywords: Silica gel, polypyrrole, Ascorbic acid, Adsorption, Isotherm

Introduction:

Ascorbic acid is commonly used in the pharmaceutical, chemical, cosmetic and food industry as antioxidant [1]. Ascorbic acid is very sensitive to light, to the action of oxidizing agents and metal ions. In the current study, the silica gel and chemically modified silica gel with polypyrrole were used for adsorption and preconcentration of ascorbic acid from aqueous solutions.

Materials and methods:

Adsorption experiments were carried out using batch system and the various empirical parameters such as adsorbent dose, initial acid concentration, contact time and temperature were studied. The data obtained in different conditions was applied to access isotherm, kinetics and thermodynamic variables and then compared with those obtained from untreated SiO₂ in the same operational adsorption conditions [2].

Result and discussion:

Scanning electron microscopy (SEM) pictures showed that the PPy polymer is coated onto silica gel as nanostructure film which the average diameter of particles is about 88 nm. It was found that in the case of SiO₂, the equilibrium sorption data were very best represented by the Freundlich isotherm ($R^2 = 0.987$), but for SiO₂/PPY nanocomposite, the equilibrium sorption data were fitted better by Langmuir isotherm ($R^2 = 0.998$). The kinetic studies showed that the adsorption of ascorbic acid on sorbent PPy/SiO₂ follows pseudo-second order kinetic which implies chemisorption mechanism[3]. Based upon the thermodynamic investigation

and the values obtained for ΔG^0 at all investigated temperatures indicate the feasibility and spontaneous nature of the sorption process. While the positive ΔG^0 values obtained for untreated SiO_2 show the non-spontaneous nature of adsorption process and more needed activation energy. The positive values obtained for both adsorbents implies endothermic nature of adsorption. However, a more positive value obtained for ΔS^0 for PPY/ SiO_2 .

Table1: thermodynamic parameters for sorption of ascorbic acid onto SiO_2 and PPY/ SiO_2

Adsorbent	T(k)	K_c	$\Delta G^0(\text{kJ/mol})$	$\Delta H^0(\text{kJ/mol})$	$\Delta S^0(\text{J/mol.k})$
SiO_2	288	0.07	6.23	39.99	117.92
	298	0.15	4.63		
	308	0.26	3.44		
	318	0.35	2.73		
PPY/ SiO_2	288	2.86	-2.52	38.77	143.49
	298	5	-3.98		
	308	8.66	-5.52		
	318	13	-6.78		

Conclusion:

The new nanocomposite material (PPY/ SiO_2) employed in this paper seems to be a promising adsorbent for sorption of drug acids from pharmacopeia industrial wastes. The finding in the current study seems to be in great importance from both analytical and environmental purposes and is reported for the first time.

References:

- [1] S. Yilmaz, M. Sadikoglu, G. Saglikoglu, S. Yagmur, G. Askin; "Determination of ascorbic acid in Tablet, Dosage Forms and Some Fruit Juices by DPV" ; Int. J. Electrochem.; 3, 1534 – 1542. Sci. 2008
- [2] R. Ansari, A. Fallah Delavar; "Application of poly 3-methylthiophene for removal of silver ion from aqueous solutions"; J of Applied Polymer.; 113, 2293–2300. Sci, 2009
- [3] Hong Zheng, Donghong Liu, Yan Zheng, Shuping Liang, Zhe Liu; "Sorption isotherm and kinetic modeling of aniline on Cr-bentonite" ; Journal of Hazardous Materials; 167, 141–147. 2009



Relationships between surface tension and bulk properties of organic liquids

M.SH.Zamany^{a*}, R. Tahery^b

^a Department of Chemistry, Faculty of sciences, Islamic Azad university, Tehran, Iran

^b Department of Chemical Engineering, Faculty of Engineering, Islamic Azad university, Tehran, Iran

Email: sh_zamany@ymail.com

Keywords: Surface tension, Bulk property, Organic liquids, Distribution function.

Introduction:

In the physical sciences, an intensive property (bulk property) is a physical property of a system that does not depend on the system size or the amount of material in the system, it is scale invariant. For example, density is an intensive property of a substance because it does not depend on the amount of that substance. In the past few years, considerable evidence has been accumulated for relationships between bulk properties and the surface tension of liquids. For organic liquids, the surface tension has been shown to be directly proportional to the function (density/ compressibility). [1]

Methods:

For a monatomic-molecular liquid such as xenon, Fowler [2] wrote a formula for the surface tension γ in terms of the assumed pair potential $\phi(r)$ and radial distribution function $g(r)$ of the bulk liquid, as

$$\gamma = \frac{\pi}{8} \rho^2 \int_0^\infty dr r^4 \frac{\partial \phi(r)}{\partial r} g(r) \quad (1)$$

Where ρ is the atomic number density of the liquid. A number of workers, and most recently Egry [3], have noticed that a formula for shear viscosity η given by Born and Green[4] involves the same structural integral as in Eq.(1), and leads to the prediction that

$$\frac{\gamma}{\eta} \left(\frac{M}{k_B T} \right)^{1/2} = \text{const.} \quad (2)$$

Where m is the atomic mass, k_B Boltzmann's constant and T is the temperature.

Results and discussion:

In this paper we obtained calculated data for organic liquids by Eq. (2). The results are listed in table 1. The product of γ with isothermal compressibility k_B for many organic liquids has a value between 20-33 pm. Values of k_B were obtained from Refs [5], [6]. $\frac{\gamma}{\eta} \left(\frac{M}{k_B T} \right)^{1/2}$ for the organic liquids actually ranges shows values between 0.1-0.9. The distances 20–33 pm were interpreted as a fraction of the surface thickness, which is the depth to which one must penetrate below the surface before the liquid takes on intensive properties characteristic of the bulk.

Conclusion:

The low values about distance parameter that explained in results and discussion section are for hydrogen-bonded liquids. The high values are for molecules that contain a strongly electronegative atom and no strongly electro positive group which results in a relatively low value of η .

Reference:

- [1] H. A. Papazian ; "Correlation of Surface Tension with Bulk Properties for Molten Alkali Halides"; International Journal of Thermo physics. 6, 533-537, 1985.
- [2] R. H. Fowler, Proc. R. Soc. London, Ser. A. 159, 229, 1937.
- [3] I. Egry, Scr. Metall. Mater. 26, 1349, 1992.
- [4] M. Born and H. S. Green, Proc. R. Soc. London, Ser. A. 190, 455, 1944.
- [5] D. R. Lide, CRC Handbook of chemistry and physics, 87th ed. 2007.



Surface tension prediction for binary solutions

M.SH.Zamany^{a*}, R. Tahery^b

^aDepartment of Chemistry, Faculty of sciences, Islamic Azad university, Tehran, Iran

^b Department of Chemical Engineering, Faculty of Engineering, Islamic Azad university,
Tehran, Iran

Email: sh_zamany@ymail.com

Keywords: Surface tension, Binary solution, Lamperski model, molecular interactions.

Introduction:

The thermodynamic and transport properties of liquids and liquid mixtures have been used to understand the molecular interactions between the components of the mixture and also for engineering applications concerning heat transfer, mass transfer, and fluid flow. One of the most striking demonstrations of the intermolecular forces is the tension at the surface of a liquid. The surface tension (γ), generally employed as a quantitative index of this tension, is defined as the force exerted in the plane of the surface per unit length (dynes/cm). Additionally, surface tension is equal to the change in the Gibbs energy in the process of formation of a unit area of the surface layers from molecules present in the bulk of the liquid phase. There are different methods and theories for surface tension calculation but in this paper we decided to use the Lamperski model that has been applied already, but there is not any report of this view that is calculated with these binary solutions. [1-4]

Methods:

The surface tension of pure i th component with the Lamperski model can be defined as:

$$\gamma = \sum_{i=1}^N \theta_i [\gamma_i + n_i RT \ln(\theta_i / v_i)] \quad (1)$$

θ_i is the surface fraction of the i th component of the solution.

The Lamperski model can be used to predict surface tension for multicomponent solutions according to the following formulas [5]:



$$\frac{\theta_2}{\nu_2} = \left(\frac{\theta_1}{\nu_1} \right)^{r_{12}} \exp \left(\frac{\gamma_1 - \gamma_2}{n_2 RT} + r_{12} - 1 \right) \quad (2)$$

θ_1 and θ_2 are the surface fractions of each component, ν_1 and ν_2 are the volume fractions of i th component, n is the semi empirical parameter can be calculated from $n_i = d/V_i$ and also r_{12} can be obtained from $r_{12} = n_2 / n_1$.

Results and discussion:

Comparison between theoretical results for surface tension of binary solutions and experimental with different materials in varied temperatures have been done and for 10 binary solutions are listed in table 1. results presented with average absolute deviations percentage. The maximum deviations are observed for polar solutions. The agreement between theoretical and experimental results is good. By using from dependence of surface fractions of alcohols solutions (methanol) on the volume fraction we can see that the presence of even a small amount of alcohol in the solution leads to its high concentration at the surface.

Conclusion:

This model can be extended to use for surface tension calculation of ternary solutions. Furthermore surface concentrations can be obtained by this model respectively. This paper shows the formula that obtained for surface tension calculation is similar to Gibbs adsorption isotherm. The results can be used to evaluate the heat transfer, flow and phase change of binary solutions.

Reference:

- [1] J. Escobedo, G. A. Mansoori; "Surface tension prediction for pure fluids"; AIChE J. 42(5), 1425-1433, 1996.
- [2] S. Lamperski; "Surface tension and adsorption from a multicomponent solution"; J. Colloid Interface Sci. 144, 153, 1991.
- [3] E. Kim, S.; "Excess volumes for 2-methyl-2-propanol + water at 5 K intervals from 303.15 to 323.15 K"; J. Chem. Eng. Data. 33, 288-292, 1988.



- [4] R. Tahery, H. Modarress, and J. Satherley; "Density and Surface Tension of Binary Mixtures of Acetonitrile + 1-Alkanol at 293.15 K"; J. Chem. Eng. Data.51, 1039-1042, 2006.

15th Physical Chemistry Conference



Adsorption of Basic Violet 16 from Aqueous Solutions by Waste Sugar Beet Pulp: Kinetic and Thermodynamic Studies

Ali Reza Harifi-Moodand FatemehHadavand-Mirzaie

Department of Chemistry, Kharazmi University, Karaj, Iran, P.O. Box 15719-14911

e-mail: alireza.harifi@gmail.com & hadavandf@yahoo.com

Keywords: Adsorption, Basic Violet 16, Beet pulp, Isotherms.

Introduction:

The environmental pollution is increasing in recent decades due to rapid industrialization and population growth throughout the world. Most of the areas situated near various industries are polluted continuously because of the disposal of industrial wastes [1]. Adsorption is a method which has gained considerable attention in the recent years [2]. The present work is an attempt to develop the waste pulp of sugar beet remaining from extraction of sugar as an efficient adsorbent for removal of a Basic violet 16 from aqueous solutions.

Experimental section:

Adsorption of Basic violet 16 was carried out by a batch technique. Experiments were conducted to observe the effect of various parameters such as pH, temperature, particle size, amount of adsorbent, concentration, and contact time. In the studying of the pH, temperature, particle size, amount of adsorbent and concentration effects, all experiments were carried out in 50 ml of the each solution in a temperature controlled shaking water bath at a constant speed of 150 rpm. Solutions were contacted with a known amount of adsorbent for 24 hours till equilibrium was attained. In order to investigation of contact time, 100 ml of Basic violet 16 solution of known concentration, pH and a known amount of the adsorbent were taken in a 2 L batch reactor circulator. The solution was vigorously stirred with a magnetic stirrer due to experimental run. Then the solutions were filtered and the filtrate was analyzed spectrophotometrically for the uptake of the dye at λ_{max} 548nm.



Results and discussion:

The adsorption studies of Basic violet 16 on Beet pulp at 25°C and varying pH range (pH 3-12) showed an approximately consistent percentage removal of the dye due to pH range.

Experimental data showed that the percentage removal of the dye has negligible tolerance with the variation of adsorbent sieve size. Therefore, the medium sieve size of particles (300-600µm) was used in all experiments. To optimize the adsorbent dose for removal of the Basic violet 16 from the aqueous solutions, adsorption was carried out with different adsorbent dosages. The dosage of the adsorbent was varied from 0.1 to 10 g/L at fixed pH, temperature, and adsorbate concentration. The adsorption capacity increases up to a maximum value (85.2%) in presence of 10/L dosage of the adsorbent.

The experimental data points were fitted to the Langmuir and Freundlich isotherms which are the most frequently used dual-parameters equations. It was observed that the adsorption of Basic violet 16 over Beet pulp fully satisfied both Langmuir and Freundlich models and straight lines were obtained in each case. This indicates uniform adsorption over the surface of the adsorbent. The value of Q_0 obtained from the Langmuir plots decreased with an increase in temperature. This also confirms that the processes are exothermic in nature. The data also show that the value of n is almost unity at all temperatures that it refers to the little heterogeneity in the surface of the adsorbent.

Two simplified kinetic models including pseudo first-order and internal particle diffusion were used to test the adsorption kinetics [3]. Results show that the intra particle diffusion is the rate determining step.

Various thermodynamic parameters were also calculated for the adsorption process. The obtained values of the thermodynamic parameters are given in Table 2. The negative value of ΔH° confirms that the adsorption process of Basic violet 16 on beet pulp is exothermic in nature and physical nature of the adsorption.

References:

- [1] Y.Verma, Toxicity assessment of dye containing industrial effluents by acute toxicity test using *Daphnia magna*. *Toxicol. Ind. Health* 2011, 27(1), 41-49.
- [2] G.Crini, Non-conventional low-cost adsorbents for dye removal: A review. *Bioresource Technol.* 2006, 97(9), 1061-1085.



- [3] Z.Aksu, I. A.Isoglu, Use of agricultural waste sugar beet pulp for the removal of Gemazol turquoise blue-G reactive dye from aqueous solution. *J. Hazard. Mater.*2006, 137, 418-430.

15th Physical Chemistry Conference



Surface Tension Prediction for Pure Compounds by Using of Different Methods

S.Shohani^{a*}, R.Tahery^b

^a Department of Chemistry, Faculty of Sciences, Islamic Azad University, Central Tehran Branch, Tehran, Iran

^b Chemical Engineering Dep., Faculty of Engineering, Islamic Azad University, Central Tehran Branch, Tehran, Iran

Email: shohani_sima@yahoo.com

Key words: Surface tension, Parachor, Pure compound, Polar

Introduction:

The surface tension is one of the interesting properties of thermodynamics, which has many applications in separation processes, adsorption, distillation, biological membranes and especially in oil industry. In the current study, the surface tension of about 50 pure compounds including alcohols, alkanes, alkenes, organic acids and cyclic compounds were calculated by five different methods and the results were compared with the experimental data.

Theory:

Macleod (1923) suggested a relation between σ and the liquid and vapor densities:

$$\sigma^{\frac{1}{4}} = [P](\rho_L - \rho_V) \quad (1)$$

Sugden (1924) has called the temperature-independent parameter [P] the parachor and indicated how it might be estimated from the structure of the molecule [1]. Brock and Bird (1955) developed this idea for nonpolar liquid and proposed that [1]:

$$\frac{\sigma}{\rho_c^{\frac{2}{3}} T_c^{\frac{1}{3}}} = (0.132\alpha_c - 0.279)(1 - T_r)^{\frac{11}{9}}$$

(2) where α_c is Riedel (1954) parameter at the critical point. Pitzer (Curl and Pitzer, 1958; Pitzer, 1995) gives a series of relations for σ that together lead to the following corresponding-states relation for σ , where ω is Acentric Factor [1]:



$$\sigma = P_c^{\frac{2}{3}} T_c^{\frac{1}{3}} \frac{1.86+1.18\omega}{19.05} \left[\frac{3.75+0.91\omega}{0.291-0.08\omega} \right]^{\frac{2}{3}} (1 - T_r)^{\frac{11}{9}} \quad (3)$$

Sastri and Rao (1995) presented the following modification [1]:

$$\sigma = K \cdot P_c^x \cdot T_b^y \cdot T_c^z \left[\frac{1-T_r}{1-T_{br}} \right]^m \quad (4)$$

The units are kelvins and bars. Values for the constants are given in reference [1], and finally Miqueu (2000) proposed the following extended scaled equation to represent the surface tension of pure compounds, where $t=1-T/T_c$ is reduced temperature [2]:

$$\sigma = K T_c \left(\frac{N_A}{V_c} \right)^{2/3} (4.35+4.14\omega) t^{1.26} (1+0.19t^{0.5}-0.25t) \quad (5)$$

Result and discussion:

We applied Equations (1) - (5) to predict surface tension of 50 pure compounds. The results show that Brock-Bird, Pitzer and Miqueu methods don't predict surface tension for alcohols, acids, and phenols.

Conclusions:

The lowest AAD% is obtained when Macleod-Sugden method is used. This is to be expected because this method is based on experimental data. The behavior of the Brock-Bird, Pitzer and Miqueu methods is nearly identical. Of the predictive methods, the Sastri-Rao method is the only one that does not give large deviations in at least some cases. The results indicate that the percentage of mean error for the five methods are: 2.68, 10.57, 12.66, 4.98, and 12.23 respectively.

References:

- [1] R.C.Reid, J. M Prausnitz, B.E. Poling, "The Properties of Gases & Liquids" 4th ed. Mc Grew Hill, 1987.
- [2] C. Miqueu, D. Broseta, J. Satherley, B. Mendiboure, J. Lachaise, A. Graciaa, "An extended scaled equation for the temperature dependence of the surface tension of pure compounds inferred from an analysis of experimental data" Fluid Phase Equilibria 172 (2000) 169-182.



The use of Scaled Particle Theory and Developed Scaled Particle Theory in Predicting the Surface Tension of Pure Compounds

S. Shohani^{a*}, R. Tahery^b

^a Department of Chemistry, Faculty of Sciences, Islamic Azad University, Central Tehran Branch, Tehran, Iran

^b Chemical Engineering Dep., Faculty of Engineering, Islamic Azad University, Central Tehran Branch, Tehran, Iran

Email: shohani_sima@yahoo.com

Key words: Surface tension, Developed Scaled Particle, Lennard-Jones parameter

Introduction:

The experimental and theoretical study of surface properties such as surface tension has received increasing attention in the different scientific research fields[1]. The scaled particle theory (SPT) of fluids was presented by Reiss et al. and is concerned primarily with systems of hard spheres [1]. The scaled particle theory of fluids is so named because it makes use of coupling parameter, which is a measure of the breadth of a molecule and its potential field rather than the amplitude of this potential [1]. By considering the fact that the surface tension of a real fluid arises from a combination of both repulsive and attractive forces between molecules, a new expression for the interfacial tension (developed SPT) has been derived from scaled particle theory (SPT) based on the work of cavity formation and the interaction energy between molecules[2]. The results indicated that the developed SPT in this work calculates the surface tensions much closer to the experimental data compared with those Reiss's SPT theory.

Theory:

A molecule is coupled formally to a fluid by letting it grow in size until it achieves the scale of its neighbors. The central idea of the development is that it is possible to write a very good estimate for the reversible work required in the production of a spherical cavity of radius r in a fluid, $W(r)$. The work of expanding the spherical cavity's radius from r to $(r + dr)$ can be



written as the sum of volume and surface contribution. For sufficiently large r , the work is related to the surface tension of fluid σ , in the following form [1]:

$$W(r) = \frac{4}{3}\pi r^3 P + 4\pi r^2 \sigma \quad (1)$$

where P is the pressure of the fluid. The resultant relation of the scaled particle theory for the surface tension calculation is presented by the following expression [1]:

$$\sigma = \frac{KT}{4\pi d_0^2} \left(12 \left(\frac{y}{1-y} \right) + 18 \left(\frac{y}{1-y} \right)^2 \right) - \frac{P d_0}{2} \quad (2)$$

where $y = \pi N d_0^3 \rho / 6$ and is the reduced density. The K , and d_0 are Boltzmann's constant, and hard sphere diameter respectively. The following equation (developed SPT) clearly shows that the surface tension of real fluid is sum of both repulsive and attractive terms [2]:

$$\sigma = \frac{KT}{4\pi d_0^2} \left(12 \left(\frac{y}{1-y} \right) + 18 \left(\frac{y}{1-y} \right)^2 \right) - \frac{P d_0}{2} - \frac{y}{4\pi d_0^2} \left[\frac{64}{3} \varepsilon + \frac{16}{d_0^6} \left(\alpha^2 \mu^2 + \frac{\mu^4}{3KT} \right) \right] \quad (3)$$

where μ is the dipole moment, α is the corresponding polarizability and (ε/K) is Lennard-Jones energy parameter. The first and the second terms are due to repulsive forces and the third term is due to attractive forces.

Results and discussion:

We used equations (2) and (3) to calculate surface tension of pure compounds including alcohols, alkanes, cycloalkanes, aromatics and noble gases. The results indicate that calculated surface tensions by the developed SPT theory are in better agreement than those calculated by the SPT theory of Reiss [2].

Conclusions:

By comparing Eq. (2), and Eq. (3), it can be seen that the second term in Eq. (3) has been neglected in the Reiss's SPT theory which causes a large deviation from experimental values of surface tension.

References:

- [1] H. Reiss, H.L. Frisch, J.L. Lebowitz, "Statistical Mechanics of Rigid Spheres" J. Chem. Phys. 31 (1959) 369-380.



- [2] R. Tahery, H. Modaress, “Lennard-Jones Energy Parameter for Pure Fluids from Scaled Particle Theory”Iran. J. Chem. Chem. Eng.26 (2007).

15th Physical Chemistry Conference



A Study Upon The Role of A B-Reducer Contained Solution In A Direct Electrodeposition of Ultrasoft and High Magnetic Moment NiFe films

Kourosh Motevalli^{a*}, Karim zare^b, Zahra Yaghoubi^c

^a Applied chemistry department, faculty of sciences, Islamic Azad university, south Tehran branch, Tehran, Iran

^b Applied chemistry department, faculty of sciences, Shahid Beheshti university, Tehran, Iran

^c Industrial Engineering faculty, Islamic Azad university, south Tehran branch, Tehran, Iran

Email: k_motevalli@azad.ac.ir

Key words: electrodeposition, ultrasoft, magnetic recording systems, biotechnological

Introduction:

The Main Aim of This Letter, is Introducing A methodology to fabricate ultrasoft NiFe nano-/microfilms directly via electrodeposition from a semineutral iron sulfate solution. Because of Using boron-reducer as the additive, the NiFe films become very soft with high magnetic moment. In addition, the film coercivity in the easy and hard axes is 6.5 and 2.5 Oersted, respectively, with a saturation polarization up to an average of 2.45 Tesla. Despite the softness, these shining and smooth films still display a high-anisotropic field of ~ 45 Oersted with permeability up to 10^4 . This kind of films can potentially be used in current and future magnetic recording systems as well as microelectronic and biotechnological devices.

The ever expanding demand of the world market leads to magnetic recording data storage devices advancing toward much smaller exterior dimension and higher capacity [1, 2]. In order to achieve very high capacity and fast recording data storage in a miniature device, an ultrasoft and high magnetic moment material is required for producing high- saturation flux density (B_s), so that the necessary flux density can be preserved on reducing device dimensions, while simultaneously achieving a low coercivity (H_c) to match the hard magnetic media with high H_c , track density, and linear density. Soft magnetic films with high moment are also widely used in modern electromagnetic devices, such as high-frequency field-amplifying components, versatile communication tools, and magnetic shielding materials in tuners.



Method and Results:

The NiFe films were electrodeposited on Si(100) wafers. A seed layer, for example, Au, Cu, or

NiFe, with thickness of 20–30 nm was sputtered onto each wafer surface as an electrical conducting layer for the electrodeposition. The $\text{Fe}_x\text{Ni}_{100-x}$ ($x = 55\text{--}68$) films were fabricated at the temperature of $40 \pm 2^\circ\text{C}$ from a solution of 0.07 mol/L $\text{NiSO}_4 \cdot 7\text{H}_2\text{O}$, 0.10 mol/L $\text{FeSO}_4 \cdot 7\text{H}_2\text{O}$, 0.5 mol/L NH_4Cl , 0.5 mol/L H_3BO_3 , and 2.8–3.2 g/L B-reducer additive. The electroplating system used was a Paddle cell with pulse DC power. During the electrodeposition of NiFe film, a magnetic field of 280 Oe was applied parallel to the substrate surface. The atomic ratio of Co to Fe in the electrodeposited films was determined by energy dispersive X-ray (EDX, JSM-6340F, JEOL Asia). While measuring H_c with the VSM possessing Helmholtz coils, high resolution of 0.01 Oe was obtained through the field control mode. The maximum relative permeability (μ_m) was calculated from easy axis M-H loops according to the formula $\mu_m = B(T)/H(T) \approx 4\pi$ magnetic moment (M , emu)/[magnetic field (H , Oe) \times film volume (cm^3)], where (M , H) refers to the turning point in the lower branch of the easy axis M-H loop. It is noted that the effect of film sample shape (normally, $1.20\text{ cm} \times 1.20\text{ cm} \times \sim 0.6\text{ }\mu\text{m}$) can be neglected due to the length and width being much larger than the thickness. The B_s values were calculated from the formula $B_s(T) = \mu_0 M_s = 4\pi \times 10^4\text{ M (emu)/film volume (cm}^3\text{)}$, where M refers to the saturation moment in the M-H loops. The B_s result is the average value obtained from a series of NiFe films having different thickness (80 nm – 2.5 μm). The dimension of the films was measured on ADM-60 Micro-Dicer. The two challenging issues (poor magnetic and mechanical properties), encountered in the preparation of high- B_s magnetic NiFe films, can simply be solved by using boron reducer in electrodeposition. The boron reducer can greatly improve the softness, magnetic moment, mechanical, and other properties of the NiFe films. Thus, the as-prepared films have potential applications in ultrahigh density and frequency magnetic recording system, biotechnological, and microelectronic devices [2]. X-ray diffraction (XRD) analysis (recorded from a powder sample) in Figure 1 shows that the added B-reducer eliminates the foreign Fe_2O_3 -phase (viz. protects Fe^{2+} from oxidation), which leads to a texture- structural change from NiFe(110) and Fe_2O_3 (209) polycrystalline to NiFe(110) single-crystalline for the Co40 Fe60 films. As a result, the film

possesses very low H_c and high theoretical B_s value ($\sim 2.45T$). Further investigation results revealed that too much of B-reducer (>10 g/L) led to an unstable plating solution and a high content of boron doping ($>2\%$) in the NiFe films. The films possess an amorphous texture, a decreased B_s , and poor anisotropy.

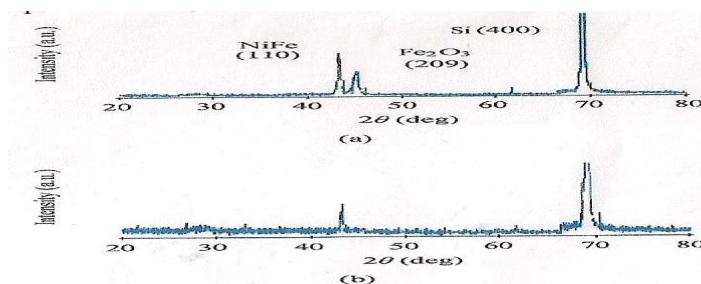


Figure 1: The 2θ XRD results of $\sim 0.6 \mu\text{m}$ Ni₄₀Fe₆₀ films on Si(100) wafer. (a) & (b) stand for without adding and adding B-reducer, respectively.

Conclusion:

The two challenging issues (poor magnetic and mechanical properties), encountered in the preparation of high- B_s magnetic NiFe films, can simply be solved by using boron reducer in electrodeposition. The boron reducer can greatly improve the softness, magnetic moment, mechanical, and other properties of the NiFe films. Thus, the as-prepared films have potential applications in ultrahigh density and frequency magnetic recording system, biotechnological, and microelectronic devices [2].

Reference:

- [1] B. Zong, Y. Wu, G. Han, et al., "Synthesis of iron oxide nanostructures by annealing electrodeposited Fe-based films," *Chemistry of Materials*, vol. 17, no. 6, pp. 1515–1520, 2005.
- [2] M. Kawasaki and Y. Kanada, "Soft magnetic film having high saturation magnetic flux density, thin-film magnetic head using the same, and manufacturing method of the same," US patent no. 6765757, August 2002.



Determined the Lyophobicity for Binary Mixture with Extended Langmuir Model

S. Hatefi Koshalshah^{*a}, R. Tahery^b

^aScience Department, Islamic Azad University, Central Tehran Branch, Tehran, Iran

^bChemical Engineering Department, Islamic Azad University, Central Tehran Branch, Tehran, Iran

Email: Sahar.Hatefi@yahoo.com

Keywords: Lyophobicity, Binary Mixture, Surface Tension, Extended Langmuir Model

Introduction:

The surface tension for the investigation of the molecular interactions in liquid mixture is the better than other experimental methods because this thermodynamic property is also easy to measure and usually presents a very strong dependence on both, the compounds constituting the mixture and their relative concentrations. The surface tension of mixture is an important physical property in mass transfer processes such as liquid-liquid extraction, gas absorption, distillation and condensation [1]. In this paper by using literature surface tension data for binary mixture, the surface mole fraction (x_B^S) and the lyophobicity (β) were derived using the extended Langmuir model at different temperature. The value of (β) is discussed based on interaction forces.

Method:

At equilibrium, the relation between the surface volume fraction (ϕ_B^S) and the bulk volume fraction (ϕ_B^S) is given by the following equation [2]:

$$\phi_B^S = \frac{\beta \phi_B}{1 + (\beta - 1) \phi_B} \quad (1)$$

The bulk volume fraction is obtained from the following equation [2]:

$$\phi_B = \frac{x_B V_B}{(x_A V_A + x_B V_B)} \quad (2)$$



V_1 and V_2 are the molar volumes. Surface tension for the binary mixture according to this model is $\sigma = \phi_A^S \sigma_A + \phi_B^S \sigma_B - \lambda \phi_A^S \phi_B^S (\sigma_A - \sigma_B)$. where the σ is the surface tension of the binary mixture, σ_A and ϕ_A^S , σ_B and ϕ_B^S are the surface tension and surface volume fraction for compound A and B, respectively. λ is the adjustable parameter which is related to structural changes. ($\lambda = \alpha - 1$)

$$\sigma = \phi_A^S \sigma_A + \phi_B^S \sigma_B$$

(3)

The combination of Eqs. (1) and (3) results in the following relation:

$$\frac{(\sigma - \sigma_A)}{(\sigma_B - \sigma)} = \beta \left(\frac{\phi_B}{\phi_A} \right) \quad (4)$$

The surface volume fractions ϕ_B^S were calculated from the following equation: $\phi_B^S = (\sigma - \sigma_A) / (\sigma_B - \sigma_A)$ and surface volume fractions ϕ_B^S were converted to surface mole fractions x_B^S using the following equation: $\phi_B^S = x_B^S V_2 / (x_A^S V_A + x_B^S V_B)$, where x_A^S and x_B^S are the surface mole fraction for compound A and B, respectively.

Results and discussion:

We used the Extended Langmuir Model for measured two adjustable parameters for 19 binary mixtures at different temperature. Two adjustable parameters (α and β) and AAD% have been calculated for studied model.

Conclusion:

The parameter β is a measure of the lyophobicity of the component with the lower surface tension. It measured the relative distribution of the molecules between the two phases. The α parameter takes the effect of the A-B interactions on surface tension $\beta > 1$ indicates that the concentration of the compound B is higher at the surface, in regard to the bulk concentration.

References:



- [1] H. Park, R.B. Thompson, N. Lanson, C. Tzoganakis, C.B. Park, and P. Chen; "Effect of Temperature and Pressure on Surface Tension of Polystyrene in Supercritical Carbon Dioxide"; J. Phys.Chem. B, 111, 3859-3868, 2007.
- [2] P. Brocos, J. Gracia-Fadrique, A. Amigo, A. Pineiro; "Application of the Extended Langmuir model to surface tension data of binary liquid mixtures" ; Fluid Phase Equilib. ; 237, 140-151, 2005.

15th Physical Chemistry Conference



Surface Tension Prediction for Liquid Organic Solvents

S. Hatefi koshalshah^{*a}, R. Tahery^b

^a Science Department, Islamic Azad University, Central Tehran Central Branch, Tehran, Iran

^b Chemical Engineering Department, Islamic Azad University, Central Tehran Branch, Tehran, Iran

Email: Sahar.Hatefi@yahoo.com

Keywords: Surface Tension, Pure Organic Solvents

Introduction:

Surface tension (ST) is an important property in the study of physics and chemistry at free surfaces. Such data are of importance to scientists, engineers, and practitioners in many fields such as chemical process and reactor engineering, flow and transport through porous media, materials selection and engineering, biomedical and biochemical engineering, electronic and electrical engineering, etc.[1]. When experimentally measured ST data are not readily available, theoretical or empirical methods may be used to establish acceptable ST values for preliminary screening purposes. Theoretical methods of calculating ST based on thermodynamics can be complex and require additional chemical properties and simplifying assumptions to complete the calculations. In this paper, we use some models for predicting surface tension of organic solvents and then compare the results.

Methods:

The first one model discussed by Sugden[2, 3] is:

$$ST = [P(\rho_l - \rho_v)]^4 \quad (1)$$

A group contribution method was proposed to calculate parachor (P).

The second method (model 2) discussed by Reid and Sherwood is [4]:

$$ST = P_c^{\frac{2}{3}} T_c^{\frac{1}{3}} [(0.133\alpha_c - 0.281)(1 - T_r)]^{\frac{11}{9}} \quad (2)$$

α_c is Riedel parameter at the critical point. Brock and Bird [5] developed Reid and Sherwood model(model 3):

$$ST = P_c^{\frac{2}{3}} T_c^{\frac{1}{3}} \phi (1 - T_r)^{\frac{11}{9}} \quad (3)$$



Gray derived following expression for surface tension (model 4) [6]:

$$ST = P_c^{\frac{2}{3}} T_c^{\frac{1}{3}} (0.3993)(1 - T_r)^{0.4} \quad (4)$$

Where P_c and T_c is the critical pressure (atm) and critical temperature (K); and T_r is the reduced temperature.

Yaws [7] has used regression analysis to derive the following equation for calculating ST (dyn/cm) at various temperatures, T (K):

$$ST = A(1 - \frac{T}{T_c})^n \quad (5)$$

Where A , n and T_c are statistically determined model constants. The fitting quality of this model was not reported. We also used eq. 5 by regression to deriving parameters A and n .

Results and Discussion:

We used eqs. (1)-(5) to predicting surface tension of 77 pure organic solvents by using four models. Absolute Average Deviation (AAD%) has been calculated for studied models .

Conclusions:

We used 4 models for predicting of pure organic solvents. Generally the results of calculations for non polar solvents is good while error of calculation for polar solvents is poor. AAD% for model 4 is lower than other models and model 4 predicts ST better than other models.

References:

- [1] C.Trevizo, C.Daniel, N.Nirmalakhandan; "Screening alternative degreasing solvents using multivariate analysis" ; Environ. Sci. Technol; 34,2587- 2595,2000.
- [2] S.Sugden; "The parachore and valency" ;J. Chem. Soc; 32 ,1924.
- [3] S.Sugden; "The variation of surface tension with Temperature and some related functions"; J. Chem. Soc. (london, Transactions); 32,125,1924.
- [4] C.R.Reid, T.K.Sherwood; "The Properties of Gases and Liquids" ; McGraw-Hill; New York;1996.



- [5] J.R.Brock, R.B.Bird; "Surface tension and the principle of corresponding states" ; AlchE J; 1:174,1955.
- [6] J.A. Gray, C.J.Brady, J.R.Cunningham, J.R.Freeman, G.M.Wilson; "Thermophysical properties of coal liquids"; Ind. Eng. Chem. Process Des. Dev; 22:410,1983.
- [7] C.L.Yaws; "Chemical properties handbook" ; McGraw-Hill; New York; 1999.

15th Physical Chemistry Conference



Adsorption of Sulfur Compounds from Liquid Fuel by Carbon Nanoparticles Dispersed in Aqueous Phase: Kinetic and equilibrium Studies

Rahimeh Naviri Fallah, Saeid Azizian*

Department of Physical Chemistry, Faculty of Chemistry, Bu-Ali Sina University, Hamedan, 65167, Iran

E-mail(s): sazizian@basu.ac.ir and minafallahh@yahoo.com

Keywords: Carbon Nanoparticles, Desulfurization, Liquid Fuel, Adsorption

Introduction:

Removal of organosulfur compounds from liquid hydrocarbon fuels have become a worldwide increasingly important issue and active research subject in environmental and energy survey. Sulfur compounds in fuels have detrimental effects in environment due to converting to sulfur oxides during combustion of transportation fuels, thereby contributing to air pollution and acid rain [1]. The primary focus of the new regulation is the reduction of sulfur in transportation fuels. The sulfur content must drop from 500 ppmw to less than 15 ppmw in diesel and from 300 ppmw to less than 30 ppmw in gasoline [2]. In the present work dispersed carbon nanoparticles (CNPs) in aqueous solution which can be prepared by a clean, cheap and convenient rout was used for adsorption of benzothiophene (BT), dibenzothiophene (DBT) and dimethyldibenzothiophene (DMDBT) from organic phase (heptane). The experiments were carried out in the batch mode form both equilibrium and kinetic point of view.

Materials and methods:

Dispersed carbon nanoparticles in aqueous phase (CNPs) were synthesized as described elsewhere [3] by using of 2 g +D-glucose and 10 ml poly (ethylene glycol) (PEG-200) and 10 ml distilled water in a microwave oven. The prepared CNPs were characterized by different methods.

The obtained solution was used for desulfurization experiments without further processing.



Apparatus:

In this two-phase system, the samples were taken from the organic phase at to measure the residual sulfur content in the organic phase using UV/Visible spectrophotometer (PG Instrument Ltd Model T80).

Result and discussion:

The efficiency of the prepared CNPs for removal of different organosulfur compounds was evaluated. The adsorption process were studied from both equilibrium and kinetics point of view. The equilibrium and kinetic data were fitted to different models and the obtained data were interpreted based on the best models. The obtained results indicated that the CNPs have favorable features for the removal of sulfur compounds.

Conclusion:

The dispersed CNPs in aqueous phase, which were prepared by simple means, can be remove sulfur compounds from liquid fuel efficiently and quickly.

Reference:

- [1] C.O. Ania, T.J. Badosz, Importance of structural and chemical heterogeneity of activated carbon surfaces for adsorption of dibenzothiophene, *Langmuir* 21, 7752-7759, 2005.
- [2] K.A. Cychosz, A.G. Wong-Foy, A.J. Matzger, Liquid phase adsorption by microporous coordination polymers: removal of organosulfur compounds, *J. Am. Chem. Soc.* 130, 6938–6939, 2008.
- [3] Zhu H, Wang X, Li Y, Wang Z, Yang F, Yang X. Microwave synthesis of fluorescent carbon nanoparticles with electrochemiluminescence properties. *Chem Comm*, 5118-5120, 2009.



FT-IR study on the interfacial interaction of novel Neutral Polymeric Bonding Agent containing NCO group with RDX

F. Gholamian^{*}, M. Ansari

Department of Chemistry and Chemistry Engineering, MalekAshtar University of Technology, Tehran, Iran

Email: Mahdi.Ansari@gmail.com

Key words: RDX, NPBA, FT-IR, Interfacial Interaction.

Introduction:

Solid propellants are energetic polymer composites filled with finely divided solid particles called fillers. Fillers aid in processing and increase the energy of the composite propellants. It is generally known that many explosives and propellants contain oxidizers as one of their principle ingredients. The crystalline oxidizers are usually inorganic compounds, such as ammonium perchlorate (AP) or potassium nitrate but can also be organic, for example cyclotrimethylenetrinitramine (RDX) or cyclotetramethylenetetramine (HMX). Also composite propellants require certain interaction between polymer and filler (oxidizer and metal component) in order to prevent separation around a particle of filler and obtaining desired mechanical properties. Poor interaction between binders and fillers are caused dewetting. If dewetting occurs between the binder and filler, the flame front propagates below the burning surfaces to produce a more rapid combustion of the propellant. Addition of bonding agent is an important way of improving the binder-filler interactions in composite propellants. A bonding agent produces an interaction between the oxidizer crystal and the binder by forming either primary or secondary bonds with the oxidizer and a primary bond with the binder [1]. In our present work, by using of Fourier Transform Infrared (FT-IR) spectrophotometer analysis we scrutinized interactions between novel Neutral Polymeric Bonding Agent (NPBA) which is containing NCO group and RDX.

Experiment:

1. Sample preparation

NPBA structure comprises four units: Acrylonitrile, Methyl Acrylate, 2-Hydroxy Ethyl Acrylate, N-Vinylpyrrolidone. In this work, by adding N-Vinylpyrrolidone, new NPBA was synthesized using a previously reported procedure [2]. Sufficiently dried RDX powder was



spread on a Teflon plate in order to make easy to remove the coagulated one later and bonding agent was dripped on it in the ratio of 1:1 (weight). To disperse bonding agent in oxidizer uniformly, 2mL acetone was added with stirring. The samples were placed vacuum at 60 °C, and degassed for 48h before any analysis.

2. Characterization

FT-IR spectra were obtained by preparing KBr pellet, using Perkin Elmer Spectrum 400 FT-IR spectrophotometer in the range of 4000-400 cm⁻¹. The resolution was 4 cm⁻¹, and the number of scans was 16.

Results and discussion:

In high frequency the intense and broad band belonging to O-H stretching vibration band which was appeared at 3446 cm⁻¹, shifted to low frequency direction for 28 cm⁻¹. The bands at 3075, 3066 and 3001 cm⁻¹ shifted to low frequency at 3071, 3060 and 2998 cm⁻¹ respectively.

Moreover the weak absorption band at 2238 cm⁻¹ corresponding to -CN group of NPBA shifted to low frequency direction for 6 cm⁻¹. Changing the position of absorption bands indicate, on the RDX surface considerable interactions have occurred and NPBA functional groups play important role in interfacial interaction between NPBA+ RDX and probably participating in the formation of hydrogen-bond.

Conclusion:

The results of the study of the interactions between RDX and NPBA, by means of the FTIR spectroscopic method, showed that the almost interfacial bonding forces arise from the hydrogen bond. Therefore, for improvement of mechanical properties of composite propellants addition of NPBA containing NCO group reinforces the bond between binder and oxidizer particles.

Reference:

- [1] J. Petković, A. Wali, D. Mijin, The Influence of Bonding Agents in Improving Interactions in Composite Propellants, Determined Using the FTIR Spectra, Scientific Technical Review 3-4 (2009) 12-16.
- [2] C. S. Kim, Filler Reinforcement Of Polyurethane Binder Using a Neutral Polymeric Bonding Agent, US Patent 4915755, (1990).



Investigating Synergism in Critical Micelle Concentration (CMC) of cationic-nonionic surfactant mixtures

A. Abolhasani^{a*}, A.R. Moghadassi^a, A. Bagheri^b, S.A. Alavi^c, A.A. Nazari Moghaddam^c

Department of Chemical Engineering, Faculty of Engineering, Arak University, Sardasht Square, Pardis of Arak University, Arak, 38156-8-8349, IRAN

^b Department of Physical Chemistry, Faculty of Chemistry, Semnan University, Semnan, Iran

^c Department of Chemical Engineering, Science and Research branch, Islamic Azad University, Tehran, Iran

Email: amirabolhasani65@yahoo.com

Keywords: Surface Tension, CMC, surfactant, Binary Mixture, Interaction parameter

Introduction:

The synergism behavior of a mixed surfactant system consisting of a nonionic surfactant (Triton x-100) and cationic surfactant (cetylpyridinium chloride C_nPC, n = 14, 16) were studied. Synergistic effects in mixtures of surfactants have been extensively studied and different theoretical approaches have been proposed [1-2]. Synergism is defined as the condition in which the properties of the mixture are better than those observed for the individual components by themselves [3]. Rubingh [4] introduced the concept of the interaction parameter, β , based on regular solution theory, which describes the synergism between two surfactants. The value of the β -parameter gives an indication of the strength of the interaction between the surfactants. In this case, β is the interaction parameter in the mixed monolayer,

$$f_1 = \exp \beta (1 - X_1)^2 \quad (1)$$

$$f_2 = \exp \beta (1 - X_2)^2 \quad (2)$$

Where β is the molecular interaction parameter:

$$\beta = \frac{\ln(y_1 C_{12}/C_1^0 X_1)}{(1 - X_1)^2} \quad (3)$$

$$\frac{(X_1)^2 \ln(y_1 C_{12}/C_1^0 X_1)}{(1 - X_1)^2 \ln[(1 - y_1) C_{12}/C_2^0 (1 - X_1)]} = 1 \quad (4)$$

Methods:

Equilibrium surface tensions were measured on the pure surfactants and mixtures of C₁₄PC: Triton x-100 and C₁₆PC: Triton x-100 (at a range of mole fractions) with a Sigma 701 Tensiometer (Germany) using a du Noüy ring in a platinum–iridium alloy. Measurements were carried out with the temperature controlled at 25 ± 1 °C by titration of a concentrated surfactant solution down to buffered Millipore water.

Result and discussion:

The surface tension for the C₁₆PC: Triton x-100 mixtures is shown in Fig. 1. From the graph it can be seen that C₁₆PC has a lower cmc (9.09×10^{-4} M) and Triton x-100 (1.67×10^{-4} M), which have cmc values in the same concentration range. For the surfactant mixtures, the surface tension values increased and approached the higher levels as the mole fraction of the nonionic surfactant in the mixtures increased.

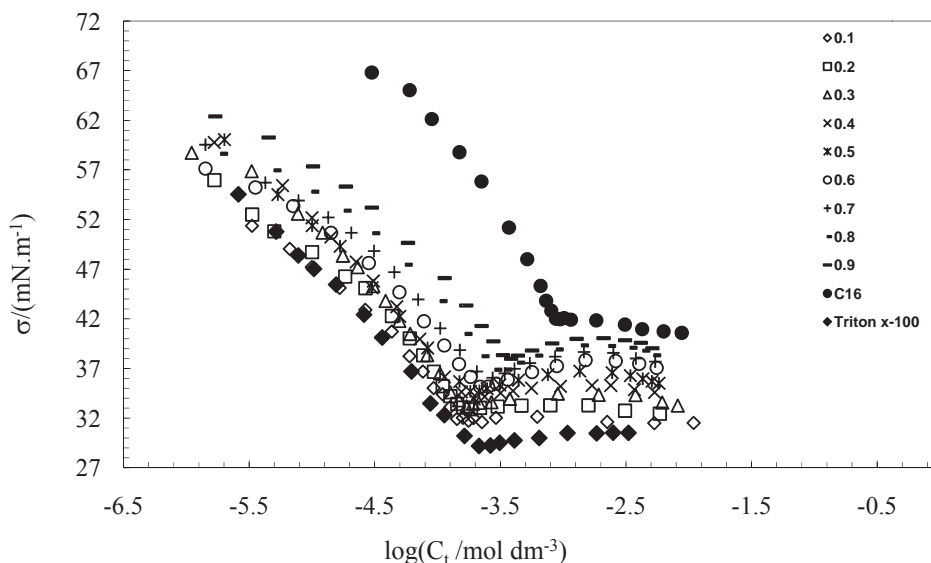


Fig. 1. Plot of the surface tension vs. the total surfactant concentration of the system C₁₆PC/TX-100 at different mole fractions of C₁₆PC in solution.

Conclusions:

From surface tension measurements it was shown that both cationic surfactants (C₁₄PC and C₁₆PC) used in the study show synergistic intermolecular interactions when mixed with the nonionic surfactant (Triton X-100). The synergistic effect is most pronounced for the mixture



with C₁₄PC: Triton X-100, which has a larger deviation from the ideal behavior than the C₁₆PC: Triton X-100.

References:

- [1] P.M. Holland, D.N. Rubingh, J. Phys. Chem. 87 (1983) 1984.
- [2] M. Bergström, Langmuir 17 (2001) 993.
- [3] M.J. Rosen, Surfactants and Interfacial Phenomena, Wiley, New York, 1989.
- [4] D.N. Rubingh, in: K.L. Mittal (Ed.), Mixed Micelle Solutions, Plenum, New York, 1979, p. 337.



Prediction and Correlation of Surface Tension Data for Binary System at Various Temperatures: DMSO - Long Chain alcohols

A.Abolhasani^{a*}, A. Bagheri^b, A.R.Moghadassi^a, A. Alavi^c, A.A. NazariMoghaddam^c

^a Department of Chemical Engineering, Faculty of Engineering, Arak University, Sardasht Square, Pardis of Arak University, Arak, 38156-8-8349, IRAN

^b Department of Physical Chemistry, Faculty of Chemistry, Semnan University, Semnan, Iran

^c Department of Chemical Engineering, Science and Research branch, Islamic Azad University, Tehran, Iran

*Email: amirabolhasani65@yahoo.com

Keywords: Surface tension, Prediction, UNIFAC, Correlation, Binary mixture

Introduction:

Surface tensions of binary mixtures of DMSO and a long chain series of aliphatic alcohols (1-propanol, 1-butanol, and 1-hexanol) were measured as a function of composition using the ring detachment method in the temperature range between (288.15 and 328.15) K. The surface tension data is used to describe quantitatively the nature, properties, and compositions of surface layers in binary liquid mixtures. The modified UNIFAC model is employed for calculation activity coefficients of surface and bulk phases. Also, the surface tension has been predicted based on the Suarez method. Correlating the surface tension of the above mentioned binary systems was performed with empirical and thermodynamic based models. The composition of the interface of a binary mixture usually differs from that of the bulk phases, and the adsorption of one chemical species at the interface can lead to a substantial reduction in the surface tension of the system [1-3].

Methods:

The surface tensions of the pure liquids and their mixtures were determined using a PC controlled KSV Sigma 701 tension balance which employs the Du Noüy ring-detachment method. The Platinum/Iridium ring was thoroughly cleaned and flamed before each measurement. Each measurement was repeated up to ten times to check for reproducibility. The uncertainty of the surface tension measurement is $\pm 0.04 \text{ mN.m}^{-1}$ of the final value of

surface tension. The temperature was kept constant by a water bath circulator (LAUDA, ECO-RE415) and with a precision of ± 0.1 K.

Result and discussion:

In all systems, the surface tension, decreased with increasing alcohol mole fraction. This trend is nonlinear and surface tension decreased rapidly with increasing alcohol concentration (see Fig. 1).

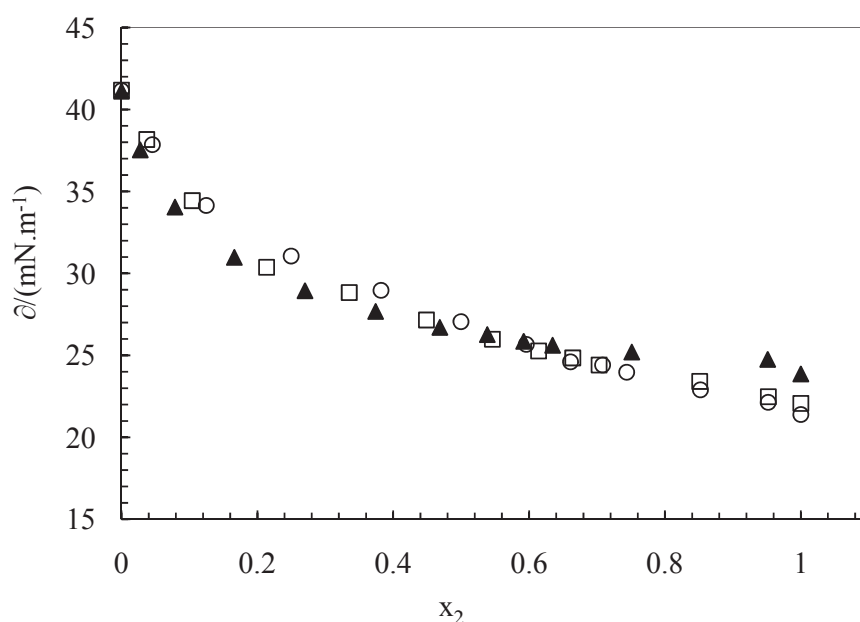


Fig. 1. Surface tension, σ , for the Alcohol/DMSO system, as a function of the mole fraction of:
(\circ)propanol, (\square)butanol and (\blacktriangle)hexanol, at 308.15 K

Conclusions:

The corresponding states models were evaluated for the estimation of the measured data. It was shown that the use of simple mixing rules can return accurate surface tension values. These methods are expected to be useful in calculating the surface tension of a large number of such liquid systems. The results obtained from the proposed methods are found to be in excellent agreement with the experimental values. The experimental results show that by adding alcohol the surface tension decreases (nonlinear) but by increasing the temperature (at constant mole fraction) the surface tension decrease linear..



References:

- [1] A. A. Rafati, E. Ghasemian, M. Abdolmaleki, J. Chem. Eng. Data 53 (2008) 1944–1949.
- [2] A. S. Skapski, J. Chem. Phys. 16 (1948) 386–389.
- [3] A. A. Rafati, E. Ghasemian, H. Iloukhani, J. Chem. Thermodyn. 41 (2009) 386–391.

15th Physical Chemistry Conference



Fixing of nickel nanoparticle on artificial vermiculite substrate in acidic media and study their catalytic properties in vegetable oil hydrogenation

S. A. Nabavi Amri^{a,*}, M. Ghaffary^a, P. Layani^a

^a Research Laboratory of Thermodynamics, Department of Chemistry, Damghan University, Damghan, Iran

* E-mail: nabavi@du.ac.ir

Keywords: nickel nanoparticle, support, vermiculite, oil hydrogenation

Introduction:

Partial hydrogenation of the carbon-to-carbon double bonds in triglycerids, especially of vegetable oils, is a major industry in many parts of the world. Despite its importance, hydrogenation mechanism is not completely clarified, until now [1]. The edible oil industry relies heavily on nickel catalysts to manufacture partially hydrogenated vegetable oil products. These catalysts offer several advantages, including high activity, low cost, and ease of separation from the processed oil [2]. Metal oxides are used in heterogeneous catalytic reactions. Large surface area of the oxides can provide a support for metal nano-particles and additives may be used to enhance catalytic activity [3]. Generally, the formation of metal nanoparticle on acidic supports always generates bifunctional catalysts. Addition of acids or acidic supports is often used to enhance the efficiency of catalysts for hydrogenation, hydrogenolysis, and hydrocracking processes [4]. The present paper focuses on the support pH effect on the catalytic hydrogenation of vegetable oil using nano-sized nickel as catalyst.

Materials and methods:

In this project, we used nickel nanoparticles, that was prepared in other projects in this laboratory in acidic medium. For fixing catalyst on support, the vermiculite slurry in water was prepared and pH of solutions was set in the range of 0-4, by adding nitric acid. After stabilizing solutions at pH values .94, 1.2, 2.73, 3.43, on the basis of its dry matter weights mixture of 15, 20, 25 wt% nickel nanoparticle were prepared in vermiculite slurry. Samples were dried, annealed and activated under hydrogen atmosphere. Activity of made catalyst was

tested in hydrogenation of oil in thermal range of 90 to 95 °C and efficiency of catalyst with saturation percentage was studied by a method which is different from popular Wijs method.

Result and discussion- Conclusion:

Chart of the amounts of saturation percentage for different concentrations in each pH is shown in figure 2. According to it:

- 1- Review of the course of curves, represents more saturation of oil in acidic pH in this range. It seems that what is common in these processes is that the hydrogenation reaction will follow the Langmuir-Hinshelwood mechanism and acidic support of catalyst helps to increase activity of catalyst with decreasing its electronic charge.
- 2- The slight differences between 3 curves, show that by using appropriate support, can reduce the percentage of the active phase in catalyst.

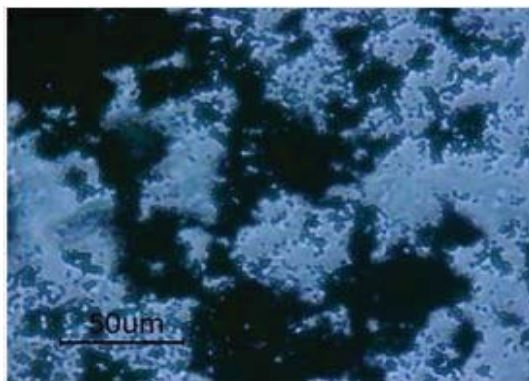


Figure 1-microscopic image of nickel nanoparticle

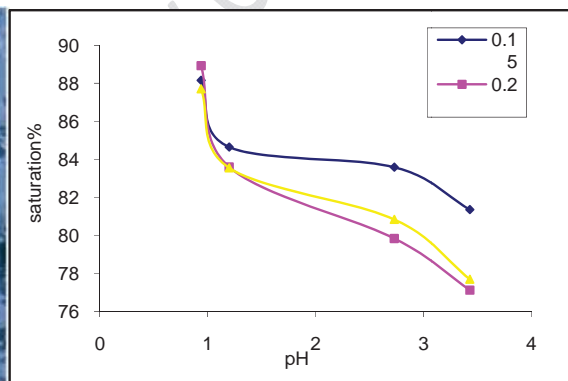


Figure 2-curve of saturation% oil- pH

References:

- [1] D. Jovanovic and et al; "The influence of the isomerization reactions on the soybean oil hydrogenation process"; J. Mol. Catal. A: chem; 159, 353-357, 2000.
- [2] A. J. Wright and et al; "Cis selectivity of mixed catalyst systems in canola oil hydrogenation"; Food Research International; 36, 797-804, 2003.
- [3] E. W. Hagaman and et al; "Surface alumina species on modified titanium dioxide: A solid-state ²⁷Al MAS and 3QMAS NMR investigation of catalyst supports"; Solid State Nucl. Magn. Reson.; 37, 82-90, 2010.
- [4] J. Huang and et al; "Tuning the support acidity of flame-made Pd/SiO₂-Al₂O₃ catalyst for chemoselective hydrogenation"; J. Catal.; 281, 352-360, 2011.



Fixing of nickel nanoparticle on artificial vermiculite substrate in acidic media and study their catalytic properties in vegetable oil hydrogenation

S. A. NabaviAmri^{a,*}, M. Ghaffary^a, P. Layani^a

^a Research Laboratory of Thermodynamics, Department of Chemistry, Damghan University, Damghan, Iran

* E-mail: nabavi@du.ac.ir

Keywords: nickel nanoparticle, support, vermiculite, oil hydrogenation

Introduction:

Partial hydrogenation of the carbon-to-carbon double bonds in triglycerids, especially of vegetable oils, is a major industry in many parts of the world. Despite its importance, hydrogenation mechanism is not completely clarified, until now[1]. The edible oil industry relies heavily on nickel catalysts to manufacture partially hydrogenated vegetable oil products. These catalysts offer several advantages, including high activity, low cost, and ease of separation from the processed oil[2]. Metal oxides are used in heterogeneous catalytic reactions. Large surface area of the oxides can provide a support for metal nano-particles and additives may be used to enhance catalytic activity[3]. Generally, the formation of metal nanoparticle on acidic supports always generates bifunctional catalysts. Addition of acids or acidic supports is often used to enhance the efficiency of catalysts for hydrogenation, hydrogenolysis, and hydrocracking processes[4]. The present paper focuses on the support pH effect on the catalytic hydrogenation of vegetable oil using nano-sized nickel as catalyst.

Materials and methods:

In this project, we used nickel nanoparticles, that was prepared in other projects in this laboratory in acidic medium. For fixing catalyst on support, the vermiculite slurry in water was prepared and pH of solutions was set in the range of 0-4, by adding nitric acid. After stabilizing solutions at pH values .94, 1.2, 2.73, 3.43, on the basis of its dry matter weights mixture of 15, 20, 25 wt% nickel nanoparticle were prepared in vermiculite slurry. Samples were dried, annealed and activated under hydrogen atmosphere. Activity of made catalyst was

tested in hydrogenation of oil in thermal range of 90 to 95 °C and efficiency of catalyst with saturation percentage was studied by a method which is different from popular Wijs method.

Result and discussion-Conclusion:

Chart of the amounts of saturation percentage for different concentrations in each pH is shown in figure 2. According to it:

- 3- Review of the course of curves, represents more saturation of oil in acidic pH in this range. It seems that what is common in these processes is that the hydrogenation reaction will follow the Langmuir-Hinshelwood mechanism and acidic support of catalyst helps to increase activity of catalyst with decreasing its electronic charge.
- 4- The slight differences between 3 curves, show that by using appropriate support, can reduce the percentage of the active phase in catalyst.

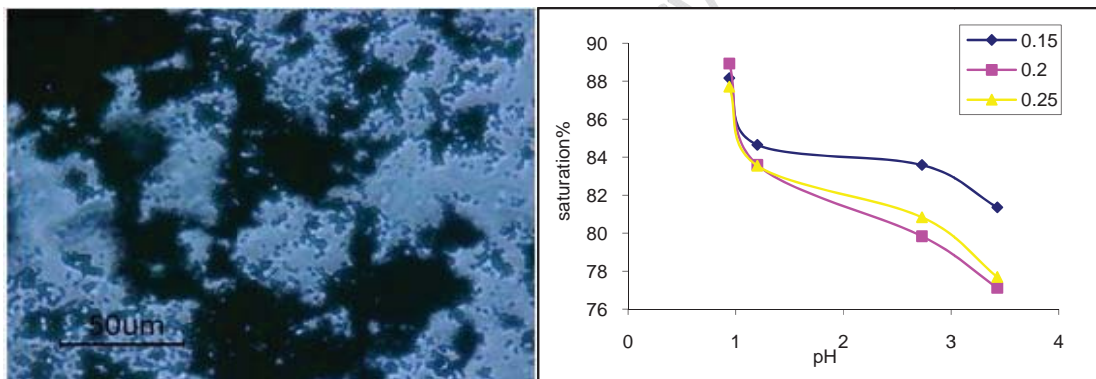


Figure 2-curve of saturation% oil- pH

Figure 1-microscopic image of nickel nanoparticle

References:

- [1] D. Jovanovic and et al; "The influence of the isomerization reactions on the soybean oil hydrogenation process"; J. Mol. Catal. A: chem; 159, 353-357, 2000.
- [2] A. J. Wright and et al; "Cis selectivity of mixed catalyst systems in canola oil hydrogenation"; Food Research International; 36, 797-804, 2003.
- [3] E. W. Hagaman and et al; "Surface alumina species on modified titanium dioxide: A solid-state ²⁷Al MAS and 3QMAS NMR investigation of catalyst supports"; Solid State Nucl. Magn. Reson.; 37, 82-90, 2010.
- [4] J. Huang and et al; "Tuning the support acidity of flame-made Pd/SiO₂-Al₂O₃ catalyst for chemoselective hydrogenation"; J. Catal.; 281, 352-360, 2011.



Application of Shereshefsky Model to Binary Mixtures: Surface Analysis for Calculating Surface Tension and Surface Parameters

F. Mosleh^{*a}, R. Tahery^b

^a Science Department, Islamic Azad University, Central Tehran Branch, Tehran, Iran

^b Chemical Engineering Department, Islamic Azad University, Central Tehran Branch, Tehran, Iran

Email: farzaneh.mosleh@gmail.com

Key words: Surface tension, Binary solution, Shereshefsky model, Surface layer

Introduction:

Surface tension is a characteristic property of fluids. It is important for the development, design and simulation of many industrial processes, such as chemical engineering, oil recovery and environmental protection [1]. There are a lot of relationships to suggest the surface tension of binary mixtures including Meissner and Michael, Tamura et al, Eberhart, Guggenheim, Winderfeld. In this paper, we applied Shereshefsky model for surface analysis and calculating the surface tension of binary solutions and some parameters regarding surface layer. The method is applicable to systems comprising components of widely different molecular sizes and the full mole fraction range

Theory and Method:

An alternative model which gives knowledge about the surface structure of binary solutions and is able to compute the excess number of molecular layers and free energy change in the surface region was developed by Shereshefsky. This model was applied to a limited number of binary solutions [2]. The surface tension σ of a binary mixture is given by the following:

$$\sigma = \sigma_1 - \frac{\Delta\sigma_0 x_{2b} e^{\Delta G_s / RT}}{1 + x_{2b} (e^{\Delta G_s / RT} - 1)} \quad (1)$$

Where σ , σ_1 , σ_2 are the surface tension of the mixture and components 1, 2 respectively. T is the absolute temperature, R is the gas constant and $\Delta\sigma_0$ is the difference between the surface tensions of pure solvent σ_1 and pure solute σ_2 , x_{2b} is the mole fraction. In Eq. (2) ΔG_s is the free energy change of replacing 1 mole of solute in the surface region and in Eq. (4), δ_2^E is the

excess number of molecular layers in the surface region. In order to calculate surface tension using Eq. (2) it is necessary to determine the slope (m) and intercept(c).

$$\frac{x_{2b}}{\Delta\sigma} = \frac{1}{\Delta\sigma_0} e^{-\Delta G_s / RT} + \frac{x_{2b}}{\Delta\sigma_0} (1 - e^{-\Delta G_s / RT}) \quad (2)$$

$$m = \frac{x_{2b}}{\Delta\sigma_0} (1 - e^{-\Delta G_s / RT}) \quad , \quad c = \frac{1}{\Delta\sigma_0} e^{-\Delta G_s / RT} \quad , \quad \Delta G_s = RT \ln(1 + m/c) \quad (3)$$

$$\Delta\sigma_0 = 1/\alpha + \beta \quad , \quad \delta_2^E = \Delta\sigma_0 \overline{A_2} / \Delta G_s \quad , \quad \overline{A_2} = (M_2 / \rho)^{2/3} N_A^{1/3} \quad (4)$$

Where M_2 and ρ are the molecular weight and the density of solute and N_A is Avogadro's number.

Results and Discussion:

We have used Shereshefsky model for predicting the surface tension of binary organic and aqueous solutions and applied it to 28 binary organic and 32 aqueous solutions at 298.15, 303.15, 308.15 and 313.15 K and excellent results are obtained. The absolute average deviations percent AAD% of aqueous and organic solutions are 1.73% and 0.56% respectively. We have also obtained the standard Gibbs energy of adsorption, ΔG_s and δ_2^E . Where experimental data is available for the standard Gibbs energy of adsorption, the agreement between the calculated and the experimental data is very good in all cases.

Conclusions:

We used Eq. (2) for both binary organic and aqueous solutions and plot $x_{2b}/\Delta\sigma$ versus x_{2b} . In some case the plot of $x_{2b}/\Delta\sigma$ versus x_{2b} is not a straight line but the results of surface tension prediction is very good. It means that the calculated surface tension is not very sensitive to the linearity of $x_{2b}/\Delta\sigma$ versus x_{2b} and for this reason this method is strongly recommended for binary solutions. It was found that generally the ΔG_s and $\Delta\sigma_0$ for aqueous solutions is greater than for the organic solutions.



Reference:

- [1] D.Fu, J.Lu, J.Liu, Y.Li;"Prediction of surface tension for pure non-polar fluids based on density functional theory"; Chem. Eng. Sci; 56, 6989-6996, 2001.
- [2] R.Tahery, H.Modarress, J.Satherley;"Surface tension prediction and thermodynamic analysis of the surface for binary solutions";Chem. Eng. Sci;60, 4935-4952, 2005.

15th Physical Chemistry Conference



Simultaneous Influence of SDS Surfactant and Uni-Univalent Salts on the Interfacial Tension of Toluene-Water: A New Insight

J.Saien*, F.Moghadamnia

Department of Applied Chemistry, Bu-Ali Sina University, Hamedan, Iran

Email: saien@basu.ac.ir

Key words: Interfacial tension, Salt, Surfactant, Modeling

Introduction:

The work done for creating a unit of new surface between two immiscible fluids is known as interfacial tension (IFT). Performing mass transfer in industrial processes such as extraction can be altered by IFT significantly, due to changes in drop hydrodynamic. The main purpose of this work is an investigation about effect of uni-univalent salts that can be found in natural and industrial waters (NaCl, KCl and KI) on IFT of toluene and solution containing low concentration of surfactant which is almost industrially inevitable due to contamination.

Materials and methods:

The chemical system of toluene-water was used. Toluene and uni-univalent salts NaCl, KCl and KI were Merck products with purity of more than 99.5%, 99.8%, 99.5% and 99.5%, respectively. Anionic surfactant sodium dodecyl sulfate (SDS) also was purchased from Merck with purity of more than 99%. Deionized water was used throughout.

Apparatus:

All interfacial tension measurements were performed at temperature 20.0 °C with a drop weight set up. Density of each salt solution was measured by mean of an Anton Paar DMA 4500 densitometer with an uncertainty of $\pm 0.01 \text{ kg.m}^{-3}$.

Result and discussion:

The IFT graph vs. surfactant concentration (Fig. 1) shows that IFTs face less reduction in the presence of SDS without any salt; however, addition of different concentrations of salts leads

to intensify this reduction in IFT. Fitting experimental data with equation of state (combination of Gibbs and Langmuir isotherms by considering salt effect) resulted in obtaining K_L (adsorption constant) and Γ_m (maximum interfacial concentration when interface is saturated). ΔG_{ads} (Gibbs free energy of adsorption) and A_m (minimum area occupied by a molecule at interface) were also obtained. Increase of K_L , Γ_m and ΔG_{ads} for each salt with increase of concentration reveals more adsorption of surfactant at interface resulting in lower amount of A_m . At high salt concentrations, the salts effect in IFT reduction are in the order of $KI > KCl > NaCl$. Meantime this order for surfactant surface concentration, Γ , is $KI > KCl > NaCl$ (Fig. 2). The strong behavior of KI stemmed from innate properties of KI salt.

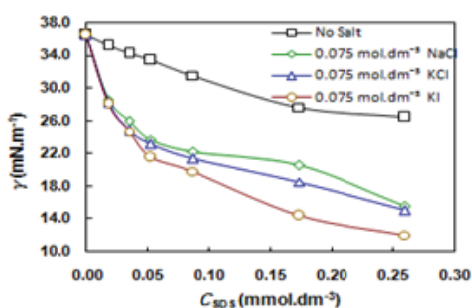


Fig 1. IFT variation VS. surfactant concentration for different salts.

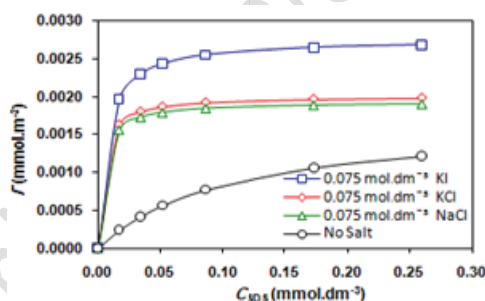


Fig 2. Γ values vs. surfactant concentration for different salts

Conclusion:

In this work simultaneous influence of SDS surfactant and three uni-univalent salts of NaCl, KCl and KI on IFT of toluene-water was investigated. Strange behavior was observed for KI at higher concentrations which caused intensive reduction in IFT in comparison to KCl and NaCl.

References:

- [1] Kumar, M. K., T. Mitra, et al. (2006). "Adsorption of Ionic Surfactants at Liquid-Liquid Interfaces in the Presence of Salt: Application in Binary Coalescence of Drops." *Industrial and Engineering Chemistry Research* 45(21): 7135-7143.
- [2] Para, G., E. Jarek, et al. (2005). "The surface tension of aqueous solutions of cetyltrimethylammonium cationic surfactants in presence of bromide and chloride counterions." *Colloids and Surfaces A: Physicochemical and Engineering Aspects* 261(1-3): 65-73.



Inhibition by cetyltrimethyl ammonium bromide of the corrosion of stainless steel in NaCl solution

Ali Yousefi^a, Soheila Javadian^{a*}

^aDepartment of chemistry, Faculty of sciences, Tarbiat modares university, Tehran, Iran

E-mail: Javadian_s@modraes.ac.ir

Key Words: Corrosion, Inhibitor, Surfactant, Impedance

Introduction:

Surfactants are compounds that can be found in a multitude of domains, from industrial settings to research laboratories and are the part of our daily lives. Due to their unique structure they can drastically modify the interfacial properties. It is well known that corrosion never stops but its scope and severity can be lessened. The main problem of using stainless steel is its dissolution in industrial water. Several methods are employed for the corrosion prevention. The addition of surfactants into aggressive media such as acid and salt solutions is one of the methods for achieving this goal. Surfactants exert the inhibition action by adsorption on the metal surfaces such that chemical structure of the ionic head (hydrophilic part) attacks the metal surface while its tail (hydrophobic part) extends to the solution face. In the present work, the inhibition effect of CTAB on the corrosion of stainless steel in 2.0 M NaCl solution was investigated by different ways [1-3].

Materials and methods:

Materials: Cetyltrimethyl ammonium bromide (CTAB) and hydrochloric acid (HCl) was obtained from Merck. The stainless steel sheets of 1 × 1 cm were abraded with a series of emery paper (grade 220–600–800–1000–1200–2000) and then washed with bidistilled water and acetone.

Methods: Electrochemical experiments were carried out in a conventional three-electrode cell with a platinum counter electrode (CE) and an Ag/AgCl reference electrode. The potential of potentiodynamic polarization curves was done from a potential of -250 mV vs. OCP, to 250 mV vs. OCP at a sweep rate of 0.5 mV s⁻¹.



Scanning electron microscopy (SEM), the specimens shown in SEM micrographs were exposed to the industrial water for a desired period of immersion under optimum conditions in the absence and presence of inhibitors.

Result and discussion:

The inhibition effect of cetyltrimethyl ammonium bromide (CTAB) on the corrosion of stainless steel in 2.0 M NaCl solution was studied by weight loss, potentiodynamic polarization, and electrochemical impedance spectroscopy (EIS) methods. The results show that CTAB is a very good inhibitor at little concentrations, and the inhibition efficiencies obtained from all methods employed are in good agreement with each other. Generally, the inhibition efficiency increased with increase of the inhibitor concentration. The obtained results show that CTAB is the best inhibitor at $5 \times 10^{-5} M$ additive concentration. Changes in impedance parameters (charge transfer resistance, R_{ct} , and double-layer capacitance, C_{dl}) were indicative of adsorption of CTAB on the metal surface, leading to the formation of a protective film. The potentiodynamic polarization measurements indicated the type of inhibition. The surface parameters of surfactant at NaCl media was calculated from its surface tension including the critical micelle concentration (CMC), maximum surface excess (Γ_{max}) and the minimum surface area (A_{min}). The free energy of micellization (ΔG_{mic}) was calculated. The surface morphology of steel sample was investigated by scanning electron microscopy (SEM).

Conclusion:

From the obtained corrosion data, it is clear that cetyltrimethyl ammonium bromide acts as a good inhibitor for the corrosion of stainless steel in 2.0 M NaCl solution. CTAB exert the inhibition action by adsorption on the metal surfaces such that chemical structure of the ionic head (hydrophilic part) attacks the metal surface while its tail (hydrophobic part) extends to the solution face.

Reference:

- [1] X. Li, S. Deng, H. Fu, CorrosionScience 53 (2011) 1529-1536.
- [2] A.M. Badiea, K.N. Mohana, CorrosionScience 51 (2009) 2231-2241.
- [3] X. Zhou, H. Yang, F. Wang, Electrochimica Acta 56 (2011) 4268-4275.



Removal of Red S-DSW (a disperse dye) from Aqueous Solution by activated carbon: A study of equilibrium adsorption isotherms

Mohsen Shabani^{*a}, Fariborz Azizinejad^a, Marjan Alikahi^a, Bita Farahany^a, Fatemeh sadat Hoseyni^a

^aDepartment Of Chemistry; Islamic Azad University; Varamin-Pishva branch; Tehran; Iran

Email: mshabani45@yahoo.com

Abstract:

The activated carbon was used for the removal of the disperse dye, Red S-DSW, from aqueous solutions. The dye adsorption experiments were carried out by using batch procedure. Experimental results have shown that in acidic pH favored the adsorption. The dye adsorption equilibrium was attained after 4 hours of contact time. The factors controlling the adsorption process were also calculated and discussed. And a maximum adsorption capacity of 59.82 mg/g of Red S-DSW was achieved. Equilibrium data were mathematically modeled using the Langmuir, Freundlich Temkin and Dubinin-Radushkevich adsorption models to describe the equilibrium isotherms at 4.64 solution pH value and 25°C temperature, and isotherm constants were determined. The Dubinin-Radushkevich isotherm was found to best fit the experimental data over the whole concentration range as indicating from the values of the correlation coefficients ($r^2 = 0.9992$).

Keywords: Adsorption isotherms, disperse dye, activated carbon

Introduction:

The treatment and disposal of dye-contaminated wastewater is one of the most serious environmental problems faced by the textile, dyeing, printing, ink, and related industries. Dyes are known pollutants that not only affecting aesthetic merit but also reducing light penetration and photosynthesis, and some are considered toxic and even carcinogenic for human health [1]. Numerous approaches, including biological treatment [2], coagulation/flocculation [3], ozone treatment [4], chemical oxidation, membrane filtration,



ion exchange, photo catalytic degradation and adsorption, have been developed to remove these compounds from colored effluents.

Among the different treatments described above, adsorption technology with no chemical degradation is attractive due to its merits of effectiveness, efficiency and economy.

Method:

The rate of dye adsorption is an important factor for disperse dye removal. Adsorption kinetic experiments were conducted by preparing a 250-mL Erlenmeyer flask containing 0.050 g L⁻¹ of activated carbon and different concentration of disperse dye solution to determine the minimum time required for adsorption to reach a steady-state condition at a fixed pH (4.64). The Erlenmeyer flasks was placed on a slow-moving platform shaker and approximately 50mL of aliquots were taken from the suspension at different time intervals of the reaction. The samples were treated with a centrifuge to separate the activated carbon from the solution. The concentration of dyes in effluent solution was analyzed by UV-vis spectrometry and relative dye adsorption (%) versus reaction time was determined.

Adsorption experiments were performed in 250-mL Erlenmeyer flask containing 50 mL of different concentrations of dyes and 0.050 g L⁻¹ of activated carbon to evaluate dye removal capability at fixed pH 4.64. To investigate the effect of adsorbent dosage, different doses of activated carbon were added to each bottle. The influence of solution pH values on dye removal was also studied by adding defined amount of the activated carbon into the Erlenmeyer flask containing 50mL of different dye solution with pH values ranging from 3 to 9. Dye adsorption isotherms were determined at initial pH 4.64 and the initial concentrations of disperse dye were varied from 20mgL⁻¹ to 120mgL⁻¹.

All batch experiments were carried out at ambient temperature (25±0.1 °C) and all the suspensions were shaken on a rotary shaker at 150rpm for 4h. The quantities of adsorbed disperse dyes were calculated by the difference of the initial and residual amounts of disperse dyes in solution divided by the weight of the adsorbent.

Results and discussion:

The effect of contact time was also investigated. It was found that dye uptake is not rapid and finally attains saturation within about 4 hours. As the pH increased, the removal rate

decreased. The pH value of the dye solution plays an important role in the whole adsorption process and particularly on the adsorption capacity.

The adsorption isotherm is the most important information, which indicates how adsorbate molecules are distributed between the liquid phase and solid phase when the adsorption process reaches equilibrium. This study adopted the Langmuir, Freundlich, Dubinin-Radushkevich (D-R) and Temkin isotherms to describe equilibrium adsorption.

Table 1 shows the isotherm parameters at 25°C. Based on the correlation coefficient (R^2), the adsorption of Disperse dye is best fitted in the D-R isotherm.

Table 1: Isotherm parameters for the removal of disperse dye by activated carbon

Langmuir constants	K_L (L/mg)	q_m (mg/g)	R^2
	0.01077	59.82	0.9639
Freundlich constants	K_F	n	R^2
	0.707725	0.9655	0.9502
D-R constants	Q_0 (mg/g)	E (kJ/mol)	R^2
	64.1933	9.7128	0.9992
Temkin constants	B_1	K_t (L/mgl)	R^2
	21.233	0.120337	0.9976

Cocclusion:

This study investigated the removal of a disperse dye from aqueous solution by activated carbon. The minimal time required to complete adsorption is 4 hours. The best pH is 4.64. For equilibrium adsorption, disperse dye was best fitted to the D-R isotherm.

References:

- [1] S.Wang, Y. Boyjoo, A. Choueib, Z.H. Zhu, Removal of dyes from aqueous solution using fly ash and red mud, Water Res. 39 (2005) 129–138.
- [2] M. Kornaros, G. Lyberatos, Biological treatment of wastewaters from a dye manufacturing company using a trickling filter, J. Hazard. Mater. 136 (2006) 95–102.
- [3] E. Guibal, J. Roussy, Coagulation and flocculation of dye-containing solutions using a biopolymer (Chitosan), React. Funct. Polym. 67 (2007) 33–42.
- [4] W. Zhao, Z. Wu, D. Wang, Ozone direct oxidation kinetics of cationic red X-GRL in aqueous solution, J. Hazard. Mater. 137 (2006) 1859–1865.



Synthesis of Mo/ZSM-5/HMS biporous catalysts with the high stability for dehydroaromatization and catalytic conversion of methane to benzene

M. R. Toosi^{*,a}, M. D. Ganji^a, M. Kalantari^b,

^b Department of Chemistry, Qaemshahr Branch, Islamic Azad University, Qaemshahr, Iran

E-mail: mertoosi@gmail.com

Keywords: Biporous catalysts, Dehydroaromatization, Methane, Benzene

Introduction:

The reaction of methane dehydroaromatization is an interesting process for conversion of natural gas to the aromatics [1, 2]. In this way, methane can be selectively converted to aromatics such as benzene and naphthalene in the absence of oxygen. Mo/HZSM-5 and W/HZSM-5 have more activity for this reaction among the transition metal catalysts supported on HZSM-5. It has been found that methane activation occurs on the reduced Mo/W species. However the main problem of these catalysts is fast deactivation due to coke deposition on the channels of zeolite [3]. In this paper we have synthesized micro/mesoporous combined materials using zeolite particles and hexagonal mesoporous silicate (HMS) as a new support for Mo catalysts and investigated their catalytic activity for conversion of methane to benzene.

Experimental:

The HMS materials were synthesized by sol-gel method similar to Pinnavaia and coworkers [4], used TEOS as the silica source and dodecylamine as the surfactant. The 6 wt. % Mo/HZSM-5/HMS and 6 wt. % W/HZSM-5/HMS catalysts were prepared by adding HZSM-5 with a desired amount of ammonium heptamolybdate and ammonium tungstate to the sol of HMS before aging and drying of gel. The IR measurements were made on powdered catalyst samples using a Biorad Infrared Spectrometer (Model FTS 40, Digilab Division) in reflective mode. Catalytic reactions were carried out in a continuous fixed-bed quartz microreactor. The pure methane was introduced into the reactor with a space velocity of 1500 ml/(gcat h). The effluent from the reactor was analyzed on-line with gas chromatograph equipped the



thermal conductive detector. The hydrocarbon products were ethylene, benzene, and naphthalene.

Results and discussion:

The FT-IR transmission spectra for fresh catalysts showed that infrared range featured absorption peaks of ZSM-5 at 550, 850, 1100, 1225, 1400, 1650, and 3340 cm^{-1} . This was shown by the presence of the infrared band at 550 cm^{-1} , assigned to the five-membered ring of the pentasil zeolite structure correspond to TO4 symmetric stretching, double-ring and bending vibrations [1, 2]. The peaks at 1220 and 1095 cm^{-1} corresponded to TO4 asymmetric stretching vibration, assigned to the external linkages (between TO4 tetrahedral) as a structure-sensitive IR band of ZSM-5 zeolite. IR spectrums of the spent catalysts showed that the Brönsted sites of zeolite decreased markedly due to the reduction of their band intensity in 3425 and 3650 cm^{-1} . The reduction of the intensity of IR band in 550 cm^{-1} indicated that the coke deposited on the entire external surface of zeolite which contained pentasil groups [3]. However, biporous ZSM-5/HMS support had a less decrease in above peaks.

Conclusion:

Our results showed that biporous catalyst had a high stability for methane dehydroaromatization. It was found that the redispersion of the ZSM-5 over the HMS could prevent the blockage of the channels of zeolite and decrease the deactivation of catalyst.

References:

- [1] C.E.A. Kirschhock, R. Ravishankar, F. Verspeurt, P.J. Grobet, P.A. Jacobs, J.A. Martens, *J. Phys. Chem., B* 103 (1999) 4965-4971.
- [2] Y. Cheng, L.-J. Wang, J.-S. Li, Y.-C. Yang, X.-Y. Sun, *Mater. Lett.* 59 (2005) 3427–3430.
- [3] B. Li, S. Li, N. Li, H. Chen, W. Zhang, X. Bao, B. Lin, *Micropor. Mesopor. Mater.* 88 (2006) 244–253.
- [4] T. Tanev, T.J. Pinnavaia, *Science* 267 (1995) 865–867



Investigation of isotherms for Adsorption of Methylene Blue dye (MB) by nano layer of electroactive polymer

M. Banimahd keivani^{* a}, H. Pourmohammad^b, R. Ansari^c,

^{* a} Department of Chemistry, Payame Noor University, Rasht, Iran

^b Department of Chemistry, Ardabil branch, Islamic Azad University, Ardabil, Iran

^cDepartment of Chemistry, Guilan University, Rasht, Iran.

Email: keivani@acecr.ac.ir

Abstract:

In this research, nano composite of polyaniline sawdust (termed as Pan/SD) was prepared via chemical polymerization of aniline on the surface of sawdust for adsorption MB from aqueous solution. The studies of adsorption were studied by using Langmuir, Freundlich equations. The results showed that Pan/SD was a good adsorption for removal of methylen blue. Finally, adsorption of MB on the surface of sawdust coated with Pan/SD was showed by using scanning electron microscopy (SEM) images.

Keywords: Methylene Blue, Nano polyaniline, Langmuir, Freundlich

Introduction:

Dyes have been extensively used in industries, such as textile, paper, printing, cosmetics, plastics and rubber, for the coloration of products [1,2]. The discharge of colored waste is not only damaging the aesthetic nature of receiving streams, but also is toxic to the aquatic life [2]. Polyaniline (Pan) is a conducting polymer that can be easily synthesized chemically from bronsted acidic aqueous solutions [3,4]. The removal dye from the wastewater, before entering rivers, is very important. For treatment of the adsorption data, both Langmuir and Freundlich isotherm were employed, therefore MB as a typical basic textile dye was selected as a test probe [4].

Methods:

Polymerization was carried out in aqueous solution. Polyaniline was obtained from Merck and Sawdust samples (SD) from walnut obtained from a local carpentry workshop. Absorbance studies were carried out on a single beam Perkin-Elmer UV-Vis

spectrophotometer with a 1 cm cell ($\lambda_{\max} = 660$ nm) was used for measuring all of absorption data.

Results and Discussion:

Langmuir and Freundlich adsorption models were used for data interpretation.

$$q_t = \frac{(C_0 - C) V}{m}$$

where q_t (mg/g) is the amount of adsorbed dye by Pan/SD at time t (min); C_0 (mg/L) and C (mg/L) are the liquid phase concentrations of the dye at time 0 (min) and t (min), respectively; V (L) is the volume of the solution, and m (g) is the weight of the Pan/SD.

Both Langmuir and Freundlich models were used to fit the isotherm experimental data. The linear form of the Langmuir isotherm equation is shown as follows:

$$q_t = \frac{1}{x_m} + \frac{1}{x_m b C_e}$$

where C_e is the equilibrium dye concentration in the solution (mg/L), X_m , the monolayer sorption capacity of the biosorbent (mg/L), and b is the Langmuir constant (L/mg) and is related to the free energy of biosorption. The linear form of the Freundlich isotherm equation is given as follows:

$$\log q_t = \log k + \frac{1}{n} \log C_e$$

where K (L/mg) and n are Freundlich sorption isotherm constants being indicative of the extent of the biosorption and the degree of nonlinearity between solution concentration and biosorption, respectively.

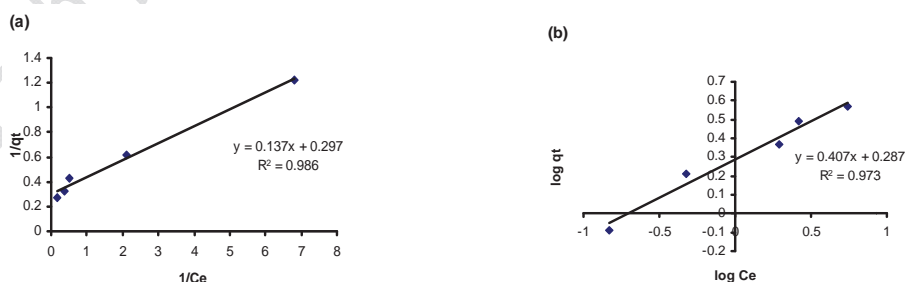


Fig.1. Langmuir plots (a) and Freundlich plots (b)

Table 1 Langmuir and Freundlich model parameters

T (K)	Langmuir model			Freundlich model		
	X_m	b (L/mg)	R^2	K (L/mg)	n	R^2
298	3.36	2.17	0.986	1.93	2.46	0.973

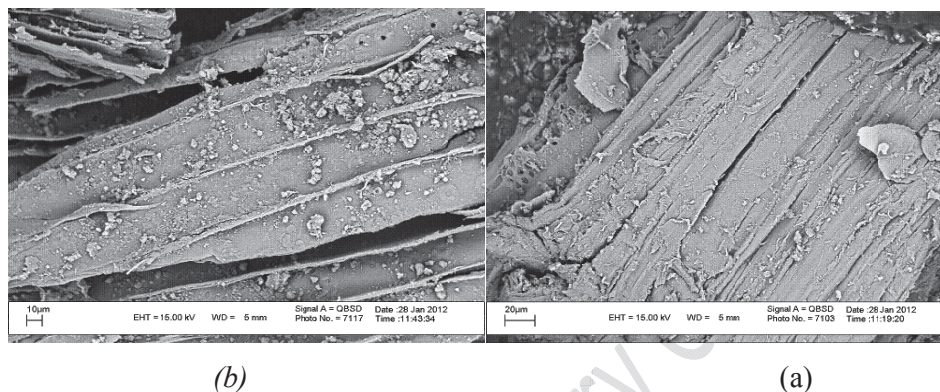


Fig. 2. SEM images of the Pan/SD before (a) and after (b) adsorption of MB.

Conclusion:

Maximum value of experimental adsorption from Langmuir isotherm is equal to 3.36 mg. also, value of $n = 2.46$ resulted from freundlich show the convenient of PAn/SD as an adsorbent for adsorptions of methylen blue.

References:

- [1] N. Kannan , M. Meenakshisundaram, *Water,Air and Soil Pollution*, (2001), 138, 289-305
- [2] K. Kadirvelu, M. Palanival , S. Rajeswari, *Bioresource Technology*, (2000),74, 263- 265
- [3] R. Ansari , A. H. Alikhani, *J. Coat. Technol. Res.*, (2009), 6 (2), 221-227
- [4] M. Banimahd Keivani, R. Ansari, A. Fallah Delavar, *J. of Appl. Polymer Science*, (2011),122 (3),804-812



Surface tension measurement of Pure Ionic Liquid, 1- hexyl-3- methyl imidazolium Bromide [HMIM][Br] in different temperature

D. Farmanzadeh*, Y. Shad, S. Yeganegi

Faculty of Chemistry, University of Mazandaran, Babolsar, Iran

Email: d.farmanzad@umz.ac.ir

Key words: Ionic liquid, Surface tension, Thermodynamic properties, Critical temperature.

Introduction:

Ionic liquids (ILs) are molten salts made up of an anion and an organic cation, they were discovered in 1914. In recent years, ILs have been widely used in chemical process and industries due to their unique properties. Therefore the knowledge of the thermodynamic properties of these ionic liquids and their mixtures with other solvents, such as surface tension, density, viscosity, electrical conductivity and refractive index, is highly important [1].

In this study, the surface tension of pure ionic liquid, [HMIM][Br], and its temperature dependency was studied. The surface thermodynamic functions, such as surface entropy and enthalpy, are derived and the critical temperature, by Guggenheim [2] equation, is estimated.

Materials and Methods:

Materials: The ionic liquid, [C6mim][Br] (mass fraction purity > 0.98), which is liquid at room temperature, is purchased and used without further purification.

Methods: The original IL bottle was opened into a glove box to avoid water adsorption, which is particularly important in this IL. All measurements were carried into the glove box and were repeated three to five times. The measurements were conducted in the 298 to 318 K temperature range at atmospheric pressure.

Apparatus:

The surface tension was measured with a Kruss K8 tensiometer using a ring method. The ring of 20 mm diameter was provided and certified by Kruss GmbH.

Result and discussion:

Effect of Temperature: The measured surface tension, σ , and its temperature dependency, $(\partial\sigma/\partial T)$, of [C6mim][Br] at 298 K temperature are reported in Table 1. Also, for comparison purposes, these values for common solvents are listed from other reference [3] in Table 1. It can be seen from Table 1 that, the surface tension of this IL is less than water and more than methanol and ethanol (normal alcohols). Whereas the amount $\partial\sigma/\partial T$ for [C6mim][Br] is less than water and normal alcohols (common solvents). This result can be interpreted as this: the ionic liquid alkyl groups are oriented toward the outside of the liquid phase, while the charged parts of IL molecules are transported to the liquid phase.

Table1. Comparing the temperature dependence of surface tension of ionic liquid [HMIM] [Br] with some common solvents.

Substance	$\sigma_{298} \text{ (m.N.m}^{-1}\text{)}$	$\partial\sigma/\partial T$	Reference
[C6mim][Br]	42.0	-0.050	This work
water	72.0	-0.168	3
methanol	22.1	-0.093	3
ethanol	21.9	-0.081	3

Thermodynamic properties: The calculated surface entropy (S^σ) and the surface enthalpy (H^σ) from $H^\sigma = \sigma - T(\partial\sigma/\partial T)$ and $S^\sigma = -(\partial\sigma/\partial T)$ at 298 K are presented in Table 2. The critical temperature (T_c^G) and the total surface energy (E^σ) of [C6mim][Br], based on of the Guggenheim equation are estimated and reported in Table 2.

Table 2. Surface thermodynamic functions for pure [C6mim][Br] at temperature T = 298 K.

IL	$10^5 S^\sigma \text{ (J. m}^{-2} \cdot \text{K}^{-1})$	$10^2 H^\sigma \text{ (J. m}^{-2})$	$10^2 E^\sigma \text{ (J. m}^{-2})$	$G^\sigma \text{ (m.J.m}^{-2})$	
[HMIM][Br]	5.0	5.7	1320	5.7	42.0

Conclusion:

The ring method has been used to measure the surface tension of IL in different temperatures. The surface tension of [C6mim][Br] IL is less than water and more than normal alcohols. The obtain results show that the effect of temperature on the surface tension of [C6mim][Br] is lower than common solvents such as water and normal alcohols.

Reference:

[1] U. Domańska, M. Królikowska, *J. Colloid. Interf. Sci.* 348, 661, **2010**.



- [2] E. A. Guggenheim, *J. Chem. Phys.* 13, 253, **1945**,
[3] B. Wohlfarth "Surface Tension of Pure Liquids and Binary Liquid Mixtures", springer, Germany, 1997.

15th Physical Chemistry Conference



Adsorption of phenol on bentonite: A study of equilibrium adsorption isotherms

Maryam Molae^a, Mohsen Shabani^{*b}, Seyed Ali Akbar Salari^a

^a Department of Chemistry; Islamic.Azad.University, Shahr-rey branch, Tehran, Iran

^b Department Of Chemistry; Islamic.Azad.University; Varamin-Pishva branch; Tehran; Iran

m.molay65@yahoo.com

Abstract:

In this study equilibrium adsorption isotherm for the removal of phenol from aqueous solution using bentonite has been investigated. Liquid phase adsorption experiments were conducted and the maximum adsorptive capacity was determined. The effect of pH was studied. Equilibrium data were mathematically modeled using the Langmuir, Freundlich and Temkin adsorption models to describe the equilibrium isotherms at 6.64 solution pH value and 25°C temperature, and isotherm constants were determined. The results indicate the potential use of the adsorbent for the removal of phenol from aqueous solution. Maximum adsorption capacity of 303.03 mg/g at 25°C at equilibrium was achieved. It was found that pH plays a major role in the adsorption process. The optimum pH for the removal of phenol from aqueous solution under the experimental conditions used in this work was 6.64. The Langmuir isotherm was found to best fit the experimental data over the whole concentration range as indicating from the values of the correlation coefficients ($r^2 > 0.9328$).

Keywords: Adsorption, Bentonite, Phenol, Isotherms

Introduction:

Phenols constitute a widespread and important class of water pollutants and are considered as priority pollutants. They are indeed discharged in the liquid effluents from various factories: Chemical, petrochemical, paper, wood, metallurgy and cocking plants [1]. They can also originate from diffuse emissions, e.g. roads and pipes tar coatings and from the use of pesticides including their transformation products, e.g. herbicides, fungicides like dinitroorthocresol (DNOC), and pentachlorophenol (PCP). Phenolic compounds are also



found in the waste waters of agroindustrial processes like the olive oil mills, tomato processing and wine distilleries [2,3].. In this study, equilibrium adsorption isotherm for the removal of phenol from aqueous solution using bentonite has been investigated. Liquid phase adsorption experiments were conducted and the maximum adsorptive capacity was determined. The effect pH was studied.

Method:

Adsorption experiments were conducted by batch mode in stoppered conical flasks. Solutions were prepared by dissolving the phenols in deionized water. For each time 0.100 g bentonite and 50 mL phenol solution were mixed in a flask, which was then shaken in a thermostat water bath.

In adsorption isotherm studies, solutions with different initial concentrations were added, the pH was adjusted at 6.64, and the equilibrium time was set as 24 h, which was enough according to the preliminary experiments. Samples were separated by filtration and the phenol concentrations were analyzed by UV spectroscopy at λ_{max} 270 nm for phenol. The uptake of the adsorbate at equilibrium, q_e (mg/g), was calculated by the following equation: $q_e = V * (C_o - C_e) / m$ where C_o and C_e are the initial and equilibrium concentrations of the phenols (mg/L). in solution, V is the volume of the solution (L) and m is the weight of the adsorbent (g).

In pH studies, the solution pH was adjusted by addition of HCl or NaOH after the mixture of phenols with Bentonite. Experiments were conducted at 25°C, samples were separated after 24 h. The initial concentration for phenol was 50 mg/L.

Results and discussion:

The effect of contact time was also investigated. It was found that dye uptake is not rapid and finally attains saturation within about 24 hours. As the pH increased, the removal rate increased. The best pH for removal of phenol by bentonite is 6.64.

The adsorption isotherm is the most important information, which indicates how adsorbate molecules are distributed between the liquid phase and solid phase when the adsorption process reaches equilibrium. This study adopted the Langmuir, Freundlich, Dubinin-Radushkevich (D-R) and Temkin isotherms to describe equilibrium adsorption.

Table 1 shows the isotherm parameters at 25°C. Based on the correlation coefficient (R^2), the adsorption of phenil is best fitted in the Langmuir isotherm.

Table 1: Isotherm parameters for the removal of phenol by activated carbon

Langmuir constants	K_L (L/mg)	q_m (mg/g)	R^2
	0.000905	303.03	0.9328
Freundlich constants	K_F	n	R^2
	4.2359	2.522	0.8114
D–R constants	Q_0 (mg/g)	E (kJ/mol)	R^2
	46.7446	11.04315	0.8663
Temkin constants	B_1	K_t (L/mgl)	R^2
	10.733	0.15242	0.718

Conclusion:

This study investigated the removal of phenol from aqueous solution by Bentonite. The minimal time required to complete adsorption is 24 hours. The best pH is 6.64. For equilibrium adsorption, phenol was best fitted to the Langmuir isotherm.

References:

- [1] F. Ramade, Dictionnaire Encyclopédique des Pollutions, Ediscience International, 2000.
- [2] G. Achilli, G.P. Cellerino, P.H. Gamache, G.M. d’Eril, Identification and determination of phenolic constituents in natural beverages and plant extracts by means of a coulometric electrode array system, Journal of Chromatography A 632 (1993) 111–117.
- [3] G.M. Hunt, E.A. Baker, Phenolic constituents of tomato cuticle, Phytochemistry 19 (1980) 1415–1419.



An experimental study on surface properties of amino acid solutions

*Mohammad Hadi Ghatee, Fatemeh Bamdad

*Department of chemistry, university of Shiraz, Shiraz, 71454, Iran

(E-mail: ghatee@susc.ac.ir)

Abstract:

The surface tension of aqueous solutions of glycine, alanine, valine, isoleucine, and leucine was measured using the capillary rise method as a function of temperature and concentration. Glycine behaves like simple salts which dissociate into cations and anions completely. Surface properties like surface entropy and surface energy have been investigated.

Keywords: Alanine, Amino acids, Glycine, Isoleucine, Leucine, Surface properties, Surface tension, valine.

Introduction:

Amino acids serve as the building blocks of proteins, which are linear chains of amino acids. Amino acids can be linked together in varying sequences to form a vast variety of proteins. Twenty amino acids are naturally incorporated into polypeptides and are called proteinogenic or standard amino acids. Amino acids are important in nutrition and are commonly used in nutrition supplements, fertilizers, food technology and industry. In industry, applications include the production of biodegradable plastics, drugs, and chiral catalysts. Studies of the surface tension of the aqueous solution of amino acids are very limited. Norihiro Matubayasi et al. [1] have studied the surface properties of four amino acid solutions. They observed a positive slope for surface tension versus concentration for the solutions of glycine and of L-alanine, and a negative slope for that of L-valine.

Method:

In this work, surface properties of five amino acid solutions have been studied. Since the amino acids are not notably surface active, a sensitive method for the surface tension measurement is needed. We will accordingly, employ the capillary rise method for the

measurement of the surface tension of solutions of the five amino acids. A homemade capillary apparatus was used to measure the liquid/vapor interface.

Result and Discussion:

The aim of this paper is calculation of surface tension of five aliphatic amino acid solutions. Also, surface entropy and surface energy of aqueous amino acid solution at different concentration were obtained. The results show the negative slope for leucine, isoleucine, alanine and, valine. However, in the case of glycine the positive slope was observed up to 0.3M concentrations with no sign of regular result for the next concentrations. The obtained results are shown in Figure 1.

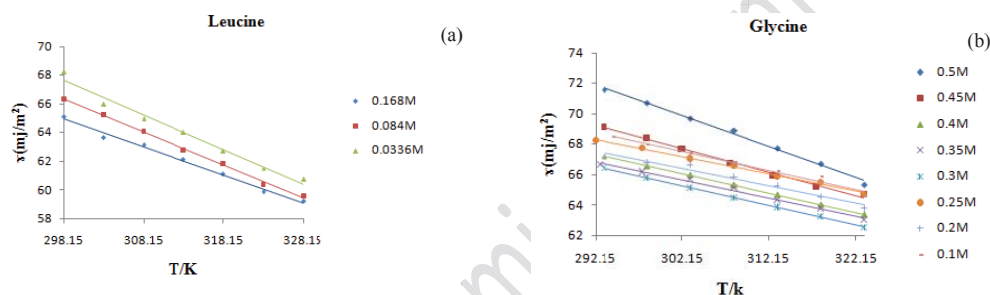


Figure1: (a) surface tension versus temprature for leucine in different concentration (b) surface tension versus temprature for glycine in different concentration.

Conclusion:

In this work surface tension of aqueous solutions of five amino acids has been studied. We have achieved the result of measurement for which was in some cases different from previous measurement and can be attributed to the method of the measurement.

References:

- [1] Norihiro Matubayasi, Hiroshi Miyamoto, Junji Namihira, Kentaro Yano, and Tomohiro Tanaka "Thermodynamic Quantities of Surface Formation of Aqueous Electrolyte Solutions" *Journal of Colloid and Interface Science* **250**, 431–437 (2002).



Nano silica phosphoric acid as an efficient eco-friendly catalyst for synthesis of aryl 14H-dibenzo[a,j] xanthenes in thermal and solvent-free conditions

A. Bamoniri^{a*}, A. Abbasi jeshvaghan^b

^a Department of Chemistry, faculty of Science, Kashan University, Iran.

^b Department of Chemistry, faculty of Science, Kashan University, Iran.

E-mail: bamoniri @ kashanu.ac.ir

Keywords: Xanthenes, Aldehyde, Dibenzo[a,j]xanthenes, Nano silica phosphoric acid

Introduction:

Nanoparticles such as silica have been widely used to reinforce polymer systems and fabricate nanocomposite[1,2]. Silica phosphoric acid (SPA) is a solid acid which can be used for different organic functional group transformations either as reagent or as catalyst under heterogeneous conditions [3]. In continuation of our investigation about application of solid acids, here we wish to report a new application of silica phosphoric acid (SPA) for the synthesis of 14H dibenzo[a,j]xanthenes derivatives in thermal and solvent-free conditions. First silica phosphoric acid was prepared. By using this catalyst, various aromatic aldehyde reaction with β -naphthol and converted to their corresponding aryl 14H-dibenzo[a,j] xanthenes in good to excellent yields.

Material and Methods:

Preparation of Nano-SPA:

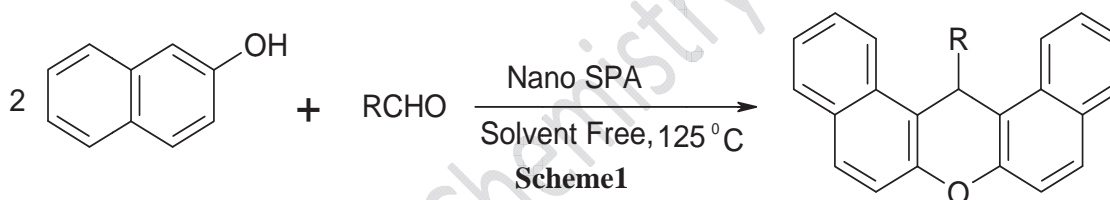
For preparation of the resin "nano silica phosphoric acid", it must be using nano silica chloride (reaction between nano silica gel and thionyl chloride), and then by the addition of anhydrous H₃PO₄ with CH₂Cl₂ (2×50 ml). Nano silica phosphoric acid was obtained as a white powder. (9.8 g, 0.1 mol) to a suspension of nano-silica chloride (94.5 g) in CH₂Cl₂ (200 ml) and vigorous stirring for 2h. Then the reaction mixture was filtered and the residue washed.

Preparation of 14H-dibenzo[a,j] xanthenes derivatives:

A mixture of the aldehyde (1 mmol), β -naphthol (2 mmol), nano-SPA (0.2g) was stirred at 125°C for the appropriate time according to Table 1. Completion of the reaction was indicated by TLC. After completion, the mixture was washed with CHCl₃ (10 ml) and filtered to recover the catalyst. The solvent was evaporated and the crude product recrystallized from EtOH to afford pure.

Results and discussion:

In this work we have described the facile, efficient synthesis of xanthene derivatives in the presence of nano silica phosphoric acid under solvent-free conditions at 125°C (Scheme 1). The optimum amount of catalyst was examined using the reaction of 4-methylbenzaldehyde and β -naphthol under solvent-free conditions at 125°C.



Conclusion :

We have demonstrated a simple method for the synthesis of 14-alkyl-14H-dibenzo[a,j]xanthenes using nano silica phosphoric acid as a reduced waste and ease of separation and recovery, environmentally friendly with respect to corrosiveness, safety, and efficient catalyst. High yields, and easy workup are the advantages of this protocol.

References :

- [1] Pinnavia T.J; Beall G.W “ Polymer–clay nanocomposites. New York”; John Wiley & Sons Ltd **2000**.
- [2] Dresselhaus M.S.; Dresselhaus G.; Avouris P ”editors Carbon nanotubes: synthesis, structure, properties and applications. Springer” p. 447, **2001**.



- [3] Zolfigol M.A; Shirini F; Zamani K.; Ghofrani E; “Silica phosphoric ACID/ NaNO_2 as a novel heterogeneous system for the coupling of thiols to their corresponding disulfides”, *Phosphorus, Sulfur, and Silicon and the related elements*; 179, 2177-2188, **2004**.

15th Physical Chemistry Conference



Half-metallic Ferromagnetism in the Zinc-blende MS(M=Li, Na & K) under Pressure and Stress

Z. Kamkar^{*a}, Z. Soltani^b

^aDepartment of Physics, Payame Noor University of Shiraz.

^bDepartment of Physics, Shiraz Branch, Islamic Azad University, Shiraz, Iran.

Email: ze.kamkar@yahoo.com

Keywords: Half-metallic, Ferromagnet, Spintronic, Density functional theory, Stress

Introduction:

Half-metallic ferromagnets, where one of the two spin channels is metallic while the other has an energy gap around the Fermi energy, attract increasing research interest in nano-electronics as potential materials for spintronic device applications; in particular, as a source of spin-polarized carriers injected into semiconductors[1]. Crystal structure of half-metal in zinc-blende are appropriate with structure of semiconductors in group III-V, so they can grow epitaxially on this semiconductors. If the lattice parameters of both compounds are slightly different, stress is entered to the system along the growth. In this case with changing the lattice parameter along the direction perpendicular to the surface, the supernatant system becomes tetragonal. Therefore in order to study the interface between half-metals and semiconductors, at first it must be determined whether these compounds maintain their half-metallic properties under stress caused by growth on semiconductors? In this article we investigate this issue and study the half-metallic property of zinc-blende MS (M=Li, Na & KS) under pressure and stress. First time Gao et al.[2] were investigated these compounds especially in the NaCl structure.

Methods:

Our calculations are based on density functional theory and for performing them we used PWscf computational code of ESPRESSO software.



Result&discussion:

Calculations of the total density of states (DOS) for each compound show that, there is an energy gap of about 5.19, 3.83 and 3.22 eV for LiS, NaS and KS, respectively in the majority-spin channel; while the minority-spin electrons are metallic, so all three compounds exhibit half-metallic ferromagnetism. The half-metallic gaps are 0.1, 0.52 and 0.71 eV for LiS, NaS and KS, respectively. The results show that the total magnetic moment is an integer value of $1\mu_B$ per formula unit, which it is a basic condition for the existence of half-metallic properties[1]. In all compounds the most contribution of total magnetic moment is related to S atoms. Our results are in agreement with Gao's et al [2] (see the following analysis in Table 1). Since the half-metallic ferromagnetism grown on the semiconductors by means of molecular-beam epitaxy (MBE) [3] as a substrate, therefore in order to study the stability of the half-metallicity under stress, we investigate the total magnetic moment at first, against the lattice contraction; then in the deviation from cubic to tetragonal structure. The results show that the half-metallicity is found to be robust against the lattice contraction up to 5%, 40% and 47% for LiS, NaS and KS, respectively.

Table 1 : The calculated equilibrium lattice constant (a), half-metallic gap (HM gap), total magnetic moment (μ_{tot}), M (M= Li, Na and K) magnetic moment (μ_M), S magnetic moment (μ_S).

Compounds	a (Å)		HMgap (eV)		m_{tot} (m_B)		m_M (m_B)	m_S (m_B)
	This work	Gao	This work	Gao	This work	Gao	This work	This work
LiS	5.59	5.58	0.10	0.03	1.00	1.00	0.001	0.998
NaS	6.37	6.34	0.52	0.46	1.00	1.00	-0.027	1.026
KS	7.32	7.28	0.71	0.65	1.00	1.00	-0.032	1.030

To investigate the half-metallicity in tetragonal phase of these compounds, we calculate the total energy as a function of c/a and the DOS. The results show that, the half-metallicity is stable in a tetragonal distorted, the HM gap is 0.1, 0.5 and 0.6 respectively, for LiS, NaS and KS; That is reduced from the same one in cubic phase, but is still considerable.

Conclusion:

We used first-principles calculations based on density functional theory to investigate the electronic structure and magnetic properties of zinc-blende MS under pressure and stress. The



stability of MS half-metallicity in tetragonal structure is hopeful, so we can use these results to predict proper substrates to fabricate a thin layer of these compounds for spintronic applications.

References:

- [1] M. Moradi, Z. Soltani, *J. Appl. Phys.* **105**, (2009) 023701.
- [2] G.Y. Gao , K.L. Yao , M.H. Song , Z.L. Liu , *J. M, M.M* **323** (2011)2652-2657.
- [3] Akinaga H, Manago T and Shairai M 2000 Japan . *J. Appl.Phys.* **239** L1118.



An investigation on interfacial interaction of AP and Tris-(2-hydroxyethyl)-isocyanurate via FT-IR and FT-Raman

F. Gholamian*, R. Mojaradfar, M. Ansari

Department of Chemistry and Chemistry Engineering, MalekAshtar University of Technology, Tehran, Iran

Email: Mojaradfar@gmail.com

Key words: AP, Bonding Agent, FT-Raman, Interfacial Interaction.

Introduction:

Composite propellants are nonhomogeneous propellants and comprise primarily crystalline oxidizers and metal fuels uniformly suspended in a resin binder. The crystalline oxidizers are usually inorganic compounds, such as ammonium perchlorate (AP) or potassium nitrate but can also be organic, for example cyclotrimethylenetrinitramine (RDX) or cyclotetramethylenetetramine (HMX). The high solid loading requires an interaction between the binder and the filler in order to prevent dewetting, i.e., separation around a particle of filler. If dewetting occurs between the binder and filler, the flame front propagates below the burning surface to produce a more rapid combustion of the propellant [1]. Attempts to improve the binder-filler interaction in composite propellants have included the addition of bonding agents. A bonding agent produces an interaction between the oxidizer crystal and the binder by forming either primary or secondary bonds with the oxidizer and a primary bond with the binder. Bonding agent by producing chemical or physical bond between binder and oxidizer, prevent dewetting and improve mechanical and aging properties [2]. In our studies FT-IR and FT-Raman were used to study the interaction between Tris-(2-hydroxyethyl)-isocyanurate as a bonding agent and AP.

Experiment

1. Sample preparation:

Sufficiently dried AP powder was spread on a Teflon plate in order to make easy to remove the coagulated one later and bonding agent was dripped on it in the ratio of 1:1 (weight). To disperse bonding agent (Tris-(2-hydroxyethyl)-isocyanurate) in oxidizer uniformly, 2mL



acetone was added with stirring. The samples were placed vacuum at 60 °C, and degassed for 48h before any analysis.

2. Characterization :

FT-IR spectra were obtained by preparing KBr pellet, using Perkin Elmer Spectrum 400 FT-IR spectrophotometer in the range of 4000-400 cm⁻¹.

FT-Raman spectra were recorded by means of a Nicolet 950 dedicated spectrometer (Nd-YAG laser, 1064 nm, 50 mW laser power) and corrected to the white light background. 1024 spectra were averaged in order to improve the signal to noise ratio.

Results and discussion:

The results of FT-IR study of the interactions between Tris-(2-hydroxyethyl) -isocyanurate (THEIC) and AP is evident that spectral changes have occurred. The frequencies of OH stretching vibrations of THEIC (3487 cm⁻¹, 3368 cm⁻¹ and 3252 cm⁻¹) changed. Also the band at 625 cm⁻¹ belonging to Cl-O bending vibration shifted downward to 613 cm⁻¹. The results show that hydrogen bonds are formed between Cl-O of perchlorate and O-H of THEIC. Also the frequency of the C=O stretching vibrations of THEIC shifted downwards from 1684 cm⁻¹ to 1676 cm⁻¹. These changes indicate N-H...O=C hydrogen bond was formed. FT-Raman study shows the C-H stretching vibrations of THEIC disappeared and new band at 2989 cm⁻¹ was appeared, so the author suggested the presence of -C-H...O-Cl interaction. Also the frequency of C-N-C stretching vibration at 914 cm⁻¹ was disappeared. Thus, it is reasonable to draw the conclusion that the strong interaction between AP and THEIC have occurred.

Conclusion:

The results of observation of the interaction between AP and THEIC, by means of the FTIR and FT-Raman suggested that strong intermolecular interactions between oxidizer and bonding agent have occurred. Also the results have proved that the bonds between AP and THEIC are almost hydrogen bonds.

Reference:

- [1] J. Petković, A. Wali, D. Mijin, The Influence of Bonding Agents in Improving Interactions in Composite Propellants, Determined Using the FTIR Spectra, Scientific Technical Review 3-4 (2009) 12-16.



[2] Cucksee et al, Bonding agent system for improved propellant agent and low temperature physical properties, US Patent 4090893, (1978).

15th Physical Chemistry Conference



FT-Raman and FT-IR study on interfacial interaction of Tris-(2-hydroxyethyl)-isocyanurate with ADN

F. Gholamian*, R. Mojaradfar, M. Ansari

Department of Chemistry and Chemistry Engineering, MalekAshtar University of Technology, Tehran, Iran

Email: Mojaradfar@gmail.com

Key words: ADN, THEIC, FT-Raman, Interfacial Interaction.

Introduction:

Solid propellants are energetic polymer composites filled with finely divided solid particles. The high solid loading requires a tight adhesion between the binder and the filler in order to prevent dewetting, i.e. separation around a filler particle, which causes severe problems to the mechanical properties of propellants and the performance of rocket motor. One way of improving mechanical properties of solid propellants is to add suitable bonding agents. Bonding agent can be adsorbed on solid particles and produce a layer on solid particles and this bonding agent can react chemically with the binder. Thus bonding agent by producing chemical or physical bond between binder and oxidizer, prevent dewetting and improve mechanical and aging properties [1]. Ammonium dinitramide (ADN) is a potential oxidizer for use in propellant formulations. The molecular structure of ADN, $\text{NH}_4^+ \text{N}(\text{NO}_2)_2^-$ consists of an ammonium cation and dinitramide anion. ADN has some interesting chemical properties. It is stable between pH 3 and 15, but slowly decomposes in concentrated acid. It is sensitive energetic materials. It is also considered as a potential replacement of ammonium perchlorate (AP) due to its halogen-free combustion products, which are not detrimental to the Earth's atmosphere [2]. In our present work, by using of FT-IR and FT-Raman analysis we scrutinized interactions between Tris-(2-hydroxyethyl)-isocyanurate (THEIC) bonding agent and ADN.

Experiment:

1. Sample preparation:

Sufficiently dried AP powder was spread on a Teflon plate in order to make easy to remove the coagulated one later and bonding agent was dripped on it in the ratio of 1:1 (weight). To



disperse bonding agent (Tris-(2-hydroxyethyl)-isocyanurate) in oxidizer uniformly, 2mL acetone was added with stirring. The samples were placed vacuum at 60 °C, and degassed for 48h before any analysis.

2.Characterization:

FT-IR spectra were obtained by preparing KBr pellet, using Perkin Elmer Spectrum 400 FT-IR spectrophotometer in the range of 4000-400 cm^{-1} .

FT-Raman spectra in the 3600–100 cm^{-1} range were measured from samples, using the Nd-YAG laser excitation (50 mW) at 1064 nm with a Bruker RFS 1000 and a Nicolet Raman System 950 spectrometer under a 2 cm^{-1} resolution.

Results and discussion:

It was evident that FT-IR spectral changes have occurred in the spectrum of ADN+ THEIC. The frequencies of OH stretching vibrations of THEIC at 3487 cm^{-1} and 3252 cm^{-1} changed and the frequency at 3368 disappeared. Also the bands at 1519 cm^{-1} and 1398 cm^{-1} are attributed to -NO₂ stretching mode shifted downwards. Changing the position of absorption bands indicate interfacial interaction in the oxidizer surface. The author suggested that O-H in THEIC can participate an interaction with -NO₂ groups of ADN. The intense band due to the C=O stretching vibration of THEIC produces a maxima at about 1684 cm^{-1} which was reduced in intensity and shifted downward in interaction with ADN. In FT-Raman spectrum with absorption bands at 1471 cm^{-1} and 1197 cm^{-1} related to -NO₂ group shifted downward as a result of intermolecular interaction and the hydrogen bonding formation between THEIC and ADN. Also the intensity of band belonging to C=O stretching vibration at 1757 cm^{-1} reduced extremely.

Conclusion:

The results of the study of the interactions between ADN and the THEIC, by means of the FTIR and FT-Raman spectroscopic methods, showed that the interfacial bonding force arises from the hydrogen bonding forces. If the essential role of bonding agents is placed on producing a toughly bonded and high modulus layer at ADN surface, THEIC is recommended.



Reference:

- [1] Weishang, W. Wenhui, J. Zhanning, D. Jianwu, and T. Huiming, Investigation on Interfacial Bonding in HMX-Containing Model Propellant Composite, *Propellants, Explosives, Pyrotechnics* 20, 327-329, (1995).
- [2] A. L. Ramaswamy, Energetic-Material Combustion Experiments on Propellant Formulations Containing Prilled Ammonium Dinitramide, *Combustion, Explosion, and Shock Waves*, 36, 119-124, (2000).

15th Physical Chemistry Conference



Adsorption of Eosin Y using polyaniline-beach sand nanocomposite: kinetic and thermodynamic studies

M. Nazmi^a, R. Ansari *, A. Mohammad-khah, F. Mizani

^a Chemistry Department, Faculty of science, University of Guilan, Rasht, Iran

Email: ransari@guilan.ac.ir

Keywords: Beach Sand, polyaniline, Eosin Y, Adsorption, Isotherm

Introduction:

Eosin Y (EY), an anionic dye is used in the fields of dyeing, printing, leather, printing ink and fluorescent pigment, etc [1]. The safe removal of such a dye is the prime aim of our present research and this is accomplished by using a novel adsorbent introduced in the current work.

Materials and methods:

In this study, Beach Sand (BS) was collected from the north of Iran (Bandar Anzali) in depth of 0-25 cm from seaside. Polyaniline (Pani) was synthesized chemically, then coated onto (BS) via cast solution method [2]. The data obtained in batch model and the effect of pH, initial dye concentration, temperature and etc have been examined. The data investigated in different conditions was applied to access isotherm, kinetics and thermodynamic parameters.

Result and discussion:

Surface analysis of BS before and after polymer coating using scanning electron microscopy (SEM) showed that the nanostructure polymer with a diameter of about 65 nm coated onto the BS improves the porosity of the adsorbent and therefore enhance the performance of dye sorption. The calculated kinetic parameters of BS and Pani/BS are given in Table.1. The high value of regression coefficient (R^2) and good agreement between experimental q_e and calculated q_e from the pseudo second-order kinetic model, clearly confirm that the EY dye sorption on modified sorbent is mainly happened via chemisorption process. The values

associated with the thermodynamic parameters represented in Table 2, showed that the sorption of EY dye onto Pani/BS is a spontaneous process with endothermic nature.

Table 1: Comparison of the different kinetic model parameters at 25 °C

Adsorbent	Pseudo-first-order model			Pseudo-second order model			
	q_{e1}	k_1	R^2	q_{e2}	k_2	$q_e(\text{exp})$	R^2
	(mg/g)	(g/mg.min)		(mg/g)	(g/mg.min)	(mg/g)	
BS	4.39	0.048	0.903	0.882	0.11	4.85	0.883
Pani/BS	6.89	0.097	0.812	16.39	0.47	15.74	0.999

The positive value obtained for entropy changes also implies the increase of disorderness of the system in the course of sorption process which determines the spontaneity of the sorption process. However; in the case of unmodified BS, the spontaneity of the sorption process is mainly determined by enthalpy factor.

Table 2: thermodynamic parameters for sorption of EY onto BS and Pani/ BS

Adsorbent	T(k)	K_c	ΔG^0 (kJ/mol)	ΔH^0 (kJ/mol)	ΔS^0 (J/mol.k)
BS	273	0.06	6.36	-25.1	-111.3
	298	0.06	6.81		
	323	0.02	9.97		
	348	0.01	14.2		
	373	0.004	17.1		
Pani/ BS	273	1.84	-13.8	15.2	59.28
	298	2.31	-20.7		
	323	3.84	-36.1		
	348	6.04	-52.0		
	373	11.1	-74.8		

Conclusion:

Beach sand was found as a very economic and environmental friendly material substrate for coating by PANi (pani/BS) as a new nonconventional nanocomposite adsorbent for anionic dye removal from water or wastewaters.



References:

- [1] I. Poullos, E. Micropoulou, R. Panou, E. Kostopoulou; "Photooxidation of Eosin Y in the presence of semiconducting oxide"; *J. Appl. Cat. B: Environmental*; 41,345 (2003).
- [2] R. Ansari, A. H. Alikhani; "Application of Polyaniline/Nylon composites coating for corrosion protection of steel"; *J of Coating Technology and Research*; 6(2), 221-227 (2009).

15th Physical Chemistry Conference



Prediction of surface properties of binary refrigerant mixtures with density (volume) based model

A. Bagheri^a, F. Varaminian^{b*}, S. Khosharay^b

^a Department of Physical Chemistry, Faculty of Chemistry, Semnan University, Semnan, Iran

^b Department of Chemical, Gas and Petroleum Engineering, Semnan University, Semnan, Iran

* E-mail: fvaraminian@semnan.ac.ir

Keywords: Surface Tension, Refrigerant Mixtures, Surface Composition

Introduction:

Surface tension is an important, but often overlooked fluid physical parameter that plays an important role in technical processes such as heat transfer, flow, and phase-change characteristic of the working fluid [1]. Laaksonen and Kulmala [2] proposed an equation for surface tension of binary liquid mixtures:

$$\begin{aligned} \gamma &= \gamma_1 \varphi_1^S \\ &+ \gamma_2 \varphi_2^S \end{aligned} \quad (1)$$

where φ^S is surface volume fraction. In addition to surface tensions of pure components, pure molar volumes of components and surface mole fractions are required in order to calculate surface tension of mixture, so phase equilibrium between the bulk liquid and surface phase should be considered. Considering the surface layer as a separate phase, the chemical potential of a component i in the bulk liquid and surface phases can be given by:

$$\begin{aligned} \mu_{i,B} &= \mu_{i,B}^0 \\ &+ RT \ln \left(\frac{f_{i,B}}{f_i^0} \right) \end{aligned} \quad (2)$$

$$\begin{aligned} \mu_{i,S} \\ = \mu_{i,S}^0 + RT \ln \left(\frac{f_{i,S}}{f_i^0} \right) \\ - \gamma \bar{A}_i \end{aligned} \quad (3)$$

where γ is the surface tension of mixture, μ the chemical potential, f the fugacity, and \bar{A}_i is partial molar surface area of component i in the solution. Indexes i and S denote the i th component and surface phase. For a pure component:

$$\begin{aligned} \mu_{i,S}^0 - \mu_{i,B}^0 \\ = \gamma_i A_i \end{aligned} \quad (4)$$

At equilibrium, the chemical potentials of phases are equal:

$$\begin{aligned} \mu_{i,B} \\ = \mu_{i,S} \end{aligned} \quad (5)$$

Combination of Eqs. (2) to (5):

$$\begin{aligned} \gamma \bar{A}_i \\ = \gamma_i A_i \\ + RT \ln \left(\frac{f_{i,S}}{f_{i,B}} \right) \end{aligned} \quad (6)$$

The partial molar area of component i is considered equal to the molar area of i , so Eq. (6) simplified:

$$\begin{aligned} \gamma \\ = \gamma_i \\ + \frac{RT}{A_i} \ln \left(\frac{f_{i,S}}{f_{i,B}} \right) \end{aligned} \quad (7)$$

The VTPR EOS [3] is used to calculate the fugacities and phase equilibrium.

Result and discussion:

The surface tension and properties of R125+R152a and R32+R227ea are determined at different temperatures and compared with experimental data.

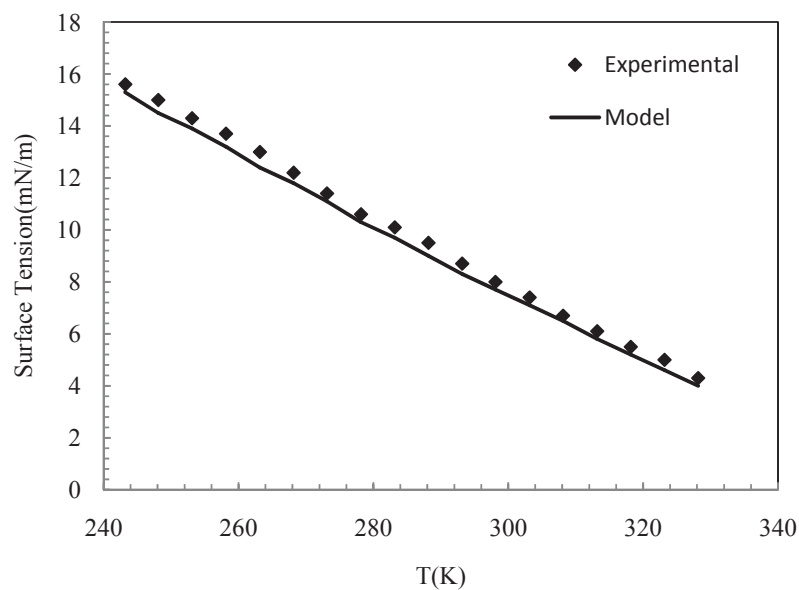


Fig.1. Surface tension vs. temperature for the 29.96 mass% R125/70.04 mass% R152a mixture. (♦) Experimental data [4]; and (—) model

Conclusions:

The combination of the Laaksonen and Kulmala model and the VTPR EOS is used to determine the surface tensions of binary refrigerant mixtures. The present model allowed the satisfactory determination of the surface tensions for the binary refrigerant mixtures.

References:

- [1] G. Zhao, S. Bi, J. Wu, Z. Liu, J. Chem. Eng. Data. 55 (2010) 3077.
- [2] A. Laaksonen, M. Kulmala, J. Chem. Phys. 95 (1991) 6745.
- [3] H. Lin, Y.Y. Duan, Fluid Phase Equilib. 233 (2005) 194.
- [4] S. Bi, G. Zhao, J. Wu, Fluid Phase Equilib. 287 (2009) 23.



Boron doped diamond like carbon nanocrystal by HFCVD

M. Dadashbab^{a*}, M. Ghoranneiss^b, M. R. Hantehzadeh^c

a.b.c Plasma Physics Research Center, Science and Research Branch, Islamic Azad University, Tehran, Iran

Email: dadashbaba@yahoo.com

Key words: Icosahedral, HFCVD, Boron Carbide, Cauliflowers

Introduction:

Diamond-like carbon (DLC) is an amorphous carbon material made of random networks of sp^3 and sp^2 hybrid bonds. DLC material with high sp^3 content has similar properties as single crystal or polycrystalline diamond in that they are hard, electrically insulating, chemically inert, very good heat conductors, that they show high electron and hole mobility, negative electron affinity, high breakdown field, light weight, large band gaps (> 2 eV), and a high index of refraction ($n > 2$). The aim of this research is to present experimental results on the synthesis of DLC and B_4C , nanostructure, chemical composition, deposition rate using hot filament chemical vapour deposition (HFCVD) and to discuss the influence of boron content on the surface morphology, crystallographic structure of the deposited films [1-2].

Materials and methods:

DLC films with different boron-doping levels were produced using solutions with varying boron (B) concentrations, i.e., 0.00626, 0.0125, 0.025 and 0.05 molar (a), (b), (c), (d) named respectively. The growth process was triggered upon introducing hydrogen gas (H_2) passing through ethanol as B_2O_3 solution in various concentrations in ethanol. Initially, Fe films were sputtered on the P-type silicon wafer. A pure hydrogen gas flow rate of approximately 100 sccm and a total pressure of 15 Torr. The substrate temperature was 500 °C. Prior to synthesis, etching was performed in H_2 ambient for 10 minutes. The deposition duration of all samples was kept at 30 min in this research.

Result and discussion:

All XRD peaks at 23.60°, 40.32°, 48.25°, 53.40°, 75.43°, 80.55° originated from $B_{13}C_2$. According to XRD results, the average diameter of nanocrystals was between 0.8-7 nm.



calculated by debye-scherr formula. The results of FE-SEM, TEM showed that the films possess an amorphous cauliflower-like structure [3-4]. Raman spectroscopy shows that one of the B_4C modes is found around 275 cm^{-1} - 325 cm^{-1} and other B_4C modes at $650\text{--}1000\text{ cm}^{-1}$ also put the same scaling characteristic on view. The whole selection rules can be disregarded while at a higher degree of disorder, and the total density of phonons can be observed. Particularly, at 1350 cm^{-1} and 1580 cm^{-1} , phonons can be observed illustrating the existence of microcrystalline graphite and the scattering intensity in the $1400\text{--}1600\text{ cm}^{-1}$ region will be due to non-diamond-carbon impurities. The size of the graphite crystallites is inversely proportional to the I_D/I_G ratio, in other words, $I_D/I_G = C/L_a$, where L_a is the sp^2 correlation length or in-plane crystallite size. The broadening of G-band along with the simultaneous decrease of I_D/I_G , accompanied by the coexistent downshift in both G and D peaks, originate from incorporating B into DLC films facilitates the formation of a film with a boosted sp^3 bonding structure and the decrease the intensity of G and D peaks may stem from disrupting the vibrational behavior of the film and diminution of polarizability in the molecules of the lattice. One of the factors inducing the decrease of polarizability may be the promotion of a great fraction of δ bonds between B-C atoms. Due to the grain size reduction and the subsequent phonon confinement which induces phonons away from Γ to be involved with $q=1/L_a$. In accordance with Tuinstra-Koenig formula, L_a decreases with the increase of the intensity of D-band which appears as a result of boron defects in the structure from 73 to 42 nm. TEM images illustrate that the size of produced clusters is Average 22 nm [5-6].

Conclusion:

According to XRD patterns, SEM images and Raman spectra, the structure of the film was determined as DLC along with grown boron carbide icosahedrals ($B_{13}C_2$) in its texture. The size of these icosahedrals was between 0.8-7 nm. The decrease observed in the intensity of G and D peaks may stem from disrupting the vibrational behavior of the film and diminution of polarizability in the molecules of the lattice.

Reference:

- [1] Z.Q. Ma, B.X. Liu. *Ins in solar cell*. Solar Energy Materials & Solar Cells 69 (2001)



- [3] T Fujii¹, Y Mori¹, H Hyodo, and K Kimura. Joint AIRAPT-22 & HPCJ-50 IOP Publishing Journal of Physics: Conference Series 215 (2010) 012011
- [4] R.M. Mohanty, K. Balasubramanian and S.K. Seshadri. Raw Materials, Processing, Properties, Degradation and Healing
- [5] Fanchini G, McCauley JW, Chhowalla M. Physical Review Letters 2006;97:035502
- [6] R. Kostic, M. Miric^α, T. Radic, M. Radovic, R. Gajic and Z.V. Popovic. Vol. 116 (2009) Acta Physica Polonica A No. 4

15th Physical Chemistry Conference



The synergism between nanostructured CdS and CdO in photocatalytic degradation of methylene blue

H. Farsi^{a,b}, S.Z. Askari^{a,*}

^a Department of Chemistry, University of Birjand, P.O. Box: 97175-615, Birjand, Iran

^b Solar Energy Research Department, University of Birjand, Birjand, Iran

Email: sz_askari208@yahoo.com

Key words: Nanostructure, cadmium oxide, cadmium sulfide, photocatalyst, methylene blue

Introduction:

Sulphide photocatalysts, which have narrow band gaps and valence bands at relatively negative potentials compared to oxides, are good candidates for visible light-driven photocatalysts. Among the available sulphide semiconductors nanosized CdS is an interesting photocatalyst material, since it has a narrow band gap (2.4 eV). However, the photocatalytic properties of CdS are limited as a consequence of its photocorrosion under visible light irradiation [1]. Nevertheless, there are strategies for reducing photocorrosion and increasing the photocatalyst efficiency of CdS, which one of them is combining the CdS semiconductor with other semiconductors with different energy. The optoelectronic properties of CdO make these materials interesting as semiconductors for combining with CdS. CdO exhibits a band gap in the interval 2.2–2.4 eV with high transmittance and very low resistance. There are interesting results showing the increase in CdS activity for samples mixed with CdO [2, 3]. In this work, we have developed a simple route for preparing of CdO-CdS nanocomposites and studied photocatalytic degradation of methylene blue using the prepared nanocomposites.

Materials and methods:

(NH₄)₂S, Cd(NO₃)₂·4H₂O, NaOH were Merck products and Methylene blue, MB, purchased from Aldrich. All chemical materials were used without further purifications and all solutions prepared using double-distilled water. The CdS_xO_{1-x} nanocomposites where x=0, 0.25, 0.5, 0.75 and 1 were prepared by coprecipitation method by controlling the ratio of (NH₄)₂S to NaOH in a solution which is added to 0.4M Cd(NO₃)₂ and refluxing the reaction mixture for 10 hours at 120°C. The morphology and crystal structure of deposited materials was studied



by TEM and XRD. Finally, the catalytic degradation of MB on the surface of all samples was measured in dark and the presence of sun light at 1.5 P.M. The converted amount of MB was determined by the absorption peak height in λ_{max} of MB using UV-Vis spectroscopy.

Apparatus:

The crystal structure of the obtained materials was investigated by using of a Bruker, Advane D8 diffractometer with Cu-K α radiation ($\lambda=0.15404$ nm). The morphology and particle size of the nanocomposites was studied by Zeiss-EM 10C TEM. UV-Vis studies were carried out by Shimadzu UV-2501 PC, UV-Vis spectrometer.

Results and discussion:

The kinetics studies verified a first order rate law for degradation of MB on the surface of all samples in the both dark (catalytic degradation) and presenting light (photocatalytic degradation). Also, the rate constant for photocatalytic degradation of MB was around ten times more than its catalytic degradation. All composites showed more activities for catalytic degradation of MB compared to pure CdS and CdO emphasizing on a contact synergism between CdS and CdO. Also, the photocatalytic activities of nanocomposites were more than pure CdS and CdO unless CdS_{0.5}O_{0.5}, emphasizing a different mechanism for synergism between CdS and CdO in the presence of light. It is claimed that photogenerated electrons in these composite systems move from CdS to the attached CdO, while photogenerated holes remain in CdS. This charge-carrier separation therefore stops charge recombination improving the photocatalytic activity of CdS.

Conclusion:

Our studies showed the existance a synergism between CdS and CdO in their nanocomposites for both catalytic and photocatalytic degradation of MB. The maximum measured rate constant for photocatalytic degradation of MB was $13.0 \times 10^{-3} \text{ min}^{-1}$ which belonged to nano-CdO_{0.25}S_{0.75}.

References:

- [1] D. Missner, R. Memming, B. Castening, J. Phys. Chem., **92** (1988) 3476.



- [2] N. Bühler, K. Meier, J.F. Reber, J. Phys. Chem., **88** (1984) 3261.
[3] R.M. Navarro, F. del Valle, J.L.G. Fierro, Int. J. Hydrogen Energy, **33** (2008) 4265.

15th Physical Chemistry Conference



Ultrasound-treated TiO₂ for removal of anionic surfactant

P. Pourahmadi, M.A. Zanjanchi*, M. Arvand

Department of Chemistry, Faculty of Science, University of Guilan, Rasht, 41335-1914, Iran

E-mail address: zanjanchi@guilan.ac.ir

Key words: TiO₂, Mesoporous, Ultrasound, surfactant

Introduction:

Surfactants are one of the most common pollutants that can be found in wastewaters and water resources. They also act as mediators for other pollutants like oils, pesticides and organochlorine compounds. Biodegradation of surfactants is a common methodology for purification of unsafe waters. Mesoporous TiO₂ may be considered as a suitable material offering excellent characteristics. We use it as expedient material for testing their adsorption properties [1].

Materials and methods:

Mesoporous TiO₂ crystals were synthesized from TiCl₄ via sol-gel process in the presence of cetyltrimethylammonium bromide (CTAB), which was used as a structure-directing agent. Adsorption of an anionic surfactant (sodium dodecyl sulfate: SDS) was performed using the pure and ultrasound-treated TiO₂ samples.

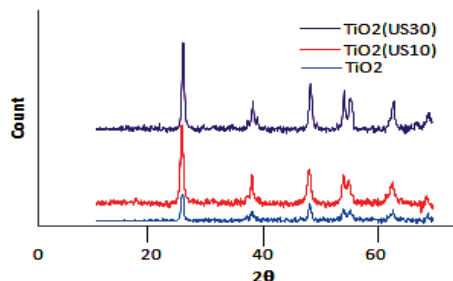
Apparatus:

The structural and textural properties of our prepared mesoporous TiO₂ were investigated by X-ray diffractometry (Philips PW1840, using CuK α irradiation) and nitrogen adsorption measurement (Sibata SA-1100).

Result and discussion:

XRD and BET measurements indicate that the TiO₂ samples possesses anatase crystalline lattice and specific surface area 254 m² g⁻¹, respectively. The cationic template was removed by ultrasound waves irradiated on TiO₂ samples for various times. The sonicated samples loss

parts of their template according to the time of sonication [2]. Figure shows the XRD patterns for two $\text{TiO}_2(\text{US10})$ and $\text{TiO}_2(\text{US30})$ samples treated in ultrasonic bath for 10 and 30 min, respectively. They have been compared with that of the pure mesopore TiO_2 . Adsorption of SDS on the pure and sonicated TiO_2 samples were investigated. The Table shows the amount of SDS removal for different samples. It shows that the as-synthesized TiO_2 was not able to adsorb high amounts of SDS, most probably due to the restricted space for diffusion. In order to increase the space, different amounts of CTAB were expelled out of the pores of TiO_2 using ultrasound treatment. The increase in adsorption capacity may be attributed to the formation of the exposed positive charged layers to negative SDS molecules which provide suitable conditions for adsorption.



Sample	% CTAB residual	% Removal SDS
TiO_2	100	38
$\text{TiO}_2(\text{US5})$	79	54
$\text{TiO}_2(\text{US10})$	58	61
$\text{TiO}_2(\text{US20})$	49	26
$\text{TiO}_2(\text{US30})$	40	10

Conclusion:

Ultrasound-treated TiO_2 shows high capability for the removal of SDS from aqueous environment.

References

- [1] A. Ariapad, M.A. Zanjanchi, M. Arvand, Desalination 284 (2012) 142–149
- [2] M.A. Zanjanchi, H. Golmojdeh, M. Arvand, Journal of Hazardous Materials 169 (2009) 233–239



Kinetics and thermodynamic study of aniline adsorption by SBA-15 with non-ionic substrate (P123) from aqueous solution

A. Baghernazari Baghban^{a*}, M. Bahmaie^a, A. Naeemy^{b, c}, S. Pourmand^a

^a Department of Chemistry, Islamic Azad University, North Tehran Branch, Tehran, Iran

^c Department of Drug and Food Control, Faculty of Pharmacy, Tehran University of Medical Sciences, Tehran, Iran

E-mail address: amirbaghernazari@yahoo.com (a.baghernazari)

Key words: Aniline, Equilibrium Isotherm Study, Mesopore, SBA-15.

Introduction:

Phenols and phenolic compounds in general are currently produced by industries like petroleum refining, leather and textile, and olive oil production; thus a significant amount of these compounds is present in the corresponding wastewater [1]. The amount of aniline produced in US and China is over 457,000 and 80,000 t per year, respectively. There were more than 150 kinds of down-stream products of aniline. Aniline has great harmful effect for public health and environmental quality, so more and more rigorous limits on the letting amount of aniline have been established. Especially, aniline-contained wastewater has brought a series of serious environmental problem because of its high toxicity and accumulation in the environment. Adsorption technology in particular has been used for the removal of organic compounds from wastewater [2]. Mesoporous silicates (SBA and MCM types) offer a number of potential advantages of nanoporous materials (IUPAC classification [3]), as adsorbents including larger pore volume and diameter, high surface area and regular channel type structures [4].

In this work, we studied the aniline adsorption on a mesoporous SBA-15 with non-ionic substrate (P123) from its aqueous solution and a comparison of five isotherms such as Langmuir, Freundlich and Redlich–Peterson, have been applied to the experiment of aniline sorption on this nano adsorbent.



Materials and methods:

Pluronic P123 (EO₂₀–PO₇₀EO₂₀), Tetraethoxysilane (TEOS, 98%), RHCl₃.4H₂O, Acetic acid, sodium acetate, sodium hydrogen phosphate, sodium dihydrogen phosphate, hydrochloric acid, sulfuric acid, nitric acid, Aniline, were products of Merck (Darmstadt, Germany).

Apparatus:

IR spectra were recorded on a FT-IR spectrometer Perkin-Elmmer/ Spectrum Gx by KBr pellet method. UV-Visible Varian, Cary 100 bio (Salt lake city, Australia) was used for measuring the concentration of Aniline. X-ray diffraction (XRD) analysis was recorded on a (Smart APEX CCD, Bruker, Germany).

Result and discussion:

Adsorption of Aniline on P123–SBA-15 is studied. It is found that P123–SBA-15 shows significant adsorption for Aniline. Batch adsorption studies have been carried out to find the optimum value of various parameters, such as contact time (40 min), pH (6.5) and adsorbent dose (40 mg). A recovery of 88% was obtained for the aniline with 1.5 M HCl as eluting agent. Kinetic adsorption data were analyzed by adsorption and desorption time of Aniline on mesopore. The equilibrium adsorption data of Aniline were analyzed by five isotherm models such as Langmuir, Freundlich and Redlich–Peterson. Langmuir isotherm parameters obtained from the four Langmuir linear equations by using linear method. The coefficient of determination for both theoretical Langmuir-1 and Redlich–Peterson isotherms were higher than those obtained for Freundlich isotherm, indicating that the adsorption system is more likely monolayer coverage of the SBA-15 surface by the aniline. The value of the apparent energy of adsorption from the Dubinin-Radushkevich isotherm, which was calculated 3.9601 KJ/mol.

Conclusion:

The Aniline adsorption was due to immobilized ligand- aniline interactions. The mesopores also present the advantage of high adsorption capacity, good reusability and high chemical stability. The sorption/desorption of aniline takes place in moderate time, making the analytical procedure reasonably fast.



Reference:

- [1] F. Cermola, M. Dellagrecia, A. Pollio, F. Temussi, *Chemosphere*, **55**, 1035 (2004).
- [2] S.P. Kamble, P.A. Mangrulkar, A.K. Bansiwai, *Chem. Eng. J.* **138**, 73 (2008).

15th Physical Chemistry Conference



Waterproofing material for inhibition of ammonium nitrate hygroscopicity by microencapsulation

A. Eslami^{*a}, S.G. Hosseini^b R. Mahmodi^a

^a Faculty of Chemistry, University of Mazandaran, P.O. Box 47416-95447, Babolsar, Iran

^b Department of Chemistry, Malek Ashtar University of Technology, P.O. Box 16765-3454, Tehran, Iran

Email: Eslami@umz.ac.ir

Keyword: Ammonium nitrate, Solvent/non-solvent, Microencapsulation, Hygroscopicity

Introduction:

Composite propellant based on ammonium perchlorate (AP) as oxidizer is extensively used in rocket and satellites launch vehicles [1]. However, global environment impact restricts AP-based propellant because of their HCl exhaust. Therefore, efforts are on to find out propellants with clean exhaust. In this view, ammonium nitrate (AN) can be considered as effective alternative for AP in the field of propellant and explosive with the advantageous that it is cheap, easily available and forming no HCl on firing [2]. It is more than half a century that AN is being used as a fertilizer and up to now no ecological problems has been reported [3]. However, the main disadvantage for the application of AN as solid propellant oxidizer is its dimensional instability due to occurrence of polymorphic transition near the propellant processing and storage temperature and its high hygroscopic [1]. In this study, the attempts are aimed at overcoming the hygroscopicity problem of ammonium nitrate through its microencapsulation with waterproofing material, nitrocellulose (NC).

Experimental:

Phase stabilized AN was prepared through its coating with NC. The coating experiments were performed using a solvent /non-solvent method which works based on the coacervation principle, in which acetone and n-hexane were used as solvent and non-solvent, respectively. The microencapsulation experiment variables (percent of stabilizer, addition time of non-solvent, stirring speed of the mixture and the volume of non-solvent) were changed as shown below.



Trial number	Stabilizer NC (%)	Stirring speed of the mixture (rpm)	Non-solvent volume(ml)	Time (min)
1	2	30	10	20
2	4	60	20	40
3	6	90	30	60

Result and discussion:

Gravimetric analysis of the samples of ammonium nitrate coated with waterproofing material, as well as uncoated ammonium nitrate, were conducted at different relative humidity under controlled condition using appropriate saturated salt solution {KCl (73% RH), $\text{Ca}(\text{NO}_3)_2$ (53%), MgCl_2 (33%), NaCl (65%)} and different exposure time. The result indicate that NC is a waterproofing for AN. Attempts were made to confirm the waterproofing ability of NC to ammonium nitrate using XRD patterns as an experimental tool.

Conclusion:

The NC has been found to be the waterproofing material for AN. The coating of AN with 4 percent NC decreases the hygroscopicity of AN drastically. X-ray diffraction and DSC studies revealed that NC-coated AN was non- hygroscopic. In fact, the hygroscopicity of AN which is responsible for the restricted use of AN as a solid propellant oxidizer decreases upon its microencapsulation with NC.

References:

- [1] S. Mathew, K. Krishnan, K. N. Ninan; *Propell. Explos. Pyrot.* 23 (1998) 150-154
- [2] S. Mathew, K. Krishnan, K. N. Ninan; *Defence Sci. J.* 49 (1999) 65-69
- [3] A. O. R. Sudhakar, S. Mathew, *Thermochim. Acta* 451 (2006) 5-9